OVERLAND FLOW MODELLING USING APPROXIMATE CONVECTION-DIFFUSION EQUATIONS
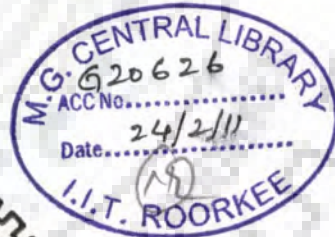
A THESIS

Submitted in partial fulfilment of the
requirements for the award of the degree
of

DOCTOR OF PHILOSOPHY

in

HYDROLOGY

by

KALE RAVINDRA VITTHAL

DEPARTMENT OF HYDROLOGY
INDIAN INSTITUTE OF TECHNOLOGY ROORKEE
ROORKEE-247 667 (INDIA)
AUGUST, 2010

INDIAN INSTITUTE OF TECHNOLOGY ROORKEE
ROORKEE

CANDIDATE'S DECLARATION

I hereby certify that the work which is being presented in the thesis entitled **OVERLAND FLOW MODELLING USING APPROXIMATE CONVECTION-DIFFUSION EQUATIONS** in partial fulfilment of the requirements for the award of the degree of Doctor of Philosophy and submitted in the Department of Hydrology, Indian Institute of Technology Roorkee, Roorkee is an authentic record of my own work carried out during a period from July 2004 to August 2010 under the supervision of Dr. M. Perumal, Professor, Department of Hydrology, Indian Institute of Technology Roorkee, Roorkee.

The matter presented in this thesis has not been submitted by me for the award of any other degree of this or any other Institute.

(KALE RAVINDRA VITTHAL)

This is to certify that the above statement made by the candidate is correct to the best of my knowledge.

(M. Perumal)
Supervisor

Date: August 31, 2010

The Ph. D. Viva-Voce Examination of **Mr. Kale Ravindra Vitthal**, Research Scholar, has been held on ...., 2010.

Signature of Supervisor   Signature of External Examiner

ABSTRACT

This study deals with the development of variable parameter Muskingum overland flow routing methods as an extension of the variable parameter Muskingum discharge hydrograph (VPMD) river routing method advocated by *Perumal* in 1994 and the variable parameter Muskingum stage hydrograph (VPMS) river routing method developed by *Perumal and Ranga Raju* in 1998, after duly accounting for the occurrence of uniform rainfall over the plane. Both these VPMD and VPMS overland flow routing methods, like the corresponding channel routing methods, have been developed from the approximate convection-diffusion (ACD) equations in discharge and flow depth formulations, respectively, which are directly derived from the Saint-Venant equations (SVE). The routing parameters of these methods expressed in terms of flow and plane characteristics are varied by accounting for the longitudinal gradient of the water depth in their relationships in a way consistent with the variation built into the solutions of the SVE. The Hortonian overland flow modelling is accomplished by coupling the Green-Ampt (GA) infiltration model with the VPMD and VPMS overland flow routing model frameworks. All these methods are studied herein for their strengths and weaknesses in reproducing the benchmark solutions of the full SVE and its variants. The present study is conducted with the following four objectives: 1) To extend the VPMD channel routing method for overland flow modelling studies and to compare its performance with those of other currently used methods; 2) To extend the VPMS channel routing method for overland flow modelling studies and to compare its performance with those of other currently used methods, and with that of the corresponding VPMD overland flow routing method; 3) To develop the applicability criteria for the above methods; and 4) To apply the above methods for Hortonian overland flow generation and to compare the performance of these methods with those of other currently used methods.

The VPMD overland flow routing method is also applied as a component model for runoff generation from a level V-catchment wherein the channel routing is accomplished using the VPMD channel routing method. The interception loss required for runoff computation of the V-catchment is accounted using a ϕ-index type method. The operational performance evaluation of the VPMD method is extensively carried out using the hypothetical overland flow data available in literature, besides the hypothetical numerical solutions obtained from the use of SVE, the laboratory and field overland flow data. Further, the VPMD solutions are evaluated by comparing with the corresponding analytical

solutions of the kinematic wave (KW) equation. The numerical study of the VPMD method reveals that it is not necessary to strictly follow the Courant condition $C_{un} \approx 1$ as used in the conventional solution methods for preserving the numerical stability. However, to preserve the solution accuracy and efficient mass conservation ($EVOL \ll 5\%$), the Courant condition may vary in the range $0.1 < C_{un} < 10$. The proposed VPMD method is found to be advantageous over the currently available numerical overland flow simulation methods because of its unconditional numerical stability, high accuracy level, and higher degree of flexibility in the selection of the computational spatial and temporal grid sizes; thus, making it amenable for coupling with various land surface schemes (LSSs) available for meso and micro-scale catchment modelling studies for assessing the impact of land use and climate changes on catchment runoff.

The operational performance of the VPMS method is also extensively evaluated using the same data set as used for evaluating the VPMD overland flow routing method. The efficacy of the VPMS solutions are compared with the corresponding VPMD solutions to verify the merits and demerits of using flow depth as an operating variable in the overland flow models in lieu of using the discharge variable. The results reveal that the VPMS method provides comparatively more flexibility in selecting the computational time interval and slightly more accuracy level in reproducing the overland flow depth hydrographs than the VPMD and KW methods. Hence, the VPMS method is amenable for meso and micro-scale catchment modelling, especially dealing with sediment erosion problem, by coupling with various LSSs.

In order to be consistent with the criterion used for the classification of one-dimensional flood waves derived from the SVE and their applicability limits, a novel applicability criterion based on the magnitude of scaled longitudinal flow depth gradient $(1/s_0)(\partial y / \partial x)_e$ is developed for both the VPMD and VPMS overland flow routing methods. In practice, the applicability limits of the variants of the SVE for overland flow modelling are commonly assessed using the kinematic wave number (k) and $(kF_{rp}^2)_e (=1/\mu)$ (where, F_{rp} is the Froude number). In this study, the physical basis of the applicability criterion 'μ' is established as: $\mu = (m+1)(1/s_0)(\partial y / \partial x)_e$, where m is the exponent of the Manning's (⅔) or Chezy's (½) friction law. A total of 2268 numerical experiments, each for the VPMD and VPMS methods were conducted to formulate the applicability criteria. The applicability limits of the VPMD and VPMS overland flow routing methods are assessed and quantified by comparing the routing results arrived at the outlet of an overland flow plane for various

hypothetical cases, comprising of different combinations of rainfall intensities, overland flow plane lengths and slopes, and Manning's roughness coefficients, with the corresponding benchmark solutions of the full SVE and ACD equations. Such evaluation reveals that at 95% accuracy level of these performance evaluation measures, the applicability limits of the VPMD and VPMS overland flow methods can be fixed at: $(1/s_0)(\partial y/\partial x) \leq 0.6$ and $(1/s_0)(\partial y/\partial x) \leq 0.35$, respectively. Hence, the VPMD method can be successfully used over the entire applicability range of the KW and to a greater extent of the applicability limits of the diffusive wave models. However, the applicability limit of the VPMS method is restricted as compared to that of the VPMD method for overland flow modelling, which is contrary to the applicability limits of the corresponding channel routing methods.

Further, for simulating the Hortonian overland flow process, the GA infiltration model is coupled with the VPMD and VPMS overland flow routing methods through sink/source type coupling to develop the VPMD-GA and VPMS-GA models, respectively. These two methods are well-tested by using the numerical experiment data accounting for the spatial heterogeneity in the model framework. The simulation results reveal that these overland flow routing methods are capable of closely reproducing the solutions of the hydrodynamic and characteristic-based KW models. Although, the source/sink type coupling is not able to ensure full volume conservation as compared to the full dynamic, sequential-iterative, and decoupling approaches, it provides liberty from the numerical complexity and ensuring simplicity in modelling. Furthermore, these models are very simple to formulate, unconditionally stable, accurate, CPU-run time efficient, and provide relatively wide flexibility in the computational grid sizes selection. Hence, these VPMD-GA and VPMS-GA coupled overland flow routing methods can also be used for basin modelling of different scales.

ACKNOWLEDGEMENTS

TABLE OF CONTENTS

LIST OF FIGURES

LIST OF TABLES

NOTATIONS

The following symbols are used in this thesis:

A	=	channel cross-sectional area of flow [L^2];
a	=	soil parameter in equation (6.12)[-];
a_c^*	=	non-dimensional convective acceleration term [-];
a_l^*	=	non-dimensional local acceleration term [-];
A_M	=	channel cross sectional area in the Muskingum sub-reach at section M of Figures 2.1, 3.2 and 4.2 [L^2];
a_p^*	=	non-dimensional pressure gradient term [-];
A_0	=	cross sectional area of flowing water corresponding to Q_0 [L^2];
A_3	=	channel cross sectional area in the Muskingum sub-reach at section 3 of Figures 2.1, 3.2 and 4.2 corresponding to the flow depth Y_3 [L^2];
B	=	$\partial A / \partial Y$ = channel top width [L];
b	=	soil parameter in equation (6.12) [-];
B_{SP}	=	Smith-Parlange infiltration model parameter [L];
B_0	=	$(\partial A / \partial Y)_0$ = top width of the channel cross-section corresponding to Q_0 or Y_0 [L];
C	=	celerity of flood wave in a rectangular channel [LT^{-1}];
c	=	celerity of the overland flow wave [LT^{-1}];
C_c	=	Muskingum channel flow routing coefficient for the first sub-reach when $t \geq \Delta t$ and for the rest of the sub-reaches when $t = \Delta t$ [-];
$C_{c1}, C_{c2}, C_{c3},$ C_{c4}	=	coefficients of the Muskingum channel flow routing equation [-];
CD	=	coefficient of determination [-];
c_d	=	wave celerity of the dynamic wave [LT^{-1}];
C_f	=	Manning's or Chezy's friction coefficient [-];
C_h	=	Chezy's roughness coefficient [-];
c_{max}	=	maximum value of c for the considered rainfall-runoff event [LT^{-1}];
C_p	=	Muskingum overland flow routing coefficient for the first sub-reach when $t \geq \Delta t$ and for the rest of the sub-reaches when $t = \Delta t$ [-];
CRM	=	coefficient of residual mass (in percentage) [-];
C_{un}	=	Courant number [-];
C_0	=	reference flood wave celerity corresponding to Q_0 or Y_0 [LT^{-1}];
c_0	=	reference wave celerity corresponding to q_0 or y_0 [LT^{-1}];

C_1, C_2, C_3, C_4	=	coefficients of the Muskingum overland flow routing equation [-];
c_3	=	celerity of the overland flow wave in the Muskingum sub-reach at section 3 of Figures 3.1, 4.1 and 6.1 [LT^{-1}];
D	=	hydraulic diffusivity coefficient of overland flow wave [L^2T^{-1}];
D_h	=	hydraulic diffusivity coefficient of channel flood wave [L^2T^{-1}];
$D^{\bullet}$	=	non-dimensional rainfall duration which is ratio of rainfall duration, t_r to the estimated time to equilibrium using the analytical KW approach [-];
$EVOL$	=	percentage error in the volume conservation [-];
F	=	cumulative infiltration depth since start of the infiltration [L];
f	=	water infiltration rate into the soil at the computational node [LT^{-1}];
F_p	=	cumulative infiltration depth at the time of ponding [L];
F_{rc}	=	Froude number in the channel flow routing [-];
F_{rp}	=	Froude number at the end of the overland flow plane routing sub-reach [-];
$(F_{rp})_e$	=	value of F_{rp} at the end of the overland flow plane at equilibrium [-];
F_{rcM}	=	Froude number in the Muskingum sub-reach at the midsection M of Figures 2.1, 3.2 and 4.2 [-];
F_{rpM}	=	Froude number in the Muskingum sub-reach at the midsection M of Figures 3.1, 4.1 and 6.1 [-];
$(F_{rp})_{min}$	=	minimum value of F_{rp} for the considered rainfall-runoff event [-];
$(F_{rc})_0$	=	Froude number corresponding to Q_0 or Y_0 [-];
$(F_{rp})_0$	=	Froude number corresponding to q_0 or y_0 [-];
F_1	=	cumulative infiltration depth at time $(t - \Delta t)$ [L];
F_2	=	cumulative infiltration depth at the current time level t for the considered sub-reach [L];
$f_2^{(avg)}$	=	average infiltration over a time interval Δt [LT^{-1}];
g	=	acceleration due to gravity [LT^{-2}];
I	=	inflow discharge in the Muskingum sub-reach at section 1 of Figures 2.1, 3.2 and 4.2 [L^3T^{-1}];
i	=	inflow discharge in the Muskingum sub-reach at section 1 of Figures 3.1, 4.1 and 6.1 [L^2T^{-1}];
I_a	=	rate of loss due to abstraction [LT^{-1}];
I_1	=	inflow discharges to the Muskingum routing sub-reach of the channel at previous time level [L^3T^{-1}];
i_1	=	inflow runoff discharge to the computational reach of the overland flow plane at the previous time level [L^2T^{-1}];
I_2	=	inflow discharges to the Muskingum routing sub-reach of the channel at current time level [L^3T^{-1}];

i_2	=	inflow runoff discharge to the computational reach of the overland flow plane at current time level $[L^2T^{-1}]$;
K	=	wave travel time parameter of the Muskingum overland flow routing equation $[T]$;
k	=	kinematic wave number $[-]$;
K_{av}	=	average saturated hydraulic conductivity $[LT^{-1}]$;
K_c	=	flood wave travel time parameter of the Muskingum channel flow routing equation $[T]$;
k_{min}	=	minimum value of k for the considered rainfall-runoff event $[-]$;
K_s	=	saturated hydraulic conductivity of the soil $[LT^{-1}]$;
KF	=	$1/n$ = constant in the explicit applicability criteria advocated by *Hager and Hager* [1985] $[-]$;
$k(F_{rp}^2)_e$	=	applicability criterion parameter estimated at equilibrium $[-]$;
$\left\|kF_{rp}^2\right\|_{min}$	=	minimum value of applicability criterion kF_{rp}^2 for the considered rainfall-runoff event $[-]$;
L	=	length of the overland flow plane $[L]$;
l	=	distance between the midsection and the normal discharge section of the Muskingum sub-reach as shown in Figures 3.1, 4.1 and 6.1 $[L]$;
L_c	=	distance between the midsection and the normal discharge section of the Muskingum sub-reach as shown in Figures 2.1, 3.2 and 4.2 $[L]$;
L_{CH}	=	length of the channel $[L]$;
L_L	=	length of the left hand side overland plane in the V-catchment $[L]$;
L_R	=	length of the right hand side overland flow in the V-catchment $[L]$;
m	=	exponent which depends on the friction law (i.e., the Manning's friction law or the Chezy's friction law) used $[-]$;
N	=	total number of outflow runoff hydrograph ordinates $[-]$;
n	=	Manning's roughness coefficient of the overland flow plane reach $[-]$;
n_c	=	Manning's roughness coefficient of the channel reach $[-]$;
P	=	wetted perimeter of the channel flow section $[L]$;
Q	=	outflow discharge from the Muskingum sub-reach at section 2 of Figures 2.1, 3.2 and 4.2 $[L^3T^{-1}]$;
q	=	flow rate per unit width of the overland flow plane $[L^2T^{-1}]$;
$\overset{\bullet}{q}$	=	normal runoff discharge corresponding to the flow depth y or y_e $[L^2T^{-1}]$;
q_{ci}	=	ith ordinate of the computed outflow runoff hydrograph at the downstream end of the overland flow plane/ channel in the V-catchment $[L^2T^{-1}]$;
q_e	=	runoff discharge at the end of an overland flow plane at equilibrium

$[L^2T^{-1}]$;

$q_{e,ACD}$	=	estimated value of q_e using the ACD momentum equation $[L^2T^{-1}]$;
$q_{e,Actual}$	=	actual value of q_e $[L^2T^{-1}]$;
$q_e/q^{\cdot}$	=	normalized equilibrium discharge [-];
Q_L	=	net lateral channel inflow/unit width of the overland flow plane $[L^2T^{-1}]$;
q_L	=	net rate of lateral inflow per unit area of the overland flow plane or average lateral inflow rate within the computational reach over Δt $[LT^{-1}]$;
q_{LH}	=	unit width discharge from the left hand side overland flow plane $[L^2T^{-1}]$;
Q_M	=	discharge in the Muskingum sub-reach at the midsection M of Figures 2.1, 3.2 and 4.2 $[L^3T^{-1}]$;
q_M	=	discharge in the Muskingum sub-reach at the midsection M of Figures 3.1, 4.1 and 6.1 $[L^2T^{-1}]$;
q_{oi}	=	ith ordinate of the observed/benchmark model outflow runoff hydrograph at the downstream end of the overland flow plane/ channel in the V-catchment $[L^2T^{-1}]$;
$\overline{q}_{oi}$	=	mean of the observed/benchmark model outflow runoff hydrograph ordinates at the downstream end of the overland flow plane/ channel in the V-catchment $[L^2T^{-1}]$;
q_{pc}	=	computed peak runoff discharge $[L^2T^{-1}]$;
q_{perr}	=	percentage error in peak runoff estimation [-];
q_{po}	=	observed/benchmark model peak runoff discharge $[L^2T^{-1}]$;
q_{RH}	=	unit width discharge from the right hand side overland flow plane $[L^2T^{-1}]$;
$Q_L V / Ag$	=	momentum component due to lateral inflow or outflow in the channel flow routing momentum equation [-];
$q_L v / gy$	=	momentum component due to lateral inflow or outflow in the overland flow routing momentum equation [-];
Q_0	=	reference discharge corresponding to the reference stage Y_o $[L^3T^{-1}]$;
q_0	=	reference overland flow discharge $[L^2T^{-1}]$;
Q_1	=	outflow discharges from the Muskingum routing sub-reach of the channel at previous time level $[L^3T^{-1}]$;
q_1	=	outflow runoff discharge from the computational reach of the overland flow plane at the previous time level $[L^2T^{-1}]$;
Q_2	=	outflow discharges from the Muskingum routing sub-reach of the channel at current time level $[L^3T^{-1}]$;
q_2	=	outflow runoff discharge from the computational reach of the

		overland flow plane at the current time level [L^2T^{-1}];
Q_3	=	normal discharge in the Muskingum sub-reach at section 3 of Figures 2.1, 3.2 and 4.2 [L^3T^{-1}];
q_3	=	normal discharge in the Muskingum sub-reach at section 3 of Figures 3.1, 4.1 and 6.1 [L^2T^{-1}];
R	=	A/P = hydraulic mean radius of the channel flow section [L];
r	=	rate of rainfall per unit area occurring for a duration t_r [LT^{-1}];
R_d	=	accumulated runoff depth [L];
r_e	=	rainfall intensity at equilibrium [LT^{-1}];
R_M	=	hydraulic mean radius in the Muskingum sub-reach at section M of Figures 2.1, 3.2 and 4.2 [L];
R^2	=	coefficient of correlation [-];
S	=	channel storage [L^3];
S_f	=	energy slope of the channel water surface [-];
s_f	=	energy slope of the overland flow water surface [-];
S_r	=	soil sorptivity [$LT^{0.5}$];
S_0	=	channel bed slope [LL^{-1}];
s_0	=	overland flow plane slope [LL^{-1}];
T	=	total simulation time [T];
t	=	time variable in the overland or channel flow routing, which is the cumulative simulation time in terms of Δt from the beginning or it is the time elapsed from the start of infiltration [T];
t_e	=	time to equilibrium arrived at by using the analytical kinematic wave approach [T];
t_p	=	time to ponding [T];
t_{pc}	=	computed time to peak runoff [T];
t_{perr}	=	error in time to peak runoff [T];
t_{po}	=	observed/benchmark time to peak runoff [T];
t_r	=	duration of rainfall event [T];
t_s	=	ponding time at the potential infiltration rate [T];
V	=	velocity of the channel flow [LT^{-1}];
v	=	velocity of the overland flow [LT^{-1}];
V_C	=	total volume calculated at the outlet of the overland flow plane/channel in the V-catchment [L^3];
V_{Er}	=	total volume of effective rainfall falling over the overland flow plane/V-catchment for the duration equal to the duration of the effective rainfall [L^3];

V_M	=	channel flow velocity in the Muskingum sub-reach at section M of Figures 2.1, 3.2 and 4.2 $[LT^{-1}]$;
v_M	=	overland flow velocity in the Muskingum sub-reach at section M of Figures 3.1, 4.1 and 6.1 corresponding to y_M $[LT^{-1}]$;
V_{vn}	=	Vedernikov number [-];
V_0	=	reference flow velocity corresponding to Q_0 or Y_0 $[LT^{-1}]$;
v_0	=	reference flow velocity corresponding to q_0 or y_0 $[LT^{-1}]$;
V_3	=	normal flow velocity in the Muskingum sub-reach at section 3 of Figures 2.1, 3.2 and 4.2 $[LT^{-1}]$;
v_3	=	normal flow velocity in the Muskingum sub-reach at section 3 of Figures 3.1, 4.1 and 6.1 $[LT^{-1}]$;
X	=	space variable for the channel [L];
x	=	space variable for the overland flow plane [L];
Y	=	channel flow depth (stage) [L];
y	=	overland flow depth [L];
Y_d	=	flow depth (stage) in the Muskingum routing sub-reach at section 2 of Figures 2.1, 3.2 and 4.2 corresponding to the outflow discharge Q_2 [L];
y_d	=	outflow runoff depth at the end of the computational sub-reach of the overland flow plane corresponding to the outflow discharge q_2 [L];
$Y_{d,1}$	=	outflow runoff flow depth from the computational sub-reach of the channel at previous time level [L];
$y_{d,1}$	=	outflow runoff flow depth at the downstream end of the computational sub-reach of the overland flow plane at previous time level [L];
$Y_{d,2}$	=	outflow runoff flow depth from the computational sub-reach of the channel at current time level [L];
$y_{d,2}$	=	outflow runoff flow depth at the downstream end of the computational sub-reach of the overland flow plane at current time level [L];
y_e	=	flow depth at the end of the overland flow plane at equilibrium [L];
$y_{e,ACD}$	=	estimated value of y_e using the ACD momentum equation (5.15) [L];
$y_{e,SVE}$	=	estimated value of y_e using the Saint-Venant Equations [L];
Y_M	=	channel flow depth (stage) in the Muskingum sub-reach at the midsection M of Figures 2.1, 3.2 and 4.2 [L];
y_M	=	overland flow depth in the Muskingum sub-reach at the midsection M of Figures 3.1, 4.1 and 6.1 [L];
Y_u	=	flow depth (stage) in the Muskingum sub-reach of the channel at section 1 of Figures 2.1, 3.2 and 4.2 [L];
y_u	=	flow depth in the Muskingum sub-reach of the overland flow plane at

		section 1 of Figures 3.1, 4.1 and 6.1 [L];
$Y_{u,1}$	=	inflow runoff flow depth at the upstream end of the computational sub-reach of the channel at the previous time level [L];
$y_{u,1}$	=	inflow runoff flow depth at the upstream end of the computational sub-reach of the overland flow plane at previous time level [L];
$Y_{u,2}$	=	inflow runoff flow depth at the upstream end of the computational sub-reach of the channel at current time level [L];
$y_{u,2}$	=	inflow runoff flow depth at the upstream end of the computational sub-reach of the overland flow plane at current time level [L];
Y_0	=	reference runoff flow depth (stage) corresponding to the reference discharge Q_o [L];
y_o	=	reference runoff flow depth corresponding to the reference discharge q_o [L];
Y_3	=	normal flow depth (stage) in the Muskingum sub-reach at section 3 of Figures 2.1, 3.2 and 4.2 [L];
y_3	=	normal flow depth in the Muskingum sub-reach at section 3 of Figures 3.1, 4.1 and 6.1 [L];
z	=	depth of the wetting front below the ground surface [L];
Z_s	=	depth below the ground surface where a stable water table may exist [L];
$(V/g)(\partial V/\partial X)$	=	convective acceleration gradient in the channel flow routing [-];
$(v/g)(\partial v/\partial x)$	=	convective acceleration gradient in the overland flow routing [-];
$(1/g)(\partial V/\partial t)$	=	local acceleration gradient in the channel flow routing [-];
$(1/g)(\partial v/\partial t)$	=	local acceleration gradient in the overland flow routing [-];
$(1/S_o)(\partial Y/\partial X)$	=	dimensionless longitudinal flow depth gradient in the channel flow routing [-];
$(1/s_o)(\partial y/\partial x)$	=	dimensionless longitudinal flow depth gradient (also known as pressure gradient term) in the overland flow routing [-];
$(1/S_o)(\partial y/\partial x)_e$	=	applicability criterion for the ACD equations based VPMD and VPMS overland flow routing methods [-];
$(1/S_o)(\partial y/\partial x)_{max}$	=	maximum value of $(1/S_o)(\partial y/\partial x)$ [-];
$(\partial A/\partial Y)_M$	=	B_M, surface width of the channel flow in the Muskingum sub-reach at section M of Figures 2.1, 3.2 and 4.2 [L];
$\partial Y/\partial X$	=	longitudinal flow depth gradient in the channel flow routing [-];
$\partial y/\partial x$	=	longitudinal flow depth gradient in the overland flow routing [-];
η_q	=	Nash–Sutcliffe efficiency for discharge hydrograph simulation (in percentage) [-];
μ	=	$1/(kF_{rp}^2)_e$ = applicability criterion parameter advocated by *Daluz*

		Vieira, [1983] [-];
ϕ-index	=	I_a = interception loss rate [LT^{-1}]
ψ	=	soil suction at water wetting front [L];
ψ_0	=	initial suction at the wetting front [L];
θ	=	spatial weighting parameter of the Muskingum overland flow routing [-];
θ_c	=	spatial weighting parameter of the Muskingum channel flow routing [-];
θ_i	=	initial soil water content [-];
θ_{max}	=	maximum value of θ occurring corresponding to the minimum discharge at the end of the considered sub-reach of the overland flow plane [-];
θ_{min}	=	minimum value of θ occurring corresponding to the maximum discharge at the end of the considered sub-reach of the overland flow plane [-];
θ_s	=	saturated soil water content [-];
$\Delta\theta$	=	volumetric soil water content at the wetting front which is equal to $(\theta_s - \theta_i)$ [-];
Δt	=	routing time step [T];
ΔX	=	routing space step of the channel [L]; and
Δx	=	routing space step of the overland flow plane [L].

ABBREVIATIONS

The following abbreviations are used in this thesis:

ACD	=	Approximate Convection–Diffusion;
ANNs	=	Artificial Neural Networks;
ASAE	=	American Society of Agricultural Engineers;
ASCE	=	American Society of Civil Engineers;
CATHY	=	CATchment HYdrology;
CVFE	=	Control Volume Finite Element;
CPU	=	Central Processing Unit;
DEM	=	Digital Elevation Model;
DRiFt	=	Discharge River Forecast;
DTMs	=	Digital Terrain Models;
DW	=	Diffusive Wave;
FL	=	Fuzzy Logic;
FVM	=	Finite Volume Method;
GA	=	Green-Ampt;
GANN	=	Geomorphology based Artificial Neural Networks;
GIUH	=	Geomorphologic Instantaneous Unit Hydrograph;
GP	=	Genetic Programming;
HEC	=	Hydrologic Engineering Centre;
HEC-HMS	=	HEC-Hydrologic Modeling System;
IAHS	=	International Association of Hydrological Sciences;
IFD	=	Integrated Finite Difference;
IUH	=	Instantaneous Unit Hydrograph;
KW	=	Kinematic Wave;
LSS(s)	=	Land-Surface Scheme(s);
MC	=	Muskingum–Cunge;
MCT	=	Muskingum-Cunge-Todini;
NERC	=	Natural Environment Research Council;
NRCS	=	Natural Resources Conservation Service;
PIHM	=	Penn State Integrated Hydrologic Model;
PUB	=	Predictions in Ungauged Basins;
SCS	=	Soil Conservation Services;

SHE	=	Système Hydrologique Européen;
SIT	=	Sequential Iterative Approach;
SNIT	=	Sequential Non-Iterative Approach;
SRH-W	=	Sedimentation and River Hydraulics-Watershed;
SVE	=	Saint-Venant Equation(s);
TUH	=	Finite Period Unit Hydrograph;
UH	=	Unit Hydrograph;
UK	=	United Kingdom;
USA	=	United States of America;
USACE	=	U.S. Army Corps of Engineers;
USDA	=	U. S. Department of Agriculture;
VPM	=	Variable Parameter Muskingum;
VPMC	=	Variable Parameter Muskingum–Cunge;
VPMD	=	Variable Parameter Muskingum Discharge hydrograph;
VPMD-GA	=	Coupled surface VPMD and subsurface GA model;
VPMS	=	Variable Parameter Muskingum Stage hydrograph;
VPMS-GA	=	Coupled surface VPMS and subsurface GA model;
WFIUH	=	Width Function based Instantaneous Unit Hydrograph;
1DS1DSS	=	One-Dimensional Surface and One-Dimensional Sub-Surface; and
1DS2DSS	=	One-Dimensional Surface and Two-Dimensional Sub-Surface.

1 INTRODUCTION

1.1 GENERAL

Overland flow is the beginning of the hydrological runoff process by which the precipitation fallen on the land surface is transported down the slope as a sheet flow before draining into different forms of streams. Overland flow is an important component of the hydrological processes which can be categorized as the Hortonian (infiltration excess) and the Dunne (saturation excess) overland flows and both of which are influenced by the dynamic interaction between the spatially and temporally varying climatic and physiographic factors, such as rainfall, infiltration, ground cover, land use, soil, and topography. As the impacts of fast changing land use activity and global climate change on the hydrological regimes of the river basins are becoming an accepted reality [*McCarthy et al.*, 2002; *Milly et al.*, 2002], their assessment requires a better understanding of the dynamic interactions between climate, topography-morphology, soil and vegetation cover. The assessment of the impacts of these dynamic interactions on water and land resources is possible through the employment of suitable physically based catchment models [*Freeze and Harlan*, 1969; *Beven and Kirkby*, 1979; *Loague and Freeze*, 1985; *Abbott et al.*, 1986a, 1986b; *Todini*, 1988; *Dunne*, 1983; *Loague*, 1990; *Grayson et al.*, 1992; *Paniconi and Wood*, 1993; *Woolhiser*, 1996; *Yu*, 2000; *Singh and Woolhiser*, 2002; *Wong*, 2006, *Todini*, 2009] and conceptual catchment models [*Beven*, 1989, 1993, 2001, 2002a, 2002b]. In practice, the distributed models are now widely used in the hillslope and catchment (surface water) hydrological studies to represent approximately the spatial variability and pathways of water through a catchment. However, modelling the interactions among the various hydrological component processes poses a great challenge to the modellers. In this regard, the overland flow simulation is of no exception, and its accurate estimation is essential for addressing a variety of hydrological and environmental problems such as flood estimation for the design of hydraulic structures, flood regulation, design and management of agricultural surface drainage systems and urban stormwater systems, soil erosion control, waste water management, hydrologic responses to land use or land cover changes, land-atmosphere interaction, hydrologic forecasting etc. Among the various headwater catchment runoff estimation models, the models based on the basic equations governing the flow process of

rainfall-runoff transformation phenomenon are more useful to deal with the gauged, semi-gauged, and ungauged field problems.

The overland flow process is most often treated as the one-dimensional gradually varied unsteady flow governed by the Saint-Venant equations (SVE), described by the partial differential equations of the continuity and momentum of flow. However, the operational use of the SVE is severely hindered by the requirement of high computational skill, extensive topographical data, and knowledge of initial and boundary conditions under unsteady flow situation. Further, these equations are too complicated to solve analytically and, therefore, require the use of numerical methods. Moreover, the stability of numerical methods depends on the dynamic wave celerity, even for the flow cases with negligible inertia [*Ferrick*, 1985] and, to circumvent these numerical problems, *Ferrick* [1985] advocated the use of appropriate wave type equations. Furthermore, many researchers [*Woolhiser and Liggett*, 1967; *Morris*, 1979, 1980; *Morris and Woolhiser*, 1980; *Daluz Viera*, 1983; *Hager and Hager*, 1985; *Govindaraju et al.*, 1988a, 1988b, *Richardson and Julien*, 1994; *Singh*, 2002, 2003, *Singh and Woolhiser*, 2002] suggested that the use of approximations of the Saint-Venant equations, such as the kinematic wave (KW) and the diffusion wave (DW) equations is appropriate for many hydrological problems of interest. In order to model the overland flow formed due to complex rainfall pattern occurring over complex catchment geometry, the modellers have to rely on various numerical schemes, i.e., the finite difference and finite element methods for the solutions of the SVE and their variants [*Liggett and Woolhiser*, 1967; *Chow et al.*, 1988; *Singh*, 1996]. Such numerical schemes employed for arriving at the solutions require the use of very short time-steps in order to ensure stability of the results [*Johnson and Miller*, 1997; *Nunes et al.*, 2005]. In this regard, *Huang and Song* [1985] argued that the instability arising due to the use of numerical schemes severely restricts the allowable spatial and temporal grid sizes, Δx and Δt, respectively, when the Froude number is very small. Further, it is noted that the overland flow estimation is more sensitive to changes in the computational grid sizes than in the case of routing in channels [*Molnár and Julien*, 2000]. Moreover, almost all the numerical schemes are prone to phase error, oscillations in the solution, and uncontrolled numerical diffusion and dispersion in varied degrees depending on the type of numerical scheme (*viz.*, backward, forward, and centered) employed in the computations [*Zienkiewicz*, 1977; *Croley and Hunt*, 1981; *Hromadka and DeVeries*, 1988; *Holden and Stephenson*, 1995; *Ponce*, 1991; *Lal*, 1998a, 1998b; *Jaber and Mohtar*, 2001, 2002]. The numerical problems associated with these numerical methods can be minimized up to a certain extent

by considering different forms of simplifications of the momentum equation of the SVE, but cannot be eliminated completely. *Henderson* [1966] and *Dooge* [1973] have also recommended the use of appropriate approximations to the SVE for many hydrological flow descriptions. One such approximation is the Approximate Convection-Diffusion (ACD) equations, recently introduced by *Perumal and Ranga Raju* [1999], which are directly derived from the SVE.

The simplified flood routing methods such as the Muskingum method and its variants have been successfully used for routing flood waves in basin-scale and continental-scale models [*Zhao and Liu,* 1995; *Yu,* 2000; *Nawarathna et al.,* 2005; *USACE,* 2006]. Over the past three decades, numerous variable parameter Muskingum (VPM) flood routing methods [*Ponce and Chaganti,* 1994; *Perumal,* 1994a, 1994b; *Perumal and Ranga Raju,* 1998a, 1998b; *Todini,* 2007; *Price,* 2009] have been developed which have an immense potential for meso- and macro-scale field applications due to their excellent computational efficiency, essential modelling accuracy and sufficient independence on the computational grid sizes [*Chow et al.,* 1988; *Ponce,* 1989; *USACE,* 2006]. The variable parameter Muskingum discharge (VPMD) [*Perumal,* 1994a, 1994b] and the variable parameter Muskingum stage (VPMS) [*Perumal and Ranga Raju,* 1998a, 1998b] hydrographs routing methods developed based on the ACD equations have been found useful in solving river routing problems [*Perumal et al.,* 2001, 2007]. Although a number of simplified flood routing methods have been developed so far, the one based on the variable parameter Muskingum-Cunge (VPMC) method [*Ponce and Yevjevich,* 1978; *Ponce and Chaganti,* 1994] is widely used in practice. However, it has been shown by *Perumal and Sahoo,* [2007] that the VPMC method is only applicable over a small range of the physical diffusion equation. Although the theories proposed by *Cunge* [1969] and *Perumal* [1994a, 1994b] attempt to give physical interpretation to the classical Muskingum routing method, the interpretation given by the latter is able to explain all the features of the classical Muskingum method including the formation of the well-known "initial dip" in the beginning of the Muskingum solution. In line with this argument, *Heatherman* [2004] pointed out that a thorough insight into the Muskingum method [*McCarthy,* 1938] can be gained using the interpretation proposed by *Perumal* [1994a, 1994b] rather than that given by *Cunge* [1969].

A comparative study among the VPMC, VPMD, and VPMS channel routing methods clearly shows that the VPMD and VPMS methods have a wider applicability ranges than the VPMC method [*Perumal and Sahoo,* 2007], which can be attributed to the physical basis of their development. Further, *Perumal and Sahoo* [2008] demonstrated that within

their applicability limit, the VPMD and VPMS methods are more volume conservative than the VPMC method. Moreover, the VPMD and VPMS methods are the only simplified variable parameter Muskingum methods which have the capability of estimating the discharge and stage variables simultaneously at any location of the channel reach similar to that of the solutions of the SVE. Although, the Muskingum-Cunge-Todini (MCT) method [*Todini*, 2007] has the capability to estimate both the stage and discharge variables, the stage is estimated at the middle of the channel reach, upstream to the routed discharge hydrograph estimation point. Therefore, the use of algorithms of the VPMD and VPMS methods have been found more useful in solving the unsteady channel flow problems [*Perumal et al.*, 2001, 2004, 2007, 2010a,2010b]. However, the potential capabilities of these methods to solve the overland flow problems remain unexplored. Only limited attempts have been made in literature to apply the simplified Muskingum method, namely, the Muskingum-Cunge method [*Ponce*, 1986] and the variable parameter Muskingum-Cunge method [Orlandini *and Rosso*, 1996] for overland flow modelling. Therefore, an equally simple, computationally efficient and, more importantly, volume conservative physically based overland flow routing methods need to be developed based on the approaches employed in the development of the VPMD and VPMS channel routing methods.

1.2 SCOPE OF THE OVERLAND FLOW MODELLING USING THE APPROXIMATE CONVECTION-DIFFUSION (ACD) EQUATIONS

In light of the above discussion in Section 1.1, the overland flow modelling using the Approximate Convection-Diffusion (ACD) equations can be briefly summarized as below:

a) Though the computational capability of the present-day computers is not a limitation, the full Saint-Venant equations cannot be used for meso- and macro-scale basin modelling due to the numerical problems which arise in the solution scheme, and also due to the burden caused by the requirement of a large database to account for the spatial and temporal variability, which is difficult to obtain in real-world field problems.

b) The physically based VPMD routing method which is structurally simple, unconditionally stable, independent of the computational grid size, and capable of simulating the local flow depth corresponding to the simulated discharge, can be used as an alternative to the physically based distributed models such as the KW and DW models which are solved using the conventional numerical schemes.

c) The physically based VPMS routing method is the only simplified method available for flood routing in river channels which is capable of routing the stage and computing the corresponding discharge at any downstream river site. This method has a higher applicability range than the VPMD and VPMC methods for channel routing. Hence, there is a need to evaluate this method for overland flow estimation studies. Note that the computation of flow depth in the overland flow modelling is important for the hydrological problems like solute transport and soil erosion studies.

d) Since infiltration loss is a major component in overland flow modelling studies of the natural catchments, the VPMD and VPMS methods can be coupled with a suitable infiltration model for modelling the Hortonian overland flow.

e) In literature, a varied number of applicability criteria have been used to determine the applicability limits of the overland flow and channel flow routing models. Hence, the use of the VPMD and VPMS methods for overland flow modelling would also enable to develop the applicability criteria of these methods.

1.3 OBJECTIVES

In light of the potential usefulness of the simplified flood routing methods as brought out in section (1.1) and considering the scope of the ACD equations for overland flow modelling as presented in section (1.2), it is proposed to focus this study on the extension of the physically based variable parameter Muskingum discharge and stage channel routing methods [*Perumal, 1994a, 1994b; Perumal and Ranga Raju, 1998a, 1998b*] for overland flow modelling by incorporating the lateral flow in the form of rainfall. The broad aim of this study is to develop and verify two different simplified VPM methods in flow depth and discharge formulations using the ACD equations [*Perumal and Ranga Raju, 1999*] for overland flow modelling. It is expected that these developed methods would be capable of realistically simulating the runoff at the downstream end of an overland flow plane in the same manner as the VPMD and VPMS methods have been employed for flood routing studies. The specific objectives of this study are:

1) To extend the VPMD channel routing method for overland flow modelling studies and to compare its performance with those of other currently used methods.

2) To extend the VPMS channel routing method for overland flow modelling studies and to compare its performance with those of other currently used methods, and with that of the corresponding VPMD overland flow routing method.

3) To develop the applicability criteria for the above methods; and

4) To apply the above methods for the Hortonian overland flow generation and to compare the performances of these models with those of the currently used methods.

1.4 SCOPE OF THE STUDY

The scope of the present study can be summarized as below:

a) Improved computational methods required for overland flow runoff estimation would be developed. This study will thoroughly bring out the features and limitations of these methods by testing these methodologies over a wide range of hypothetical and field observed rainfall-runoff data.

b) A number of criteria for assessing the field applicability of different simplified routing methods based on kinematic and diffusion waves are available in literature. Unlike in the case of channel routing, the variable parameter Muskingum method is still not popular for overland flow routing and, hence, the applicability limits of these methods for modelling overland flow are not well-established. Hence, this study proposes the development of applicability criteria for these variable parameter Muskingum methods, namely, the VPMD and VPMS methods.

c) This study would also bring out the suitability and accuracy of these simplified overland flow routing methods for modelling the Hortonian overland flow.

d) Since the developed variable parameter simplified routing methods would use a lumped approach in their model frameworks, these methods are more amenable to account for a coarser computational grid scale suitable for the hydrological simulation of the land surface schemes (LSSs) of the climate change models. Thus these simplified methods hold a great promise in coupling with the LSSs of the climate change models and the basin-scale hydrological models.

1.5 LIMITATIONS OF THE STUDY

The limitations of the present study can be enlisted as follows:

a) Since both the proposed VPMS and VPMD overland flow routing methods assume approximately linear variation of flow depth and/or discharge over the computational routing space-step over the plane, and in the channel of a level V-

catchment, these methods are not suitable for application when all the terms of the Saint-Venant's momentum equation are of the same order of magnitude, and

b) These simplified overland flow routing methods are not suitable for application in the presence of downstream disturbances.

1.6 THESIS LAYOUT

This thesis constitutes a total of seven chapters. The relevance of the ACD equations for overland flow modelling is presented in Chapter 1 along with the objectives, scope and limitations of the study. The review of literature is presented in Chapter 2.

In Chapter 3, corresponding to the first objective, the VPMD channel routing method [*Perumal*, 1994a, 1994b] has been extended for overland flow modelling by incorporating distributed lateral inflow in the model framework. The evaluation of the proposed extended VPMD method (henceforth, termed as the VPMD method or model) for overland flow modelling is extensively carried out based on the assessment of comparison of the simulated runoff hydrographs with the corresponding benchmark hydrographs obtained by the analytical solutions of the KW and DW models, and the numerical solutions of the SVE, DW and KW models. Besides, the field and experimental overland flow hydrographs available in literature have also been considered as the benchmark hydrographs for their simulation using the proposed method.

In Chapter 4, Corresponding to the second objective, the VPMS channel routing method has been extended for overland flow routing by incorporating the distributed lateral flow in the model structure. The routing performance of this extended VPMS method (henceforth, termed as the VPMS method or model) has also been verified by conducting similar experiments as used for verifying the VPMD method presented in Chapter 3.

In Chapter 5, corresponding to the third objective, a novel applicability criterion based on the magnitude of the longitudinal water depth gradient, $(1/s_0)(\partial y/\partial x)_e$ is developed for quantifying and assessing the applicability limits of the VPMD and VPMS methods for overland flow modelling studies, where s_0 is the slope of overland flow plane and $(\partial y/\partial x)_e$ is the longitudinal gradient of the flow depth corresponding to the equilibrium condition.

In Chapter 6, dealing with the fourth objective, the capabilities of the VPMD and VPMS methods have been evaluated for studying the overland flow generation over an infiltrating

land surface by coupling these methods with the Green-Ampt (GA) infiltration model which are referred herein as the VPMD-GA and VPMS-GA models.

Chapter 7 presents the conclusions of this study and provides recommendations for future work.

The FORTRAN codes used in this thesis for numerical routing experiments and field applications are given in Appendices I–III. Izzard's experimental data used in this study have been compiled in Appendix–IV.

2 REVIEW OF LITERATURE

2.1 GENERAL

For a long time, the subject of catchment routing and, thus, the overland flow modelling has been of interest to the hydraulic and hydrologic research community. Catchment routing refers to the estimation of flow in space and time within a catchment by transforming effective rainfall into runoff [Ponce, 1989]. This task is accomplished in a lumped mode or in a distributed mode. The methods for catchment routing are generally identical to those used in the reservoir and channel routing. Historically, the researchers relied on two modelling approaches for catchment routing: 1) hydrologic routing methods and 2) deterministic methods based on the process-based distributed models, known as the hydraulic routing methods [Ponce, 1989]. The hydrologic routing methods are usually data driven techniques which employ the observed inflow-outflow data for the estimation of model parameters. This classification is based on the degree of incorporation of the physical laws governing the rainfall to runoff transformation into the model framework, and by the rationalization of model parameters. Based on this classification, a plethora of rainfall-runoff models have been proposed in practice ranging from simple data driven model to complex hydrodynamic models. This chapter presents a detailed review on the classification of rainfall-runoff models in general and the simplified hydraulic routing methods in particular with emphasis on the description of the Variable Parameter Muskingum Discharge (VPMD) and Variable Parameter Muskingum Stage (VPMS) channel routing methods. These methods form the basis for the development of the overland flow methods proposed in this study. The review also discusses on the Hortonian overland flow models and the available applicability criteria for overland flow modelling using the DW and KW models.

2.2 CLASSIFICATION OF RAINFALL–RUNOFF MODELS

2.2.1 Hydrologic Routing Methods

The hydrologic methods of catchment routing can use conceptual, parametric and black box models, all of which may be categorized as data driven models, including the Artificial

Neural Networks (ANNs) models. In the conceptual models, the heuristic or empirical functions are used to represent the water balance dynamics which is deemed to be qualitatively reasonable; whereas, the black box models relate the input and output by arbitrary functions and, therefore, they lack in representing the inherent physical significance. These models are less rigorous and simpler in approach. The conceptual model finds its roots in the quantitative and qualitative description of a physical system. The quantitative description is based partly on the available database for the model parameterization, while the qualitative description is based on the data used for an identical physical system in a situation of non-availability of data for model parameterization. The rational method proposed by *Mulvany* [1850] gives a clear description of the concept of time of concentration and its relation to the maximum runoff. It is capable of estimating the peak flow, but not the flood volume and, thus, its use is limited to the impervious small catchments in which the flow dynamics is mainly driven by kinematic process [*Todini*, 2009]. Many years latter, *Sherman* [1932] pioneered the unit hydrograph (UH) theory based on the principle of superposition of effects which propelled substantial changes in the development of rainfall-runoff models. This theory enables the reproduction of runoff hydrograph using the rainfall data sampled at constant time intervals. With the introduction of system theory, two major types of hydrographs, viz., instantaneous unit hydrograph (IUH) and finite period unit hydrograph (TUH) [*O'Donnell*, 1966] were considered based on the interpretation of UH as a response of linear, contributing, and dynamic stationary system. The introduction of the IUH concept helped to segregate the physically meaningful and data driven models [*Todini*, 2009]. If the shape of the IUH or the TUH cannot be defined *a priori* on the physical ground and both the shape and relevant parameters are estimated using the measurements, then the resulting model is categorized as a data driven model [*Natale and Todini*, 1976a; 1976b]. Subsequently, the attempt to relate the catchment geomorphology to the catchment response through an IUH leads directly to the development of the geomorphologic instantaneous unit hydrograph theory (GIUH) [*Rodriguez-Iturbe and Valdes*, 1979]. A GIUH consists of two components, one relevant to the geomorphology and the other to the hydraulic aspect describing the movement of a drop of water along a stream [*Franchini and O'Connell*, 1996]. However, it was demonstrated by *Franchini and O'Connell* [1996] that the GIUH velocity parameter lacks the physical interpretation, in contrast to the physically consistent hydraulic parameters of the width function based IUH (WFIUH) [*Naden*, 1992]. The conceptual and data-driven black box models were extensively used in the past, resulting in the development of a plethora of such

rainfall-runoff models in the form of the GIUH based techniques [e.g., *Franchini and O'Connell*, 1996; *Gyasi-Agyei*, 1996; *Karvonen et al.*, 1999; *López et al.*, 2005; *Sahoo et al.*, 2006; *Bhadra, et al.*, 2008, *Nourani et al.*, 2009]; semi-distributed event-based DRiFt (Discharge River Forecast) rainfall-runoff model that uses the geomorphologic TUH [*Giannoni et al.*, 2000]; genetic programming (GP) based data-driven black box model [*Savic et al.* 1999; *Whigham and Crapper*, 2001; *Liong et al.* 2002]; artificial neural networks (ANNs) based black box models [*ASCE Task Committee*, 2000; *Sajikumar and Thandaveswara*, 1999; *Jain and Prasad Indurthy*, 2003; *Chua et al.*, 2008]; three-layer ANN based UH theory [*Hjelmfelt and Wang*, 1993a, 1993b, 1993c]; geomorphology based ANN (GANN) [*Zhang and Govindaraju*, 2003]; and intelligent computing tools based on fuzzy logic (FL) and ANNs [e.g., *Chang and Chen*, 2001; *Talei, et al.*, 2010]. The extension of the IUH and TUH approaches faces with the problem of determination of effective rainfall, separation of runoff from the base flow and to derive the IUH/TUH shape factor and/or their parameters from the observed data. For runoff estimation of the ungauged and semi-gauged catchments, the regionalization of parameters can be carried out utilizing the data from hydro-meteorologically similar regions or by using the morphological details of the ungauged basins. However, the regionalization of parameters is a nontrivial task due to the difficulty in determining the hydro-meteorologically similar basins. Use of empirical models such as ANNs, for catchment modelling further increases the loss of physics as the simulation results of these models are less robust and may sometime diverse outside the range of training set [*Cameron et al.*, 2002; *Gaume and Gosset*, 2003]. Further, several studies [*ASCE Task Committee*, 2000; *Gupta et al.*, 2000; *Hsu et al.*, 1997; *Zhang and Govindaraju*, 2000] argued for more cautious approaches that include consideration of the relevant physics and statistical principles in an effort to make the ANNs more useful as a practical and research tool. Fundamentally, the empirical methods such as the ANNs models are considered as the interpolation formulas and their use for extrapolation outside the range of the underlying data sets used for calibration of the parameters involves the risk of large errors [*Klemeš*, 1982]. Moreover, since the ANNs, genetic algorithm and FL based soft computing tools are not based on the physical processes, the uncertainty of these models involved in the prediction of hydrological responses such as the catchment runoff limits their use in the meso- and macro-scale basin models, especially when used for predictions in ungauged basins.

Conceptual models are also the data-driven techniques that are based on a spatially lumped form of the continuity equation, often called the water balance, and a flux relation

11

expressing storage as a function of inflow and outflow [*Singh*, 1988]. Models based on the use of IUH may also be classified as conceptual models. For example, the physical interpretation of the IUH can be accomplished by defining the shape of the IUH *a priori* as an integral solution of a set of linear and linearized differential equations, and by computing the parameter values as a function of physical characteristics of the phenomenon [*Todini*, 2009]. Similarly, the simplified overland flow model may be considered as a conceptual model in which the overland flow plane or channel reach is treated as a lumped system, and with the use of lumped continuity equation and a nonlinear storage equation one may arrive at the solution [*Dooge*, 1973]. The calibration of such hydrologic methods is carried out based on the past measurements. However, the Saint-Venant equations (SVE) are capable of modelling the overland flow and channel flow in a physically distributed manner. Note that since the solution procedures of the full Saint-Venant equations which require the use of numerical methods could not be attempted till the mid-fifties [*Stoker*, 1957], these hydrologic routing methods were developed as a simple alternative to the full Saint-Venant equations for field applications.

Using the storage equation, *Horton* [1938] and *Izzard* [1944, 1946] developed methods to simulate the overland flow. The Nash model [*Nash*, 1960] developed based on the concept of routing through a series of linear reservoirs and applied for rainfall-runoff modelling and flood routing in channels [*Dooge*, 1973], accounts for the convection and diffusion characteristics of the flood wave through the parameters of number of linear reservoirs-in-series and reservoir coefficient, respectively. The use of linear storage equation in the classical hydrologic routing methods presumes that all the discharges of different magnitudes in a flood wave travel at the same wave speed which, however, is in contradiction with the nonlinear dynamics of the flood wave propagation. To circumvent this deficiency in the linear methods, hydrologic methods based on nonlinear storage equations were proposed by various researchers [e.g., *Laurenson*, 1962]. Since the hydrologic storage routing methods may be linked to the hydrodynamics-based methods [*Weinmann and Laurenson*, 1979; *Zoppou and O'Neill*, 1982], the classification of routing methods as hydrologic or hydraulic has become more synthetic. For instance, when the Nash model [*Nash*, 1960] parameter denoting the number of linear reservoirs in a reach is an integer, the Nash model conceptually represents the Kalinin–Milyukov method that is derived indirectly from the Saint-Venant equations [*Dooge*, 1973]. Further, the widely used classical Muskingum routing method [*McCarthy*, 1938], which is based on a linear storage routing concept, employs two routing parameters, viz., the travel time, accounting for the

convection dynamics of the flood wave, and the weighting parameter, accounting for the diffusion characteristics of the flood wave. The Muskingum method, conventionally considered as a hydrologic storage routing method, can be linked to the hydrodynamics-based methods as investigated by *Apollov et al.* [1964], *Cunge* [1969], *Dooge* [1973], and *Dooge et al.,* [1982]. Further, through the moment matching technique, *Dooge* [1973] showed that most of the linear storage routing methods may be linked to the hydrodynamics-based methods when the routing parameters can be related to the channel and flow characteristics as described by the linearized Saint-Venant equations. These typical examples reveal that some of the storage routing methods are also derivable as a simplification of the physically based hydrodynamics methods. Consequently, the real distinction between the hydrologic and hydraulic methods should be on the basis of the estimation of the routing parameters of the method. If the parameters of the storage routing method are estimated using the inflow, outflow, and the corresponding storage information, then it may be categorized as the hydrologic method; and if they are estimated using the established relationships based on the channel and flow characteristics, then it may be categorized as the hydraulic routing method [*Perumal,* 1995] or the physically based hydrologic routing method [*Kundzewicz,* 1986]. A brief description on the hydraulic routing method and its different simplifications are given below.

2.2.2 Hydraulic Routing Methods

Incorporation of overland flow component is an essential step towards developing a spatially distributed physically based modelling tool. Generally, the overland flow component is best represented mathematically by the full SVE describing the mass and momentum balance of the one-dimensional flow. As the analytical solution of the full SVE is difficult, various researchers have used explicit and implicit numerical schemes to solve the full SVE for the simulation of runoff from the overland flow planes and channels [*Woolhiser and Liggett,* 1967; *Strelkoff,* 1970; *Abbott et al.,* 1986a, 1986b; *Bathurst,* 1986; *Singh and Bhallamudi,* 1998; *Fielder and Ramirez,* 2000; *Graham and Butts,* 2005; *Yeh et al.* 2004, 2006]. However, the operational use of the SVE is severely hindered by the requirement of high computational skill, extensive topographical data, and the requirement of boundary conditions at one or more locations in the domain under unsteady flow conditions of many situations of practical importance [*Tan,* 1992]. Therefore, the use of SVE is advisable only when the simplified variants of the SVE, such as the kinematic wave (KW) and diffusion wave (DW) models are not applicable. Further, the stability of the

explicit numerical methods depends on the dynamic wave celerity, even for the flow cases having negligible inertia [*Ferrick*, 1985]. To circumvent these numerical problems *Ferrick* [1985] suggested the use of appropriate wave type equations. *Henderson* [1966] and *Dooge* [1973] have also recommended the use of appropriate approximations to the SVE for describing many hydrological flow problems. Further, many researchers [*Woolhiser and Liggett*, 1967; *Morris*, 1979, 1980; *Morris and Woolhiser*, 1980; *Woolhiser*, 1982; *Daluz Vieira*, 1983; *Govindaraju et al.*, 1988a, 1988b, *Richardson and Julien*, 1994; *Singh*, 1996, 2001, 2002, 2003] suggested that a greater degree of sophistication can be achieved, without ignoring fundamental mechanism, by evolving simplified approximations to the full SVE for describing the overland flow process. On the basis of simplifications of the full SVE, two different models have been evolved: 1) the kinematic wave model and 2) the diffusion wave or the zero-inertia model. The governing equations of these models are given as [*Singh*, 1996]

$$\frac{\partial q}{\partial t} + c \frac{\partial q}{\partial x} = cq_L \qquad \text{(Kinematic wave model)} \qquad (2.1)$$

$$\frac{\partial q}{\partial t} + c \frac{\partial q}{\partial x} = D \frac{\partial^2 q}{\partial x^2} + cq_L \qquad \text{(Diffusion wave model)} \qquad (2.2)$$

where q = flow rate per unit width of the flow plane; q_L = net lateral inflow rate per unit area; c = celerity of the flood wave; $D = \dfrac{q}{2s_0}$ = hydraulic diffusivity coefficient; s_0 = bed slope; and the notations x and t denote the space and time variables, respectively.

For describing the unsteady flow in channel and overland planes, the KW theory was introduced by *Lighthill and Whitham* [1955] and independently conceived by *Iwagaski* [1955]. *Wooding* [1965a, 1965b, 1966] was probably one of the first researchers to apply the kinematic wave theory for overland flow simulation. *Woolhiser and Liggett* [1967] was the first to present accurately the overland flow solutions for the rising hydrograph simulation over a plane. Since then a number of studies based on the KW models have been developed for the simulation of surface runoff generation of the catchments. *Singh* [1996] presents a comprehensive review of a number of studies available for runoff generation using the KW theory. Further, for evaluating the accuracy of the KW theory, the experimental study by *Langford and Turner* [1973] involving single overland flow plane with rough, uneven surface and constant slope shows that accounting of simplified assumptions of shallow flow over smooth surface does not have a major role that might lead to a significant solution error in predicting the overland flow behavior. *Langford and Turner*

[1973] described the observed hysteresis in the storage-discharge curve in terms of the KW theory, but neglecting the momentum due to overland flow and rain. This suggests that a certain amount of averaging in time and space is permissible. Regarding the applicability of the KW models for overland flow simulation, *Woolhiser and Liggett* [1967] emphasized that the use of the kinematic wave approximation is more appropriate to describe the overland flow, if the conditions of kinematic wave number $k > 20$ and Froude number $F_{rp} \geq 0.5$ are met at the end of the overland flow plane. In addition to these criteria, *Morris and Woolhiser* [1980] provided an additional criterion that $kF_{rp}^2 \geq 5$ on the consideration that the criteria recommended by *Woolhiser and Liggett* [1967] are necessary but not sufficient. When $5 \leq k \leq 20$, the choice among the use of DW and KW approximations for describing the overland flow phenomenon depends on the Froude number, F_{rp}. However, *Daluz Vieira* [1983] surmised that when $k < 5$ and $F_{rp} > 1$, the solution using the full SVE is a better choice. Consequently, *Singh* [2002] advocated that the nature of runoff generation in many circumstances can indeed be approximated quite closely by the KW theory within certain limit of applicability; however, outside these limits, the diffusion wave or dynamic wave solutions are necessary. To overcome the limitations of the KW model and to take into account the downstream boundary conditions, various models based on DW equations were evolved [*Singh*, 1996; *DiGiammarco et al.*, 1996; *Wang and Hjelmfelt*, 1998; *Jain and Singh*, 2005; *Santillana and Dawson*, 2009; *Lai*, 2009]. Furthermore, to provide a reliability check, *Kazezyılmaz-Alhan et al.* [2005] have investigated various finite difference numerical schemes to solve the KW and DW equations for the simulation of the one-dimensional overland flow. *Gottardi and Venutelli* [2008] proposed the solution of the KW and DW equations based on an accurate time integration method which is applicable under the non-uniform rainfall intensity and spatially varying roughness conditions for the overland flow simulation.

Most of the above described models use discharge as the operating variable, but only few overland flow routing methods which use flow depth as the operating variable are available in literature. *Govindaraju and Kavvas* [1991] presented an overland flow routing method using flow depth as the operating variable based on the modified DW model. Similarly, *Govindarju et al.* [1988a, 1988b, 1990] presented overland flow depth analytical solutions based on the KW and DW equations. There are also other models derived as the averaged form of the continuity and momentum equations [e.g., *Morita and Yen*, 2002] to predict the overland flow response involving the flow depth.

The use of numerical schemes for overland flow modelling is needed when the catchment is subjected to complex rainfall pattern occurring over complex catchment geometry. However, for simple rainfall patterns and catchment geometry, analytical solutions of the KW and DW equations are available which can be used as a benchmark model to test the newly developed models [*Singh*, 1996]. In this regard, the classical analytical solution of the KW arrived at by *Woolhiser* [1974] for overland flow simulation over a plane and the semi-analytical solution presented by *Overton and Meadows* [1976, p.73] for runoff simulation in a level V-catchment could be used as a benchmark model. Further, the approximate analytical solution given by *Govindaraju et al.* [1990] for overland flow simulation on steep terrains based on the solution of the DW equation could be appropriate to serve as a benchmark model to test the efficacy of the newly developed model. For the last four decades, numerous researchers have presented a plethora of numerical and analytical methods which find their place in well refereed textbooks [e.g. *Abbott*, 1979; *Chow et al.*, 1988; *Eagleson*, 1970; *Overton and Meadows*, 1976, *Ponce*, 1989; *Singh*, 1996]. Notably, *Morita and Yen* [2002] have reviewed various numerical schemes for solving the KW and DW equations used in the overland flow modelling. With the use of these varieties of numerical solutions of the full SVE and their variants, a number of physically based watershed models are available following the blue print proposed by *Freeze and Harlan* [1969]. An excellent review of these hydrological models has been presented by *Singh* [1995], *Singh and Woolhiser* [2002], *Loague and VanderKwaak* [2004], and *Kampf and Burges* [2007].

In most of the earlier studies, the resistance to flow due to the ground surface and vegetation is considered to be constant for the whole computational reach length. In fact, the surface resistance depends on the overland flow depth, wetted perimeter, length of flow path, and nature and height of vegetation. Further, the advanced techniques such as the terrestrial laser scanning for understanding the overland flow hydraulics, may enable the investigation of catchment roughnesses over a complex morphology [*Smith et al.*, 2007]. In such a case, accurate estimation of the overland flow depth can provide a greater potential for modelling development. Moreover, in the soil erosion study, detachment of soil particles has a direct relationship with the depth of runoff; hence, accurate prediction of the average flow depth within a spatial grid is also an important aspect of overland flow modelling studies [*Bathurst et al.*, 1995, pp. 575-576]. The accurate estimation of flow depth hydrograph is also essential for implementing the gully erosion control measures for

16

designing the soil conservation structures along the stream. Therefore, the depth of overland flow is also an important variable in catchment system modelling.

A comprehensive review of literature reveals that for the runoff simulation from a basin due to a complex rainfall pattern occurring over a complex catchment geometry, the modelers have to rely on various numerical schemes, i.e., the finite difference, finite volume and finite element methods for the solutions of the SVE and their variants [*Liggett and Woolhiser*, 1967; *Chow et al.*, 1988; *Singh*, 1996, *Morita and Yen*, 2002; *Qu and Duffy*, 2007, *Jones et al.*, 2008; *Heng et al.*, 2009]. Such numerical schemes employed in the solutions require the use of very short temporal and spatial grid sizes in order to ensure the stability of the results [*Johnson and Miller*, 1997; *Nunes et al.*, 2005]. In this regard, *Huang and Song* [1985] argued that the instability of the numerical schemes severely restricts the allowable spatial and temporal grid sizes, Δx and Δt, respectively, when the magnitude of the Froude number is very small. Further, it is noted that the flow on the overland cells is more sensitive to changes in computational grid sizes than those used in channel flow studies [*Molnár and Julien*, 2000]. In fact almost all the numerical schemes are prone to phase error, oscillations in the solution, and uncontrolled numerical diffusion and dispersion in varied degree depending on the type of numerical schemes (*viz.*, backward, forward, and centered) employed in the computations [*Zienkiewicz*, 1977; *Croley and Hunt*, 1985; *Hromadka and DeVeries*, 1988; *Holden and Stephenson*, 1995; *Ponce*, 1991; *Lal*, 1998a, 1998b; *Jaber and Mohtar*, 2001, 2002, *Qu*, 2005]. The stability and accuracy of the numerical solutions of the SVE and its variants generally depend on the structure of the numerical scheme, selected time step, and computational grid size. The stability of the forward and backward schemes usually depends on the Courant (i.e., the Courant-Friedrichs-Levy) condition [*Richtmyer and Morton*, 1967]. Although, the central difference schemes are unconditionally stable, these schemes when used for solving the advection dominated flows have inherent oscillatory properties that reduce the accuracy of the solution or even completely destroy it [*Gresho and Lee*, 1981]. The numerical errors associated with numerical schemes used in the solution of the diffusion flow models increase with the decrease in the bed roughness, surface slope, wavelength of the water profile, and with the increase in flow depth [*Lal*, 1998a]. These problems associated with these numerical methods can be minimized to a certain extent by considering varied degree of simplifications to the SVE, but cannot be eliminated completely. In light of these shortcomings, a modelling tool is required which is structurally simple and easy to apply for

overland flow simulation while consistently retaining a higher degree of modelling efficiency. The parameters of such a model should have some reasonable physical basis linked to the basin and flow characteristics as envisaged by *Woolhiser* [1996], and the model developed with such features should have wider applicability range than the KW approximation. One such scheme could be experimented using the approximate convection-diffusion (ACD) equations, introduced by *Perumal and Ranga Raju* [1999], which have been directly derived from the SVE.

2.3 SIMPLIFIED HYDRAULIC ROUTING METHODS

2.3.1 Muskingum Routing Method for Channel Flow Routing

2.3.1.1 Classical Muskingum method

The classical Muskingum method [*McCarthy*, 1938], which is coined after its first application to the Muskingum River, a tributary of the Ohio River in the USA, is a linear storage routing method being widely used in practice [*Singh*, 1988]. This method combines the lumped continuity equation

$$\frac{\mathrm{d}S}{\mathrm{d}t} = I - Q \tag{2.3}$$

with the linear storage equation

$$S = K_c\left[\theta_c I + (1-\theta_c)Q\right] \tag{2.4}$$

to arrive at the difference equation which on simplification leads to the Muskingum routing equation as

$$Q_2 = C_{c1}I_2 + C_{c2}I_1 + C_{c3}Q_1 \tag{2.5}$$

where S is the storage volume, I is the inflow discharge, Q is the outflow discharge, K_C is the channel flood wave travel time, θ_c is the weighting parameter, the suffix 1 and 2 denotes the ordinate at previous and current time level, respectively, Δt is the routing time step, and the coefficients C_{c1}, C_{c2}, and C_{c3} are expressed as

$$C_{c1} = \frac{-K_c\theta_c + 0.5\Delta t}{K_c(1-\theta_c) + 0.5\Delta t} \tag{2.6a}$$

$$C_{c2} = \frac{K_c\theta_c + 0.5\Delta t}{K_c(1-\theta_c) + 0.5\Delta t} \tag{2.6b}$$

$$C_{c3} = \frac{K_c(1-\theta_c) - 0.5\Delta t}{K_c(1-\theta_c) + 0.5\Delta t} \qquad (2.6c)$$

where $C_{c1} + C_{c2} + C_{c3} = 1.0$, which shows the mass conserving ability of the classical Muskingum method. The routing parameters K_c and θ_c of this method are computed by using the historical flood events by trial and error approach. To calculate the value of θ_c, the storage S is plotted against the corresponding weighted discharge value $[\theta_c I + (1-\theta_c)Q]$ in equation (2.4) for different trial values of θ_c resulting in various sizes of loops; and the value of θ_c which gives the narrowest loop of this plot is considered as the appropriate one for its use in the model.

2.3.1.2 Physically based Muskingum routing methods

Constant Parameter Muskingum routing methods: Several attempts have been made by various researchers [*Dooge and Harley*, 1967; *Cunge*, 1969; *Dooge et al.*, 1982] to link the routing parameters K_c and θ_c of the classical Muskingum method with the flow and channel characteristics using the hydrodynamics principles to transform it into a physically based method. Although, *Dooge and Harley* [1967] presented the Muskingum parameter relationships with the wide rectangular channel and flow characteristics through the moment matching technique [*Nash*, 1960], and *Dooge et al.* [1982] later arrived at the same relationships for any shape of prismatic channel and for any type of friction law, it is the *Cunge*'s [1969] matched diffusivity approach which has become more popular as the "Muskingum–Cunge (MC) method." By matching the numerical diffusivity of the approximate linear kinematic wave equation, derived from the classical Muskingum difference equation, with the physical diffusivity of the linear convection–diffusion equation, *Cunge* [1969] arrived at the relationship for K_c and θ_c for wide rectangular channels as

$$K_c = \frac{\Delta X}{C_0} \qquad (2.7)$$

$$\theta_c = \frac{1}{2} - \frac{Q_0}{2S_0 B_0 C_0 \Delta X} \qquad (2.8)$$

where ΔX is the channel sub-reach length, C_0 is the flood wave celerity corresponding to the reference discharge Q_0, S_0 is the bed slope of the channel, and B_0 is the top width of the

channel cross section corresponding to Q_0.

Using a more refined difference scheme to represent the Muskingum routing equation and based on the matched diffusivity concept, *Koussis* [1976, 1978, 1980, 1983] arrived at an alternate relationship for θ_c different from that given by equation (2.8). However, a comparison between the *Cunge*'s and *Koussis*' approaches shows that both the approaches lead to the same coefficients of the Muskingum routing equation and the differences in the form of the weighting parameter of both the schemes are only apparent [*Perumal*, 1989].

Variable Parameter Muskingum Methods for Channel Flow Routing: Over the past two decades, numerous variable parameter Muskingum (VPM) flood routing methods [*Ponce and Yevjevich*, 1978; *Price*, 1985; *Wang and Singh* 1992; *Ponce and Chaganti*, 1994; *Perumal*, 1994a, 1994b; *Perumal and Ranga Raju*, 1998a, 1998b; *Lamberti and Pilati*, 1996; *Todini*, 2007; *Price*, 2009] have been developed which have an immense potential for meso- and macro-scale field applications due to their excellent computational efficiency, essential modelling accuracy and sufficient independence on the computational grid sizes [*Chow et al.*, 1988; *Ponce*, 1989; *USACE*, 2006]. The variable parameter Muskingum discharge (VPMD) [*Perumal*, 1994a, 1994b] routing method developed based on the approximate convection-diffusion equations, introduced by *Perumal and Ranga Raju* [1999] in discharge variable formulation has been found useful for solving river routing problems [*Perumal et al.*, 2001, *Heatherman*, 2008]. Although a number of simplified flood routing methods have been developed so far, the Muskingum-Cunge method and the variable parameter Muskingum-Cunge (VPMC) method [*NERC*, 1975; *Ponce and Yevjevich*, 1978; *Ponce and Chaganti*, 1994] are widely used in practice. However, the physical justification of the VPMC method based on the concept of matching the physical and numerical diffusion is questionable [*Perumal*, 2010] on the pretext that since this method is based on the concept of matching the numerical diffusion with the Hayami's physical diffusion equation [*Hayami*, 1951], the method should work for the entire range of the physical diffusion equation. However, it is a well-known fact that the VPMC method is only applicable for a small range [*Perumal and Sahoo*, 2007] of the physical diffusion equation. Although the theories proposed by *Cunge* [1969] and *Perumal* [1994a, 1994b] attempt to give physical interpretation to the classical Muskingum routing method, the interpretation given by the latter is able to explain all the features of the classical Muskingum method, including the formation of the well-known "initial dip" at the beginning of the Muskingum solution. In line with this argument, *Heatherman* [2004, 2008]

has pointed out that a thorough insight into the Muskingum method [*McCarthy*, 1938] can be gained using the interpretation proposed by *Perumal* [1994a, 1994b] rather than that given by *Cunge* [1969]. This view point is in line with the recommendation of *Woolhiser* [1996] suggesting that any simplified method should be based on strong and valid physical reasoning and a model should work well for the right reasons [*Klemeš*, 1986; *Bergström*, 1991]. Further, a study made by *Perumal and Sahoo* [2007] on the applicability criteria of the VPMC, VPMD and VPMS methods clearly brought out that the VPMD method has a wider applicability range than that of the VPMC method for channel routing, which can be attributed to the physical basis of the development of the VPMD method. The VPMD method preserves volume more accurately than the VPMC method [*Perumal and Sahoo*, 2008] when it is applied within its applicability range. Further, unlike any other simplified Muskingum method, it is also capable of simultaneously estimating stage (flow depth) corresponding to the routed discharge.

The VPMD method [*Perumal*, 1994a, 1994b] was originally developed for channel/river flow routing without accounting for the lateral flow. Hence, the VPMD method could be extended for overland flow modelling accounting for the lateral flow. Since, the VPMD method is used in this thesis for overland flow modelling, a detailed theoretical background of this method is given below.

2.3.2 Theoretical Background of the VPMD Method

The VPMD routing method [*Perumal*, 1994a, 1994b] is directly derived from the full Saint-Venant equations of continuity and momentum governing the one-dimensional unsteady flow in channels and rivers, respectively, given by

$$\frac{\partial Q}{\partial X} + \frac{\partial A}{\partial t} = 0 \tag{2.9}$$

$$S_f = S_o - \frac{\partial Y}{\partial X} - \frac{V}{g}\frac{\partial V}{\partial X} - \frac{1}{g}\frac{\partial V}{\partial t} \tag{2.10}$$

where Q is the discharge, A is the flow area, S_o is the bed slope, S_f is the energy slope, g is the acceleration due to gravity, V is the average velocity over cross section, Y is the depth of flow, and the notations X and t denote the space and time variables, respectively.

The parameters of the VPMD method vary at every routing time interval, and they are related to the channel and flow characteristics by the same relationships as established for the physically based Muskingum method [*Apollov et al.*, 1964; *Cunge*, 1969; *Dooge et al.*,

1982]. The VPMD method is based on the hypothesis that during the steady flow in a river reach having any shape of prismatic cross section, the stage and, hence, the cross sectional area of flow at any point of the reach is uniquely related to the discharge at the same location defining the steady flow rating curve. However, this situation is altered during the unsteady flow, as conceptualized in the definition sketch of Figure 2.1 of the VPMD routing reach of length ΔX, in which the same unique relationship is maintained between the stage and the corresponding steady discharge at any given instant of time, recorded not at the same section, but at a dynamic downstream section (section 3 in Figure 2.1) preceding the corresponding steady stage section (midsection in Figure 2.1). For the sake of better understanding of the VPMD routing method, a brief description of it is presented herein.
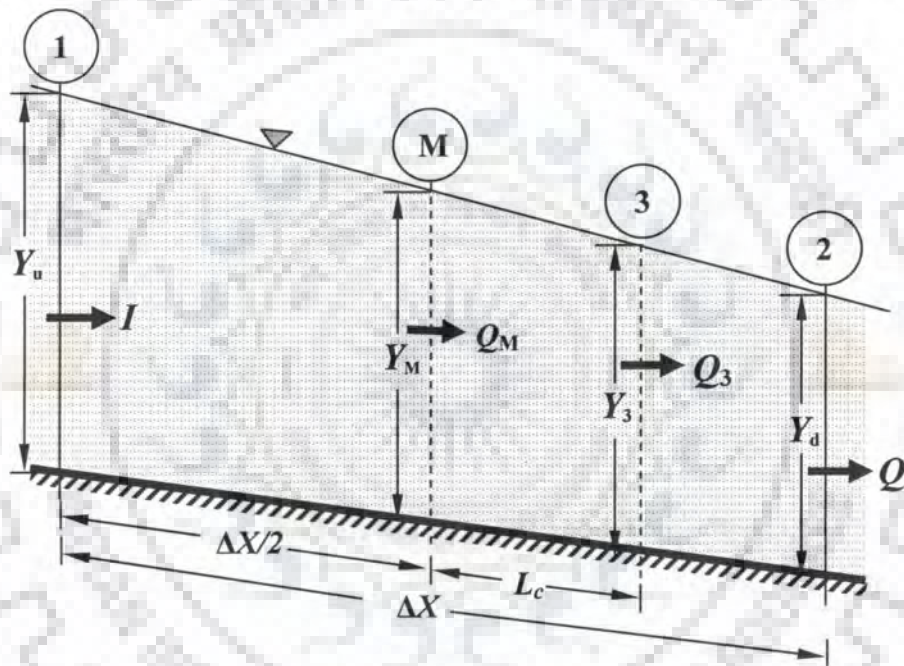
Figure 2.1 Definition sketch of the variable parameter Muskingum computational reach. I, Q_M, Q_3, and Q are the discharges at sections 1, M, 3, and 2, respectively; and the corresponding stage variables are Y_u, Y_M, Y_3, and Y_d, respectively [after *Sahoo*, 2007].

The derivation of the VPMD routing method involves some assumptions which facilitate the simplification of the unsteady flow dynamics by assuming the channel reach to be prismatic, the longitudinal flow depth gradient, $\partial Y/\partial X$, the convective acceleration gradient, $(V/g)(\partial V/\partial X)$, and the local acceleration gradient, $(1/g)(\partial V/\partial t)$, all remain approximately constant at any instant of time in a given computational routing reach and the magnitudes of multiples of the derivatives of flow and section variables with respect to both time and distance are negligible. The last two assumptions imply that the friction slope S_f is approximately

constant over the computational reach length and the variation of discharge is approximately linear (i.e., $\partial^2 Q/\partial X^2 \approx 0$). It has been shown by *Perumal* [1994a] and *Perumal and Ranga Raju* [1999] that the use of approximately constant S_f and the Manning's or Chezy's friction law governing the unsteady flow enable to arrive at the simplified momentum equation expressed as

$$\frac{\partial Q}{\partial X} = V\left[\frac{\partial A}{\partial Y} + mP\frac{\partial R}{\partial Y}\right]\left[\frac{\partial Y}{\partial X}\right] \tag{2.11}$$

where R is the hydraulic mean radius ($= A/P$), P is the wetted perimeter, and m is an exponent which depends on the friction law used ($m = \frac{2}{3}$ for the Manning's friction law; $m = \frac{1}{2}$ for the Chezy's friction law).

Using equation (2.11), the celerity, C, of the flood wave can be estimated as [e.g., *NERC, 1975*]

$$C = \frac{\partial Q}{\partial A} = \left[1 + m\left(\frac{P\partial R/\partial Y}{\partial A/\partial Y}\right)\right]V \tag{2.12}$$

Using equations (2.9), (2.10), (2.12), and the expression for discharge $Q = AV$, along with the assumption that all the terms of the friction slope S_f remains constant at any instant of time, the term S_f using the friction law, S_f can be expressed as [*Perumal, 1994a*]

$$S_f = S_o\left[1 - \frac{1}{S_o}\frac{\partial Y}{\partial X}\left\{1 - \left[mF_{rc}\left(\frac{P\partial R/\partial Y}{\partial A/\partial Y}\right)\right]^2\right\}\right] \tag{2.13}$$

where the Froude number, F_{rc}, is expressed as

$$F_{rc} = \left(\frac{V^2 \partial A/\partial Y}{gA}\right)^{1/2} \tag{2.14}$$

Using equation (2.13) in the expression for discharge Q_M at the middle of the computational channel reach (i.e., section M in Figure 2.1), based on the Manning's friction law, and its simplification based on the binomial series expansion leads to the simplified expression for Q_M as

$$Q_M = Q_3 - \frac{Q_3 \left[1 - m^2 (F_{rc}^2)_M \left(\dfrac{P \partial R / \partial Y}{\partial A / \partial Y} \right)_M^2 \right]}{2 S_o \left. \dfrac{\partial A}{\partial Y} \right|_3 \left[1 + m \left(\dfrac{P \partial R / \partial Y}{\partial A / \partial Y} \right)_3 \right] V_3} \left. \frac{\partial Q}{\partial X} \right|_3 \tag{2.15}$$

Equation (2.15) expresses the discharge Q_M in terms of discharge Q_3, which is the normal discharge corresponding to the flow depth Y_M at the middle of the reach. Since the discharge also varies approximately linearly, the term adjunct to $(\partial Q / \partial X)_3$ in equation (2.15) represents the distance L_c between the midsection M and the downstream section 3 where the normal discharge Q_3 passes, as shown in Figure 2.1. Hence, the distance L_c is expressed as

$$L_c = \frac{Q_3 \left[1 - m^2 (F_{rc}^2)_M \left(\dfrac{P \partial R / \partial Y}{\partial A / \partial Y} \right)_M^2 \right]}{2 S_o \left. \dfrac{\partial A}{\partial Y} \right|_3 \left[1 + m \left(\dfrac{P \partial R / \partial Y}{\partial A / \partial Y} \right)_3 \right] V_3} \tag{2.16}$$

where the subscripts M and 3 attached with different variables denote these variables at sections M and 3, respectively.

Further, *Perumal and Ranga Raju* [1999] proposed a new wave type equation, known as the ACD equation in discharge form as

$$\frac{\partial Q}{\partial t} + C \frac{\partial Q}{\partial X} = 0 \tag{2.17}$$

Note that equation (2.17) is a special case of the diffusive wave equation

$$\frac{\partial Q}{\partial t} + C \frac{\partial Q}{\partial X} = D_h \frac{\partial^2 Q}{\partial X^2} \tag{2.18}$$

where D_h is the hydraulic diffusivity coefficient of channel flood wave [$L^2 T^{-1}$];

Perumal and Ranga Raju [1999] have clarified that although the form of the ACD equation (2.17) is similar to that of the well-known kinematic wave equation [*Lighthill and Whitham*, 1955], it is capable of approximately modelling a flood wave in the transition range between the zero-inertia wave, governed by *Hayami*'s [1951] convection–diffusion equation and the kinematic wave, including the latter. The basis behind this inference is that

the right hand side of equation (2.17) is zero because of the assumption $\partial^2 Q / \partial X^2 \approx 0$, but the diffusivity coefficient associated with this term $D_h \neq 0$. This enables the application of equation (2.17) for modelling the lower order diffusive flood waves, including the kinematic wave. This inference, however, contradicts the conventional perception that equation (2.17) is strictly applicable for modelling the kinematic flood waves only.

Applying equations (2.12) and (2.17) at section 3 of Figure 2.1 and its simplification leads to [*Perumal*, 1994a, 1994b] the governing differential equation of the Muskingum routing, using discharge as the operating variable, and it is expressed as

$$I - Q = \frac{\Delta X}{\left[1 + m\left(\dfrac{P\partial R / \partial Y}{\partial A / \partial Y}\right)_3\right]V_3} \times \frac{\partial}{\partial t}\left[Q + \left(\frac{1}{2} - \frac{L_c}{\Delta X}\right)(I - Q)\right] \tag{2.19}$$

where I and Q denote the discharges at the upstream and downstream of the Muskingum reach, respectively. Using the analogy between the governing differential equation of the Muskingum method in discharge formulation:

$$I - Q = \frac{\partial S}{\partial t} = \frac{\partial}{\partial t}\left[K_c\left(\theta_c I + (1 - \theta_c)Q\right)\right] \tag{2.20}$$

and equation (2.19), it is inferred that the travel time, K_c of the Muskingum discharge routing method can be expressed as

$$K_c = \frac{\Delta X}{\left[1 + m\left(\dfrac{P\partial R / \partial Y}{\partial A / \partial Y}\right)_3\right]V_3} \tag{2.21}$$

and the weighting parameter, θ_c, after substituting for L_c from equation (2.16), can be obtained as

$$\theta_c = \frac{1}{2} - \frac{Q_3\left[1 - m^2(F_{rc}^2)_M\left(\dfrac{P\partial R / \partial Y}{\partial A / \partial Y}\right)_M^2\right]}{2S_o\left.\dfrac{\partial A}{\partial Y}\right|_3\left[1 + m\left(\dfrac{P\partial R / \partial Y}{\partial A / \partial Y}\right)_3\right]V_3\Delta X} \tag{2.22}$$

Assuming the magnitude of the inertial terms to be negligible in natural flood waves [*Henderson*, 1966; *Price*, 1985], equation (2.22) can be modified using $(F_{rc})_M \approx 0$ as

$$\theta_c = \frac{1}{2} - \frac{Q_3}{2S_o \left.\dfrac{\partial A}{\partial Y}\right|_3 \left[1 + m\left(\dfrac{P\partial R/\partial Y}{\partial A/\partial Y}\right)_3\right] V_3 \Delta X} \tag{2.23}$$

For a wide rectangular channel section, the parameters K_c and θ_c, respectively, reduces to following form:

$$K_c = \frac{\Delta X}{(1+m)V_3} \tag{2.24}$$

$$\theta_c = \frac{1}{2} - \frac{Q_3 \left[1 - m^2 (F_{rc}^2)_M\right]}{2S_o (1+m)V_3 \Delta X} \tag{2.25}$$

Substituting equations (2.21) and (2.23) in equation (2.19) and using the classical Muskingum difference scheme [McCarthy, 1938], the differential equation (2.19) is converted to a difference equation which on algebraic operation reduces to the Muskingum routing equation expressed as

$$Q_2 = C_{c1} I_2 + C_{c2} I_1 + C_{c3} Q_1 \tag{2.26}$$

where I_2 and Q_2, denote the upstream and downstream discharges at current time level, respectively; I_1 and Q_1, denote the upstream and downstream discharges at previous time level, respectively; and the coefficients C_{c1}, C_{c2}, and C_{c3} are expressed as given by equations (2.6a)–(2.6c).

For estimating the stage hydrograph corresponding to the routed discharge hydrograph, the flow depth Y_d corresponding to the routed discharge Q can be estimated using equation (2.11) as

$$Y_d = Y_M + \frac{Q - Q_M}{\left.\dfrac{\partial A}{\partial Y}\right|_M \left[1 + m\left(\dfrac{P\partial R/\partial Y}{\partial A/\partial Y}\right)_M\right] V_M} \tag{2.27}$$

in which Y_M is estimated iteratively using the Manning's equation:

$$Q_3 = \frac{1}{n_c} A_M R_M^{2/3} S_o^{1/2} \tag{2.28}$$

The above simplified hydraulic VPMD method, which is directly derived from the Saint-Venant equations for routing floods in channels having any shape of prismatic cross section, allows the simultaneous computation of discharge hydrograph as well as the corresponding stage hydrograph.

2.3.3 Theoretical Background of the VPMS Method

Since, this thesis makes use of the VPMS channel routing method advocated by *Perumal and Ranga Raju* [1998a, 1998b], a detailed description of this method is given below. The VPMS method has been developed using the following concept [*Perumal and Ranga Raju, 1998a, 1998b*]: During steady flow in a river reach having any shape of prismatic cross section, the stage and, hence, the cross sectional area of flow at any point of the reach is uniquely related to the discharge at the same location defining the steady flow rating curve. However, this situation is altered during unsteady flow, as conceptualized in the definition sketch (Figure 2.1) of the variable parameter Muskingum routing reach of length ΔX, in which the same unique relationship is maintained between the stage and the corresponding steady discharge at any given instant of time, recorded not at the same section, but at a downstream section (section 3 in Figure 2.1) preceding the corresponding steady stage section (midsection in Figure 2.1).

The VPMS routing method is derived from the Saint-Venant equations (2.9) and (2.10), which govern the one-dimensional unsteady flow in channels and rivers without considering lateral flow. The derivation of the method involves some assumptions which enable the simplification of the unsteady flow process by assuming the channel reach to be prismatic and the longitudinal water surface gradient, the convective and the local acceleration gradients remain approximately constant at any instant of time in a given channel reach. The latter assumption implies that the friction slope, S_f, is approximately constant over the computational reach length at any instant of time and, hence, the flow depth varies approximately linearly over the Muskingum reach. It has been shown by *Perumal and Ranga Raju* [1998a, 1998b, 1999] that the use of the assumption of approximately constant S_f and the Manning's friction law governing the unsteady flow enable to arrive at the simplified momentum equation expressed by equation (2.11) as in the case of the derivation of the VPMD method. This equation (2.11) defines the longitudinal variation of discharge over the computational channel reach. For estimating the celerity, C, of the flood wave, equation (2.12) can also be used herein. Note that the application of equation (2.12) for unsteady flow in rectangular channels yields the same celerity relationship as given in the

report of the *Natural Environment Research Council (NERC)* [1975]. Further, using equations (2.9), (2.10), (2.11), and the expression of discharge using Manning's friction law, one can express the friction slope S_f by equation (2.13).

Now, use of equation (2.13) in the expression for discharge Q_M at the middle of the computational channel reach, using the Manning's friction law, and its simplification based on binomial series expansion leads to the simplified expression for Q_M same as given by equation (2.15). This equation (2.15) expresses the discharge Q_M in terms of normal discharge Q_3, corresponding to Y_M, the flow depth at the middle of the reach. The section 3 (in Figure 2.1), where Q_3 passes corresponding to Y_M, is located at a distance L_c downstream of the midsection and can be expressed by equation (2.16).

Use of equations (2.9), (2.11), and (2.12) leads to the expression [*Perumal and Ranga Raju, 1998a, 1998b*]

$$\frac{\partial Y}{\partial t} + C\frac{\partial Y}{\partial X} = 0 \tag{2.29}$$

It was pointed out by *Perumal and Ranga Raju* [1998a, 1998b] that although the form of equation (2.29) is same as that of the well-known kinematic wave equation [*Lighthill and Whitham*, 1955], it is capable of approximately modelling a flood wave in the transition range between the zero-inertia wave, governed by the convection–diffusion equation [*Hayami*, 1951], and the kinematic wave, including the latter. The characteristic of this new wave type governed by equation (2.29), termed as the ACD equation in stage formulation, has been investigated in detail by *Perumal and Ranga Raju* [1999].

Applying equations (2.12) and (2.29) at section 3 of Figure 2.1, its simplification leads to the governing differential equation of the Muskingum type routing [*Perumal and Ranga Raju, 1998a, 1998b*] using stage as the operating variable in place of discharge, and it is expressed as

$$Y_u - Y_d = \frac{\Delta X}{\left[1 + m\left(\dfrac{P\partial R/\partial Y}{\partial A/\partial Y}\right)_3\right]V_3} \times \frac{\partial}{\partial t}\left[Y_d + \left(\frac{1}{2} - \frac{L_c}{\Delta X}\right)(Y_u - Y_d)\right] \tag{2.30}$$

where Y_u and Y_d denote the stages at the upstream and downstream of the reach.

Using the similarity between the governing differential equation of the Muskingum method in stage formulation expressed by equation (2.30) and that of the equation (2.20) in

discharge formulation, the Muskingum type routing equation in stage formulation can be obtained as:

$$Y_{d,2} = C_{c1}Y_{u,2} + C_{c2}Y_{u,1} + C_{c3}Y_{d,1} \qquad (2.31)$$

where $Y_{u,2}$ and $Y_{d,2}$ denote the upstream and downstream stages at current time level, respectively; $Y_{u,1}$ and $Y_{d,1}$ denote the upstream and downstream stages at the previous time level, respectively; and the coefficients C_{c1}, C_{c2}, and C_{c3} are expressed by equations (2.6a)–(2.6c), respectively, which are the same as that of the VPMD routing method, including the expressions for the parameters K_c and θ_c, respectively given by equations (2.21) and (2.22).

For estimating the discharge hydrograph corresponding to the routed stage hydrograph, the discharge Q corresponding to the routed stage Y_d can be estimated using equation (2.11) as

$$Q = Q_M + \left.\frac{\partial A}{\partial Y}\right|_M \left[1 + m\left(\frac{P\partial R / \partial Y}{\partial A / \partial Y} \right)_M \right] V_M (Y_d - Y_M) \qquad (2.32)$$

Since the VPMS method was originally developed for river flood routing studies [*Perumal and Ranga Raju*, 1998], it could be further extended for overland flow routing studies accounting for lateral flow.

2.3.4 Muskingum Routing Method for Overland Flow Routing

Only limited attempts have been made to verify the application of the Muskingum-Cunge method for overland flow modelling. *Ponce* [1986] was the first researcher to apply the Muskingum-Cunge method for overland flow modelling and reported that this approach has better convergence properties than the methods based on the solutions of the kinematic wave equation using the conventional numerical scheme approach. *Ponce* [1986] found that the accuracy of the Muskingum-Cunge method is independent of the computational grid size used in the solution scheme. The Muskingum-Cunge method was further used by *Ponce and Klabunde* [1999] for modelling runoff from a parking lot without any comparison with the observed data. *Holden and Stephenson* [1988] advocated that the overland flow modelling using the Muskingum-Cunge method is always preferred over the KW and DW models because of its simplicity, stability and consistency in accuracy. The approach of *Ponce* [1986] was further extended by *Orlandini and Rosso* [1996, 1998] to

simulate the runoff in a cascade of planes through a digital elevation model (DEM) based conceptual network to study the effect of catchment topography and river networks on the runoff generation process. *Orlandini and Rosso* [1996, 1998] employed the VPMC method to route the overland and channel flows, and found that this method is computationally inexpensive and able to preserve accuracy of the solution with scale independence. However, much details about the verification of the VPMC method for overland flow computation have not been provided in this study, besides with no details on the applicability limit of the method and its accuracy (including the ability to conserve mass) for different spatial and temporal grid sizes. Subsequently, this model was extended by *Brath and Montanari* [2003] to verify the effect of spatial variability of soil infiltration parameters on the simulated river flow by distributed modelling under different climatic scenarios. Recently, *Moretti and Montanari* [2007] used the VPMC method for simulation of the overland and channel flows in the AFFDEF model, a spatially distributed (grid-based) model, which is able to simulate the continuous time series of river flows at any time step and at any location in the catchment. They found that the main strength of the AFFDEF model is its computational efficiency. Although, the VPMC method is capable of varying the parameters systematically, the variation is not consistent with the variation built-in into the SVE solution [*Perumal*, 1994a]. The proper way of varying these parameters of the Muskingum method would be to account for the longitudinal gradient of the flow depth in their relationships in a way consistent with the variation built into the Saint-Venant solution [*Perumal*, 1994a]. Though, nearly 25 years have passed since the demonstration of the applicability of the Muskingum-Cunge method for overland flow modelling [*Ponce*, 1986], no attempt has been made till date to exclusively study the strength and weakness of either the constant parameter Muskingum-Cunge method or the VPMC method with regard to the accuracy, stability and applicability of the solutions of the method in comparison with the solutions of the SVE and DW model. A systematic investigative study on these lines is required for recommending the use of the Muskingum overland flow routing method for field applications over that of the conventional numerical solution based methods.

2.4 HORTONIAN OVERLAND FLOW MODELLING

Although, the two forms of runoff generation mechanisms, viz., the infiltration excess (Hortonian) and saturation excess (Dunne) are often treated as separate mechanisms, they are interrelated and may co-exist due to uneven distribution of the soil hydraulic properties [*Kollet and Maxwell*, 2006]. Generally, the Hortonian runoff generation mechanism

dominates over the basin in the dessert and semi-arid regions due to poor development of soil structure with the lack of dense vegetative cover and organic matter [*Sivapalan et al.,* 1987]. Since the Dunne runoff generation is not significant during single storm and short storm events as compared to the Hortonian overland flow mechanism, this mechanism is generally ignored in the event based overland flow models.

Moreover, the dynamic interaction between the temporally and spatially varied unsteady overland flow and infiltrating subsurface flow is very complex in nature. The rainfall intensity, its duration, aerial distribution characteristics, climatic factors, topographic features, land surface characteristics, and soil characteristics (viz., antecedent moisture condition, hydraulic properties, and water table condition) have a strong influence on the runoff generation process. However, it is not feasible to incorporate the influence of all these factors in the rainfall-runoff modelling. Hence, the objective in the model development should be the utilization of simplified assumptions which retain the most important characteristics of the physical hydrologic system [*Smith and Woolhiser,* 1971]. Further, the real world physically based overland flow models cannot be totally physically based as the model itself includes the empirical statement of the roughness coefficient described by any of the friction laws. However, the physically based approach can reconcile the differences in the empirical results and lay a firm foundation for the hydrological development [*Woolhiser,* 1996; *Wong,* 2006].

2.4.1 Hortonian Overland Flow Models

During the last three decades, a plethora of physically based distributed models ranging from the simple to complex task performing models for the Hortonian runoff generation have been advocated by several researchers and found their place in well refereed textbooks and research articles [e.g. *Singh,* 1995; *Singh,* 1996; *Singh and Woolhiser,* 2002; *Kampf and Burges,* 2007]. A pioneering approach to the physically based distributed modelling of the surface runoff was initiated with the development of a simplified model of an open book or V-shaped catchment [*Wooding,* 1966]. A first attempt was made by *Smith and Woolhiser* [1971] to introduce the KW overland flow model coupled with the Richards equation to simulate the catchment response from an infiltrating plane, wherein the infiltration equation and the overland flow model over a cascade plane were solved using a nonlinear Crank-Nicholson implicit finite difference scheme and a second order accurate explicit difference method (i.e., single-step Lax-Wendroff scheme), respectively. They also surmised that the overland flow gets initiated only when the top soil layer becomes saturated which is the

widely accepted concept in the physically based distributed models for the Hortonian overland flow simulation. However, this study lacks in the specific description on the time of ponding and potential infiltration rate. Subsequently, a number of overland flow models in the form of the SVE or its variants coupled with different infiltration models were developed by various researchers to simulate the Hortonian overland flow generation process. Some of these models include: the one-dimensional surface and two-dimensional subsurface model of *Akan and Yen* [1981]; the overland flow model of *Yen and Akan* [1984] based on the concept of rainfall intensity exceeding the infiltration capacity of the soil; the KW approximation of *Woolhiser et al.* [1996] coupled with the Smith-Parlange [*Smith and Parlange*, 1978] infiltration equation as an extension of the study by *Smith and Hebbert* [1979] introducing a simple technique for simulating the flow concentration in the rills and small channels; a simplified model of *Govindaraju et al.* [1992] using an eigen-function expansion by coupling with the KW approximation for two-dimensional overland flow routing; a coupled kinematic runoff routing scheme with a two-dimensional (radial plus vertical) subsurface model of *Pohll et al.* [1996] to study the seepage beneath a nuclear subsidence crater in Nevada; both the one-dimensional and two-dimensional Richards equations coupled with the one-dimensional SVE conjunctive surface-subsurface numerical model of *Singh and Bhallamudi* [1998], namely, 1DS1DSS and 1DS2DSS models, respectively; an one-dimensional Richards equation coupled with two-dimensional shallow water equations of *Gandolfi and Savi* [2000]; a three-dimensional modified Richards equation coupled with the non-inertia approximation/diffusion wave conjunctive model of *Morita and Yen* [2002]; an one-dimensional Richards equation coupled with the two-dimensional surface flow conjunctive model of *Downer and Ogden* [2003]; the one-dimensional Richards equation (for unsaturated flow) and three-dimensional finite element solver (for saturated flow) coupled with the SVE integrated models of *Graham and Butts* [2005]; a fully integrated physically based three-dimensional saturated-unsaturated flow equation coupled with the DW model of *Pandey and Huyakorn* [2004]; the generalized Darcy-Richards equation coupled with the surface flow routing implicit models of *Ababou and Tr'egarot* [2002] and *Weill et al.* [2009]; a finite volume scheme of *Heng et al.* [2009] for coupling the SVE with the multiparticle size class Hairsine-Rose soil erosion model; a coupled fully implicit finite volume model of *He et al.* [2008] which uses the depth-averaged two-dimensional DW equation for overland flow routing and three-dimensional mixed form of the Richards equation for variable saturated subsurface flow to simulate the response of wetlands and agricultural watersheds. The conjunctive models of *VanderKwaak*

and Loague [2001], *Morita and Yen* [2002], *Panday and Huyakorn* [2004], and *Jones et al.* [2008] which couple the Richards equation with a varied level of approximations of the SVE that rely on some form of the exchange flux using the concept of conductance; whereas, the integrated model of *Kollet and Maxwell* [2006] relies on the continuity of pressure head and fluxes at the ground surface in the coupling approach.

Similarly, a number of researchers have used the Green-Ampt (GA) infiltration model and its variants as a submodel of the Hortonian overland flow model. These works include: the coupled KW approximation of *Rovey et al.* [1977] with the GA infiltration model of *Mein and Larson* [1973] and *Smith and Hebbert* [1979], the KW approximation coupled with the GA infiltration model to determine the time of concentration and peak runoff rate from a converging basin [*Akan*, 1988]; a two-dimensional DW model coupled with the GA equation to simulate a single event storm [*James and Kim*, 1990]; an analytical model of *Robinson and Sivapalan* [1996] based on the generalization of the classic work of Horton and Rose's approximation [*Horton*, 1938; *Rose et al.*, 1982] for the piston displacement model coupled with the KW approximation to describe the surface and subsurface storm flows; a DEM based physically based distributed model of *Wang and Hjelmfelt* [1998] formulated by coupling the DW equations with the GA infiltration model; the two-dimensional hydrodynamic equations coupled with the GA infiltration equation for simulating the surface flow with the spatial variable infiltration and microtopograpy [*Fiedler and Ramirez*, 2000]; a GA model coupled with the two-dimensional SVE [*Esteves et al.*, 2000]; the integrated KW overland flow and Muskingum-Cunge channel flow models coupled with the GA model [*Yu*, 2000]; the KW approximation coupled with the GA model in the HEC-HMS environment [*USACE*, 2006]; the GA model coupled in the CASC2D model [*Downer et al.*, 2002]; an one-dimensional KW conjunctive model of *Liu and Singh* [2004] coupled with the modified GA equation by considering the effect of microtopography, slope gradient, and vegetative land surface cover to account for the hydrological system response; and the KW coupled GA models of *Reddy et al.* [2007], *Meng et al.* [2008], *Vieux et al.* [2009], and *Castaings et al.* [2009]. The details on the implementation of the GA infiltration model in the hydrological model framework for the subsurface flow routing are given by *Vieux* [2004a, 2004b]. Note that when the catchment scale is large, the conceptual model of surface microtopography advocated by *Woolhiser et al.* [1996] is not appropriate. Further, *Singh and Bhallamudi* [1998] concluded that the two dimensional effects in the 1DS2DSS model are only marginal and the application of the 1DS1DSS model gives satisfactory results.

The physical description of the flow path of water through the catchment to the stream is a very complex hydrological process, and it is evidenced that the rainfall-runoff record is only amenable to satisfy the models of very limited complexity [*Jakeman and Hornberger,* 1993]. Hence, the application of the complex models is quite challenging, especially for the large spatial scale due to uncertainties involved in the reasonable parameter estimation. In most of the practical situations, the KW approximation is valid for land slopes greater than about 0.001 [*Woolhiser and Liggett,* 1967, p. 763]; however, in very flat grassy slopes, it is necessary to use the SVE when the kinematic wave number is less than 5 [e.g., *Daluz Vieira,* 1983] or at least the DW equation [*Morris and Woolhiser,* 1980]. Similarly, for many cases of practical interest involving very high subcritical flows on the flat slopes, the DW equation is appropriate [*Gonwa and Kavvas,* 1986]. Moreover, after the commencement of rain and before ponding on the ground surface (i.e., zero initial depth as the true condition), the numerical solution of the SVE and its variants gets aborted since the flow depth appears in the denominator of several terms. After ponding, the flow depth is generally small and the corresponding small numerical oscillations can destroy the solution [*Fiedler and Ramirez,* 2000]. Further, the numerical schemes are prone to phase error, uncontrolled numerical dispersion [*Hromadka and DeVeries,* 1988; *Holden and Stephenson,* 1995; *Lal,* 1998a, 1998b; *Jaber and Mohtar,* 2001, 2002], instability and conversion problems [*Liggett and Wolhiser,* 1967]. The numerical integration scheme used for the solution of the shallow surface flow equation combined with the subsurface flow equation results in numerical instability problem due to the non-linearity of equations and boundary conditions used for their coupling. Hence, there is a need to go for the simplified physically based schemes which are devoid of the complication of numerical schemes used in the solutions of the SVE and its variants while maintaining the numerical stability and required model efficiency. One such approach could be based on the use of the Approximate Convection-Diffusion (ACD) equations advocated by *Perumal and Ranga Raju* [1999], which are directly derived from the SVE. Based on the ACD equations, two simplified routing methods *viz.,* VPMD and VPMS have been proposed for river routing purposes. These two models have the capability to estimate both the stage and discharge variables simultaneously at the end of the routing reach. The robustness of these river routing models for their field applicability has been verified by *Perumal et al.* [2001] (for the VPMD method); and *Perumal et al.,* [2007, 2010a, 2010b] (for the VPMS method). Alternative simplified model, namely, the VPMC method have also been extensively used both for the river [NERC, 1975; *Ponce and Yevjevich,* 1978, *Price,* 1985, *Ponce and Chaganti,*

1994]and overland flood routing studies [*Ponce*, 1986, 1989]. *Orlandini and Rosso* [1996] used the VPMC method to describe the surface runoff dynamics for a large catchment area utilizing the spatial data in the form of the digital elevation models (DEMs) and digital terrain models (DTMs). Further, the recently, introduced CATchment HYdrology (CATHY) model [*Camporese et al.*, 2010] couples the Richards equation for describing the flow process in variably saturated porous media coupled with the VPMC model for routing runoff from the hillslope and channel cells. Note that, in the VPMC method, the model parameters (viz., weighting parameter and travel time) are linked to the channel and flow characteristics based on the concept of matching the numerical diffusion with the hydraulic diffusion described by the diffusion coefficient. As discussed earlier, the physical justification of the VPMC method based on the concept of matching the physical and numerical diffusions is questionable [*Perumal*, 2010] on the pretext that since this method is based on the concept of matching the numerical diffusion with the Hayami's physical diffusion equation [*Hayami*, 1951], the method should work for the entire range of the physical diffusion equation. But it is a well-known fact that the VPMC method is only applicable for a small range [*Perumal and Sahoo*, 2007] of the physical diffusion equation.

Since the subsurface flow component has a direct impact on the direct surface runoff generation as overland flow, it has an equal importance as the surface flow component. Among the various infiltration models reported in the literature, the Richards and GA equations are mostly used as the submodels of the Hortonian overland flow models. The widespread use of the GA model may be attributed to its physical basis of development [*Mein and Larson*, 1971; *Morel-Seytox and Khanji*, 1974] which provides comparable results with that of the Richards equation [*Mein and Larson*, 1971; *Hsu et al.*, 2002] and, at the catchment scale, it is not a data intensive model as compared to the Richards equation. Moreover, the GA equation is an approximation of the Richards equation and is least complicated than the numerical solution of the Richards equation without much loss of computational accuracy [*Hsu et al.*, 2002; *Freeze*, 1974]. Hence, due to the sophisticated nature of the GA infiltration model, it has become the key infiltration model in recent overland flow modelling studies [also see *Philip*, 1983].

2.4.2 Coupling Approaches

The coupling of surface and subsurface flow dynamics is a very important step in an integrated physically based watershed model. Generally, the surface and subsurface flow components are interrelated by a pressure head and source/sink term such as the infiltration

35

rate (exchange flux) at the interface. If there exists a continuity of interface between the surface and subsurface sub-domains such as in case of the under laying permeable soil layer, the continuity of the pressure and exchange-flux is applied. However, when the under laying soil layer is less permeable, there exists a discontinuity at the interface, thus two coupling approaches, namely, the continuity or discontinuity approach can be used. With the continuous pressure and fluxes, the continuity approach can be used; however, it requires the numerical discritization into excessive number of computational grid points. In the discontinuity approach, an ad hoc exchange flux term can be used [*Huang and Yeh*, 2009]. Notably, *Morita and Yen* [2002] classified the surface and subsurface sub-domain coupling approaches into three categories: i) fully coupled (simultaneous solution), ii) alternative iterative coupling, and iii) external coupling (decoupling). Similarly, *Holzbecher et al.* [2005] and *Gunduz* [2006] have also described the coupling approaches in the hydrologic models by means of links and feedbacks between the surface and subsurface sub-domains. The links can be either one-way or two-way interfaces between the surface and subsurface sub-domains. The two-way links with feedbacks between the surface and subsurface sub-domains can be implemented with simultaneous solution of the flux term representing the interaction between these two sub-domains, known as the fully coupled approach or first order coupling [see *Kampf and Burger*, 2007]. Alternatively, the two way links with feedbacks can also be implemented by solving the surface and subsurface flow equations separately and the discontinuous interface between the surface and subsurface sub-domains is maintained by iterative updating of the exchange flux and subsurface boundary. Such a coupling process is known as the sequential iterative approach (SIT) [*Holzbecher and Vasiliev*, 2005] or alternative coupling approach. Further, the one-way link between the sub-domains can be implemented by solving for flow in one domain and, subsequently, the solution for that domain at the surface and subsurface interfaces is used as the boundary condition for the adjacent domain. In other words, the infiltration rate is computed by using the surface flow equations from a preceding time step. This approach is known as the sequential non-iterative approach (SNIT) [*Holzbecher and Vasiliev*, 2005] or time-lagged, decoupled approach. A thorough comparative study of all these coupling approaches by *Huang and Yeh* [2009] revealed that all the three approaches can be applied for continuous or discontinuous interface conditions. The fully coupling approach considers the surface and subsurface as a continuum and, hence, it guarantees the mass conservation across the interface. Further, this approach is convenient only when the same time step is used for the surface and subsurface water flow computations. Although, it is the most

36

accurate, this approach is very difficult to implement, and the CPU run time is expensive with limited field applicability. The SIT and SNIT approaches provide flexibility in selecting the number of time steps for overland flow within the single time steps for subsurface flow. Although, the accuracy of the SIT approach is somewhat better than the SNIT approach, the latter approach is advantageous as it is easier to implement and CPU run time efficient than the former approach. These SIT and SNIT approaches have the high field applicability than the fully coupling approach. Moreover, the SNIT approach can reduce half of the CPU run time without significantly affecting the accuracy of the solution [*Singh and Bhallamudi*, 1998]. All these three types of coupling approaches are applied only when the surface and subsurface sub-domains are equally important to the modeler. However, when the focus is only at one sub-domain, whereas, the other sub-domain is of least importance which is required only to compute some approximate effect on the primary sub-domain, it is convenient to use the primitive sink type coupling. In this type of coupling, the interacting exchange flux (i.e., infiltration rate) is considered as the sink or source in the overland flow routing equation. Indeed, there exists no direct link between the surface and subsurface sub-domains and, hence, the sink type coupling is always referred as the no-coupling approach [*Gunduz*, 2006], which is again simpler and computationally efficient than any other coupling approaches that can be used when the Green-Ampt or Philips or Horton equation is used for computation of flow in the subsurface domain without solving the surface flow routing equations. Further, this coupling approach is in harmony with the limited data availability for field application and, hence, it is still finding a wide application area in the field of hydrologic modelling studies [e.g., *Gunduz*, 2006; *Tayfur et al.*, 1993; *Fiedler and Ramirez*, 2000; *Esteves et al.*, 2000; *Castillo et al.*, 2003; *Liu and Singh*, 2004].

2.5 APPLICABILITY CRITERIA OF THE OVERLAND FLOW METHODS

Due to the availability of a number of simplifications to the SVE in literature, various researchers tried to evaluate the adequacy of these overland flow models under varied field and rainfall conditions using different applicability criteria. *Woolhiser and Liggett* [1967] is probably the first to advocate a non-dimensional criterion, the kinematic wave number (k), for judging the goodness of the KW approximation in overland flow modelling, expressed

as
$$k = \frac{s_0 L}{y_e F_{rp}^2} \tag{2.33}$$

where L = length of the overland plane [L]; y_e = depth of flow at the end of the plane at

equilibrium [L]; and F_{rp} = Froude number at the end of the plane at equilibrium.

With the increase of the value of k, the solution of the SVE for the rising hydrograph approaches the solution of the KW approximation. In the subsequent studies [*Daulz Vieira* 1983; *Govindaraju et al.*, 1988a, 1988b; *Moramarco and Singh*, 2002], the kinematic wave number was found as a key parameter for establishing the applicability limits of both the KW and DW overland flow models. The KW approximation may be used instead of the SVE, if $k > 20$ and $F_{rp} \geq 0.5$ [*Woolhiser and Liggett*, 1967], which should only be applicable for the rising limb of the runoff hydrograph without formation of the front face. However, when the lateral inflow continuously contributes along the flow path leading to higher flow depth at the downstream end of the plane, the possibility of front face formation is very rare. Further, while solving the SVE for subcritical, critical, and supercritical flows considering the critical flow depth as the lower boundary condition, *Al-Mashidani and Taylor* [1974] confirmed the findings of *Woolhiser and Liggett* [1967] that the kinematic wave number k could be used for validating the KW approximation; and suggested that its value should be higher without the necessity of the imposed condition: $F_{rp} < 2$.

Similarly, *Miller and Cunge* [1975] derived an applicability criterion based on the Froude number by balancing the dynamic and kinematic wave celerities in open channel flow, wherein the dynamic and kinematic waves are equally important. According to this criterion, $F_{rp} = 1.5$ or 2 when Chezy's or Manning's friction law is used, respectively, and during this, the dynamic wave dampens out rapidly. Subsequently, the study by *Miller and Cunge* [1975] established that the KW approximation would not be appropriate to describe such highly supercritical flows owing to the fact that the dynamic wave celerity diverges from the KW celerity. It is a well known fact that when the overland flow is in a subcritical flow range, the typical Froude numbers are $0 < F_{rp} < 0.2$, except for the case of extreme excess precipitation envisaged during the thunderstorms [*Hager and Hager*, 1985]; hence, the criterion by *Miller and Cunge* [1975] is not generally useful. Subsequently, *Morris and Woolhiser* [1980] modified the criterion of *Woolhiser and Liggett* [1967] to provide an additional criterion of $(kF_{rp}^2)_e \geq 5$, if the KW approximation is to be used accounting for the rising and recession hydrographs for the conditions of rainfall ceasing before or after an equilibrium flow condition has reached. Further, *Daluz Vieira* [1983] extended the work of *Morris and Woolhiser* [1980] to develop the applicability criteria for examining the appropriateness of the kinematic, diffusion and gravity wave approximations to the SVE by accounting for the critical-flow-depth and zero-depth-gradient as the lower boundary

conditions with constant lateral flow contribution. On the basis of the graphical representation of the $F_{rp} - k$ field by *Daluz Vieira* [1983], it may be surmised that when $k > 5$, the KW and DW approximation zones are identical; when $k > 50$, the KW approximation is appropriate for overland flow modelling instead of the full SVE solution; when $5 \leq k \leq 20$, the choice among the KW and DW approximations depends on the value of F_{rp}; when $k < 5$ and $F_{rp} > 1$, the overland flow modelling should be carried out by using the full SVE solution or else the gravity wave solution may be used; and when $k < 5$, the critical-flow-depth lower boundary condition criterion has a significant effect as compared to that of the zero-depth-gradient downstream boundary condition. *Hager and Hager* [1985] surmised that the use of these entire criteria set out for deciding the appropriateness of the KW approximation is substantially accurate. Alternatively, these criteria k and kF_{rp}^2 can be obtained as [*Morris and Woolhiser*, 1980; *Stephenson and Meadows*, 1986; *Wong*, 1992, 2005]:

$$k = 1.725 \times 10^6 \frac{n^{1.2} s_0^{0.4} L^{0.2}}{r_e^{0.8}} \tag{2.34a}$$

$$k(F_{rp}^2)_e = 8585.81 \times \frac{s_0^{1.3} L^{0.4}}{n^{0.6} r_e^{0.6}} \tag{2.34b}$$

where r_e = rainfall intensity at equilibrium (mm/h); L = overland plane length in metre; and n = Manning's roughness coefficient.

Further, *Hager and Hager* [1985] advocated the explicit criteria for KW models as: (i) $KF\sqrt{s_0} < 3$, except for the dynamical effect (*viz.*, roll waves), and (ii) $r(KF)^3 \sqrt{s_0}/g^2 < 0.07$, except for the diffusive effect, where r is rainfall intensity and $KF = 1/n$. Based on the $F_{rp} - (kF_{rp}^2)_e$ plot developed using the effect of the upstream depth boundary condition, *Pearson* [1989] recommended a criterion to justify the validity of the KW approximation expressed as: $k > 3 + 5/F_{rp}^2$ applicable for the overland flow modelling and not for the channel flow routing. A study by *Singh and Aravamuthan* [1995, 1997] revealed that for channel flow routing, the DW and KW approximations are satisfied when $(kF_{rp}^2)_e > 7.5$ and 30, respectively. Various other workers [*Fread*, 1985; *Afouda*, 1980a, 1980b] also tried to develop applicability criteria for the KW and DW approximations. A detailed investigation of errors involved with these simplifications was studied by *Parlange et al.* [1990], *Singh* [1994a, 1994b], and *Singh and Aravamuthan* [1995, 1997] for channel

flow condition. While investigating on the appropriateness of using the KW and DW equations for modelling under the condition of spatially varying rainfall excess, *Moramarco and Singh* [2002] found that the modelling errors are independent of rainfall excess distribution for $(kF_{rp}^2)_e > 5$; and recommended that the KW approximation (critical-flow-depth as the lower boundary condition) is reasonably accurate when $(kF_{rp}^2)_e \geq 20$ and $(kF_{rp}^2)_e \geq 35$, if rainfall excess occurs over the whole plane and if it is concentrated within a portion of the plane, respectively; and the corresponding applicability limits for the DW approximation are $(kF_{rp}^2)_e \geq 15$ and $(kF_{rp}^2)_e \geq 30$, respectively. Similarly, with the zero-depth-gradient lower boundary condition, the corresponding applicability limits are $(kF_{rp}^2)_e \geq 10$ and $(kF_{rp}^2)_e \geq 15$ for the KW approximation, and $(kF_{rp}^2)_e \geq 7.5$ and $(kF_{rp}^2)_e \geq 12.5$ for the DW approximation, respectively.

In general, for the implementation of the downstream boundary conditions in overland flow modelling, there are two school of thoughts prevail: i) that imposing the downstream boundary such as the critical flow depth and zero-depth-gradient boundary conditions has little or no influence on the outflow hydrograph [e.g., *Al-Mashidani and Taylor*, 1974; *Morris*, 1979; *Govindaraju et al.*, 1988a, 1988b; *Gottardi and Venutelli*, 2008]; and ii) that the lower downstream boundary condition significantly affect the simulation results when $k < 5$ and for a lower value of F_{rp} [e.g., *Daulz Vieira*, 1983; *Moramarco and Singh*, 2002]. *Gottardi and Venutelli* [2008] pointed out that the selection of the downstream boundary condition is not necessarily meaningful, but only for mathematical convenience it could be imposed in the hydrological modelling. Moreover, the critical-flow-depth downstream boundary condition is a stringent condition which might lead to problems in certain range of parameter values while seeking a numerical solution [*Govindaraju et al.*, 1988a, 1988b]. Further, it is relatively easier to incorporate the downstream boundary effect in river routing schemes, but not in the overland flow modelling schemes due to the spatially varying topology, land use, vegetation, and geomorphology. Hence, although there are some theoretical investigations carried out in support of using the downstream boundary condition in overland flow modelling [*Morris and Woolhiser*, 1980, *Daluz Vieira*, 1983; *Moramarco and Singh*, 2002], however, its proper implementation in the practical catchment modelling studies is hardly known. Moreover, the geographical referencing used for this will result in unnecessary burden on the modeled runoff hydrograph prediction due to parameter uncertainty introduced out of self-delusion of the modelers [*Beven*, 1993]. *Kampf and*

Burges [2007] opined that although the numerical models are capable of solving the boundary value problems, these models always face with the challenge of assigning accurate boundary conditions which are often a nontrivial task. Note that the boundary conditions such as the catchment divide can be incorporated very easily and quite accurately into the model framework, but it is extremely difficult to define the hydrodynamic boundary such as the catchment overland flow plane outlet due to dynamic nature. Since the assigned downstream boundary conditions influence the routing solutions, their effect may extend well beyond the location of the interest. Hence, the error involved with the estimated runoff hydrograph by incorporating the downstream boundary condition could be much higher than those simulated without incorporating the boundary condition.

Several authors have also examined the applicability zones of KW, DW, and gravity wave approximations in the main river channel [*Dooge and Harley*, 1967; *Weinmann and Laurenson*, 1979; *Ferrick*, 1985; *Fread*, 1985; *Dooge and Napiórskowski*, 1987; *Ponce*, 1993; *Fread and Hsu*, 1993; *Moussa and Bocquillon*, 1996; *Moussa and Bocquillon*, 2000; *Tsai*, 2003; *Moramarco et al.*, 2008a, 2008b]. Notably, based on the linear stability analysis of the perturbation characteristics of a flood wave (i.e., propagation celerity and logarithmic decrement), *Ponce et al.* [1978] developed the applicability criteria for the KW and DW applications for open channel flow routing without accounting for the lateral inflow contribution. The basic disadvantages of using the linear stability analysis are: a) its incapability to describe perceptible subsidence caused due to downstream traveling wave front, b) possibility of break-down when the flow traverses over a dry porous bed [*Singh*, 1996, p. 568], and c) its inability to account for the nonlinear characteristics of the flood wave that exists in nature [*Perumal and Sahoo*, 2007]. Although the applicability criteria of *Ponce et al.* [1978] is questionable in practice [*Zoppu and O'neill*, 1982; *Perumal and Sahoo*, 2007], it is still in use for examining the appropriateness of the KW and DW approximations for overland flow modelling [e.g. *Orlandini and Rosso*, 1998; *Santillana and Dawson*, 2009]. Based on the magnitude of the scaled flow depth gradient $(1/S_0)(\partial Y/\partial X)$, *Perumal and Sahoo* [2007] developed the applicability criteria of the VPMD, VPMS, and VPMC river routing methods as $(1/S_0)(\partial Y/\partial X)_{max} \leq 0.43$, 0.63 and 0.11, respectively (where S_0 is the channel bed slope, Y is the flow depth (stage) in the open channel, and X is the space variable). The logic behind the development of this criterion is that the scaled flow depth gradient $(1/S_0)(\partial Y/\partial X)$ is used for the classification of flood waves [*Henderson*, 1966; *NERC*, 1975] and, hence, it is more appropriate to use the

same to establish the applicability limit. Previously, such a criterion was advocated by *Price* [1985] while assessing the applicability limit for the simplified river routing model developed by him. The presence of $(1/S_0)(\partial Y/\partial X)$ signifies a diffusive flood wave, and its absence signifies a kinematic flood wave. In fact, the form of the momentum equation in the KW approximation is $S_0 \cong S_f$, implying that the free water surface should be approximately parallel to the channel bed slope, i.e., $(1/S_0)(\partial Y/\partial X) \ll 1$ [*Singh*, 1996]. Similarly, *Hunt* [1982] and *Gill* [1984] also attempted to derive the criteria for the KW approximation based on the comparison of gradient terms in the momentum equation as: $(m^2 F_{rc}^2/S_0)(\partial Y/\partial X) \ll 1$ and $[(1-m^2 F_{rc}^2)/S_0](\partial Y/\partial X) \ll 1$, where F_{rc} is the Froude number in the open channel flow.

A study by *Richardson and Julien* [1994] reveals that (i) at equilibrium, a_l^* is always larger during the rising limb than a_c^*, (ii) for supercritical flow, $F_{rp} > 1.4$, $a_l^* > a_c^* > a_p^*$, (iii) for subcritical flow, $F_{rp} < 0.4$, $a_p^* > a_l^* > a_c^*$, and (iv) the relative magnitude of acceleration terms ($a_l^* > a_c^* > a_p^*$) for supercritical flow are always in contrast with the open channel flow ($a_p^* > a_c^* > a_l^*$), where $a_p^* =$ non-dimensional pressure gradient term of the SVE, $a_l^* =$ non-dimensional local acceleration term of the SVE, and $a_c^* =$ non-dimensional convective acceleration term of the SVE. Although, the open channel flow and shallow overland flow processes resemble to each other, there is a basic difference in the magnitudes of inertial and pressure gradient terms in the momentum equation [*Richardson and Julien*, 1994]. When k is large, the magnitude of the non-dimensional acceleration terms are small as compared to the overland plane slope (s_0). Hence, the KW approximation is valid only when k and F_{rp} are large. Under subcritical overland flow conditions, the DW approximation can be used to improve the error caused by the KW approximation. Moreover, the order of magnitudes of the inertial and pressure gradient terms in the open channel and shallow overland flows are significantly different [*Richardson and Julien*, 1994]. Therefore, the applicability criteria advocated for a routing scheme used for the open channel flow without accounting for the lateral inflow may not be admissible to the overland flow modelling with significant and continuous lateral inflows. Consequently, the applicability criteria advocated by *Perumal and Sahoo* [2007] for the VPMD and VPMS river flow routing models may not be appropriate for their use in the overland flow modelling, which receives significant and continuous lateral inflows; and, hence, warrants

for the development of applicability criteria for these models in the context of overland flow modelling.

2.6 CONCLUDING REMARKS

On the basis of literature review presented in this Chapter, it can be surmised that:

a) The main disadvantages associated with the numerical solution of the complete hydrodynamic wave model are the requirement of (fictitious) boundary conditions at one or more locations in the domain, numerical instability, and computational limitations in most of the situations of practical importance [*Tan*, 1992]. Under such circumstances the use of approximation to the SVE, viz., KW, DW, and gravity wave methods are feasible within their respective applicability limits. However, the stability and accuracy problems arise while using the SVE and its variants due to the numerical dispersion, diffusion, and oscillation. These problems associated with these numerical methods can be minimized to a certain extent by considering varied degree of simplifications to the SVE, but cannot be eliminated completely. In light of these shortcomings, a novel modelling tool is required which is structurally simple and easy to apply for overland flow simulation by maintaining a higher degree of modelling efficiency. The parameters of such a model should have reasonable physical basis linking to the basin and flow characteristics [*Woolhiser*, 1996], with a wider applicability range of the model beyond the applicability range of the KW approximation.

b) Among the multitude of approaches available for the physical interpretation of the Muskingum method, the approaches based on the VPMD and VPMS methods may be considered as appropriate since these methods are able to explain many features of the Muskingum method than by the other available approaches. These VPMD and VPMS methods have been developed using the ACD equations [*Perumal and Ranga Raju*, 1999] in discharge and stage formulations, respectively. The ACD equations are capable of modelling the physical diffusion, in a limited sense, in the transition range between that governed by the diffusive and kinematic waves with the latter wave type being a special case.

c) The use of the VPMD method has been found useful for solving the unsteady channel flow problems [*Perumal et al.*, 2001, 2004]. However, the potential capabilities of these methods to solve the overland flow problem remain unexplored.

Because of the sound theoretical basis of the VPMD routing method, it has strong potential for its application to overland flow modelling.

d) Only a few overland flow routing methods which use flow depth as the operating variable are available in literature. It may be noted that the VPMS river routing method has a higher applicability range than the VPMD and VPMC river routing methods [*Perumal and Sahoo*, 2007]. Since the VPMS method has been originally developed for river routing without accounting for the lateral flow contribution, this method can be explored by extending its applicability to the realm of overland flow modelling.

e) The order of magnitudes of the inertial and pressure gradient terms in the open channel and shallow overland flows are significantly different [*Richardson and Julien*, 1994]. Hence, the applicability criteria advocated for a routing scheme used for the open channel flow without accounting for lateral inflow may not be admissible to the overland flow modelling with significant and continuous lateral flow contribution. Consequently, the applicability criteria advocated by *Perumal and Sahoo* [2007] for the VPMD and VPMS river flow routing models may not be appropriate for their application in overland flow modelling; and, hence, this warrants for the development of applicability criteria of these models in the context of overland flow modelling.

f) As stated earlier, the VPMD and VPMS methods have a wider applicability range and improved performance than the VPMC method [*Perumal and Sahoo*, 2007]. Hence, there is a need to test the VPMD and VPMS overland flow routing methods by coupling with the infiltration models to simulate the Hortonian overland flow process.

3

OVERLAND FLOW MODELLING USING THE VARIABLE PARAMETER MUSKINGUM DISCHARGE ROUTING METHOD AND ITS EVALUATION

3.1 GENERAL

This chapter presents the development of a simple and numerically stable physically based method to simulate overland flow following the approach used in the development of the variable parameter Muskingum method proposed by *Perumal* [1994a]. The operational performance of this method is extensively carried out using the observed rainfall-runoff data available in literature based on various evaluation measures. Besides, the simulation results are also evaluated with the analytical solutions of the kinematic wave equation, and the various numerical method solutions of the SVE, and diffusive and kinematic wave equations. The VPMD method is also coupled with a ϕ-index infiltration type interception model to account for the interception losses. The sensitivity of the method for varying the computational space and temporal grid sizes have also been studied.

3.2 FORMULATION OF THE OVERLAND FLOW MODEL

The term overland flow broadly includes thin sheet of flow and may also include flows over rilled and irregular surfaces or flow in small channels which results in useful abstraction [*Woolhiser*, 1974]. However, for the sake of mathematical simplicity, it is assumed that the flow is occurring over a plane surface. In such a situation, considering the flow behaviour to be one-dimensional, it can be described by the well known Saint-Venant equations consisting of the continuity and momentum equations. In many situations, it has been found that the continuity equation and the simplified form of the momentum equation obtained by eliminating and curtailing some of the terms are found to describe the one-dimensional flow very well [*Henderson*, 1966]. *Perumal* [1994a, 1994b] made one such simplification and used the continuity equation and the simplified momentum equation to develop the VPMD method. This method was developed for routing the gradually varying unsteady flow in channel or river reach having a prismatic rectangular cross section, without considering lateral flow in the reach. As the form of the routing equation is same as that of

the classical Muskingum method involving the same parameters, it was considered appropriate to name this method as the variable parameter Muskingum method. This method is capable of varying its parameters in a physically based manner at every routing time interval relating them to channel and flow characteristics in a manner consistent with the variation built-in in the SVE solution. Based on the same concept, *Perumal and Ranga Raju* [1998a, 1998b] proposed a simplified variable parameter Muskingum-type stage-hydrograph routing method which uses the same form of the routing equation as that of the Muskingum method, but replacing the discharge variable by the stage variable. Therefore, to differentiate the variable parameter Muskingum routing using the discharge and stage variables, it was proposed to identify these methods as the Variable Parameter Muskingum Discharge (VPMD) and the Variable Parameter Muskingum Stage routing (VPMS) methods, respectively. In the present study, the VPMD channel routing method [*Perumal*, 1994a] has been extended for overland flow modelling by incorporating the distributed lateral flow in the model framework. Henceforth, for the sake of brevity, the VPMD overland flow routing method is referred as the VPMD method.

3.2.1 Concept of the Proposed Overland Flow Model

During the steady state flow condition in a overland flow strip, there exists a one-to-one relationship between the flow depth or the cross-sectional area of the flow and the discharge at any location defining the steady state flow-depth relationship at that location. But during unsteady flow situation, there exists no unique relationship between the flow depth and the discharge at any location, but the same unique relationship exists between the flow depth at a given section and the corresponding steady discharge, occurring somewhere downstream from that section. This condition is depicted in Figure 3.1 which defines the Muskingum routing reach considered for the overland flow study. This figure clearly shows that within the sub-reach of length Δx, at any instant of time t, the flow depth, y_M at the middle of the reach is uniquely related with the discharge q_3 passing at a location l downstream from the mid-section of the reach.

3.2.2 Governing Equations

The VPMD method for overland flow modelling is derived from the full Saint-Venant equations considering lateral flow, which govern the one-dimensional flow over a plane. These equations applied to a unit width of the overland flow plane are expressed by the continuity and momentum equations, respectively, as [*Singh*, 1996]

46
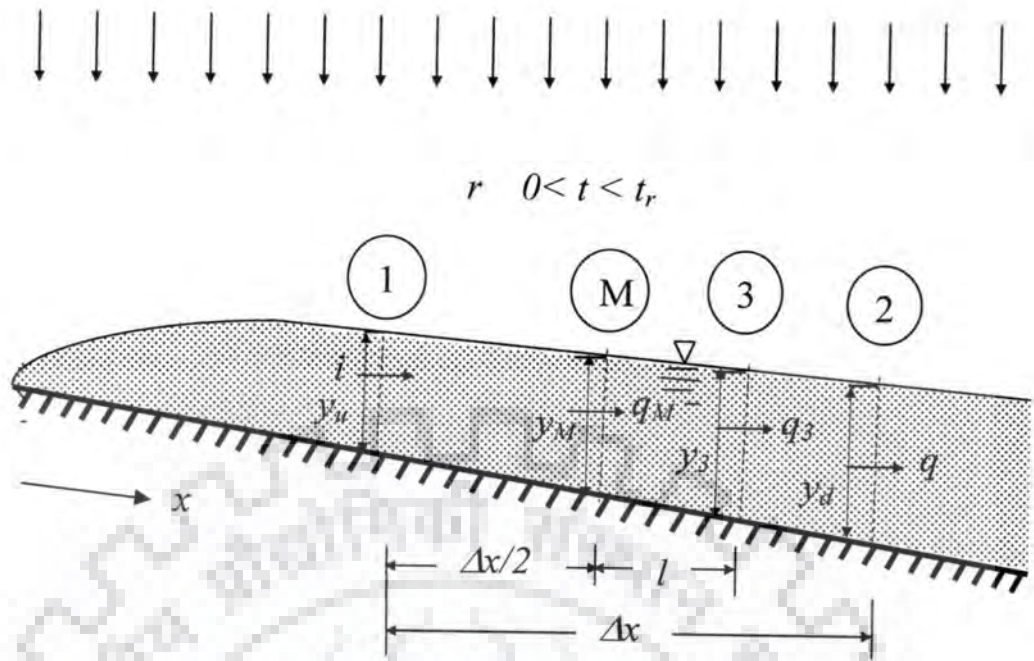
Figure 3.1 Schematic sketch of the Muskingum reach governing the overland flow over an impervious surface.

$$\frac{\partial q}{\partial x} + \frac{\partial y}{\partial t} = q_L \tag{3.1}$$

$$s_f = s_0 - \left(\frac{\partial y}{\partial x}\right) - \left(\frac{1}{g}\right)\left(\frac{\partial v}{\partial t}\right) - \left(\frac{v}{g}\right)\left(\frac{\partial v}{\partial x}\right) - \left(\frac{q_L v}{gy}\right) \tag{3.2}$$

where q = flow rate per unit width of the flow plane [$L^2 T^{-1}$], y = flow depth [L], s_f = energy slope [LL^{-1}], g = acceleration due to gravity [LT^{-2}], v = flow velocity [$L\ T^{-1}$], s_0 = the bed slope [LL^{-1}], q_L = net rate of lateral inflow per unit area [LT^{-1}] expressed as

$$q_L = r - I_a \tag{3.3}$$

where, r = the rate of rainfall per unit area occurring for a duration t_r, and I_a = the rate of loss due to abstraction. An order of magnitude analysis of equation (3.2) reveals that the momentum due to lateral inflow or outflow has a negligible effect on the flow dynamics [*Eagleson*, 1970; *Henderson*, 1966], and, hence, the term ($q_L v / gy$) is neglected in the analysis.

3.2.3 Assumptions

The assumptions used in the derivation of this VPMD method are:

a) A uniform thin sheet flow of runoff developing over an overland flow plane resembles to that of a shallow water unsteady flow in a wide prismatic rectangular cross-section channel reach;

b) There is lateral inflow due to rainfall and/or outflow due to the interception and infiltration losses uniform over the computational reach;

c) The momentum due to lateral inflow and/or outflow is assumed to be negligible;

d) The slope of the water surface ($\partial y/\partial x$), the slope due to local acceleration $(1/g)(\partial v/\partial t)$ and the slope due to convective acceleration $(v/g)(\partial v/\partial x)$ all remain constant at any instant of time in a given routing reach. This assumption implies that the friction slopes s_f is constant over the computation reach of length Δx and, accordingly, the flow depth variation is linear over this reach Δx;

e) The multiple of the derivatives of flow and section variables with respect to both time and space are negligible; and

f) At any instant of the time during unsteady flow, the steady flow relationship is applicable between the flow depth at the middle of the computational reach and the discharge passing somewhere downstream of it.

Assumptions (d – f) are employed in the VPMD channel routing method without considering lateral flow [*Perumal*, 1994a].

3.2.4 Derivation of the VPMD Method for Overland Flow Modelling

The discharge at any section of the unit width of the overland flow plane reach may be expressed as:

$$q = vy \tag{3.4}$$

Equation (3.4) can be rewritten after incorporating velocity v expressed by the Manning's friction law as

$$q = \frac{1}{n} y^{5/3} s_f^{1/2} \tag{3.5}$$

where, n is the Manning's roughness coefficient. It may be noted that for the unit width overland flow plane strip, the hydraulic radius is equal to the overland flow depth.

48

Differentiating equation (3.5) with reference to x and invoking assumption (d) of constant s_f over the length Δx, the resulting expression may be written as

$$\frac{\partial q}{\partial x} = (5/3) v \frac{\partial y}{\partial x} \qquad (3.6)$$

Using equation (3.6), the celerity of flow wave may be expressed as

$$c = \frac{\partial q}{\partial y} = \frac{5}{3} v \qquad (3.7)$$

Due to the assumption of linearly varying flow depth over a computational reach, the celerity of the overland flow governed by equation (3.7) is not unique, as in the case of the KW model [*Ponce*, 1986], for the same flow depth occurring in the rising and falling limbs of the runoff hydrograph.

Differentiation of equation (3.6) with reference to x and invoking assumption (e) that the multiples of derivatives of flow and section variables with reference to x and t are negligible, the resulting expression can be written as

$$\frac{\partial^2 q}{\partial x^2} = 0 \qquad (3.8)$$

Equation (3.8) implies that the runoff discharge is also varying linearly over the computational reach considered.

The use of equations (3.1), (3.4), (3.6) and (3.7) and also the assumption of negligible momentum due to lateral inflow contribution enables one to arrive at the equation for the local acceleration term, which can be expressed as

$$\frac{1}{g} \frac{\partial v}{\partial t} = -\frac{10}{9} \frac{\partial y}{\partial x} F_{rp}^2 \qquad (3.9)$$

where F_{rp} = Froude number of the overland flow expressed as $F_{rp} = v / \sqrt{gy}$.

Further, the use of equation (3.4) and (3.6) leads to the expression for the convective acceleration term which can be written as

$$\frac{v}{g} \frac{\partial v}{\partial x} = \frac{2}{3} \frac{\partial y}{\partial x} F_{rp}^2 \qquad (3.10)$$

Using equations (3.9) and (3.10) in equation (3.2) leads to the expression for the friction slope (s_f) as

$$s_f = s_0 \left[1 - \frac{1}{s_0} \frac{\partial y}{\partial x} \left\{ 1 - \frac{4}{9} F_{rp}^2 \right\} \right] \qquad (3.11)$$

49

The term $(2/3)F_{rp}$ given in the squared form in equation (3.11) is known as the Vedernikov number, V_{vn} [Chow, 1959; *Jolly and Yevjevich*, 1971; *Ponce*, 1991] which defines the criterion for the amplification of the overland flow, when $V_{vn} > 1$.

3.2.4.1 Weighted runoff discharge location

Using equation (3.11) in equation (3.5) for expressing the discharge q_M at the middle of the considered computational flow reach of Δx, and eliminating higher order terms of the $\frac{1}{s_0}\frac{\partial y}{\partial x}\left\{1 - \frac{4}{9}F_{rp}^2\right\}$ in the binomial series expansion of equation (3.11), leads to the expression for q_M as

$$q_M = q_3 - \frac{q_3\left(1 - (4/9)F_{rp}^2\right)_M}{2s_0(5/3)v_3}\frac{\partial q}{\partial x}\bigg|_3 = q_3 - l\frac{\partial q}{\partial x}\bigg|_3 \tag{3.12}$$

in which

$$q_3 = \frac{1}{n}y_M^{5/3}s_0^{1/2} \tag{3.13}$$

where, the subscripts M and 3, respectively, denote the mid-section and section '3' of the computational reach length Δx. In equation (3.12), the discharge q_M is expressed in terms of normal discharge, q_3, which is uniquely related to y_M by the steady-state relationship. Therefore, the adjunct term of $\partial q/\partial x|_3$ denotes the length l of the location of section (3) downstream from the mid-section of the computational reach, at which the normal discharge q_3 corresponding to the flow depth y_M passes during unsteady flow.

3.2.4.2 Derivation of the Approximate Convection-Diffusion (ACD) equation for overland flow

Differentiation of equation (3.5) with respect to t gives

$$\frac{\partial q}{\partial t} = (5/3)v\frac{\partial y}{\partial t} + \frac{y^{5/3}}{2n}s_f^{-1/2}\frac{\partial s_f}{\partial t} \tag{3.14}$$

The expression for the term $(\partial s_f/\partial t)$ in equation (3.14) can be obtained by differentiation of equation (3.2) with reference to t, and using equation (3.10) and the assumption (d) that $(1/g)(\partial v/\partial t)$ remains constant at any instant of time over a given computational reach, which leads to

$$\frac{\partial s_f}{\partial t} = -\left(1 - \frac{2}{3}F_{rp}^{2}\right)\frac{\partial^2 y}{\partial x \partial t} \qquad (3.15)$$

Differentiating equation (3.1) with reference to x and using equation (3.8) in equation (3.15) leads to

$$\frac{\partial s_f}{\partial t} = 0 \qquad (3.16)$$

Therefore, equation (3.14) can be rewritten using equation (3.16) as

$$\frac{\partial q}{\partial t} = (5/3)v\frac{\partial y}{\partial t} \qquad (3.17)$$

Using equations (3.7) and (3.17) in equation (3.1) leads to the governing equation of the overland flow model as

$$\frac{\partial q}{\partial t} + c\frac{\partial q}{\partial x} = cq_L \qquad (3.18)$$

This simplified governing equation is used in the development of the VPMD method for overland flow modelling and is referred to as the Approximate Convection-Diffusion (ACD) equation. Note that the form of equation (3.18) is similar to the form of the kinematic wave equation expressed by *Ponce* [1986]. Although, the ACD equation and the kinematic wave equation resemble each other having the same form, the ACD equation is capable of modelling the overland flow in an approximate manner in the transition range of the unsteady overland flow governed by the diffusion and kinematic waves (including the latter) in a way similar to the VPMD method developed for routing floods in channels [*Perumal and Ranga Raju*, 1999]. The basis behind this inference is that the right hand side of equation (3.18) does not contain the diffusion term ($D\partial^2 q/\partial x^2$) due to equation (3.8), but the diffusion coefficient $D \neq 0$. This enables the application of equation (3.18) for overland flow modelling in the range of lower order shallow diffusive flood waves, including the kinematic waves. However, this remark seems to be contradictory with the conventional perception that equation (3.18) is strictly applicable for modelling the overland flow in the kinematic wave range only.

3.2.4.3 Routing equation of the proposed overland flow model

Since the discharge is varying linearly, the normal discharge, corresponding to flow depth y_M, which passes at section (3) at any instant of time can be expressed based on the linear variation of flow over Δx in terms of inflow (i), and outflow (q) as

$$q_3 = q + \left(\frac{\Delta x}{2} - l\right)\left(\frac{i-q}{\Delta x}\right) = q + \left(\frac{1}{2} - \frac{l}{\Delta x}\right)(i-q) \tag{3.19}$$

Application of the governing equation (3.18) of the ACD wave to section '3' as depicted in Figure 3.1, leads to the expression

$$\left.\frac{\partial q}{\partial x}\right|_3 = -\left(\frac{1}{c}\frac{\partial q}{\partial t}\right)_3 + q_L \tag{3.20}$$

Further, due to linear variation of discharge, one can write

$$\left.\frac{\partial q}{\partial x}\right|_3 = \left.\frac{\partial q}{\partial x}\right|_2 = \frac{q-i}{\Delta x} \tag{3.21}$$

Using equations (3.19) and (3.21) in equation (3.20) leads to the expression

$$i - q + q_L\Delta x = \frac{\Delta x}{c_3}\frac{\partial}{\partial t}\left[q + \left(\frac{1}{2} - \frac{l}{\Delta x}\right)(i-q)\right] \tag{3.22}$$

Equation (3.22) has the same form as that of the governing differential equation of the Muskingum method with its parameters K and θ expressed as

$$K = \frac{\Delta x}{c_3} \tag{3.23}$$

Substituting the expression for l in equation (3.22) from equation (3.12), the expression for θ can be given as

$$\theta = \frac{1}{2} - \frac{q_3\left(1-(4/9)F_{rpM}^2\right)}{2s_0 c_3 \Delta x} \tag{3.24}$$

The numerical approximation of equation (3.22) leads to a form similar to the routing equation for overland flow modelling developed by *Ponce* [1986] using the Muskingum-Cunge method and can be expressed on the space-time computational grid as

$$q_2 = C_1 i_2 + C_2 i_1 + C_3 q_1 + C_4 q_L \Delta x \tag{3.25}$$

where q_2 = the outflow runoff discharge from the computational reach at current time level; i_2 = the inflow runoff discharge to the computational reach at current time level; i_1 = the inflow runoff discharge to the computational reach at the previous time level; q_1 = the outflow runoff discharge from the computational reach at the previous time level; and q_L = average lateral inflow rate within the computational reach over Δt. The routing coefficients $C_1, C_2, C_3,$ and C_4 are given by

$$C_1 = \frac{-K\theta + 0.5\Delta t}{K(1-\theta) + 0.5\Delta t} \tag{3.26}$$

52

$$C_2 = \frac{K\theta + 0.5\Delta t}{K(1-\theta) + 0.5\Delta t} \tag{3.27}$$

$$C_3 = \frac{K(1-\theta) - 0.5\Delta t}{K(1-\theta) + 0.5\Delta t} \tag{3.28}$$

$$C_4 = \frac{\Delta t}{K(1-\theta) + 0.5\Delta t} \tag{3.29}$$

3.2.4.4 Runoff flow depth computations

The runoff flow depth y_d at the end of the computational sub-reach corresponding to the outflow q_2 is estimated from equation (3.6) as

$$y_d = y_M + \frac{(q_2 - q_M)}{(5/3)v_M} \tag{3.30}$$

in which y_M is estimated directly from the normal runoff discharge relationship given by equation (3.13). The discharge q_M at middle of the computational reach is obtained by taking the mean of inflow and outflow discharge at current time level.

3.3 VPMD CHANNEL FLOW ROUTING METHOD CONSIDERING LATERAL FLOW

Channel flow routing is required to compute runoff discharge of a catchment. The VPMD channel flow routing method developed by *Perumal* [1994a] without considering lateral flow is modified for channel flow routing of the V-catchment studied herein, considering lateral flow, as formulated below:

The continuity and momentum equations of the one-dimensional channel routing are given as

$$\frac{\partial Q}{\partial X} + \frac{\partial A}{\partial t} = Q_L \tag{3.31}$$

$$S_f = S_0 - \left(\frac{\partial Y}{\partial X}\right) - \left(\frac{1}{g}\right)\left(\frac{\partial V}{\partial t}\right) - \left(\frac{V}{g}\right)\left(\frac{\partial V}{\partial X}\right) - \left(\frac{Q_L V}{Ag}\right) \tag{3.32}$$

where Q = the channel flow rate [L^3T^{-1}]; A = the channel cross-sectional area of flow [L^2]; S_f = the channel energy slope [LL^{-1}]; g = acceleration due to gravity [LT^{-2}]; V = velocity of the channel flow [LT^{-1}]; S_0 = the channel bed slope [LL^{-1}]; the notations X and t denote the space and time variables, respectively; and Q_L = net lateral channel flow/unit width of the overland flow plane, given as

$$Q_L = [q_{RH} + q_{LH} + (q_L \times B)] \tag{3.33}$$

where q_{RH} = unit width discharge from the right hand side overland flow plane ; q_{LH} = unit width discharge from the left hand side overland flow plane ; B = width of the channel; and q_L = net rainfall rate same as used for the overland flow plane.

The discharge is given as

$$Q = A \frac{1}{n_c} R^{2/3} S_f^{1/2} \tag{3.34}$$

where, n_c is the Manning's roughness coefficient of the channel, and R is the hydraulic radius of the channel flow section.

The development of the VPMD routing method for flow routing in a rectangular channel can be obtained in a similar manner as given for the overland flow simulation described earlier by following the same assumptions (b-f) applied for overland flow modelling, but for the entire channel width of B. Further, a similar definition sketch by replacing the variables $i, q, y_u, y_d, y_M, q_3, q_M, \Delta x$, and l with inflow (I), Outflow (Q), stage at upstream, downstream and at mid-section $(Y_u, Y_d$ and $Y_M)$, normal discharge Q_3 corresponding to Y_M, discharge at the mid-section (Q_M) of the computational routing reach of ΔX and the location of section-3 at L_c distance in downstream of the mid-section of computational reach, respectively, is applicable for the channel flow routing as shown in Figure 3.2. The interested reader may also refer the work of *Perumal* [1994a, 1994b] for the detailed derivation of the VPMD method applicable for flow routing in rectangular channels. In this section only a brief development of the channel flow routing equation is presented.

The approximate convection-diffusion (ACD) equation applicable for the channel flow routing [*Perumal and Ranga Raju*, 1999] considering uniform lateral flow contribution can be expressed in a form similar to that of the overland flow as

$$\frac{\partial Q}{\partial t} + C \frac{\partial Q}{\partial X} = CQ_L \tag{3.35}$$

where C = wave celerity of the flood wave in rectangular channel $[LT^{-1}]$ expressed as

$$C = \frac{\partial Q}{\partial A} = \left[1 + \frac{2}{3} \left(\frac{P \partial R / \partial Y}{\partial A / \partial Y} \right) \right] V \tag{3.36}$$

where R = the hydraulic radius (A/P) of the channel section [L]; and P = the wetted perimeter of the channel section [L].

$$q_{LH} + q_{RH}$$
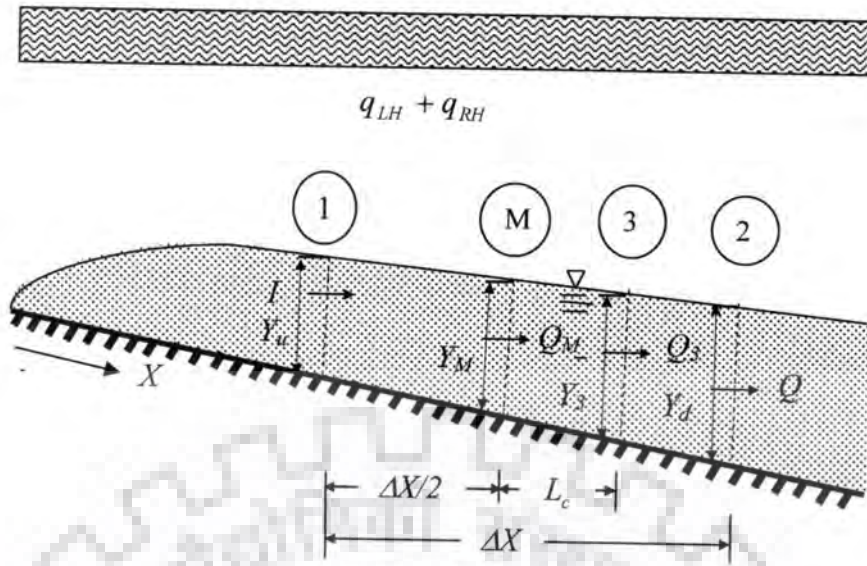
Figure 3.2 Schematic sketch of the Muskingum reach governing flow in a rectangular channel reach.

Employing the assumption of linearly varying discharge over the computational reach ΔX, the discharge Q_M passing at the mid-section of the computational reach is expressed in terms of discharge Q_3 which is uniquely related to the stage Y_M, expressed as [*Perumal, 1994a*]

$$Q_M = Q_3 - \frac{Q_3 \left[1 - \frac{4}{9} F_{rc_M}^2 \left(\frac{P\partial R/\partial Y}{\partial A/\partial Y}\right)_M^2\right]}{2S_0 \left.\frac{\partial A}{\partial Y}\right|_3 \left[1 + \frac{2}{3}\left(\frac{P\partial R/\partial Y}{\partial A/\partial Y}\right)_3\right] V_3} \left.\frac{\partial Q}{\partial X}\right|_3 = Q_3 - L_c \left.\frac{\partial Q}{\partial X}\right|_3 \tag{3.37}$$

Further, the VPMD channel routing method arrives at a similar form of the routing equation as that of the Muskingum method applied for the overland flow routing, given by equation (3.25), by replacing the parameters K by K_c and θ by θ_c. The parameters K_c and θ_c are expressed as

$$K_c = \frac{\Delta X}{\left[1 + \frac{2}{3}\left(\frac{P\partial R/\partial Y}{\partial A/\partial Y}\right)_3\right] V_3} \tag{3.38}$$

$$\theta_c = \frac{1}{2} - \frac{Q_3\left[1 - \frac{4}{9}F_{rc}^2\left(\frac{P\partial R/\partial Y}{\partial A/\partial Y}\right)^2\right]_M}{2S_0\frac{\partial A}{\partial Y}\bigg|_3\left[1 + \frac{2}{3}\left(\frac{P\partial R/\partial Y}{\partial A/\partial Y}\right)_3\right]V_3\Delta X} \qquad (3.39)$$

3.4 V-CATCHMENT RUNOFF COMPUTATION PROCEDURE USING THE VPMD METHOD

The V-catchment comprises of two overland flow planes on either sides of a central rectangular channel which contribute runoff into the rectangular channel, wherein the V-catchment river routing using the VPMD method is carried out. Such an assembling of the V-catchment resembles to a simplified model of catchment idealized by an open book geometry [Wooding, 1965a, 1965b, 1966]. Therefore, the runoff computation of the V-catchment involves the routing of the rainfall generated flow over the overland flow plane which in turn contributes to the channel as lateral flow, thus, generating runoff in the channel requiring channel routing of the V-catchment. This process of runoff generation at the outlet of the V-catchment is simulated by coupling the overland flow routing algorithm with the channel flow routing algorithm as described below.

3.4.1 Overland Flow Routing

The application of the VPMD method for overland flow computation requires the subdivision of the overland flow plane along the sloping direction into a number of unit width strips each of which is bounded on the upper end by the watershed ridge and at the lower end, the overland flow is contributed to the collector channel. Each of these strips is divided into a cascade of equal number of sub-reaches of length Δx suitable for the application of the VPMD method. The following step-by-step solution procedure is adopted for each routing time-step of the VPMD method while routing flow over each of the sub-reaches of Δx. As there is no flow of water at the upstream end of the computational sub-reach immediately adjacent to the ridge of the V-catchment, the overland flow routing process is implemented using two types of routing procedures:

3.4.1.1 Routing procedure for the first sub-reach when $t \geq \Delta t$ and for the rest of the sub-reaches when $t = \Delta t$

1) Temporally varying continuous rainfall input can be subdivided into number of pulses of equal duration Δt which corresponds to the temporal grid size used for

routing computations. In a similar manner, a uniform abstraction corresponding to each pulse is also specified, if abstraction is considered. Thus, the net lateral inflow rate over the considered strip is computed using equation (3.3).

2) Considering zero initial flow over the overland flow strip, estimate the reference discharge q_0 for the first routing interval Δt to estimate the VPMD parameters and, similarly, for all the succeeding time increments at the outlet of the first sub-reach using the expression:

$$q_0 = \frac{(q_L \Delta x) + q_1}{2}; \; q_1 = 0, \text{when } t = \Delta t \tag{3.40}$$

where, q_1 = the outflow runoff discharge from the computational reach at the previous time level; and t represents the cumulative simulation time in terms of Δt from the beginning, which is bounded by the total simulation time, T as an upper limit.

3) Estimate the value of travel time, K corresponding to the reference discharge, q_0 as

$$K = \Delta x / c_0 \tag{3.41}$$

where, c_0 = wave celerity computed corresponding to q_0 which is estimated using equation (3.7).

4) The routing coefficient C_p is estimated as

$$C_p = \frac{K - 0.5\Delta t}{K + 0.5\Delta t}; \tag{3.42}$$

5) Estimate the outflow runoff discharge q_2 at current time using the VPMD routing equation as

$$q_2 = C_p q_1 + (1 - C_p) q_L \Delta x \tag{3.43}$$

The runoff discharge estimated by equation (3.43) at the end of the first computational routing sub-reach becomes inflow to the subsequent routing sub-reach. The routing of this inflow for $t > \Delta t$ in the subsequent sub-reaches requires a different routing procedure which is described below:

3.4.1.2 Routing procedure for the second and subsequent sub-reaches when $t > \Delta t$

1) The same procedure as given in step 1(section 3.4.1.1) is used for the discritization of the continuous rainfall of varying intensity over-time into number of pulses of equal duration Δt.

2) Estimate the reference discharge q_0 by using the three point average method of *Ponce and Yevjevich* [1978] as

$$q_0 = \frac{i_2 + i_1 + q_1}{3} \tag{3.44}$$

3) Estimate the value of travel time K corresponding to the reference discharge q_0 using equation (3.41).

4) Estimate the weighting coefficient θ corresponding to the reference discharge, q_0 as

$$\theta = \frac{1}{2} - \frac{q_0\left(1 - \frac{4}{9}F_{rp_0}^2\right)}{2s_0(5/3)v_0\Delta x} \tag{3.45}$$

where s_0 = overland flow plane slope; v_0 = velocity corresponding to q_0; and F_{rp_0} = Froude's number corresponding to q_0.

5) The routing coefficients C_1, C_2, C_3 and C_4 can be computed using equations (3.26), (3.27), (3.28), and (3.29), respectively.

6) The unrefined estimate of outflow runoff discharge q_2 at the end of current routing time step is estimated using the recursive VPMD routing equation (3.25).

7) Estimate the normal runoff discharge at section 3 (Figure 3.1) using equation

$$q_3 = \theta i_2 + (1-\theta)q_2 \tag{3.46}$$

8) Using the value of q_3, compute the corresponding flow depth, y_M at the middle of the computational sub-reach, using the assumption (f) as

$$y_M = \left(\frac{q_3 n}{\sqrt{s_0}}\right)^{(3/5)} \tag{3.47}$$

9) Estimate q_M at the middle of the computational sub-reach as

$$q_M = 0.5(i_2 + q_2) \tag{3.48}$$

10) Estimate the flow velocity at the midsection of the computational sub-reach as

$$v_M = q_M / y_M \tag{3.49}$$

11) Estimate the Froude number at the midsection of the computational sub-reach as

$$F_{rp_M} = q_M / \sqrt{g(y_M)^3} \tag{3.50}$$

12) Estimate the flow depth y_3 at section 3 (Figure 3.1) using the assumption (d) as

$$y_3 = y_M + \frac{q_3 - q_M}{(5/3)v_M}$$ (3.51)

13) Estimate the flow velocity corresponding to y_3 as

$$v_3 = q_3 / y_3$$ (3.52)

14) Estimate the revised $K = \Delta x / ((5/3)v_3)$.

15) Estimate the revised value of θ for the considered computational sub-reach using equation (3.24).

16) Repeat steps 5 to 15 to estimate the refined outflow runoff discharge q_2 using equation (3.25).

17) Compute the outflow runoff depth y_d corresponding to q_2, given by equation (3.30) as

$$y_d = y_M + \frac{q_2 - q_M}{(5/3)v_M}$$ (3.53)

It is considered that the approximation involved in the computation of θ, using the approximate location 'l' of the weighted runoff discharge, would not affect the accuracy of the routing solution based on this procedure.

3.4.2 Channel Flow Routing

The application of the VPMD method for routing runoff in the channel which receives the zero inflow at the upper end but uniform runoff discharge contribution along the flow path from both the overland flow planes on either side requires the subdivision of channel into a number of equal sub-reaches of length ΔX. Similar to the flow computation adopted for overland flow plane, two separate flow routing procedures are adopted: first one for the upstream sub-reach of the channel when $t \geq \Delta t$ and for other sub-reaches when $t = \Delta t$, and the other for the rest of the channel sub-reaches when $t > \Delta t$.

3.4.2.1 Routing procedure for the first sub-reach when $t \geq \Delta t$ and for the rest of the sub-reaches when $t = \Delta t$

1) Considering zero initial flow, the reference discharge Q_0 at current time step is estimated as

$$Q_0 = \frac{(Q_L \Delta X) + Q_1}{2}; \quad Q_1 = 0, \text{ when } t = \Delta t$$ (3.54)

where t represents the cumulative simulation time in terms of Δt from the beginning, which is bounded by the total simulation time, T as an upper limit, and Q_L is the sum of the average overland flow discharge/unit width along the channel and the direct rainfall over the channel flow surface/unit width across the channel section.

2) Estimate the channel flood wave travel time, K_c corresponding to the reference discharge, Q_0 as

$$K_c = \Delta X / C_0 \qquad (3.55)$$

where C_0 = wave celerity corresponding to Q_0 which is estimated using the equation

$$C_0 = \left[1 + \frac{2}{3} \left(\frac{P \partial R / \partial Y}{\partial A / \partial Y} \right) \right] V_0 \qquad (3.56)$$

where V_0 = channel flow velocity corresponding to Q_0.

3) The routing coefficients C_c is estimated as

$$C_c = \frac{K_c - 0.5 \Delta t}{K_c + 0.5 \Delta t} \qquad (3.57)$$

4) Estimate of the outflow runoff discharge Q_2 at current time step using the recursive VPMD routing equation as

$$Q_2 = C_c Q_1 + (1 - C_c) Q_L \Delta X \qquad (3.58)$$

The runoff discharge estimated by equation (3.58) at the end of the computational routing sub-reach becomes inflow to the subsequent routing sub-reach.

3.4.2.2 Routing procedure for the second and subsequent sub-reaches when $t > \Delta t$

1) Estimate the reference discharge, Q_0 by using the three point average method [*Ponce and Yevjevich*, 1978]

$$Q_0 = \frac{I_2 + I_1 + Q_1}{3} \qquad (3.59)$$

2) Estimate the routing parameter K_c corresponding to the reference discharge, Q_0 using equations (3.55) and (3.56).

3) Estimate the weighting coefficient, θ_c corresponding to Q_0 as:

$$\theta_c = \frac{1}{2} - \frac{Q_0\left[1 - \frac{4}{9}(F_{rc})_0^2\left(\frac{P\partial R/\partial Y}{\partial A/\partial Y}\right)\right]_0}{2S_0V_0\Delta X\left(\frac{\partial A}{\partial Y}\right)_0\left[1 + \frac{2}{3}\left(\frac{P\partial R/\partial Y}{\partial A/\partial Y}\right)_0\right]}$$

(3.60)

where S_0 = channel bed slope; V_0 = flood wave velocity corresponding to Q_0; $(F_{rc})_0$ = Froude's number corresponding to Q_0; and A, P, and R are the flow area, perimeter, and hydraulic radius, respectively, computed corresponding to Q_0.

4) The coefficients C_{c1}, C_{c2}, C_{c3} and C_{c4} are estimated as

$$C_{c1} = \frac{-K_c\theta_c + 0.5\Delta t}{K_c(1-\theta_c) + 0.5\Delta t}$$

(3.61)

$$C_{c2} = \frac{K_c\theta_c + 0.5\Delta t}{K_c(1-\theta_c) + 0.5\Delta t}$$

(3.62)

$$C_{c3} = \frac{K_c(1-\theta_c) - 0.5\Delta t}{K_c(1-\theta_c) + 0.5\Delta t}$$

(3.63)

$$C_{c4} = \frac{\Delta t}{K_c(1-\theta_c) + 0.5\Delta t}$$

(3.64)

5) The unrefined estimate of outflow runoff discharge Q_2 at the end of the current time step is estimated using the recursive VPMD routing equation as

$$Q_2 = C_{c1}I_2 + C_{c2}I_1 + C_{c3}Q_1 + C_{c4}Q_L\Delta X$$

(3.65)

6) Estimate the normal runoff discharge at section 3 (Figure 3.2) using equation

$$Q_3 = \theta_c I_2 + (1-\theta_c)Q_2$$

(3.66)

7) Knowing Q_3, compute the corresponding flow depth, Y_M at the middle of the computational sub-reach using the Newton-Raphson method based on the relationship:

$$Q_3 = \frac{1}{n_c} A_M R_M^{2/3} S_0^{1/2}$$

(3.67)

8) Estimate Q_M at the middle of the routing sub-reach as

$$Q_M = 0.5(I_2 + Q_2)$$

(3.68)

9) Estimate the flow velocity at the midsection of the routing sub-reach as

$$V_M = Q_M/A_M$$

(3.69)

61

10) Estimate the Froude's number at the midsection of the routing sub-reach as

$$(F_{rc})_M = Q_M \left[(\partial A/\partial Y)_M / (g A_M^3) \right]^{(1/2)} \qquad (3.70)$$

11) Estimate the flow depth Y_3 at section 3 (Figure 3.2) as

$$Y_3 = Y_M + \cfrac{Q_3 - Q_M}{\left. \dfrac{\partial A}{\partial Y} \right|_M \left\{ 1 + \dfrac{2}{3} \left(\dfrac{P \partial R / \partial Y}{\partial A / \partial Y} \right)_M \right\} V_M} \qquad (3.71)$$

12) Estimate the flow area A_3 corresponding to Y_3.

13) Estimate the flow velocity corresponding to A_3.

14) Estimate the revised value of K_c as

$$K_c = \Delta X / C \qquad (3.72)$$

where the flood wave celerity C for a rectangular channel reach is estimated using the Manning's friction law as

$$C = \left[\frac{5}{3} - \frac{4}{3} \frac{Y_3}{(B + 2Y_3)} \right]_3 V_3 \qquad (3.73)$$

15) Estimate the revised value θ_c for the rectangular channel reach using the Manning's friction law as

$$\theta_c = \frac{1}{2} - \cfrac{Q_3 \left[1 - \dfrac{4}{9} (F_{rc})_M^2 \left(1 - 2 \dfrac{Y_M}{(B + 2Y_M)} \right)^2 \right]}{2 S_0 B \left[\dfrac{5}{3} - \dfrac{4}{3} \dfrac{Y_3}{(B + 2Y_3)} \right] V_3 \Delta X} \qquad (3.74)$$

16) Repeat steps 4 to 15 to estimate the refined value of outflow discharge, Q_2 at the end of the current time step using equation (3.65).

17) Compute the outflow stage Y_d corresponding to Q_2 at current time step as

$$Y_d = Y_M + \cfrac{Q_2 - Q_M}{\left. \dfrac{\partial A}{\partial Y} \right|_M \left\{ 1 + \dfrac{2}{3} \dfrac{Y_M}{(B + 2Y_M)} \right\} V_M} \qquad (3.75)$$

Following the procedure as presented in this section 3.4, a FORTRAN code is developed for the estimation of the runoff and flow depth at the outlet of the V-catchment, which is given in Appendix –I.

3.5 PERFORMANCE EVALUATION CRITERIA

Any hydrological model has mainly three kinds of error sources in the model estimations related to the input error, the parameter error and the model error. The physically based models are more susceptible to the parameter error due to the availability of limited data set such as the estimates of semi-empirical parameters representing the areal distribution. The model errors are inbuilt error and can vary according to the approximation involved and assumptions used in the model development, and the numerical accuracy and stability of the solution technique. All the three types of the errors constitute total model error. Therefore, the performance evaluation of the model is a necessary step in the modelling process. According to *Willmott et al.* [1985], the model performance evaluation consists of operational and scientific evaluation. The operational evaluation is an assessment of the model accuracy and precision. Accuracy of the model is the ability of the model to predict the values in close accordance with the corresponding set of the observed values. Precision is the measure of the degree to which model estimated values match precisely the linear function of the observed values. The scientific model evaluation consists of the assessment of consistency between the model estimated results and the prevailing scientific theory [*Willmott et al.*, 1985].

In this regard, *Loague and Green* [1991], *Loague* [1992] *and the ASCE Task Committee* [1993] presented various statistical model performance evaluation criteria on the consideration that assessment of single criterion is not adequate to judge the overall fit between the computed and observed/benchmark solution in view of multi-objectiveness involved in the hydrological modelling. The prerequisite to use these criteria is the setting of accuracy and precision level for the model depending upon the flow process to be modeled. The model performance evaluation criteria to be adopted mainly depend on the purpose for which the model is being used. In case of the overland flow modelling, the conservation of mass is an important factor which is required to be fulfilled by the model in question. The various other criteria adopted in the present study are given below.

3.5.1 Model Efficiency

The goodness of fit for the runoff hydrograph can be described by the coefficient of efficiency, generally known as the Nash-Sutcliffe criterion [*Nash and Sutcliffe*, 1970], recommended by the *ASCE Task Committee* [1993]. The Nash-Sutcliffe efficiency, η_q for discharge hydrograph simulation is given as

$$\eta_q = \left[1 - \frac{\sum\limits_{i=1}^{N}(q_{oi} - q_{ci})^2}{\sum\limits_{i=1}^{N}(q_{oi} - \bar{q}_{oi})^2} \right] \times 100 \tag{3.76}$$

where q_{oi} = ith ordinate of the observed/benchmark model outflow runoff hydrograph at the downstream end; q_{ci} = ith ordinate of the computed outflow runoff hydrograph at the downstream end; $\bar{q}_{oi}$ = mean of the observed/benchmark model outflow runoff hydrograph ordinates at the downstream end; and N = total number of outflow runoff hydrograph ordinates to be simulated. The maximum value of η_q is 100 % which indicates the exact reproduction of the benchmark hydrograph. An efficiency $\eta_q > 90.0\%$ indicates a very satisfactory performance, while a value between $80.0\% < \eta_q < 90.0$, indicates fairly good performance and $\eta_q < 80.0\%$ indicates unsatisfactory performance [*Shamseldin*, 1997].

3.5.2 Coefficient of Determination

The coefficient of determination (CD) measures the proportion of total variance of the observed data explained by the model simulated data. The CD is given as

$$CD = \sum_{i=1}^{N}(q_{oi} - \bar{q}_{oi})^2 \Big/ \sum_{i=1}^{N}(q_{ci} - \bar{q}_{oi})^2 \tag{3.77}$$

3.5.3 Coefficient of Residual Mass

$$CRM = \left(\sum_{i=1}^{N} q_{oi} - \sum_{i=1}^{N} q_{ci} \right) \Big/ \sum_{i=1}^{N} q_{oi} \times 100 \tag{3.78}$$

3.5.4 Conservation of Mass

The relative error in the computed flow volume by the VPMD method considering the total effective rainfall as input is given by

$$EVOL = (V_c - V_{Er})/V_{Er} \times 100 \tag{3.79}$$

where V_C = total volume calculated at the outlet of the overland flow plane/channel in the V-catchment; and V_{Er} = total volume of effective rainfall falling over the overland flow plane/V-catchment for the duration equal to the duration of the effective rainfall. The negative value of $EVOL$ indicates a loss of the mass whereas the positive $EVOL$ value indicates gain of mass. The $EVOL = 0$ indicates the 100% mass conservation by the model.

3.5.5 Peak Runoff Reproduction

The percentage error in peak runoff estimated by the VPMD method is given as

$$q_{perr} = \left(\frac{q_{pc}}{q_{po}} - 1 \right) \times 100$$

(3.80)

where q_{pc} = computed peak runoff discharge; and q_{po} = observed/benchmark model peak runoff discharge. A negative error indicates under-estimation and a positive error indicates over-estimation of the peak of the benchmark solution.

3.5.6 Time to Peak Runoff Production

The error in time to peak runoff (in minute) can be expressed as

$$t_{perr} = t_{pc} - t_{po}$$

(3.81)

where t_{perr} = error in time to peak runoff (min); t_{pc} = computed time to peak runoff (min); and t_{po} = observed/benchmark time to peak runoff (min). A negative and a positive error indicates early and late arrival of the peak, respectively, with reference to the peak of the benchmark solution.

Equations (3.76), (3.77), (3.78), and (3.80) are applicable to the V-catchment runoff simulation study by using the computed and corresponding observed/benchmark model runoff discharges at the outlet of the channel. The best performing hydrological model should have η_q, CD, and CRM values close to 100%, 1.0 and 0.0%, respectively.

3.6 APPLICATION

The VPMD overland flow model, presented in section-3.2, is applied to simulate runoff from overland flow planes with each of the plane characterized by a given set of slope of the plane, s_0 and the Manning's roughness coefficient, n or the Chezy's roughness coefficient, C_h. The evaluation of the proposed method is extensively carried out based on the assessment of comparison of the simulated runoff hydrographs with the corresponding benchmark overland flow hydrographs simulated for a unit width of the considered plane. Different benchmark solutions were obtained depending on the nature of the input such as semi-infinite uniform intensity rainfall, uniform intensity rainfall of duration $t_r < t_e$, $t_r = t_e$ and $t_r > t_e$, where t_e is the time to equilibrium or time of concentration of the considered

overland flow strip for a given uniform intensity of rainfall. The benchmark overland flow hydrographs consist of hydrographs simulated for hypothetical rainfall inputs on hypothetical overland flow planes or strips, and the observed hydrographs simulated either in laboratory or field experimental overland flow study facilities for specified rainfall input patterns. The hypothetical solutions were obtained using different approaches: 1) Analytical solutions of the KW equation [*Overton and Brakenseik*, 1973; *Overton and Meadows*, 1976; *Woolhiser*, 1974], 2) Approximate analytical solutions of the diffusive wave equation [*Govindaraju et al.*, 1990], 3) Solution of the full SVE using the explicit finite difference method, 4) Runoff hydrographs simulated using the time integration method for the solution of the KW and DW equations [*Kazezyılmaz-Alhan et al.*, 2005; *Gottardi and Venuteli*, 2008], and 5) Solutions of the DW model proposed by *Lai* [2009]. While arriving at the full SVE solutions using the explicit numerical method, the stability of the numerical solution was ensured by satisfying the Courant condition, i.e., $\Delta t < \Delta x / (v + c_d)$, where c_d is the wave celerity of the dynamic wave [*Chow et al.*, 1988]. The performance of the VPMD method was also investigated by comparing its solutions with the observed hydrographs recorded corresponding to eight laboratory experimental storm events of complex rainfall input pattern conducted by *Izzard* [1942, 1944]. The data of these events have been reported by *Maksimović and Radojković* [1986] and they are produced at the end of this thesis (Appendix- IV). Also the data of ten natural rainfall-runoff events recorded in the outdoor experimental laboratory facility developed by *Wong* [2009] at the Nanyang Technological University, Singapore were used for studying the proposed VPMD overland flow model. This facility consists of asphalt and concrete overland flow planes, and a concrete level V-catchment.

3.6.1 The Rising Runoff Hydrograph Simulations

3.6.1.1 Results

The performance of the VPMD method for simulating the rising part of the overland flow hydrograph is evaluated using the standard experimental data of *Morgali and Linsely* [1965], quite often used by researchers [for example, *Govindaraju et al.*, 1990; *Gottardi and Venutelli*, 2008] of the overland flow studies. The Soil Conservation Services (SCS) (now, the NRCS) experimental plot used in this study consists of 21.945 m (72 ft) plane with 3.81 cm (1.5 in) thick soil turf overlying an impervious surface. The slope of this experimental plane was $s_0 = 0.04$. Two different semi-infinite spatially uniform intensity of rainfall of

$r = 9.30$ cm/h (3.66 in/h) and $r = 4.8$ cm/h (1.89 in/h) were applied in simulating the rising overland flow hydrographs. The Manning's roughness coefficients estimated by *Morgali and Linsely* [1965] for the two rainfall intensities of $r = 9.30$ cm/h and $r = 4.8$ cm/h were $n = 0.5$ and 0.4 m$^{-1/3}$ /s, respectively. The same values of the Manning's n were used by *Gottardi and Venutelli* [2008] while evaluating these events of *Morgali and Linsely* [1965] using their DW model. While studying these events using the approximate DW model based on Chezy's roughness coefficient, *Govindaraju et al.,* [1990] worked out the Chezy's roughness coefficient $C_h = 0.994$ m$^{1/2}$/s (1.8 ft$^{1/2}$/s) and 1.336 m$^{1/2}$/s (2.42 ft$^{1/2}$/s) for the rainfall intensities of 9.30 and 4.8 cm/h, respectively.

Figure 3.3a shows the observed experimental runoff hydrograph of the *Morgali and Linsley* [1965] for the rainfall intensity of 9.30 cm/h along with the corresponding solution of the VPMD method obtained based on the solution procedure described in section 3.4.1 for overland flow estimation using the Chezy's friction law. Also the corresponding solutions of the analytical KW solution [*Overton and Brakenseik,* 1973; *Overton and Meadows,* 1976; *Woolhiser,* 1974], explicit numerical solution of the SVE, and the approximate analytical solution of DW, which is also known as the one-term solution of the DW [*Govindaraju et al.* 1990] based on the Chezy's friction law ($C_h = 0.994$) are also presented. Similarly, Figure 3.3b shows the comparison of the same observed runoff hydrograph shown in Figure 3.3a, with the solutions of all the methods employed in Figure 3.3a, but based on the Manning's roughness coefficient, except the one-term approximate solution of the DW [*Govindaraju et al.* 1990] which can be obtained only for the Chezy's friction law. In addition to these methods, Figure 3.3b also shows the DW solution results of the *Gottardi and Venutelli* [2008] based on the accurate time integration method. The simulated runoff hydrograph at the outlet of the unit width strip of the overland flow plane is obtained using the VPMD and the numerical SVE method by dividing the unit width strip into 55 and 30 sub-reaches, respectively. The corresponding time intervals used were $\Delta t = 3$s and 0.125s, respectively. In order to ensure the successful simulations of the overland flow using the VPMD method, a small time and space grid sizes have been used for this example. However, it is to be noted that the use of larger Δx and Δt values for the VPMD simulations are possible and further details on this aspect would be presented while discussing the sensitivity analysis of the VPMD method solutions for different temporal and spatial grid sizes.
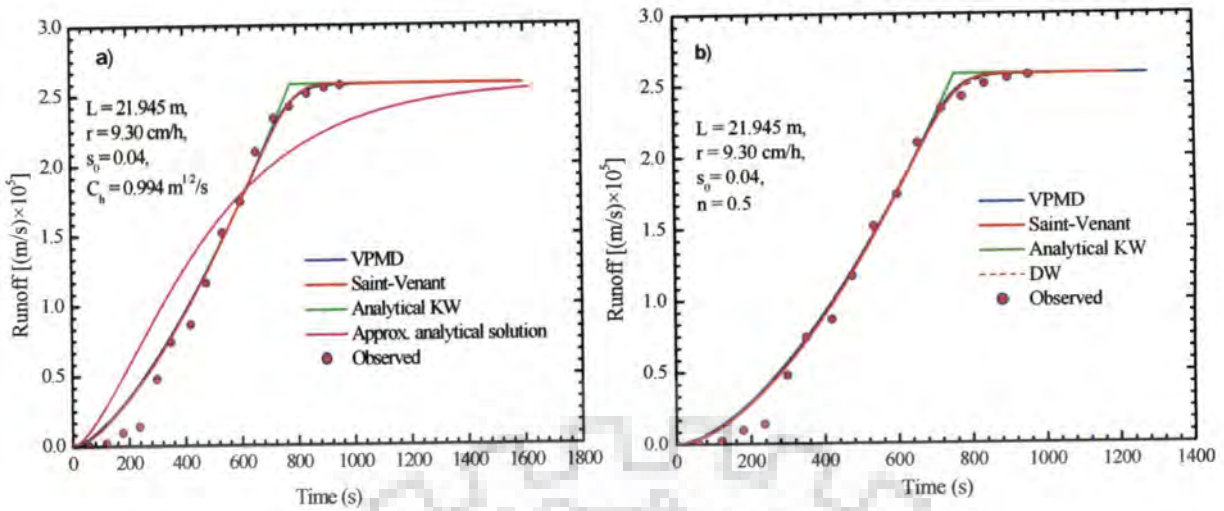
Figure 3.3 Comparison of the VPMD method simulated runoff hydrographs with a) observed runoff values from *Morgali and Linsely* [1965], approximate analytical solution [*Govindaraju et al.*, 1990], classical analytical solution of the KW and the explicit method numerical solution of the SVE using the Chezy's friction law, and b) observed hydrograph of *Morgali and Linsely* [1965], the DW solution of *Gottardi and Venutelli* [2008], the classical analytical solution of the KW and the explicit method numerical solution of the SVE using the Manning's friction law.

3.6.1.2 Discussion

It has been brought out by *Perumal and Ranga Raju* [1999] that the approximate Convection-Diffusion (ACD) equations in stage and discharge formulations are capable of modelling the flood waves in the transition range of the applicability domains governed by the diffusive wave and the kinematic wave, including the latter. As the VPMD routing method has been developed from the ACD equation in discharge formulation, one of the ways of demonstrating its capability for overland flow modelling is to apply the same first in the kinematic wave range and then, subsequently, demonstrate its capability for its application in the diffusive wave range. Accordingly, the rainfall-runoff simulations presented in Figures 3.3a and 3.3b were meant for demonstrating the suitability of the VPMD method for overland flow modelling in the kinematic wave range. In this context, the kinematic wave number (k) given by *Woolhiser and Liggett* [1967] and the parameter $k(F_{rp})_e^2$ are used to assess the flow regime. Accordingly, the recommended values

of k, $k(F_{rp})_e^2$ are > 20 and > 5, respectively, when the overland flow process is governed by the kinematic wave equation. The kinematic wave number can be expressed as

$$k = \frac{s_0 L}{y_e (F_{rp})_e^2}$$

(2.33)

where, y_e is the computed flow depth at the outlet of the plane corresponding to equilibrium discharge condition and $(F_{rp})_e$ is the corresponding Froude number. Based on equation (2.33), k and $k(F_{rp})_e^2$ can be expressed using the Manning's friction law as [*Morris and Woolhiser*, 1980; *Stephenson and Meadows*, 1986; *Wong*, 1992, 2005]:

$$k = 1.725 \times 10^6 \frac{n^{1.2} s_0^{0.4} L^{0.2}}{r_e^{0.8}}$$

(2.34a)

$$k(F_{rp})_e^2 = 8585.81 \times \frac{s_0^{1.3} L^{0.4}}{n^{0.6} r_e^{0.6}}$$

(2.34b)

Similarly, the corresponding expressions based on the Chezy's friction law can be expressed as

$$k = 2.247 \times 10^5 \frac{C_h^{-1.335} s_0^{0.335} L^{0.335}}{r_e^{0.665}}$$

(3.82a)

$$k(F_{rp})_e^2 = 22905.5 \times \frac{C_h^{0.665} s_0^{1.335} L^{0.335}}{r_e^{0.665}}$$

(3.82b)

where r_e is the rainfall intensity at equilibrium (mm/h) and plane length L in metre.

In the present example, the estimated k, $k(F_p)_e^2$ and $(F_{rp})_e$ values based on equation (3.82) were 10646.34, 42.89 and 0.063 corresponding to the observed results shown in Figure 3.3a. Similarly these values were estimated as 10232.75, 44.93 and 0.066 corresponding to the observed runoff results shown in Figure 3.3b. The corresponding estimates based on the VPMD method solutions were 10953.31, 43.43 and 0.063, and 10332.64, 44.76, and 0.066, pertaining to the results shown in Figure 3.3a and 3.3b, respectively. Therefore, it can be inferred from these estimates of the applicability limits that the flow regimes are well within the KW applicability limit as established both based on the relationships given by equations (2.34) and (3.82), and the VPMD simulations. The respective estimates also closely agree with each other. The estimates of the time of

equilibrium or concentration (t_e) in seconds arrived at by using the analytical KW approach with use of the Manning's and Chezy's roughness coefficients, respectively are expressed as [*Overton and Meadows*, 1976]

$$t_e = (1/(r_e)^{0.4})(nL/\sqrt{s_0})^{0.6} \tag{3.83a}$$

$$t_e = (1/(r_e)^{0.4})(L/C_h\sqrt{s_0})^{0.6} \tag{3.83b}$$

where r_e = equilibrium rainfall rate (m/s). The estimates of time of equilibrium or concentration (t_e) were 12.98 min and 12.60 min when applied using the Chezy's and the Manning's friction law, respectively. Further, the performance of the VPMD method is evaluated statistically using various performance assessment measures given in section 3.5. The various measures such as the Nash Sutcliffe efficiency (η_a), CRM (%), CD and the percentage error in simulating the peak of the runoff hydrograph (q_{perr}) estimated in comparison with the observed data and the simulated runoff hydrographs obtained using the analytical KW solution, the numerical solution of the SVE based on the explicit method and the DW solution (only for Figure 3.3b), all shown in Figures 3.3a and 3.3b, are presented in Table 3.1. It can be inferred from these results that the VPMD method is able to closely simulate the behavior of the overland flow as given by the observed hydrographs. It can be inferred from the estimated CRM values of -6.17 and -5.60 %, corresponding to Figures 3.3a and 3.3b, respectively, the presence of some error in mass conservation as compared to that of the observed hydrographs which may be attributed to the non-consideration of initial interception loss caused by the ground and detention storage due to the presence of grass on the plane which resulted in the discrepancy of the computed flow in the initial few minutes of simulation. Otherwise, as compared with the other models, especially the numerical SVE solution, the VPMD method is able to conserve the mass accurately. Further, the value of CD close to 1 suggests a very close agreement of the VPMD method with that of the DW and SVE solutions. The values of q_{perr} nearly zero in all the cases indicate that the VPMD method is able to accurately reproduce the peak of the runoff hydrograph. It can also be inferred from the Nash-Sutcliffe efficiency criterion values that the simulated hydrographs by the VPMD method are in very close agreement with the solutions of SVE, DW and the analytical KW, except with one-term solution of *Govindaraju et al.* [1990]. Therefore, it can

Table 3.1 Evaluation of the rising hydrographs simulated by the VPMD method with those of other methods

Simulations Shown in Figure	Benchmark Solution	Performance Evaluation Measures				CPU-time (s) for VPMD	CPU-time (s) for SVE	Applicability Criteria			
		η_q (%)	CRM (%)	CD	q_{perr} (%)			Method	k	kF_{rp}^2	F_{rp}
3a	Observed	98.52	-6.17	1.11	0.48	0.11		Analytical KW			
	Analytical KW	99.95	-0.11	1.02	0.00	0.14			10646.30	42.89	0.06
	Explicit SVE	99.98	-0.40	1.01	0.00	0.16	3.828	VPMD	10953.31	43.43	0.06
3b	Observed	99.05	-5.60	1.05	0.48	0.11		Analytical KW			
	Analytical KW	99.96	-0.32	1.02	0.00	0.13			10232.80	44.93	0.07
	Explicit SVE	99.95	-0.55	1.01	0.00	0.16	3.531	VPMD	10332.64	44.76	0.07
	DW	99.97	-0.30	0.98	0.00	0.11					
4a	Observed	84.69	-26.89	0.89	0.25	0.11		Analytical KW			
	Analytical KW	99.98	-0.22	1.01	-0.01	0.13			11134.30	81.04	0.08
	Explicit SVE	99.97	-0.41	1.01	-0.17	0.14	5.641	VPMD	11413.66	82.40	0.08
4b	Observed	98.06	-7.91	1.10	0.63	0.11		Analytical KW			
	Analytical KW	99.98	-0.18	1.01	-0.01	0.13			16523.60	66.57	0.06
	Explicit SVE	99.98	-0.47	1.01	-0.12	0.14	4.563	VPMD	16956.28	67.61	0.06
4c	Observed	94.64	-16.28	0.94	0.25	0.11		Analytical KW			
	Analytical KW	99.97	-0.40	1.01	0.00	0.13			13284.90	76.39	0.08
	Explicit SVE	99.95	-0.60	1.01	-0.09	0.16	5.875	VPMD			
	DW	93.66	-14.1	0.88	0.03	0.13			13369.95	76.20	0.08
4d	Observed	98.99	-2.16	1.09	0.25	0.11		Analytical KW			
	Analytical KW	99.95	-1.00	1.01	0.00	0.13			17364.10	66.81	0.06
	Explicit SVE	99.96	-0.67	1.01	-0.05	0.11	4.922	VPMD			
	DW	99.94	-1.43	0.98	0.02	0.11			17487.11	66.63	0.06

be inferred that the considered rainfall-runoff event is indeed kinematic in nature. Further, the comparison of the VPMD method simulated hydrograph with the observed data elucidates that the use of the Manning's friction law for the overland flow simulation results in a better performance by the VPMD method as compared to that based on the use of the Chezy's friction law. This is corroborated by the study of *Overton* [1972] wherein it was concluded after studying the rising portion of 214 runoff hydrographs generated on the uniform concrete or simulated turf surfaces that the kinematic wave models produce solution with 15% and 19% standard error, when the Manning's and Chezy's laws were used for the computations, respectively, in fitting the observed runoff hydrographs.

Since the modeller often resorts to the simplest and the faster computation scheme, one of the most pertinent criteria in hydrological model application to large catchment is the CPU time required for the execution of the computer program. In the present example, although a very fine grid size was chosen for the runoff simulation by the VPMD method, the required computation times were less than 0.11 s for the simulation of for both the observed runoff hydrographs as shown in the Figure 3.3a and 3.3b, whereas the computation times required for the same events by the numerical SVE solution were 3.828 s and 3.531 s, respectively, as can be seen from the Table 3.1(for Figure 3.3a and 3.3b). It may be noted that the CPU times presented in Table 3.1 for the simulations of the VPMD method in reproducing different benchmark solutions include also the computation times used in estimating the evaluation measures for assessing the reproduction of the benchmark solutions. This clearly suggests that despite of the same modelling accuracy, the proposed method has an advantage of faster solution, which is a pertinent consideration for its application to large catchment modelling [*Camporese et al.*, 2010].

Figure 3.4 shows the simulated hydrographs by the VPMD method in comparison with the other solutions and observed hydrographs, presented in the same form as in Figure 3.3, but for the rainfall intensity of 4.8 cm/h. It may be inferred from this figure that the Chezy's roughness coefficient $C_h = 1.336$ as recommended by *Govindaraju et al.* [1990] and the Manning's roughness coefficient $n = 0.4$ as recommended by *Morgali and Linsely* [1965] for this case are not appropriate. This inference can be verified from the poor estimates of performance evaluation measures arrived at for the cases corresponding to Figures 3.4a and 3.4c as described in Table 3.1, wherein the values of η_q, CRM, CD and q_{perr} have been estimated by comparing the solution of the VPMD method with the corresponding observed hydrographs, the analytical KW solution, the numerical solutions of the SVE and the DW
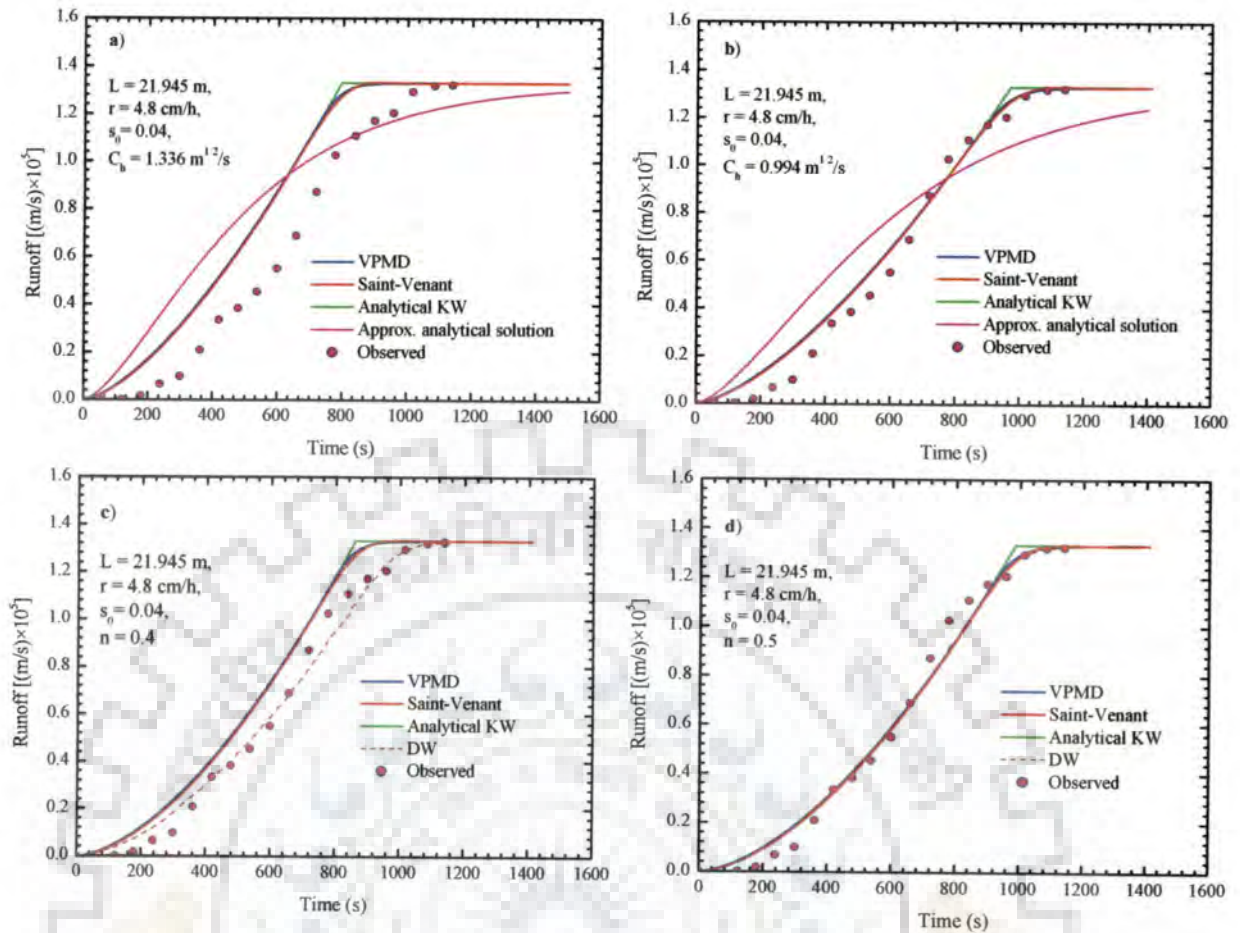
Figure 3.4 Comparison of the VPMD method simulated runoff hydrographs with the observed hydrograph of *Morgali and Linsely* [1965], and with the solutions of other methods as used in Figure 3.3 with a) $C_h = 1.336$ b) $C_h = 0.994$ c) $n = 0.4$ and d) $n = 0.5$.

solution. This inference is corroborated very clearly from, Figures 3.4a and 3.4c which reveal that with the use of the recommended $C_h = 1.336$ and $n = 0.4$, respectively, the simulated runoff hydrographs by the VPMD method, the SVE solution, the analytical solution of the KW and the one-term solution of the DW all deviate by a greater degree from the observed runoff hydrograph and from the simulated results of *Gottardi and Venutelli* [2008] for the DW method. It is surmised that this deviation may be attributed to the inappropriate values of the friction coefficients used for the simulation of these events. This inference enables one to be cautious that from the reliable catchment modelling point of view, not only an appropriate hydrological model is important to accurately model the rainfall-runoff process, but also the use of appropriate model parameters is equally important.

However, with the use of Chezy's and Manning's frictrion coefficients as used for the event of 9.30 cm/h rainfall intensity as shown in Figure 3.3, the accurate reproductions of the observed hydrograph corresponding to the event with rainfall intensity of 4.8 cm/h could

be achieved. The simulated hydrographs of the VPMD method in comparison with the observed hydrographs and the other solution methods are shown in Figures 3.4b ($C_h = 0.994$) and 4d ($n = 0.5$) for the Chezy's and Manning's coefficient, respectively. The runoff hydrographs simulated by the VPMD method, SVE solution, analytical solution and the one-term solution of the DW are all able to closely match the observed hydrograph. Furthermore, the performance measures η_q, CRM, CD and q_{perr} estimated using the VPMD method solution in comparison with the observed hydrograph and the simulated runoff hydrographs using the analytical solution of the KW, the SVE solution and the DW solutions (only for the case d), all shown in Figure 3.4b and 3.4d, are presented in Table 3.1. It can be concluded from this analysis that the use of the correct friction coefficient would be resulting in improved overland flow simulation process. Further, similar conclusions as arrived at for the events simulated corresponding to Figure 3.3 can be applicable for this case also. Consequently, the estimated values of time of equilibrium, t_e were 13.28 min for $C_h = 1.336$, 16.18 min for $C_h = 0.994$, 14.36 min for $n = 0.4$, and 16.42 min for $n = 0.5$. It is inferred from these results that the friction coefficient has also impact on the time of concentration of the catchment. The CPU times required for the solutions using the VPMD and SVE methods for the simulation of the event as depicted in the Figures 3.4a-3.4d are shown in Table 3.1. These results, as in the earlier study, demonstrate the efficiency of the VPMD method over that of the numerical SVE solution. Furthermore, the estimated k, $k(F_{rp})_e^2$ and $(F_{rp})_e$ values estimated using the analytical KW approach and by the VPMD method for all the four cases shown in Figure 3.4 are presented in Table 3.1. It is surmised from this analysis that the flow is well within the KW applicability regime and k, $k(F_p)_e^2$ and $(F_p)_e$ estimated using the VPMD method are in close agreement with the respective estimates of the analytical solutions of the kinematic wave. Furthermore, a careful examination of these applicability criteria values estimated for 9.30 cm/h and 4.8 cm/h intensities indicate that with the decrease in rainfall intensity there is an over all increase in the estimates of k, $k(F_{rp})_e^2$ and $(F_{rp})_e$, suggesting close adherence of the mean flow conditions to the kinematic wave theory, provided all the other conditions remain same.

3.6.2 Overland Flow Hydrographs for Pulse Rainfall Input

While the capability of the VPMD method to simulate the rising part of the hydrographs has been demonstrated in the earlier section, its capability to simulate the recession limb of the hydrographs also needs to be demonstrated. This aspect is studied herein by simulating the entire overland flow hydrographs for a pulse input. The simulated overland flow

hydrographs by the VPMD method are compared with the numerical SVE solutions, the classical analytical solutions of the KW and the solutions of the time integration method of the DW equation [*Gottardi and Venutelli*, 2008] for assessing the ability of the method to reproduce the rising as well as the falling limbs of the overland flow hydrographs. The example presented by *Gottardi and Venutelli* [2008] for a pulse input with a rainfall duration $t_r > t_e$, the time of equilibrium of the overland flow strip, is used here for the comparison purpose. Using the same rainfall intensity two different cases were also studied, with $t_r < t_e$ and $t_r = t_e$, to demonstrate the capability of the VPMD method to simulate the partial equilibrium hydrographs. *Gottardi and Venutelli* [2008] used the spatially uniform and steady rainfall of intensity $r = 6$ cm/h (2.3622 in/h) falling over the unit width strip of the sloping plane having a length $L = 200$ m. The plane is characterised by a slope $s_0 = 0.001$ and a Manning's roughness coefficient $n = 0.03$. The three different cases studied herein are designated as (1) Case I ($t_r < t_e$), (2) Case II ($t_r = t_e$), and (3) Case III ($t_r > t_e$) which is the study of *Gottardi and Venutelli* [2008]. The rainfall durations (t_r) considered are 25 minute, 31.6 minute and 1 h for cases I, II and III, respectively. The computed time of equilibrium for this watershed by analytical kinematic wave approach is $t_e = 31.6$ min, which forms the basis to select these three cases under consideration.

The steady state flow depths y_e at the end of overland flow plane computed with the VPMD method and the SVE solutions are 0.0326 m and 0.032 m, respectively. Note that the t_e and y_e values reported herein are the same as estimated by *Gottardi and Venutelli* [2008]. The analytically estimated k, $k(F_{rp})_e^2$ and $(F_{rp})_e$ corresponding to the equilibrium flow condition are 176.61, 6.32 and 0.19, respectively. Though these estimates very well satisfy the kinematic wave applicability limit, the magnitude of $k(F_{rp})_e^2$ very close to 5 suggests that the generated overland flow is nearly kinematic in nature. Using the VPMD method, the estimated k, kF_{rp}^2 and F_{rp} for the case III ($t_r > t_e$) are 187.15, 6.13 and 0.18, while the corresponding value of k estimated by *Gottardi and Venutelli* [2008] was $k = 188$. As compared to the applicability criteria measures estimated for the analytical kinematic wave solution for case III, the corresponding VPMD method computed k is slightly higher, while the corresponding estimates of kF_{rp}^2 and F_{rp} are comparatively lower as expected due to the accounting of diffusion present in the system by the VPMD method. Similarly, using the flow depth estimated by the VPMD method at the end of the plane enables one to compute the k using equation (2.33), kF_{rp}^2 and F_{rp} corresponding to the other

cases of t_r i.e., for case I and II, as 239.13, 7.87 and 0.18 and 198.51, 6.63, 0.18, respectively. It can be inferred from these results that the rainfall duration also influences the applicability criteria, as the case of $t_r < t_e$ results in increased estimates of k, $kF_{rp_e}^2$ and F_{rp}.

The simulated runoff hydrographs for all these three cases are shown in Figure 3.5. It is seen from Figure 3.5b that the VPMD method is able to very closely reproduce the rising as well as the recession limbs of the runoff hydrographs simulated using the numerical solution of the SVE and the DW solution by *Gottardi and Venutelli* [2008] (for case III). It can also be inferred from Figure 3.5b that the simulated runoff hydrograph of the VPMD and DW of the considered rainfall event is not fully kinematic in nature as the simulations deviate from the classical analytical solution of KW at the upper end, thus, demonstrating the presence of diffusion in the runoff generation. Analysis of the results of case I ($t_r < t_e$) demonstrate that the VPMD method solution begin to recede immediately after the rainfall ceases, which is a realistic simulation of the considered event. However, the analytical KW solution fails to capture the instantaneous start of the recession phase due to its inherent assumption that the flow is kinematic at any location. The recession limbs of the runoff hydrographs simulated by the proposed method for all the three cases are in well agreement with the SVE solution exhibiting the comparatively slower recession rate, especially at the lower portion of hydrographs, in comparison with the analytical KW solution which recedes faster in the absence of diffusion. This inference can also be made based on the performance measures computed for all these three cases using finer and coarser grid sizes as presented in Table 3.2. Although, the grid sizes considered herein do not strictly follow the Courant condition, there is almost no significant impact on the accuracy of the VPMD method. The performance evaluation measures such as η_q, CRM, CD, q_{perr} and t_{perr} computed in comparison with the SVE solution and the analytical KW solutions are able to demonstrate the adequacy of the VPMD method for the overland flow modelling to simulate the runoff hydrographs accurately and efficiently, which closely simulate the SVE solutions rather than the analytical KW solution. However, it should be noted herein especially, for case I in which the rainfall ceases well before the equilibrium time that the use of $\Delta t = 12$ s might have led to slightly higher errors in the computed volumes by the VPMD method as compared to those of cases II and III. This may probably be attributed to the inability of the method to capture accurately the transient changes tacking place in the physical system. Therefore, it may be inferred that the restrictions on the selection of Δx and Δt also needed depending on the duration of the rainfall event considered for the study and existing flow
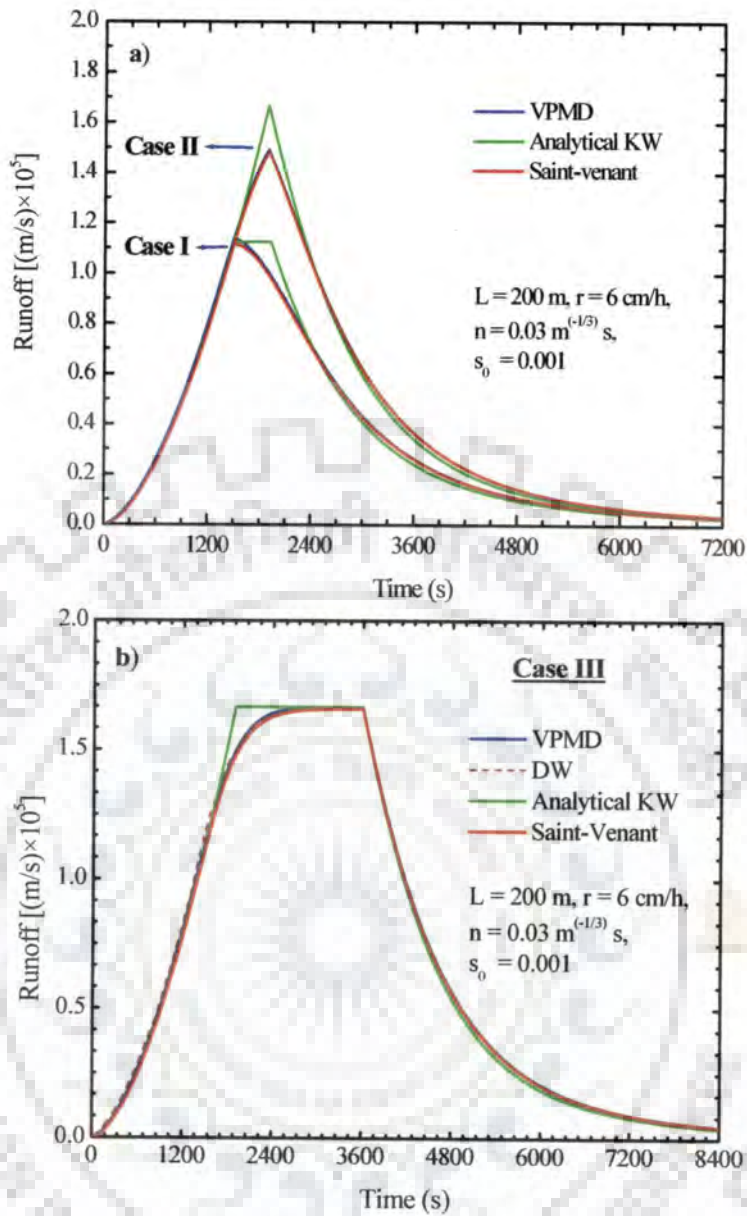
Figure 3.5 Comparison of the simulated runoff hydrographs of the VPMD method with the analytical solutions of the KW model, numerical solutions of the SVE and the DW solution of *Gottardi and Venutelli* [2008] considering three cases: (I) $t_r < t_e$ (II) $t_r = t_e$ and (III) $t_r > t_e$.

conditions. The CPU-time required for the execution of the VPMD solution is much less than that required for the SVE solution, which, however, also depends on the selection of Δx and Δt. Overall, it can be concluded from these example cases that the proposed method is able to accurately reproduce the runoff hydrographs of the SVE solution and the DW solution rather than the analytical solution of the KW and, thus, demonstrating the capability of the VPMD method, to describe the overland flow process in the transition

Table 3. 2 Performance evaluation of the VPMD method for runoff hydrograph simulations considering three durations of pulse rainfall inputs: $t_r < t_e$ (Case I), $t_r = t_e$ (Case II) and $t_r > t_e$ (Case III)

Case	Δx (m)	Δt (s)	$\dfrac{\Delta x}{\Delta t}$	c_{max}	Performance Evaluation Measures in Simulating the Benchmark Solutions by the VPMD Method									Error in Volume and Run-time			
					Benchmark Solutions									VPMD		Saint-Venant	
					Saint-Venant					KW Analytical Solution							
					η_q (%)	CRM (%)	CD	q_{perr} (%)	t_{perr} (min)	η_q (%)	CRM (%)	CD	q_{perr} (%)	EVOL (%)	CPU-time (s)	EVOL (%)	CPU-time (s)
I	0.5	12	0.04	0.15	99.93	-1.82	0.96	2.47	0.00	99.62	-1.78	1.03	1.45	0.86	1.69	-0.96	14.02
	5.0	12	0.42	0.15	99.91	-2.13	0.96	2.86	0.00	99.61	-2.10	1.03	1.84	1.17	0.38		
II	0.5	10	0.05	0.17	99.97	-1.15	0.98	0.72	-0.17	99.55	-1.03	1.08	-10.43	0.37	2.52	-0.78	14.09
	5.0	10	0.50	0.17	99.96	-1.38	0.98	0.85	-0.17	99.55	-1.20	1.08	-10.31	0.60	0.94		
III	0.5	12	0.04	0.17	99.98	-1.11	0.98	0.36	0.00	99.77	-0.64	1.05	0.00	0.28	1.72	-0.50	21.95
	5.0	12	0.42	0.17	99.97	-1.23	0.98	0.36	0.00	99.77	-0.73	1.05	0.00	0.40	0.67		

range between the kinematic wave, and that of the DW and SVE.

The capability of the VPMD method is further verified using the rainfall-runoff study of *Lai* [2009] who developed diffusive wave equations, using the hybrid mesh method (SRH-W) based on the finite-volume formulation, for overland flow simulation. The rainfall-runoff events studied by *Lai* [2009] were also studied earlier by *Govindaraju et al.* [1988 a, 1988b] and *Therrien et al.* [2003] to verify their overland flow simulation methods. The overland flow plane used in this study is characterised by a slope of $s_0 = 0.01$ and the hydrograph is simulated at the end of plane at $L = 100$ m. Two cases were considered for the simulation study: Case I) rainfall intensity $r = 1440$ cm/h, Manning's roughness coefficient $n = 0.0548$, with a reported kinematic wave number and Froude number being 10 and 0.5, respectively. Case II) rainfall of intensity $r = 972$ cm/h, Manning's roughness coefficient $n = 0.0155$, and a reported kinematic wave number and Froude number being 3 and 1.5, respectively. While the case I event is characterised by an estimate of $kF_{rp}^2 = 2.5$ and that of case II by an estimate of $kF_{rp}^2 = 6.75$.

For the example of case I, the analytically computed $t_e = 1.68$ min using equation (3.83a) with $k = 9.92$, $k(F_{rp})_e^2 = 2.49$ and $(F_{rp})_e = 0.5$ using equation (2.34a, b) and that for case II, $t_e = 0.92$ min with $k = 2.99$, $k(F_{rp})_e^2 = 6.71$ and $(F_{rp})_e = 1.5$. These estimates are the same as those reported by *Lai* [2009]. One may infer that the flow conditions in both these cases are beyond the applicability range of the KW model and they may fall in-between the applicability range of the diffusion and kinematic waves. Moreover, the diffusion wave equation is a good approximation to the dynamic wave equations, if the kinematic wave number is not too small [*i. e.* when $k > 5$] [*Daluz Vieira*, 1983] . The previous solutions such as those of DW by *Lai* [2009], KW by *Govindaraju et al.* [1988a, 1988b] and DW by *Therrien et al.* [2003] [as quoted by *Lai*, 2009] used the zero-depth gradient downstream boundary conditions. *Lai* [2009] had used a spatial grid size of $\Delta x = 1$m in the DW solution. Further, he has reported that for case I, stable solution may be obtained by the explicit scheme using $\Delta t \leq 0.015$s (actually used 0.01s), while an implicit scheme can allow the use of $\Delta t \leq 5$s without hampering the solution accuracy. Similarly, for case II, the use of $\Delta t < 0.015$s and $\Delta t \leq 1$s may be admissible, respectively, for the explicit and implicit schemes. The same spatial grid size is used in this study for simulation using the VPMD method with the use of $\Delta t = 1$s and 0.5s for case I and II, respectively. However, it was found during the present investigation that the use of larger computational

grid size in the VPMD method solution much larger than that prescribed for the implicit scheme, can be used without facing any stability problem and with acceptable accuracy.

Figure 3.6 shows the non-dimensional runoff hydrographs (non-dimensionalised with respect to time of equilibrium computed by using the analytical kinematic wave solution) simulated using the VPMD method at the end of the overland flow plane for both the cases under discussion along with the corresponding analytical solutions of the KW, numerical solutions of the SVE, solutions of the DW by *Therrien et al.*, 2003, the KW solutions of *Govindaraju et al.* [1988a, 1988b], and the SVE solutions of *Daluz Vieira* [1983] as presented by *Lai* [2009]. It is seen from Figure 3.6a that the VPMD method is able to reproduce the runoff hydrograph of the SVE solution with $\eta_q = 99.59$ %, $CRM = -0.54$ %, $CD = 1.08$, and $t_{perr} = -2.52$ min. It can be inferred that the VPMD simulated runoff hydrograph is also able to reproduce both the DW solutions as well as both the SVE solutions closely.

In the simulation study of case II event, the VPMD method solution is able to reproduce the runoff hydrograph with $\eta_q = 95.79$ %, $CRM = -0.84$ %, and $CD = 1.24$ in comparison with the SVE solution, and $\eta_q = 99.76$ %, $CRM = 0.03$ %, and $CD = 1.03$ in comparison with the analytical KW solution. It is inferred from these estimates of performance evaluation measures that the VPMD method simulates the runoff hydrograph comparatively close to the KW solution rather than with the SVE solution. The same inference can also be made from Figure 3.6b which clearly shows that there is no any significant difference between the DW and the VPMD solutions. These inferences imply that neither the KW nor the DW or the VPMD solutions are reasonably good approximations to the SVE solution in reproducing the rising limb of the hydrograph. The deviations between the other solutions under consideration and that of the SVE are visible due to fact that the Froude number $(F_{rp})_e > 1$, i.e. the flow is in the supercritical regime and, therefore, in such a situation the inertial terms are dominant. Further, *Daluz Vieira* [1983] concluded that when $(F_{rp})_e \to \infty$ and $k < 5$, the gravity wave solution approaches the SVE solution and, thus, it may be appropriate to use the SVE only for simulation of such events. Furthermore, in both of these cases corresponding to Figures 3.6a and 3.6b, the emphasis must be given to the realistic physical conditions responsible for the generation as well as the governance of overland flow mechanism. As assessment of overland flow generations as shown in Figure 3.6 draws attention to two important issues: a) such a high intensity rainfall cannot occur even during
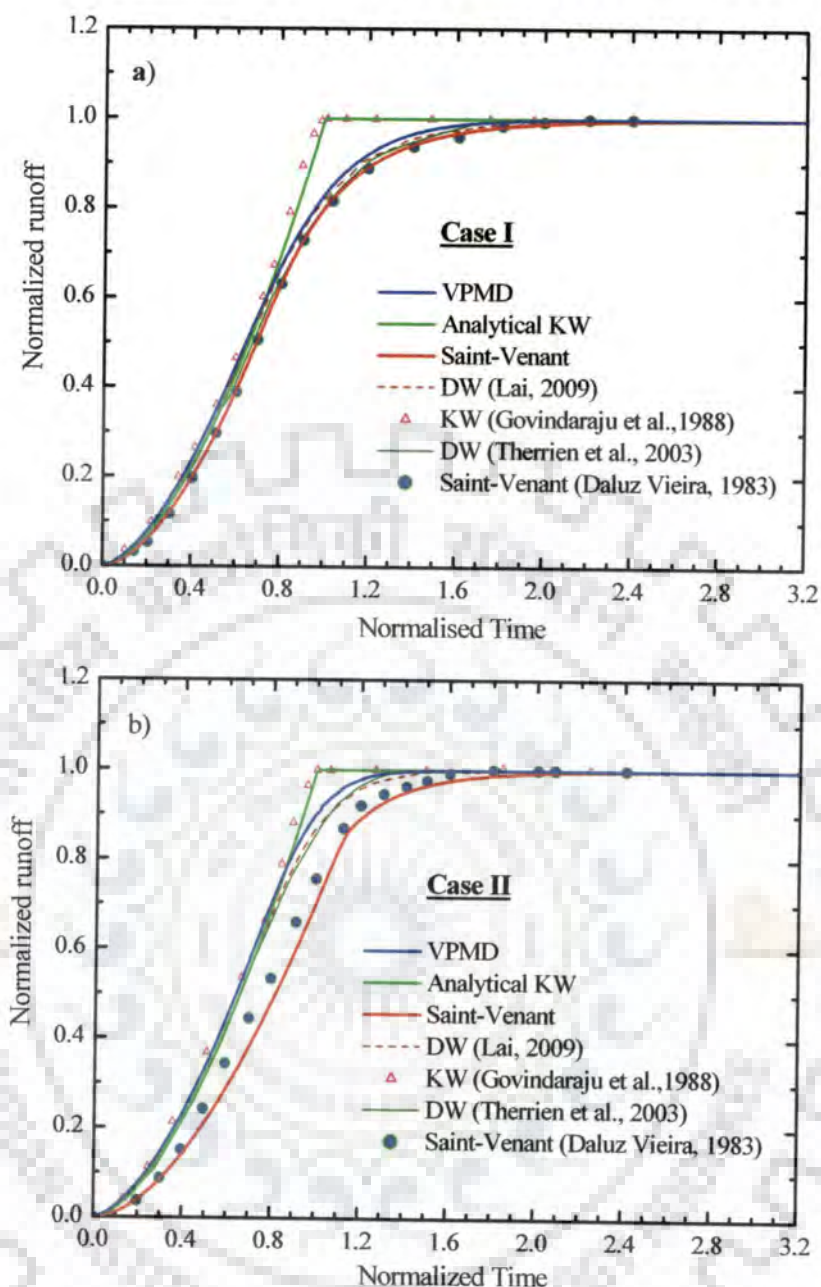
Figure 3.6 Comparison of the VPMD method simulated runoff hydrographs with various other solutions using the example of *Lai* [2009].

a thunder storm, and b) under such a situation, consideration of the generated flow as overland flow may not be appropriate as the flow no longer corresponds to a thin sheet flow as per the definition of overland flow, rather, it could be considered as a concentrated channel flow. The corresponding estimated equilibrium flow depths of the SVE solutions at the end of the planes were 0.423 and 0.176 m, respectively, for the runoff hydrographs shown in Figures 3.6a and 3.6b which are far greater than that of a thin sheet flow. Though

81

both the overland flow and channel flow processes are governed by the same equations, the scale effects due to differing order of magnitudes of flow depths in them make these processes different from each other. As a consequence of these scale effects, the main features of these flow processes such as attenuation and transition may differ from each other.

The generation of the overland flow hydrograph using the VPMD is also studied for a pulse input studied by *Kazezyılmaz-Alhan et al.* [2005] using the solutions of the DW equation arrived at based on the explicit and implicit finite difference schemes. These solutions are also compared with the analytical solution of the KW and the numerical solution of the SVE. The hypothetical solutions presented by *Kazezyılmaz-Alhan et al.* [2005] are used herein to demonstrate the capability of the proposed VPMD method to reproduce the overland flow solutions in the diffusive wave range. The spatially uniform rainfall of intensity $r = 5.08$ cm/h is applied for a duration of 30.0 minutes over a 182.88 m long plane. The plane is characterised by a uniform bed slope of $s_0 = 0.0016$ and a Manning's roughness coefficient $n = 0.025$. The runoff hydrograph is simulated at the end of the unit width plane.

Considering the runoff event to be kinematic in nature, the time to equilibrium is estimated as $t_e = 24.89$ min (1493.79 s) and the applicability criteria parameters are estimated as $k = 192.18$, $k(F_{rp})_e^2 = 13.85$ and $(F_{rp})_e = 0.27$, while the corresponding parameters for the VPMD method are computed as $k = 198.21$, $kF_{rp}^2 = 13.74$ and $F_{rp} = 0.26$. These results suggest that the applicability parameters estimated by the analytical kinematic wave approach and that by the VPMD method are in good agreement. On the basis of these results, one can surmise that the considered event could be reasonably simulated by the KW model. To simulate the runoff using the VPMD method, the unit width strip of the overland plane is divided into 69 sub-reaches as used in the case of the DW solutions by *Kazezyılmaz-Alhan et al.* [2005] based on both the implicit and explicit methods and using a temporal grid size of $\Delta t = 3$ s. Although, *Kazezyılmaz-Alhan et al.* [2005] concluded that MacCromack scheme is more efficient than the implicit and explicit methods widely used for the solutions of the DW, it is seen from their study that there is no any significant differences exhibited by theses three solutions. Due to this inference McCormack solution results are not used herein for comparison. The results of simulation by the VPMD method along with the analytical solution of KW, numerical solution of the SVE and the solutions of DW based on implicit and explicit methods are shown in Figure 3.7. The VPMD method solution matches near perfectly with the SVE solution, including
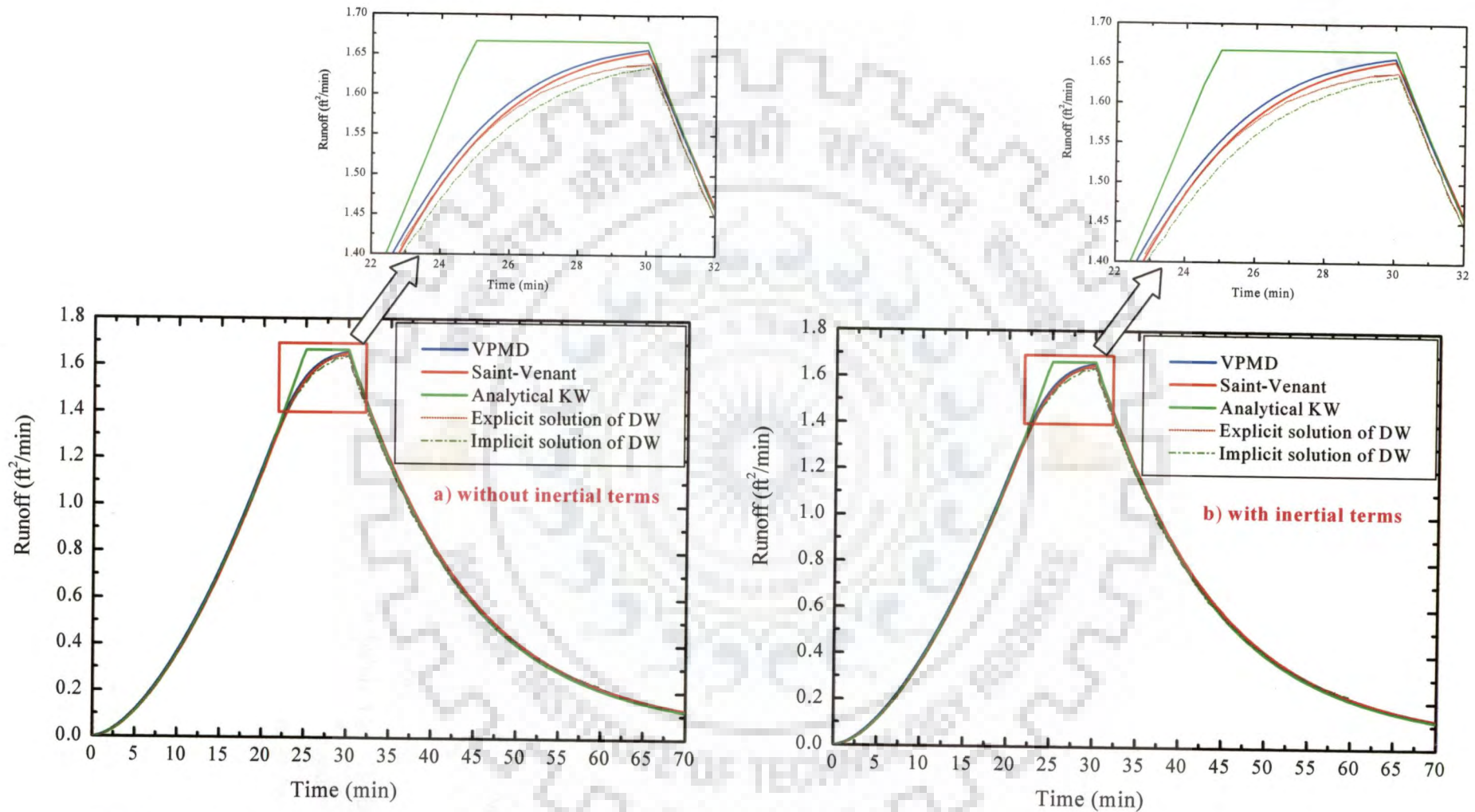
Figure 3.7 Comparison of the simulated runoff hydrographs by the VPMD method with the SVE solution, the analytical solution of the KW and the simulated runoff hydrograph by *Kazezyımaz-Alhan et al.* [2005], using explicit and implicit methods for DW solutions.

the peak of the runoff hydrograph as shown in the inset. There is also a good agreement between the solutions of the VPMD method and those of DW equation based on both the numerical schemes, except that the former solution display a slightly better edge in matching the SVE solution, around the peak region of the runoff hydrograph. As compared to the implicit scheme, the explicit scheme displays a better accuracy in matching with the solutions of the SVE and VPMD methods. *Lal* [1998b] has arrived at the same conclusion while evaluating the implicit and explicit schemes for the SVE solutions. The results also show that the VPMD method solution is in well agreement with the analytical KW solution except nearer the peak region of the runoff hydrograph where the overland flow process is not strictly kinematic and exhibits small diffusivity. This inference can also be verified from the performance evaluation measures estimated for the VPMD method solution, but without the consideration of inertial terms, i.e., $\left(1-(4/9)F_{rpM}^{2}\right)$ in equation(3.24), which is able to reproduce the SVE solution hydrograph closely with $\eta_q = 99.98$ %, $CRM = -0.60$ %, $CD = 0.99$, $q_{perr} = 0.22$ and $t_{perr} = 0.0$ min, while the estimated performance evaluation measures are $\eta_q = 99.98$ %, $CRM = -0.60$ %, $CD = 0.99$, $q_{perr} = 0.25$ and $t_{perr} = 0.0$ min, when the inertial terms are considered in equation (3.24). The corresponding estimated performance evaluation measures by the VPMD method solutions in comparison with the simulated runoff hydrograph by the analytical KW solution are $\eta_q = 99.87$ %, $CRM = -0.42$ %, $CD = 1.03$, $q_{perr} = -0.51$ and $t_{perr} = 5.0$ min and $\eta_q = 99.87$ %, $CRM = -0.43$ %, $CD = 1.04$, $q_{perr} = -0.48$ and $t_{perr} = 5.0$ min, without and with accounting of inertial terms in equation (3.24), respectively. It is seen from these results that the solution by the VPMD method are not close to analytical KW solution as compared to the SVE solution. Consequently, these results clearly indicate that accounting of the inertial terms in the VPMD method solution does not show any change in the simulation performance by the VPMD method. The estimated volume error of $EVOL = -3.62$ indicating under-estimation of input mass, may be attributed to the termination of the VPMD simulation process well before the complete draining of the detention storage. Note that the total simulation time used in the current case is 90 minutes, which is 30 minute higher than those used by the *Kazezyılmaz-Alhan et al.* [2005]. The study by *Kazezyılmaz-Alhan et al.* [2005] does not consider the volume error aspects. The CPU-time required for the execution of the VPMD solution is 0.495 s while it is 4.06 s for the SVE solution with the use of $\Delta t = 0.125$ s and the same $\Delta x = 2.65$ m as used in the solution of the VPMD method. Therefore, it can be

inferred from all these results that the VPMD method is accurate as well as computationally more efficient than the other numerical schemes used for the solution of the SVE and DW.

3.7 VARIATION OF WEIGHTING PARAMETER

While applying the VPMD method for flood routing in channels, *Perumal* [1994a] studied the variation of the weighting parameter θ used in the VPMD method with reference to the inflow discharge at every routing time interval. *Perumal* [1994a] investigated this variation using the generalized relationship established for the weighting parameter while developing the VPMD method from the SVE. The relationship between θ and the channel and flow characteristics is given as

$$\theta = \frac{1}{2} - \frac{l}{\Delta x} \tag{3.24}$$

where, Δx is the selected sub-reach length and l is the distance between the mid-section and that downstream section where the normal discharge corresponding to the depth at the mid-section passes at the same instant of time. It can be inferred from the relationship of θ given by equation (3.24) that θ can never exceed 0.5 as the least magnitude of l could be zero, at which the flood propagation is strictly kinematic in nature. Using an example of flood propagation in a steep channel, *Perumal* [1994b] showed that θ was varying very close to 0.5, but always < 0.5 as the flood propagation even in a steep river reach exhibits a small amount of diffusion. *Perumal's* [1994a] study further showed that at the lower end, the magnitude of θ could be $\theta < 0$ for a small routing sub-reach length when $l > 0.5 \Delta x$, i.e., when the flow section wherein the normal discharge corresponding to the flow depth at the mid-section of the sub-reach passes is located downstream of the outflow section of the considered routing sub-reach. While the same theoretical interpretation for the variation of θ could be applicable for modelling the overland flow simulation using the VPMD method, it has to be kept in mind that the magnitude of θ estimated for overland flow simulation at any time is also influenced by the lateral flow, which was considered absent while applying the VPMD method for routing in channels. In view of these considerations it is desirable to investigate the variation of θ when simulating the overland flow using the VPMD method. The nature of variation of θ along the plane length is demonstrated using the example of *Kazezyılmaz-Alhan et al.* [2005] as studied in the previous section, wherein 182.88 m plane is subdivided into 69 sub-reaches. The θ values estimated corresponding to the overland flow simulations at the end of 2nd, 35th and 69th (end of the plane) sub-reaches are
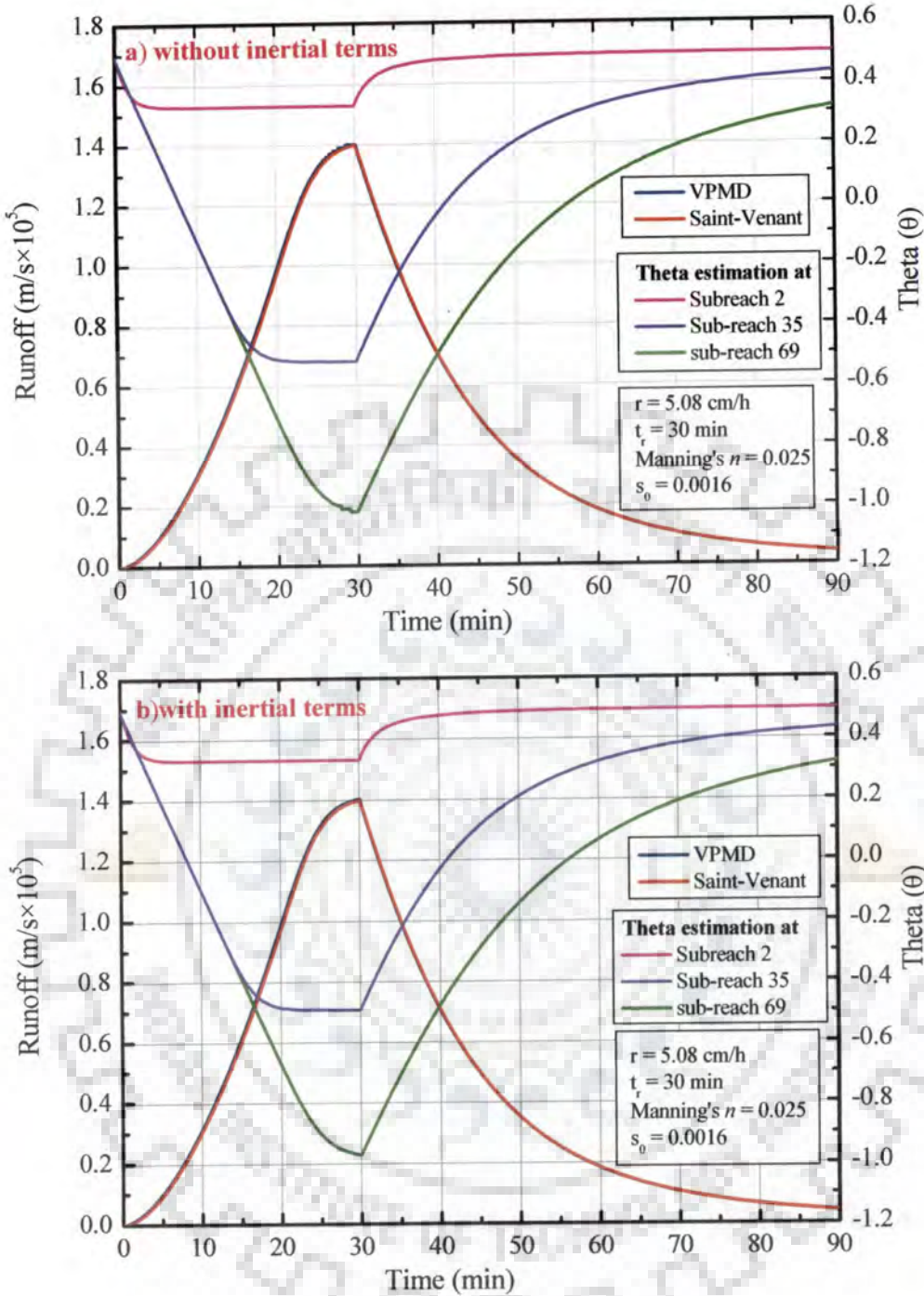
Figure 3.8 Temporal variation of θ estimated at the end of 2nd, 35th and last (69th) routing sub-reaches by the VPMD method along with the simulated runoff hydrograph at the end of the overland flow plane by the VPMD and SVE methods.

shown in Figure 3.8, along with the runoff hydrograph at the end of the overland flow plane. It is inferred from Figure 3.8a that the computed θ values vary from ≈ 0.5, but < 0.5, to negative values as runoff hydrograph rises rapidly. The values of the weighting parameter

estimated at the end of the 2nd sub-reach vary in the range of 0.33 and 0.497, with a minimum weighting parameter values $\theta_{min} = 0.33$ occurring corresponding to maximum discharge at the end of the considered sub-reach. However, in case of the 35th and the 69th sub-reaches, the negative values of θ_{min} were estimated with the maximum negative values of -0.52 and -1.02, respectively, occurring corresponding to the peak discharges at the downstream end of the respective sub-reaches. With the accounting of the inertial terms in the runoff hydrograph simulation by the VPMD method, the θ_{max} and θ_{min} estimated, respectively during the simulation were 0.497 and 0.33; 0.49 and -0.49; and 0.49 and -0.97 at the respective downstream ends of the 2nd, 35th and 69th sub-reaches. It can be inferred from these results that the θ_{min} values estimated for these three sub-reaches are slightly lower than those corresponding estimates arrived at without consideration of the inertial terms. These inferences can also be seen from Figure 3.8b. The magnitude of maximum negative values of θ estimated for sub-reach increases with the increase in the magnitude of discharge to be routed, which is consistent with the relationship of θ given by equation (3.24). The systematic variation of θ as exhibited in Figure 3.8 indicates the unconditional stability offered by the VPMD method.

3.8 ACCURACY OF THE VPMD METHOD

The accuracy of the proposed VPMD method mainly depends on the adherence to the assumptions involved in the development of the method by the considered overland flow simulation process. Accordingly, there are three major sources of approximations involved in the application of the method for overland flow generation:

(i) approximation with reference to the use of the assumption of linear variation of flow depth in the considered routing reach;

(ii) approximation with reference to the use of the assumption that multiples of derivatives of the flow variables are negligible; and

(iii) approximation that arises due to the binomial series expansion of the energy slope in estimating the distance l between the mid-section and the normal flow section of the routing sub-reach.

The error introduced due to the first approximation can be minimized by reducing the length of the routing sub-reach Δx. Though the validity of the second assumption requires the validity of the first assumption, it also requires the use of smaller Δt to enable the

requirement of linear variation of the flow depth and the flow velocity along time. However, if truncation error introduced by the third assumption related to the approximation of the energy slope by retaining only the first two terms is significant, then the routing using an increased number of sub-reaches would compound the inaccuracy in the solution which may lead to numerical instability problems. But *Perumal* [1994b] pointed out that such a situation develops only when $[(1/S_0)\partial Y/\partial X]$ is nearer to unity. Fortunately such a situation generally does not arise in overland flow planes as they are characterised by comparatively larger bed slopes than that of the channel and river beds. As the VPMD method for overland flow study has the same governing equation as that used for flood routing in channels, it is surmised that at least the same limit may hold good for the overland flow modelling also. However, a detailed study in this regard is required. Based on a detailed analysis, *Perumal and Sahoo* [2007] have specified an applicability limit of the VPMD method for flood routing in channels as $\dfrac{1}{S_0}\dfrac{\partial Y}{\partial X} < 0.43$. In view of these theoretical considerations related to the accuracy of the VPMD solutions, it is pertinent to study the effects of spatial and temporal grid sizes, which have implications related to the first and second assumptions, respectively, on the capability of the VPMD method to closely simulate the benchmark solutions of overland flow runoff.

3.8.1 Effect of Spatial Grid Size Variations on the Solution Accuracy

Overland flow simulation results of the VPMD method are also greatly influenced by the solution scheme used. In this regard it is pertinent to note the suggestion given by *Kampf and Burges* [2007] who state that "the solution's procedure for representing coupled process, determining time steps, tracking mass balance, and evaluating convergence are all important considerations in evaluating simulation output". Therefore, it is an important step in model verification to study the impact of computational spatial and temporal grid sizes on the overall performance of the model and its accuracy. In order to study the sensitivity analysis of spatial grid size on the accuracy of the simulated overland flow hydrographs, the example of *Gottardi and Venutelli* [2008], already considered earlier as illustrated in Figure 3.5b is employed. Different sizes of Δx ranging from 0.05 to 50 m were used to simulate the overland flow hydrographs at the end of 200 m length of a unit width strip plane. The results of the simulated hydrographs for all the considered numerical experiments are shown in Figure 3.9 along with the benchmark hydrograph. It can be inferred from this figure that
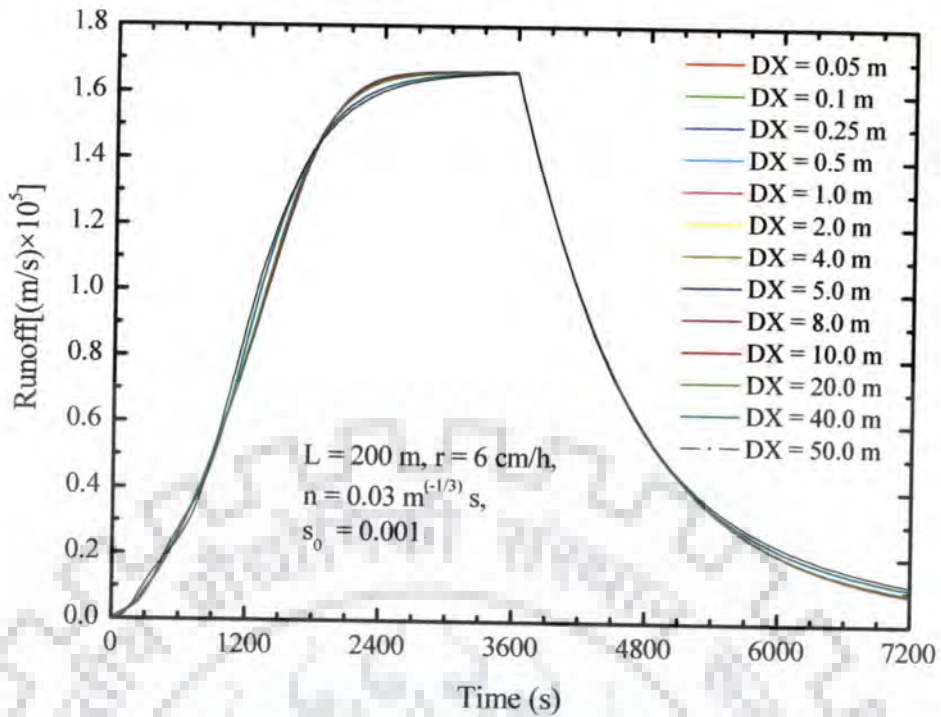
Figure 3.9 Effect of spatial grid size variations on the simulations.

when Δx is varying from 0.05 to 20 m, no significant difference is seen between the benchmark and the simulated hydrographs, and the VPMD method may be considered as an accurate method. However, when the chosen Δx sizes of 40 m and 50 m were used for the solution using the VPMD method, the corresponding simulated hydrographs are not close to the benchmark hydrograph in comparison with the simulations arrived at using the grid sizes in the range of 0.05 to 20 m. However, this inference may be qualified only in a relative sense, but not in an absolute sense. The relative inability of the VPMD method to reproduce the benchmark solution closely for these cases may be attributed to the non-adherence of the assumption of linear variation of flow depth by the VPMD method.

It is worthwhile to analyse the accuracy of the solutions arrived at using different spatial grid sizes from the perspective of accuracy criteria given for other similar methods such as the kinematic wave solution of the HEC-HMS model [*USACE*, 2000]. To preserve the accuracy of the kinematic wave based overland flow simulation, the HEC-HMS model adopts the use of the criterion $C_{un} \approx 1$, where $C_{un} = c(\Delta t / \Delta x)$ and it denotes the Courant number. But it is to be noted that HEC-HMS solves the kinematic wave equation using the conventional explicit numerical scheme which requires such criterion in order to control the numerical diffusion in the solution. However, the ACD equation, based on which the

VPMD method has been developed, is directly derived from the Saint-Venant equations and it has the inherent feature to preserve the accuracy and stability of the solution without exhibiting numerical diffusion. Table 3.3 demonstrates the accuracy of the VPMD method solution for the considered example of *Gottardi and venutelli* [2008] despite the violation of the condition given by the HEC-HMS model in simulating the overland flow hydrograph using the KW.

It is seen from Table 3.3 that for all the numerical experiments with $\Delta x \leq 20$ m, there is no significant change in the estimated Nash-Sutcliffe efficiency value of 99.98 implying that all these simulations very closely reproduce the considered SVE benchmark solutions. Besides, the other performance measures such as the mass conservation criterion ($EVOL$), CRM, CD are very close to the ideal values of 0%, 0.0% and 1.0, respectively. However, relatively large error in the performance measures were estimated for the numerical

Table 3.3 Performance evaluation of the VPMD method solutions for spatial grid size variations

Δx (m)	$\dfrac{\Delta x}{\Delta t}$	c_{max}	Courant Number C_{un}	θ_{max}	θ_{min}	Performance Evaluation Measures						CPU -time (s)
						η_q (%)	CRM (%)	CD	$EVOL$ (%)	q_{perr} (%)	t_{perr} (min)	
0.05	0.004	0.174	41.739	0.500	-200.75	99.98	-1.11	0.98	0.28	0.36	0.00	14.86
0.10	0.008	0.174	20.868	0.500	-100.12	99.98	-1.10	0.98	0.27	0.36	0.00	7.61
0.25	0.021	0.174	8.346	0.500	-39.739	99.98	-1.10	0.98	0.27	0.36	0.00	3.17
0.50	0.042	0.174	4.172	0.500	-19.612	99.98	-1.11	0.98	0.28	0.36	0.00	1.70
1.00	0.083	0.174	2.085	0.499	-9.549	99.98	-1.13	0.98	0.30	0.36	0.00	0.95
2.00	0.167	0.174	1.041	0.499	-4.517	99.98	-1.16	0.98	0.33	0.36	0.00	0.58
4.00	0.333	0.173	0.520	0.499	-2.001	99.97	-1.21	0.98	0.38	0.36	0.00	0.39
5.00	0.417	0.173	0.415	0.499	-1.498	99.97	-1.23	0.98	0.40	0.36	0.00	0.36
8.00	0.667	0.173	0.259	0.498	-0.743	99.97	-1.32	0.98	0.49	0.36	0.00	0.33
10.00	0.833	0.172	0.207	0.498	-0.492	99.97	-1.38	0.98	0.55	0.35	0.00	0.30
20.00	1.667	0.170	0.102	0.498	0.012	99.96	-1.84	0.99	1.01	0.33	0.00	0.25
40.00	3.333	0.167	0.050	0.497	0.263	99.86	-3.30	1.00	2.45	0.18	0.00	0.25
50.00	4.167	0.165	0.040	0.497	0.314	99.74	-4.27	1.01	3.41	0.05	0.00	0.23

experiments with $\Delta x = 40$ m and 50 m, especially with regard to CRM and $EVOL$ estimates. Considering the fulfillment of all the performance measures, it may be considered from the evaluations of the pertinent characteristics of the solution as presented in Table 3.3 that the solution of the VPMD method is not sensitive to the adopted spatial grid size up to

20 m and the corresponding simulations can be considered very accurate in reproducing the benchmark hydrograph.

It is seen from Table 3.3, that there is no significant change in the estimated Nash-Sutcliffe efficiency for all the considered Δx values. However, the VPMD method is able to preserve the mass conservation with *EVOL* estimate < 1% only when $\Delta x \leq 20$ m. Similarly, *CRM* and *CD* are also close to the ideal performance indicators when $\Delta x \leq 20$ m. These performance measures are estimated with large degree of error, when $\Delta x > 20$ m. Indeed, the grid ratio ($\Delta x / \Delta t$), maximum celerity (c_{max}), Courant number (C_{un}), θ_{min} (which is estimated at the downstream end of overland flow plane for the highest runoff discharge value) and θ_{max} all computed for each Δx case are given in Table 3.3. It can be inferred from these results that if the condition $C_{un} \approx 1$ has to satisfy as recommend in the HEC-HMS model, then only the use of $\Delta x = 2$ m is allowed and this will be too restrictive as compared to the use of $\Delta x = 20$ m for the KW solution. In turn, this requires a larger computational time (CPU time) over the case of using $\Delta x = 20$ m which however, is characterised by $C_{un} = 0.102$. Therefore, it is inferred from this analysis that strictly following the Courant condition is not necessary to preserve the solution accuracy. Further, the θ_{max} value estimated below 0.5 in all the cases indicates that the method is unconditionally stable. The results presented in Table 3.3 also demonstrate that the use of large space intervals up to $\Delta x = 50$ m do not cause any numerical or stability problem, while, the explicit numerical scheme for the SVE solution is non-convergent even for a small space grid size of 0.05 m. Further, it can be seen from Table 3.3, that the weighting parameter θ_{min} ranges from 0.314 ($\Delta x = 50$ m) to -200.76 ($\Delta x = 0.05$ m) contrary to the conventional notion that the minimum Muskingum weighting parameter is zero. It can be inferred from the analysis of spatial grid size impacts on the solution accuracy of the VPMD method that the ability to use longer space interval while preserving the accuracy will have an important implication in the large catchment/basin modelling. This inference has been substantiated by *Molnár and Julien* [2000] who concluded that coarser grid sizes can be used for rainfall-runoff modelling, especially when events of higher rainfall intensity and longer duration occurs.

3.8.2 Effect of Temporal Grid Size Variations on the Solution Accuracy

The same example of *Gottardi and Venutelli* [2008] already considered earlier as in the case of Figure 3.5b, is further employed to examine the impact of temporal grid size variations on the solution performance and accuracy, using pre-selected Δt ranging from 1 s to 360 s and $\Delta x = 0.5$ m in all the numerical experiments. It can be seen from Figure 3.10, that the VPMD method is able to produce the benchmark hydrograph with consistent accuracy for Δt ranging from 1s to 30s. However, any further increase in the time interval results in the
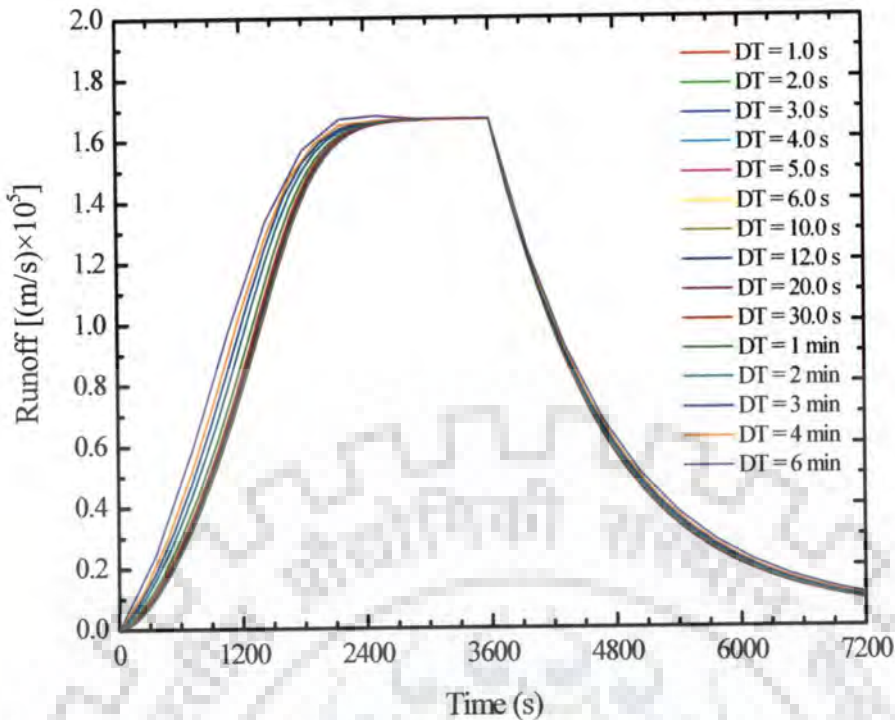
Figure 3.10 Effect of temporal grid size variations on the simulations.

deviation of the hydrograph towards the left, especially, greater on the rising limb of the hydrograph than on the recession limb. This can also be verified from the computed performance criteria as shown in Table 3.4. Similarly, too small Δt values would not yield enhanced accuracy of the solution and only resulting in higher CPU time. On the other hand, the use of higher temporal grid size results in early arrival of the rising part of the overland flow hydrograph causing volume error due to increased volume of the generated runoff.

The close examination of the results shown in Table 3.4 clearly demonstrates that the satisfaction of the criterion $C_{un} \approx 1$, allow only the use of $\Delta t = 3$ s. However, the use of $\Delta t > 3$ s, does not affect the solution accuracy and the performance of the method. Therefore, it can be inferred that the satisfaction of this criterion is not needed when using the VPMD method and it leads to more computation time. It is also inferred from this study that the inaccuracy of the solution occurs when the Courant number exceeds the threshold value of $C_{un} \approx 10.0$. However, this statement required to be verified with extensive testing of the proposed method for various rainfall intensities and slope conditions. Moreover, the choice of computational temporal grid size also depends on the time of concentration, duration of rainfall and the time interval of the rainfall data made available. Note that *Orlandini and Rosso* [1996] reported the threshold value of the Courant number for the VPMC method as 3 and reported fluctuations in the estimated discharge response when

Table 3.4 Performance evaluation of the VPMD method solutions for temporal grid size variations

Δt (s)	$\dfrac{\Delta x}{\Delta t}$	c_{max}	Courant Number C_{un}	θ_{max}	θ_{min}	Performance Evaluation Measures						CPU-time (s)
						η_q (%)	CRM (%)	CD	EVOL (%)	q_{perr} (%)	t_{perr} (min)	
1.00	0.500	0.174	0.348	0.4996	-19.612	100.00	-0.46	0.99	-0.37	0.36	0.00	18.08
2.00	0.250	0.174	0.695	0.4996	-19.612	100.00	-0.53	0.99	-0.29	0.36	0.00	9.22
3.00	0.167	0.174	1.043	0.4996	-19.612	99.99	-0.60	0.99	-0.22	0.36	0.00	6.22
4.00	0.125	0.174	1.391	0.4996	-19.612	99.99	-0.66	0.99	-0.16	0.36	0.00	4.56
5.00	0.100	0.174	1.738	0.49961	-19.612	99.99	-0.73	0.99	-0.10	0.36	0.00	3.80
6.00	0.083	0.174	2.086	0.49961	-19.612	99.99	-0.78	0.99	-0.04	0.36	0.00	3.19
10.00	0.050	0.174	3.477	0.49961	-19.612	99.98	-1.00	0.99	0.18	0.36	0.00	2.00
12.00	0.042	0.174	4.172	0.49961	-19.612	99.98	-1.11	0.98	0.28	0.36	0.00	1.70
20.00	0.025	0.174	6.953	0.49961	-19.612	99.96	-1.50	0.98	0.66	0.36	0.00	1.08
30.00	0.017	0.174	10.430	0.49961	-19.612	99.92	-1.94	0.98	1.11	0.36	0.00	0.78
60.00	0.008	0.174	20.860	0.49961	-19.612	99.79	-3.14	0.96	2.29	0.36	0.00	0.49
120.00	0.004	0.174	41.720	0.49992	-19.613	99.42	-5.14	0.95	4.28	0.36	0.00	0.25
180.00	0.003	0.174	62.580	0.4999	-19.613	99.00	-6.82	0.93	5.96	0.36	-9.00	0.16
240.00	0.002	0.174	83.471	0.49988	-19.622	98.56	-8.29	0.92	7.64	0.45	-16.00	0.13
360.00	0.001	0.174	125.548	0.49979	-19.717	97.71	-10.82	0.90	10.02	1.16	-18.00	0.09

used beyond this limit. It can be inferred from the above discussion that the VPMD method provides more stable and accurate solutions with the use of larger space and time resolutions not restricted by the Courant condition $C_{un} = 1$.

The impacts of different combinations of Δx and Δt on the performance of the VPMD overland flow routing method, especially on the three performance evaluation measures such as $EVOL$, q_{perr} and η_q are shown in Figure 3.11. It can be seen from this figure that the use of the different combinations of Δx and Δt does not have a significant impact on the estimated peak discharge of the runoff hydrograph estimation, and the Nash-Sutcliffe efficiency, but the volume error increases beyond 1% for all the combinations of Δx and Δt shown therein, except for the combinations of $\Delta x = 0.5$ m and $\Delta t = 12$ s; and $\Delta x = 5$ m and $\Delta t = 12$ s.

3.9 TIME-VARYING RAINFALL CASES

The capability of the VPMD method to estimate runoff in response to time varying rainfall is evaluated using the hypothetical cases as used by *Govindaraju et al.* [1990]. The configurations of the overland flow planes and the associated rainfall details studied are
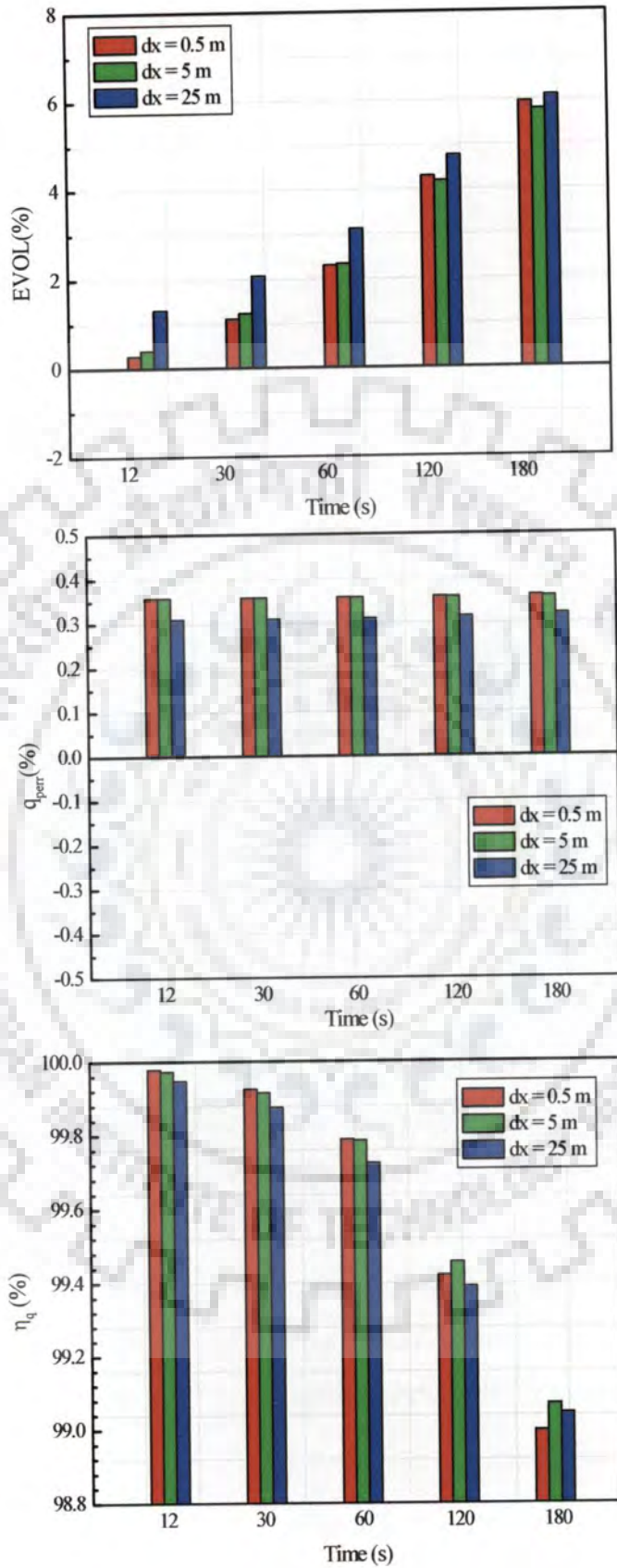
Figure 3.11 Effect of spatial and temporal grid sizes variations on the performance evaluation measures.

given in Table 3.5. The simulated hydrographs by the VPMD method for these inputs are compared with the corresponding numerical solutions of the SVE, the approximate analytical solution of *Govindaraju et al.* [1990] and the numerical solution of the SVE given by *Govindaraju et al.* [1990], and the numerical solutions of the KW and DW equations of *Gottardi and Venutelli* [2008] as shown in Figure 3.12. It can be seen from the results presented for case –I that the simulated hydrograph of the VPMD method is not matching perfectly with the SVE solution, although it has better performance than the KW solution and the approximate analytical solution. This can also corroborated with the performance evaluation measures such as η_q, CRM, CD, q_{perr} and t_{perr} given in Table 3.6 (Case I). The DW solution of *Gottardi and Venutelli* [2008] is also showing over prediction around the peak region as compared to the SVE solution; however, it reproduces the SVE solution closely than the VPMD method solution. However, the VPMD method solution coincides with the recession limb of the DW equations solution and both these solutions over predict the recession limb of the SVE solution. The unsatisfactory performance of the VPMD method may be attributed to the lower F_{rp} and $k(F_{rp})^2$ value which is even beyond the applicability limits of the DW equations. However, as the estimates of the applicability criteria parameters $(F_{rp})_{min}$ and $\left|kF_{rp}^2\right|_{min}$ increase (as seen from Table 3.6), the performance of the VPMD method solution is also improved. Therefore, in cases II and III, even when the flow conditions are well within the applicability limit of the DW equation with $(F_{rp})_{min}$ = 0.016 and 0.017 and $\left|kF_{rp}^2\right|_{min}$ = 1.10 and 1.31, respectively, the performance of the VPMD solution is in close agreement with that of the SVE demonstrating the capability of the VPMD method to simulate events governed by the diffusive wave.

For cases IV and V, VI the flow conditions are well within the KW applicability limit, and, hence, the simulated hydrographs by the VPMD method display perfect match with the SVE solution and the DW equations solution as expected. This inference can also be corroborated from the performance evaluation measures computed for these cases which are given in Table 3.6. It is inferred from Figure 3.12 that the approximate analytical solution is not able to perfectly match the VPMD, SVE and DW solutions, but able to produce the hydrograph in an approximate manner in all the cases. It is revealed from Table 3.6 that the Courant number in all the cases is not following the criteria $C_{un} \approx 1$, once again confirming that this criterion is not required in arriving at the VPMD solution. It can be inferred from the results given in Table 3.6 that the VPMD method solution is able to

Table 3.5 Details of the overland flow planes and the time varying rainfall events considered for the VPMD method applications

Event	Length, $L\,(m)$	Chezy's $C(m^{1/2}/s)$	Slope S_0	Rainfall r (cm/h) vs Time $t\,(s)$
I^*	21.945	1.336	0.001	10.16, $0 \le t \le 600$ 5.08, $600 \le t \le 1200$ 10.16, $1200 \le t \le 1800$ 5.08, $1800 \le t \le 2400$ 0, $t > 2400$
II	21.945	1.336	0.002	Same as case I^*
III	21.945	1.336	0.0023	Same as case I^*
IV	21.945	1.336	0.007	Same as case I^*
V^*	21.945	1.767	0.04	5.08, $0 \le t \le 600$ 10.16, $600 \le t \le 1200$ 5.08, $1200 \le t \le 1800$ 10.16, $1800 \le t \le 2400$ 0, $t > 2400$
VI^*	21.945	1.767	0.04	10.16, $0 \le t \le 600$ 5.08, $600 \le t \le 1200$ 10.16, $1200 \le t \le 1800$ 5.08, $1800 \le t \le 2400$ 0, $t > 2400$

*Indicates the hypothetical variable rainfall-runoff simulation cases employed by *Govindaraju et al.* [1990] in the verification of their developed approximate analytical solution known as the one-term solution

Table 3.6 Performance evaluation of the VPMD method for different time-varying rainfall events

Event	Δx (m)	Courant Number	η_q (%)	CRM (%)	CD	q_{perr} (%)	t_{perr} (min)	EVOL (%) VPMD	CPU-time (s) VPMD	EVOL (%) Saint-Venant	CPU-time (s) Saint-Venant	k_{min}	F_{rp}	$\lfloor kF_{rp}^2 \rfloor_{min}$
I^*	0.51	0.12	96.50	-0.53	1.18	-16.21	0.00	0.29	0.97	-0.28	5.23	6099.9	0.009	0.494
	2.19	0.03	97.25	-1.34	1.13	-13.90	0.00	1.09	0.58			5849.3	0.009	0.492
II	0.51	0.18	99.60	-0.55	0.99	-4.74	3.40	0.46	0.95	-0.23	4.94	4478.8	0.016	1.102
	2.19	0.04	99.63	-1.34	0.98	-3.76	2.90	1.25	0.58			4519.7	0.016	1.105
III	0.51	0.20	99.75	-0.57	0.98	-3.35	0.20	0.49	0.95	-0.22	5.05	4365.4	0.017	1.309
	2.19	0.05	99.76	-1.35	0.97	-2.57	0.10	1.27	0.66			4417.6	0.017	1.315
IV	0.51	0.32	99.99	-0.64	0.99	-0.04	0.00	0.62	0.95	-0.15	4.73	4648.4	0.034	5.285
	2.19	0.07	99.99	-1.23	0.99	0.10	0.00	1.21	0.59			4681.3	0.034	5.332
V^*	0.51	0.75	99.99	-0.40	1.00	-0.05	0.00	0.38	0.44	-0.04	3.20	4742.6	0.112	59.707
	2.19	0.17	99.99	-0.65	1.00	-0.55	20.0	0.63	0.28			4794.8	0.112	60.371
IV^*	0.51	0.75	99.98	-0.58	0.99	-0.05	0.00	0.55	0.45	-0.04	3.64	4742.6	0.112	59.707
	2.19	0.17	99.96	-0.84	1.00	-0.55	0.00	0.82	0.28			4794.8	0.112	60.371
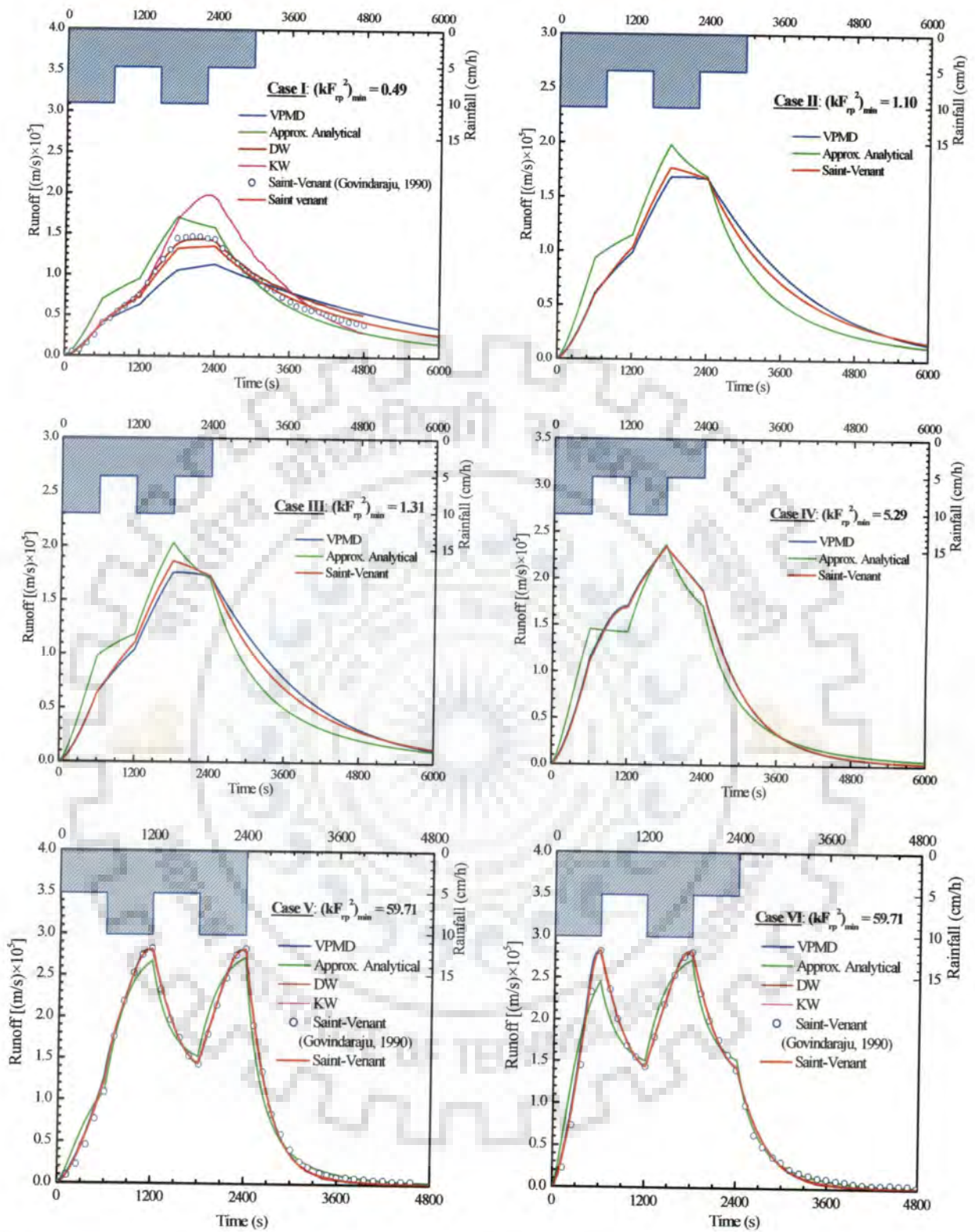
Figure 3.12 Comparison of the runoff hydrographs simulated using the VPMD method with those obtained using the approximate analytical solution method [*Govindaraju et al.*, 1990], the numerical solution of the SVE and the simulated runoff hydrographs using the KW and DW solutions of *Gottardi and Venutelli* [2008].

97

perform efficiently in all the cases, when $kF_{rp}^2 > 1.0$, and the CPU-time required for the solution is much less than the numerical solution of the SVE.

3.10 FIELD VERIFICATION WITH IZZARD'S DATA

The classical overland flow laboratory experiments conducted by *Izzard* in USA during 1942-43 were among the first systematic study carried out on the overland flow process under controlled conditions. Even more than half-a-century later, since the experimental study was reported by *Izzard* [1944], these results continue to serve as the basic data for model verification of the newly developed overland flow models. Therefore, the performance of the VPMD method under complex rainfall pattern is further investigated by comparing its solution with the eight selected overland flow events of the Izaard's experimental study [as reported by *Maksimović and Radojković*, 1986]. The data utilized in the present study were collected from two different experimental plots each having a width 1.83 m and a length of 21.95 m, and each characterized by different surfaces to define two uniform roughness values, *viz.*, (I) smooth asphalt surface and (II) dense blue grass turf sod placed directly upon roofing paper with transverse slats. Considering typical variability of the rainfall pattern, the runoff events of 34, 35, 36 and 50 corresponding to smooth asphalt surface and the runoff events of 301, 302, 318 and 319 corresponding to the plane characterized by dense blue grass turf sod as reported by *Maksimović and Radojković*, [1986] were considered for the study. The runoff flow data of these eight rainfall-runoff events are given in Appendix-IV.

The various plane characteristics and rainfall conditions corresponding to these selected events used for the verification of the developed method are summarized in Table 3.7. In order to evaluate the Manning's roughness coefficient required to simulate the runoff hydrograph, the practice of matching the observed hydrograph closely using the simulated hydrograph is adopted [*Woolhiser*, 1975; *Engman*, 1986]. Following the approach of *Wong and Lim* [2006], the Manning's n is computed for each runoff event based on the sensitivity analysis tests carried out by varying n from 0.010 to 0.018 for the asphalt experimental surface, while from 0.21 to 0.38 for the dense blue grass sod experimental surface by assessing the reproduction performance using the Nash-Sutcliffe efficiency (η_q).The obtained optimum Manning's roughness coefficients, with the event number written within the adjacent brackets, are 0.016 (34), 0.017 (35), 0.015 (36), 0.015 (50), 0.36 (301), 0.27 (302), 0.25 (318) and 0.38 (319). These values are nearer to those recommended values (0.010-0.013 for the asphalt plane and 0.38-0.63 for the dense blue grass turf) by

Table 3.7 Details of Izzard's experimental events considered for the VPMD method application

Surface Cover, Length of Planes and Constant Slopes (s_0),					
Asphalt, 21.95 m, 0.005			Dense Blue Grass Turf, 21.95 m , 0.01		
Event	Manning's n	Rainfall Intensity r (cm/h) Versus Time $t(s)$	Event	Manning's n	Rainfall Intensity r (cm/h) Versus Time $t(s)$
34	0.015	9.756, $0 \leq t \leq 420$ 0, $t > 420$	301	0.28 0.36*	9.678, $0 \leq t \leq 1680$ 0, $t > 1680$
35	0.015	4.752, $0 \leq t \leq 600$ 9.474, $600 \leq t \leq$ 1080 0, $t > 1080$	302	0.28	4.65, $0 \leq t \leq 1800$ 0, $t > 1800$
36	0.015	9.702, $0 \leq t \leq 480$ 0, $480 \leq t \leq 540$ 9.702, $540 \leq t \leq 780$ 0, $t > 780$	318	0.28	4.524, $0 \leq t \leq 1320$ 9.096, $1320 \leq t \leq$ 1980 0, $t > 1980$
50	0.015	4.8, $0 \leq t \leq 120$ 9.6, $120 \leq t \leq 420$ 0, $420 \leq t \leq 540$ 9.6, $540 \leq t \leq 840$ 0, $840 \leq t \leq 960$ 4.8, $960 \leq t \leq 1320$ 0, $t > 1320$	319	0.28 0.38*	9.348, $0 \leq t \leq 1140$ 0, $1140 \leq t \leq 1440$ 9.348, $1440 \leq t \leq$ 1890 0, $t > 1890$

*Additional Manning's n used to verify the effect of increased roughness. Note that Manning's n for these events are chosen based on the sensitivity analysis tests.

Woolhiser [1975] and *Engman* [1986]. Therefore, a uniform value of Manning's roughness coefficient of $n = 0.015$ for the asphalt plane and a value of $n = 0.28$ for the dense blue grass turf were used in the simulation of all the events considered in this study. However, the differences between the employed and the calibrated roughness values are high for the events 301 and 319 and, therefore, the corresponding calibrated roughness values for these events are also used in the performance verification of the VPMD method. The variation ranges of the minimum computed criteria using a finer grid size are: $k_{min} = 64.89 - 66.41$, $(F_{rp})_{min} \cong 0.60 - 0.61$ and $\left| kF_{rp}^2 \right|_{min} = 23.79 - 24.22$ for the asphalt plane events; whereas, they are $k_{min} = 2951.52 - 5233.87$, $(F_{rp})_{min} = 0.05 - 0.06$, and $\left| kF_{rp}^2 \right|_{min} = 10.06 - 15.72$ for

the dense blue grass turf events. The use of the calibrated Manning's roughness coefficients identified for each of the events is also causing changes in the computed applicability criteria: for the event 301 with $n = 0.36$, the estimated criteria are $k_{min} = 4015.82$ (2951.52), $(F_{rp})_{min} = 0.05$ (0.06), and $\left[kF_{rp}^2\right]_{min} = 8.62$ (10.06), and for the event 319 with $n = 0.38$, the estimated criteria are $k_{min} = 4456.66$ (3033.47), $(F_{rp})_{min} = 0.04$ (0.06), and $\left[kF_{rp}^2\right]_{min} = 8.66$ (10.28). The value given in the adjacent brackets corresponds to those simulations obtained with the adopted uniform Manning's roughness coefficient of $n = 0.28$. These results suggest that the flow conditions in all the events are well within the KW applicability limits.

The typical runoff hydrograph simulation results by the proposed method along with the observed hydrographs and the corresponding numerical solutions of the SVE are shown in Figure 3.13. It can be revealed from these results that the VPMD method has the ability to reproduce the observed data accurately; besides, it matches perfectly with the solution of the SVE for all the considered events. It is interesting to note that, particularly, for the cases of rainfall-runoff events on asphalt plane, *Izzard* observed a sudden increase of discharge immediately after the cessation of rain as shown in Figure 3.13 (Events 36 and 50). This sudden spike observed in the discharge hydrograph is due to sudden reduction of the surface roughness caused by the termination of the impact of the rain drops on the surface of the overland flow [*Izzard*, 1944, as quoted by *Maksimović and Radojković*, 1986]. However, for dense blue grass turf, such an instant rise of runoff discharge was not observed when rainfall ceased.

The estimated performance measures of the VPMD simulations in comparison with the observed hydrographs and the numerical SVE's solutions are shown in Table 3.8 along with the chosen Δx and Δt values used in the computations. The computed Courant number for each event is also given therein. It is seen from Table 3.8 that theses performance measures varying in the range of $\eta_q = 94.07 - 96.14$ %, $CRM = (-3.41) - (-6.38)$ %, $CD = 1.24 - 1.30$, $q_{perr} = (0.01) - (-0.08)$ % and $t_{perr} = 1.88 - 2.23$ minutes, for the runoff events on the asphalt plane, while $\eta_q = 83.67 - 97.03$ %, $CRM = (-2.82) - (-16.87)$ %, $CD = 0.79 - 1.33$, $q_{perr} = (-0.09) - (-6.32)$ % and $t_{perr} = (-0.80) - 2$ minutes for the events on the dense blue grass turf. It can be inferred from these results that the VPMD method is able to produce all the runoff hydrographs of the considered events with $\eta_q > 90.0$ % (except in case of event 319), which suggest the suitability of the VPMD method for overland flow generation in practice. The estimated error in mass conservation for all the events and computations using
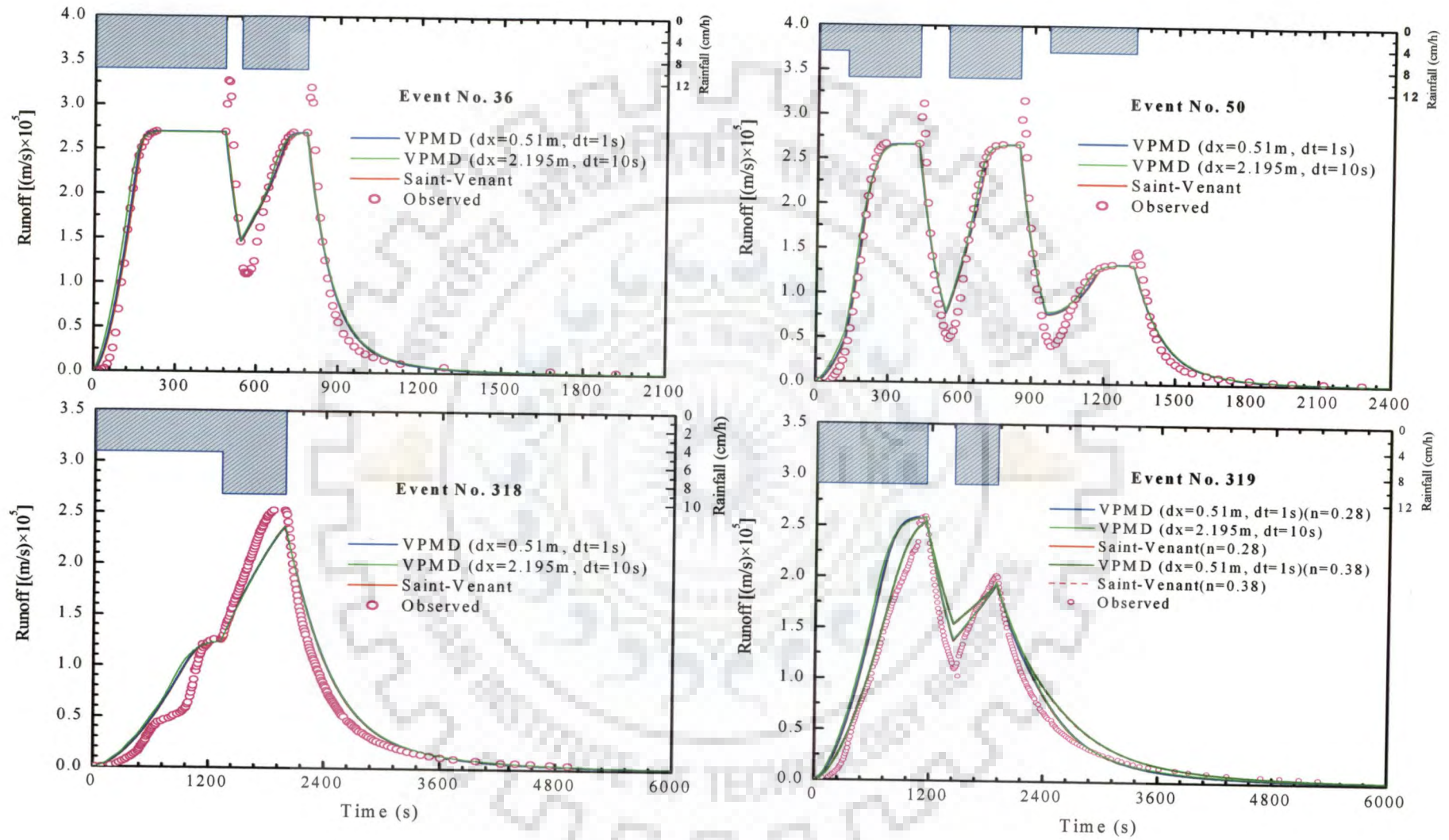
Figure 3.13 Izzard's experimental hydrographs and the corresponding simulated hydrographs of the VPMD and SVE methods.

Table 3.8 Verification of the VPMD method using Izzard data given in Table 3.7 (*Izzard*, 1942, 1944)

Event No.	Δx (m)	Δt (s)	Courant Number (C_{un})	Performance Evaluation Measures											VPMD		Saint-Venant	
				Comparison with Observed Data					Comparison with SVE Solution									
				η_q (%)	CRM (%)	CD	q_{perr} (%)	t_{perr} (min)	η_q (%)	CRM (%)	CD	q_{perr} (%)	t_{perr} (min)	EVOL (%)	CPU-time (s)	EVOL (%)	CPU-time (s)
34	0.51	1	0.42	96.14	-3.49	1.24	-0.04	1.88	99.97	-0.72	0.99	0.00	1.22	0.46	0.39	-0.25	3.75
	2.20	5	0.48	94.99	-6.24	1.24	-0.04	3.33	99.77	-2.61	0.99	0.00	2.67	2.34	0.16		
35	0.51	1	0.42	95.05	-6.38	1.30	0.01	2.05	99.99	-0.24	1.00	0.00	0.72	-0.06	0.41	-0.29	2.14
	2.20	10	0.95	93.15	-9.56	1.33	0.01	5.17	99.89	-1.37	1.01	0.00	3.83	1.07	0.14		
36	0.51	1	0.42	94.07	-3.41	1.26	-0.04	2.02	99.98	-0.48	1.00	0.00	1.43	0.26	0.39	-0.21	2.06
	2.20	10	0.96	92.43	-7.38	1.24	-0.04	-0.17	99.64	-2.62	0.99	0.00	3.50	2.40	0.16		
50	0.51	1	0.42	95.36	-4.44	1.24	-0.08	2.23	99.98	-0.37	1.00	0.00	-6.60	0.12	0.45	-0.24	2.42
	2.20	10	0.96	94.33	-7.09	1.23	-0.09	2.33	99.76	-2.16	0.99	-0.01	-6.50	1.91	0.17		
301	0.51	1	0.09	89.52	-16.74	0.79	-1.56	-0.80	100.00	-0.41	1.00	0.02	5.20	0.20	2.11	-0.20	3.95
	2.20	10	0.20	87.17	-18.52	0.79	-1.57	-0.17	99.93	-2.06	0.99	0.01	5.83	1.85	0.67		
	0.51*	1	0.08	95.34	-12.29	0.93	-1.56	-0.17	100.00	-0.47	1.00	0.02	1.17	0.17	2.09	-0.30	3.45
302	0.51	1	0.07	97.03	-2.82	0.82	-0.98	-0.17	100.00	-0.41	1.00	0.02	3.50	0.20	2.31	-0.29	4.36
	2.20	10	0.15	96.97	-4.76	0.82	-1.03	-0.17	99.93	-2.27	0.99	-0.03	3.50	2.06	0.41		
318	0.51	1	0.08	93.02	-6.57	1.33	-6.32	2.00	100.00	-0.35	1.00	-0.18	0.00	0.20	2.41	-0.20	2.70
	2.20	10	0.19	92.53	-7.05	1.35	-6.34	2.00	99.96	-1.89	1.00	-0.20	0.00	1.75	0.41		
319	0.51	1	0.09	83.67	-16.87	0.81	-0.09	0.17	100.00	-0.51	0.99	0.05	0.00	0.39	2.58	-0.16	4.08
	2.20	10	0.20	80.51	-18.63	0.80	-0.43	0.17	99.91	-2.64	0.98	-0.29	0.00	2.53	0.42		
	0.51*	1	0.07	92.52	-12.30	0.95	-2.16	0.17	100.00	-0.58	0.99	0.18	0.00	0.40	2.47	-0.20	4.41

* The simulation using calibrated Manning's n for the event

finer grid sizes, $EVOL < 0.46$ (-0.06-0.46) %, indicates the good mass conservation ability of the method. The low performance of the VPMD method in simulating some of the events is not due to the inadequacy of the method, rather it is due to improper values of the roughness coefficients used for these events. This can be inferred from the simulation of events 319 and 301 where the use of optimum roughness values ($n = 0.38$ and 0.36) causes improvement in the model performances as indicated by the estimates of η_q which increases from 84.19 to 92.55 % for the event 319 and from 90.01 to 95.40 % for the event 301. Accordingly, other performance measures also show corresponding improvement. Thus, it can be inferred that the improper selection of the roughness coefficient also drastically affects the model performance rather than assigning the cause of poor performance to the computational grid size used in the simulation, as seen from Figure 3.13 (event 319). Besides, the comparison of the VPMD method solution with the numerical solution of the SVE also shows that $\eta_q \cong 100.0$ %, and $CD \cong 1.0$ for all the simulated events with CRM varying in the range of -0.27 to -3.37 %. The errors in the computed peak runoff and the time to peak are also almost negligible. These measures indicate that the VPMD method is able to produce the results as accurately as that of the SVE. However, the inability of both the methods to account for other factors influencing the runoff generation process in the experiments results in the inaccurate reproduction of the observed runoff hydrographs. The use of coarser temporal grid size causes lower solution performance and also affects the mass conserving ability of the VPMD method as can be seen from Table 3.8. The use of higher Δt causes the slight shifting of hydrograph toward the left, especially in the rising limb of the first hydrograph of the multi-peak hydrograph case as shown in Figure 3.13 (Events 36 and 50). However, the difference is very negligible and, hence, it is appropriate to conclude that the inaccuracy of the VPMD method solution caused due to the use of larger time interval can be improved with use of appropriate finer temporal grid size, though it does not significantly change the response of the catchment. Consequently, it is assumed that when $C_{un} \geq 1$, the accuracy of the solution scheme will be preserved. However, it is interesting to note that though the computed C_{un} for coarser grid size is close to 1 than those for the finer grid size, the use of finer grid size gives better accuracy than that of using the coarser grid size as shown in Table 3.8, specifically for the event numbers 35, 36 and 50. It clearly brings out that it is not necessary that the satisfaction of the criterion $C_{un} \approx 1$ preserves the accuracy of the scheme, unless and until the computational temporal grid size is appropriate. Therefore, the VPMD method, like

other numerical methods, is more sensitive to the use of computational temporal grid size than the spatial grid size. The CPU-run time efficiency is dependent on the grid size, as a very finer grid size causes a larger run time but it can be improved by the use of appropriate larger grid size as shown in Table 3.8.

3.11 FIELD VERIFICATION USING WONG'S EXPERIMENTAL DATA

The data of ten natural rainfall-runoff events which occurred over the outdoor experimental laboratory facility, developed by *Wong* and his co-workers at the Nanyang Technological University, Singapore, during the period between October 2002 and December 2002 [*Wong and Lim*, 2006; *Wong*, 2009] were used for studying the proposed VPMD overland flow method. This facility consists of asphalt and concrete overland flow planes, and a concrete level V-catchment as shown in Figure 3.14. Their experimental plot consists of four testing bays and one collection chamber. The two bays were prepared with asphalt surface and the other two were prepared with concrete surface. The dimensions of the bays were 25 m long by 1 m wide. The asphalt plane and concrete plane were developed with a slope of 2% surrounded by a 1 m high concrete wall along the length and at the upstream end of the section. Each event of the natural rainfall studied herein was recorded by using the tipping bucket raingauges located at 6.25 m from each ends of the bays. The weigh tanks which placed at the end of experimental bays were properly calibrated to enable the recording of outflow runoff discharge, using an electromagnetic flow meter. The rainfall and runoff data from the ten storms occurring over theses experimental plot were logged at every 15 s. These ten events consists of a variety of runoff hydrographs, such as hydrographs with one major peak (Events 7 and 9), hydrographs with two major peaks with a higher first peak (Events 3 and 5), hydrographs with two major peaks with a second higher peak (Events 1 and 2), and hydrographs with multiple peaks (Events 4, 6, 8 and 10).

According to *Wong and Lim* [2006], there was always some time lag between the commencement of rainfall and the corresponding runoff. It was also reported by *Wong and Lim* [2006] that prior to the experiments the plots were dry, and, hence, some quantity of rain got lost due interception by the planes, channel and side walls between the commencements of rain and runoff which may be referred as "initial loss". The quantity of water intercepted in this manner ranged from 0.30 to 5.49 mm which may be attributed to the antecedent meteorological conditions and rainfall pattern [*Wong*, 2008]. *Wong and Lim* [2006] had attempted to account for this interception loss with the use of four kinds of loss models which are generally preferred in practice [*Pilgrim and Cordery*, 1993]. These loss models are (1) the proportional loss model; (2) the initial and proportional loss model; (3)
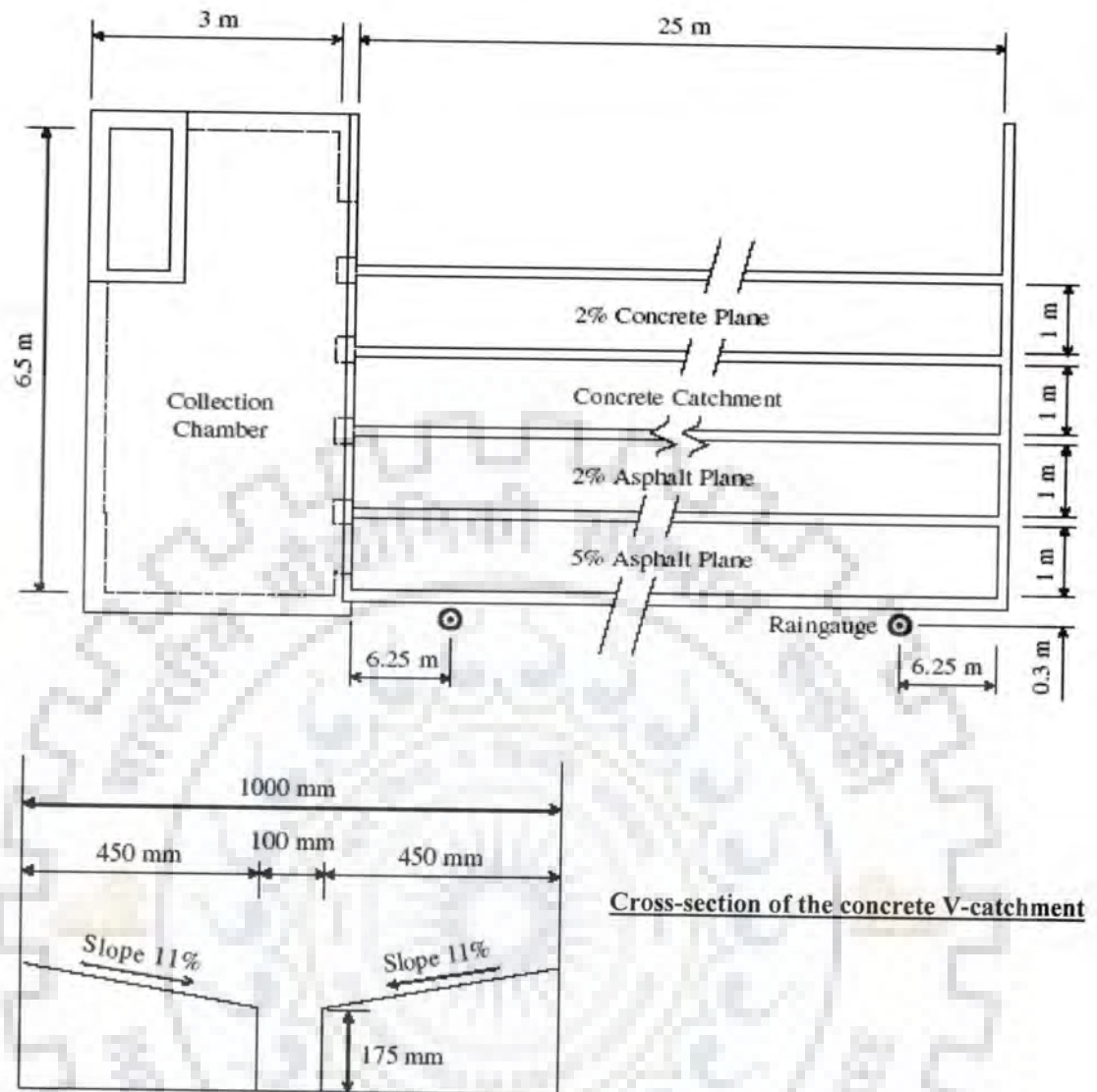
Figure 3.14 Plan view of experimental facility [After *Wong and Lim*, 2006].

the upperbound loss model which is termed as ϕ-*index* loss model and (4) the initial and upperbound loss model. However, they found that the ϕ-*index* loss model is accurate as well as simple to use due to the requirement of calibration of only one parameter. Therefore, it was decided to couple this model with the VPMD model frame-work to account for the interception loss *i.e* I_a in equation (3.3). The expression for the runoff causing rainfall considering the ϕ-*index* infiltration type interception loss model can be written as [*Wong*, 2008]

$$\sum (r - I_a) \times (\Delta t / 60.0) = R_d \qquad (3.84)$$

where, R_d is the accumulated runoff depth expressed in cm. *Wong and Lim* [2006] considered the rainfall, r and interception loss, I_a in cm/h. The temporal grid size Δt was

expressed in minutes. Further, for periods when $r < I_a$, $(r - I_a) = 0$. Note that, henceforth, the notation I_a is termed as ϕ-*index* as it has similar connotation as infiltration loss with nearly uniform interception of the rainfall by the bay boundary wall and the initial wetting of the dry surface. It was noted from the considered events that the interception loss was varying from event to event and it was very difficult to account for the initial losses accurately in advance, although the physical specifications of the catchments are primarily known. *Chua et al.* [2008] carried out the impact of using the same index for all the events. However, the purpose of the present study is to examine how accurately the VPMD method can simulate the observed hydrographs of the *Wong and Lim* [2006] and, hence, the ϕ-index computed separately for each of the events is directly used in this study.

3.11.1 Results of Asphalt Plane Study

The rainfall-runoff data observed for the asphalt plane is summarized in Table 3.9 with similar ϕ-index values as reported by *Chua et al.* [2008]. It can be inferred from Table 3.9 that the ϕ-index is highly variable among the events with the high intensity rainfall of short duration causing a high interception loss rate. Further, the period without rainfall between two storm events also have impact on the ϕ-index as it can be seen that for the rainfall occurring within the same week as in the case of event 2, the estimated interception loss is less than that of the event 1. Similar is the case for event 7 wherein a very small interception ϕ-index was noted as this event was preceded by a previous day rainfall. Therefore, it can be surmised that the antecedent rainfall condition plays an important role in the interception loss rate to be used in the computations.

In the present study, the chosen $\Delta x = 0.5$ m and $\Delta t = 3$ s were used in the simulation of all the events, though it was found that the use of higher spatial and temporal grid sizes was possible without causing any significant accuracy problem. The numerical solutions of the SVE were obtained with the use of $\Delta x = 1.0$ m and $\Delta t = 0.125$ s for the events 1 to 4 and 0.5 s for the events 5 to 10. *Wong* [2008] used a value of the Manning's $n = 0.013$ with the consideration of only wet portion of the events and the same value has been adopted in the present investigation for events over the asphalt plane. This selected value of n falls well within the recommended value by *Engman* [1986]. The variation range of the computed minimum magnitude applicability criteria are $k_{min} = 66.51 - 142.32$, $\left| kF_{rp}^2 \right|_{min} = 126.39 - 223.80$ and $(F_{rp})_{min} = 1.25 - 1.38$. It may be inferred from the $(F_{rp})_{min}$ values that the flow generated in all the experiments were supercritical and the flow regimes are well within the KW applicability limits.

Table 3.9 Details of the rainfall-runoff events studied by *Wong* [2009] over the asphalt plane

Event	Date	Duration	ϕ-Index	Rainfall			Runoff			Remark
				Peak Intensity	Average Intensity	Total Depth	Peak Flow	Average Flow	Total Depth	
		(min)	(cm/h)	(cm/h)	(cm/h)	(cm)	(L/s)	(L/s)	(cm)	
1	6-Oct-02	40	0.583	14.400	3.340	2.227	0.670	0.197	1.900	Double peak
2	14-Oct-02	80	0.265	14.400	1.992	2.656	0.824	0.125	2.412	Double peak
3	27-Oct-02	40	0.988	21.600	4.317	2.878	0.973	0.263	2.541	Double peak
4	3-Nov-02	120	0.187	14.400	1.750	3.500	0.816	0.112	3.230	Multiple peak
5	13-Nov-02	30	0.628	14.400	3.260	1.630	0.590	0.185	1.341	Double peak
6	17-Nov-02	100	0.271	14.400	2.574	4.289	0.760	0.164	3.953	Multiple peak
7	18-Nov-02	120	0.021	9.600	0.840	1.681	0.528	0.057	1.640	Single peak
8	22-Nov-02	90	0.080	12.000	1.905	2.857	0.655	0.126	2.738	Multiple peak
9	5-Dec-02	100	0.146	14.400	1.656	2.760	0.883	0.106	2.553	Single peak
10	7-Dec-02	100	0.174	7.200	1.193	1.988	0.342	0.074	1.772	Multiple peak

The simulated runoff hydrographs of the typical events of the Wong's experimental study using the VPMD method are shown in Figure 3.15. It can be seen that the simulated hydrographs are well in agreement with the observed hydrographs of complex natural rainfall patterns. Furthermore, the perfect match between the solutions of that VPMD and the numerical solution of the SVE can be observed in all these figures. It is apparent from Figure 3.15 (event 1, 4 and 5) that during the initial portion of the event, the simulated hydrographs overestimate the observed hydrographs. Such a discrepancy in hydrograph simulations may be attributed to the inappropriate accounting of the actual interception loss rate which is initially higher than that considered by the loss model. However, in case of event 9, the rainfall intensity was small nearly equal to the considered interception loss during initial period of the event and, hence, there is not much discrepancy visible between the simulated and observed runoff hydrographs. The simulated results for all the ten events can also be verified with the performance evaluation criteria estimated as given in Table 3.10 by comparing the VPMD method results with the observed hydrographs and with the corresponding SVE solutions for the considered grid sizes along with the estimated c_{max} values and the Courant numbers (C_{un}). It can be seen that the Nash-Sutcliffe efficiency (η_q) for each of the event is always higher than 95.0%, except for the events 5 and 10, for which the estimated η_q values are 92.96% and 90.18%, respectively. The lower η_q for the event 5, may be attributed to the assigning of inappropriate interception loss which is less at the beginning of rainfall event and is higher at the later part of the event as revealed by the simulated hydrograph which over-estimates the earlier peak and under estimates the later peaks. Similarly, in case of event 10 associated with multiple storms which are sufficiently isolated and also have a lower peak discharge, the same reasoning as assigned for event 5 may be attributed. Thus, it can be surmised that even if accurate loss is known in all these events, the accurate distribution of the same is also equally important. Thus, the use of higher interception ϕ-index during the initial period of the rainfall event rather than uniform rate would lead to minimization of such discrepancies in the overall hydrograph simulation. The Nash-Sutcliffe efficiency (η_q) estimates for all the simulated events by the VPMD method and those obtained by *Chua et al.* [2008] based on KW model are expected to be nearly same. But this study results are slightly better, as *Chua et al.* [2008] have used Manning's $n = 0.011$ which is a lower estimate than that used in the present investigation. Furthermore, the computed coefficient of determination (CD) values for all the events are close to 1, except for the events 5 and 10, which demonstrate the robust performance of the proposed method.
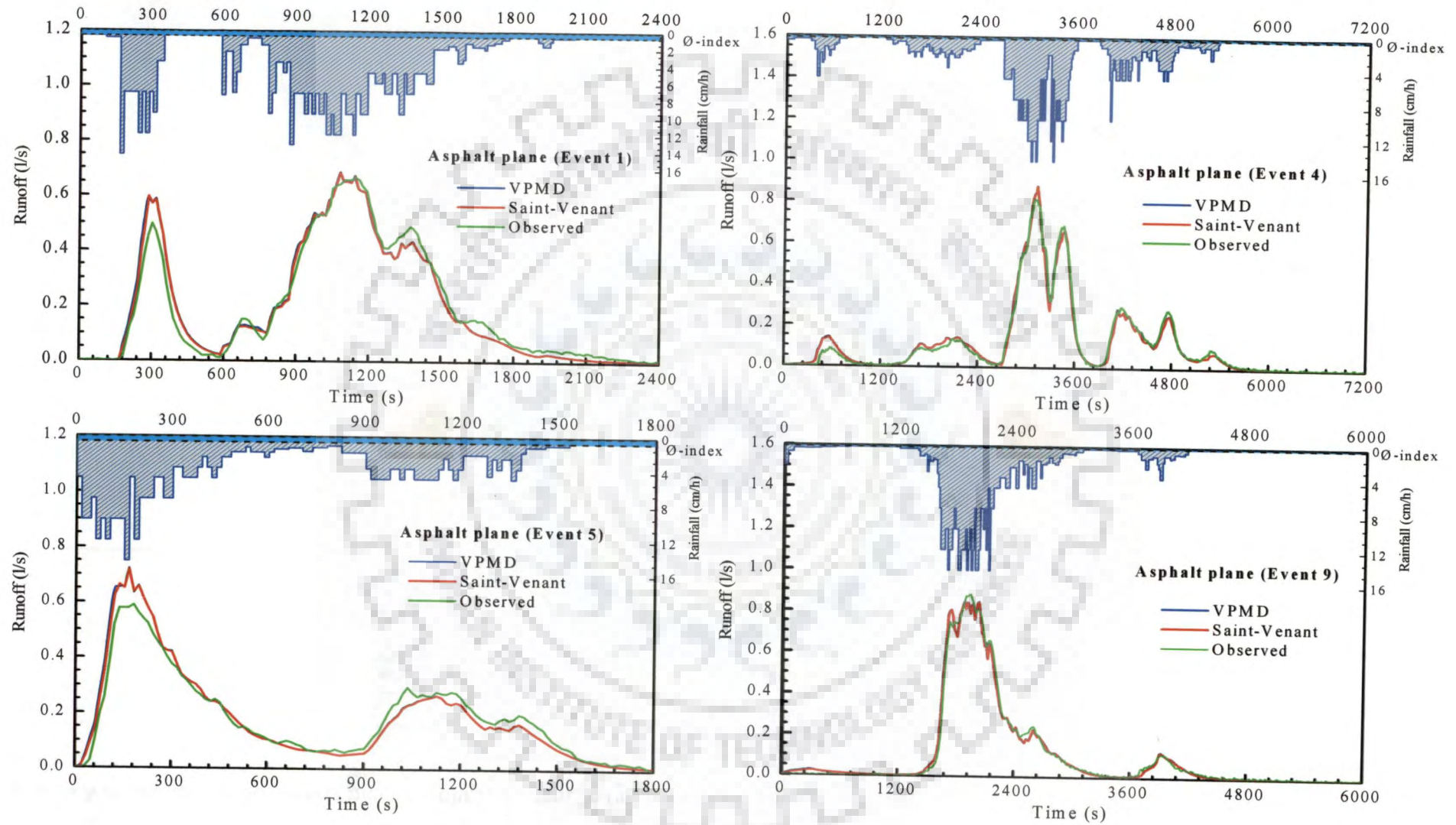
Figure 3.15 Typical experimental study hydrographs of *Wong* [2009] over the asphalt plane and the corresponding simulations by the VPMD and SVE methods

Table 3.10 Verification of the VPMD method solutions using Wong's rainfall-runoff events over the asphalt plane and with the corresponding SVE solutions

| Event | $\dfrac{\Delta x}{\Delta t}$ (m/s) | c_{max} (m/s) | Courant Number (C_{un}) | Performance Evaluation Measures | | | | | | | | | | VPMD | | Saint-Venant | |
| | | | | Comparison with the Observed Data | | | | | Comparison with the SVE Solution | | | | | | | | |
				η_q (%)	CRM (%)	CD	q_{perr} (%)	t_{perr} (min)	η_q (%)	CRM (%)	CD	q_{perr} (%)	t_{perr} (min)	EVOL (%)	CPU-time (s)	EVOL (%)	CPU-time (s)
1	0.17	0.38	2.27	96.83	-0.69	0.95	2.67	-1.00	99.92	-1.02	0.99	0.20	0.00	1.02	1.02	-0.01	3.30
2	0.17	0.40	2.42	98.56	-0.60	1.00	-1.29	0.00	99.99	-0.63	0.99	0.37	0.00	0.62	1.31	-0.04	3.88
3	0.17	0.45	2.71	99.19	-0.69	0.98	10.47	-0.05	99.96	-0.71	0.99	2.75	-0.05	0.69	1.19	-0.03	3.98
4	0.17	0.42	2.50	98.76	-0.42	1.03	7.78	0.50	99.99	-0.43	0.99	0.17	0.00	0.42	1.38	-0.03	4.38
5	0.17	0.39	2.31	92.96	-0.23	0.75	22.51	-0.25	99.93	-0.88	0.98	0.46	0.00	0.87	0.91	-0.02	2.24
6	0.17	0.39	2.37	96.01	-0.36	0.91	0.89	-0.50	99.98	-0.37	0.99	0.20	0.00	0.36	1.18	-0.01	2.03
7	0.17	0.35	2.08	98.84	-0.16	0.96	5.05	0.00	100.00	-0.26	1.00	0.19	0.00	0.26	1.44	-0.02	2.00
8	0.17	0.36	2.17	95.57	-0.34	1.00	-6.22	0.00	99.98	-0.44	0.99	0.01	0.00	0.43	1.38	-0.01	1.95
9	0.17	0.41	2.46	99.20	-0.37	1.03	-3.82	-1.00	100.00	-0.38	1.00	0.01	0.00	0.37	1.38	-0.02	4.11
10	0.17	0.31	1.85	90.18	-0.43	0.85	21.35	-37.75	99.98	-0.45	0.99	0.77	0.00	0.45	1.22	-0.01	3.38

The CRM and EVOL are less than 1%, demonstrating the mass conservation ability of the method. It is interesting to note that the efficient mass conservative method not necessarily mean that the simulation results will be accurate, as it can be verified from the results of events 5 and 10 as the volume conservation deals with integrated water depth of rainfall and loss but not their distribution within the simulation period. The performance measures estimated for the VPMD method solutions in comparison with the numerical solution of the SVE elucidate that there is perfect match between both the solutions for all the events. The Courant numbers estimated for all these simulations always remained in the range 1.85 – 2.71, defying the required Courant number condition of $C_{un} \approx 1$ as used in the HEC-HMS model.

3.11.2 Results for the Concrete Plane

The evaluation of the VPMD method was further carried out by comparing the simulated runoff hydrographs with the observed overland flow hydrographs of the concrete plane as summarized in Table 3.11. Following the study of *Wong* [2008], the same Manning's roughness coefficient $n = 0.010$ was used in these simulations. Same computational grid sizes of $\Delta x = 0.5$ m and $\Delta t = 3$ s as used for the asphalt plane were used herein for the simulation of rainfall-runoff events. The variation range of the minimum computed applicability criteria are $k_{min} = 45.99 – 94.22$, $\left[kF_{rp}^{2} \right]_{min} = 142.21 – 243.45$ and $(F_{rp})_{min} = 1.61 – 1.76$. It may be surmised from these results that the flows are supercritical and flow regimes are well within the KW applicability range. The simulation results for typical events are shown in Figure 3.16. It can be inferred from these figures that the simulated runoff hydrographs are well in agreement with the observed hydrograph and perfectly coincide with the numerical solutions of the SVE. Table 3.12 shows the modelling accuracy as well as the mass conservation ability of the proposed method. Further, similar conclusions as arrived for the runoff simulation over the asphalt plane using the VPMD method can be arrived at for the runoff simulations over this concrete plane also. In this case also the Courant number was varying between 2.28 – 3.26, without causing any significant inaccuracy in the solution for deviating from the condition of $C_{un} = 1$ as recommended in HEC-HMS model.

Table 3.11 Details of rainfall-runoff events studied by *Wong* [2009] over the concrete plane

Event	Date	Duration	φ-Index	Rainfall			Runoff			Remark
				Peak Intensity	Average Intensity	Total Depth	Peak Flow	Average Flow	Total Depth	
		(min)	(cm/h)	(cm/h)	(cm/h)	(cm)	(L/s)	(L/s)	(cm)	
1	6-Oct-02	40	0.635	14.400	3.340	2.227	0.641	0.194	1.877	Double peak
2	14-Oct-02	80	0.481	14.400	1.992	2.656	0.758	0.118	2.269	Double peak
3	27-Oct-02	40	1.675	21.600	4.317	2.878	0.912	0.241	2.329	Double peak
4	3-Nov-02	120	0.348	14.400	1.750	3.500	0.745	0.105	3.024	Multiple peak
5	13-Nov-02	30	0.673	14.400	3.260	1.630	0.601	0.182	1.322	Double peak
6	17-Nov-02	100	0.398	14.400	2.574	4.289	0.730	0.158	3.807	Multiple peak
7	18-Nov-02	120	0.065	9.600	0.840	1.681	0.495	0.054	1.572	Single peak
8	22-Nov-02	90	0.182	12.000	1.905	2.857	0.601	0.121	2.624	Multiple peak
9	5-Dec-02	100	0.051	14.400	1.656	2.760	0.832	0.111	2.676	Single peak
10	7-Dec-02	100	0.152	7.200	1.193	1.988	0.352	0.075	1.796	Multiple peak
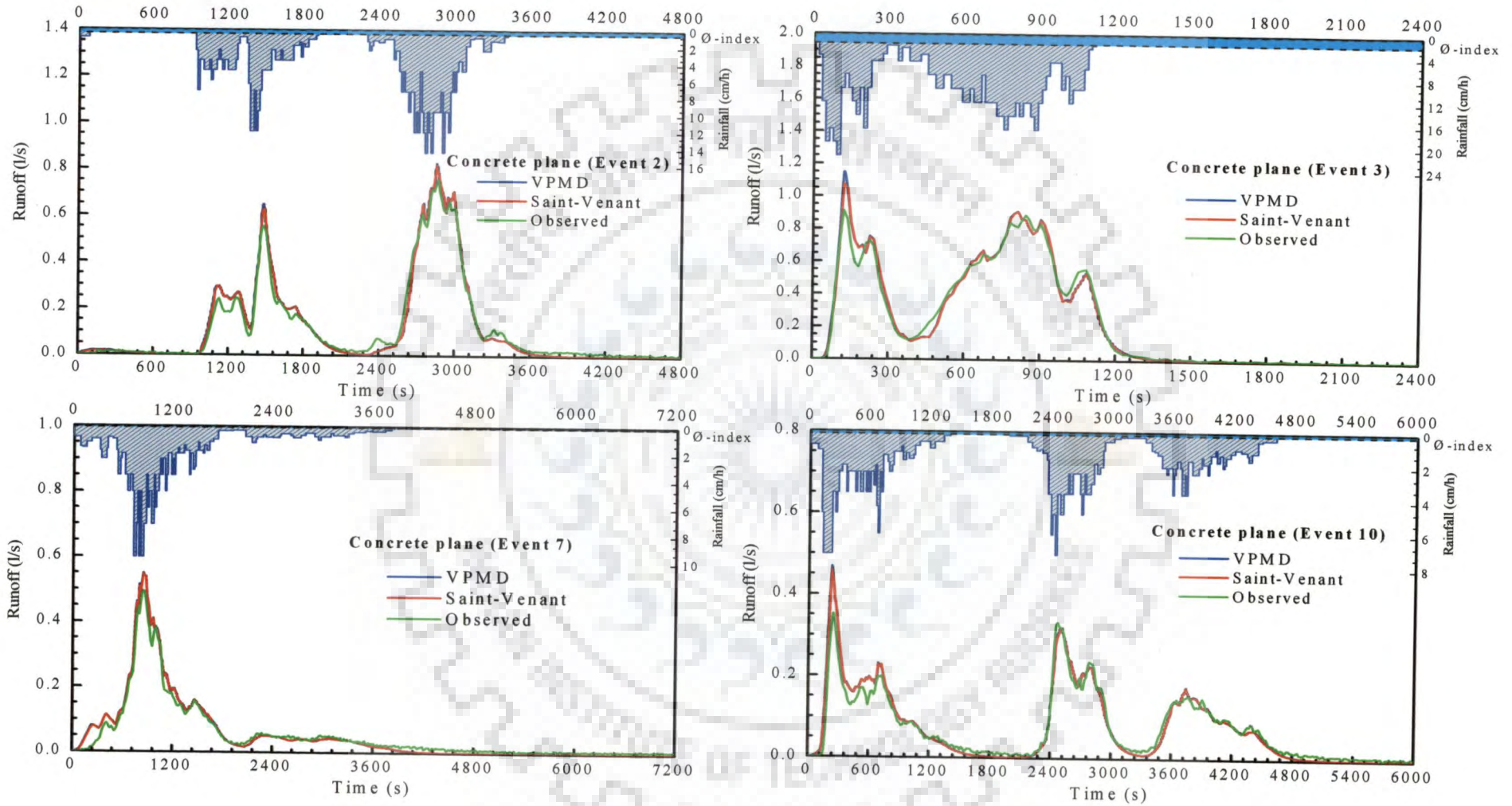
Figure 3.16 Typical experimental study hydrographs of Wong over the concrete plane and the corresponding simulations by the VPMD and SVE methods.

Table 3.12 Verification of the VPMD method using Wong's rainfall-runoff events over concrete plane and with the corresponding SVE solutions

Event	$\dfrac{\Delta x}{\Delta t}$ (m/s)	c_{max} (m/s)	Courant Number (C_{un})	Performance Evaluation Measures													
				Comparison with the Observed Data					Comparison with the SVE Solution					VPMD		Saint-Venant	
				η_q (%)	CRM (%)	CD	q_{perr} (%)	t_{perr} (min)	η_q (%)	CRM (%)	CD	q_{perr} (%)	t_{perr} (min)	EVOL (%)	CPU-time (s)	EVOL (%)	CPU-time (s)
1	0.17	0.45	2.68	93.05	-0.92	0.81	9.92	0.50	99.94	-1.07	0.99	0.44	0.00	1.08	1.95	-0.03	3.24
2	0.17	0.48	2.86	97.81	-0.70	0.87	9.34	-0.25	99.98	-0.69	0.99	0.76	0.00	0.68	1.30	-0.03	3.30
3	0.17	0.54	3.26	98.11	-0.83	0.91	25.96	0.00	99.93	-0.82	0.99	6.83	0.00	0.79	1.16	-0.03	2.91
4	0.17	0.49	2.92	98.08	-0.53	0.84	17.06	0.50	99.99	-0.52	0.99	0.26	0.00	0.51	1.41	-0.02	3.44
5	0.17	0.45	2.71	93.21	-0.40	0.72	20.61	0.00	99.93	-0.87	0.98	0.42	0.00	0.86	0.88	-0.02	1.97
6	0.17	0.46	2.77	97.12	-0.43	0.84	5.03	-0.50	99.97	-0.43	0.99	0.41	-0.50	0.42	1.45	-0.01	2.22
7	0.17	0.40	2.42	96.33	-0.30	0.78	11.18	0.00	100.00	-0.28	1.00	0.33	0.00	0.28	1.38	-0.03	3.24
8	0.17	0.42	2.53	96.97	-0.48	0.86	1.79	0.00	99.98	-0.48	0.99	0.13	0.00	0.46	1.30	-0.03	3.38
9	0.17	0.49	2.91	98.89	-0.32	0.89	4.37	-0.55	100.00	-0.36	1.00	0.19	-0.05	0.35	1.39	-0.03	2.95
10	0.17	0.38	2.28	93.34	-0.41	0.77	33.21	-0.25	99.98	-0.42	0.99	1.87	0.00	0.42	1.36	-0.03	3.22

3.12   RUNOFF ROUTING ON THE V-CATCHMENT

The capability and robustness of the proposed VPMD method for routing runoff on the overland flow plane as well as in the channel were further investigated by comparing the simulated runoff hydrographs arrived at the end of the channel in the level V-catchment with the corresponding hydrographs of other solution methods, including the runoff hydrographs of *Wong and Lim* [2006].

3.12.1 Synthetic Example

The overland flow coupled with rectangular channel routing is verified using the rainfall-runoff example of *DiGiammarco et al.* [1996] on level V-catchment. The schematic presentation of the V-Catchment is shown in Figure 3.17. The simulation is conducted with
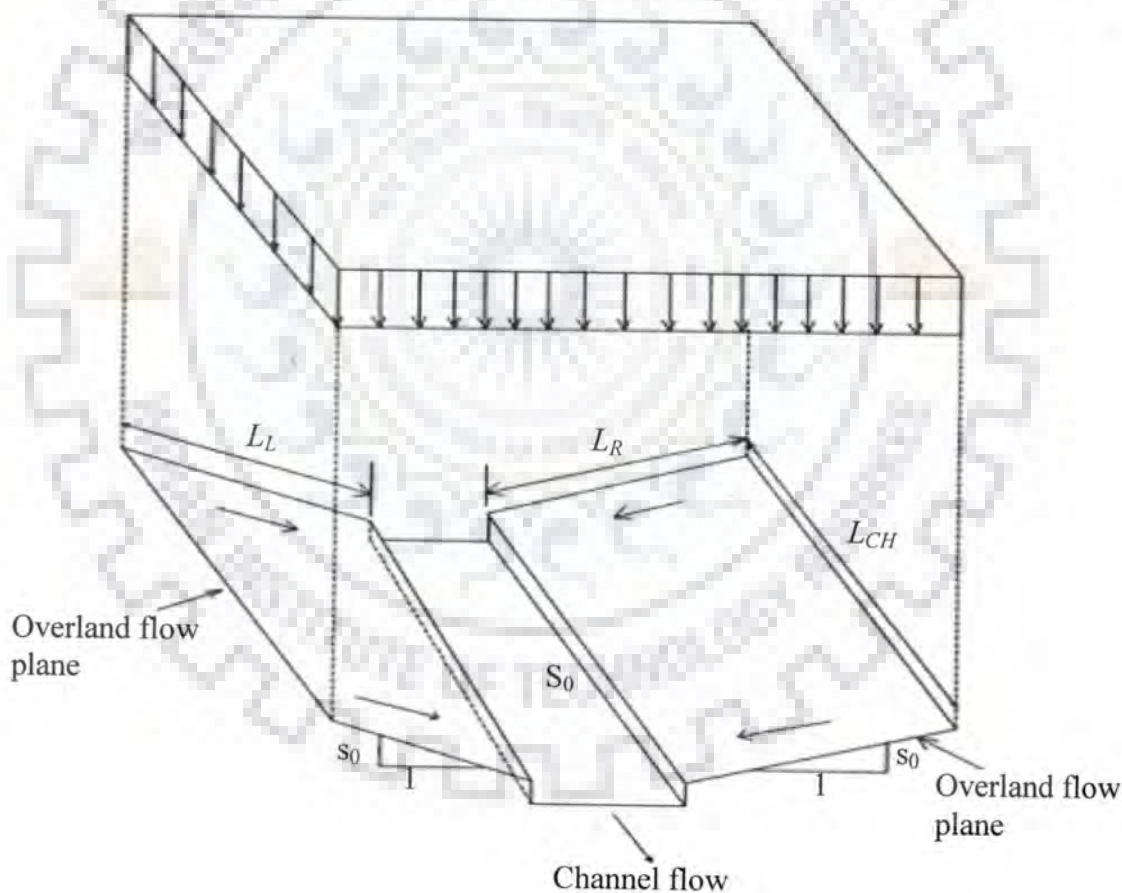
Figure 3.17 Schematic presentation of the level V-catchment.

a constant rainfall intensity $r = 1.08$ cm/h for a duration $t_r = 90.0$ min occurring over an impervious surfaces. The symmetric V-catchment consists of two planes, with sizes 800 m (L_R and L_L) × 1000 m width, which are connected to a channel having a length of 1000 m

(L_{CH}) and 20 m width in a middle of the catchment. The longitudinal slope of the channel is 0.02. Both overland flow planes are flat and inclined perpendicular towards channel with a slope of 0.05. The applied Manning's roughness coefficient are $n = 0.015$ for the overland flow plane and $n_c = 0.15$ for the channel as given by *DiGiammarco et al.* [1996], although unrealistic in natural conditions. The overland flow planes and channel are considered initially dry. Further, it is assumed that the precipitation falling on the channel is not affecting the flow characteristics.

The runoff hydrograph estimated by the VPMD method at the outlet of the level V-catchment in response to the semi-infinite spatially uniform constant rainfall intensity applied over the entire V-catchment was also compared with the corresponding runoff hydrograph arrived at as a semi-analytical solution of the KW model presented by *Overton and Brakensiek* [1973]. The simulated runoff hydrograph at the valley side is also compared with the published results for several solution approaches presented by *DiGiammarco et al.* [1996]. Besides, the comparison is also made with the numerical solution of the SVE for overland flow plane. Similarly, the VPMD method simulated runoff hydrograph at the outlet of the channel is also compared with the corresponding simulated hydrograph obtained using the HEC-HMS model [*USACE*, 2006] and with various other solutions presented by *DiGiammarco et al.* [1996]. These other solutions include the methods based on the control volume finite element (CVFE) method applied to the DW solution, the classical integrated finite difference (IFD) method and that of the SHE model developed based on conventional finite difference scheme [*Bathurst*, 1986]. The HEC-HMS model [*USACE*, 2006] solves the KW equations using the finite difference scheme. The runoff hydrograph at the outlet of the valley side of the overland flow plane having a dimension 800m × 100 m is estimated using the VPMD method to facilitate its comparison with the various solutions presented by *DiGiammarco et al.* [1996]. Consequently, the overland flow plane is divided into 8, 80, 800 and 4000 sub-reaches, while the channel is divided into 10, 99 (maximum sub-reaches division allowable in the HEC-HMS model), 1000 and 5000 sub-reaches. The simulations were made using four Δt values 10 s, 60 s, 120 s and 180 s to examine the impacts of the spatial and temporal grid sizes on the accuracy of the solution. It was found that the selected smaller or larger spatial grid sizes do not have significant impact on the accuracy of the model. However, inaccuracy is introduced in the solution when $\Delta t > 60$ s in a manner similar to the results shown in Figure 3.10, in terms of shifting of the rising limb of the hydrograph towards the left of the benchmark solution without

making much influence on the recession limb. This shifting is directly proportional to the increase in Δt as inferred earlier while discussing the results shown in Figure 3.10. The numerical solution of the SVE using the explicit numerical scheme for the plane requires the use of $\Delta x \geq 5$ m in order to avoid convergence problem.

The simulated runoff hydrograph and the corresponding flow depth hydrograph estimated at the outlet of the valley side and its comparison with other approaches solutions are shown in Figure 3.18 (a and, c). Figure 3.18 (a) elucidate that the VPMD method solution has a good agreement with the other methods used for the comparison. Further, it is interesting to note that the analytically obtained applicability criteria for the plane are $k = 1912.34$, $k(F_{rp})_e^2 = 7550.38$ and $(F_{rp})_e = 1.98$, while that obtained by the VPMD method are $k = 1914.48$, $kF_{rp}^2 = 7550.18$ and $F_{rp} = 1.985$. Attention is drawn to the estimated magnitude of the Froude number $F_{rp} > 1.5$, resulting in supercritical flow state. Therefore, careful observation of Figure 3.18 (a) shows periodic pulsating waves motion on the rising and recession limb of the hydrograph. This phenomenon is due to the formation of roll waves [*Iwasa*, 1954; *Jolly and Yevjevich*, 1971; *Ponce* 1991; *Perumal*, 1992; *Liu et al.*, 2005; *Zanuttigh and Lamberti*, 2007]. This might be the possible reason, which leads to the "overshoot" of the CVFE and IFD methods solutions during the rising limb of the overland flow hydrograph [Figure 3.18 (a)]. Furthermore, it can be seen from the results of using the Quadratic Petrov-Galerkin scheme for the KW model [*Carpena et al.*, 1993] and the PIHM model which used the finite volume method (FVM) [see *Qu*, 2005] that such a tendency of overshooting can be observed, especially when $F_{rp} > 1.5$. Consequently, for such a situation $\theta > 0.5$, this leads to the amplification of flow. As shown in Figure 3.18(b) that the use of inertial terms in the solution of the VPMD method resulted in the estimated $\theta > 0.5$, at different locations along the flow path except at the end of 2nd sub-reach. However, ignoring the inertial term in the runoff hydrograph simulation by the VPMD method resulted in $\theta < 0.5$. Even then no any significant difference can be seen on the simulated runoff hydrograph at the end of overland flow plane due to the reason that the flow characteristics are not much dynamic to induce significant wave amplification, even though $(F_{rp})_e$ is still close to 1.5. Indeed, in the supercritical regime of the overland flow, the inertial terms become dominant over the longitudinal slope gradient $\partial y / \partial x$ and, hence, accounting the inertial term will enable one to handle the flow situation wherein the possibility of roll wave formation exists. Thus, it can be inferred from this discussion that even the higher values of Froude number
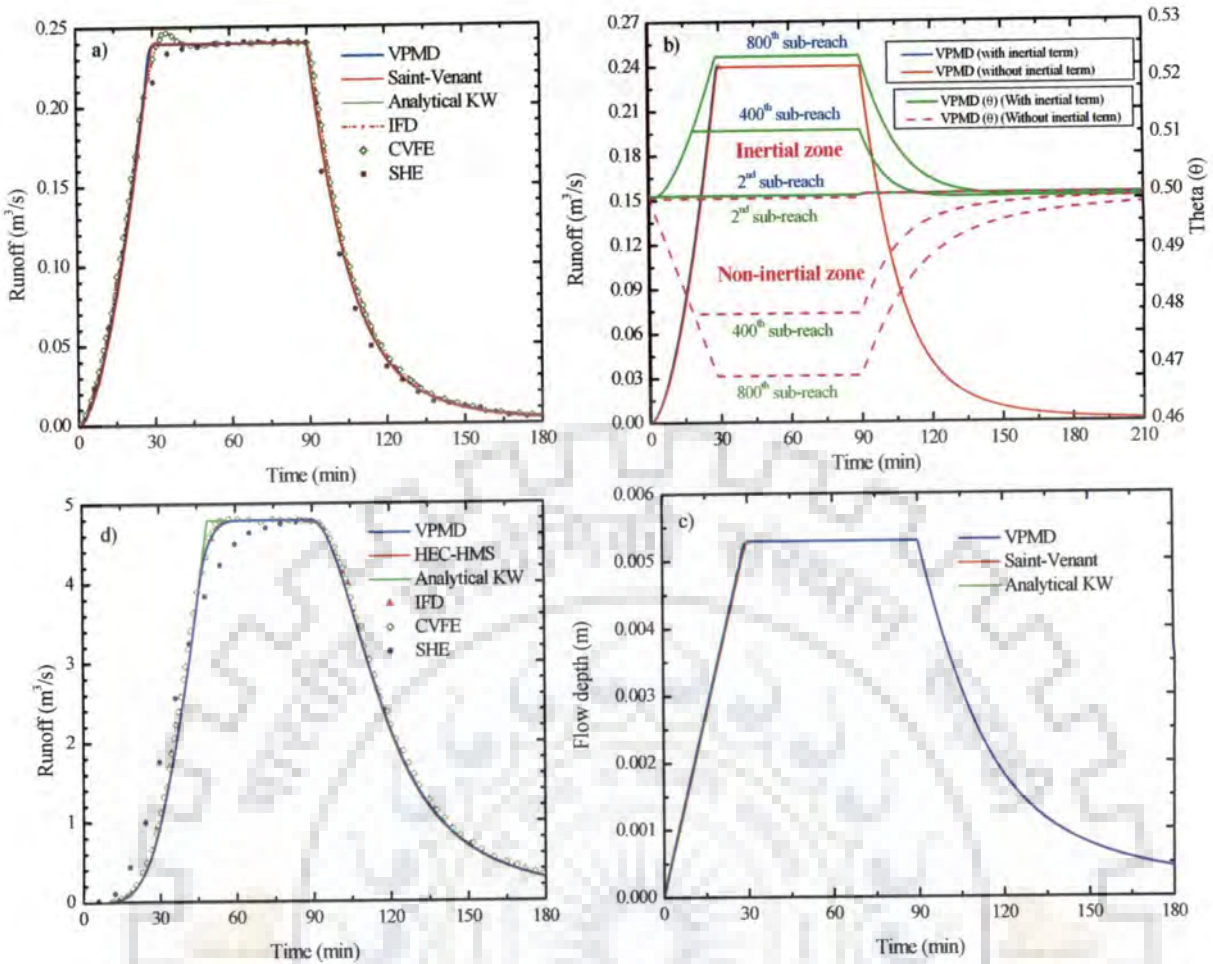
Figure 3.18 Comparison of the VPMD method simulated runoff hydrographs (a) at the outlet of the valley side (b) at the outlet of the valley side showing the effect of inclusion and exclusion of the inertial terms along with the temporal variation of θ at different locations of the overland flow plane (c) simulated flow depth hydrographs at the outlet of valley side (d) runoff hydrograph at the outlet of the level V-catchment (recession simulations not available for both the analytical method and the SHE model). Number of sub-reaches used for the plane and the channel are 80 and 99 (except in Figure 3.18b), respectively, and for $\Delta t = 10s$.

do not make any significant difference between the estimated θ values and, thus, on the simulated hydrographs by accounting or ignoring the inertial terms in equation (3.24), provided that the Vedernikov number $V_{vn} < 1$, where V_{vn} is ratio of the relative celerity of kinematic waves to the relative celerity of dynamic waves. This inference is also true in case of the effect of θ due to inclusion or exclusion of the inertial terms on the simulated hydrographs as depicted in Figure 3.8. Therefore, *Ponce's* [1991] viewpoint that the

Vedernikov number has a significant role for extending the hydraulic diffusivity to the realm dynamic waves is not correct. However, accounting of the inertial terms in equation (3.24) yields $\theta > 0.5$ when $F_{rp} > 1.5$ for which $V_{vn} > 1$ [*Ponce*, 1991; *Perumal*, 1992]. This condition results in the amplification of the flood waves or formation of the roll waves. This confirms that the Vedernikov number and Craya's criteria [*Craya*, 1952] are one and the same [*Jolly and Yevjevich*, 1971; *Ponce*, 1991]. Therefore, it is surmised that the Vedernikov number only serves the purpose as an criterion to detect the formation of roll waves in gradually varied flow conditions as in the case of overland flow modelling after the time of equilibrium is reached at any location in the plane.

The runoff hydrograph estimated at the outlet of the V-catchment [Figure 3.18 (d)] using the VPMD method clearly shows that the VPMD method has a very good agreement with CVFE, IFD and HEC-HMS model results. Note that the same spatial grid size used as in the VPMD method solution is also used for the HEC-HMS model. The estimated applicability criteria by the VPMD method for the channel are $k = 686.42$, $kF_{rp}^2 = 44.57$ and $F_{rp} = 0.25$. As the estimated Froude number $F_{rp} < 1$ and, hence, the estimated hydrograph by the VPMD method is smooth. Also, CVEF and IFD methods solution do not show overshooting as in case of the corresponding overland flow plane hydrographs. The other performance measures $\eta_q = 100$ %, $CRM = -0.42$ %, $CD = 1.0$, $q_{perr} = -0.0002$ % and the $t_{perr} = 1.17$ min when compared with the simulated runoff hydrograph obtained using the HEC-HMS model.

3.12.2 Verification with Wong's Experimental V-Catchment Results

The VPMD method was also used to simulate the V-catchment experimental results of *Wong* [2009]. The runoff data was observed at the channel outlet of the 25 m² area of the experimental concrete V-catchment (25 m long and 1 m wide) subjected to natural rainfall. The concrete catchment comprises of two identical planes draining into a centrally placed rectangular channel as shown in Figure 3.14. Each plane is 25 m wide and 0.45 m long with a slope of 11% towards the channel. The rectangular channel is 0.1 m wide and 0.175 m deep with a bed slope of 2%. The Manning's roughness coefficient adopted is 0.015 both for the overland flow planes and the channel as no observed overland runoff hydrographs were available at the outlet of the overland flow plane where the flow is contributed to the channel. The present experimental study uses the natural rainfall data which is the basic difference in comparison with all the previously studied experimental results wherein the

laboratory simulated rainfall was applied. The rainfall-runoff data was recorded at 15 s (0.25 min) interval. Data for ten storm events were obtained for the period between October 2002 to December 2002. A summary of the ten events is provided in Table 3.13.

Table 3.13 Details of rainfall-runoff events studied by *Wong* [2009] over the concrete V-catchment

Event	Date	Duration	ϕ-Index	Rainfall			Runoff from the Concrete Catchment			Remark
				Peak Intensity	Average Intensity	Total Depth	Peak Flow	Average Flow	Total Depth	
		(min)	(cm/h)	(cm/h)	(cm/h)	(cm)	(L/s)	(L/s)	(cm)	
1	6-Oct-02	40	0.654	14.400	3.340	2.227	0.713	0.194	1.869	Double peak
2	14-Oct-02	80	0.371	14.400	1.992	2.656	0.858	0.122	2.340	Double peak
3	27-Oct-02	40	1.215	21.600	4.320	2.88	1.004	0.256	2.470	Double peak
4	3-Nov-02	120	0.117	14.400	1.750	3.500	0.868	0.115	3.327	Multiple peak
5	13-Nov-02	30	0.546	14.400	3.260	1.630	0.644	0.190	1.376	Double peak
6	17-Nov-02	100	0.189	14.400	2.574	4.289	0.782	0.168	4.048	Multiple peak
7	18-Nov-02	120	0.015	9.600	0.840	1.681	0.548	0.057	1.651	Single peak
8	22-Nov-02	90	0.125	12.000	1.905	2.857	0.647	0.124	2.682	Multiple peak
9	5-Dec-02	100	0.076	14.400	1.656	2.760	0.927	0.110	2.641	Single peak
10	7-Dec-02	100	0.094	7.200	1.193	1.988	0.395	0.078	1.866	Multiple peak

The simulation results showing the runoff hydrograph as well as the corresponding flow depth hydrograph at the channel outlet of the V-catchment for some typical events are shown in Figure 3.19. These results demonstrate the capability and efficacy of the VPMD method to simulate both the overland flow and channel flow routings involved in a watershed such as the considered V-catchment. This is one of the major advantages of the VPMD method over the other rainfall-runoff algorithms which use two different algorithms to simulate the overland flow and channel flow routing as two different processes. In order to demonstrate the role of the Courant number in the selection of spatial and temporal computational grid sizes and their impact on the solution accuracy, simulations were made by adopting two different temporal sizes, 1s and 3s. The grid sizes used, kinematic wave celerities and Courant numbers are presented in Table 3.14 along with the different performance measures used for the assessment of the VPMD method solution to reproduce the observed runoff hydrographs. It is inferred from the results that the estimated Nash-

Sutcliffe efficiency $\eta_q > 95\%$ for all the events except those of the events 1, 5 and 10 which may be attributed to the improper accounting of the interception loss rate in the initial period by the ϕ - index interception loss model. Further, the η_q obtained for the ten events are very similar to those obtained using the KW model by *Wong and Lim* [2006]. The identical results by the VPMD and KW methods solutions are expected as computed $k_{min} =$ 14.57- 27.69, $\left|kF_{rp}^2\right|_{min} = 22.54 - 42.71$ and $(F_{rp})_{min} = 1.24 - 1.25$ for finer grid size, while $k_{min} = 14.52$- 27.69, $\left|kF_{rp}^2\right|_{min} = 22.46 - 42.71$ and $(F_{rp})_{min} = 1.24 - 1.25$ for coarser grid size. The estimated $EVOL < 1.16$ for all the studied events demonstrates that the VPMD method solution is able to efficiently conserve the mass. The estimated time to peak of the runoff hydrographs (t_{perr}) is nearly the same as the observed time to peak as revealed by the corresponding error estimates. It is also revealed while simulating all the events with the same grid sizes, the maximum kinematic wave celerity estimated depends on the applied peak rainfall intensity, as the lower peak rainfall intensity of event 10 estimates a lower $c_{max} = 0.1$, while a higher peak rainfall intensity of event 3 estimates a higher $c_{max} = 0.15$ as overland flow is a nonlinear process and the degree of nonlinearity of the generated runoff is directly proportional to the intensity of the rainfall. Therefore, in order to appropriately capture the runoff variation, a smaller temporal grid size needs to be employed in the simulation. It may be noted that uniform spatial and temporal grid sizes were used in simulating all the considered ten events without the need for enforcing the Courant condition $C_{un} \approx 1$, as has been done in the HEC-HMS model to avoid the numerical diffusion in the solution. In the present investigation, it can be clearly seen from the Table 3.14, that Courant number C_{un} varies between 1.11 - 5.0 for the planes and 0.26 - 1.01 for the channel which are different from the recommended value $C_{un} = 1$ by the U. S. Army Corps of Engineers [USACE, 2006] without causing any significant difference in the simulated results and with $EVOL \ll 5\%$. This justifies the use of threshold Courant number values ranging between 0.10 - 10 as already advocated in section 3.8.2, which do not cause significant error in the simulation results. Thus, it is inferred from this discussion that the proposed method is able to simulate the rainfall-runoff events of the considered experimental V-catchment with negligible mass conservation errors and the solution algorithm is robust and run-time efficient.
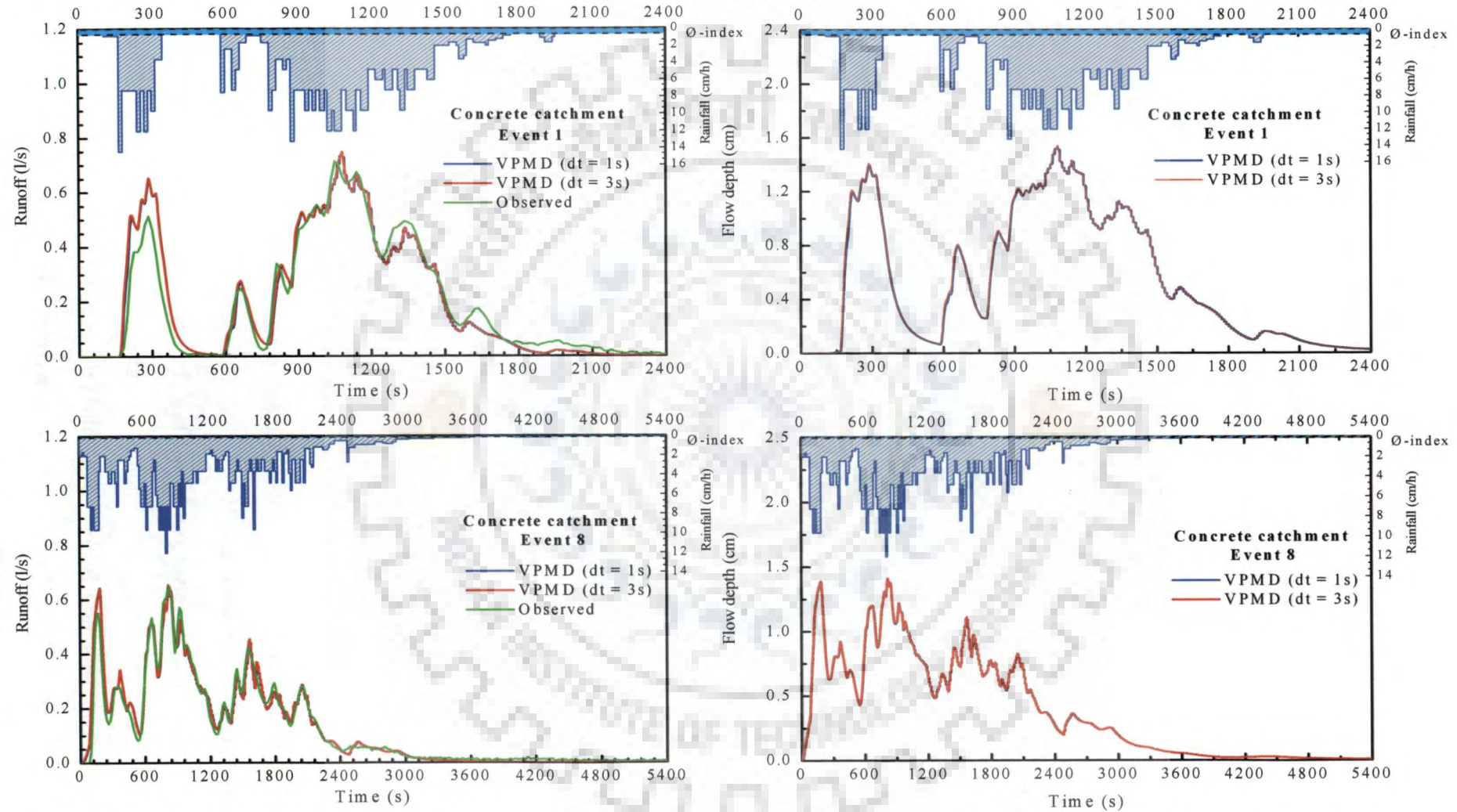
Figure 3.19 Simulated runoff and flow depth hydrographs by the VPMD method at the outlet of the V-catchment for some typical rainfall-runoff events of the *Wong's* [2009] study.

Table 3.14 Verification of the VPMD method using *Wong's* [2009] rainfall-runoff events over concrete V-catchment (number of sub-reaches for the plane and channel are 5 and 10, respectively.)

Event	Grid Ratio, Wave Celerity and Courant Number						Performance Evaluation Measures					Errors in the Computed Peak Discharge and the Time to Peak					
	Plane			Channel			η_q (%)	CRM (%)	CD	EVOL (%)	CPU-time (s)	q_{pc} (m³/s)	t_{pc} (min)	q_{po} (m³/s)	t_{po} (min)	q_{perr} (%)	t_{perr} (min)
	$\dfrac{\Delta x}{\Delta t}$	c_{max}	C_{un}	$\dfrac{\Delta x_c}{\Delta t}$	c_{max}	C_{un}											
1	0.09	0.13	1.41	2.50	0.72	0.29	93.85	-1.18	0.91	1.16	1.44	0.75	18.00	0.71	17.50	4.52	0.50
	0.03	0.13	4.30	0.83	0.72	0.87	93.28	-2.18	0.90	2.21	0.56	0.75	18.00	0.71	17.50	4.88	0.50
2	0.09	0.13	1.42	2.50	0.75	0.30	97.41	-0.66	1.00	0.63	3.41	0.84	47.52	0.86	46.75	-1.66	0.77
	0.03	0.13	4.31	0.83	0.75	0.90	97.38	-1.19	0.99	1.17	1.45	0.85	47.50	0.86	46.75	-1.30	0.75
3	0.09	0.15	1.65	2.50	0.84	0.34	97.64	-0.58	0.94	0.57	1.72	1.29	2.00	1.00	2.00	28.02	0.00
	0.03	0.15	4.98	0.83	0.84	1.01	97.57	-1.06	0.93	1.06	0.75	1.29	2.00	1.00	2.00	28.73	0.00
4	0.09	0.13	1.43	2.50	0.76	0.30	97.94	-0.44	1.01	0.44	3.55	0.89	51.07	0.87	51.25	2.57	-0.18
	0.03	0.13	4.36	0.83	0.76	0.91	98.00	-0.84	1.00	0.85	0.75	0.89	52.00	0.87	51.25	2.86	0.75
5	0.09	0.13	1.42	2.50	0.73	0.29	94.06	-0.44	0.78	0.60	1.19	0.75	2.77	0.64	2.75	16.50	0.02
	0.03	0.13	4.28	0.83	0.73	0.87	93.09	-0.99	0.78	1.16	0.53	0.76	2.75	0.64	2.75	17.53	0.00
6	0.09	0.13	1.43	2.50	0.74	0.30	95.46	-0.42	0.90	0.40	3.63	0.82	16.28	0.78	16.50	4.48	-0.22
	0.03	0.13	4.34	0.83	0.74	0.89	95.17	-0.78	0.89	0.78	1.58	0.82	16.25	0.78	16.50	4.90	-0.25
7	0.09	0.11	1.22	2.50	0.67	0.27	97.70	-0.25	0.93	0.28	3.73	0.58	14.07	0.55	12.50	6.42	1.57
	0.03	0.11	3.69	0.83	0.67	0.81	97.67	-0.51	0.92	0.55	1.58	0.59	14.05	0.55	12.50	6.91	1.55
8	0.09	0.12	1.33	2.50	0.70	0.28	96.98	-0.50	0.95	0.50	3.42	0.65	13.53	0.65	13.75	0.57	-0.22
	0.03	0.12	4.02	0.83	0.70	0.84	96.87	-0.95	0.94	0.96	1.49	0.65	13.55	0.65	13.75	1.03	-0.20
9	0.09	0.13	1.44	2.50	0.77	0.31	98.95	-0.35	1.04	0.35	3.44	0.92	30.65	0.93	30.75	-1.11	-0.10
	0.03	0.13	4.36	0.83	0.77	0.92	98.89	-0.65	1.03	0.67	1.52	0.92	30.65	0.93	30.75	-0.99	-0.10
10	0.09	0.10	1.08	2.50	0.64	0.26	92.89	-0.31	0.83	0.34	3.44	0.49	3.75	0.40	3.75	24.86	0.00
	0.03	0.10	3.27	0.83	0.64	0.77	92.58	-0.60	0.83	0.63	1.53	0.49	3.75	0.40	3.75	24.87	0.00

3.13 IMPACT OF INITIALLY HIGHER INTERCEPTION LOSS RATE

As seen in the previous sections while applying the VPMD method for overland flow simulation over the asphalt and concrete planes, the use of constant interception loss rate over the total period of the considered event resulted in over-prediction of the runoff hydrograph in the initial period by the VPMD method, as shown in Figures 3.15, 3.16 and 3.19. This overprediction is attributed to the under-specification of the interception loss in the initial period of the events and similar trend is observed while applying the KW model by *Wong and Lim* [2006]. In general, most of the interception loss occurs during the initial storm period and the rate of interception approaches zero thereafter. To prove this viewpoint, it is envisaged to select a higher interception loss rate during the initial period, especially, for the period of rise and recession of the first major peak runoff hydrograph of a multi-peak storm event, by conserving mass using equation (3.84).

A summary of the computation of the interception loss rates for the initial as well as for the later period until the cessation of the rainfall of the events on asphalt plane is presented in Table 3.15. Note that the event 7 is with a single major peak and the total loss in the event 8 by interception is very less and, hence, initial higher interception loss rates are not applicable for these events. It was also found from these results that accounting of initially higher interception loss rate resulted in the increase of k_{min} and kF_{rp}^2 while reduction in F_{rp}. It can be seen from Table 3.16 that the total losses relative to the total rainfall depth of all the events considered for analysis were in the range of 7.428-17.669 %. The sufficiently isolated first major storm from the consecutive storms for the events 1, 5 and 10 justifies the use of higher interception loss rate initially, rather than a uniform rate, which is reflected in the overall improvement of runoff hydrograph reproduction as shown in Figure 3.20 (events 1 and 5). This can also be verified from the improvement achieved in the performance

Table 3.15 Summary of rainfall distribution over the asphalt plane considering initial higher interception loss rate

Event	Duration	ϕ-Index	Duration used for ϕ-Index Calculations (min)			Rainfall Depth	Total Rainfall Depth	Runoff Depth	Total Runoff Depth
			Start	End	Total				
	(min)	(cm/h)				(cm)	(cm)	(cm)	(cm)
1	40	2.521	0.00	9.75	9.75	0.459	2.227	0.284	1.901
		0.330	9.75	40.00	30.25	1.768		1.617	
2	80	1.447	0.00	23.00	23.00	0.493	2.656	0.272	2.412
		0.027	23.00	80.00	57.00	2.163		2.140	
3	40	2.099	0.00	6.75	6.75	0.928	2.878	0.698	2.541
		0.415	6.75	40.00	33.25	1.950		1.843	
4	120	0.846	0.00	17.50	17.50	0.232	3.500	0.096	3.230
		0.112	17.50	120.00	102.50	3.268		3.134	
5	30	1.104	0.00	14.00	14.00	1.045	1.630	0.789	1.341
		0.123	14.00	30.00	16.00	0.585		0.553	
6	100	1.863	0.00	10.75	10.75	0.740	4.289	0.480	3.953
		0.062	10.75	100.00	89.25	3.549		3.472	
9	100	0.188	0.00	59.50	59.50	2.533	2.760	2.350	2.550
		0.033	59.50	100.00	40.50	0.227		0.205	
10	100	1.961	0.00	6.75	6.75	0.375	1.988	0.190	1.772
		0.026	6.75	100.00	93.25	1.613		1.582	

measures criteria as shown in Table 3.17 over those respective measures given in Table 3.10. It is seen from these comparisons that initially very light rainfall rate almost equal to the considered interception loss rate causes higher lag time for the events 2, 4 and 9 (Table 3.16). Alternatively, for concentrated storms from the beginning as in the event 3 that the use of higher interception loss rate during the initial period of the event shows only slight improvement. Furthermore, a critical examination of Table 3.16 reveals that approximately 90% interception loss of the event occurs during the initial 28.75-59.5% time period of the rainfall for the events 2, 5, 6 and 9. Similar analyses were carried out for the overland flow studies of the concrete plane and V-catchment also, and the typical improved reproductions are shown in Figure 3.20.

Table 3.16 Summary of time lag and relative interception loss for the selected events on asphalt plane using the estimated initial high loss rate

Event	Total Event Duration (min)	Lag Time (min)	Duration for Loss Rate Calculation (min)	Rainfall Depth (cm)	Runoff Depth (cm)	Interception Loss for the Selected Duration (cm)	Total Loss of the Event (cm)	Interception Loss (% Total Loss)	Interception Loss (% Total Rainfall Depth)	Total Loss (% Rainfall Depth)	Time Period (% Total Event Duration)
1	40	2.75	9.75	0.459	0.284	0.175	0.326	53.681	7.858	14.639	24.375
			30.25	1.768	1.617	0.151		46.319	6.780		75.625
2	80	16.25	23.00	0.493	0.272	0.221	0.244	90.574	8.321	9.187	28.750
			57.00	2.163	2.140	0.023		9.426	0.866		71.250
3	40	0.75	6.75	0.928	0.698	0.230	0.337	68.249	7.992	11.710	16.875
			33.25	1.950	1.843	0.107		31.751	3.718		83.125
4	120	7.00	17.50	0.232	0.096	0.136	0.270	50.370	3.886	7.714	14.583
			102.50	3.268	3.134	0.134		49.630	3.829		85.417
5	30	0.25	14.00	1.045	0.789	0.256	0.288	88.889	15.706	17.669	46.667
			16.00	0.585	0.553	0.032		11.111	1.963		53.333
6	100	3.00	10.75	0.740	0.480	0.260	0.337	77.151	6.062	7.857	10.750
			89.25	3.549	3.472	0.077		22.849	1.795		89.250
9	100	21.00	59.50	2.533	2.350	0.183	0.205	89.202	6.626	7.428	59.500
			40.50	0.227	0.205	0.022		10.798	0.802		40.500
10	100	2.25	6.75	0.375	0.190	0.185	0.216	85.745	9.320	10.869	6.750
			93.25	1.613	1.582	0.031		14.255	1.549		93.250
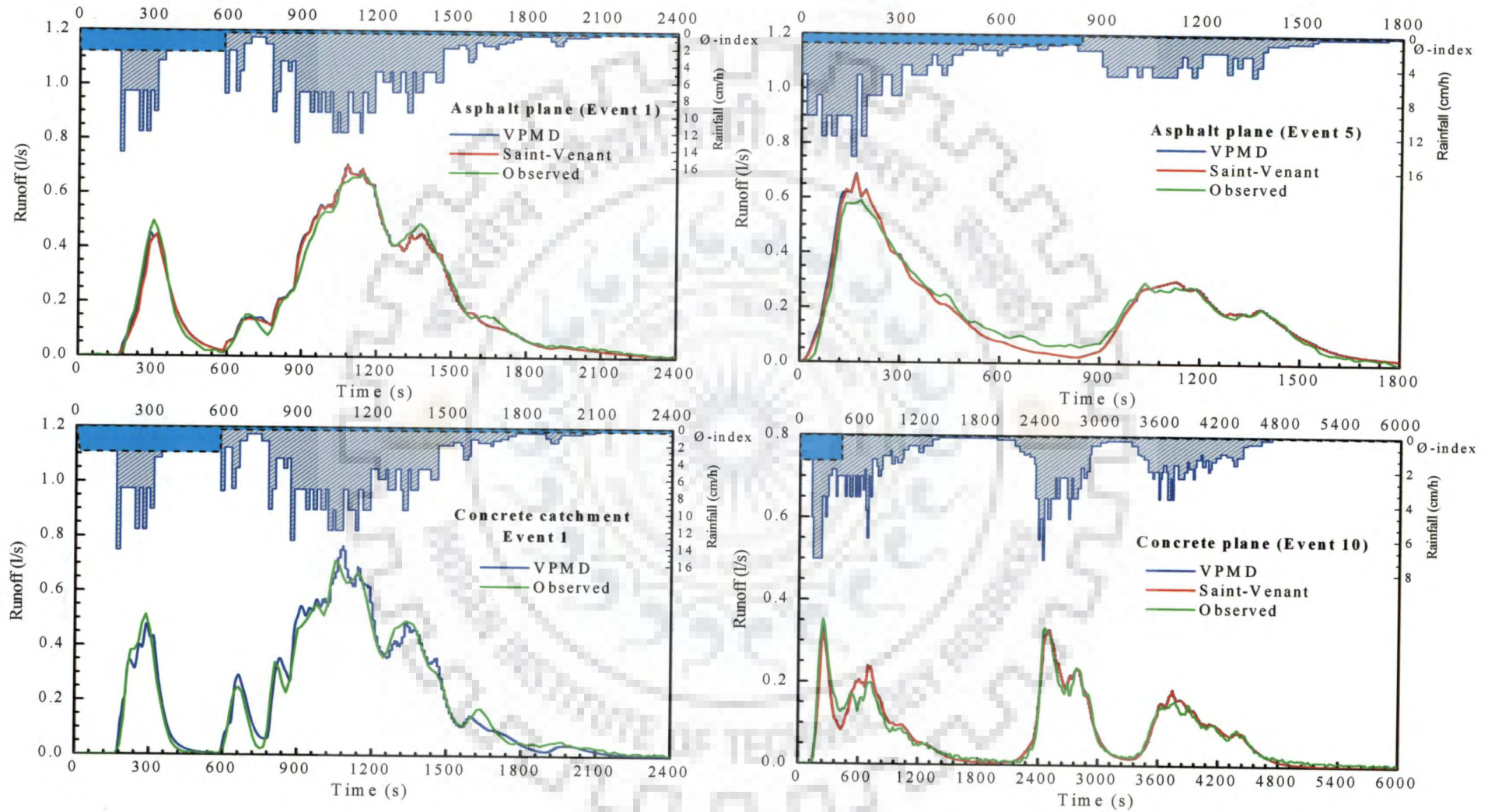
Figure 3.20 Typical simulated runoff hydrographs of the *Wong's* study on the asphalt plane, concrete plane and concrete V-catchment considering initial higher interception loss rates.

Table 3.17 Verification of the VPMD method as in Table 3.10, but considering higher initial interception loss rate

| Event | $\dfrac{\Delta x}{\Delta t}$ (m/s) | c_{max} (m/s) | Courant Number (C_{un}) | Performance Evaluation Measures | | | | | | | | | | VPMD | | Saint-Venant | |
| | | | | Comparison with Observed Data | | | | | Comparison with SVE Solution | | | | | | | | |
				η_q (%)	CRM (%)	CD	q_{perr} (%)	t_{perr} (min)	η_q (%)	CRM (%)	CD	q_{perr} (%)	t_{perr} (min)	EVOL (%)	CPU-time (s)	EVOL (%)	CPU-time (s)
1	0.17	0.38	2.29	98.76	-0.66	0.99	5.47	-1.00	99.95	-1.03	0.99	0.23	0.00	1.03	1.20	-0.01	3.73
2	0.17	0.41	2.44	99.15	-0.48	0.98	0.92	0.00	99.99	-0.56	0.99	0.38	0.00	0.55	1.31	-0.04	3.17
3	0.17	0.44	2.62	99.08	-0.74	0.96	1.58	11.25	99.95	-0.76	0.99	0.07	0.00	0.75	1.20	-0.03	3.42
4	0.17	0.42	2.50	99.15	-0.42	1.00	8.43	0.50	99.99	-0.42	0.99	0.17	0.00	0.41	1.41	-0.03	3.59
5	0.17	0.38	2.27	95.67	0.37	0.83	16.72	-0.25	99.93	-0.88	0.98	0.55	0.00	0.88	0.91	-0.02	2.86
6	0.17	0.40	2.38	98.47	-0.36	0.95	2.86	-0.50	99.98	-0.40	0.99	0.23	0.00	0.40	1.38	-0.01	2.06
9	0.17	0.41	2.46	99.21	-0.27	1.04	-4.16	-1.00	100.00	-0.39	1.00	0.02	0.00	0.38	1.39	-0.02	2.09
10	0.17	0.28	1.68	95.92	-0.44	1.04	-4.21	0.00	99.97	-0.52	0.99	0.19	0.00	0.51	1.38	-0.01	2.81

3.14 SUMMARY AND CONCLUDING REMARKS

This study presents the development of the VPMD routing method for runoff generation from the overland flow planes and for estimating the runoff hydrograph at the outlet of a level V-catchment by incorporating channel routing accounting for the distributed lateral flow in the form of overland flow. The evaluation of the proposed method for overland flow modelling is extensively carried out through the assessment of comparison of the simulated runoff hydrographs with the corresponding hydrographs simulated by the analytical KW solution, approximate analytical solution, numerical solution of the full SVE, and the runoff hydrographs extracted from the available publications in the form of experimental rainfall-runoff data as well as hypothetical rainfall-runoff data generated based on the KW and DW models. The performance of the proposed VPMD method is evaluated using different evaluation measures, *viz.*, Nash-Sutcliffe efficiency (η_q, %), coefficient of residual mass (CRM, %), coefficient of determination (CD), percentage error in volume conservation, and percentage error in peak runoff production. The performance of the VPMD routing method under complex rainfall pattern is further investigated by comparing its solutions with the simulated runoff hydrograph for Izzard's data and runoff data collected for natural rainfall events from an outdoor laboratory experimental facility. Similarly, the performance of the VPMD method for the simulation of discharge hydrographs and corresponding flow depth hydrographs at the valley side as well as at the outlet of a V-catchment were verified by comparing the results with the analytical solution of the KW equation, HEC-HMS model results, simulation results of a hypothetical study and with the Wong's observed data for natural rainfall input. In order to account interception loss in the rainfall-runoff data of Wong's study, the VPMD method was coupled with a ϕ-index interception loss model. All these studies on V-catchment runoff simulation reveal that the simulated runoff hydrographs by the VPMD method are in good agreement with the observed data, SVE solution, and the solutions of the DW and KW equations; whereas the VPMD method is also found to yield solution better than the KW solution and the approximate analytical solutions of the diffusive wave model, when this method is applied beyond the kinematic wave range and well into the applicability range of the DW model. Besides, the close reproduction of the runoff hydrographs recorded at the downstream end of the overland flow plane/ channel and that simulated by the SVE solutions at the end of the overland flow plane demonstrates that the VPMD method can be confidently used for catchment modelling studies.

Further, it was found that the proposed VPMD method is unconditionally stable. The role of the Courant condition in preservation of the solution accuracy was investigated using the numerical experiments and found that it was not necessary to strictly follow this condition ($C_{un} \approx 1$) for the applicability of the VPMD method. Further, to preserve the solution accuracy and efficient mass conservation ($EVOL \ll 5\%$), Courant condition can vary in the range $0.1 < C_{un} < 10.0$. Further, the study revealed that the model accuracy also depends on the use of appropriate and accurate input parameters such as the roughness coefficient. Overall, the applicability range of the proposed method falls in the transition range between the DW and KW models, including the full range of the latter model. Thus, this approach is efficient alternative to the SVE and its variants solutions in modelling surface runoff in a natural catchment, especially when the stringent requirement of the downstream boundary condition restricts the use of these solutions. Consequently, the study demonstrates that the VPMD method is advantageous over the existing overland flow models because of its unconditional numerical stability with good accuracy even with the use of larger computational spatial and temporal grid sizes, and inexpensive computations. Hence, the proposed VPMD method can be confidently used for meso- and macro-scale catchment modelling studies.

4 OVERLAND FLOW MODELLING USING THE VARIABLE PARAMETER MUSKINGUM STAGE-HYDROGRAPH ROUTING METHOD AND ITS EVALUATION

4.1 GENERAL

Considering the better attributes of the VPMS channel routing method, it is proposed in this study to extend the VPMS channel routing method, using flow depth as the operational variable, for overland flow modelling in the presence of rainfall and overland flow as lateral flow over the planes and in the channel of V-catchments, respectively. The operational performance of the method is extensively carried out using the observed rainfall-runoff data available in literature, based on various evaluation measures. Besides, the simulation results are also evaluated with the analytical solutions of the kinematic wave equation, and the various numerical method solutions of the Saint-Venant, diffusive and kinematic wave equations. To bring out the merits and demerits of using flow depth as an operating variable in overland flow modelling instead of discharge variable, the simulation results of the proposed VPMS method are also compared with the results of the variable parameter discharge-hydrograph (VPMD) routing method. Further, the VPMS overland flow model is coupled with a ϕ-index infiltration type interception loss model to account for the interception losses. The current study also investigates the issue of scale problem that arises due to the routing of small overland flow depth as compared to the larger flow depth (stage) realized in channel routing. The sensitivity of the method for varying computational space and temporal grid sizes has also been studied.

4.2 FORMULATION OF THE OVERLAND FLOW MODEL

The overland flow may be treated as the shallow water flow per unit width of the plane with similarity to the section characteristics as in the case of unit width section of the wide rectangular channels [*Woolhiser*, 1974; *Govindarju and Kavvas*, 1991]. The dynamics of overland flow mechanism can be described by the well-known Saint-Venant equations (SVE). In many situations, it has been found that the continuity equation and the simplified form of the momentum equation obtained by eliminating and curtailing some of the terms of

the momentum equation of the SVE are found to describe the one dimensional flow very well [*Henderson*, 1966]. Hence, the method derived directly from the SVE could be applied with ample confidence for catchment modelling provided that it is capable of efficiently and accurately simulating the flow behaviour of the KW and, up to certain extent, the DW equations as applicable in mild to low sloping overland flow area. *Perumal and Ranga Raju* [1998a, 1998b] has made one such a simplification and used the continuity equation and the simplified momentum equation to develop the VPMS method. This method was developed for routing the gradually varying unsteady flow depth (stage) and, thus, the flow discharge in the channel or river reach having prismatic cross section, without considering lateral flow in the reach. This method is capable of varying its parameters in a physically based manner at every routing time interval relating them to channel and flow characteristics. This method is based on the same concept as that of the variable parameter Muskingum discharge-hydrograph routing method [*Perumal*, 1994a, 1994b] and also uses the same form of the routing equation as that of the Muskingum method, but replacing discharge variable by the stage variable. In the present study, the VPMS routing method [*Perumal and Ranga Raju*, 1998a] has been extended for overland flow modelling using overland flow depth as the operating variable and by incorporating the distributed lateral flow (rainfall) in the model framework.

4.2.1 Concept of the Proposed Overland Flow Model

During steady state flow conditions in a overland flow strip, a one-to-one relationship prevails between the flow depth or the cross sectional area of the flow and the discharge at any location defining the steady state flow-depth relationship at that location. But, during the unsteady flow situation, there exists no such unique relationship between the flow depth and the discharge at any location, but the same unique relationship exists between the flow depth at a given section and the corresponding steady state discharge, occurring somewhere downstream from that section depending on the existing hydraulic control at the downstream location and the prevailing flow condition in the computational routing reach in question. This condition is depicted in Figure 4.1, which also defines the Muskingum overland plane routing reach. This figure clearly shows that within the sub-reach of length Δx, at any instant of time t, the flow depth, y_M at the mid-section of the reach is uniquely related with the discharge q_3 passing at a location l (section 3 in Figure 4.1) downstream from the mid-section of the reach.
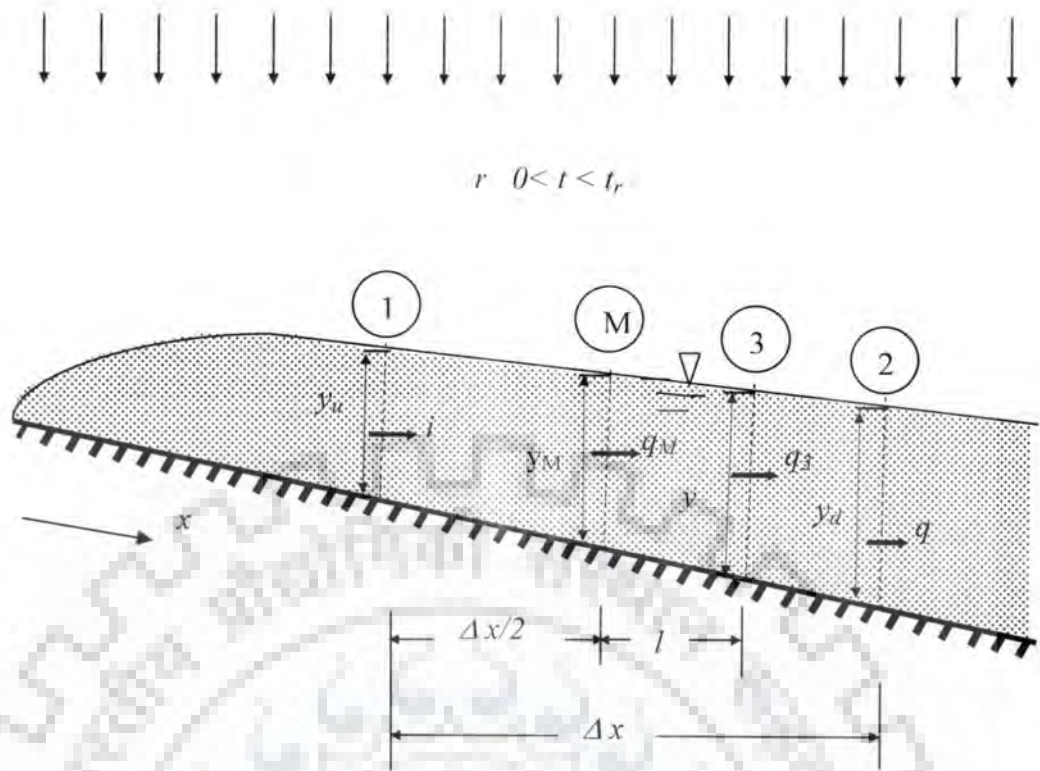
Figure 4.1 Schematic sketch of the Muskingum reach governing the overland flow depth variation over an impervious surface.

4.2.2 Governing Equations

The VPMS method for overland flow modelling is derived from the full Saint-Venant equations considering lateral flow, which govern the one-dimensional flow over a plane. The equations applied to a unit width overland flow plane are expressed by the continuity and momentum equations, respectively, as

$$\frac{\partial q}{\partial x} + \frac{\partial y}{\partial t} = q_L \tag{4.1}$$

$$s_f = s_0 - \left(\frac{\partial y}{\partial x}\right) - \left(\frac{1}{g}\right)\left(\frac{\partial v}{\partial t}\right) - \left(\frac{v}{g}\right)\left(\frac{\partial v}{\partial x}\right) - \left(\frac{q_L v}{gy}\right) \tag{4.2}$$

where q= flow rate per unit width of the flow plane $[L^2T^{-1}]$, y = flow depth [L], s_f= energy slope $[LL^{-1}]$, g = acceleration due to gravity $[LT^{-2}]$, v = flow velocity $[L\,T^{-1}]$, s_0 is the bed slope $[LL^{-1}]$, q_L = net rate of lateral inflow per unit area $[LT^{-1}]$ expressed as

133

$$q_L = r - I_a \qquad\qquad (4.3)$$

where r = the rate of rainfall per unit area occurring for a duration t_r, and I_a = the rate of loss due to abstraction. The magnitudes of pressure gradient term $(\partial y / \partial x)$, and acceleration terms $(1/g)(\partial v / \partial t)$ and $(v/g)(\partial v / \partial x)$ are small in comparison with s_0 in many circumstances, and under this situation the application of the approximate momentum equation of the SVE obtained by elimination or approximation of some of these terms may be sufficient. An order of the magnitude analysis of equation (4.2) reveals that the momentum due to lateral inflow or outflow has a negligible effect on the flow dynamics [*Eagleson*, 1970; *Henderson*, 1966], and, hence, the term $(q_L v / gy)$ can be neglected in equation (4.2) without facing any inaccuracy problem.

4.2.3 Assumptions

The assumptions used in the derivation of this VPMS method are:

a) A uniform thin sheet flow of runoff developing over an overland flow plane resembles to that of a shallow water unsteady flow in a wide prismatic rectangular cross-section channel reach;

b) There is lateral inflow due to rainfall and/or outflow due to interception losses and infiltration losses from the computational reach;

c) The momentum due to the lateral inflow and/or outflow is assumed to be negligible;

d) The longitudinal pressure gradient $(\partial y / \partial x)$ and the longitudinal gradients due to both local acceleration $(1/g)(\partial v / \partial t)$ and convection acceleration $(v/g)(\partial v / \partial x)$ all remain constant at any instant of time in a given computational routing reach. This assumption implies that the friction slope s_f is constant over the computational reach of length Δx and, accordingly, the flow depth variation is linear over this reach Δx;

e) The multiplication of derivatives of flow and section variable with respect to both time and space are negligible; and

f) At any instant of time during unsteady flow, the steady flow relationship is applicable between the flow depth at the middle of the computational reach and the discharge passing somewhere downstream of it.

134

Assumptions (d–f) are employed in the VPMS channel routing method without considering lateral flow [*Perumal and Ranga Raju*, 1998a].

4.2.4 Derivation of the VPMS Method for Overland Flow Modelling

The discharge at any section of the unit width of the overland flow plane reach may be expressed as:

$$q = vy$$

(4.4)

For the unit width of overland flow plane, the hydraulic radius at any location of the strip can be considered equal to the flow depth. Consequently, equation (4.4) can be expressed using the Manning's friction law as

$$q = \frac{1}{n} y^{5/3} s_f^{1/2}$$

(4.5)

where, n is the Manning's roughness coefficient.

Differentiating equation (4.5) with respect to x and invoking the assumption (d) that s_f is constant over the length Δx, the resulting expression can be written as

$$\frac{\partial q}{\partial x} = (5/3) v \frac{\partial y}{\partial x}$$

(4.6)

Using equation (4.6), the celerity of overland flow wave can be expressed as

$$c = \frac{\partial q}{\partial y} = \frac{5}{3} v$$

(4.7)

Due to the assumption of linearly varying flow depth over a computational sub-reach, the celerity of the overland flow governed by equation (4.7) is not unique, for the same runoff discharge occurring in the rising and falling limbs of the runoff hydrograph, as in case of the kinematic wave model [*Ponce*, 1986].

The use of equations (4.1), (4.4), (4.6) and (4.7) and also the assumption of negligible momentum due to lateral inflow contribution enable one to arrive at the equation for the local acceleration term which can be expressed as

$$\frac{1}{g} \frac{\partial v}{\partial t} = -\frac{10}{9} \frac{\partial y}{\partial x} F_p^2$$

(4.8)

where, F_{rp} = Froude number of the overland flow expressed as: $F_{rp} = v / \sqrt{gy}$.

Further, the use of equation (4.4) and (4.6) leads to the expression for the convective acceleration term, which can be written as

$$\frac{v}{g} \frac{\partial v}{\partial x} = \frac{2}{3} \frac{\partial y}{\partial x} F_{rp}^2 \tag{4.9}$$

Further, the substitution of equations (4.8) and (4.9) in equation (4.2) leads to the expression for the friction slope (s_f) as

$$s_f = s_0 \left[1 - \frac{1}{s_0} \frac{\partial y}{\partial x} \left\{ 1 - \frac{4}{9} F_{rp}^2 \right\} \right] \tag{4.10}$$

and the term $(4/9) F_{rp}^2$ is represented as V_{vn}^2, where V_{vn} is known as the Vedernikov number [*Chow*, 1959; *Jolly and Yevjevich*, 1971; *Ponce*, 1991] which defines the criterion for the amplification of the overland flow. Vedernikov number is defined as the ratio of the relative celerity of kinematic waves to the relative celerity of dynamic waves.

4.2.4.1 Weighted runoff discharge location

Using equation (4.10) in equation (4.5) for expressing the discharge q_M at the middle of the considered computational flow reach of Δx, and eliminating the higher order terms of the binomial series expansion of $s_0^{1/2} \left[\frac{1}{s_0} \frac{\partial y}{\partial x} \left\{ 1 - \frac{4}{9} F_{rp}^2 \right\} \right]^{1/2}$, leads to the expression for q_M as

$$q_M = q_3 - \frac{q_3 \left(1 - (4/9) F_{rp}^2 \right)_M}{2 s_0} \left. \frac{\partial y}{\partial x} \right|_3 \tag{4.11a}$$

Using equations (4.6) and (4.7) in equation (4.11a) leads to

$$q_M = q_3 - l \left. \frac{\partial q}{\partial x} \right|_3 \tag{4.11b}$$

where l denotes the location of section (3), at which the normal discharge q_3 corresponding to the flow depth y_M passes during unsteady flow for overland flow and it is expressed as

$$l = \frac{q_3 \left(1 - (4/9) F_{rp}^2 \right)_M}{2 s_0 c} \tag{4.12}$$

In equation (4.11), the discharge q_M is expressed in terms of the normal discharge, q_3, which is uniquely related to y_M by the steady-state relationship as

$$q_3 = \frac{1}{n} y_M^{5/3} s_0^{1/2} \tag{4.13}$$

where, the subscripts M and 3 denote the mid-section and section '3' of the computational reach of length Δx.

4.2.4.2 Derivation of the approximate convection diffusion (ACD) equation in flow depth form

Use of equations (4.6) and (4.7) in equation (4.1), leads to the expression

$$\frac{\partial y}{\partial t} + c \frac{\partial y}{\partial x} = q_L \tag{4.14}$$

This simplified governing equation is used in the development of the VPMS method for overland flow modelling and is referred to as the Approximate Convection Diffusion (ACD) equation, which implies that the shallow overland flow wave is characterized by constant friction slope s_f at any instant of time and, hence, the flow depth varies approximately linearly over the computational sub-reach. Note that the form of equation (4.14) is similar to the form of the kinematic equation expressed in the flow depth form by *Lighthill and Whitham* [1955] and *Govindaraju and Kavvas* [1991]. Although, the ACD and the kinematic wave equations in flow depth formulation resemble each other, the ACD equation is capable of modelling the overland flow in an approximate manner in the transition range of the unsteady overland flow governed by the diffusive wave and the kinematic wave (including the latter) [*Perumal and Ranga Raju*, 1999; *Perumal et al.*, 2007]. The basis behind this inference is that the right hand side of equation (4.14) does not contain the diffusion term ($D \partial^2 y / \partial x^2$), but the diffusivity coefficient $D \neq 0$, where $D = q_0 / (2s_0)$ corresponding to unit width overland flow plane as described by *Lighthill and Whitham* [1955]. This enables the application of equation (4.14) for overland flow modelling in the range of lower order shallow diffusive flood waves, including the kinematic waves. Since the kinematic wave equation is derived by neglecting the pressure term and all the inertial terms in the momentum equation (4.2), it does not display any physical attenuation [*Ponce*, 1986]. Hence, the kinematic wave equation is also considered as the special case of equation (4.14), when $\partial y / \partial x \approx 0$. However, this statement seems to be contradictory with the conventional perception that equation (4.14) is strictly applicable for modelling the overland flow in the kinematic wave range only.

137

4.2.4.3 Routing equation of the VPMS overland flow model

Applying equation (4.7) and (4.14) at section '3' and rearranging the terms leads to expression

$$c_3 \left.\frac{\partial y}{\partial x}\right|_3 = -\left.\frac{\partial y}{\partial t}\right|_3 + q_{L_3} \tag{4.15}$$

Employing the assumption of linear variation of flow depth along the computational routing reach of Δx, one can write

$$\left.\frac{\partial y}{\partial x}\right|_3 = \left.\frac{\partial y}{\partial x}\right|_2 = \frac{y_d - y_u}{\Delta x} \tag{4.16}$$

Similarly, using the same assumption, the flow depth at the weighted section '3' can be written as

$$y_3 = y_d + \left(\frac{1}{2} - \frac{l}{\Delta x}\right)\left(\frac{y_u - y_d}{\Delta x}\right) \tag{4.17}$$

where, y_u and y_d denote the flow depths at the upstream and downstream ends of the computational routing reach.

Substituting equations (4.16) and (4.17) in equation (4.15) leads to the expression

$$(y_u - y_d) + Kq_L = \frac{\Delta x}{c_3}\frac{\partial}{\partial t}\left[y_d + \left(\frac{1}{2} - \frac{l}{\Delta x}\right)(y_u - y_d)\right] \tag{4.18}$$

Using the similarity between the governing differential equation of the Muskingum method in the discharge formulation and that of equation (4.18), the travel time K can be expressed as

$$K = \frac{\Delta x}{c_3} \tag{4.19}$$

Substituting the expression for l in equation (4.18) from equation (4.11), the expression for the Muskingum weighting parameter θ can be given as

$$\theta = \frac{1}{2} - \frac{q_3\left(1 - (4/9)F_{rpM}^2\right)}{2s_0 c_3 \Delta x} \tag{4.20}$$

Using the parameters K and θ given in equations (4.19) and (4.20) enables one to reduce equation (4.18) to the form analogous to the conventional Muskingum equation in discharge formulation, and can be written as

$$(y_u - y_d) + Kq_L = \frac{\partial}{\partial t}\left[K(\theta y_u + (1 - \theta)y_d)\right] \tag{4.21}$$

138

The numerical approximation of equation (4.21) leads to the derivation similar to the Muskingum routing equation using flow depth as the operating variable, instead of discharge variable, accounting for the lateral inflow and can be expressed on the space-time computational grid as

$$y_{d,2} = C_1 y_{u,2} + C_2 y_{u,1} + C_3 y_{d,1} + C_4 K q_L \tag{4.22}$$

where $y_{d,2}$ = the outflow runoff flow depth at the downstream end of the computational sub-reach at current time level; $y_{u,2}$ = the inflow runoff flow depth at the upstream end of the computational sub-reach at current time level; $y_{d,1}$ = the outflow runoff flow depth at the downstream end of the computational sub-reach at the previous time level; $y_{u,1}$ = the inflow runoff flow depth at the upstream end of the computational sub-reach at the previous time level; and q_L = average lateral inflow rate within the computational reach over Δt. The routing coefficients C_1, C_2, C_3, and C_4 are expressed as

$$C_1 = \frac{-K\theta + 0.5\Delta t}{K(1-\theta) + 0.5\Delta t} \tag{4.23}$$

$$C_2 = \frac{K\theta + 0.5\Delta t}{K(1-\theta) + 0.5\Delta t} \tag{4.24}$$

$$C_3 = \frac{K(1-\theta) - 0.5\Delta t}{K(1-\theta) + 0.5\Delta t} \tag{4.25}$$

$$C_4 = \frac{\Delta t}{K(1-\theta) + 0.5\Delta t} \tag{4.26}$$

4.2.4.4 Runoff discharge computations

Similar to the VPMD method [Chapter 3, section 3.2.4.4], which enables the simultaneous computations of the runoff flow depth corresponding to an estimated runoff discharge, the proposed VPMS method is also capable of simultaneously calculating the runoff discharge corresponding to a routed flow depth arrived at using equation (4.22). The runoff discharge q_2 corresponding to an estimated flow depth y_d is computed using equation (4.6) as

$$q_2 = q_3 + (5/3) v_3 (y_d - y_3) \tag{4.27}$$

The flow and section variables at the section '3' are estimated using the flow depth information y_u and y_d and the assumption of linear variation of flow depth along the computational reach.

4.3 VPMS CHANNEL FLOW ROUTING METHOD CONSIDERING LATERAL FLOW

Channel flow routing is required to compute the runoff discharge at the outlet of a V-catchment. The VPMS channel flow routing method developed by *Perumal and Ranga Raju* [1998a] is modified for the channel flow depth routing of the V-catchment, considering lateral flow, as formulated below:

The continuity and momentum equations are given as

$$\frac{\partial Q}{\partial X} + \frac{\partial A}{\partial t} = Q_L \tag{4.28}$$

$$S_f = S_0 - \left(\frac{\partial Y}{\partial X}\right) - \left(\frac{1}{g}\right)\left(\frac{\partial V}{\partial t}\right) - \left(\frac{V}{g}\right)\left(\frac{\partial V}{\partial X}\right) - \left(\frac{Q_L V}{Ag}\right) \tag{4.29}$$

where Q = the channel flow rate [L^3T^{-1}]; A = the channel cross-sectional area of flow [L^2]; S_f = the channel energy slope [LL^{-1}]; g = acceleration due to gravity [LT^{-2}]; V = velocity of the channel flow [LT^{-1}]; S_0 = the channel bed slope [LL^{-1}]; the notations X and t denote the space and time variables, respectively; and Q_L = net lateral channel flow/unit width of the overland flow plane given as

$$Q_L = [q_{RH} + q_{LH} + (q_L \times B)] \tag{4.30}$$

where q_{RH} = unit width discharge from the right hand side overland flow plane; q_{LH} = unit width discharge from the left hand side overland flow plane; B = width of the channel; and q_L = net rainfall rate same as used for the overland flow plane. However, the rainfall falling over the channel flow surface is very small as compared to the draining surface area of the V-catchment and, hence, the term q_L is often neglected in equation (4.30).

The runoff discharge is given as

$$Q = A\frac{1}{n_c} R^{2/3} S_f^{1/2} \tag{4.31}$$

where, n_c is the Manning's roughness coefficient of the channel reach.

The development of the VPMS routing method for channel flow can be obtained in a similar manner as given for the overland flow described earlier following the same assumptions (b-f) applied for the overland flow modelling. Further, the similar definition sketch by replacing the variables i, q, y_u, y_d, y_M, q_3, q_M, Δx, and l with inflow (I), outflow (Q), stage or flow depth at the upstream, downstream and at mid-section (Y_u, Y_d

140

and Y_M), normal discharge Q_3 corresponding to Y_M, discharge at the mid-section (Q_M) of the computational routing reach of ΔX and the location of section-3 at L_c distance downstream of the mid-section of computational reach, respectively, are applicable for the channel flow routing as shown in Figure 4.2. The interested readers may refer the work by *Perumal and Ranga Raju* [1998a, 1998b] and *Perumal et al.* [2007] for the detailed derivation of the VPMS channel flow routing method. In this section, only a brief development of the channel flow routing equation is presented.
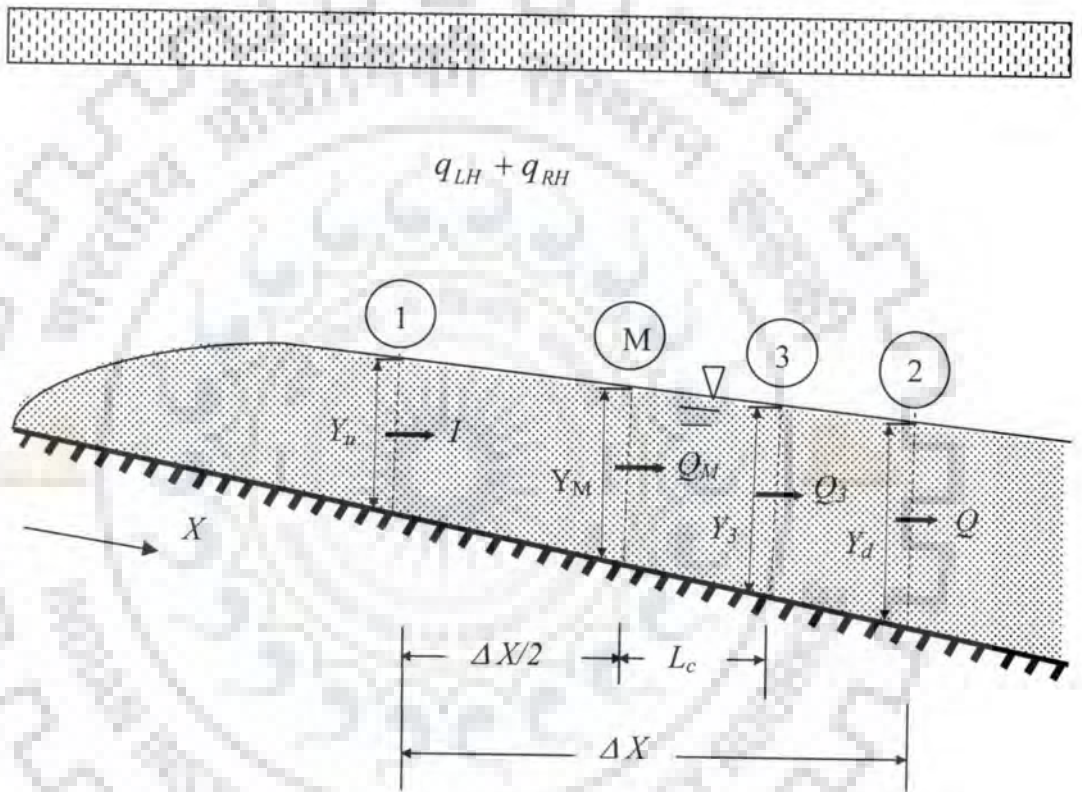
Figure 4.2 Schematic sketch of the Muskingum reach governing the flow depth variation in a rectangular channel reach.

The ACD equation in flow depth formulation required for the channel flow routing with uniform contribution of the lateral inflow/outflow can be expressed in a similar form as that applicable for the overland flow as

$$\frac{\partial Y}{\partial t} + C\frac{\partial Y}{\partial X} = Q_L \tag{4.32}$$

where C = wave celerity of flood wave in the channel [LT^{-1}] expressed as

$$C = \frac{\partial Q}{\partial A} = \left[1 + \frac{2}{3}\left(\frac{P\,\partial R/\partial Y}{\partial A/\partial Y}\right)\right]V \qquad (4.33)$$

where R = hydraulic radius (A/P) [L]; and P = wetted perimeter [L].

Employing the assumption of linearly varying flow depth over the computational reach, ΔX, the discharge Q_M at the mid-section of the computational reach is expressed in terms of discharge Q_3, which is uniquely related to flow depth Y_M. The unsteady runoff discharge at the middle of the computational routing reach can be expressed as [*Perumal and Ranga Raju*, 1998a]

$$Q_M = Q_3 - \frac{Q_3\left[1 - \frac{4}{9}F_{rc_M}^2\left(\frac{P\,\partial R/\partial Y}{\partial A/\partial Y}\right)_M^2\right]}{2S_0\left.\frac{\partial A}{\partial Y}\right|_3\left[1 + \frac{2}{3}\left(\frac{P\,\partial R/\partial Y}{\partial A/\partial Y}\right)_3\right]V_3}\left.\frac{\partial Q}{\partial X}\right|_3 = Q_3 - L_c\left.\frac{\partial Q}{\partial X}\right|_3 \qquad (4.34)$$

where, the location of the weighted runoff discharge L_c can be expressed as

$$L_c = \frac{Q_3\left[1 - \frac{4}{9}F_{rc_M}^2\left(\frac{P\,\partial R/\partial Y}{\partial A/\partial Y}\right)_M^2\right]}{2S_0\left.\frac{\partial A}{\partial Y}\right|_3\left[1 + \frac{2}{3}\left(\frac{P\,\partial R/\partial Y}{\partial A/\partial Y}\right)_3\right]V_3} \qquad (4.35)$$

Further, the VPMS channel flow routing method arrives at the same expression of the parameter K_c and θ_c expressed for the VPMD routing method as

$$K_c = \frac{\Delta X}{\left[1 + \frac{2}{3}\left(\frac{P\,\partial R/\partial Y}{\partial A/\partial Y}\right)_3\right]V_3} \qquad (4.36)$$

$$\theta_c = \frac{1}{2} - \frac{Q_3\left[1 - \frac{4}{9}F_{rc}^2\left(\frac{P\,\partial R/\partial Y}{\partial A/\partial Y}\right)^2\right]_M}{2S_0\left.\frac{\partial A}{\partial Y}\right|_3\left[1 + \frac{2}{3}\left(\frac{P\,\partial R/\partial Y}{\partial A/\partial Y}\right)_3\right]V_3\Delta X} \qquad (4.37)$$

4.4 V-CATCHMENT RUNOFF COMPUTATION PROCEDURE USING THE VPMS METHOD

The V-catchment considered in this study comprises of two same size overland flow planes on either side of the rectangular channel located at the middle of the catchment which

receives runoff from the overland flow planes. Such an assembling of the V-catchment resembles to a simplified model of catchment idealized by an open book geometry [*Wooding*, 1965a, 1965b, 1966]. Therefore, the runoff computation of the V-catchment involves the routing of the rainfall generated flow over the overland flow plane which in turn contributes to the channel as lateral flow, thus, generated runoff in the channel requiring channel routing of the V-catchment. This process of runoff generation at the outlet of the V-catchment is simulated by coupling the overland flow routing algorithm with the channel flow routing algorithm as described below.

4.4.1 Overland Flow Routing

The application of the VPMS method for overland flow computation requires the subdivision of the overland flow plane along the sloping direction into a number of unit width strips each of which is bounded on the upper end by the watershed ridge and at the lower end, the overland flow generated from the plane is contributed to the collector channel. Each of these strips is divided into a cascade of equal number of sub-reaches of length Δx suitable for the application of the VPMS method. The following step-by-step solution procedure is adopted for each routing time-step of the VPMS method while routing flow over each of the sub-reaches of Δx of the overland flow strip. As there is no flow of water at the upstream end of the computational sub-reach corresponding to the ridge of the V-catchment, the overland flow routing process is implemented using two types of routing procedures:

4.4.1.1 Routing procedure for the first sub-reach when $t \geq \Delta t$ and for the rest of the sub-reaches when $t = \Delta t$

1) Temporally varying continuous rainfall input can be subdivided into a number of pulses of equal duration Δt which also corresponds to that of the routing time interval. In a similar manner, a uniform abstraction corresponding to each pulse is also specified. Thus, the net lateral inflow rate over the considered strip is computed using equation (4.3).

2) Considering zero initial overland flow depth over the overland flow strip, estimate the reference water flow depth, y_0 for the first routing time interval Δt to estimate the VPMS parameters and similarly, for all the succeeding time increments at the outlet of the first sub-reach using the expression

$$y_0 = \frac{(q_L \times \Delta t) + y_{d,1}}{2}; \qquad y_{d,1} = 0, \text{ when } t = \Delta t \qquad (4.38)$$

where, t represents the cumulative simulation time in terms of Δt from the beginning, which is bounded by the total simulation time, T as an upper limit.

3) Estimate the value of travel time, K corresponding to the reference flow depth y_0 as

$$K = \Delta x / c_0 \qquad (4.39)$$

where, c_0 = wave celerity computed corresponding to y_0 which is estimated using equation (4.7), in which the reference flow velocity v_0 is estimated using y_0 by using the expression as

$$v_0 = \frac{1}{n} y_0^{2/3} s_f^{1/2} \qquad (4.40)$$

4) The routing coefficient C_p is estimated as

$$C_p = \frac{K - 0.5\Delta t}{K + 0.5\Delta t}; \qquad (4.41)$$

5) Estimate the outflow runoff flow depth $y_{d,2}$ at the current time step using the VPMS routing equation as

$$y_{d,2} = C_p y_{d,1} + (1 - C_p) K q_L \qquad (4.42)$$

The overland runoff flow depth estimated by equation (4.42) at the end of the first computational routing sub-reach becomes runoff flow depth at the upstream end of the subsequent routing sub-reach. The routing of this upstream flow depth for $t > \Delta t$ requires a different routing procedure which is described below:

4.4.1.2 Routing procedure for the second and subsequent sub-reaches when $t > \Delta t$

1) The same procedure as given in step 1 of section 4.4.1.1 is used for the discritization of the continuous rainfall of variable intensity into number of pulses of equal duration Δt.

2) Estimate the reference runoff flow depth y_0 by using the three point average method as

$$y_0 = \frac{y_{u,2} + y_{u,1} + y_{d,1}}{3} \qquad (4.43)$$

3) Estimate the value of travel time K corresponding to the reference runoff flow depth y_0 using equation (4.39).

144

4) Estimate the weighting coefficient θ corresponding to the reference runoff flow depth, y_0 as

$$\theta = \frac{1}{2} - \frac{y_0\left(1 - \frac{4}{9}F_{rp_0}^2\right)}{2s_0(5/3)\Delta x} \qquad (4.44)$$

where s_0 = overland flow plane slope; and F_{rp_0} = Froude's number corresponding to y_0.

5) The routing coefficients C_1, C_2, C_3 and C_4 can be computed using equations (4.23), (4.24), (4.25), and (4.26), respectively.

6) The unrefined estimate of the outflow runoff flow depth $y_{d,2}$ at the current routing time step is estimated by using the recursive VPMS routing equation (4.22).

7) Estimate the normal runoff flow depth at section '3' (Figure 4.1) using equation

$$y_3 = \theta y_{u,2} + (1-\theta)y_{d,2} \qquad (4.45)$$

8) Estimate the normal runoff flow depth , y_M at the middle of the computational sub-reach as

$$y_M = \frac{y_{u,2} + y_{d,2}}{2} \qquad (4.46)$$

9) Estimate the flow velocity, v_3 at section '3' by

$$v_3 = \frac{1}{n}\frac{y_M}{y_3}(y_M)^{2/3}s_0^{1/2} \qquad (4.47)$$

10) Estimate the flow velocity, v_M at the middle of the computational sub-reach corresponding to y_M as

$$v_M = \frac{1}{n}y_M^{2/3}\sqrt{s_0} \qquad (4.48)$$

11) Estimate q_3 and q_M corresponding to v_3 and y_3; and v_M and y_M, respectively.

12) Estimate the Froude's number at the mid-section of the computational sub-reach as

$$F_{rp_M} = q_M / \sqrt{g(y_M)^3} \qquad (4.49)$$

13) Estimate the revised $K = \Delta x / c_3$.

14) Estimate the revised value of θ for the considered computational sub-reach using equation (4.20).

15) Repeat steps 5 to 14 to estimate the refined outflow runoff flow depth $y_{d,2}$ using equation (4.22) as in step 6.

145

16) Compute the outflow runoff discharge q_2 corresponding to $y_{d,2}$ given by equation (4.27) as

$$q_2 = q_3 + (5/3)v_3\left[y_{d,2} - y_3\right] \tag{4.50}$$

It is considered that the approximation involved in the computation of θ using the approximate location 'l' of the weighted runoff discharge, would not affect the accuracy of the routing solution based on this procedure.

4.4.2 Channel Flow Routing

The application of the VPMS method for routing runoff in the channel which has zero inflow depth at the upper end, but receives uniform runoff contribution along the flow path from both the overland flow planes on either side of the channel requires the subdivision of channel into number of equal sub-reaches of length ΔX. Similar to the flow computation adopted for the overland flow plane, two separate flow routing procedures, one for the upstream sub-reach of the channel for $t \geq \Delta t$ and for the rest of the sub-reaches for $t = \Delta t$; the other, for flow routing in the rest of the channel sub-reaches for time $t > \Delta t$.

4.4.2.1 Routing procedure for the first sub-reach when $t \geq \Delta t$ and for the rest of the sub-reaches when $t = \Delta t$

1) Considering zero initial runoff flow depth estimate the reference flow depth, Y_0 at current time step is estimated as

$$Y_0 = \frac{\left[\dfrac{(q_{RH} + q_{LH})\Delta t}{B} + q_L\Delta t\right] + Y_{d,1}}{2}; \qquad Y_{d,1} = 0, \text{when } t = \Delta t \tag{4.51}$$

where t represents the cumulative simulation time in terms of Δt from the beginning, which is bounded by the total simulation time, T as an upper limit; q_{RH} and q_{LH} are the unit width runoff discharge from the right and left hand side overland flow planes; and q_L is the direct net rainfall rate over the channel flow surface. Note that when $Y_0 = 0$, the estimated flow depth and the runoff discharge at the end of computational routing reach is set equal to zero and the computations are carried out for the next time level.

2) Estimate the channel flood wave travel time, K_c corresponding to the reference runoff flow depth, Y_0 as

$$K_c = \Delta X / C_0 \tag{4.52}$$

where C_0 = wave celerity corresponding to Y_0 which is estimated using the equation

$$C_0 = \left[1 + \frac{2}{3}\left(\frac{P \partial R / \partial Y}{\partial A / \partial Y}\right)\right] V_0 \tag{4.53}$$

where V_0 = channel flow velocity corresponding to Y_0.

3) The routing coefficients C_c is estimated as

$$C_c = \frac{K_c - 0.5\Delta t}{K_c + 0.5\Delta t} \tag{4.54}$$

4) Estimate the outflow runoff flow depth $Y_{d,2}$ at the downstream end of the computational reach at current time step using the recursive VPMS routing equation as

$$Y_{d,2} = C_c Y_{d,1} + (1 - C_c) K Q_L \tag{4.55}$$

The runoff flow depth estimated by equation (4.55) at the end of the first computational routing sub-reach becomes runoff flow depth at the upper end of the subsequent routing sub-reach.

4.4.2.2 Routing procedure for the second and subsequent sub-reaches when $t > \Delta t$

1) Estimate the reference runoff flow depth, Y_0 by using the three point average method

$$Y_0 = \frac{Y_{u,2} + Y_{u,1} + Y_{d,1}}{3} \tag{4.56}$$

where $Y_{u,1}$ = the inflow runoff flow depth at the upstream end of the computational sub-reach of the channel at the previous time level; $Y_{u,2}$ = the inflow runoff flow depth at the upstream end of the computational sub-reach of the channel at current time level; and $Y_{d,1}$ = the outflow runoff flow depth at the downstream end of the computational sub-reach of the channel at the previous time level.

2) Estimate the routing parameter K_c corresponding to the reference runoff flow depth, Y_0 using equations (4.52) and (4.53).

147

3) Estimate the weighting coefficient, θ_c corresponding to Y_0 as:

$$\theta_c = \frac{1}{2} - \frac{Q_0\left[1 - \frac{4}{9}(F_{rc})_0^2\left(1 - 2\frac{Y_0}{(B+2Y_0)}\right)^2\right]}{2S_0B\left[\frac{5}{3} - \frac{4}{3}\frac{Y_0}{(B+2Y_0)}\right]V_0\Delta X} \tag{4.57}$$

where S_0 = the channel bed slope; V_0 = flood wave velocity corresponding to Y_0; $(F_{rc})_0$ = Froude's number corresponding to Y_0.

4) The coefficients C_{c1}, C_{c2}, C_{c3} and C_{c4} are estimated as

$$C_{c1} = \frac{-K_c\theta_c + 0.5\Delta t}{K_c(1-\theta_c) + 0.5\Delta t} \tag{4.58}$$

$$C_{c2} = \frac{K_c\theta_c + 0.5\Delta t}{K_c(1-\theta_c) + 0.5\Delta t} \tag{4.59}$$

$$C_{c3} = \frac{K_c(1-\theta_c) - 0.5\Delta t}{K_c(1-\theta_c) + 0.5\Delta t} \tag{4.60}$$

$$C_{c4} = \frac{\Delta t}{K_c(1-\theta_c) + 0.5\Delta t} \tag{4.61}$$

5) The unrefined estimate of outflow runoff flow depth $Y_{d,2}$ from the computational sub-reach of the channel at current time step is estimated using the recursive VPMS routing equation

$$Y_{d,2} = C_{c1}Y_{u,2} + C_{c2}Y_{u,1} + C_{c3}Y_{d,1} + C_{c4}KQ_L \tag{4.62}$$

Estimate the normal stage at section 3 (Figure 4.2) using

$$Y_3 = \theta_c Y_{u,2} + (1-\theta_c)Y_{d,2} \tag{4.63}$$

6) Estimate the stage Y_M at the middle of the computational routing sub-reach using equation

$$Y_M = \frac{Y_{u,2} + Y_{d,2}}{2} \tag{4.64}$$

7) Estimate the flow velocity V_3 at section '3' by using equation

$$V_3 = \frac{1}{n_c}\frac{Y_M}{Y_3}R_M^{2/3}\sqrt{S_0} \tag{4.65}$$

148

8) Estimate the flow velocity V_M approximately at the mid-section of the routing sub-reach corresponding to Y_M as

$$V_M = \frac{1}{n_c} R_M^{2/3} \sqrt{S_0}$$

(4.66)

9) Estimate Q_3 and Q_M corresponding to V_3 and A_3; and V_M and A_M, respectively.

10) Estimate the Froude's number at the midsection of the routing sub-reach as

$$(F_{rc})_M = Q_M \left[(\partial A/\partial Y)_M / (g A_M^3) \right]^{(1/2)}$$

(4.67)

11) Estimate the revised value of K_c as

$$K_c = \Delta X / C$$

(4.68)

where the flood wave celerity C for a rectangular channel reach is estimated using the Manning's friction law, as

$$C = \left[\frac{5}{3} - \frac{4}{3} \frac{Y_3}{(B+2Y_3)} \right] V_3$$

(4.69)

12) Estimate the revised value θ_c for the considered channel sub-reach using the Manning's friction law as

$$\theta_c = \frac{1}{2} - \frac{Q_3 \left[1 - \frac{4}{9}(F_{rc})_M^2 \left(1 - 2 \frac{Y_M}{(B+2Y_M)} \right)^2 \right]}{2 S_0 B \left[\frac{5}{3} - \frac{4}{3} \frac{Y_3}{(B+2Y_3)} \right] V_3 \Delta X}$$

(4.70)

13) Repeat steps 4 to 12 to estimate the refined value of outflow runoff flow depth at the downstream end of the computational routing sub-reach using equation (4.62).

14) Compute the outflow runoff discharge, Q_2 from the computational channel sub-reach corresponding to $Y_{d,2}$ using equation

$$Q_2 = Q_3 + \left. \frac{\partial Q}{\partial Y} \right|_3 \left[Y_{d,2} - Y_3 \right]$$

(4.71)

Following the procedure as presented in this section 4.4, a FORTRAN code is developed for the estimation of the runoff and flow depth at the outlet of the V-catchment and is given in Appendix –II.

4.5 PERFORMANCE EVALUATION MEASURES

The results simulated by this VPMS method in reproducing the benchmark solutions are evaluated using the same performance evaluation measures as adopted for the evaluation of simulations of the VPMD method as described in section 3.5 of chapter 3.

4.6 APPLICATION

The VPMS overland flow model, presented in section-4.2, is applied to simulate runoff from overland flow planes with each of the plane characterized by a given set of slope of the plane, s_0 and the Manning's roughness coefficient, n or the Chezy's roughness coefficient, C_h. The evaluation of the proposed method is extensively carried out based on the assessment of comparison of the simulated runoff hydrographs for a unit width of the considered plane with the corresponding simulated benchmark overland flow hydrographs. Different benchmark solutions were obtained depending on the nature of the input such as semi-infinite uniform intensity rainfall, uniform intensity rainfall of duration $t_r < t_e$, $t_r = t_e$ and $t_r > t_e$, where t_e is the time to equilibrium or time of concentration of the considered overland flow strip for a given uniform intensity of rainfall. The benchmark solutions consist of hydrographs simulated for hypothetical rainfall inputs on hypothetical overland flow planes or strips, and the hydrographs observed either in laboratory or field experimental overland flow study facilities for specified rainfall input patterns. The hypothetical solutions were obtained using different approaches: 1) Analytical solutions of the KW equation [*Overton and Brakenseik*, 1973; *Overton and Meadows*, 1976; *Woolhiser*, 1974], 2) Approximate analytical solutions of the diffusive wave equation [*Govindaraju et al.*, 1990], 3) Solution of the full SVE using the explicit finite difference method, 4) Solution of the VPMD method [*Chapter* 3] 5) Runoff hydrographs simulated using the time integration method for the solution of the KW and DW equations [*Kazezyılmaz-Alhan et al.*, 2005; *Gottardi and Venuteli*, 2008], and 6) Solutions of the DW model proposed by *Lai* [2009]. While arriving at the full SVE solutions using the explicit numerical method, the stability of the numerical solution was ensured by satisfying the Courant condition, i.e., $\Delta t < \Delta x/(v+c_d)$, where c_d is the wave celerity of the dynamic wave [*Chow et al.*, 1988]. The performance of the VPMS method was also investigated by comparing its solutions with the observed hydrographs recorded corresponding to eight laboratory experimental storm events of complex pattern of rainfall input, conducted by *Izzard* [1942, 1944]. The data of these events have been reported by *Maksimović and Radojković* [1986]. Also the data of ten natural rainfall-runoff events recorded in the outdoor experimental laboratory facility developed by *Wong* [2009] at the Nanyang Technological University, Singapore were used for studying the proposed VPMS overland flow model. This facility consists of asphalt and concrete overland flow planes, and a concrete level V-catchment. Note that all

the numerical examples and experimental data used for the evaluation of the VPMS overland flow routing method have been already used for the evaluation of the VPMD overland flow routing method presented in chapter 3 and, therefore, at some places the input data are repeated for the sake of better understanding.

4.6.1 The Rising Runoff Hydrograph Cases

4.6.1.1 Results

The performance of the VPMS method for simulating the rising part of the overland flow hydrograph is evaluated using the standard experimental data of *Morgali and Linsely* [1965], quite often used by researchers [for example, *Govindaraju et al.,* 1990; *Gottardi and Venutelli,* 2008] of the overland flow studies. The Soil Conservation Services (SCS) (now, the NRCS) experimental plot used in this study consists of 21.945 m (72 ft) plane with 3.81 cm (1.5 in) thick soil turf overlying an impervious surface. The slope of this experimental plane was $s_0 = 0.04$. Two different semi-infinite spatially uniform intensity of rainfall of $r = 9.30$ cm/h (3.66 in/h) and $r = 4.8$ cm/h (1.89 in/h) were applied in simulating the rising overland flow hydrographs. The Manning's roughness coefficients estimated by *Morgali and Linsely* [1965] for the two rainfall intensities of $r = 9.30$ cm/h and $r = 4.8$ cm/h were $n = 0.5$ and 0.4 m$^{-1/3}$ /s, respectively. The same values of the Manning's n were used by *Gottardi and Venutelli* [2008] while evaluating these events of *Morgali and Linsely* [1965] using their DW model. While studying these events using the approximate DW model based on the Chezy's roughness coefficient, *Govindaraju et al.,* [1990] estimated the Chezy's roughness coefficient $C_h = 0.994$ m$^{1/2}$/s (1.8 ft$^{1/2}$/s) and 1.336 m$^{1/2}$/s (2.42 ft$^{1/2}$/s) for the rainfall intensities of 9.30 and 4.8 cm/h, respectively.

Figure 4.3a shows the observed experimental runoff hydrograph of the *Morgali and Linsley* [1965] for the rainfall intensity of 9.30 cm/h along with the corresponding solution of the VPMS method obtained using the solution procedure described in section 4.4.1 for overland flow estimation using the Chezy's friction law. Also the corresponding solutions of the VPMD method, the analytical KW solution [*Overton and Brakenseik*, 1973; *Overton and Meadows*, 1976; *Woolhiser*, 1974], explicit numerical solution of the SVE, and the approximate analytical solution of DW, which is also known as the one-term solution of the DW [*Govindaraju et al.* 1990] based on the Chezy's friction law ($C_h = 0.994$) are also presented. Similarly, Figure 4.3b shows the comparison of the same observed runoff hydrograph shown in Figure 4.3a, with the solutions of all the methods employed in Figure
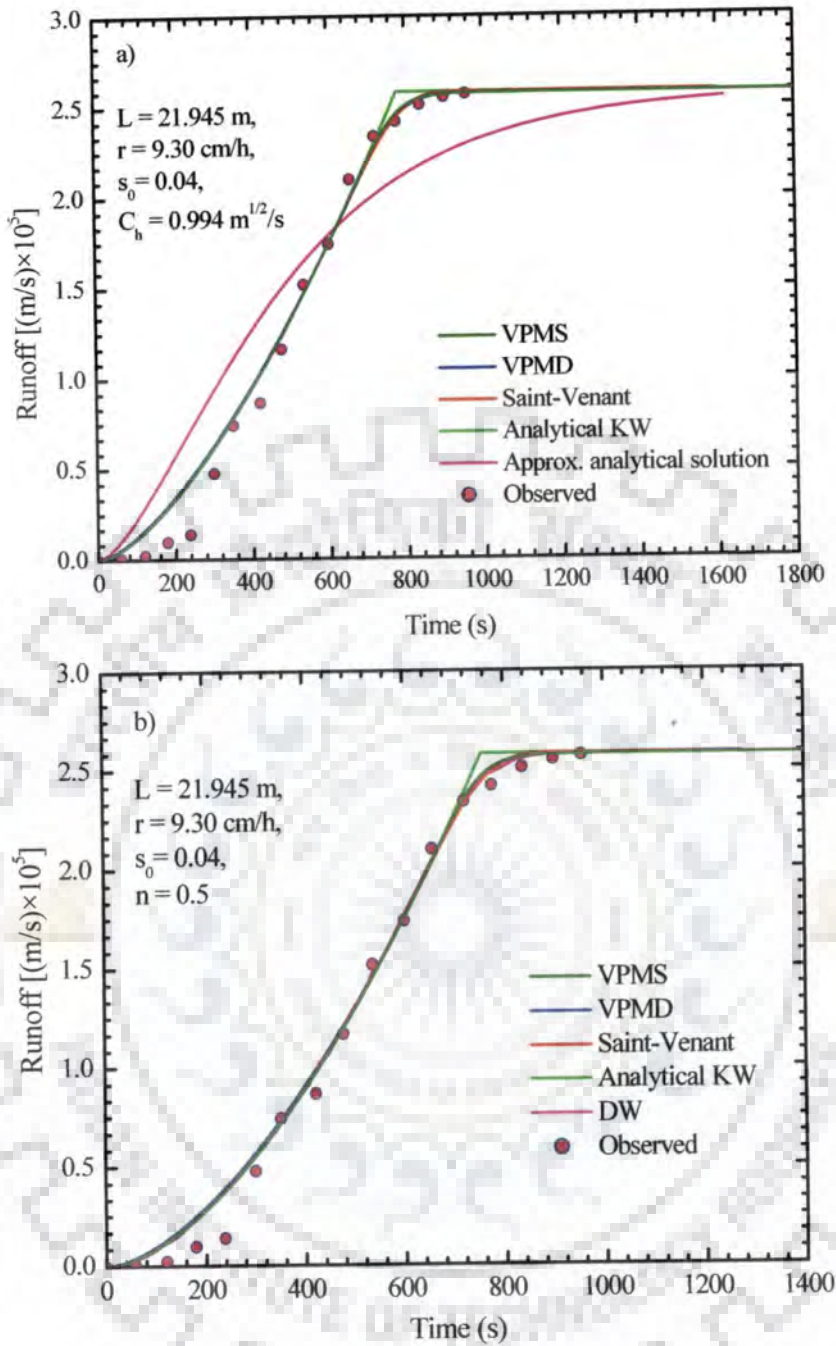
Figure 4.3 Comparison of the VPMS method simulated runoff hydrographs with a) observed hydrograph of *Morgali and Linsely* [1965], the VPMD method solution, the approximate analytical solution [*Govindaraju et al., 1990*], the classical analytical solution of the KW and the explicit method numerical solution of the SVE using the Chezy's friction law, and b) observed hydrograph of *Morgali and Linsely* [1965], the VPMD method solution, the DW solution of *Gottardi and Venutelli* [2008], the classical analytical solution of the KW and the explicit method numerical solution of SVE using the Manning's friction law.

4.3a except the one-term approximate solution of the DW [*Govindaraju et al.* 1990] which can be obtained only using the Chezy's friction law, but based on the Manning's roughness law. In addition to these methods, Figure 4.3b also shows the DW solution result of the *Gottardi and Venutelli* [2008] based on the accurate time integration method. The simulated runoff hydrograph at the outlet of the unit width strip of the overland flow plane is obtained using the VPMS and the numerical SVE method by dividing the unit width strip into 55 and 30 sub-reaches, respectively. The corresponding time intervals used were $\Delta t = 3$ s and 0.125 s, respectively. The same computational grid size as used in the VPMD method is adopted for the VPMS method solutions to facilitate the comparison of these two computational methods. In order to ensure the successful simulations of the overland flow using the VPMS method, a small temporal and spatial grid sizes have been used for this example. However, it is to be noted that the use of higher Δx and Δt values for the VPMS simulations are possible and further details on this aspect would be presented while discussing the sensitivity analysis of the VPMS method solutions for different temporal and spatial grid sizes.

4.6.1.2 Discussion

It has been brought out by *Perumal and Ranga Raju* [1999] that the approximate Convection-Diffusion (ACD) equations in stage and discharge formulations are capable of modelling the flood waves in the transition range of the applicability domains governed by the diffusive wave and the kinematic wave, including the latter. As the VPMS routing method has been developed from the ACD equation in flow depth (stage) formulation, one of the ways of demonstrating its capability for overland flow modelling is to apply the same first in the kinematic wave range and then, subsequently, demonstrate its capability for its application in the diffusive wave range. Accordingly, the rainfall-runoff simulations presented in Figures 4.3a and 4.3b were meant for demonstrating the suitability of the VPMS method for overland flow modelling in the kinematic wave range. In this context, the kinematic wave number (k) given by *Woolhiser and Liggett* [1967] and the parameter $k(F_{rp}^2)_e$ are used to assess the flow regime. These criteria state that when $k > 20$ and $k(F_{rp})_e^2 > 5$, the KW models can be used for overland flow simulations with acceptable

accuracy rather than using the full SVE [*Morris and Woolhiser*, 1980]. These applicability

parameters are expressed as

$$k = \frac{s_0 L}{y_e (F_{rp}^2)_e} \qquad (2.33)$$

$$k = 1.725 \times 10^6 \frac{n^{1.2} s_0^{0.4} L^{0.2}}{r_e^{0.8}} \qquad k(F_{rp}^2)_e = 8585.81 \times \frac{s_0^{1.3} L^{0.4}}{n^{0.6} r_e^{0.6}} \qquad (2.34a, b)$$

$$k = 2.247 \times 10^5 \frac{C_h^{-1.335} s_0^{0.335} L^{0.335}}{r_e^{0.665}} \qquad k(F_{rp}^2)_e = 22905.5 \times \frac{C_h^{0.665} s_0^{1.335} L^{0.335}}{r_e^{0.665}} \qquad (3.82a, b)$$

where, y_e is the computed flow depth at the outlet of the plane corresponding to equilibrium

discharge condition and $(F_{rp})_e$ is the corresponding Froude number. Note that equations

(2.34a, b) and (3.82a, b) are applicable when the Manning's and Chezy's friction laws have

been employed, respectively, in the simulation of the overland flow hydrograph.

In the present example, the estimated k, $k(F_{rp}^2)_e$ and $(F_{rp})_e$ values based on equation

(3.82), i.e., based on the Chezy's friction law, were 10646.34, 42.89 and 0.063

corresponding to the observed results shown in Figure 4.3a. Similarly these values

estimated based on the Manning's friction law were 10232.75, 44.93 and 0.066

corresponding to the observed runoff results shown in Figure 4.3b. The corresponding

estimates based on the VPMS method solutions were 10802.25, 43.50, and 0.063, and

10212.26, 44.82, and 0.066, pertaining to the results shown in Figure 4.3a and 4.3b,

respectively. Therefore, it can be inferred from these estimates of the applicability limits

that the flow regimes are well within the KW applicability limit as established both based

on the relationships given by equations (2.34) and (3.82), and the VPMS simulations. The

respective estimates also closely agree with each other. The estimates of the time of

equilibrium, t_e in seconds arrived at by the analytical kinematic wave approach using

equation (3.83a, b) were 12.98 min and 12.60 min when applied using the Chezy's and the

Manning's friction law, respectively. Further, the performance of the VPMS method is

evaluated using various performance assessment measures given in section 3.5. The various measures such as the Nash-Sutcliffe efficiency (η_q), CRM (%), CD and the percentage error in simulating the peak of the runoff hydrograph (q_{perr}) estimated in comparison with the observed data and the simulated runoff hydrographs obtained using the analytical KW and the DW solutions (only for Figure 4.3b), all shown in Figures 4.3a and 4.3b, are presented in Table 4.1. Similarly, the performance evaluation measures estimated in comparison with the numerical solution of the SVE based on the explicit method along with those for the VPMD method are presented in Table 4.2. It can be inferred from these results that the VPMS method is able to closely simulate the behavior of the overland flow as given by the observed hydrographs. It can be inferred from the estimated CRM values of -4.94 and -3.89%, corresponding to Figures 4.3a and 4.3b, respectively, the presence of some error in mass conservation as compared to that of the observed hydrographs which may be attributed to the non-consideration of initial interception loss caused by the ground and detention storage due to the presence of grass on the plane resulting in the discrepancy of the computed flow in the initial few minutes of simulation. Otherwise, as compared with the other models, especially the numerical SVE solution, the VPMS method is able to conserve the mass accurately. Further, the value of CD close to 1 suggests a very close agreement of the VPMS method with that of the DW and SVE solutions. It can also be inferred from the Nash-Sutcliffe efficiency criterion values that the simulated hydrographs by the VPMS method are in very close agreement with the solutions of SVE, DW and the analytical KW, except with one-term solution of *Govindaraju et al.* [1990]. Therefore, it may be considered that the analysed rainfall-runoff event is indeed kinematic in nature. Further, the comparison of the VPMS method simulated hydrograph with the observed data elucidates that the use of the Manning's friction law for the overland flow simulation results in a better performance by the VPMS method as compared to that based on the use of the Chezy's friction law. It can also be revealed from Table 4.2 that the performance parameters η_q,

Table 4.1 Evaluation of the rising hydrographs simulated by the VPMS method with those of other methods

Simulations Shown in Figure	Benchmark Solution	Performance Evaluation Measures				CPU-time (s) for VPMS Method	CPU-time (s) for SVE Method	Applicability Criteria			
		η_q (%)	CRM (%)	CD	q_{perr} (%)			Method	k	kF_{rp}^2	F_{rp}
3a	Observed	98.72	-4.94	1.12	0.25	0.16	3.828	Analytical KW	10646.3	42.89	0.06
	Analytical KW	99.95	0.41	1.01	-0.23	0.14		VPMS	10802.25	43.50	0.06
3b	Observed	99.29	-3.89	1.06	0.26	0.125		Analytical KW	10232.8	44.93	0.07
	Analytical KW	99.98	0.34	1.01	-0.21	0.157	3.531				
	DW	99.92	1.33	0.98	-0.21	0.140		VPMS	10212.26	44.82	0.07
4a	Observed	85.94	-25.72	0.90	0.05	0.157	5.641	Analytical KW	11134.3	81.04	0.08
	Analytical KW	99.99	0.28	1.01	-0.21	0.172		VPMS	11336.26	82.51	0.09
4b	Observed	98.30	-6.75	1.10	0.43	0.156	4.563	Analytical KW	16523.6	66.57	0.06
	Analytical KW	99.98	0.35	1.01	-0.21	0.156		VPMS	16811.20	67.69	0.06
4c	Observed	95.61	-14.67	0.95	0.07	0.157		Analytical KW	13284.9	76.39	0.08
	Analytical KW	99.99	0.27	1.01	-0.18	0.172	5.875				
	DW	94.72	-12.63	0.88	-0.16	0.141		VPMS	13284.13	76.29	0.08
4d	Observed	98.95	-0.53	1.10	0.07	0.125		Analytical KW	17364.1	66.81	0.06
	Analytical KW	99.97	0.48	1.02	-0.18	0.141	4.922				
	DW	99.99	0.05	0.99	-0.16	0.125		VPMS	17355.10	66.71	0.06

Table 4.2 Evaluation of the rising hydrographs simulations by the VPMS and VPMD methods with the solution of the Saint-Venant equations

Simulations Shown in Figure	Rainfall Intensity (cm/h)	Roughness Coefficient	Performance Evaluation Measures Estimated Using the SVE as a Benchmark Solution								CPU Run-time		
			VPMS				VPMD				VPMS	VPMD	SVE[*]
			η_q (%)	CRM (%)	CD	q_{perr} (%)	η_q (%)	CRM (%)	CD	q_{perr} (%)	CPU-time (s)	CPU-time (s)	CPU-time (s)
3a	9.30	$C_h = 0.994$	100.0	0.13	1.00	-0.23	99.98	-0.40	1.01	0.00	0.172	0.156	3.828
3b	9.30	$n = 0.5$	100.0	0.11	1.00	-0.21	99.95	-0.55	1.01	0.00	0.172	0.156	3.531
4b	4.8	$C_h = 0.994$	99.99	0.07	1.00	-0.31	99.98	-0.47	1.01	-0.12	0.172	0.141	4.563
4d	4.8	$n = 0.5$	99.99	0.05	1.00	-0.23	99.96	-0.67	1.01	-0.05	0.172	0.109	4.922

[*] the computational grid sizes are different ($\Delta x = 0.73$ m and $\Delta t = 0.125$ s) than that used for the solutions of the VPMS and VPMD methods
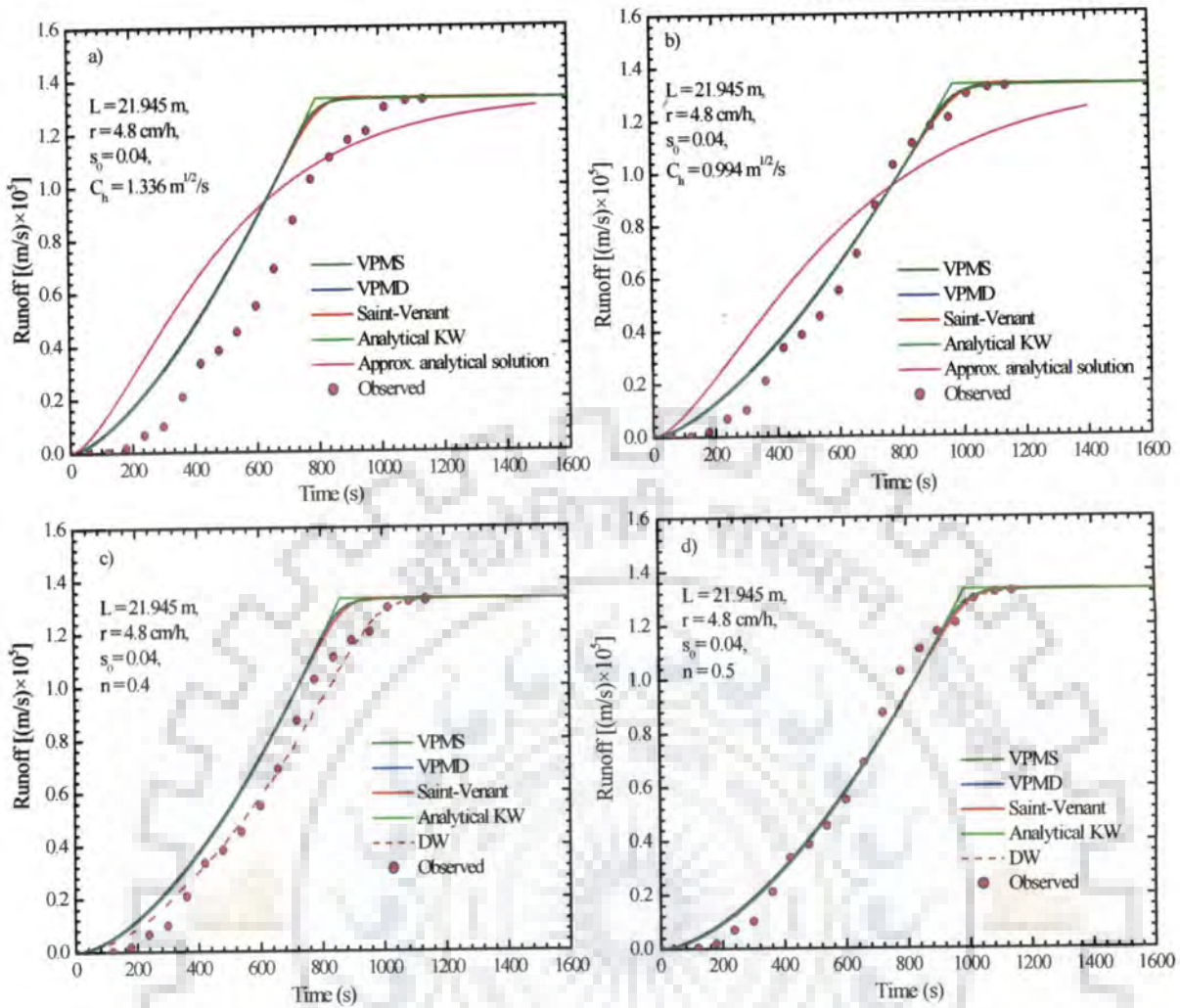
Figure 4.4 Comparison of the VPMS method simulated runoff hydrographs with the observed hydrograph of *Morgali and Linsely* [1965], and with other solutions used as in Figure 4.3 with a) $C_h = 1.336$ b) $C_h = 0.994$ c) $n = 0.4$ and d) $n = 0.5$.

CRM, and CD estimated for the VPMS method in comparison with the SVE solution are relatively better than those obtained for the VPMD method, except that the VPMS method shows slightly higher error in the estimation of peak discharge of the runoff hydrograph, q_{perr}. Although a very fine grid size was chosen for runoff simulation by the VPMS and VPMD methods, the computation times for both runoff hydrographs simulations as shown in the Figure 4.3a and 4.3b are almost same and they are very small as compared with that of the SVE solution to simulate the same event. Computation time is one of the vital considerations in the selection of any scheme in hydrological model applications, especially to large basin studies. The computation time for the corresponding SVE solution of the overland flow simulation is approximately 24 times higher than that of the VPMS method.

Figure 4.4 shows the simulated hydrographs by the VPMS method in comparison with the other solutions and observed hydrographs, presented in the same form as in Figure 4.3, but for the rainfall intensity of 4.8 cm/h. It may be inferred from this figure that the Chezy's roughness coefficient ($C_h = 1.336$) recommended by *Govindaraju et al.* [1990] and the Manning's roughness coefficient ($n = 0.4$) recommended by *Morgali and Linsely* [1965] for this case are not appropriate. This inference can be verified from the poor performance evaluation measures estimated for the cases corresponding to Figures 4.4a and 4.4c as described in Tables 4.1, wherein the values of η_q, CRM, CD and q_{perr} have been estimated by comparing the solutions of the VPMS method with the corresponding observed hydrographs, the analytical KW solutions and the DW solutions. This inference is corroborated very clearly from Figures 4.4a and 4.4c which reveal that with the use of the recommended $C_h = 1.336$ and $n = 0.4$, respectively, the simulated runoff hydrographs by the VPMS and VPMD methods, the SVE solution, the analytical solution of the KW and the one-term solution of the DW all deviate by a greater degree from the observed runoff hydrograph and from the simulated results of *Gottardi and Venutelli* [2008] for the DW method. It is surmised that this deviation may be attributed to the inappropriate values of the friction coefficients used for the simulation of these events. This inference enables one to be cautious that from the reliable catchment modelling point of view, not only an appropriate hydrological model is important to accurately model the rainfall-runoff process, but also the use of appropriate model parameters is equally important.

However, with the use of Chezy's and Manning's frictrion coefficients as used for the event of 9.30 cm/h rainfall intensity as shown in Figure 4.3, the accurate reproductions of the observed hydrograph corresponding to the event with rainfall intensity of 4.8 cm/h could be achieved. The simulated hydrographs of the VPMS method in comparison with the observed hydrographs and the other solution methods are shown in Figures 4.4b ($C_h = 0.994$) and 4d ($n = 0.5$) based on the use of Chezy's and Manning's friction laws, respectively. The runoff hydrographs simulated by the VPMS and VPMD methods, the SVE solution, the analytical solution and the one-term solution of the DW are all able to closely match the observed hydrograph. Furthermore, the performance measures η_q, CRM, CD and q_{perr} estimated using the VPMS method solution in comparison with the observed hydrograph and the simulated runoff hydrographs using the analytical solution of the KW and the DW solutions (only for the case d), all shown in Figure 4.4b and 4.4d, are presented

in Table 4.1. Similarly, the estimated performance evaluation measures for the VPMS and VPMD methods in comparison with the SVE solution, all shown in Figure 4.4b and 4.4d, are presented in Table 4.2. It can be concluded from this analysis that the use of the correct friction coefficient would be resulting in improved overland flow simulation process. Further, similar conclusions as arrived at for the events simulated corresponding to Figure 4.3 can be applicable for this case also. Consequently, the estimated values of time of equilibrium, t_e were 13.28 min for $C_h = 1.336$, 16.18 min for $C_h = 0.994$, 14.36 min for $n = 0.4$, and 16.42 min for $n = 0.5$. It is inferred from these results that the friction coefficient has also impact on the time of concentration of the catchment. The CPU times required for the solutions using the VPMS, VPMD and SVE methods for the simulation of the event as depicted in the Figures 4.4a-4.4d are shown in Table 4.2. These results, as in the earlier study, demonstrate the computational efficiency of the VPMS method over that of the numerical SVE solution. Furthermore, the estimated k, $k(F_{rp}^2)_e$ and $(F_{rp})_e$ values estimated using the analytical KW approach and by the VPMS method for all the four cases, shown in Figure 4.4, are presented in Table 4.1. It is surmised from this analysis that the flow is well within the KW applicability regime and k, $k(F_{rp}^2)_e$ and $(F_{rp})_e$ estimated using the VPMS method are in close agreement with the respective estimates of the analytical solutions of the kinematic wave. Furthermore, a careful examination of these applicability criteria values estimated for 9.30 cm/h and 4.8 cm/h intensities indicate that with the decrease in rainfall intensity there is an overall increase in the estimates of k, $k(F_{rp})_e^2$ and $(F_{rp})_e$, suggesting close adherence to the kinematic flow conditions, provided all the other physical conditions remain the same.

4.6.2 Overland Flow Hydrographs for Pulse Rainfall Input

While the capability of the VPMS method to simulate the rising part of the hydrograph has been demonstrated in the earlier section, its capability to simulate the recession limb of the hydrograph also needs to be demonstrated. This aspect is studied herein by simulating the entire overland flow hydrograph for a pulse input. The simulated overland flow hydrographs by the VPMS method are compared with the corresponding numerical SVE solutions, the classical analytical solutions of the KW and the solutions of the time integration method of the DW equation [*Gottardi and Venutelli*, 2008] for assessing the ability of the method to reproduce the rising as well as the falling limbs of the overland flow hydrographs. The

example presented by *Gottardi and Venutelli* [2008] for a pulse input with a rainfall duration $t_r > t_e$, the time of equilibrium of the overland flow strip, is used here for the comparison purpose. Using the same rainfall intensity two different cases were also studied, with $t_r < t_e$ and $t_r = t_e$ to demonstrate the capability of the VPMS method to simulate the partial equilibrium hydrographs. *Gottardi and Venutelli* [2008] used the spatially uniform and steady rainfall of intensity $r = 6$ cm/h (2.3622 in/h) falling over a unit width strip of sloping plane having a length $L = 200$ m. The plane is characterised by a slope $s_0 = 0.001$ and a Manning's roughness coefficient $n = 0.03$. The three different cases studied herein are designated as (1) Case I ($t_r < t_e$), (2) Case II ($t_r = t_e$), and (3) Case III ($t_r > t_e$) which is the study of *Gottardi and Venutelli* [2008]. The rainfall durations (t_r) considered are 25 minute, 31.6 minute and 1 h for cases I, II and III, respectively. The time of equilibrium for this watershed by analytical kinematic wave approach using equation (3.83a) is $t_e = 31.6$ min, which forms the basis for selecting these three cases under consideration.

The steady state flow depths y_e at the end of the overland flow plane computed with the VPMS and VPMD methods and the SVE solution are 0.033, 0.033 and 0.032 m, respectively. Note that the t_e and y_e values reported herein are the same as estimated by *Gottardi and Venutelli* [2008]. The analytically estimated k, $k(F_{rp}^2)_e$ and $(F_{rp})_e$ corresponding to the equilibrium flow condition are 176.61, 6.32 and 0.19, respectively. Though these estimates very well satisfy the kinematic wave applicability criteria, the magnitude of $k(F_{rp}^2)_e$ very close to 5 suggests that the generated overland flow is nearly kinematic in nature. Using the VPMS and VPMD methods, the estimated k, kF_{rp}^2 and F_{rp} for the case III ($t_r > t_e$) are 171.72, 6.18 and 0.19 and 187.79, 6.14 and 0.18, respectively, while the corresponding value of k estimated by *Gottardi and Venutelli* [2008] was $k = 188$. As compared to the applicability criteria measures estimated for the analytical kinematic wave solution for case III, the corresponding VPMS method computed k, kF_{rp}^2 and F_{rp} are comparatively lower as expected due to the accounting of diffusion present in the system by the VPMS method. Similarly, as compared to the k estimated for the VPMD method for case III, the corresponding VPMS method estimated k is slightly lower, while the corresponding estimate of F_{rp} is comparatively higher than that of the VPMD method.

161

However, both of these methods give almost equal estimate of the kF_{rp}^2. The difference in the magnitude of k by the VPMS and VPMD method may be attributed to the binomial series expansion involved in the derivation of these methods. The longitudinal gradient of water depth ($\partial y/\partial x$) involved in the binomial series expansion is obtained directly in the VPMS method, while it is obtained indirectly in the VPMD method [*Perumal and Ranga Raju*, 1998b]. Therefore, the truncation error introduced by the binomial series expansion, especially in the diffusion wave applicability range leads to somewhat different estimation of applicability criteria for both of these methods. However, if the truncation error due to a binomial series expansion is not significant, especially near the applicability range of the kinematic wave, then the estimation of these applicability criteria measures by both of these methods would be nearly equal. Similarly, for other cases of t_r, i.e. cases I and II, using the flow depths estimated by the VPMS and VPMD methods at the end of plane in equation (2.33) enables one to compute the k, kF_{rp}^2 and F_{rp}. The estimated applicability criteria for the VPMS method are 243.15, 8.04 and 0.18 and 192.42, 6.74, 0.19, respectively for case I, II, while the corresponding estimates for the VPMD method are 235.16, 7.76 and 0.17 and 198.52, 6.61, and 0.18, respectively. It can be inferred from these results that the rainfall duration also influences the applicability criteria, as the case of $t_r < t_e$ results in increased estimates of k, kF_{rp}^2 and F_{rp}.

The simulated runoff hydrographs for all these three cases are shown in Figure 4.5. It is seen from Figure 4.5b that the VPMS method is able to very closely reproduce the rising as well as the recession limbs of the runoff hydrographs simulated using the numerical solution of the SVE, the VPMD method [*Chapter* 3] and the DW solution by *Gottardi and Venutelli* [2008] (for case III). It can also be inferred from Figure 4.5b that the simulated runoff hydrographs of the VPMS, VPMD and DW of the considered rainfall event is not fully kinematic in nature as the simulations deviate away from the classical analytical solution of KW at the upper end, thus, demonstrating the presence of diffusion in the runoff generation. Analysis of the results of case I ($t_r < t_e$) demonstrate that the VPMS method solution begins to recede immediately after the rainfall ceases, which is a realistic simulation of the considered event. However, the analytical KW solution fails to capture the instantaneous start of the recession phase due to its inherent assumption that the flow is kinematic at any location. The recession limbs of the runoff hydrographs simulated by the proposed method for all the three cases are in well agreement with the SVE solution exhibiting the
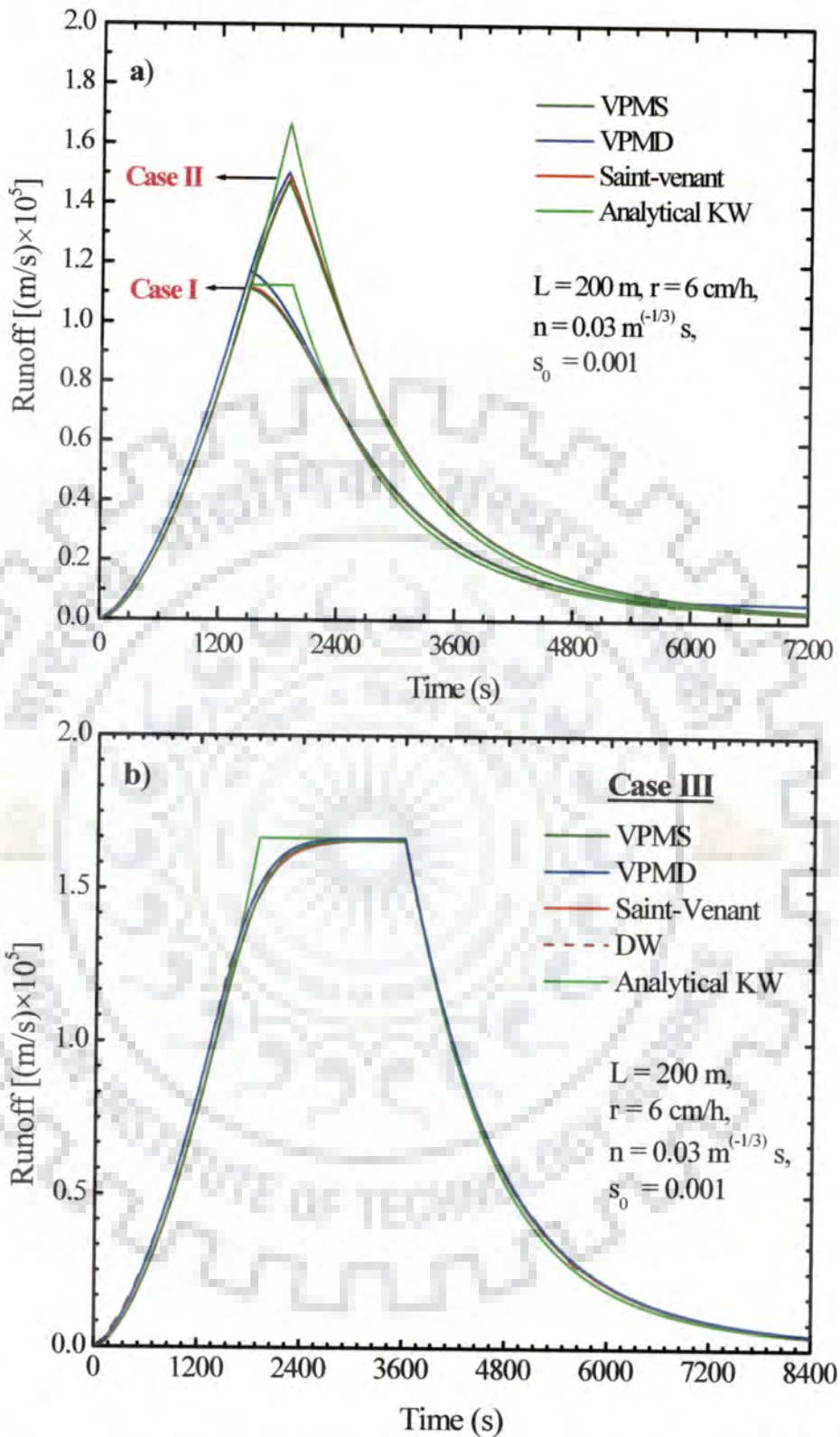
Figure 4.5 Comparison of simulated runoff hydrograph by the VPMS method with the VPMD method, analytical solution of the KW model, numerical solution of the SVE and the DW solution of *Gottardi and Venutelli* [2008] considering three cases: (I) $t_r < t_e$ (II) $t_r = t_e$ and (III) $t_r > t_e$.

comparatively slower recession rate, especially at the lower portion of hydrographs, in comparison with the analytical KW solution which recedes faster in the absence of diffusion. It can also be seen that there is no any significant difference between the runoff hydrographs simulated by the VPMD and VPMS methods. However, for cases I and II, the runoff peak as well as the rising limb simulated by the VPMD method are slightly overestimated as compared to those by the SVE and VPMS methods. The overestimation of the rising limb by the VPMD method is attributed to the use of higher temporal grid size Δt. But, VPMS method is able to reproduce the solution accurately, even with the use of such a larger temporal grid size. To simulate the runoff hydrographs as shown in Figure 4.5, computational grid sizes used for the solutions of the VPMS and VPMD methods were $\Delta x = 0.5$ m and $\Delta t = 30$ s, while the corresponding grid size for the SVE solution were $\Delta x = 1$ m and $\Delta t = 0.125$ s.

These inferences can also be made based on the performance measures computed for all these three cases using finer and coarser grid sizes as presented in Table 4.3. Although, the grid sizes considered herein do not strictly follow the Courant condition, there is almost no significant impact on the accuracy of the VPMS method. The performance evaluation measures such as η_q, CRM , CD, q_{perr} and t_{perr} computed in comparison with the SVE solution and the analytical KW solutions are able to demonstrate the adequacy of the VPMS method for overland flow modelling to simulate the runoff hydrographs accurately and efficiently, which closely simulate the SVE solutions rather than the analytical KW solution. Similarly, the performance evaluation measures computed for the VPMD method in comparison with the SVE solution for all these three cases are shown in Table 4.3, in order to facilitate its comparison with the VPMS method. The comparison of these performance evaluation measures computed for the VPMS and VPMD methods clearly brings out that even with the use of higher temporal grid size Δt, the VPMS method provides relatively better runoff hydrograph simulations than those using the VPMD method. The volume conservation error estimates, EVOL of the VPMS method for all the three cases with the consideration of three computational grid sizes ($\Delta x = 0.1, 0.5, 5.0$ m and constant $\Delta t = 30$ s) are very close to those estimated using the SVE solution and are relatively less than those estimated for the VPMD method. However, differences in the solutions of both of these methods increases with the increase in the spatial grid size due to the violation of the assumption of linear variation of the runoff discharge and flow depth used in the VPMD and VPMS methods. It can be noted that the VPMD method is slightly restrictive in the use of time step Δt than the VPMS method. Although finer spatial grid sizes were used for runoff hydrograph simulation by the VPMD and VPMS methods, the

Table 4.3 Performance evaluation of the VPMS method in comparison with the VPMD method solution for runoff hydrograph simulations considering three durations of pulse rainfall inputs: $t_r < t_e$ (Case I), $t_r = t_e$ (Case II) and $t_r > t_e$ (Case III)

Case	Δx (m)	Δt (s)	$\dfrac{\Delta x}{\Delta t}$	c_{max}	Analy KW η_q (%)	η_q (%)	CRM (%)	CD	q_{perr} (%)	t_{perr} (min)	η_q (%)	CRM (%)	CD	q_{perr} (%)	EVOL (%)	CPU-time (s)	EVOL (%)	CPU-time (s)	EVOL (%)	CPU-time (s)
I	5.0	30	0.167	0.15	99.53	99.99	0.42	1.01	-0.11	0.00	99.67	-4.10	0.92	5.54	-1.36	0.28	3.11	0.27		
	0.5	30	0.017	0.15	99.55	100.0	-0.21	1.00	-0.04	0.00	99.71	-3.80	0.92	5.15	-0.74	0.95	2.81	0.80	-0.96	14.02
	0.1	30	0.003	0.15	99.56	100.0	-0.30	1.00	-0.03	0.00	99.70	-3.86	0.92	5.25	-0.65	3.75	2.88	3.16		
II	5.0	30	0.167	0.17	99.38	99.97	1.13	1.02	-0.64	0.00	99.80	-2.63	0.96	1.97	-1.89	0.39	1.84	0.38		
	0.5	30	0.017	0.17	99.43	99.99	0.50	1.01	-0.18	0.00	99.83	-2.39	0.96	1.87	-1.27	1.06	1.60	0.92	-0.78	14.09
	0.1	30	0.003	0.17	99.43	99.99	0.41	1.01	-0.13	0.00	99.82	-2.45	0.96	1.90	-1.18	3.75	1.66	3.27		
III	5.0	30	0.167	0.17	99.70	100.0	0.40	1.01	-0.68	0.00	99.91	-2.06	0.98	0.36	-1.22	0.30	1.23	0.25		
	0.5	30	0.017	0.17	99.73	100.0	-0.21	1.00	-0.08	0.00	99.92	-1.94	0.98	0.36	-0.61	0.94	1.11	0.78	-0.50	21.95
	0.1	30	0.003	0.17	99.74	100.0	-0.31	1.00	0.01	0.00	99.92	-1.97	0.98	0.36	-0.52	3.91	1.13	3.17		

Column groupings: Under "Bench Mark Solution for Estimation of Performance evaluation Measures" — Analy KW (η_q); Saint-Venant split into VPMS (η_q, CRM, CD, q_{perr}, t_{perr}) and VPMD (η_q, CRM, CD, q_{perr}). Under "Error In Volume and Run-Time" — VPMS (EVOL, CPU-time), VPMD (EVOL, CPU-time), SVE (EVOL, CPU-time).

computational times required for both these methods are nearly same when the same grid sizes have been used and which are nearly 15-73 times lower as compared to that required for the SVE solution. Overall, these numerical experiments suggest that the VPMS method is a reasonable approximation of the SVE like those of the VPMD and DW equations.

The capability of the VPMS method is further verified using the rainfall-runoff study of *Lai* [2009] who solved diffusive wave equations using hybrid mesh method (SRH-W) based on finite-volume formulation for overland flow simulation. The rainfall-runoff event studied by *Lai* [2009] were also studied earlier by *Govindaraju et al.* [1988 a, 1988b] and *Therrien et al.* [2003] to verify their methods. The overland flow plane used in this study is characterised by a slope of $s_0 = 0.01$ and the hydrograph is simulated at the end of plane at $L = 100$ m. Two cases were considered for the simulation study: Case I) rainfall intensity $r = 1440$ cm/h, Manning's roughness coefficient $n=0.0548$, with a reported kinematic wave number and Froude number is 10 and 0.5, respectively. Case II) rainfall of intensity $r = 972$ cm/h, Manning's roughness coefficient $n=0.0155$, and a reported kinematic wave number and Froude number is 3 and 1.5, respectively. While the case I event is characterised by an estimate of $kF_{rp}^2 = 2.5$ and that of case II by an estimate of $kF_{rp}^2 = 6.75$.

For the example of case I, the analytically computed t_e using equation (3.83a) is $t_e = 1.68$ min and the corresponding applicability criteria estimated using equation (2.34a,b) are $k = 9.92$, $k(F_{rp})_e^2 = 2.49$ and $(F_{rp})_e = 0.5$; while, for the case II, the corresponding estimates are $t_e = 0.92$ min, $k = 2.99$, $k(F_{rp})_e^2 = 6.71$ and $(F_{rp})_e = 1.5$. These estimates are the same as those reported by *Lai* [2009]. One may infer that the flow conditions in both of these cases are beyond the applicability range of the kinematic wave model and they may fall in-between the applicability range of the diffusion and kinematic waves. Moreover, the diffusion wave equation is a good approximation to the dynamic wave equation, if the kinematic wave number is not too small [*i. e.* $k > 5$]. The previous solutions of this case such as those of DW by *Lai* [2009], KW by *Govindaraju et al.* [1988a, 1988b] and DW by *Therrien et al.* [2003] [see *Lai*, 2009] used the zero-depth gradient downstream boundary conditions. *Lai* [2009] had used a spatial grid size of $\Delta x = 1$m for the DW solution. Further, he reported that for case I, the stable solution may be obtained by the explicit scheme using $\Delta t \leq 0.015$ s (actually used 0.01 s), while an implicit scheme can allow the use of $\Delta t \leq 5$ s without hampering the solution accuracy. Similarly, for case II, he reported the use of $\Delta t <$

0.015 s and $\Delta t \leq 1$ s may be admissible, respectively, for the explicit and implicit schemes. The same spatial grid size is used in this study for simulation using the VPMS method and VPMD method [*Chapter* 3, section 3.6.2] with the use of $\Delta t = 1$ s and 0.5 s for case I and II, respectively. The kinematic wave and diffusion wave solutions do not take into account the effect of inertial terms, hence the term $\left(1-(4/9)F_{rp_M}^2\right)$ in equation (4.20) is ignored during computation to facilitate the comparison with the solutions by *Lai* [2009]. The effect of inclusion of this term on the simulation of the runoff process is evaluated separately for the same example. However, it was found during the present investigation that the use of larger computational temporal grid sizes (20s and 6s for case I and II, respectively) in the VPMS method solution than those prescribed for implicit scheme by *Lai* [2009], can be used without facing any stability problem and with acceptable accuracy.

Figure 4.6 shows the non-dimensional runoff hydrographs (non-dimensionalised with respect to the time of equilibrium computed using the analytical kinematic wave solution on the x-axis and with equilibrium discharge on the y-axis) simulated using the VPMS method at the end of the overland flow plane for both the cases under discussion along with the corresponding analytical solutions of the KW, numerical solutions of the SVE, the VPMD method solution, solutions of the DW [*Therrien et al.*, 2003], the KW solutions of *Govindaraju et al.* [1988a, 1988b], and the SVE solutions of *Daluz Vieira* [1983] as presented by *Lai* [2009]. It is seen from Figure 4.6a that the VPMS and VPMD methods are able to reproduce runoff hydrograph of the SVE solution with $\eta_q = 99.05$ and 99.59 %, $CRM = 1.54$ and -0.54 %, and $CD = 1.10$ and 1.08, respectively. Similarly, the VPMS and VPMD methods are also able to reproduce runoff hydrograph of the analytical KW solution with the evaluation measures: $\eta_q = 97.52$ and 98.79 %, $CRM = 2.50$ and 0.44 %, $CD = 1.03$ and 1.02, respectively. It can be inferred that the VPMS method simulated runoff hydrograph is also able to reproduce the SVE solutions, both the DW solutions and the VPMD method solution closely rather than those based on the kinematic wave solutions. Thus, it can be inferred that the VPMS method has higher applicability range than the kinematic wave solution. As compared with the VPMD method solution, the VPMS method solution has slightly lower performance for this particular case.

In the simulation study of case II event, the VPMS and VPMD methods solutions are able to reproduce the runoff hydrograph with $\eta_q = 96.54$ and 95.79 %, $CRM = -0.16$ and
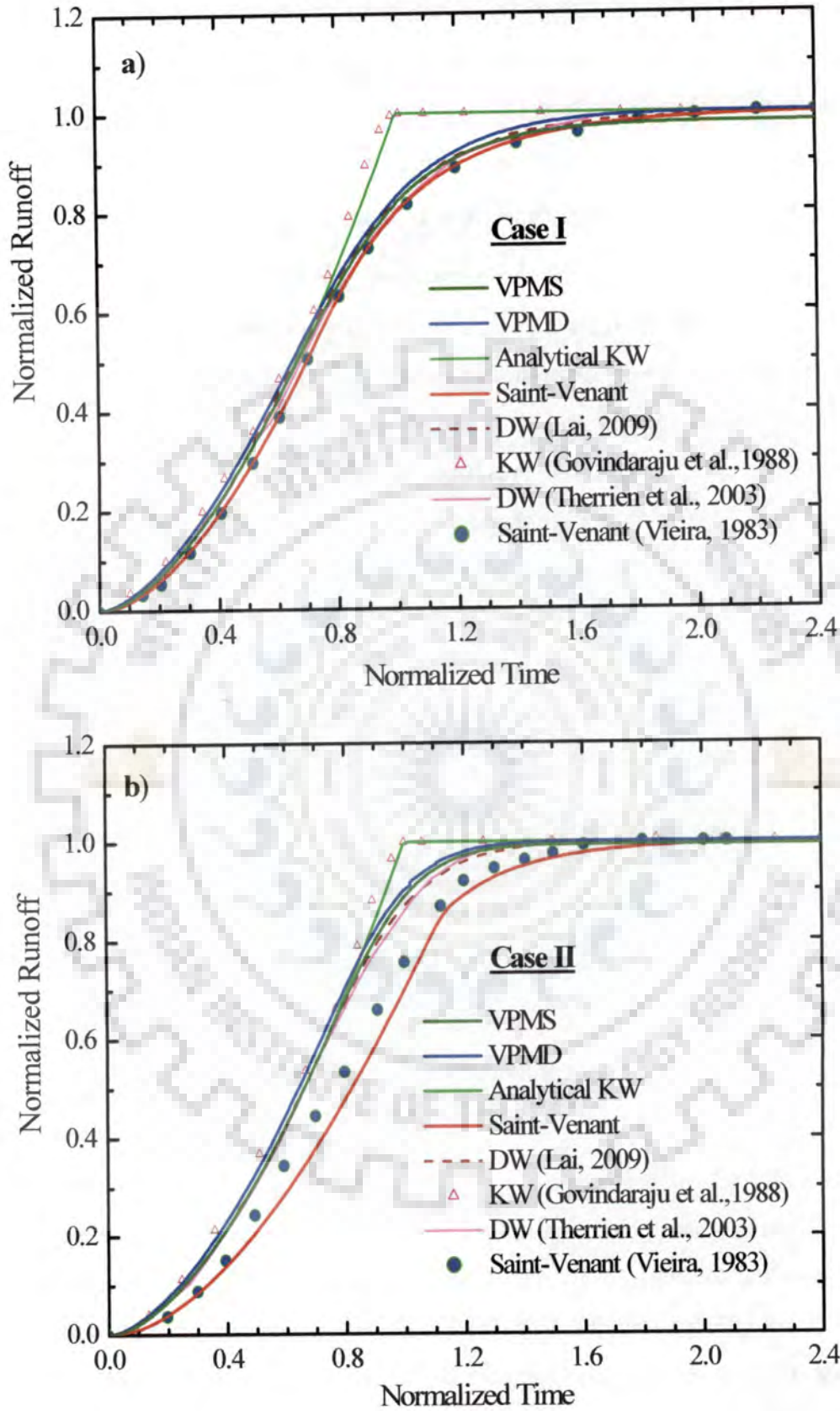
Figure 4.6. Comparison of the VPMS method simulated runoff hydrographs with various other solutions using the example of *Lai* [2009].

-0.84 %, and CD = 1.22 and 1.24, in comparison with the SVE solution and with η_q = 99.56 and 99.76 %, CRM = 0.69 and 0.03 %, and CD = 1.0 and 1.03, in comparison with analytical KW solution, respectively. It is inferred from these performance evaluation measures that the VPMS method simulated runoff hydrograph is slightly better than the VPMD method simulated runoff hydrograph, and the simulated runoff hydrographs of both the methods are comparatively closer to the KW solution rather than to the SVE solution. The same inference can be made from Figure 4.6b which clearly shows that there is no any significant difference between the DW and both the VPMS and VPMD methods solutions. These inferences imply that neither the KW nor the DW or the VPMS and VPMD solutions are reasonably good approximations to the SVE solution in reproducing the rising limb of the hydrograph. The deviations between the other solutions under consideration and that of the SVE may be attributed to the overland flow condition exemplified by the Froude number $(F_{rp})_e > 1$, i.e. the flow is in the supercritical regime and, therefore, in such a situation the inertial terms are dominant. Further, *Daluz Vieira* [1983] concluded that when $(F_{rp})_e \rightarrow \infty$ and $k < 5$, the gravity wave solution approaches the SVE solution and, thus, it may be appropriate to use the SVE only for simulation of such events rather than the simplified models derived from the SVE.

Furthermore, in both these cases corresponding to Figure 4.6a and 4.6b, the emphasis must be given to the realistic physical conditions responsible for the generation of flow as well as the governance of the overland flow mechanism. An assessment of the overland flow hydrograph simulations as shown in Figure 4.6 draws attention to two important issues: a) such a high intensity rainfall cannot occur even during a thunder storm, and b) under such a situation consideration of the generated flow as overland flow may not be appropriate as the flow no longer corresponds to a thin sheet flow as per the definition of overland flow, rather, it could be considered as a concentrated channel flow. The corresponding estimated equilibrium flow depths of the SVE solutions at the end of the planes were 0.423 and 0.176 m, respectively, for the runoff hydrographs shown in Figures 4.6a and 4.6b which are far greater than that of a thin sheet flow. Though both the overland flow and channel flow processes are governed by the same equations, the scale effects due to differing order of magnitudes of flow depths in them make these processes different from each other. As a consequence of these scale effects, the main features of these flow processes such as attenuation and translation may differ from each other. Regarding this perspective, *Richardson and Julien*, [1994] pointed out that the relative magnitudes of the

acceleration terms are such that $(a_l^* > a_c^* > a_p^*)$ for the supercritical overland flow with $F_{rp} >$ 1.4 which differs from $(a_p^* > a_l^* > a_c^*)$ for the subcritical overland flow with $F_{rp} < 0.4$ which in all the cases are in contrast with $(a_p^* > a_c^* > a_l^*)$ for the open channel flow, where $a_p^* =$ pressure gradient term, $a_l^* =$ local acceleration term and $a_c^* =$ convective acceleration term, all are in non-dimensional form. Therefore, it can be inferred that the VPMS and VPMD methods are suitable to use in the transition range between the DW and KW solution including the full range of latter solution. However, this requires further investigation with the consideration of realistic overland flow runoff generation input parameters.

The generation of overland flow hydrograph using the VPMS method is also studied for a pulse input using the solutions of the DW equation arrived at based on the explicit and implicit schemes by *Kazezyılmaz-Alhan et al.* [2005]. These solutions are also compared with the VPMD method solution [*Chapter* 3, section 3.6.2], the analytical solution of the KW and the numerical solution of the SVE. The hypothetical solution presented by *Kazezyılmaz-Alhan et al.* [2005] is used herein to demonstrate the capability of the proposed VPMS method to reproduce the overland flow solutions in the diffusive wave range. The spatially uniform rainfall of intensity $r = 5.08$ cm/h is applied for a duration of 30.0 min over a 182.88 m long plane. The plane is characterised by a uniform bed slope of $s_0 = 0.0016$ and a Manning's roughness coefficient $n = 0.025$. The runoff hydrograph is simulated at the end of the unit width plane for a duration of 90 minutes, which may ensure the total draining of the entire input rainfall volume.

Considering the runoff event to be kinematic in nature, the time to equilibrium is estimated as $t_e = 24.89$ min, $k = 192.18$, $k(F_{rp}^2)_e = 13.85$ and $(F_{rp})_e = 0.27$ while the corresponding VPMS and VPMD methods estimates are $k = 190.86$ and 198.21, $kF_{rp}^2 = 13.78$ and 13.74 and $F_{rp} = 0.27$ and 0.26, respectively. These results suggest that the applicability criteria parameters estimated by the analytical kinematic wave approach and the VPMS and VPMD methods are in a good agreement. On the basis of these results, one can surmise that the considered event could be reasonably simulated by the KW model. To simulate the runoff using the VPMS and VPMD methods, the unit width strip of the overland plane is divided into 69 sub-reaches as used in the case of the DW solutions by *Kazezyılmaz-Alhan et al.* [2005] based on the implicit and explicit methods using temporal grid size of $\Delta t = 10$ s. An additional test run by dividing the unit width strip of the overland plane into 69 sub-reaches and with $\Delta t = 30$ s is carried out to analyze the impact of larger computational grid size on the error of the computed peak discharge of runoff

hydrograph. *Kazezyılmaz-Alhan et al.* [2005] claimed that the MacCormack scheme is more efficient in terms of using a higher temporal grid size than that could be used in the widely employed explicit and implicit numerical schemes of the DW equation, eventhough they could use a maximum of $\Delta t = 6$ s only for the MacCormack scheme [see *Kazezyılmaz-Alhan and Medina Jr.*, 2007]. It is seen from their study that there is no any significant difference seen among theses three solutions. Due to this reason, the MacCormack scheme solution results are not used herein for comparison. The results of simulation of the VPMS method along with the VPMD method solution, the analytical solution of KW, numerical solution of the SVE and the solutions of DW based on implicit and explicit methods are shown in Figure 4.7. The VPMS method solution matches near perfectly with the SVE solution, including the peak of the runoff hydrograph as shown in the enlarged inset. As compared to the VPMD method solution, for both the finer as well as coarser grid sizes, the VPMS method solution has a slight better edge in matching the SVE solution. In the vicinity of peak of the runoff hydrograph, the VPMD method shows slight over-prediction as seen in the inset, although it is better than the DW solution based on the explicit method. There is also a good agreement between the solutions of the VPMS method and those of the DW equation based on both the numerical schemes, except that the former solution display a slightly better edge in matching the SVE solution, around the peak region of the runoff hydrograph. As compared to the implicit scheme, the explicit scheme displays a better accuracy in matching with the solutions of the SVE, VPMS and VPMD methods. *Lal* [1998b] has arrived at the same conclusion while evaluating the implicit and explicit schemes for the SVE solutions. The results also show that the VPMS method solution is well in agreement with the analytical KW solution except nearer the peak region of the runoff hydrograph, where the overland flow process is not strictly kinematic and exhibits small diffusivity. This inference can also be verified from the performance evaluation measures estimated for the VPMS and VPMD methods, with the consideration of the inertial terms, i.e. $\left(1-(4/9)F_{rpM}^{2}\right)$ as in equation (4.20), which is able to reproduce the SVE solution hydrograph closely with $\eta_q = 100.0$ and 99.98 %, $CRM = 0.15$ and -0.60 %, $CD = 1.0$ and 0.99, $q_{perr} = -0.15$ and 0.25 % and $t_{perr} = 0.0$ and 0.0 min, respectively, while the corresponding estimated performance evaluation measures are $\eta_q = 100.0$ and 99.98 %, $CRM = 0.17$ and -0.60 %, $CD = 1.0$ and 0.99, $q_{perr} = -0.21$ and 0.22 % and $t_{perr} = 0.0$ and 0.0 min, respectively, when the inertial term, i.e. $\left(1-(4/9)F_{rpM}^{2}\right)$ is ignored in equation (4.20). The corresponding estimated performance evaluation measures by

171
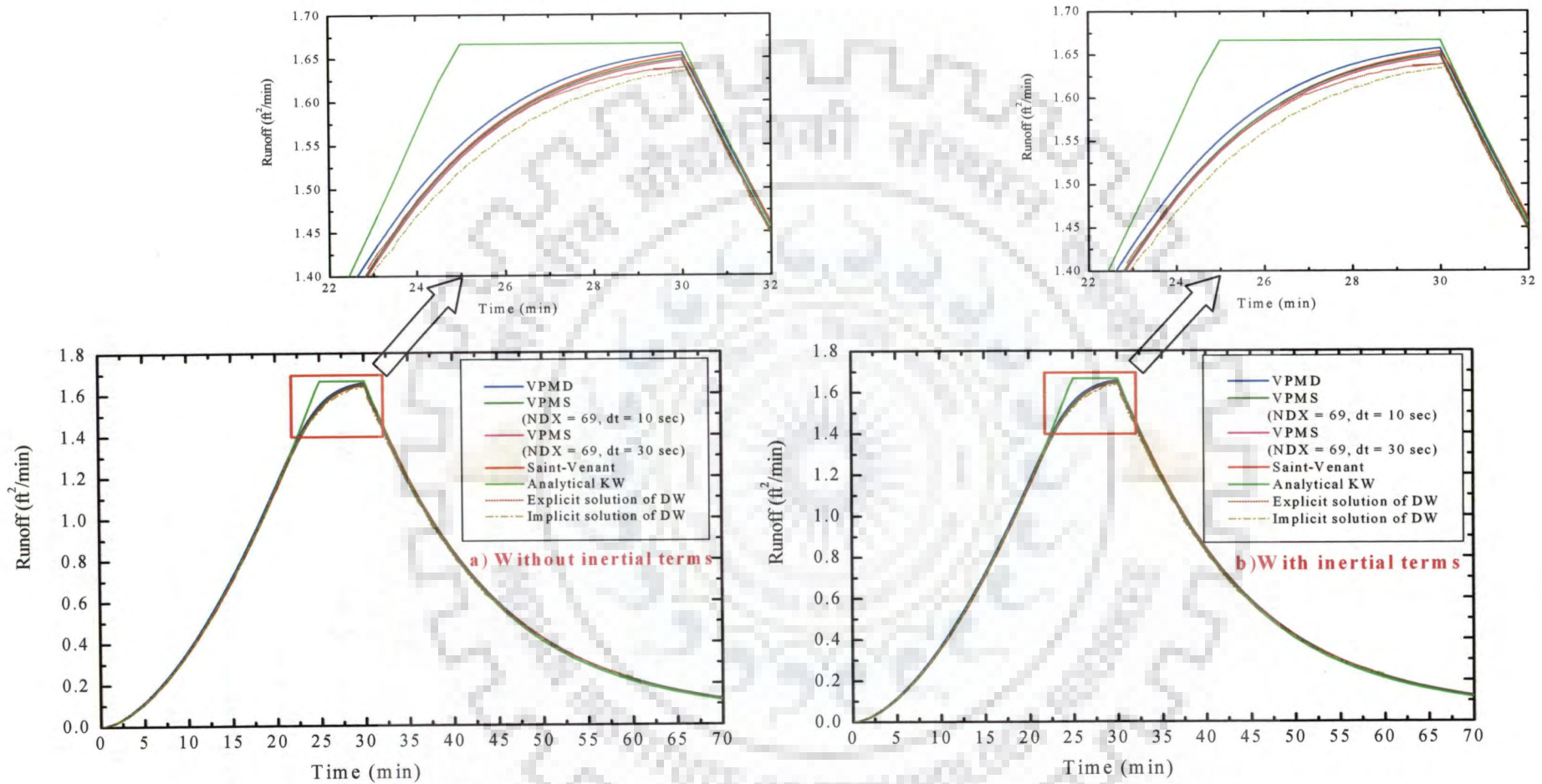
Figure 4.7 Comparison of the simulated runoff hydrograph by the VPMS method with the VPMD method solution, the SVE solution, the analytical solution of the KW and the simulated runoff hydrograph by *Kazezyımaz-Alhan et al.* [2005] using the explicit and implicit methods for DW solutions.

the VPMS and VPMD method solutions in comparison with the simulated runoff hydrograph by the analytical KW solution are η_q = 99.84 and 99.87 %, CRM = 0.32 and -0.43 %, CD = 1.05 and 1.04, q_{perr} = -0.89 and -0.48 % and t_{perr} = 5.0 and 5.0 min, and η_q = 99.84 and 99.87 %, CRM = 0.34 and -0.42 %, CD = 1.05 and 1.03, q_{perr} = -0.94 and -0.51 % and t_{perr} = 5.0 and 5.0 min, respectively, with and without accounting of the inertial terms in equation (4.20), respectively. It is seen from these results that the solutions by the VPMS and VPMD methods are not close to the analytical KW solution as compared to the SVE solution. Consequently, these results clearly indicate that accounting of the inertial terms in the VPMS and VPMD methods solution does not show any significant change in the simulation performance of these methods, when the existing flow conditions are in a subcritical state. The estimated volume errors of $EVOL$ = -4.35% and -3.62%, by the VPMS and VPMD method respectively, indicating the underestimation of input mass may be attributed to the termination of the VPMS and VPMD simulation process well before the complete draining of the detention storage. Note that the total simulation time used in the current case is 90 minutes, which is 30 minutes higher than that used by *Kazezyılmaz-Alhan et al.* [2005]. It may be noted that the study by *Kazezyılmaz-Alhan et al.* [2005] does not consider the volume error criterion. The CPU-time required for the execution of the VPMS and VPMD solutions are 0.625 s and 0.495 s, respectively, while it is 4.06 s for SVE solution with the use of Δt = 0.125 s and Δx = 2.65 m, and same spatial grid size have also been as used in the solutions of the VPMS and VPMD methods. Therefore, it can be inferred from all these simulated results that the VPMS method, like that of the VPMD method, is accurate as well as computationally more efficient than the numerical schemes used in the solution of the SVE and the DW equation.

4.7 VARIATION OF WEIGHTING COEFFICIENT

While applying the VPMS method for flood routing in channels, *Perumal and Ranga Raju* [1998a] studied the variation of the weighting parameter θ used in the VPMS method with reference to the inflow discharge at every routing time level. *Perumal and Ranga Raju* [1998a] investigated this variation using the generalized relationship established for the weighting parameter while developing the VPMS method from the SVE. The relationship between θ and the channel flow characteristics is given as

$$\theta = \frac{1}{2} - \frac{l}{\Delta x}$$

(4.20)

173

where, Δx is the selected sub-reach length and l is the distance between the mid-section and that downstream section where the normal discharge corresponding to the depth at the mid-section passes at the same instant of time. It can be inferred from the relationship of θ given by equation (4.20) that θ can never exceed 0.5 as the least magnitude of l could be zero, at which the flood propagation is strictly kinematic in nature. Using an example of flood propagation in a steep channel, *Perumal and Ranga Raju* [1998b] showed that θ was varying very close to 0.5, but always < 0.5 as the flood propagation even in a steep river reach exhibits a small amount of diffusion. *Perumal and Ranga Raju's* [1998a] study further showed that at the lower end, the magnitude of $\theta < 0$ for a small routing sub-reach length when $l > 0.5 \Delta x$, i.e., when the flow section wherein the normal discharge corresponding to the flow depth at the mid-section of the sub-reach passes is located downstream of the outflow section of the considered routing sub-reach. While the same theoretical interpretation for the variation of θ could be applicable for modelling the overland flow simulation using the VPMS method, it has to be kept in mind that the magnitude of θ estimated for overland flow simulation at any time is also influenced by the lateral flow, which was considered absent while applying the VPMS method for routing in channels. In view of these considerations it is desirable to investigate the variation of θ when simulating the overland flow using the VPMS method.

The nature of variation of θ along the plane length is demonstrated using the example of *Kazezyılmaz-Alhan et al.* [2005] as studied in the previous section, wherein 182.88 m plane is subdivided into 69 sub-reaches. The θ values estimated corresponding to the overland flow simulations at the end of 2nd, 35th and 69th (end of the plane) sub-reaches by the VPMS and VPMD methods are shown in Figure 4.8, along with the corresponding runoff hydrograph at the end of the overland flow plane. It is inferred from Figure 4.8a that the computed θ values by the respective solutions of both the methods are almost perfectly matches with each other. Further, the values of computed θ vary from ≈ 0.5, but < 0.5, to negative values as runoff hydrograph rises rapidly. The values of the weighting parameter estimated by the VPMS method at the end of the 2nd sub-reach vary in the range of 0.35 to 0.5, with a minimum weighting parameter values $\theta_{min} = 0.35$ occurring corresponding to maximum discharge at the end of the considered sub-reach. However, in case of the 35th and the 69th sub-reaches, the negative values of θ_{min} were estimated with the maximum negative values of -0.52 and -1.03, respectively, occurring corresponding to the peak discharges at the downstream end of the respective sub-reaches. The corresponding minimum and maximum values of θ were 0.33 and 0.497 at the end of 2nd sub-reach and the negative values of θ_{min} were -0.52 and -1.02 at the end the 35th and the 69th sub-reaches, respectively, with the VPMD method solution. It can be seen that there is slight difference
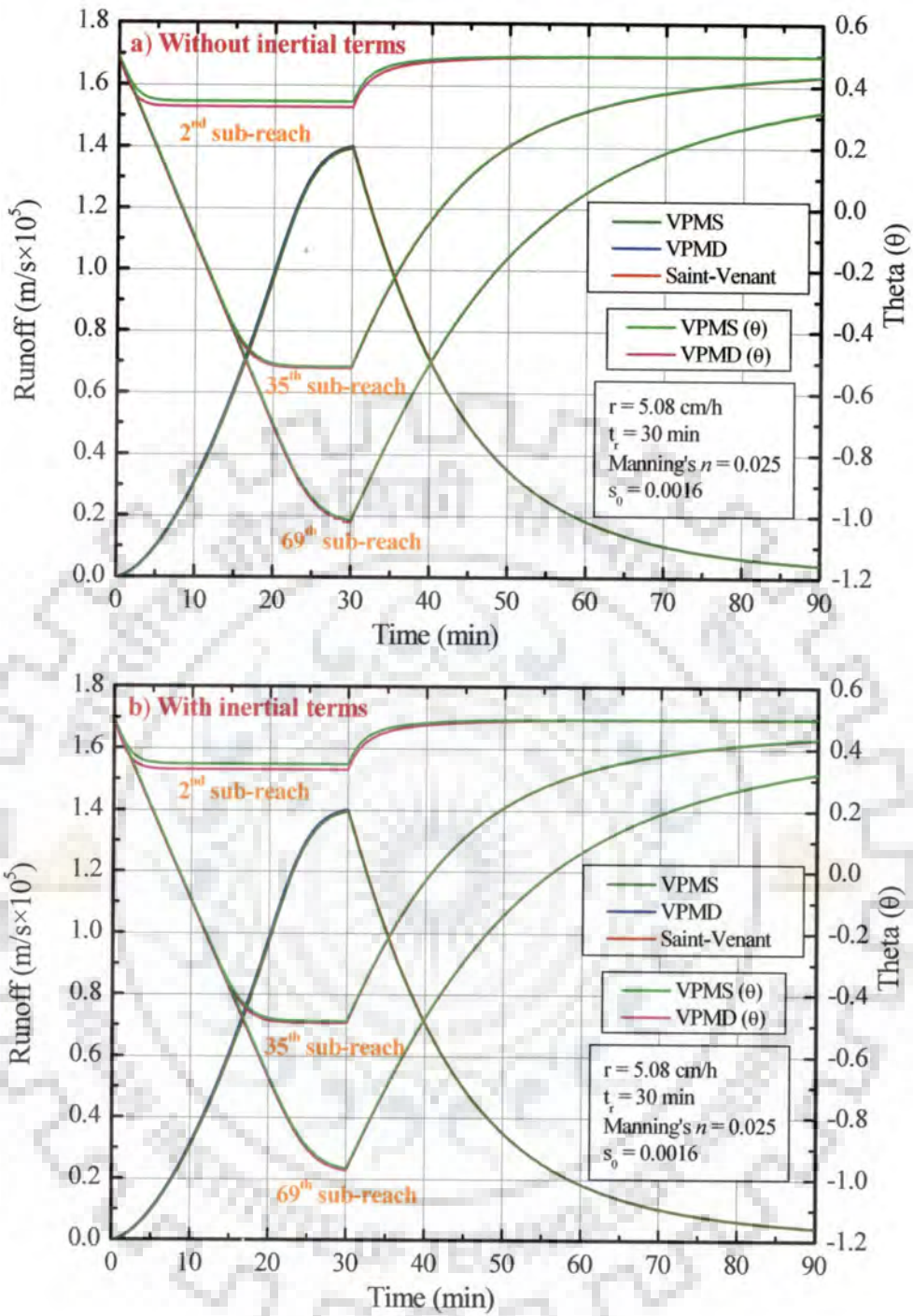
Figure 4.8 Temporal variation of θ estimated at the end of 2nd, 35th and the last (69th) routing sub-reaches by the VPMS and VPMD methods along with the runoff hydrographs simulated at the end of the overland flow plane by the VPMS, VPMD and SVE methods.

in estimated θ_{min} by both the VPMS and VPMD method at the end of the 2nd sub-reach, which may be attributed to the use of larger spatial grid size for which the assumption of linearly varying flow depth employed in the VPMS method may not hold good as that of the assumption of linearly varying discharge employed in the VPMD method. However, at the

end of the 35th and 69th sub-reaches, a substantial depth of flow gets developed due to lateral inflow contribution along the strip displaying no difference between the θ estimates of both the methods. With the accounting of inertial terms in the runoff hydrograph simulation by the VPMS method, the θ_{max} and θ_{min} estimated, respectively during the simulation were 0.50 and 0.35; 0.49 and -0.49; and 0.49 and -0.97 at the respective downstream ends of the 2nd, 35th and 69th sub-reaches. While, the corresponding estimates by the VPMD method simulations were 0.497 and 0.33; 0.49 and -0.49; and 0.49 and -0.97 at the respective downstream ends of the 2nd, 35th and 69th sub-reaches. It can be inferred from these results that the θ_{min} values estimated for all these three sub-reaches are slightly lower than those corresponding estimates arrived at without consideration of the inertial terms. These inferences can also be seen from Figure 4.8b. The magnitudes of maximum negative values of θ estimated for each of the sub-reaches increases with the increase in the magnitude of discharge to be routed, which is consistent with the relationship of θ given by equation (4.20). The systematic variation of θ as exhibited in Figure 4.8 indicates the unconditional stability offered by the VPMS and VPMD methods. Further, it can be surmised that when the variation of θ estimated by the VPMS and VPMD methods matches with each other, it is expected that there would be a perfect match between the simulated runoff hydrographs of both the methods.

4.8 ACCURACY OF THE METHOD

The accuracy of the proposed VPMS method, as in the case of the VPMD method, mainly depends on the adherence to the assumptions involved in the development of the method by the considered overland flow simulation process. Accordingly, there are three major sources of approximations involved in the application of the method for overland flow generation:

(i) approximation with reference to the use of the assumption of linear variation of flow depth in the considered routing reach;

(ii) approximation with reference to the use of the assumption that multiplications of derivatives of the flow variables are negligible; and

(iii) approximation that arises due to the binomial series expansion of the energy slope in estimating the distance l between the mid-section and the normal flow section of the routing sub-reach.

The error introduced due to the first approximation can be minimized by reducing the length of the routing sub-reach Δx. Though the validity of the second assumption requires the validity of the first assumption, it also requires the use of smaller Δt to enable the requirement of linear variation of the flow depth and the flow velocity along time. However,

if the truncation error introduced by the third assumption related to the approximation of the energy slope by retaining only the first two terms is significant, then the routing using an increased number of sub-reaches would compound the inaccuracy in the solution which may lead to numerical instability problems. But *Perumal and Ranga Raju* [1998b] pointed out that such a situation develops only when $[(1/S_0)\partial Y/\partial X]$ is nearer to unity. It is to be noted that the VPMS method has the advantage of direct computation of $\partial y/\partial x$, whereas in the VPMD method y and $\partial y/\partial x$ is computed indirectly. Therefore, computed y and $\partial y/\partial x$ computed by the VPMS method are slightly more accurate than the corresponding estimates of the VPMD method, if the applicability criteria $[(1/S_0)\partial Y/\partial X]$ nearer to unity is satisfied. Fortunately such a situation *i.e* $[(1/S_0)\partial Y/\partial X] > 1$ generally does not arise in overland flow planes as they are characterised by comparatively larger bed slopes than that of the channel and river beds. As the VPMS method for overland flow study has the same governing equation as that used for flood routing in channels, it is surmised that at least the same limit may hold good for the overland flow modelling also. However, a detailed study in this regard is required. Based on a detailed analysis, *Perumal and Sahoo* [2007] have specified the applicability limit of the VPMS method for flood routing in channels as $\dfrac{1}{S_0}\dfrac{\partial Y}{\partial X} < 0.63$ when discharge computations are required. In view of these theoretical considerations related to the accuracy of the VPMS solutions, it is pertinent to study the effects of spatial and temporal grid sizes which have implications related to the first and second assumptions, respectively, on the capability of the VPMS method to closely simulate the benchmark overland flow runoff.

4.8.1 Effect of Spatial Grid Size on the Solution Accuracy

In order to study the sensitivity analysis of spatial grid size on the accuracy of the simulated overland flow hydrographs, the example of *Gottardi and Venutelli* [2008], already considered earlier as illustrated in Figure 4.5b is employed. Different sizes of Δx ranging from 0.1 to 40 m were used to simulate overland flow hydrographs at the end of 200 m length of a unit width strip plane. The results of the simulated hydrographs for all the considered numerical experiments are shown in Figure 4.9. It can be inferred from this figure that when Δx is varying from 0.1 to 10 m, no significant difference is seen between the benchmark and the simulated hydrographs, and the VPMS method may be considered as an accurate method. However, when the chosen $\Delta x > 10$ m were used, the corresponding
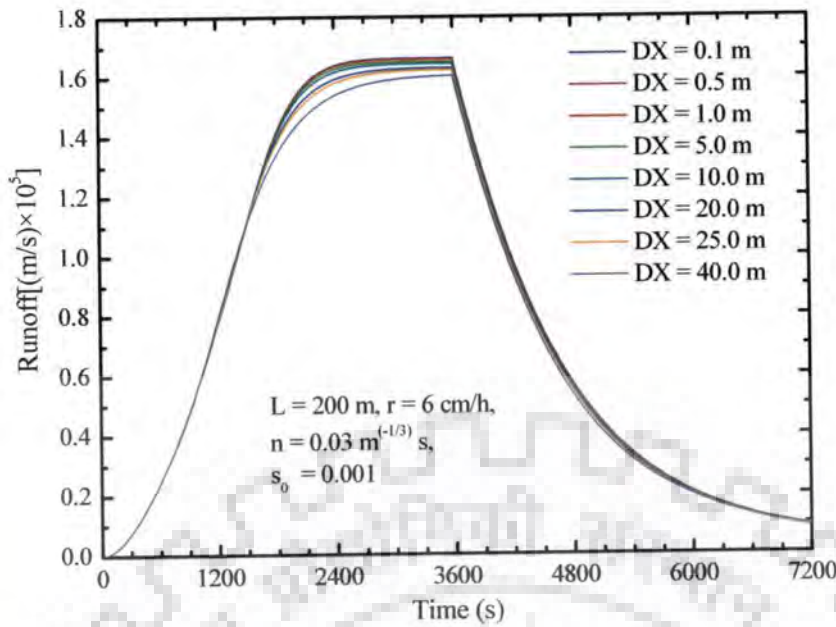
Figure 4.9 Effect of spatial grid size variations on the simulations.

simulated hydrographs using the VPMS method are not close to the benchmark hydrograph in comparison with the simulations arrived at using the grid sizes in the range of 0.1 to 10 m. However, this inference may be qualified only in a relative sense, but not in an absolute sense. The relative inability of the VPMS method to reproduce the benchmark solution closely for $\Delta x > 10$ m may be attributed to the non-adherence of the assumption of linear variation of flow depth over Δx by the considered simulation using the VPMS method. Further, it is noted that with identical computational and input conditions, the VPMD method allows the use of $\Delta x \leq 20$ m. Therefore, it is inferred that the VPMS method requires the use of relatively small Δx as compared to the VPMD method.

It is worthwhile to analyse the accuracy of the solutions arrived at using different spatial grid sizes from the perspective of accuracy criteria given for other similar methods. In case of linear analysis of the kinematic wave model, *Holden and Stephenson* [1995] stated that to maintain the numerical stability, the grid ratio must be greater than or equal to the wave celerity c, i.e., $\Delta x / \Delta t \geq c$, where c is the average kinematic wave celerity over the grid size Δx. But the kinematic wave celerity is a function of runoff flow depth, so it varies with time and location. Moreover, this condition is only a guideline for the stability preservation of the explicit method without any firm warranty; hence it is a necessary, but not a sufficient condition [*Chow* et al. 1988, pp. 293-294]. Such a condition is not applicable for the implicit scheme. Consequently, to preserve the accuracy of the kinematic wave based overland flow simulation, HEC-HMS model [*USACE*, 2000] adopts the use of the criterion

178

$C_{un} \approx 1$, where $C_{un} = c(\Delta t / \Delta x)$ and it denotes the Courant number. But it is to be noted that HEC-HMS solves the kinematic wave equation using the conventional explicit numerical scheme which requires such a criterion in order to control the numerical diffusion in the solution. However, as the governing equation of the VPMS method known as the approximate convection-diffusion equation [*Perumal and Ranga Raju*, 1999] is directly derived from the Saint-Venant equations governing the one-dimensional flow, it has the inherent feature to preserve the accuracy and stability of the solution without exhibiting numerical diffusion. Table 4.4 demonstrates the accuracy of the VPMS method solution for the considered example of *Gottardi and venutelli* [2008] despite the violation of the condition given by the HEC-HMS model in simulating the overland flow hydrograph governed by the KW.

It is seen from Table 4.4 that for all the numerical experiments with $\Delta x \leq 10$ m, there is no significant change in the estimated Nash-Sutcliffe efficiency value of 99.99 implying that all these simulations very closely reproduce the considered SVE benchmark solution. Besides, the other performance measures such as the mass conservation criterion (*EVOL*), *CRM* , *CD* are very close to the ideal values of 0.0%, 0.0% and 1.0, respectively. However, relatively large error performance measures were estimated for the numerical experiments with $\Delta x = 20$, 25 m and 40 m, especially with regard to *CRM* and *EVOL* estimates. Considering the fulfillment of all the performance measures, it may be considered from the evaluations of the pertinent characteristics of the solution as presented in Table 4.4 that the solution of the VPMS method is not sensitive to the adopted spatial grid size up to 10 m and the corresponding simulations can be considered very accurate in reproducing the benchmark hydrograph.

Table 4.4 also gives the grid ratio ($\Delta x / \Delta t$), maximum celerity (c_{max}), Courant number (C_{un}), θ_{min} (which is estimated at the downstream end of overland flow plane for the highest runoff discharge value) and θ_{max} for each Δx case. It can be inferred from these results that if the condition $C_{un} \approx 1$ has to satisfy as recommended in the HEC-HMS model, then only the use of $\Delta x = 2$ m is allowed and this will be too restrictive as compared to the use of $\Delta x = 10$ m for the KW solution. In turn, this requires a larger computational time (CPU time) over that of the case of using $\Delta x = 10$ m which however, is characterised by $C_{un} = 0.21$. Therefore, it is inferred from this analysis that strictly following the Courant condition is not necessary to preserve the solution accuracy of the VPMS method. Further,

Table 4.4 Performance evaluation of the VPMS method solutions for spatial grid size variations

Δx (m)	$\dfrac{\Delta x}{\Delta t}$	c_{max}	Courant Number C_{un}	θ_{max}	θ_{min}	η_q (%)	CRM (%)	CD	EVOL %	q_{perr} (%)	t_{perr} (min)	CPU -time (s)
0.1	0.008	0.174	20.86	0.500	-98.205	100.00	-0.25	1.00	-0.58	0.10	-1.20	9.31
0.5	0.042	0.174	4.17	0.500	-19.220	100.00	-0.16	1.00	-0.66	0.01	-0.20	2.05
1.0	0.083	0.174	2.08	0.500	-9.348	100.00	-0.07	1.00	-0.75	-0.08	0.00	1.13
5.0	0.417	0.173	0.41	0.499	-1.453	100.00	0.41	1.01	-1.23	-0.55	0.00	0.39
10.0	0.833	0.171	0.21	0.499	-0.467	99.99	0.88	1.02	-1.69	-0.99	0.00	0.30
20.0	1.667	0.169	0.10	0.498	0.026	99.94	1.68	1.04	-2.49	-1.77	0.00	0.27
25.0	2.083	0.168	0.08	0.498	0.125	99.91	2.06	1.05	-2.86	-2.15	0.00	0.25
40.0	3.333	0.164	0.05	0.499	0.273	99.72	3.15	1.10	-3.94	-3.33	0.00	0.22

the θ_{max} value estimated below 0.5 in all the cases indicates that the method is unconditionally stable. The results presented in Table 4.4 also demonstrate that the use of large space intervals up to $\Delta x = 40$ m do not cause any numerical or stability problem, while the explicit numerical scheme for the SVE solution is non-convergent even for a small space grid size of 0.1 m. Further, it can be seen from Table 4.4 that the weighting parameter θ_{min} ranges from 0.273 ($\Delta x = 40$ m) to -98.205 ($\Delta x = 0.1$ m) contrary to the conventional notion that the minimum Muskingum weighting parameter is zero. It can be inferred from the analysis of spatial grid size impacts on the solution accuracy of the VPMS method that the ability to use larger spatial grid size while preserving the accuracy has an important implication in the large basin modelling.

4.8.2 Effect of Temporal Grid Size on the Solution Accuracy

The same example of *Gottardi and Venutelli* [2008] considered earlier as referred to the case of Figure 4.5b is further employed to examine the impact of temporal grid size on the solution performance and accuracy using pre-selected Δt ranging from 2 s to 360 s and with a uniform $\Delta x = 0.5$ m for each Δt, in all the numerical experiments. It can be seen from Figure 4.10, that the VPMS method is able to produce the simulated hydrograph with consistent accuracy for Δt ranging from 2s to 180s. However, any further increase in the
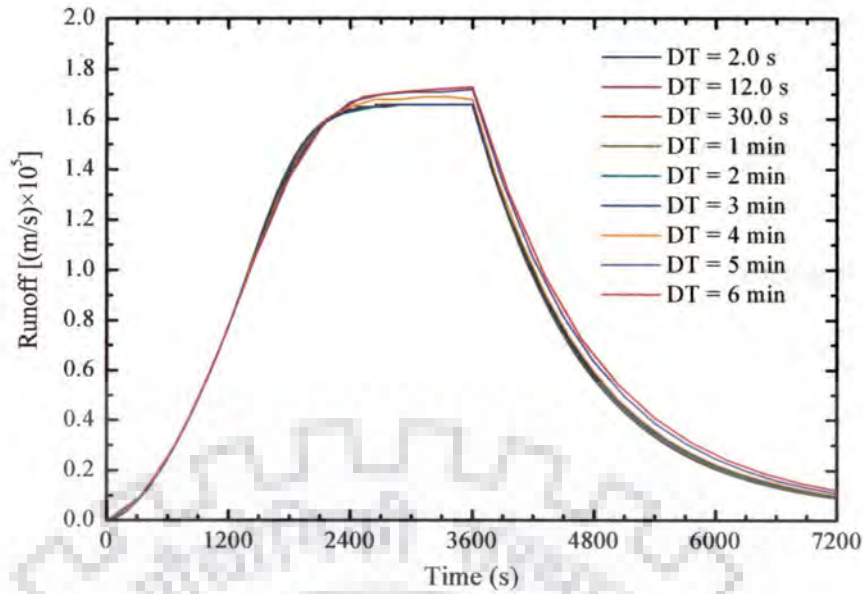
Figure 4.10 Effect of temporal grid size variations on the simulations.

Table 4.5 Performance evaluation of the VPMS method solutions for temporal grid size variations

Δt (s)	$\dfrac{\Delta x}{\Delta t}$	c_{max}	Courant Number C_{un}	θ_{max}	θ_{min}	Performance Evaluation Measures						CPU-time (s)
						η_q (%)	CRM (%)	CD	EVOL %	q_{perr} (%)	t_{perr} (min)	
2	0.250	0.174	0.70	0.500	-19.227	100.00	-0.14	1.00	-0.68	0.07	-0.07	11.31
12	0.042	0.174	4.17	0.500	-19.220	100.00	-0.16	1.00	-0.66	0.01	-0.20	2.05
30	0.017	0.174	10.42	0.500	-19.210	100.00	-0.21	1.00	-0.61	-0.08	0.00	0.94
60	0.008	0.174	20.83	0.500	-19.199	100.00	-0.35	1.00	-0.47	-0.17	0.00	0.56
120	0.004	0.174	41.64	0.500	-19.189	99.99	-0.71	1.00	-0.12	-0.25	0.00	0.28
180	0.003	0.174	62.46	0.500	-19.185	99.98	-1.15	1.00	0.32	-0.29	-9.00	0.19
240	0.002	0.175	83.91	0.500	-19.386	99.95	-2.14	0.98	1.50	1.52	-8.00	0.14
300	0.002	0.176	105.59	0.500	-19.578	99.74	-4.46	0.96	3.61	3.30	0.00	0.11
360	0.001	0.177	127.24	0.499	-19.675	99.52	-7.06	0.95	6.19	4.31	0.00	0.09

time interval results in overestimation of runoff in the vicinity of equilibrium state of runoff hydrograph and at the lower portion of recession limb. Note that by keeping the same input and computational conditions, the VPMD method reproduces the hydrograph with consistent accuracy for $\Delta t \le 30s$ [*Chapter* 3, section 3.9.2]. Therefore, it is inferred that the VPMS method allows the use of larger temporal grid size than that of the VPMD method. This can also be verified from the computed performance evaluation measures as shown in

181

Table 4.5. Similarly, too small Δt values would not yield enhanced accuracy of the solution and only resulting in higher CPU time. On the other hand, the use of higher temporal grid size results in the over estimation of the equilibrium discharge and also delay in the recession part of the overland flow hydrograph causing volume error due to increased volume of the generated runoff.

It can be seen from the results shown in Table 4.5 that the computed c_{max} and θ_{min} are nearly constant irrespective of the variation of temporal grid size. Further, the close examination of the performance evaluation measures clearly demonstrate that the satisfaction of the criteria $C_{un} \approx 1$, allow only the use of $\Delta t \approx 3$ s. However, the use of $\Delta t >$ 3 s does not affect the solution accuracy and performance of the method. Therefore, it can be inferred that the satisfaction of this criterion is not needed when using the VPMS method and it leads to increased computation time. Moreover, the temporal grid size selection also depends upon the time of concentration, duration of the rainfall and the recorded rainfall time interval. Hence, it is better to use that temporal grid size identified by trial and error approach which would not give significantly different simulated results for two different, but close time intervals. Based on the above discussion, it can be argued that the VPMS method is more flexible in the selection of the temporal grid size which enables very fast computation.

The impact of different combinations of Δx and Δt on the performance and solution accuracy of the VPMS method, especially on three performance evaluation measures such as $EVOL$, q_{perr} and η_q are shown in Figure 4.11. It can be seen that the accuracy of the solution is greatly influenced by the selection of grid size with the combination of larger Δx and Δt. It can be seen that if $\Delta x \leq 10$ and $\Delta t \leq 180$, the simulation results are consistently accurate with $q_{perr} \leq 2.0$ %, $EVOL \leq 2.0$ % and with Nash-Sutcliffe efficiency $(\eta_q) \approx 100$ %. The grid sizes with the combination of larger Δx and Δt resulted in poor performance due to inaccurate simulation by the VPMS method. Similarly, the use of grid sizes with a combination of very small Δx and a very larger Δt is also not appropriate. Therefore, it is always better to select optimum combinations of Δx and Δt as envisaged in Figure 4.11.
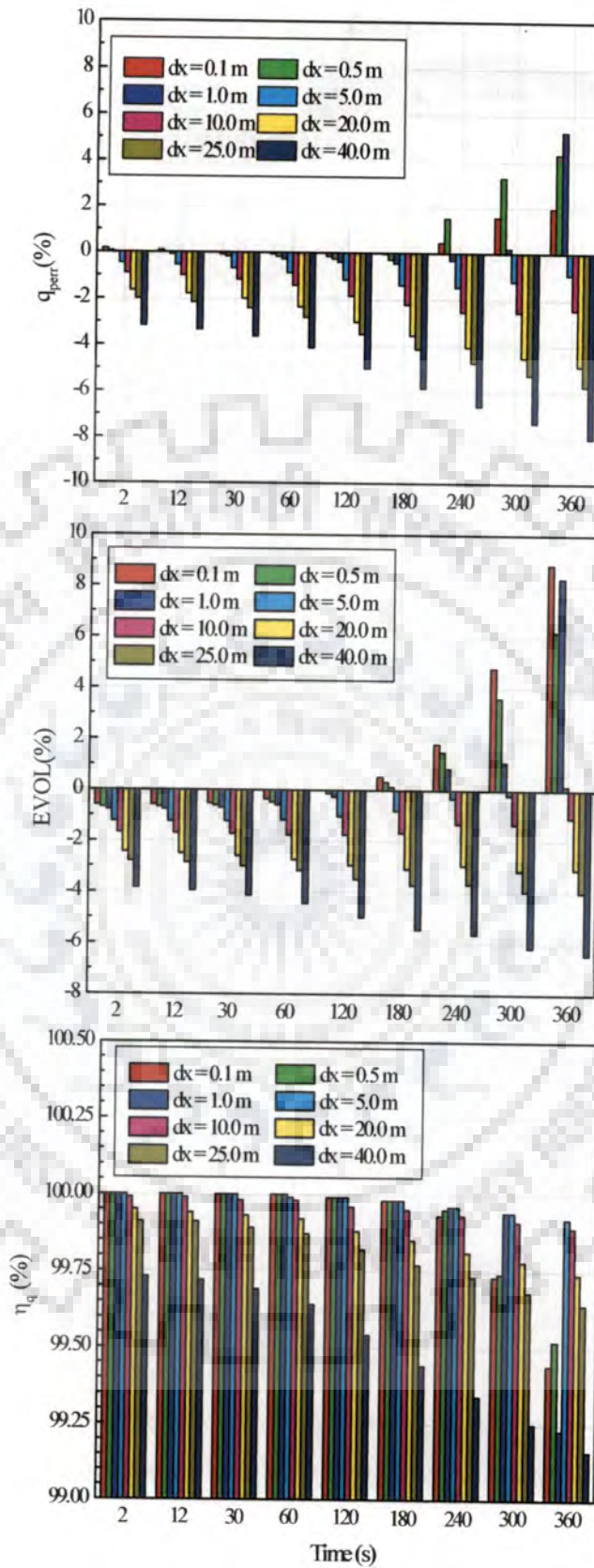
Figure 4.11 Effect of spatial and temporal grid size variations on the performance evaluation measures.

4.9 TIME-VARYING RAINFALL CASES

The capability of the VPMS method to estimate runoff in response to time varying rainfall is evaluated using the hypothetical cases as used by *Govindaraju et al.* [1990]. The configurations of the overland flow planes and associated rainfall details studied are given in Table 3.5. Figure 4.12 shows the simulated hydrographs of the VPMS method for time varying inputs which are compared with the corresponding VPMD method solutions, the numerical solutions of the SVE, the approximate analytical solutions [*Govindaraju et al.* 1990] and the numerical solution of the SVE given by *Govindaraju et al.* [1990] and the numerical solutions of the KW and DW equations [*Gottardi and Venutelli*, 2008]. It can be seen from the results presented for case I that the simulated hydrograph of the VPMS method like that of the VPMD method is not matching with the SVE solution, although it has better performance than the KW solution and the approximate analytical solution. However, the simulated runoff hydrograph of the VPMD method solution is slightly better than that of the VPMS method, although the VPMS method solution coincides with the recession limb of the SVE solution. It can also be corroborated with the performance evaluation measures such as η_q, CRM, CD, q_{perr} and t_{perr} for the VPMS and VPMD methods as given in Table 4.6 (Case I). Therefore, it can be inferred that the VPMS method has slightly lower applicability range than the VPMD method for the overland flow modelling which is contrary to the applicability limit advocated for these methods for routing floods in channels [*Perumal and Sahoo*, 2007]. This contradiction may be attributed to the scale problem caused due to the formation of a very small runoff flow depth in overland flow modelling. Due to this small flow depth, the estimated $\partial y / \partial x$ over the computational space grid may not be significant in comparison with the corresponding estimate over the channel spatial grid size. The DW solution of *Gottardi and Venutelli* [2008] is also showing over prediction around the peak region as compared to the SVE solution; however it reproduces the SVE solution closely than the VPMS and VPMD method solutions. The unsatisfactory performance of the VPMS method may be attributed to the lower F_{rp} and $k(F_{rp})^2$ values, although $k \approx 3000$, which is even beyond the applicability limits of the DW equations. These results corroborate the finding by *Morris and Woolhiser* [1980] that the criterion $k(F_{rp})^2$ plays an important role in judging the applicability limits of the KW and DW models for overland flow modelling. However, as the estimates of the applicability criteria parameters $(F_{rp})_{\min}$ and $\left[kF_{rp}^2\right]_{\min}$ increase (as
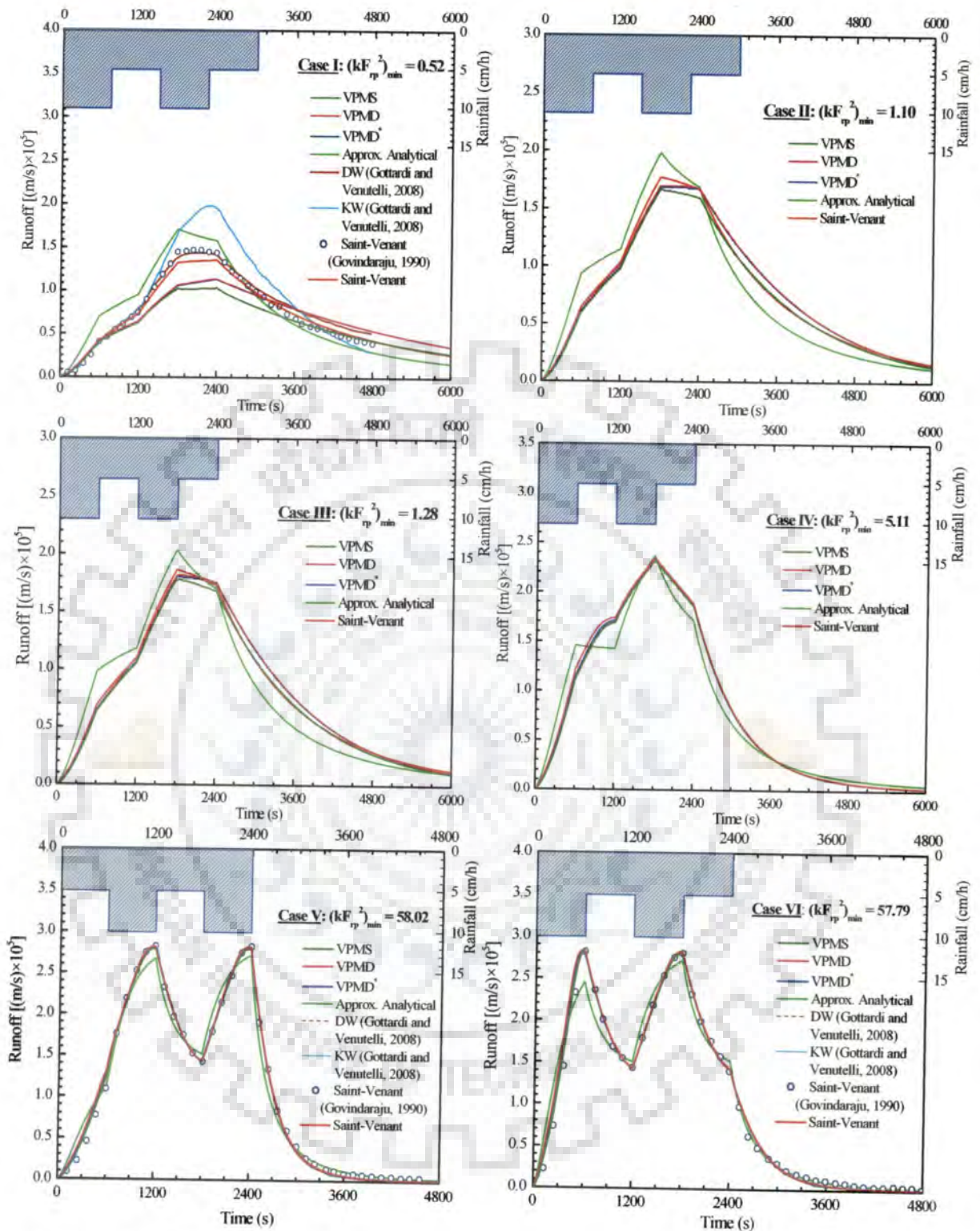
Figure 4.12 Comparison of the runoff hydrographs simulated using the VPMS method with those obtained with the VPMD method, approximate analytical solution [*Govindaraju et al.*, 1990], the numerical solution of the SVE and the simulated runoff hydrographs using the KW and DW solutions by *Gottardi and Venutelli* [2008] for time varying rainfall cases. Note that VPMD* presents the VPMD method simulated runoff hydrographs with grid size of $\Delta x = 0.51$ m and $\Delta t = 6$ s.

Table 4.6 Performance evaluation of the VPMS method and its comparison with the VPMD method solutions for different time-varying rainfall events

Event	Δx (m)	Δt (s)	$\dfrac{\Delta x}{\Delta t}$	c_{max}	Courant Number (C_{ur})	VPMS η_q (%)	CRM (%)	CD	q_{perr} (%)	t_{perr} (min)	EVOL (%)	CPU-time (s)	VPMD η_q (%)	CRM (%)	CD	q_{perr} (%)	t_{perr} (min)	EVOL (%)	CPU-time (s)	Saint-Venant EVOL (%)	CPU-time (s)	k_{min}	$(F_{rp})_{min}$	$\left|kF_p^2\right|_{min}$
I*	0.51	15	0.034	0.010	0.30	95.47	13.01	1.46	-23.80	0.0	-13.22	0.70	96.56	-0.72	1.17	-16.10	0.00	0.48	0.58			3022	0.013	0.55
	0.51	30	0.017	0.010	0.60	95.43	13.12	1.47	-23.87	0.0	-13.34	0.53	96.65	-0.97	1.17	-15.96	0.00	0.73	0.48	-0.28	5.23	2879	0.013	0.52
	0.05	30	0.002	0.010	5.67	96.38	5.75	1.34	-21.12	0.0	-5.99	1.59	96.48	-0.62	1.18	-16.64	0.00	0.37	1.09			2802	0.013	0.51
II	0.51	15	0.034	0.016	0.46	99.75	4.44	1.07	-5.79	0.0	-4.53	0.67	99.61	-1.05	0.98	-4.46	3.00	0.96	0.56			3142	0.019	1.14
	0.51	30	0.017	0.016	0.92	99.73	4.53	1.08	-5.98	0.0	-4.61	0.55	99.60	-1.77	0.97	-4.07	2.50	1.68	0.52	-0.23	4.94	3012	0.019	1.10
	0.05	30	0.002	0.016	8.65	99.82	2.48	1.04	-4.84	0.0	-2.56	1.59	99.60	-1.76	0.98	-4.31	2.50	1.67	1.09			2950	0.019	1.07
III	0.51	15	0.034	0.017	0.50	99.85	3.59	1.05	-4.29	0	-3.67	0.67	99.75	-1.11	0.98	-3.02	0	1.03	0.59			3205	0.020	1.34
	0.51	30	0.017	0.017	1.00	99.84	3.66	1.06	-4.48	0	-3.74	0.55	99.73	-1.87	0.96	-2.55	0	1.79	0.52	-0.22	5.05	3063	0.020	1.28
	0.05	30	0.002	0.017	8.50	99.90	2.01	1.03	-3.41	0	-2.09	1.61	99.73	-1.87	0.97	-2.71	0	1.8	1.11			3004	0.020	1.26
IV	0.51	15	0.034	0.027	0.80	99.99	0.81	1.01	-1.10	0.0	-0.83	0.67	99.97	-1.27	0.98	0.02	0.00	1.24	0.59			4138	0.036	5.27
	0.51	30	0.017	0.027	1.60	99.99	0.79	1.02	-1.27	0.0	-0.81	0.53	99.91	-2.13	0.97	0.11	0.00	2.10	0.52	-0.15	4.73	4015	0.036	5.11
	0.05	30	0.002	0.027	14.95	100.00	0.18	1.00	-0.71	0.0	-0.20	1.61	99.90	-2.13	0.97	0.10	0.00	2.11	1.09			3963	0.036	5.05
V*	0.51	15	0.034	0.063	1.86	100.00	0.42	1.01	-0.59	20.0	-0.44	0.20	99.98	-0.74	0.99	-0.03	0.00	0.72	0.19			4670	0.113	59.45
	0.51	30	0.017	0.063	3.73	99.99	0.48	1.02	-0.68	20.0	-0.50	0.17	99.95	-1.37	0.99	0.12	-0.50	1.35	0.16	-0.04	3.20	4558	0.113	58.02
	0.05	30	0.002	0.064	34.87	99.99	-0.14	1.00	0.05	20.0	0.12	0.39	99.95	-1.39	0.99	0.30	19.50	1.37	0.27			4501	0.113	57.30
VI*	0.51	15	0.034	0.063	1.86	100.00	0.40	1.01	-0.59	0.0	-0.42	0.19	99.92	-1.05	0.98	-0.03	0.00	1.02	0.17			4670	0.113	59.45
	0.51	30	0.017	0.064	3.73	99.99	0.44	1.01	-0.17	-20.0	-0.47	0.16	99.80	-1.81	0.97	0.45	-20.50	1.79	0.14	-0.04	3.64	4539	0.113	57.79
	0.05	30	0.002	0.064	34.97	100.00	-0.18	1.00	0.91	-20.0	0.15	0.39	99.79	-1.86	0.97	0.95	-20.50	1.84	0.30			4471	0.113	56.92

seen from Table 4.6), the performance of the VPMS method solution is also improved. Therefore, for cases II and III, even when the flow conditions are well within the DW equation applicability limit as $(F_{rp})_{min} = 0.019$ and 0.020 and $\left[kF_{rp}^2\right]_{min} = 1.10$ and 1.28, respectively, the performance of the VPMS solution is in close agreement with that of the SVE demonstrating the capability of the VPMS solution to simulate events governed by the diffusive wave.

For Case IV, $\left[kF_p^2\right]_{min} \cong 5$, hence it is the lower limit of the applicability the KW models. It can be seen from Figure 4.12 (case IV) that the simulated runoff hydrographs by the VPMS and VPMD methods perfectly match with each other and also exactly coincide with the SVE solution. For cases V and VI, the flow conditions are well within the KW applicability limit, and, hence the simulated hydrographs by the VPMS method display perfect match with the SVE solution, the VPMD method solution, the solutions of DW equations [Gottardi and venutelli, 2008] and also with the KW models solution as expected. This inference can also be corroborated from the performance evaluation measures computed for these cases as presented in Table 4.6. It is inferred from Figure 4.12 that the approximate analytical solution is not able to perfectly match the VPMS, VPMD, SVE and DW solutions, but able to produce the hydrograph in an approximate manner in all the cases. Note that the runoff hydrographs shown in Figure 4.12 have been estimated with the grid sizes of $\Delta x = 0.51$ m and $\Delta t = 30$ s in the computations of the VPMS and VPMD methods. An additional combination of grid sizes $\Delta x = 0.51$ m and $\Delta t = 6$ s was also used in the computations by the VPMD method, designated as VPMD* in Figure 4.12. It is revealed from Table 4.6 that the Courant number in all the cases is not following the criteria $C_{un} \approx 1$, once again confirming that this criterion is not required in arriving at the VPMS solution. As discussed in the earlier Section 4.8, the VPMS method is able to provide wide flexibility in the selection of the temporal grid sizes, but with a restriction of spatial grid size, without violating the assumption of linear variation of y over the selected Δx, and, therefore, there is insignificant effect on the performance evaluation measures. However, the use of a small spatial grid size is advisable as it results in less error in the peak of the runoff hydrograph estimation. Furthermore, the comparison of the VPMS and VPMD methods as shown in Table 4.6 reveals that from case II onwards, the performance of the

VPMS method is slightly better than the VPMD method for the selected grid sizes as reflected in the performance evaluation measures. Further, it is also true that the use of larger temporal grid size as used in the VPMS method is not applicable in the case of the VPMD method. This inference can be verified from the performance evaluation measures such as η_q, CRM, CD computed for the former method which are slightly better than those of the latter method. However, error in the peak discharge of runoff hydrograph estimation is less for the VPMD method as compared to the VPMS method. Further, the VPMS method is capable of conserving the volume very efficiently, as $EVOL \ll 1.0$ % (except case I II and III), provided that the selected grid size is appropriate. The VPMD method is also efficiently able to preserve the volume, however, it requires the use of relatively smaller Δt as compared to the VPMS method solution. Overall, it can be inferred from the results given in Table 4.6 that the VPMS method solution is able to perform efficiently in all the cases, when $kF_{rp}^2 > 1.0$, and the CPU-time required for the solution is nearly same as the VPMD method which, however, is much less than that required for the numerical solution of the SVE.

4.10 VERIFICATION USING IZZARD'S EXPERIMENTAL DATA

The same set of *Izzard's* [1944] numerical experiments [as reported by *Maksimović and Radojković,* 1986] used for evaluating the VPMD method as described in section (3.10) is also used herein for verifying the overland flow simulation capability of the VPMS method. The plane characteristics and rainfall inputs used for the verification of the developed method are summarized in Table 3.7. In order to evaluate the Manning's roughness coefficient required to simulate the runoff hydrograph, the practice of matching the observed hydrograph closely using the simulated hydrograph is adopted [*Woolhiser,* 1975; *Engman,* 1986]. Following the approach of *Wong and Lim* [2006], the Manning's n is computed for each runoff event based on the sensitivity analysis tests carried out by varying n from 0.010 to 0.018 for the asphalt experimental surface, while from 0.21 to 0.38 for the dense blue grass sod experimental surface by assessing the reproduction performance using the Nash-Sutcliffe efficiency (η_q). The obtained optimum Manning's roughness coefficients with the event number written within the adjacent brackets are 0.016 (34), 0.017 (35), 0.015

(36), 0.015 (50), 0.36 (301), 0.27 (302), 0.25 (318) and 0.38 (319). These values are nearer to those recommended values (0.010-0.013 for the asphalt plane and 0.38-0.63 for the dense blue grass turf) by *Woolhiser* [1975] and *Engman* [1986]. Therefore, a uniform value of Manning's roughness coefficient of $n=0.015$ for the asphalt plane and a value of $n=0.28$ for the dense blue grass turf were used in the simulation of all the events considered in this study. However, the differences between the employed and the calibrated roughness values are high for the events 301 and 319, and, therefore, the corresponding calibrated values for these events are also used in the performance verification of the VPMS method. The variation range of the minimum computed criteria using a finer grid size $k_{min} = 63.74$ - 65.25, $(F_{rp})_{min} \cong 0.61$ and $\left| kF_{rp}^2 \right|_{min} = 23.93$ - 24.36 for the asphalt plane events; whereas, $k_{min} = 2815.27$ - 5081.30, $(F_{rp})_{min} \cong 0.06$, and $\left| kF_{rp}^2 \right|_{min} = 10.17$-15.83 for the dense blue grass turf events. The use of calibrated Manning's roughness coefficient identified for each event is also causing change in the computed applicability criteria: for the event 301 with $n=0.36$, $k_{min} = 3799.10$ (2815.27), $(F_{rp})_{min} = 0.05$ (0.06), and $\left| kF_{rp}^2 \right|_{min} = 8.73$ (10.17) and for the event 319 with $n=0.38$, the estimated criteria are $k_{min} = 4240.83$ (2897.58), $(F_{rp})_{min} = 0.05$ (0.06), and $\left| kF_{rp}^2 \right|_{min} = 8.75$ (10.39). The values given in the adjacent brackets correspond to those simulations obtained with the adopted uniform Manning's roughness coefficient of $n=0.28$. These results suggest that the flow conditions in all the events are well within the KW applicability limits.

The typical runoff hydrograph simulation results by the proposed method along with the observed hydrographs and the corresponding VPMD method solutions and the numerical solutions of the SVE are shown in Figure 4.13. In these figures, the VPMS and VPMD method solutions are obtained with finer as well as with coarser computational grid sizes. It is already demonstrated in Section 4.8.1 that the VPMS method requires the use of relatively smaller spatial grid size, but higher temporal grid size can be used as compared to those admissible in the computations of the VPMD method. Therefore, the computations by the VPMS and VPMD methods are performed using different grid sizes based on the requirement of each individual method. It can be seen from these results that the VPMS has the ability to reproduce the observed hydrographs accurately; beside it matches perfectly
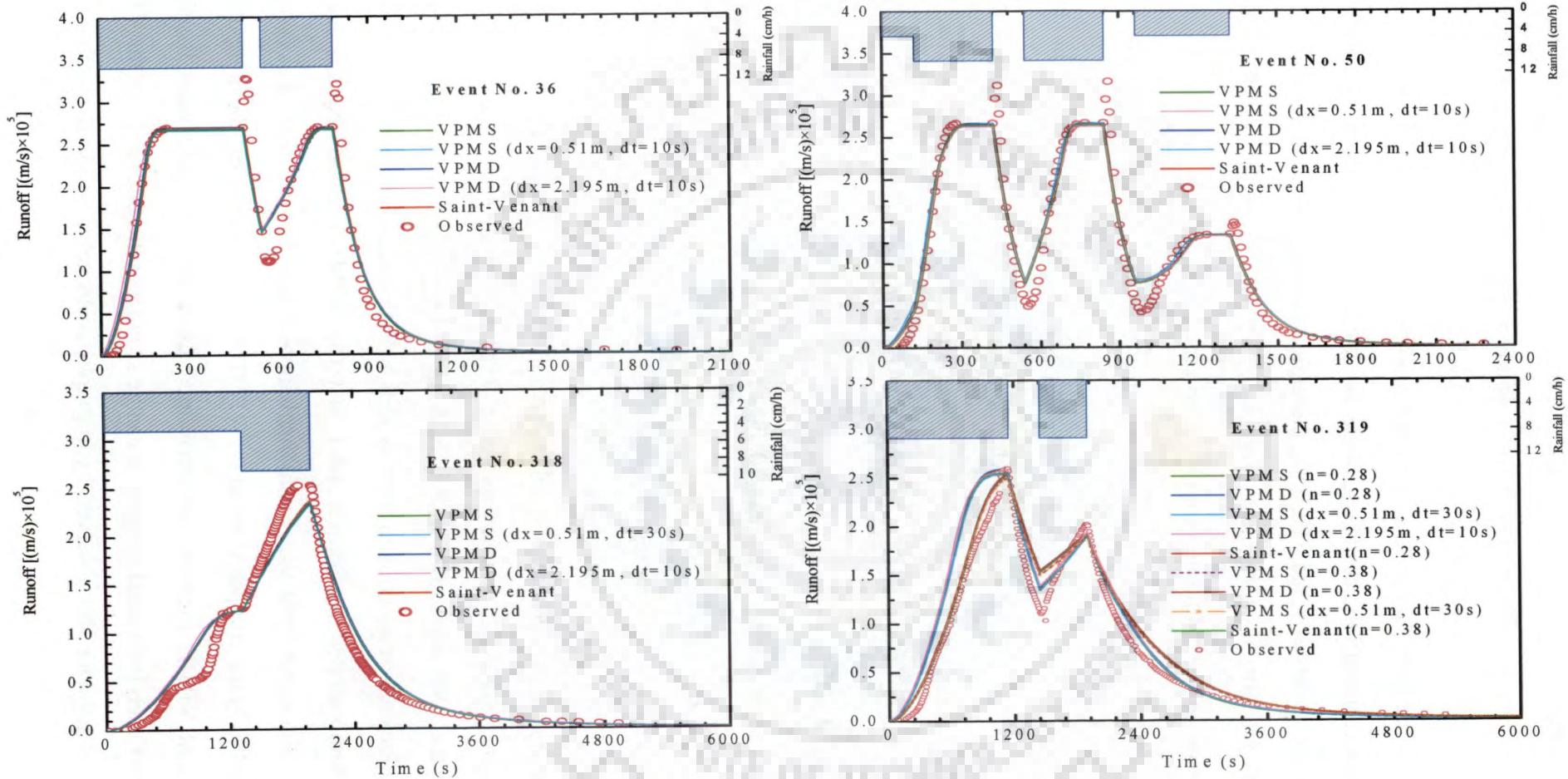
Figure 4.13 Izzard's experimental hydrographs and the corresponding simulated hydrographs of the VPMS, VPMD and SVE methods. Effect of larger grid size on the solution accuracy of the VPMS and VPMD methods is also shown. In event No. 319, the effect of Manning's roughness coefficient on the simulation outputs is also shown.

with the solutions of the VPMD method and the numerical solutions of the SVE. The selected larger temporal grid size in the computations by the VPMD method resulted in the early rise of the rising limb of the runoff hydrograph; however the VPMS method is comparatively insensitive for the use of such small or large temporal grid size in the computations. These results are consistent with the conclusions arrived at in the earlier in Sections 4.8.2. It is interesting to note that, particularly, for the cases of rainfall-runoff events on asphalt plane, *Izzard* observed a sudden increase of discharge immediately after the cessation of rainfall as shown in Figure 4.13 (Events 36 and 50). This sudden spike observed in the discharge hydrograph is due to sudden reduction in the surface roughness caused by the termination of the impact of the rain drops on the surface of the overland flow [*Izzard*, 1944, as quoted by *Maksimović and Radojković*, 1986]. However, in case of the runoff events over dense blue grass turf, such an instant rise of runoff discharge was not observed when rainfall ceased.

The estimated performance measures of the VPMS simulations in comparison with the observed hydrographs and the numerical SVE solutions are shown in Table 4.7 along with the chosen Δx and Δt values used in the computations. The computed Courant number for each event is also given therein. It can be seen from Table 4.7 that these performance measures varying in the range of η_q =90.57 - 94.94 %, CRM =(-3.61) – (0.59) %, CD =1.29 – 1.42, q_{perr} =(-18.27) – (-10.71) % and the t_{perr} =(-3.57) –(-0.30) minutes, for rainfall-runoff events on the asphalt plane, while η_q =85.40 - 97.45 %, CRM =(-14.88) - (-1.53) %, CD =0.82 – 1.35, q_{perr} =(-7.14) – (-1.71) % and the t_{perr} = (-4.20) – (2.0) minutes for the experiments on the dense blue grass sod turf. It can be inferred from these results that the VPMS method is able to produce all the runoff hydrographs of the considered events with η_q >90.0 % (except in case of event 319) which indicates a very satisfactory performance of the method and also suggests the suitability of the method for overland flow generation in practice. The estimated errors in mass conservation for all the events simulated using finer grid sizes falls in the range of $EVOL$ < (-1.71)-(-0.84) % which indicates the good mass conservation ability of the method. The poor performance of the VPMS method in simulating some of the events is not due to the inadequacy of the method, rather it is due to improper values of the roughness coefficients used for the simulation of these events. This can be inferred from the simulation of events 319 and 301 where the use of optimum roughness values (n=0.38 and 0.36) causes improvement in the model performances as indicated by the estimates of η_q which increases from 85.40 to 94.04 % for

Table 4.7 Verification of the VPMS method using Izzard data given in Table 3.7 (*Izzard*, 1942, 1944)

Event No.	Manning's n	Δx (m)	Δt (s)	Courant Number (C_{un})	Comparison with Observed Data					Comparison with SVE Solution					VPMS		Saint-Venant	
					η_q (%)	CRM (%)	CD	q_{perr} (%)	t_{perr} (min)	η_q (%)	CRM (%)	CD	q_{perr} (%)	t_{perr} (min)	EVOL (%)	CPU-time (s)	EVOL (%)	CPU-time (s)
34	0.015	0.51	1	0.42	96.32	-1.70	1.26	-0.77	1.52	99.99	0.62	1.01	-0.72	0.85	-0.88	0.47	-0.25	3.75
		0.51	5	2.10	96.25	-1.67	1.27	-1.07	1.25	99.98	0.66	1.02	-1.03	0.58	-0.92	0.20		
35	0.015	0.51	1	0.42	95.27	-5.29	1.31	-0.71	1.85	99.99	0.61	1.01	-0.72	0.52	-0.90	0.47	-0.29	2.14
		0.51	10	4.14	95.00	-5.84	1.34	-1.29	0.50	99.97	0.93	1.03	-1.30	-0.83	-1.22	0.17		
36	0.015	0.51	1	0.42	94.25	-2.06	1.27	-0.77	1.23	99.98	0.64	1.01	-0.72	0.65	-0.86	0.45	-0.21	2.06
		0.51	10	4.19	94.45	-2.33	1.27	-1.21	-4.67	99.97	0.82	1.03	-1.16	-1.00	-1.04	0.17		
50	0.015	0.51	1	0.42	95.51	-3.32	1.25	-0.80	2.20	99.98	0.59	1.01	-0.72	-6.63	-0.84	0.53	-0.24	2.42
		0.51	10	4.17	95.17	-3.25	1.28	-1.28	7.67	99.97	0.75	1.03	-1.20	-1.17	-1.00	0.19		
301	0.28	0.51	1	0.09	90.80	-14.66	0.82	-3.20	-4.20	99.97	1.51	1.03	-1.65	1.80	-1.71	2.44	-0.20	3.95
		0.51	30	2.65	92.30	-13.54	0.86	-3.63	-3.17	99.96	1.47	1.04	-2.08	2.83	-1.68	0.33		
	0.36	0.51	1	0.08	96.55	-10.10	0.96	-3.45	-0.67	99.96	1.70	1.03	-1.89	0.67	-2.00	2.39	-0.30	3.45
		0.51	30	2.27	97.06	-9.10	0.99	-3.82	-0.17	99.96	1.62	1.04	-2.27	1.17	-1.91	0.30		
302	0.28	0.51	2	0.13	97.45	-1.53	0.84	-2.10	-0.37	99.99	0.99	1.02	-1.11	3.30	-1.19	1.73	-0.29	4.36
		0.51	30	1.98	98.06	-2.63	0.85	-2.43	-0.17	99.98	0.89	1.02	-1.44	3.50	-1.10	0.45		
318	0.28	0.51	2	0.17	93.42	-5.08	1.35	-7.14	2.00	99.98	1.22	1.02	-1.05	0.00	-1.36	1.69	-0.20	2.70
		0.51	30	2.53	93.62	-5.01	1.34	-7.83	2.00	99.97	1.16	1.03	-1.79	0.00	-1.30	0.42		
319	0.28	0.51	2	0.17	85.40	-14.88	0.84	-1.71	0.17	99.98	1.39	1.03	-1.57	0.00	-1.50	1.70	-0.16	4.08
		0.51	30	2.61	85.10	-15.19	0.85	-2.11	0.17	99.97	1.27	1.03	-1.97	0.00	-1.36	0.42		
	0.38	0.51	2	0.14	94.04	-10.18	0.99	-3.61	0.17	99.97	1.60	1.03	-1.30	0.00	-1.77	1.72	-0.20	4.41
		0.51	30	2.16	94.14	-8.99	1.01	-4.84	0.17	99.97	1.45	1.03	-1.67	0.00	-1.61	0.42		

the event 319 and from 90.80 to 96.55 % for the event 301. Accordingly, other performance measures also show corresponding improvement. Thus, it can be inferred that the improper selection of the roughness coefficient also drastically affects the model performance rather than attributing the cause of poor performance on the computational grid size used in the simulation, as seen from Figure 4.13 (event 319). Besides, the comparison of the VPMS method solution with the numerical solution of the SVE also shows that $\eta_q \cong 99.99$ % and $CD \cong 1.01$ for all the simulated events with CRM varying in the range of $0.59 - 1.7$ %. The error in the computed peak runoff q_{perr} varying in the range of -0.72- 1.89%, where negative sign denote the underestimation of peak runoff and the error in the time to peak computations t_{perr} are also almost negligible. These measures indicate that the VPMS method is able to produce the results as accurately as that of the SVE solution. Similarly, the simulated hydrographs for all the considered events by the VPMS and VPMD methods are identical as shown in Figure 4.13. The use of coarser temporal grid size causes lower solution performance and also affect the mass conserving ability of the VPMS method as can be seen from Table 4.7, although it has very marginal impact. It is also inferred from the results that the strict satisfaction of the Courant condition i.e. $C_{un} \approx 1$ is not necessary. However, the inability of all the considered methods to account for other factors such as depression storage and interception losses influencing the runoff generation process in the experiments results in the inability of accurate reproduction of the observed runoff hydrographs. The CPU-run time efficiency is dependent on the grid size as a very finer grid size causes a larger run time, but it can be improved by the use of appropriate larger grid size as shown in Table 4.7.

4.11 FIELD VERIFICATION USING WONG'S EXPERIMENTAL DATA

The same set of ten natural rainfall-runoff events recorded by *Wong and Lim* [2006] and used for verifying the VPMD method in section 3.11 were also used for studying the proposed VPMS overland flow routing method. This facility consists of asphalt and concrete overland flow planes, and a concrete level V-catchment. Their experimental plots consist of four testing bays and one collection chamber. Two bays consisting of a plane and V-catchment were prepared with asphalt surface and the other two similar set-ups were prepared with concrete surface, though the asphalt V-catchment was not used in the experiments. The dimensions of the bays were 25 m long by 1 m wide. The asphalt plane and concrete plane were developed with a slope of 2% and each plane was surrounded by a

1 m high concrete wall along the length and at the upstream end of the section. Each event studied herein of the natural rainfall was recorded by using the tipping bucket raingauges located at 6.25 m from each ends of the bays. The weigh tanks which placed at the end of experimental bays were properly calibrated to enable the recording of outflow runoff discharge using an electromagnetic flow meter. The rainfall and runoff data from ten storms occurring over these experimental plots were logged at every 15 s. These ten events consist of a variety of runoff hydrographs, such as hydrographs with one major peak (Events 7 and 9), hydrographs with two major peaks with a higher first peak (Events 3 and 5), hydrographs with two major peaks with a second higher peak (Events 1 and 2), and hydrographs with multiple peaks (Events 4, 6, 8 and 10).

The same uniform interception loss model as adopted by *Wong and Lim* [2006] and denoted in equation (4.3) as I_a, has been used herein to verify the VPMS method. The same loss model was used for verifying the VPMD method as described in section 3.11. The expression for the accumulated runoff depth R_d in cm can be written as [*Wong*, 2008]

$$R_d = \sum (r - I_a) \times (\Delta t / 60.0) \tag{3.84}$$

Wong and Lim [2006] considered the rainfall, r and interception loss, I_a in cm/h. The temporal grid size Δt was expressed in minutes. Further, for periods when $r < I_a$, $(r - I_a) = 0$. Note that, henceforth, the notation I_a is termed as ϕ-*index* as it has similar connotation as infiltration loss with nearly uniform interception of the rainfall by the bay boundary wall and the initial wetting of the dry surface. It was noted from the considered events that the interception loss was varying from event to event and it was very difficult to account for the initial losses accurately in advance, although the physical specifications of the catchments are primarily known. *Chua et al.* [2008] carried out the impact of using the same ϕ-index for all the events. However, the purpose of the present study is to examine how accurately the VPMS method can simulate the observed hydrographs of the *Wong and Lim* [2006] and, hence, the ϕ-index computed separately for each of the events is directly used in this study.

4.11.1 Results of Asphalt Plane Study

The rainfall-runoff data observed for the asphalt plane is summarized in Table 3.9 with similar ϕ-index values as reported by *Chua et al.* [2008]. It can be surmised that the antecedent rainfall condition plays an important role in the interception loss rate to be

computed. In the present study, two different grid sizes were chosen to demonstrate the capability of the proposed VPMS method in the simulation of the observed rainfall-runoff events and simultaneously analyze the grid size impacts on the solution accuracy. Thus, the chosen computational grid sizes for the VPMS and VPMD methods were $\Delta x = 0.51$ m, $\Delta t = 3$ s; and $\Delta x = 0.51$ m, $\Delta t = 15$ s. The numerical solutions of the SVE were obtained with use of $\Delta x = 1.0$ m for all the events studied herein and $\Delta t = 0.125$ s for the events 1 to 4, and 0.5 s for the events 5 to 10. *Wong* [2008] has used a value of Manning's $n = 0.013$ with the consideration of only wet portion of the events and the same value has been adopted in the present investigation for simulating the events over the asphalt plane. This selected values of n falls well within the recommended value by *Engman* [1986]. The variation range of the computed minimum magnitude of applicability criteria were $k_{min} = 67.44 - 144.04$, $\left| kF_{rp}^{2} \right|_{min} = 127.98 - 226.12$ and $(F_{rp})_{min} = 1.25 - 1.38$. It may be inferred from the $(F_{rp})_{min}$ values that the flow generated in all the experiments were supercritical and the flow regimes are well within the KW applicability limits.

The simulated runoff hydrographs of the typical events of the Wong's experimental study using the VPMS are shown in Figure 4.14. It can be seen that the simulated hydrographs are well in agreement with the observed hydrographs of complex natural rainfall patterns. Further, the perfect match between the VPMS and VPMD methods and the numerical solution of the SVE can be observed in all these figures. It is apparent from Figure 4.14 (event 1, 4 and 5) that during the initial portion of the event, the simulated hydrographs overestimate the observed hydrographs. Such a discrepancy in hydrograph simulations may be attributed to the inappropriate accounting of the actual interception loss rate which is initially higher than that considered by the loss model. However, in case of event 9, the rainfall intensity during initial period was small nearly equal to the considered interception loss and, hence, there is not much discrepancy seen between the simulated and the observed runoff hydrographs. Consequently, the simulated runoff hydrographs by the VPMS method using two different temporal grid sizes $\Delta t = 3$ s and 15s with a uniform
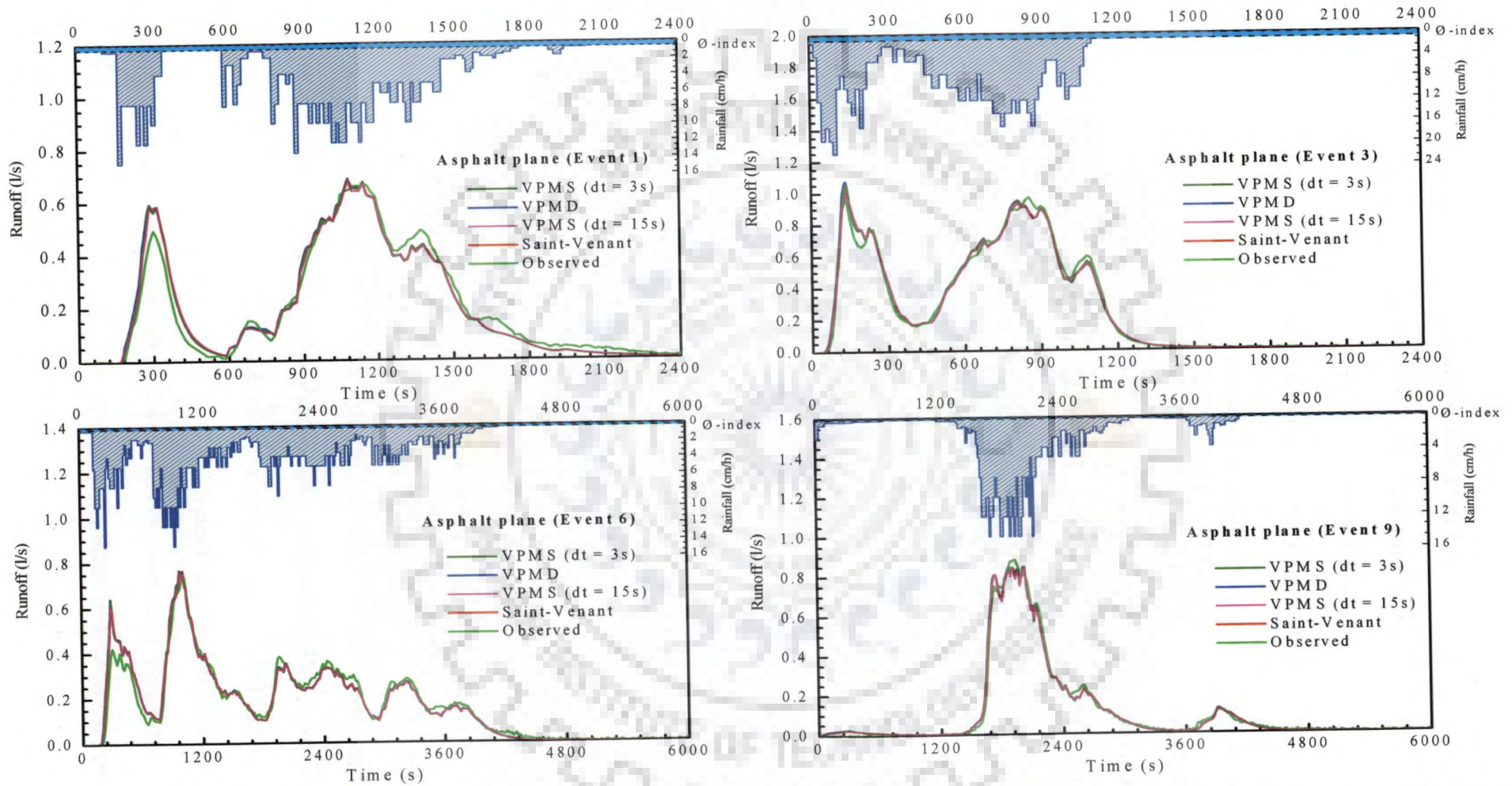
Figure 4.14 Typical experimental study hydrographs of Wong [2009] over the asphalt plane and the corresponding simulations by the VPMS, VPMD and SVE methods along with the demonstration of the computational grid sizes impacts on the runoff hydrograph generation by the VPMS method.

spatial grid size $\Delta x = 0.51$ m for both the temporal grid sizes are presented in Figure 4.14. It can be clearly seen from this figure that the differences in the simulated hydrographs due to the use of two different temporal grid sizes are not significant except that there is a slight underestimation of the peak runoff of the hydrographs of the multi-peaks runoff hydrograph. The simulated results for all the ten events can also be verified with the performance evaluation measures estimated as given in Table 4.8 by comparing the VPMS method simulation with the corresponding observed hydrographs and with the corresponding SVE solutions for the considered two different temporal grid sizes. The estimated c_{max} values and the Courant numbers (C_{un}) for each of the simulations are also shown therein. The Nash-Sutcliffe efficiency criteria computed by the VPMD method for all the events in comparison with the observed hydrographs are also presented therein. It can be seen that the Nash-Sutcliffe efficiency (η_q) for each of the events is always higher than 95.0%, except for the events 5 and 10, for which the estimated η_q values are 94.11% and 90.81%, respectively.. The lower η_q for the event 5 associated with multiple storms, may be attributed to the assigning of inappropriate interception loss rate which is less than that of the actual rate at the beginning of rainfall event and is higher than the actual rate at the later part of the event as inferred from the simulated hydrograph, which over-estimates the earlier peak and under estimates the later peaks. Similarly, in case of event 10 associated with multiple storms which are sufficiently isolated and also has relatively lower peak discharge in comparison with that of event 5, the same reasoning as assigned for event 5 may be attributed. Thus, it can be surmised that even if accurate volume loss is known in all these events, the accurate distribution of the same is also equally important. Thus, the use of higher interception ϕ-index during the initial period of the rainfall event rather than uniform rate would lead to minimization of such discrepancies in the overall hydrograph simulation. The Nash-Sutcliffe efficiency (η_q) estimates for all the simulated events by the VPMS method and those obtained by *Chua et al.* [2008] based on KW model are expected to be nearly same. But, the present study simulation results are slightly better than that of *Chua et al.* [2008] as they have used Manning's $n = 0.011$ which is a lower estimate than that used in the present investigation. Furthermore, the computed coefficient of determination (CD) values for all the events are close to 1, except for the events 5 and 10, which demonstrate the robust performance of the proposed method. The CRM and EVOL

Table 4.8 Verification of the VPMS method solutions using Wong's [2009] rainfall-runoff events over the asphalt plane, and their comparison with the corresponding VPMD method and SVE solutions

Event	$\dfrac{\Delta x}{\Delta t}$ (m/s)	c_{max} (m/s)	Courant Number (C_{un})	Performance Evaluation Measures															
				Comparison With the Observed Data						Comparison With the SVE Solution					VPMS		Saint-Venant	
				η_q (%) (VPMS)	η_q (%) (VPMD)	CRM (%)	CD	q_{perr} (%)	t_{perr} (min)	η_q (%)	CRM (%)	CD	q_{perr} (%)	t_{perr} (min)	EVOL (%)	CPU-time (s)	EVOL (%)	CPU-time (s)
1	0.167	0.38	2.26	97.21	96.83	0.54	0.96	2.06	-1.00	99.99	0.22	1.01	-0.40	0.00	-0.22	1.20	-0.01	3.30
	0.033	0.38	11.26	97.15		0.64	0.98	1.05	-1.00	99.94	0.32	1.03	-1.38	0.00	-0.06	0.57		
2	0.167	0.40	2.41	98.63	98.56	0.29	1.01	-2.20	0.00	100.00	0.26	1.01	-0.56	0.00	-0.27	1.45	-0.04	3.88
	0.033	0.40	12.01	98.57		0.54	1.03	-3.45	0.00	99.97	0.51	1.02	-1.83	0.00	-0.44	0.67		
3	0.167	0.45	2.69	99.28	99.19	0.25	1.00	8.32	0.00	100.00	0.24	1.01	0.75	0.00	-0.26	1.34	-0.03	3.98
	0.033	0.44	13.18	99.16		0.36	1.02	2.70	0.00	99.95	0.35	1.02	-4.48	0.00	-0.29	0.56		
4	0.167	0.42	2.49	98.75	98.76	0.27	1.04	7.24	0.50	100.00	0.27	1.01	-0.33	0.00	-0.28	1.52	-0.03	4.38
	0.033	0.41	12.43	98.78		0.57	1.06	6.19	0.50	99.97	0.56	1.02	-1.31	0.00	-0.59	0.80		
5	0.167	0.38	2.31	94.11	92.96	0.85	0.77	21.89	-0.25	99.99	0.21	1.01	-0.06	0.00	-0.21	0.99	-0.02	2.24
	0.033	0.38	11.48	94.27		0.94	0.78	20.74	-0.25	99.98	0.28	1.01	-1.00	0.00	-0.08	0.47		
6	0.167	0.39	2.36	96.31	96.01	0.29	0.92	0.32	-0.50	100.00	0.28	1.01	-0.38	0.00	-0.29	1.52	-0.01	2.03
	0.033	0.39	11.77	96.32		0.69	0.94	-0.44	-0.50	99.97	0.68	1.02	-1.13	0.00	-0.65	0.70		
7	0.167	0.35	2.08	98.90	98.84	0.38	0.97	4.64	0.00	100.00	0.27	1.01	-0.19	0.00	-0.28	1.63	-0.02	2.00
	0.033	0.34	10.33	98.92		0.80	0.99	3.39	0.00	99.98	0.70	1.02	-1.39	0.00	-0.65	0.80		
8	0.167	0.36	2.16	95.81	95.57	0.37	1.02	-6.72	0.00	100.00	0.27	1.01	-0.52	0.00	-0.28	1.50	-0.01	1.95
	0.033	0.36	10.74	95.80		0.72	1.03	-8.21	0.00	99.97	0.61	1.02	-2.11	0.00	-0.66	0.70		
9	0.167	0.41	2.46	99.22	99.2	0.33	1.04	-4.44	-1.00	100.00	0.32	1.01	-0.63	0.00	-0.33	1.52	-0.02	4.11
	0.033	0.41	12.27	99.23		0.79	1.06	-4.90	-0.50	99.97	0.78	1.02	-1.11	0.50	-0.80	0.72		
10	0.167	0.31	1.84	90.81	90.18	0.22	0.86	19.35	-37.75	100.00	0.20	1.00	-0.89	0.00	-0.21	1.53	-0.01	3.38
	0.033	0.30	9.14	90.95		0.36	0.87	17.03	-37.75	99.98	0.34	1.01	-2.81	0.00	-0.31	0.72		

Note that the computations in the first row for each event are carried out with $\Delta x = 0.5$m and $\Delta t = 3$ s; whereas, the computations in the second row with $\Delta x = 0.5$ m and $\Delta t = 15$ s. The computations by the VPMD method are performed with $\Delta x = 0.5$ m and $\Delta t = 3$ s.

($EVOL$ = (-0.33) – (-0.21) %) are less than 1%, demonstrating the mass conservation ability of the method. The events 5 and 10 also show the lower CD, higher errors in the estimates of peak of the runoff hydrograph simulated (q_{perr}) and corresponding higher errors in time to peaks (t_{perr}). Except these two events, the estimated performance evaluation measures for all the other events are reasonably close to the ideal values of these measures. The performance measures estimated for the VPMS solution method in comparison with the numerical solution of the SVE elucidate that there is a perfect match between both the solutions for all the events. Similarly, the comparison of the Nash-Sutcliffe efficiency (η_q) estimates obtained for both the VPMS and VPMD solution methods (see Table 4.8) suggest that the simulations of the former method are slightly better than the latter method in a relative sense. The Courant numbers estimated for all these simulations always remained in the range 1.84 – 13.18, defying the required Courant number condition of $C_{un} \approx 1$ as used in the HEC-HMS model.

4.11.2 Results of Concrete Plane Study

The evaluation of the VPMS method was further carried out by comparing the simulated runoff hydrographs with the observed overland flow hydrographs of the concrete plane. The details of the rainfall-runoff events of the concrete plane are summarized in Table 3.11. The same Manning's roughness coefficient $n = 0.010$ as used by *Wong* [2008] was used in these simulations. The same computational grid sizes of $\Delta x = 0.51$ m and $\Delta t = 3$ s; and $\Delta x = 0.51$ m and $\Delta t = 15$ s as used for the study of the rainfall-runoff events of the asphalt plane case were used herein for the simulation of rainfall-runoff events. The variation range of the minimum computed applicability criteria are $k_{min} = 46.92 – 95.29$, $\left| kF_{rp}^{2} \right|_{min} = 144.52 – 245.83$ and $(F_{rp})_{min} = 1.61 – 1.75$. It may be surmised from these results that the flows are supercritical and flow regimes are well within the KW applicability range. The typical observed hydrographs of the rainfall-runoff events along with the VPMS, VPMD and SVE solutions are shown in Figure 4.15. It can be inferred from these figures that the simulated runoff hydrographs by the VPMS method are well in agreement with the observed hydrographs and perfectly coincide with the numerical solution of the SVE and the VPMD method. Table 4.9 shows the modelling accuracy as well as the mass conservation ability of the proposed VPMS method. Further, the similar conclusions as arrived at for the runoff simulations over the asphalt plane using the VPMS method can be arrived at for the runoff
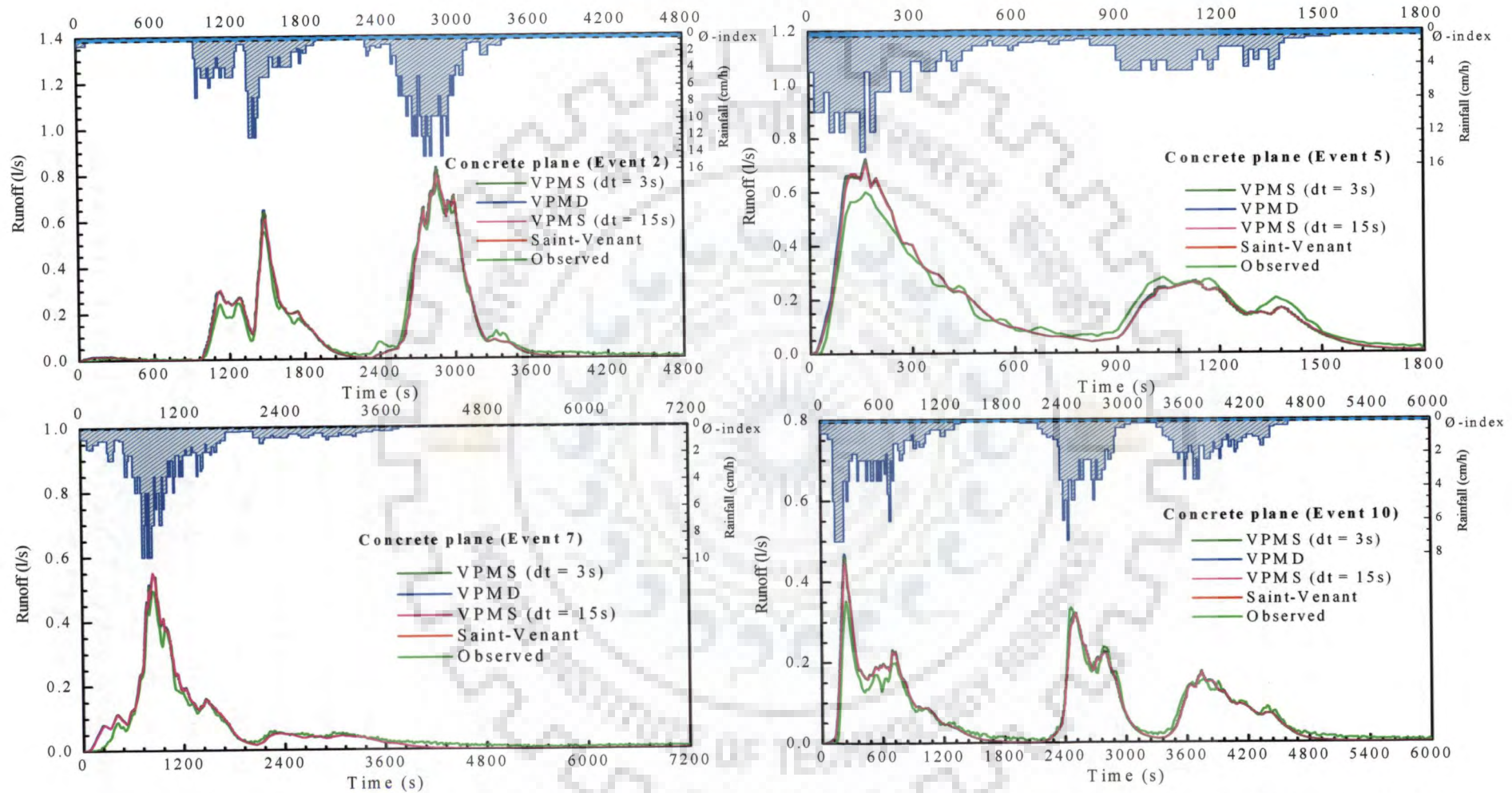
Figure 4.15 Typical experimental study hydrographs of Wong [2009] over the concrete plane and the corresponding simulations by the VPMS, VPMD and SVE methods along with the demonstration of the computational grid sizes impacts on the runoff hydrograph generation by the VPMS method.

Table 4.9 Verification of the VPMS method solutions using Wong's [2009] rainfall-runoff events over the concrete plane, and their comparison with the corresponding VPMD method and SVE solutions

Event	$\frac{\Delta x}{\Delta t}$ (m/s)	c_{max} (m/s)	Courant Number (C_{un})	Comparison with the Observed Data						Comparison with the SVE Solution					VPMS EVOL (%)	VPMS CPU-time (s)	Saint-Venant EVOL (%)	Saint-Venant CPU-time (s)
				η_q (%) (VPMS)	η_q (%) (VPMD)	CRM (%)	CD	q_{perr} (%)	t_{perr} (min)	η_q (%)	CRM (%)	CD	q_{perr} (%)	t_{perr} (min)				
1	0.167	0.45	2.7	93.55	93.05	0.40	0.82	9.10	0.50	99.99	0.25	1.01	-0.31	0.00	-0.24	2.13	-0.01	3.30
	0.033	0.44	13.2	93.69		0.51	0.83	6.96	0.50	99.96	0.34	1.02	-2.27	0.00	-0.04	0.53		
2	0.167	0.48	2.9	97.95	97.81	0.27	0.88	8.48	-0.25	100.00	0.28	1.01	-0.03	0.00	-0.28	1.45	-0.04	3.88
	0.033	0.47	14.1	98.01		0.52	0.89	5.31	-0.25	99.96	0.52	1.02	-2.96	0.00	-0.44	0.63		
3	0.167	0.54	3.2	98.34	98.11	0.26	0.92	22.78	0.10	99.99	0.26	1.01	4.14	0.10	-0.27	1.31	-0.03	3.98
	0.033	0.52	15.7	98.24		0.28	0.94	14.08	0.00	99.94	0.29	1.02	-3.24	0.00	-0.23	0.52		
4	0.167	0.49	2.9	98.19	98.08	0.27	0.85	16.46	0.50	100.00	0.28	1.01	-0.25	0.00	-0.29	1.64	-0.03	4.38
	0.033	0.48	14.5	98.40		0.56	0.86	15.79	0.50	99.96	0.57	1.02	-0.82	0.00	-0.60	0.75		
5	0.167	0.45	2.7	94.12	93.21	0.70	0.74	19.92	0.00	99.99	0.24	1.01	-0.15	0.00	-0.24	0.98	-0.02	2.24
	0.033	0.45	13.4	94.32		0.83	0.75	17.49	0.00	99.97	0.35	1.01	-2.18	0.00	-0.11	0.45		
6	0.167	0.46	2.8	97.31	97.12	0.29	0.86	4.50	-0.50	100.00	0.30	1.01	-0.10	-0.50	-0.31	1.52	-0.01	2.03
	0.033	0.46	13.8	97.28		0.72	0.87	3.90	-0.50	99.97	0.73	1.02	-0.67	-0.50	-0.68	0.72		
7	0.167	0.40	2.4	96.55	96.33	0.28	0.79	10.68	0.00	100.00	0.29	1.01	-0.13	0.00	-0.30	1.53	-0.02	2.00
	0.033	0.40	12.1	96.72		0.75	0.80	11.32	0.00	99.97	0.76	1.02	0.45	0.00	-0.71	0.72		
8	0.167	0.42	2.5	97.19	96.97	0.28	0.88	1.28	0.00	100.00	0.28	1.01	-0.36	0.00	-0.30	1.44	-0.01	1.95
	0.033	0.42	12.6	97.20		0.66	0.89	1.24	0.00	99.97	0.66	1.02	-0.40	0.00	-0.71	0.64		
9	0.167	0.48	2.9	99.00	98.89	0.38	0.90	3.64	-0.55	100.00	0.35	1.01	-0.51	-0.05	-0.36	1.52	-0.02	4.11
	0.033	0.48	14.4	99.11		0.91	0.92	1.91	-0.50	99.97	0.88	1.02	-2.17	0.00	-0.89	0.70		
10	0.167	0.38	2.3	93.83	93.34	0.25	0.78	31.19	-0.25	100.00	0.24	1.00	0.33	0.00	-0.24	1.48	-0.01	3.38
	0.033	0.37	11.2	93.94		0.47	0.79	27.67	-0.25	99.98	0.46	1.01	-2.37	0.00	-0.42	0.69		

Note that the computations in the first row for each event are carried out with $\Delta x = 0.5$ m and $\Delta t = 3$ s whereas the computations in the second row with $\Delta x = 0.5$ m and $\Delta t = 15$ s. The computations by the VPMD method are performed with $\Delta x = 0.5$ m and $\Delta t = 3$ s.

simulations over this concrete plane also. In this case also the Courant number was varying between 2.3 – 15.7, without causing any significant inaccuracy in the solutions when the condition of $C_{un} = 1$ as recommended in HEC-HMS model was not followed. Therefore, both the VPMS and VPMD methods are very flexible in the selection of the computational grid sizes in comparison with the KW overland flow solution given by the HEC-HMS model.

4.12 RUNOFF ROUTING ON THE V-CATCHMENT

The capabilities and robustness of the proposed VPMS method for routing runoff on the overland flow plane as well as flow in the channel are further investigated by comparing the simulated runoff hydrographs arrived at the end of the channel of the level V-catchment with the corresponding hydrographs of other solution methods, including the runoff hydrographs of *Wong and Lim* [2006].

4.12.1 Synthetic Example

The application of the VPMS method for runoff simulation of a V-catchment considering the component processes of overland flow simulation and the subsequent channel routing is demonstrated using the synthetic rainfall-runoff example given by *DiGiammarco et al.* [1996] on a level V-catchment. The schematic presentation of the V-Catchment is shown in Figure 3.17 and the description of the same was presented in section 3.12.1. The runoff hydrograph estimated by the VPMS method at the outlet of the level V-catchment in response to the semi-infinite spatially uniform constant rainfall intensity applied over the entire V-catchment was also compared with the corresponding runoff hydrograph arrived at as a semi-analytical KW solution presented by *Overton and Brakensiek* [1973]. The simulated runoff hydrograph at the valley side is also compared with the published results of several solution approaches presented by *DiGiammarco et al.* [1996]. Besides, the comparison is also made with the VPMD method solution and the numerical solution of the SVE for overland flow plane. Similarly, the VPMS method simulated runoff hydrograph at the outlet of the channel i.e., at the outlet of the level V-catchment, is also compared with the corresponding simulated hydrograph obtained using the HEC-HMS model [*USACE*, 2006], the VPMD method solution and with various other solutions presented by *DiGiammarco et al.* [1996]. These other solutions include the methods based on the control

202

volume finite element (CVFE) method applied to the DW solution, the classical integrated finite difference (IFD) method and that of the SHE model developed based on a conventional finite difference scheme [*Bathurst*, 1986]. The HEC-HMS model [*USACE*, 2006] solves the KW equations for both the overland flow and channel simulations using the finite difference scheme. The runoff hydrograph is estimated at the outlet of valley side of the overland flow plane having a dimension 800m × 100 m using the VPMS method to facilitate its comparison with various other solutions presented by *DiGiammarco et al.* [1996]. In the present case, the VPMS model uses the grid sizes of $\Delta x = 10$ m and $\Delta t = 10$ s for planes and channel. The same sets of computational grid sizes have been used in the runoff hydrograph simulation by the VPMD method and the HEC-HMS model. The numerical solution of the SVE using the explicit numerical scheme for the plane requires the use of $\Delta x \geq 5$ m in order to avoid convergence problem.

The simulated runoff hydrograph and the corresponding flow depth hydrograph estimated at the outlet of the valley side and its comparison with other solutions are shown in Figure 4.16 (a and, c). Figure 4.16 (a) elucidates that the VPMS method solution is in agreement with the solutions of other methods. Further, it is interesting to note that the analytically obtained applicability criteria for the plane are $k = 1912.34$, $k(F_{rp}^2)_e = 7550.38$ and $(F_{rp})_e = 1.98$, while those obtained by the VPMS and VPMD methods are $k = 1900.71$ and 1914.48, $kF_{rp}^2 = 7509.26$ and 7550.18; and $F_{rp} = 1.988$ and 1.985, respectively. Attention is drawn to the estimated magnitude of the Froude number $F_{rp} > 1.5$, resulting in supercritical flow state. A careful observation of Figure 4.16 (a) shows periodic pulsating wave motion on the rising and recession limbs of the hydrograph (not clearly visible in the Figure). This phenomenon is due to the formation of roll waves [*Iwasa*, 1954; *Jolly and Yevjevich*, 1971; *Dooge and Napiorkowski* 1987; *Ponce* 1991; *Liu et al.*, 2005; *Zanuttigh and Lamberti*, 2007]. This might be the possible reason for the "overshoot" of the CVFE and IFD methods solutions near the equilibrium condition of the overland flow hydrograph [Figure 4.16 (a)]. However, the VPMS and VPMD methods do not exhibit such behavior, but shows slight wavy motion which is not clearly visible. Consequently, for such a situation, the Muskingum weighting coefficient, $\theta > 0.5$ and this leads to the amplification of flow. As shown in the Figure 4.16(b), the use of the inertial terms in the solution of the VPMS and VPMD methods resulted in the estimated values of $\theta > 0.5$, at different
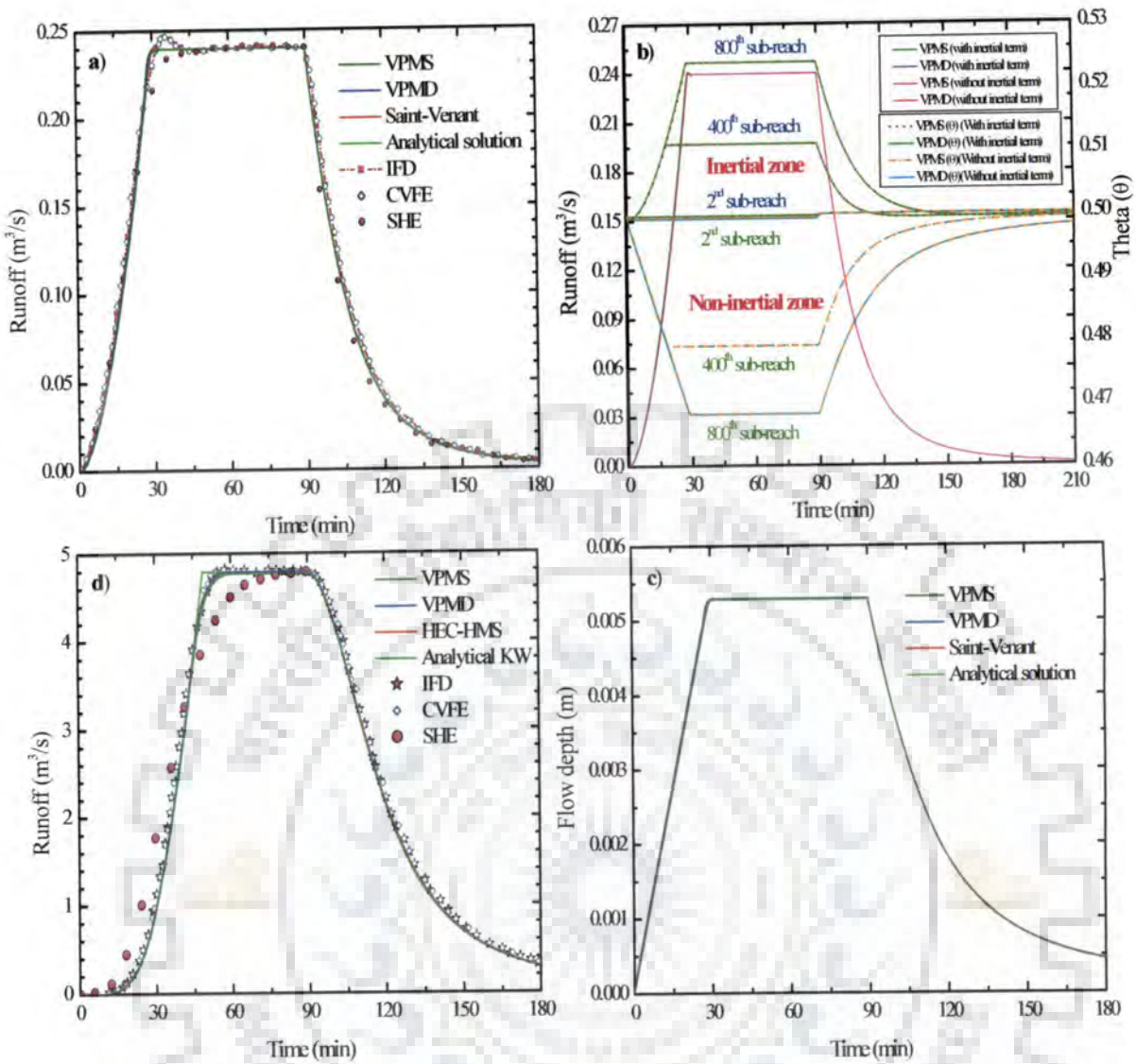
Figure 4.16 Comparison of the VPMS method simulated runoff hydrographs (a) at the outlet of the valley side (b) at the outlet of the valley side showing the effect of inclusion and exclusion of the inertial terms along with the temporal variation of θ at different locations of the overland flow plane (c) simulated flow depth hydrograph at the outlet of the valley side (d) runoff hydrograph at the outlet of the level V-catchment (recession simulations not available for both the analytical method and the SHE model). Number of sub-reaches used for the plane and the channel are 80 and 99 (except in Figure 4.16b), respectively, and for $\Delta t = 10$s.

locations along the flow path except at the end of 2nd sub-reach. However, ignoring the inertial terms in the runoff hydrograph simulation by the VPMS and VPMD methods resulted in $\theta < 0.5$. Moreover, the estimated values of θ by the VPMS and VPMD methods at different locations of the considered overland flow strip match perfectly with

each other. Consequently, the accounting or neglecting the inertial terms in the runoff hydrograph simulations do not have any significant difference on the simulated runoff hydrographs on the overland flow plane due to the reason that the flow characteristics are not very dynamic to induce significant wave amplification, even though the required criterion for wave amplification that $(F_{rp})_e > 1.5$, is satisfied. Indeed, in the supercritical regime of the overland flow, the inertial terms become dominant over the longitudinal slope gradient $\partial y / \partial x$ and, hence, accounting the inertial term will enable one to handle the flow situation wherein the possibility of roll wave formation prevails. Thus, it can be inferred from this discussion that even the higher values of Froude number do not make any significant difference between the estimated θ values with and without accounting of the inertial terms in equation (4.20), provided that the Vedernikov number $V_{vn} < 1$. The same inference is also true in case of variation of θ as depicted in Figure 4.8. However, accounting of inertial terms in equation (4.20) yields $\theta > 0.5$ when $F_{rp} > 1.5$ for which $V_{vn} > 1$ [*Ponce*, 1991]. This condition results in the amplification of flood waves or formation of roll waves. Therefore, it is surmised that the Vedernikov number only serves the purpose as an criterion to detect the formation of roll waves in gradually varied flow conditions as in the case of overland flow modelling after the time of equilibrium is reached at any location in the plane.

The runoff hydrograph estimated at the outlet of the V-catchment [Figure 4.16 (d)] using the VPMS method clearly shows that this method has a very good agreement with the VPMD method solution, CVFE, IFD and HEC-HMS model results. Note that the same spatial grid size used in the VPMS method solution is also used in the VPMD solution and the HEC-HMS model. The estimated applicability criteria by the VPMS and VPMD method at the end of channel are $k = 683.66$ and 686.42, $kF_{rp}^2 = 44.67$ and 44.57 and $F_{rp} = 0.26$ and 0.25, respectively. The Froude number $(F_{rp})_{min} < 1$, hence the estimated hydrographs by the VPMS and VPMD methods are smooth. Also, CVEF and IFD methods solution do not show overshooting as in case of the corresponding overland flow plane hydrographs.

To facilitate the decision making on the appropriate selection of the computational grid sizes to preserve the accuracy of the solution, the numerical experiments are performed by dividing the overland flow plane into 8, 80, 200, 800 and 4000 sub-reaches, while the channel is divided into 10, 99, 250, 1000 and 5000 sub-reaches with use of four Δt values
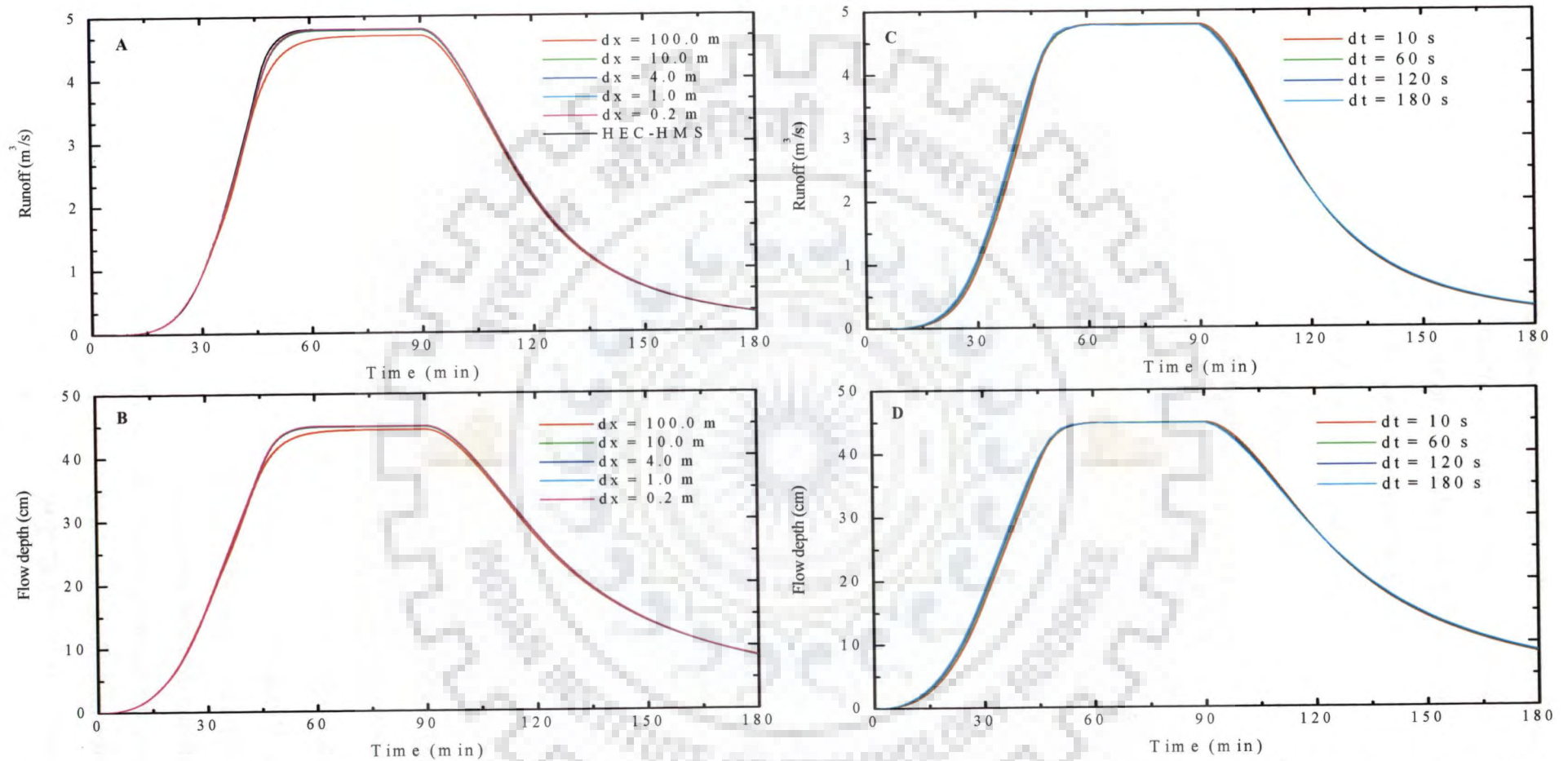
Figure 4.17 Assessment of the impacts of the computational grid sizes on the VPMS method estimated flow characteristics at the outlet of the level V-catchment on the runoff (A) and the flow depth (B) with the use of $\Delta t = 60$ s, and on runoff (C) and the flow depth (D) with the use of Δx and $\Delta X = 4.0$ m.

such as 10 s, 60 s, 120 s and 180 s. The impact of spatial grid sizes with the use of uniform temporal grid size of 10 s on the runoff and the flow depth hydrographs can be seen from Figure 4.17 (A and B). It is seen from these figures that the VPMS model is showing better performance and accuracy for the selected computational spatial grid size except for the $\Delta x = 100$ m. When a very large spatial grid size (say $\Delta x = 100$ m) is selected for the computation, the simulated hydrograph with uniform value of $\Delta t = 10$ s resulted in the underestimation of the runoff as well as of the flow depth, especially in the vicinity of equilibrium state of both the runoff and flow depth hydrograph. Similarly, the impact of the computational temporal grid size on the runoff and stage hydrograph estimated at the end of the channel in a level V-catchment with uniform spatial grid size of $\Delta x = 4$ m for both the overland flow plane and the channel can be seen from the Figure 4.17 (C and D). It can be seen that the proposed VPMS method is able to perform very well and also able to conserve the accuracy with the selected wide range of computational temporal grid size. It can be revealed from the performance evaluation measures as presented in Table 4.10 that a very large spatial grid size resulted in the poor performance of the VPMS method and can be examined from the poor estimates of the performance evaluation measures such as η_q, $EVOL$ and q_{perr}. It can also be surmised from the results presented in Table 4.10 that the use of Δx or $\Delta X \leq 10$ m and $\Delta t \leq 120$ s resulted in a very good performance and accuracy of the method. These results clearly elucidate that the VPMS method provides wide flexibility in the selection the computational grid sizes. Further, it can be noted that even though the Courant condition criteria $C_{un} \approx 1$ as used in HEC-HMS model is not strictly followed (Table 4.10), it has no any significant impact on the accuracy of the method. Further, the runoff hydrographs as shown in Figure 4.17 A and C and those computed at the end of the overland flow plane by the proposed method (Figure 4.9 and 4.10) exhibit identical computational characteristics of the method.

Table 4.10 Verification of the VPMS method for simulation of runoff from a level V-catchment using the HEC-HMS model results as a benchmark solution

Δx OR ΔX (m)	Δt	Grid Ratio	Wave Celerity and Courant Number				Performance Evaluation Measures				CPU-time (s)	q_{pc} (m³/s)	t_{pc} (min)	q_{po} (m³/s)	t_{po} (min)	Error in Computed Peak Discharge and Time to Peak	
			Plane		Channel		η_q (%)	CRM (%)	CD	EVOL (%)						q_{perr} (%)	t_{perr} (min)
			c_{max}	C_{un}	c_{max}	C_{un}											
100.0	10	10.00	0.73	0.07	0.85	0.09	99.84	2.22	1.07	-3.18	0.39	4.69	90.00	4.80	67.00	-2.20	23.00
	60	1.667	0.73	0.44	0.85	0.51	99.78	2.66	1.08	-3.62	0.23	4.65	90.00	4.80	67.00	-3.03	23.00
	120	0.833	0.73	0.87	0.85	1.02	99.67	3.07	1.10	-4.02	0.13	4.61	90.00	4.80	67.00	-3.93	23.00
	180	0.556	0.73	1.31	0.84	1.52	99.55	3.36	1.12	-4.32	0.08	4.57	90.00	4.80	67.00	-4.74	23.00
10.0	10	1.000	0.75	0.75	0.87	0.86	99.99	0.23	1.01	-1.21	1.69	4.78	68.83	4.80	67.00	-0.40	1.83
	60	0.167	0.76	4.53	0.87	5.18	99.98	0.05	1.02	-1.03	0.45	4.77	65.00	4.80	67.00	-0.68	-2.00
	120	0.083	0.76	9.10	0.87	10.36	99.95	-0.27	1.02	-0.71	0.24	4.76	62.00	4.80	67.00	-0.78	-5.00
	180	0.056	0.76	13.67	0.87	15.54	99.89	-0.65	1.02	-0.34	0.16	4.76	63.00	4.80	67.00	-0.77	-4.00
4.0	10	0.400	0.75	1.89	0.88	2.19	99.99	0.03	1.01	-1.01	3.81	4.79	66.83	4.80	67.00	-0.21	-0.17
	60	0.067	0.76	11.37	0.87	13.12	99.99	-0.26	1.01	-0.72	0.81	4.78	63.00	4.80	67.00	-0.36	-4.00
	120	0.033	0.76	22.82	0.87	26.24	99.95	-0.70	1.01	-0.29	0.41	4.78	62.00	4.80	67.00	-0.35	-5.00
	180	0.022	0.76	34.30	0.88	39.38	99.90	-1.17	1.01	0.17	0.28	4.79	63.00	4.80	67.00	-0.26	-4.00
1.0	10	0.100	0.76	7.56	0.88	8.76	99.99	-0.11	1.00	-0.87	14.33	4.80	74.33	4.80	67.00	-0.06	7.33
	60	0.017	0.76	45.57	0.88	52.56	99.99	-0.50	1.01	-0.48	2.58	4.79	63.00	4.80	67.00	-0.11	-4.00
	120	0.008	0.76	91.43	0.88	105.16	99.96	-1.02	1.01	0.03	1.30	4.80	62.00	4.80	67.00	-0.02	-5.00
	180	0.006	0.76	137.46	0.88	157.82	99.90	-1.54	1.00	0.54	0.86	4.81	63.00	4.80	67.00	0.12	-4.00
0.2	10	0.020	0.76	37.83	0.88	43.83	99.99	-0.18	1.00	-0.81	71.88	4.80	81.50	4.80	67.00	0.00	14.50
	60	0.003	0.76	227.94	0.88	262.95	99.99	-0.61	1.00	-0.37	12.09	4.80	63.00	4.80	67.00	0.00	-4.00
	120	0.002	0.76	457.53	0.88	526.22	99.96	-1.18	1.00	0.19	6.05	4.81	62.00	4.80	67.00	0.16	-5.00
	180	0.001	0.76	687.62	0.88	789.71	99.90	-1.68	1.00	0.68	4.03	4.81	63.00	4.80	67.00	0.28	-4.00

4.12.2 Verification with Wong's Experimental V-Catchment Results

The VPMS method was also used to demonstrate its ability to simulate the V-catchment experimental results recorded by *Wong* [2009]. The runoff data was observed at the channel outlet of the 25 m^2 area of the experimental concrete V-catchment (25 m long and 1 m wide) subjected to natural rainfall as described in Table 3.13. The configuration details of the V-catchment are described in section 3.12.2.

The simulation results showing the runoff hydrographs as well as the corresponding flow depth hydrographs at the channel outlet of the V-catchment for some typical events (events 1 and 4) by employing the VPMS method are shown in Figure 4.18, along with the corresponding solutions by the VPMD method. These results demonstrate the capability and efficacy of the VPMS method to simulate both the overland flow and channel flow routings involved in a watershed such as the considered V-catchment. It is revealed from these figures that the simulated runoff and the corresponding flow depth hydrographs of the VPMS and VPMD methods perfectly coincide with each other. Further, it can be observed from these figures that the VPMS method resulted in a slight underestimation of the recession portion of the runoff as well as the flow depth hydrographs, particularly, when the rainfall intensity during the event becomes very low. However, the differences involved in the reproduction of the runoff and flow depth hydrographs is very negligible. In order to demonstrate the role of the Courant number in the selection of spatial and temporal computational grid sizes and their impact on the solution accuracy, simulations were made by adopting two different temporal sizes, 1s and 3s. The grid sizes used, the corresponding kinematic wave celerities and Courant numbers computed are presented in Table 4.11 along with the different performance measures used for the assessment of the VPMS method solution to reproduce the observed runoff hydrographs. Similar performance measures for the VPMD method solution are also presented therein to facilitate the comparison of both of these methods. Similarly, it is also observed that the use of a set of larger temporal grid size
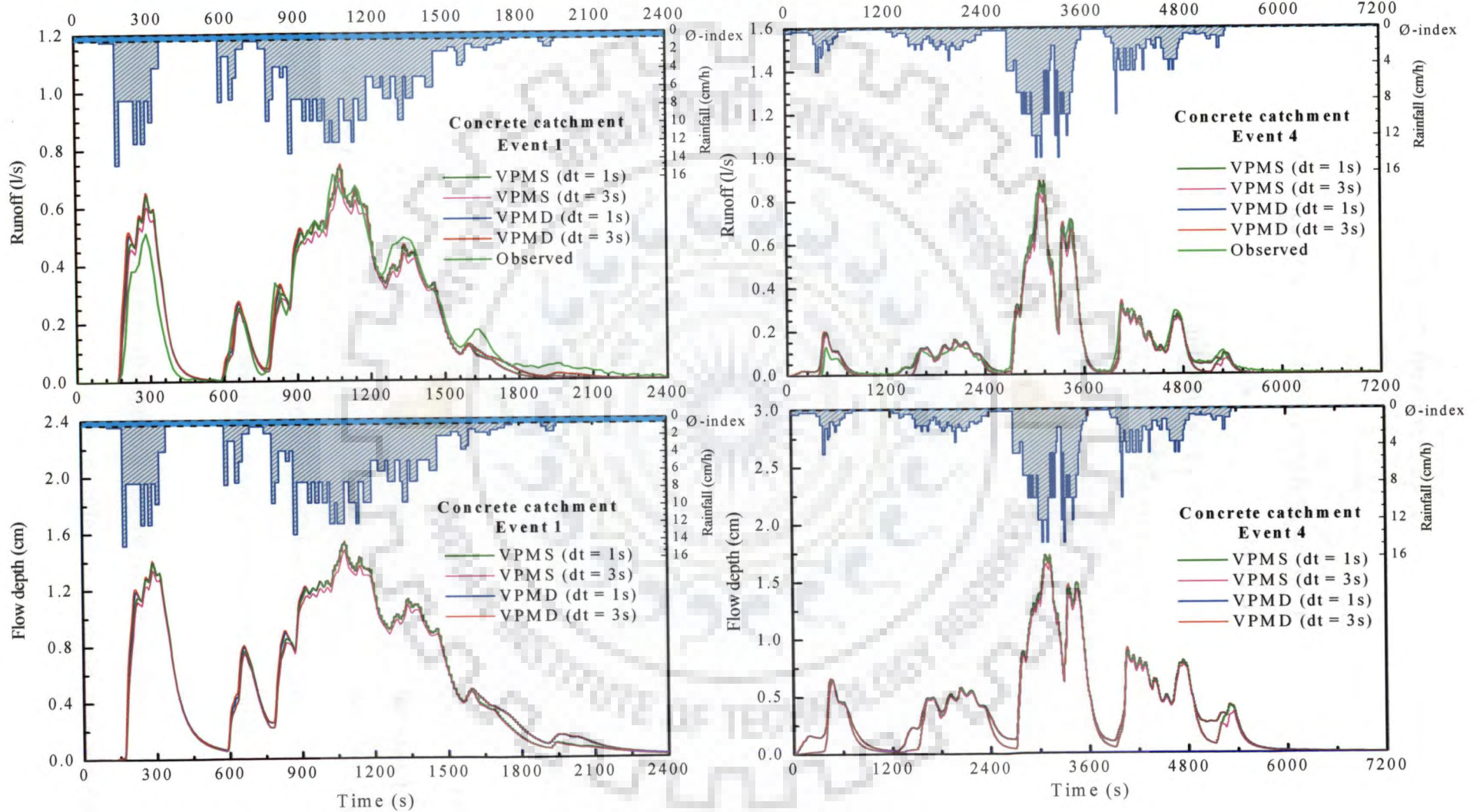
Figure 4.18 Simulated runoff and flow depth hydrographs by the VPMS and VPMD methods at the outlet of the V-catchment for some typical rainfall-runoff events of the Wong's [2009] study.

Table 4.11 Verification of the VPMS method solutions using Wong's [2009] rainfall-runoff events over the concrete level V-catchment

| Event | Grid Ratio, Wave Celerity and Courant Number | | | | | | Performance Evaluation Measures Estimated by Method | | | | | | | | | | | | | |
| | Plane* | | | Channel* | | | VPMS | | | | | | | VPMD | | | | | | |
	$\frac{\Delta x}{\Delta t}$	c_{max}	C_{un}	$\frac{\Delta x}{\Delta t}$	c_{max}	C_{un}	η_q (%)	CRM (%)	CD	EVOL (%)	CPU-time (s)	q_{per} (%)	t_{per} (min)	η_q (%)	CRM (%)	CD	EVOL (%)	CPU-time (s)	q_{per} (%)	t_{per} (min)
1	0.09	0.12	1.4	2.50	0.72	0.3	93.90	1.62	0.90	-1.67	0.77	4.12	0.50	93.85	-1.18	0.91	1.16	1.44	4.52	0.50
	0.03	0.12	4.1	0.83	0.71	0.9	94.10	6.49	1.01	-6.51	0.44	-1.80	0.50	93.28	-2.18	0.90	2.21	0.56	4.88	0.50
2	0.09	0.12	1.4	2.50	0.75	0.3	97.22	2.98	0.99	-3.01	1.86	-1.82	0.77	97.41	-0.66	1.00	0.63	3.41	-1.66	0.77
	0.03	0.12	4.1	0.83	0.74	0.9	96.75	8.58	1.11	-8.60	0.92	-7.34	0.75	97.38	-1.19	0.99	1.17	1.45	-1.30	0.75
3	0.09	0.14	1.6	2.50	0.83	0.3	97.59	0.25	0.94	-0.30	0.97	26.70	0.00	97.64	-0.58	0.94	0.57	1.72	28.02	0.00
	0.03	0.14	4.7	0.83	0.82	1.0	97.55	5.80	1.07	-5.83	0.52	18.72	0.00	97.57	-1.06	0.93	1.06	0.75	28.73	0.00
4	0.09	0.13	1.4	2.50	0.76	0.3	97.57	5.33	0.99	-5.34	2.08	2.27	0.77	97.94	-0.44	1.01	0.44	3.55	2.57	-0.18
	0.03	0.12	4.1	0.83	0.75	0.9	97.09	10.3	1.10	-10.32	1.13	-3.82	0.75	98.00	-0.84	1.00	0.85	0.75	2.86	0.75
5	0.09	0.12	1.4	2.50	0.72	0.3	93.70	3.29	0.76	-3.23	0.69	15.70	0.02	94.06	-0.44	0.78	0.60	1.19	16.50	0.02
	0.03	0.12	4.0	0.83	0.71	0.9	94.58	8.38	0.84	-8.32	0.38	9.15	0.00	93.09	-0.99	0.78	1.16	0.53	17.53	0.00
6	0.09	0.13	1.4	2.50	0.74	0.3	95.82	1.00	0.90	-1.03	2.00	3.90	-0.22	95.46	-0.42	0.90	0.40	3.63	4.48	-0.25
	0.03	0.12	4.1	0.83	0.73	0.9	96.01	5.73	1.00	-5.74	1.05	-2.42	-0.20	95.17	-0.78	0.89	0.78	1.58	4.90	-0.25
7	0.09	0.11	1.2	2.50	0.67	0.3	95.00	18.5	0.88	-18.51	1.70	5.49	1.55	97.70	-0.25	0.93	0.28	3.73	6.42	1.57
	0.03	0.11	3.5	0.83	0.66	0.8	95.00	22.2	0.97	-22.24	1.14	-0.09	1.50	97.67	-0.51	0.92	0.55	1.58	6.91	1.55
8	0.09	0.12	1.3	2.50	0.69	0.3	96.53	4.11	0.93	-4.13	1.97	-0.12	-0.20	96.98	-0.50	0.95	0.50	3.42	0.57	-0.22
	0.03	0.11	3.8	0.83	0.68	0.8	96.38	8.62	1.03	-8.62	1.00	-6.00	-0.20	96.87	-0.95	0.94	0.96	1.49	1.03	-0.20
9	0.09	0.13	1.4	2.50	0.76	0.3	98.99	6.36	1.02	-6.37	1.95	-2.23	-0.03	98.95	-0.35	1.04	0.35	3.44	-1.11	-0.10
	0.03	0.12	4.1	0.83	0.75	0.9	98.40	11.1	1.14	-11.19	1.03	-8.49	0.00	98.89	-0.65	1.03	0.67	1.52	-0.99	-0.10
10	0.09	0.10	1.1	2.50	0.64	0.3	92.53	7.17	0.81	-7.15	1.97	24.86	0.00	92.89	-0.31	0.83	0.34	3.44	24.86	0.00
	0.03	0.09	3.1	0.83	0.63	0.8	93.02	11.6	0.89	-11.62	1.03	18.09	0.00	92.58	-0.60	0.83	0.63	1.53	24.87	0.00

*Number of sub-reaches for plane and channel are 5 and 10, respectively, for the computations by the VPMS and VPMD methods

as in case of event 1 using the VPMS method, such as $\Delta x = 0.09$ m, $\Delta X = 2.5$ m and $\Delta t = 3$s, introduces some sort of underestimation of runoff or flow depth in the vicinity of high peaks of the multi-peak runoff or flow depth hydrograph (see Figure 4.18, event 1), but the overall response of the catchment remains unaffected. Similarly, when the same set of computational grid size is used in the simulation of the VPMD method solution, there is a tendency to slightly overestimate of the rising limbs in the multi-peak runoff or flow depth hydrograph. It is inferred from the results presented in Table 4.11 that for the VPMS and VPMD methods, the estimated Nash-Sutcliffe efficiency $\eta_q > 95\%$ for all the events except those of the events 1, 5 and 10 which may be attributed to the improper accounting of the interception loss rate in the initial period by the ϕ - index interception loss model. Further, the η_q obtained for the ten events are very similar to those obtained using the KW model by *Wong and Lim* [2006]. The identical results by the VPMS, VPMD and KW methods solutions are expected as computed applicability criteria by the VPMS method are $k_{min} = 60.72 - 138.89$, $\left|kF_{rp}^2\right|_{min} = 189.11 - 351.86$ and $(F_{rp})_{min} = 1.59 - 1.76$ for the plane, while $k_{min} = 14.47 - 27.52$, $\left|kF_{rp}^2\right|_{min} = 22.64 - 42.66$ and $(F_{rp})_{min} = 1.25 - 1.26$ for the channel. The comparison between the VPMS and VPMD methods reveals that the Nash-Sutcliffe efficiency, η_q and CD by both the methods in the reproduction of runoff hydrographs at the outlet of the level V-catchment is very satisfactory. Moreover, the $EVOL$ estimated for the VPMS method is slightly higher than that of the VPMD method which is attributed to the underestimation of the recession at the lower portion of the hydrograph, especially, for the very low intensity rainfall occurring during the storm event.

4.13 IMPACT OF INITIALLY HIGHER INTERCEPTION LOSS RATE

As seen in the previous sections while applying the VPMS method for overland flow simulation over the asphalt plane and the concrete planes, and in the concrete V-catchment,

the use of constant interception loss rate over the total period of the event resulted in the over-prediction of runoff hydrograph in the initial period by the VPMS method solutions as shown in Figures 4.14, 4.15 and 4.18. This over-prediction is attributed to the under-specification of the interception loss in the initial period of the events and interestingly similar trend is observed while applying kinematic wave model by *Wong and Lim* [2006]. In general, most of the interception loss occurs during the initial storm period and the rate of interception approaches zero thereafter. To prove this viewpoint, it is envisaged to select a higher interception loss rate during the initial period, especially, for the period of rise and recession of the first major peak runoff hydrograph of a multi-peak storm event, by conserving mass using equation (3.84).

Table 3.15 presents the summary of varying interception loss rates of all the 10 events considered (except event 7 and 8 for which uniform loss rate is applicable) for which higher loss rates are applicable for the initial period of the storm followed by a lower rate for the remaining period of the storm. It was also found from these results that accounting of initially higher interception loss rates resulted in the increase of k_{min} and $(kF_{rp}^2)_{min}$ and decrease in $(F_{rp})_{min}$. The sufficiently isolated first major storm from the consecutive storms for the events 1, 5 and 10 justifies the use of higher interception loss initially, rather than a uniform rate, which is reflected in the overall improvement of runoff hydrograph reproduction as shown in Figure 4.19 (events 1 and 5). This also can be verified from the improvement achieved in the performance measures criteria as shown in Table 4.12 over those respective measures given in Table 4.8. For concentrated storms recorded from the beginning, as in the event 3, the use of higher interception loss during initial period of the event shows only slight improvement. Similar analyses were carried out for the overland flow studies of the concrete plane and V-catchment also, and the typical improved reproductions of the same are shown in Figure 4.19.
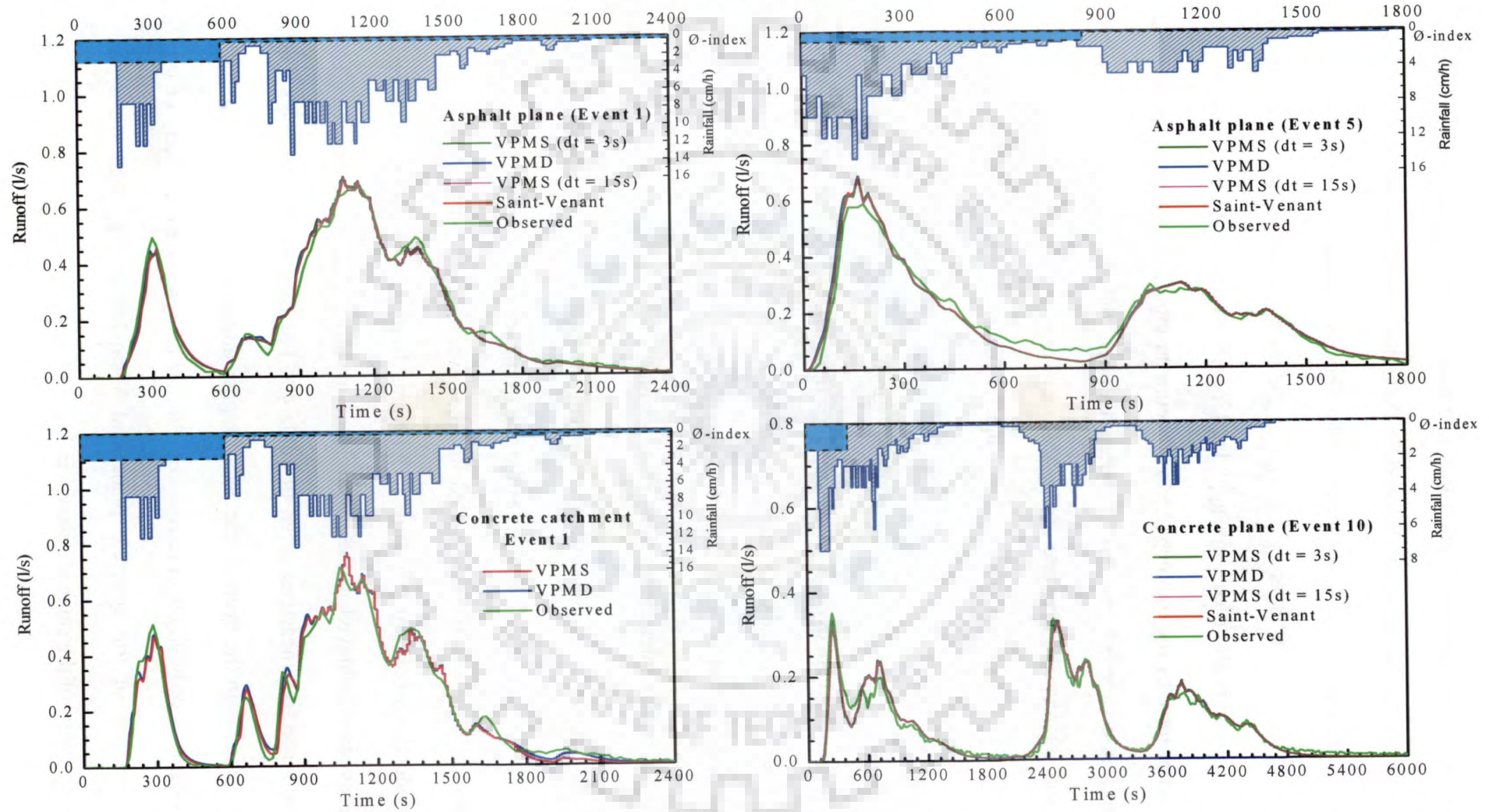
Figure 4.19 Typical simulated runoff hydrographs of the Wong's [2009] study on the asphalt and concrete planes and on the concrete V-catchment considering initial higher interception loss rates.

Table 4.12 Verification of the VPMS method as in Table 4.8, but considering higher initial interception loss rates

Event	$\frac{\Delta x}{\Delta t}$ (m/s)	c_{max} (m/s)	Courant Number (C_{un})	η_q (%) (VPMS)	η_q (%) (VPMD)	Comparison With Observed Data				Comparison With SVE Solution					VPMS		Saint-Venant	
						CRM (%)	CD	q_{perr} (%)	t_{perr} (min)	η_q (%)	CRM (%)	CD	q_{perr} (%)	t_{perr} (min)	EVOL (%)	CPU-time (s)	EVOL (%)	CPU-time (s)
1	0.167	0.38	2.3	98.68	98.76	0.61	1.00	4.83	-1.00	100.00	0.25	1.01	-0.38	0.00	-0.24	1.38	-0.01	3.73
	0.033	0.38	11.4	98.69		0.78	1.02	3.73	-1.00	99.97	0.40	1.02	-1.42	0.00	-0.18	0.59		
2	0.167	0.41	2.4	99.15	99.15	0.34	0.99	-0.03	0.00	100.00	0.27	1.01	-0.56	0.00	-0.28	1.47	-0.04	3.17
	0.033	0.40	12.1	99.09		0.63	1.01	-1.35	0.00	99.97	0.56	1.02	-1.88	0.00	-0.49	0.66		
3	0.167	0.44	2.6	99.01	99.08	0.27	0.98	0.96	11.25	100.00	0.25	1.01	-0.55	0.00	-0.26	1.41	-0.03	3.42
	0.033	0.43	13.0	99.03		0.35	0.99	-0.62	11.25	99.95	0.33	1.02	-2.11	0.00	-0.28	0.63		
4	0.167	0.42	2.5	99.15	99.15	0.27	1.01	7.88	0.50	100.00	0.27	1.01	-0.33	0.00	-0.28	1.58	-0.03	3.59
	0.033	0.42	12.5	99.19		0.58	1.03	6.85	0.50	99.97	0.58	1.02	-1.29	0.00	-0.61	0.78		
5	0.167	0.38	2.3	96.41	95.67	1.46	0.85	16.09	-0.25	99.99	0.21	1.01	0.01	0.00	-0.20	1.02	-0.02	2.86
	0.033	0.38	11.3	96.56		1.51	0.85	15.55	-0.25	99.98	0.24	1.01	-0.45	0.00	-0.04	0.50		
6	0.167	0.40	2.4	98.58	98.47	0.33	0.96	2.28	-0.50	100.00	0.28	1.01	-0.34	0.00	-0.29	1.53	-0.01	2.06
	0.033	0.40	11.9	98.66		0.73	0.97	1.57	-0.50	99.97	0.69	1.02	-1.03	0.00	-0.66	0.70		
9	0.167	0.41	2.5	99.23	99.21	0.43	1.05	-4.78	-1.00	100.00	0.32	1.01	-0.63	0.00	-0.33	1.69	-0.02	2.09
	0.033	0.41	12.3	99.23		0.88	1.07	-5.25	-0.50	99.97	0.77	1.02	-1.11	0.50	-0.79	0.77		
10	0.167	0.28	1.7	95.85	95.92	0.27	1.06	-4.79	0.00	100.00	0.20	1.00	-0.41	0.00	-0.21	1.52	-0.01	2.81
	0.033	0.28	8.3	95.98		0.43	1.07	-6.41	0.00	99.97	0.36	1.01	-2.11	0.00	-0.34	0.73		

215

4.14 SUMMARY AND CONCLUDING REMARKS

In the present study, a novel, physically distributed yet simple, computationally inexpensive, and numerically stable method based on variable parameter Muskingum stage-hydrograph (VPMS) river routing method has been proposed for routing runoff on overland flow plane and subsequently in a channel [in an idealized open book shaped V-catchment] by incorporating a uniformly distributed lateral inflow in the model framework. The evaluation of this VPMS overland flow routing method for runoff generation is extensively carried out through the assessment of comparison of the simulated runoff hydrographs with the corresponding simulated overland flow hydrographs obtained by the analytical KW solution, approximate analytical solution or one-term solution, numerical solution of the full SVE, the VPMD overland flow routing method and the runoff hydrographs extracted from the available publications in the form of experimental runoff data as well as hypothetical rainfall-runoff data generated based on the KW and DW models. The performance of the proposed VPMS method is evaluated using different evaluation measures. The performance of the VPMS routing method under complex rainfall pattern is further investigated by comparing its solutions with the simulated runoff hydrographs of Izzard's experimental data and runoff data collected for natural rainfall events from an outdoor laboratory experimental facility. Besides, the comparison of the simulated hydrographs by the VPMS method was also carried out with the corresponding solutions of the VPMD method and the SVE. Similarly, the performance of the extended VPMS method for the simulation of discharge hydrographs and the corresponding flow depth (stage) hydrographs at the valley side as well as at the outlet of a V-catchment channel are verified by comparing the results with the analytical solution of the KW equation, HEC-HMS model results, the corresponding results of the VPMD method, simulation results of hypothetical routing study and with the Wong's runoff data of the natural rainfall events. In order to account for the interception loss in the rainfall-runoff data of Wong's study, the VPMS method was coupled with ϕ-index infiltration type interception loss model. All these studies on V-catchment reveals that the VPMS method solution is in better agreement with the observed data, SVE solution, and the solutions of the DW and KW equations; whereas the VPMS method is also found to yield better solution than the KW solution and the approximate analytical solution of the diffusive wave model, when this model is applied beyond the kinematic wave applicability range, but well within the diffusive wave applicability range. A comparative study of the VPMS and VPMD method solutions for overland flow modelling reveal that the applicability range of

the VPMS method is lower than the VPMD method which is in contrast with the applicability limit specified for these methods in routing floods in channels/rivers. This contrast may be attributed to the difference in the magnitude of flow depths of these two phenomena which play an important role in the respective flow dynamics. However, the applicability range of the proposed method falls in the transition range between the DW and KW models, including the full range of the latter model. Besides, the close reproductions of the runoff hydrographs recorded at the downstream end of the overland flow plane and those simulated by the SVE solutions at the end of the overland flow plane demonstrate that the VPMS method can be confidently used for catchment modelling studies, especially when the stringent requirement of downstream boundary condition restricts the use of the SVE and its variants solutions.

Further, it was found that the proposed VPMS method is unconditionally stable. The role of the Courant condition in preserving the solution accuracy was investigated using the numerical experiments and found that it was not necessary to strictly follow this condition ($C_{un} \approx 1$) while using the VPMS method. Unlike, the conventional numerical methods, this method does not show stability or convergence problems in the solution. It is inferred from this study that it is more appropriate to select computational grid sizes based on the requirement of physical process rather than merely on the numerical computational requirements. The simulation results reveal that the VPMS method is advantageous over the existing models because of its unconditional numerical stability, flexibility in using larger computational grid sizes, and inexpensive computations. Therefore, the proposed VPMS method can be confidently used for meso- and macro-scale catchment modelling studies.

5 DEVELOPMENT OF APPLICABILITY CRITERIA FOR THE VPMD AND VPMS OVERLAND FLOW ROUTING METHODS

5.1 GENERAL

Simplified methods developed based on the kinematic wave (KW) and diffusion wave (DW) equations derived from the SVE are extensively used for overland flow modelling studies. These approximations to the SVE have been found to minimize numerical complexity, CPU-run time, and large input data requirement. Based on theoretical and practical considerations, *Singh* [2003] has justified the use of the KW model for overland flow modelling. Although, most of the practical situations of overland flow dynamics can be handled using the KW approximation, modelling of high subcritical flows over mild sloped planes warrants the use of DW models. This requirement could now be met to a larger extent using the variable parameter Muskingum discharge-hydrograph (VPMD) [*Chapter, 3*] and variable parameter Muskingum stage-hydrograph (VPMS) [*Chapter, 4*] overland flow routing methods developed from the approximate convection-diffusion (ACD) equations which have been directly derived from the SVE [*Perumal and Ranga Raju, 1999*]. These physically based VPMD and VPMS overland flow routing methods are easy to implement, accurate, free from numerical stability problem and CPU-run time efficient, which make them amenable for large scale basin modelling, although these methods have the inability to handle the downstream disturbances in the routing process. However, the applicability limits of these two methods have not yet been analyzed. The present study focuses on the development of the applicability criteria for overland flow modelling using the ACD equations both in discharge and flow depth formulations. In order to be consistent with the classification of flood waves in channels based on the magnitudes of different terms of the momentum equation of the SVE with reference to the bed slope s_0, as envisaged by *Henderson* [1966], it is opted herein also to develop the applicability criteria of the VPMD and VPMS overland flow routing methods based on the magnitude of the scaled flow depth gradient, $(1/s_0)(\partial y/\partial x)$. These applicability criteria are developed using the momentum equation of the ACD equation of the VPMD and VPMS methods along with a systematic comparison of each method's solutions with the corresponding solutions of the

SVE by conducting a number of hypothetical numerical experiments covering almost all the overland flow generation conditions of practical interest based on the considerations of 99% accuracy level of the Nash-Sutcliffe efficiency (η_q = 95 % in case of partial hydrographs generation), and 95% accuracy level of volume and peak runoff reproductions.

5.2 APPLICABILITY CRITERIA FORMULATION USING THE ACD EQUATIONS

The VPMD [*Chapter,* 3] and VPMS [*Chapter,* 4] overland flow routing methods have been developed based on the assumptions of approximate linear variation of runoff discharge and flow depth, respectively. These methods have been developed using the ACD equations in discharge and flow depth formulations [Equations (3.18) and (4.14)], respectively, expressed as

$$\frac{\partial q}{\partial t} + c\frac{\partial q}{\partial x} = cq_L \tag{5.1}$$

and

$$\frac{\partial y}{\partial t} + c\frac{\partial y}{\partial x} = q_L \tag{5.2}$$

Note that while developing the applicability criteria for the ACD equations, it is assumed that the overland flow generation due to a given intensity of rainfall takes place over an impervious surface as assumed in the previous studies by numerous authors [*Morris and Woolhiser*, 1980; *Daulaz Vieira*, 1983; *Hager and Hager*, 1985; *Pearson*, 1989].

Using the assumption of linearly varying flow depth, as used in the derivation of the ACD governing equations, leads to the simplified momentum equation governing the overland flow process as

$$\frac{\partial q}{\partial x} = c\frac{\partial y}{\partial x} \tag{5.3}$$

where q = flow per unit width of the overland flow plane strip; and c, the flood wave celerity expressed as

$$c = (1 + m)v \tag{5.4}$$

where v is the velocity and m = 2/3 when Manning's friction law is used, and m =1/2 when Chezy's friction law is used.

Using equation (5.4) in equation (5.3) results in

$$\frac{\partial q}{\partial x} = (1 + m)v\frac{\partial y}{\partial x} = \frac{(1+m)q}{y}\frac{\partial y}{\partial x} \tag{5.5}$$

When equilibrium condition is reached at the end of the unit width strip of length L, $\dfrac{\partial q}{\partial x} = r_e$ and $q_e = r_e L$. Then equation (5.5) can be modified as

$$r_e = \frac{(1+m)r_e L}{y_e} \left.\frac{\partial y}{\partial x}\right|_e \tag{5.6}$$

where y_e = depth of flow at the end of the plane at equilibrium and $(\partial y/\partial x)_e$ is the water surface gradient at equilibrium expressed as

$$\left.\frac{\partial y}{\partial x}\right|_e = \frac{y_e}{(1+m)L} \tag{5.7}$$

Using the assumption of linearly varying flow depth, the friction slope, s_f can be approximated by equation (3.11) as

$$s_f = s_0 \left[1 - \frac{1}{s_0}\frac{\partial y}{\partial x}\left(1 - m^2 F_{rp}^2\right)\right] \tag{5.8}$$

The equilibrium discharge q_e can be expressed as

$$q_e = q^* \left[1 - \frac{1}{s_0}\left.\frac{\partial y}{\partial x}\right|_e \left(1 - m^2 \left(F_{rp}^2\right)_e\right)\right]^{1/2} \tag{5.9}$$

where q^* is the normal discharge corresponding to the flow depth y_e, expressed as

$$q^* = C_f y_e^{(1+m)} s_0^{1/2} \tag{5.10}$$

where C_f = Manning's or Chezy's friction coefficient.

Substituting equation (5.10) in equation (5.9) and equation (5.7) in equation (5.9) yields

$$q_e = C_f y_e^{(m+1)} s_0^{1/2} \left[1 - \frac{y_e}{s_0(1+m)L}\left(1 - m^2 \left(F_{rp}^2\right)_e\right)\right]^{1/2} \tag{5.11}$$

Since $q_e = r_e L$, equation (5.11) can be modified as

$$r_e^2 L^2 = C_f^2 y_e^{2(m+1)} s_0 \left[1 - \frac{y_e}{s_0(1+m)L}\left(1 - m^2 \left(F_{rp}^2\right)_e\right)\right] \tag{5.12}$$

Further, the Froude number $\left(F_{rp}\right)_e$ at equilibrium can be expressed as

$$\left(F_{rp}^2\right)_e = \frac{q_e^2}{gy_e^3} = \frac{r_e^2 L^2}{gy_e^3} \tag{5.13}$$

Using equation (5.13), equation (5.12) can be modified as

$$r_e^2 L^2 = C_f^2 y_e^{2(m+1)} s_0 \left[1 - \frac{y_e}{s_0(1+m)L}\left(1 - \frac{m^2 r_e^2 L^2}{gy_e^3}\right)\right] \tag{5.14}$$

221

Using the Manning's friction law, equation (5.14) can be rewritten as

$$r_e^2 L^2 = \frac{1}{n^2} y_e^{10/3} s_0 \left[1 - \frac{3y_e}{5s_0 L} \left(1 - \frac{4}{9} \frac{r_e^2 L^2}{g y_e^3} \right) \right] \tag{5.15}$$

It may be noted that equations (5.3), (5.11) and (5.15) are alternate forms of the ACD momentum equations. Corresponding to a given value of r_e, s_0, L, and n, the equilibrium depth y_e is evaluated from equation (5.15) using the Newton-Raphson method. Then the scaled flow depth gradient is estimated from equation (5.7) as

$$\frac{1}{s_0} \frac{\partial y}{\partial x}\bigg|_e = \frac{y_e}{(1+m)s_0 L} \tag{5.16}$$

Equation (5.16) can be used as the basis for formulating the applicability criterion for the ACD equations based VPMD and VPMS overland flow routing methods. Further, the kinematic wave number k can be estimated as advocated by *Woolhiser and Liggett* [1967] for judging the goodness of the KW approximation in overland flow modelling, expressed as

$$k = \frac{s_0 L}{y_e F_{rp}^2} \tag{2.33}$$

where L = length of the overland plane (m); y_e = depth of flow at the end of the plane at equilibrium which can be estimated using equation (5.15) ; and F_{rp} = Froude number at the end of the plane at equilibrium. Similarly, the parameter $(kF_{rp}^2)_e$ can be estimated using equations (2.33) and (5.15).

The criteria k and $k(F_{rp}^2)_e$ at the equilibrium used in equation (2.33) can be obtained using the KW theory as [*Morris and Woolhiser*, 1980; *Stephenson and Meadows*, 1986; *Wong*, 1992, 2005]:

$$k = 1.725 \times 10^6 \frac{n^{1.2} s_0^{0.4} L^{0.2}}{r_e^{0.8}} \tag{2.34a}$$

$$k(F_{rp}^2)_e = 8585.81 \times \frac{s_0^{1.3} L^{0.4}}{n^{0.6} r_e^{0.6}} \tag{2.34b}$$

where r_e = rainfall intensity at equilibrium (mm/h); L = overland plane length in metre; and n= Manning's roughness coefficient.

While estimating these applicability criteria $(1/s_0)(\partial y/\partial x)$, k, F_{rp} and kF_{rp}^2 for the VPMD and VPMS overland flow routing methods, the computed maximum flow depth (i.e.,

222

the equilibrium flow depth of the complete runoff hydrograph) is used instead of the theoretically obtained flow depth estimated using equation (5.15), which enables the estimation of these applicability criteria for the complete and partial runoff hydrographs. Note the subscript 'e' is used in the subsequent sections to present the estimation of these criteria at equilibrium flow conditions for the complete runoff hydrographs; otherwise, these criteria are given for the partial equilibrium hydrographs.

The developed applicability criterion given by equation (5.16) for the VPMD and VPMS overland flow routing methods shows that it is a function of the rainfall and overland flow plane characteristics, i.e.,

$$(1/s_0)(\partial y / \partial x)\big|_e = f\{r_e, n, L, s_0\} \tag{5.17}$$

where $f\{\bullet\}$ denotes a function.

It was shown in Chapters 3 and 4 that the VPMD and VPMS overland flow routing methods are capable of modelling the overland flow in the transition range of the applicability of the DW and KW approximations, including the full range of the latter. Hence, it is expected that within the applicability range of the VPMD and VPMS overland flow routing methods given by the developed applicability criterion of equation (5.16), it would be possible to closely model the overland flow generation governed by the kinematic wave equation in all the situations and that of the diffusive wave in an approximate manner, subject to the satisfaction of the assumptions built-in in these methods.

5.3 PHYSICAL SIGNIFICANCE OF THE PARAMETER $(kF_{rp}^2)_e$

For deciding the applicability of the KW and DW approximations for overland flow modelling, *Morris and Woolhiser* [1980] and *Daluz Viera*, [1983] have proposed the applicability criteria based on the kinematic wave number, k and $(kF_{rp}^2)_e$. *Daluz Viera*, [1983] surmised that when $\mu << 2$ ($F_{rp} = 0.1$, $k = 50$), the solution of the DW approximation approaches the KW approximation, where $\mu = 1/(kF_{rp}^2)_e$. Based on the limit of $\mu << 2$, one may consider $(kF_{rp}^2)_e = 0.5$ as the lower limit for the DW solution. Note that the applicability criterion based on $(kF_{rp}^2)_e$ has been obtained using the KW approach [*Morris and Woolhiser*, 1980]. However, the physical interpretation of the parameter μ has not yet been established in literature. The physical significance of μ can be derived using

223

equations (5.16) in (2.33) as

$$\left(\frac{1}{s_0}\right)\left(\frac{\partial y}{\partial x}\right)_e = \frac{1}{(m+1)}\frac{1}{\left(kF_{rp}^2\right)_e} \tag{5.18}$$

Rearranging equation (5.18) one obtains

$$\mu = \frac{1}{\left(kF_{rp}^2\right)_e} = (m+1)\left(\frac{1}{s_0}\right)\left(\frac{\partial y}{\partial x}\right)_e \tag{5.19}$$

As per this equation when $\mu = 2$, we get $(1/s_0)(\partial y/\partial x) = 1.2$. Equation (5.19) shows that the value of μ is also a function of the exponent m of the friction law used.

5.4 NUMERICAL APPLICATION

The proposed applicability criterion $(1/s_0)(\partial y/\partial x)_e$ and the existing applicability criteria k and $(kF_{rp}^2)_e$ are evaluated by i) applying the VPMD and VPMS overland flow routing methods for generation of overland flow runoff hydrographs at the end of the unit width strip of overland flow planes for different combinations of parameters described in equation (5.17) (for both the complete and partial hydrographs cases); ii) using the alternate ACD momentum equation (5.15) to estimate y_e and subsequently using it in equations (5.16), (5.13) and (2.33) to estimate the required applicability criteria; and iii) analytical expressions of the criteria based on the KW wave approach through equations (2.34a) and (2.34b). The different input parameters, viz., rainfall rate and topographic characteristics used in the test runs are illustrated in Table 5.1. The range of different input parameters are selected based on the existing real world rainfall-runoff conditions: 1) $r \leq 0.025$ (very light rain), 2) $0.025 < r \leq 0.1$ (light rain), 3) $0.1 < r \leq 0.4$ (moderate rain), 4) $0.4 < r \leq 1.6$ (heavy rain), 5) $1.6 < r \leq 5.0$ (very heavy rain), and 6) $r > 5.0$ (extreme rain) [http://en.wikipedia.org/wiki/Rain# cite_note_1], where r is the rainfall intensity in cm/h. The overland flow plane length considered in this study ranges from 6–300 m, though the recommended maximum overland flow plane length is 100 m [Merkel, 2001]. Based on the recommendation of Engman [1986] for overland flow studies, the selected values of the Manning's roughness coefficient vary in the range 0.006–0.45 [e.g., Barros and Colello, 2001]. Similarly, the considered overland flow plane slopes range from very steep to very flat with $s_0 = 0.05–0.00002$.

Table 5.1 Various combinations of parameters used for test runs

Parameters		Values
Rainfall intensity, r (cm/h)	:	0.1, 0.4, 1.6, 6.0, 10.0, 16.0
Bed slope, s_0	:	0.05, 0.01, 0.005, 0.001, 0.0007[*], 0.0005, 0.0003, 0.0001, 0.00005, 0.00002[**]
Plane length, L (m)	:	6.0, 40.0, 100.0, 150.0, 200.0, 300.0
Manning's roughness coefficient, n	:	0.006, 0.010, 0.05, 0.1, 0.18, 0.3, 0.45

[*]Used only for the VPMS method; [**]Used only for the VPMD method

For each of the numerical test runs, the time of equilibrium is computed analytically by the KW approach [*Overton and Meadows*, 1976] as

$$t_e = (1/(r_e)^{0.4})(nL/\sqrt{s_0})^{0.6} \tag{5.20}$$

where t_e = time of equilibrium (s); and r_e = rainfall intensity (m/s).

Equation (5.20) is further used to estimate the duration of rainfall (t_r) in case of complete and partial runoff hydrographs with $t_r > t_e$ and $t_r < t_e$, respectively. Since the value of t_e computed by the KW approach for any numerical test run is always smaller than that required by the solutions of the SVE, VPMD, and VPMS methods, particularly in highly diffusive conditions, the value of t_r is considered herein as approximately five times of t_e. Similarly, to ensure complete draining of the detention storage over the overland flow plane during the recession phase of the complete or partial runoff hydrograph, the total simulation time is taken approximately five times of t_r.

One of the best ways to evaluate the efficacy of these simplified overland flow routing methods is by comparing the simulated runoff hydrographs of the VPMD and VPMS methods for the given input conditions with the corresponding stable runoff hydrographs obtained using the SVE (solved by using the explicit numerical scheme), which are considered as the benchmark solutions. A total of 2268 numerical test runs, formed by different combinations of parameters as given in Table 5.1 were used for studying each of the VPMD and VPMS methods simulations for arriving at the applicability limits of these methods.

There exists the possibility of numerical errors creeping into the benchmark solutions of the SVE to mask the physical characteristics of the actual solutions. To circumvent this

problem, it was ensured in the study that the benchmark solutions obtained using the numerical explicit scheme very well satisfied the Courant's condition [*Chow et al.*, 1988] and the obtained solutions were fully mass conservative. Similarly, to circumvent such numerical problems with the VPMD and VPMS methods solutions, the computational grid sizes were selected based on the sensitivity analysis of these methods described in Chapters 3 and 4, respectively.

Note that the maximum Vedernikov number in each of the test runs was less than 1.0 in the stable flow regime and, thus, ensuring the Froude number to be less than 1.5 for runoff estimated using the Manning's friction law, which marks the beginning of flow wave instability [*Jolly and Yevjevich*, 1971; *Ponce*, 1991; *Perumal*, 1992] leading to the formation of roll waves. This study does not consider overland flow generation with roll wave formation.

5.5. PERFORMANCE EVALUATION MEASURES

For arriving at the applicability criteria of the VPMD and VPMS methods, the same performance measures as considered in Chapter 3 for evaluating the VPMD method have been used. They are 1) closeness of reproduction of the benchmark solutions based on the Nash-Sutcliffe efficiency (η_q) criterion [*Nash and Sutcliffe*, 1970]; 2) coefficient of determination, CD; 3) coefficient of residual mass, CRM; 4) conservation of Mass, $EVOL$; 5) the percentage error in peak runoff reproduction, q_{perr}; and 6) time to peak runoff reproduction, t_{perr}. Equations (3.76) – (3.81) are used to estimate the performance measures 1-6, respectively. A negative error of q_{perr} indicates under-estimation and a positive error of q_{perr} indicates over-estimation of the peak of the benchmark solution. The best performing hydrological model should have η_q, CD, and CRM values close to 100%, 1.0, and 0.0%, respectively.

5.6. RESULTS AND DISCUSSION

5.6.1 Characteristics of the Applicability Criteria in Relation to the ACD Equations

The proposed applicability criterion $(1/s_0)(\partial y / \partial x)_e$ and the existing applicability criteria, k, F_{rp} and $\left(kF_{rp}^2\right)_e$ were evaluated using the alternative form of the ACD momentum equation given by equation (5.15) while simulating the complete overland flow hydrograph using the VPMD and VPMS methods for various combinations of uniform rainfall input and overland flow plane characteristics. Figure 5.1 shows the comparison results between

226

$\left(kF_{rp}^2\right)_e$ and the normalized discharge (q_e / q^*) estimates obtained from the simulation results of the VPMD and VPMS methods, and the corresponding estimates obtained from the application of the Newton-Raphson trial and error approach in solving for y_e of the ACD momentum equation as expressed by equation (5.15). It is inferred from this figure that the estimates of $\left(kF_{rp}^2\right)_e$ and (q_e / q^*) for all the methods closely coincide with each other, except for few cases of the VPMS method when $(kF_{rp}^2)_e < 5$. When $\left(kF_{rp}^2\right)_e \geq 30$, $(q_e / q^*) \to 1$, and the overland flow tends to be kinematic in nature and in such a condition KW solution is theoretically same as the SVE solution. When $\left(kF_{rp}^2\right)_e < 30$, $(q_e / q^*) \to 0$ when $\left(kF_{rp}^2\right)_e \to 0$. Note that the lower limit of $\left(kF_{rp}^2\right)_e$ advocated by *Morris and Woolhiser* [1980] for the overland flow modelling using KW approximation is $\left(kF_{rp}^2\right)_e = 5$. Therefore, between the limits $5 \leq \left(kF_{rp}^2\right)_e \leq 30$, the KW solution is only an approximation to the SVE solution within the practically acceptable error level. Further, it can be seen from Figure 5.1 that when $\left(kF_{rp}^2\right)_e = 5$, $(q_e / q^*) \approx 0.95$; and when $0.5 \leq \left(kF_{rp}^2\right)_e \leq 5$, the rate of decrement of the normalized equilibrium discharge is significant resulting in significant attenuation of the overland flow hydrograph in comparison with the analytical KW solution. Under such circumstances, the DW equation has been found suitable for modelling the overland flow processes with certain acceptable error level in reproducing the solutions of the SVE. The rapid decrement in the estimates of (q_e / q^*) clearly demonstrates the importance of the original inertial terms in the momentum equation of the SVE and, under such circumstances, only the solutions of the SVE can estimate the runoff hydrographs accurately. However, *Daulz Vieira* [1983] has recommended the use of DW equation for modelling the overland flow in the range of $0.5 \leq \left(kF_{rp}^2\right)_e \leq 5$. Consequently, the applicability range of the VPMD and VPMS overland flow routing methods can be fixed somewhere in-between this range with a lower limit higher than 0.5. Figure 5.1 clearly demonstrates that the VPMD and VPMS methods have a wider applicability range than that of the KW model when $q_e / q^* < 0.95$ and falls in the transition zone of the applicability between the DW and KW approximations, including the full range of the latter.

Figure 5.2 shows the variation of the normalized equilibrium discharge with $(1/s_0)(\partial y / \partial x)_e$, estimated for all the considered test runs using the ACD momentum equation, VPMD, and VPMS methods. It can be surmised from Figure 5.2 that when
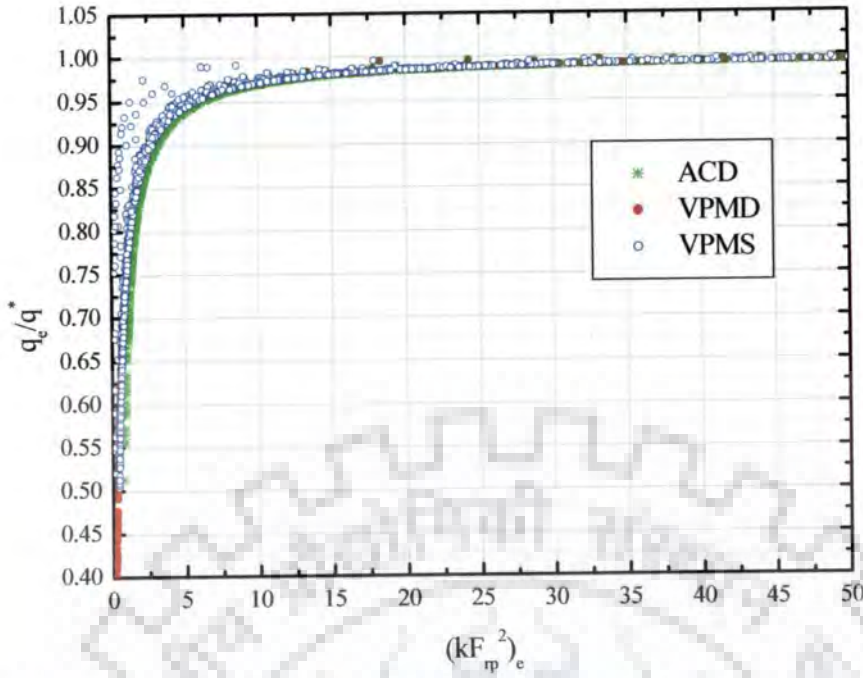
Figure 5.1 Relationship between $(kF_{rp}^2)_e$ and normalized discharge (q_e/q^*) for the ACD, VPMD, and VPMS methods.

$(1/s_0)(\partial y/\partial x)_e \leq 0.3$, the estimates of (q_e/q^*) by all the methods nearly fall on a single line and, beyond this limit, the (q_e/q^*) estimates of the VPMD and VPMS methods gradually deviate away from the corresponding estimates obtained using the ACD momentum equation. Based on equation (5.19), it may be inferred that this limit of $(1/s_0)(\partial y/\partial x)_e \leq 0.3$ corresponds to the estimate of $(kF_{rp}^2)_e = 2$ and the VPMD and VPMS solutions are capable of simulating overland flow solutions very close to the DW and KW solutions when $(kF_{rp}^2)_e \geq 2$. However, further analysis would be required to assess the acceptable approximation of the solutions of these methods in reproducing the SVE solutions and to ascertain the corresponding applicability limits of $(1/s_0)(\partial y/\partial x)_e$ of these methods. Further, when $(1/s_0)(\partial y/\partial x)_e \leq 0.5$, the estimates of (q_e/q^*) of the VPMD and VPMS methods closely match with each other, beyond which they also deviate. It can also be inferred from Figure 5.2 that for a given estimate of (q_e/q^*) of the ACD momentum equation, the estimates of $(1/s_0)(\partial y/\partial x)_e$ of the VPMD is larger than that of the VPMS method, implying that the estimated equilibrium overland flow depth of the VPMD method is larger than that of the corresponding estimate using the VPMS method. It may be recognised at this juncture that the estimate of y_e obtained from the ACD momentum
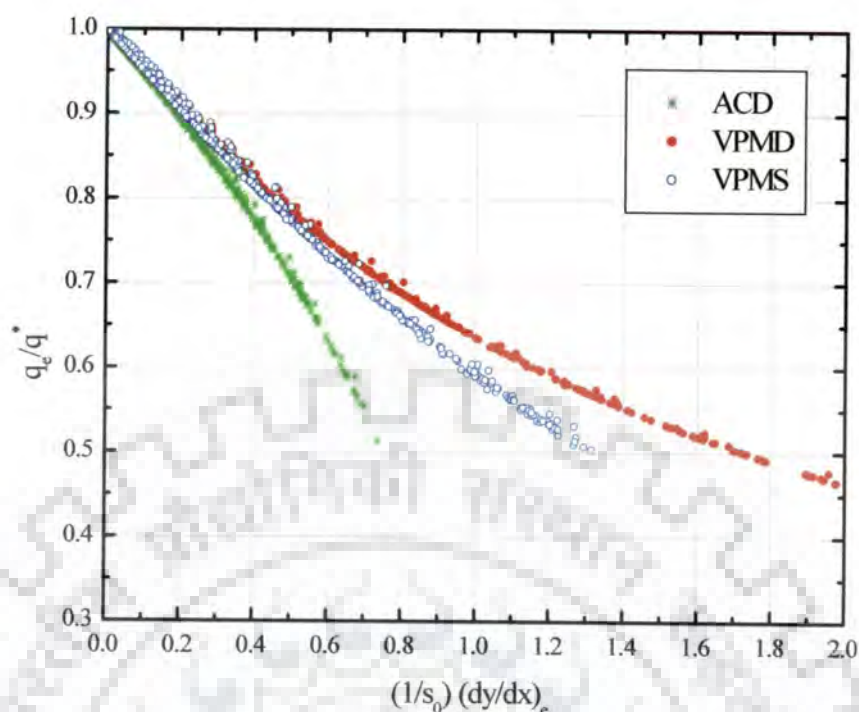
Figure 5.2 Relationship between the estimated normalized discharge (q_e/q^*) and $(1/S_0)(\partial y/\partial x)_e$ for the ACD, VPMD, and VPMS methods.

equation itself is an approximation to the corresponding estimate of the SVE. But this approximation may be acceptable up to a certain value of $(1/s_0)(\partial y/\partial x)_e$ of the SVE, i.e., $(1/s_0)(\partial y/\partial x)_e =0.43$. Therefore, the estimates of $(1/s_0)(\partial y/\partial x)_e$ obtained from the VPMD and VPMS solutions are more approximate, due to recursive nature of arriving at these solutions, than the corresponding estimate arriving at by the application of the ACD momentum equation at equilibrium condition.

Similarly, Figure 5.3 illustrates the relationship between $(1/s_0)(\partial y/\partial x)_e$ and $\left(kF_{rp}^2\right)_e$ obtained using the ACD momentum equation, and the VPMD and VPMS methods. It can be clearly seen from Figure 5.3 that $(1/s_0)(\partial y/\partial x)_e$ and $\left(kF_{rp}^2\right)_e$ are inversely proportional to each other based on equation (5.19). When $\left(kF_{rp}^2\right)_e \geq 30$, $(1/s_0)(\partial y/\partial x)_e \rightarrow 0$, signifying the absence of diffusion in the overland flow wave (i.e., kinematic). When $5\leq \left(kF_{rp}^2\right)_e \leq 30$, then $0.02\leq (1/s_0)(\partial y/\partial x)_e \leq 0.12$, implying that there is small, but perceptible diffusion present in the overland flow generation which can be modelled approximately by the KW. Further, when $\left(kF_{rp}^2\right)_e < 5$, $(1/s_0)(\partial y/\partial x)_e$ increases rapidly with the decrease in $\left(kF_{rp}^2\right)_e$ resulting in
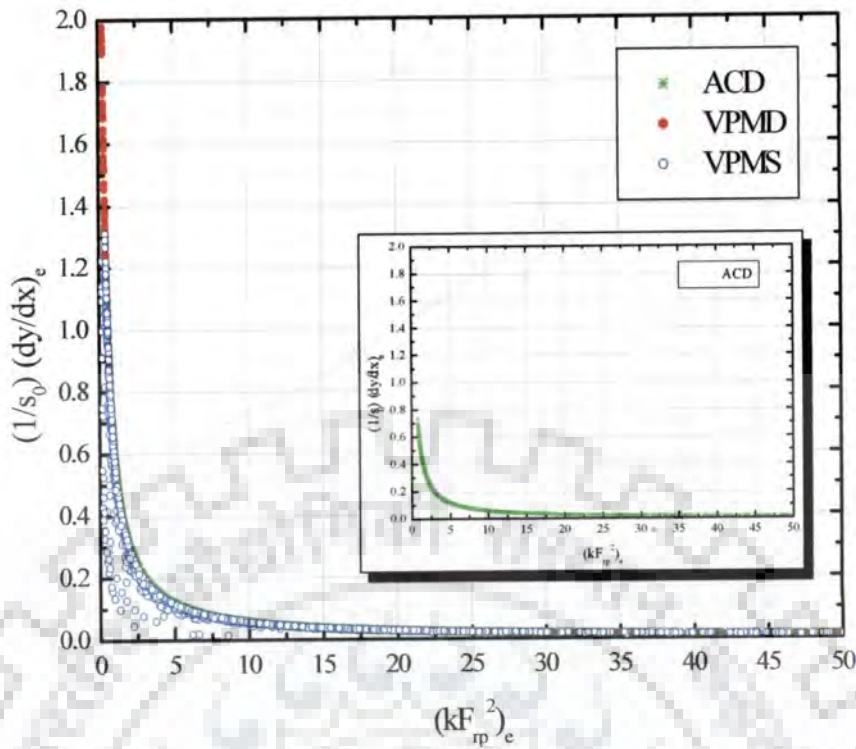
Figure 5.3 Relationship between $(kF_{rp}^2)_e$ and $(1/s_0)(\partial y / \partial x)_e$ for the ACD, VPMD, and VPMS methods.

the presence of significant diffusion in the overland flow process. As the magnitude of $(kF_{rp}^2)_e$ becomes very small, the curtailed or modified terms in the momentum equation of the SVE become important and, hence, the use of the SVE approximations, viz., the KW, the DW and the ACD equations are not appropriate to handle the overland flow modelling except the full SVE. It can be inferred from the graph shown in the inset of Figure 5.3 that the ACD momentum equation enables the estimation of equilibrium discharge up to $(1/s_0)(\partial y / \partial x)_e \leq 0.74$, and beyond which the solution of equation (5.15) for solving y_e using the Newton-Raphson method does not converge.

The VPMS method based estimates of $(1/s_0)(\partial y / \partial x)_e$ deviate away from the general trend of the relationship shown in Figure 5.3 for 57 test run cases (2.51% of the total 2268 runs) which are characterized by the Nash-Sutcliffe efficiency $\eta_q > 99$ % and for 13 test runs (0.57% of the total runs) with $\eta_q = 95 - 99$ %. The summary of the 57 test runs characterized by different input parameters such as rainfall intensity, plane length, slope and Manning's roughness coefficients used is presented in Table 5.2. The estimates of the applicability criteria for the test runs with small rainfall intensities (viz., 0.1 and 0.4 cm/h) as

230

Table 5.2. The summary of 57 test run cases simulated using the VPMS method with $\eta_q > 99\%$ which deviate away from the general trend of the relationship as shown in Figure 5.3.

Number of Test Runs (out of 2268)	Rainfall Intensity, r (cm/h)	Variation Range		
		Plane Length, L (m)	Slope, s_0	Manning's n
24 (1.06%)	0.1	6 - 40	0.001- 0.0001	0.01 – 0.45
21 (0.93%)	0.4	6 -150	0.01-0.0003	0.05 – 0.45
5 (0.22%)	1.6	6 - 100	0.001- 0.0007	0. 1 – 0.3
4 (0.18%)	6	6	0.005-0.0005	0. 006 – 0.45
1 (0.04%)	10	6	0.005	0. 45
2 (0.08%)	16	6 - 300	0.005 - 0.0007	0. 006 - 0.3

given in Table 5.2 using the VPMS method are slightly different from the corresponding estimates arrived at using the ACD momentum equation and the VPMD method in the range $0.5 \leq \left(kF_{rp}^2\right)_e \leq 5$ (see Figure 5.3), although this difference does not affect the accuracy of the VPMS method estimated runoff hydrographs when compared with the corresponding solutions of the SVE.

Although the ACD momentum equation can estimate the equilibrium discharge when $(1/s_0)(\partial y/\partial x)_e \leq 0.74$, it can be inferred from Figure 5.4a that when the applicability criterion $(1/s_0)(\partial y/\partial x)_e \leq 0.43$, the percentage error in the equilibrium overland flow depth estimation using equation (5.15) is less than 5% of the corresponding estimates of the SVE solution, as envisaged by the linear fit equation $y_{e,ACD} = 1.0443 \, y_{e,SVE} - 1.85386 \times 10^{-4}$ with coefficient of correlation $R^2 = 0.998$. In a similar way, it can be inferred from Figure 5.4b that by keeping the same applicability limit of $(1/s_0)(\partial y/\partial x)_e \leq 0.43$, the percentage error in the estimated equilibrium runoff discharge values estimated using the ACD momentum equation given by equation (5.15) is less than 5% of the corresponding equilibrium runoff discharge of the SVE solution, as seen from the linear fit equation $q_{e,ACD} = 0.9538 \, q_{e,Actual} + 5.1597 \times 10^{-6}$ with coefficient of correlation $R^2 = 0.997$. The results of Figures (5.4a) and (5.4b) demonstrate that at equilibrium condition, the ACD momentum equation tends to slightly overestimate the equilibrium flow
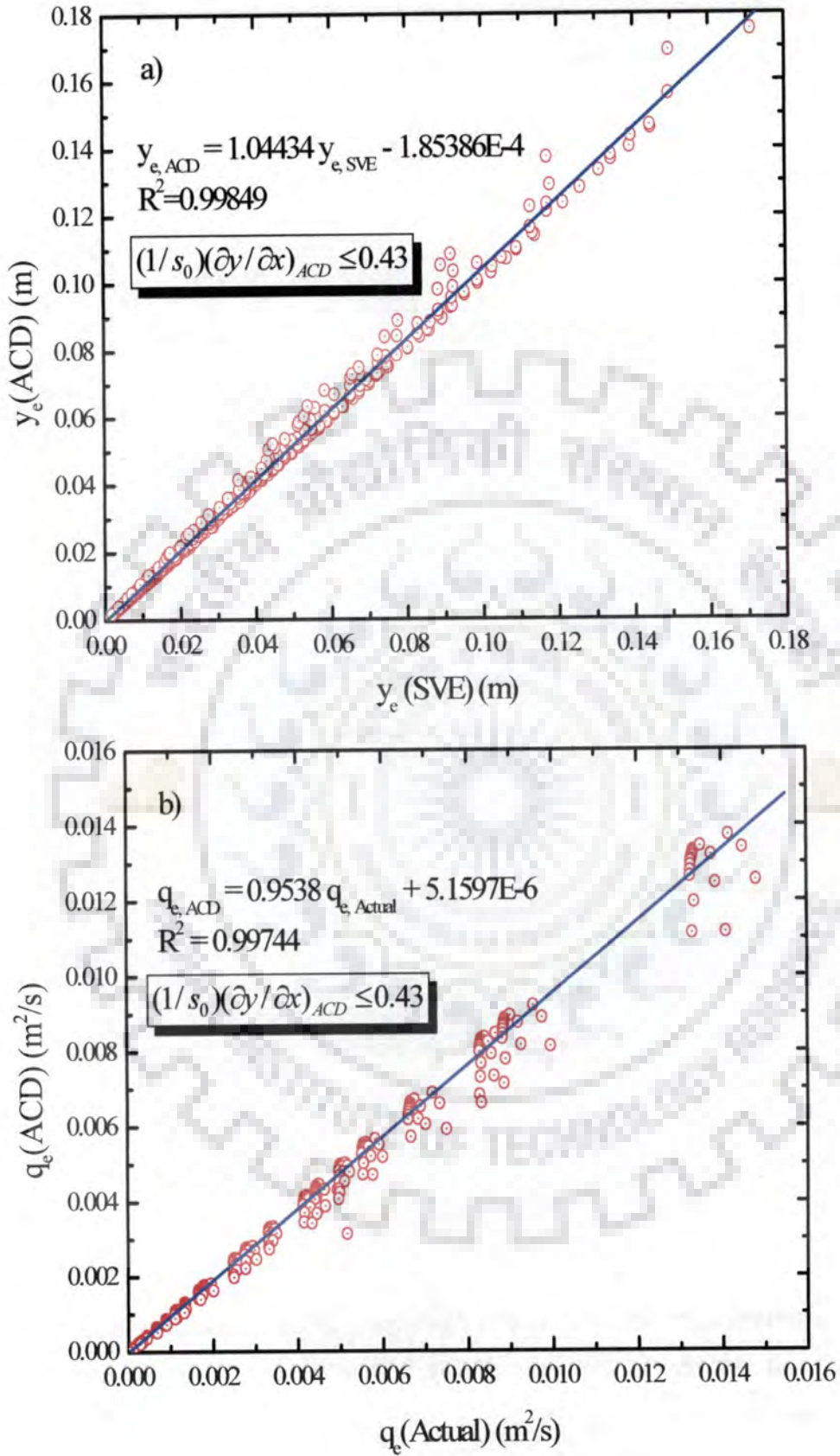
Figure 5.4 Theoretical applicability limit for application of the ACD equation.

depth and slightly underestimate the corresponding runoff discharge given by the SVE solution. The present study makes use of the estimated equilibrium flow depth of the complete hydrograph or the maximum flow depth of the partial hydrograph to estimate the applicability criterion $(1/s_0)(\partial y/\partial x)$ using equation (5.16) and subsequently, the estimate of kF_{rp}^2 using equation (5.19). But based on the analysis of the results shown in Figures 5.2 and 5.4, one can infer that there would be a possibility of overestimation of $(1/s_0)(\partial y/\partial x)_e$ or underestimation of $(kF_{rp}^2)_e$ by the VPMD and VPMS methods while routing overland flows when $(1/s_0)(\partial y/\partial x)_e > 0.43$ or $(kF_{rp}^2)_e < 1.4$. Further, from theoretical consideration that the applicability limits of the VPMD and VPMS methods should be $(1/s_0)(\partial y/\partial x)_e \ll 1$, as these methods have used the binomial series expansion of $\sqrt{s_f}$ [Perumal, 1994a; Perumal 1998a] in their development. It may be further noted that the error involved in the estimation of the equilibrium overland flow depth using the VPMD and VPMS overland flow routing methods when used for routing flows characterized by $(1/s_0)(\partial y/\partial x)_e > 0.43$ may lead to erroneous estimation of the applicability criteria $(1/s_0)(\partial y/\partial x)$ on a higher side and kF_{rp}^2 on a lower side.

The relationships between the estimates of $(1/s_0)(\partial y/\partial x)_e$ by the ACD momentum equation and those by the VPMD and VPMS methods are depicted in Figure 5.5. It is inferred from Figure 5.5 that for test runs with $(1/s_0)(\partial y/\partial x)_e < 0.35$, the estimates of the proposed applicability criteria by the VPMD and VPMS methods are the same as that of the ACD equations; however, beyond this limit, these estimates slightly deviate away from the corresponding ACD momentum equation estimates. To be consistent with the inference arrived at based on Figure 5.4, One may extend the limit of theoretical agreement of the estimates of $(1/s_0)(\partial y/\partial x)_e$ on Figure 5.5 approximately as $(1/s_0)(\partial y/\partial x)_e = 0.43$ when using the ACD equations both in discharge and flow depth formulations for modelling the overland flow process. Fixing the magnitude of $(1/s_0)(\partial y/\partial x)_e = 0.43$ as the theoretical limit is also consistent with the finding of *Perumal and Sahoo* [2007] who identified that for this limit of 0.43, the truncation error that arise due to binomial series expansion of $\sqrt{s_f}$ involved in the development of the VPMD and VPMS channel routing methods is < 5%. Further, for all the test runs with $(1/s_0)(\partial y/\partial x)_e \leq 0.5$, the estimates by the VPMD and

233
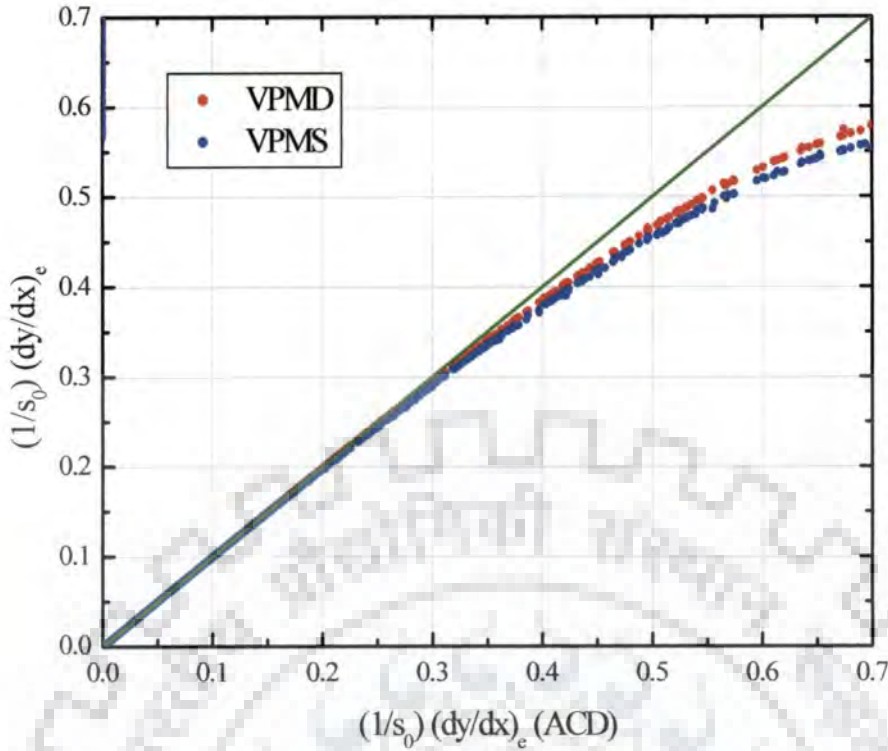
Figure 5.5 Relationship between the applicability criteria $(1/s_0)(\partial y/\partial x)_e$ estimated by the ACD equation and that by the corresponding VPMD and VPMS methods.

VPMS methods closely coincide with each other as already seen from Figure 5.2. While Figure 5.5 confirms the inference that the solutions of the VPMD and VPMS methods are able to match with the theoretical limit of applicability estimated by the ACD momentum equation on the consideration of equilibrium flow depth estimation, it does not confirm that the VPMD and VPMS methods are also able to reproduce various features of the benchmark solutions as measured by η_q (in %), CRM, CD and q_{perr} (%). Therefore, to decide on the practical limit of applicability criteria of the VPMD and VPMS overland flow routing methods beyond the use of a single criterion based on the estimation of equilibrium condition when $(1/s_0)(\partial y/\partial x)_e \leq 0.43$, evaluation based on such multiple criteria is required. Figure 5.6 brings out such an evaluation, however, with reference to the currently used criterion $(kF_{rp}^2)_e$. It can be inferred from Figure 5.6 that while the VPMD method is able to reproduce the overland flow hydrographs with desirable estimates of these performance evaluation measures nearly up to $(kF_{rp}^2)_e \approx 1$, these desirable estimates are not to be seen with the solutions of the VPMS method.

234
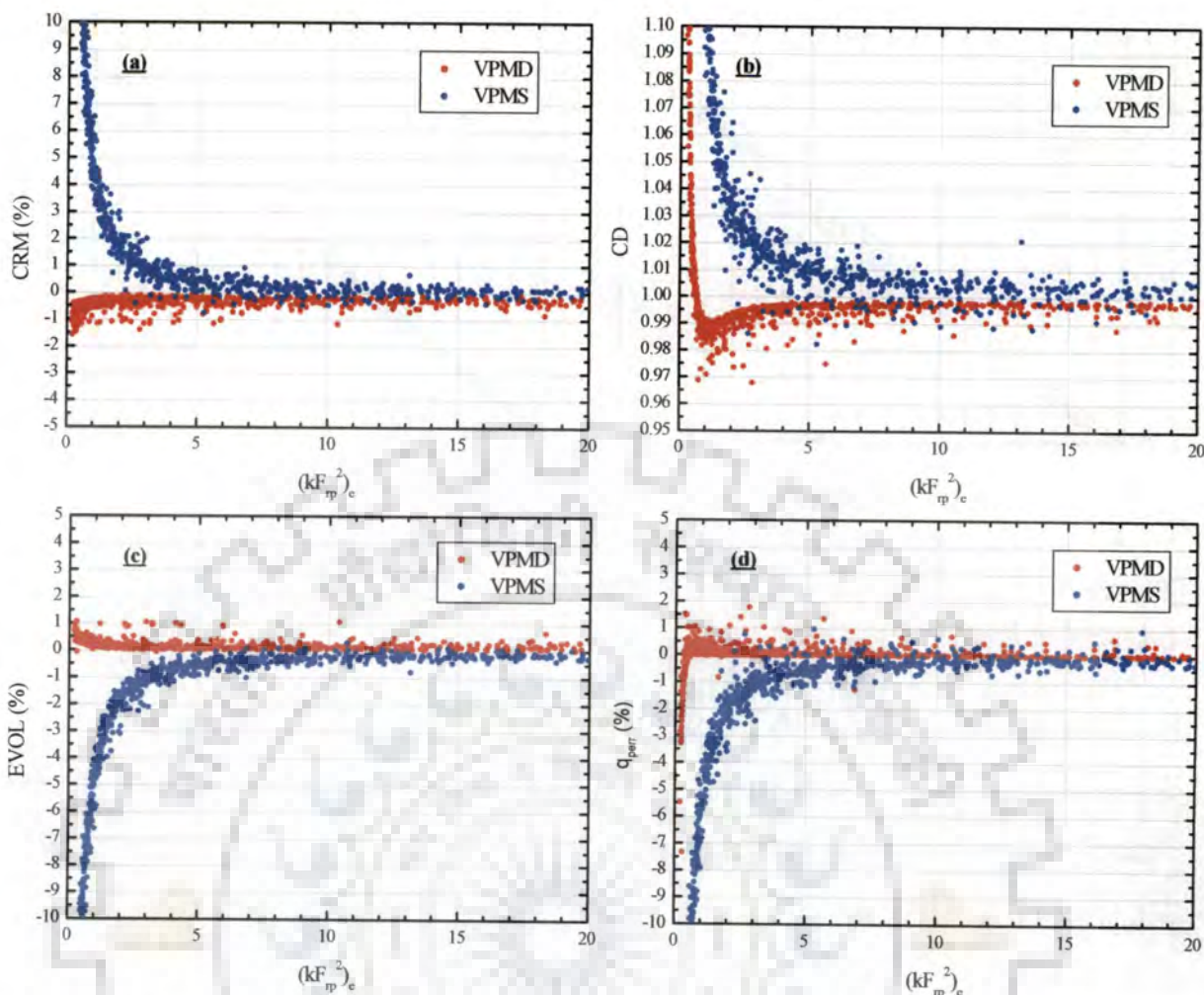
Figure 5.6 Various performance evaluation measures by the VPMD and VPMS methods with the existing applicability criteria $\left(kF_{rp}^2\right)_e$.

5.6.2 Characteristics of the Applicability Criteria in Relation to the Kinematic Wave Approach

Since the approximate momentum equation given by equation (5.3) is used in the derivation of the ACD equations, the VPMD and VPMS methods derived from these ACD equations account for the pressure gradient and inertial terms in an approximate manner and, thereby, making these methods to convect and attenuate the overland flow similar to the DW equation. Accounting of diffusion in the VPMD and VPMS methods, results in the computation of slightly higher flow depths by these methods than that estimated by the KW approach, particularly in the DW applicability range. This makes the value of $\left(kF_{rp}^2\right)_e$ in the DW range estimated by the VPMD and VPMS methods to be smaller than that estimated by the KW approach. This inference can be reconfirmed from Figure 5.7 that when $\left(kF_{rp}^2\right)_e \leq 5$,
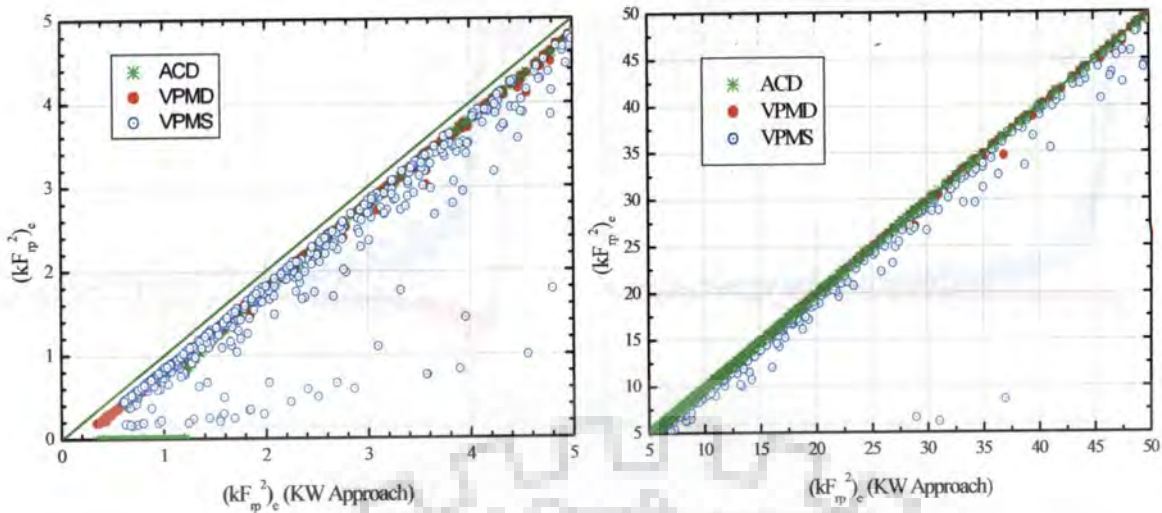
Figure 5.7 Error involved with $(kF_{rp}^2)_e$ estimated by the KW approach of *Woolhiser and Liggett* [1967] in the DW range.

the estimates of the criterion $(kF_{rp}^2)_e$ with the KW approach are always higher than those estimated using the ACD momentum equation, VPMD, and VPMS methods; and when $5 \leq (kF_{rp}^2)_e \leq 30$, although this difference is not much significant, but still there is small amount of diffusion exists as exemplified by a thick line in the lower range of Figure 5.7. Further, when $(kF_{rp}^2)_e > 30$, the difference between the ACD equations based solutions and the KW approach vanishes almost completely as shown by a thin line. This analysis conclusively proves that the KW approach is a specific case of the ACD approach, and the VPMD and VPMS methods are capable of simulating the KW solutions in totality.

5.6.3 Evaluation of the VPMD and VPMS Methods to Establish the Applicability Criteria Using the Complete Runoff Hydrographs

Figures 5.8a and 5.8b show the variation of $\eta_q (\%)$ with $(1/s_0)(\partial y/\partial x)_e$ and $(kF_{rp}^2)_e$ values estimated at the end of the overland flow plane for all the considered test run cases of the VPMD and VPMS methods in reproducing the corresponding benchmark solutions of the SVE, wherein $\eta_q = 99\%$ is used as the lower limit of the acceptable accuracy. It can be seen from Figure 5.8a that the performance of the VPMD and VPMS methods diminishes systematically with the increase of the $(1/s_0)(\partial y/\partial x)_e$ estimates, with the VPMD overland flow routing method displaying a wider applicability range than the VPMS method, which is just the reverse for the case of routing in open channel flow as brought out by *Perumal and Sahoo* [2007]. Based on this acceptable accuracy of reproduction, the various ranges of

236
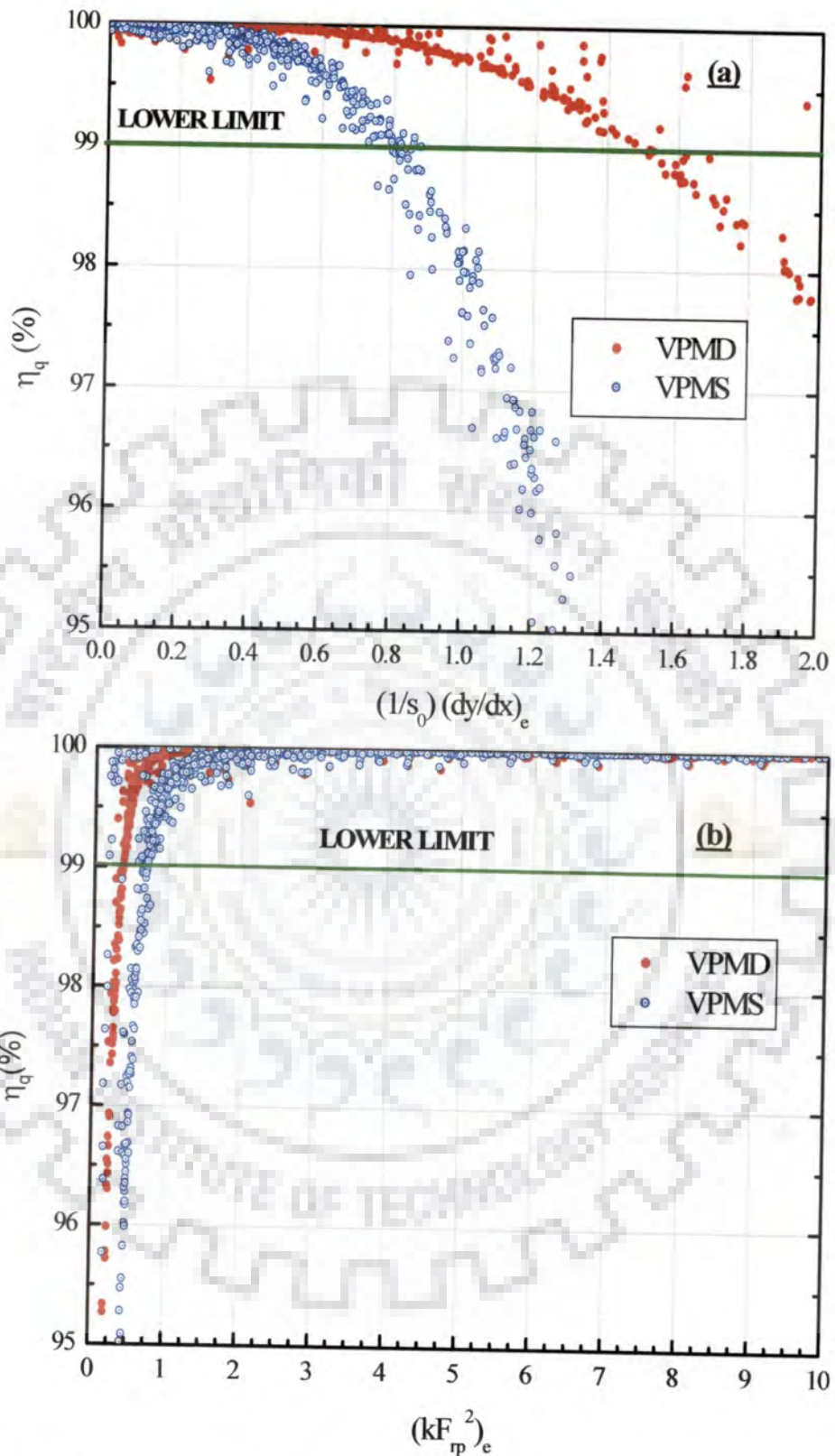
Figure 5.8 Variation of Nash-Sutcliffe efficiency, η_q (%) with (a) the proposed applicability criteria, $(1/s_0)(\partial y/\partial x)_e$ and (b) the existing applicability criteria, $(kF_{rp}^2)_e$ for the VPMD and VPMS methods.

applicability criteria estimated using the VPMD method are: $k = 6.69\text{--}624016.4$, $\left(kF_{rp}^2\right)_e = 0.31\text{--}10325.26$, $F_{rp} = 0.0023\text{--}1.49$, $q_e/q^* = 0.48\text{--}1.0$, and $(1/s_0)(\partial y/\partial x)_e = 0.000058\text{--}1.55$. The applicability criterion of the VPMD method for the complete hydrograph reproduction based on $\eta_q \geq 99\%$ can be fixed at $(1/s_0)(\partial y/\partial x)_e \leq 1.55$. However, when partial runoff hydrographs are generated using the VPMD method, then the above applicability criteria $(1/s_0)(\partial y/\partial x)_e \leq 1.55$ is not applicable. Further, the *ASCE Task Committee* [1993] recommended that the use of single performance measure such as η_q (in %) is not appropriate in view of multiple objectiveness involved in the rainfall-runoff modelling. Also the performance of the VPMD method diminishes rapidly after $(1/s_0)(\partial y/\partial x)_e > 1.2$, and, therefore, the selection of an applicability criterion for any rainfall-runoff method is desirable based on the reproduction of all the pertinent characteristics of the runoff hydrographs including that of the partial runoff hydrograph generation when $t_r < t_e$. It may be noted that it is not theoretically possible to specify the applicability criterion beyond $(1/s_0)(\partial y/\partial x)_e > 1.0$, due to the use of binomial series expansion of $\sqrt{s_f}$ in the development of VPMD and VPMS methods. The estimated values of $(1/s_0)(\partial y/\partial x)_e > 1$ occur in the VPMD method simulations due to error involved in the estimation of the equilibrium overland flow depth arrived at by the VPMD method. Similarly, for all the test runs with $\eta_q \geq 99\%$, the various applicability criteria estimated by the VPMS method are: $k = 4.28\text{--}624055.10$, $\left(kF_{rp}^2\right)_e = 0.20\text{--}10294.23$, $F_{rp} = 0.0039\text{--}1.49$, $q_e/q^* = 0.64\text{--}1.0$, and $(1/s_0)(\partial y/\partial x)_e = 0.000058\text{--}0.86$. Although the VPMS method is capable of simulating the overland flow runoff hydrographs with $\eta_q \geq 99\%$ for all the cases when $(1/s_0)(\partial y/\partial x)_e \leq 0.86$, the performance of this method is poor and diminishes rapidly when $(1/s_0)(\partial y/\partial x)_e > 0.5$. Hence, the applicability limit of the VPMS method for routing the complete runoff hydrographs can be fixed at $(1/s_0)(\partial y/\partial x)_e \leq 0.5$ with performance evaluation measures of the VPMS being: $k = 4.33\text{--}624055.10$, $\left(kF_{rp}^2\right)_e = 0.21\text{--}10294.23$, $F_{rp} = 0.0039\text{--}1.49$, $q_e/q^* = 0.77\text{--}1.0$, and $\eta_q = 99.43\text{--}100.0$ %. Note that this applicability criterion $(1/s_0)(\partial y/\partial x)_e \leq 0.5$ for the VPMS method is lower than the maximum applicability limit $(1/s_0)(\partial y/\partial x)_e \leq 0.74$ up to which the ACD momentum equation yields the equilibrium flow depth. However, under very small intensity rainfall

conditions, the lower limit of $\left(kF_{rp}^2\right)_e$ estimated by the VPMS method involves scattering errors as compared to the corresponding estimates given by the ACD momentum equation and, hence, it is recommended to estimate the lower limit of $\left(kF_{rp}^2\right)_e$ for the VPMS method by using the ACD momentum equation. While fixing the applicability criterion $(1/s_0)(\partial y/\partial x)_e \leq 0.5$ for the VPMS method, the k and $\left(kF_{rp}^2\right)_e$ values estimated by the KW approach based on equations (2.34a, b) are > 5 and > 1.34, respectively, which reconfirms the satisfaction of the proposed criterion that can take care of the suggested lower limits of k and $\left(kF_{rp}^2\right)_e$ applicable in the DW range [*Daulz Vieira*, 1983] (see Figures 5.8a and 5.8b).

Considering the suggestion of *Woolhiser and Liggett* [1967] that the applicability criteria for the KW approach should satisfy $k > 20$ and $F_{rp} \geq 0.5$, attempt has been made to verify the effect of k and F_{rp} on the solution of the VPMD and VPMS methods (Figures 5.9a and 5.9b). It can be seen from Figure 5.9a that the test runs with $F_{rp} > 0.2$ values results in better performance (with $\eta_q >> 99$ %), but those with $F_{rp} < 0.2$ values show performance with $95\% < \eta_q < 99\%$ by the VPMD and VPMS methods; although, the lower limit of $F_{rp} = 0.2$ (with $\eta_q >> 99$ %) is smaller than that prescribed for the KW approximation ($F_{rp} \geq 0.5$). As compared to the VPMS method, the solutions of the VPMD method are more accurate for the test runs with smaller Froude numbers, although a large number of test runs in this range are successfully simulated by both the VPMS and VPMD methods. Under such circumstances, the overland flow has a higher kinematic wave number which may be a reason for advocating the applicability criterion $\left(kF_{rp}^2\right)_e$ by *Morris and Woolhiser* [1980] to account for the combined effect of k and F_{rp}, as also envisaged in the proposed applicability criterion $(1/s_0)(\partial y/\partial x)_e$ expressed by equation (5.19). However, unlike $(1/s_0)(\partial y/\partial x)_e$, the applicability criterion advocated by *Morris and Woolhiser* [1980] does not account for the effect of friction law. Therefore, the use of the proposed applicability criterion based on $(1/s_0)(\partial y/\partial x)_e$ can eliminate the need to set a lower limit of the Froude number. This can be reconfirmed from Figure 5.9b, wherein the limits of F_{rp} and k for the KW advocated by *Woolhiser and Liggett* [1967] are shown. It can be surmised from Figure 5.9b that the test runs with small kinematic wave number requires the
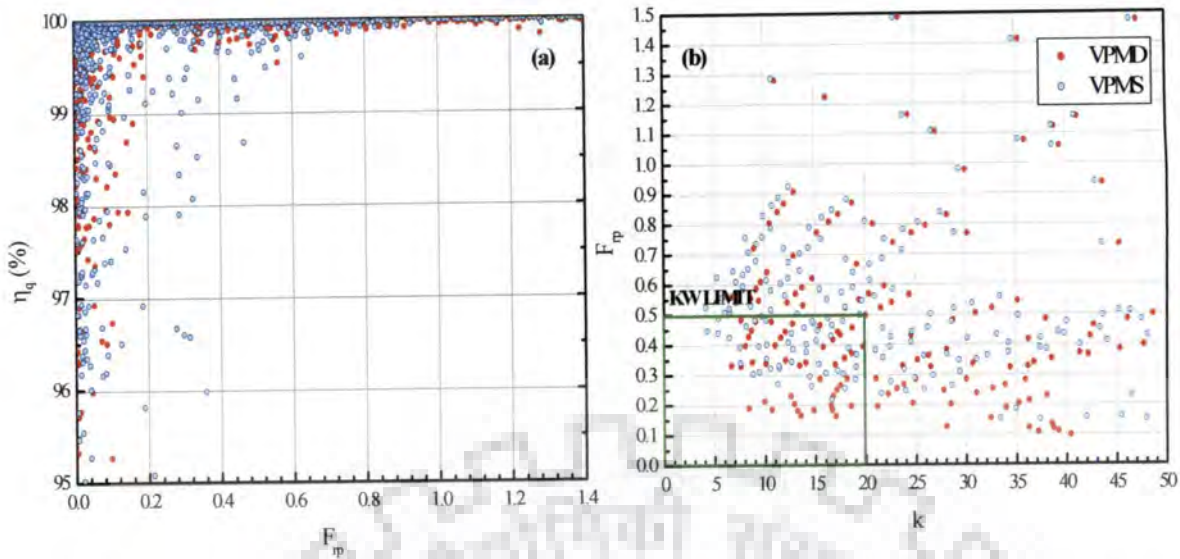
Figure 5.9 Variation of the Froude number, F_{rp} with a) Nash-Sutcliffe efficiency for the cases with $\eta_q > 95\%$ and (b) the kinematic wave number, k for the case with $\eta_q > 99\%$ using the VPMD and VPMS methods.

use of higher Froude number, although both the VPMD and VPMS methods successfully simulate the test runs with $F_{rp} < 0.5$. Similarly, for all the successful test runs with $\eta_q > 99$ %, the kinematic wave number $k > 5$, which confirms the lower limit of k for the DW approximation as advocated by *Daulz Vieira* [1983].

5.6.4 Evaluation of the VPMD and VPMS Methods to Establish the Applicability Criteria Using the Non-dimensional Complete and Partial Runoff Hydrographs

The applicability criteria for the VPMD and VPMS overland flow routing methods are also evaluated by examining the partial non-dimensional runoff hydrographs computed at the end of the overland flow plane in comparison with the corresponding solutions of the SVE and the analytical KW equation as demonstrated by *Morris and Woolhiser* [1980] for different values of k, F_{rp}, and the non-dimensional rainfall duration D^* estimated as $D^* = t_r / t_e (KW)$, wherein k and F_{rp} and D^* are computed using the analytical KW approach (see Figures 5.10-5.12). The test runs with various combinations of the parameters $r - L - s_0 - n$ and t_e used in Figures 5.10-5.12 are presented in Table 5.3.

Table 5.3 The selected numerical test runs for the demonstration of simulated non-dimensional runoff hydrographs by the VPMD and VPMS methods showing various combinations of $r - L - s_0 - n$ parameters

Test Run code	Plane Length L (m)	Manning's n	Slope s_0	Rain intensity r (cm/h)	t_e (min)
SIM558	300	0.006	0.00002	0.4	146.69
SIM1025	40	0.006	0.0001	1.6	15.52
SIM1637	300	0.01	0.0001	6	41.63
SIM1518	6	0.006	0.0005	6	1.81
SIM2031	40	0.006	0.0005	10	4.60
SIM1538	100	0.006	0.0001	6	15.85
SIM2112	100	0.01	0.0005	10	10.83
SIM2525	6	0.006	0.0007	16	1.1
SIM2023	6	0.006	0.0003	10	1.72
SIM2527	6	0.006	0.0003	16	1.42
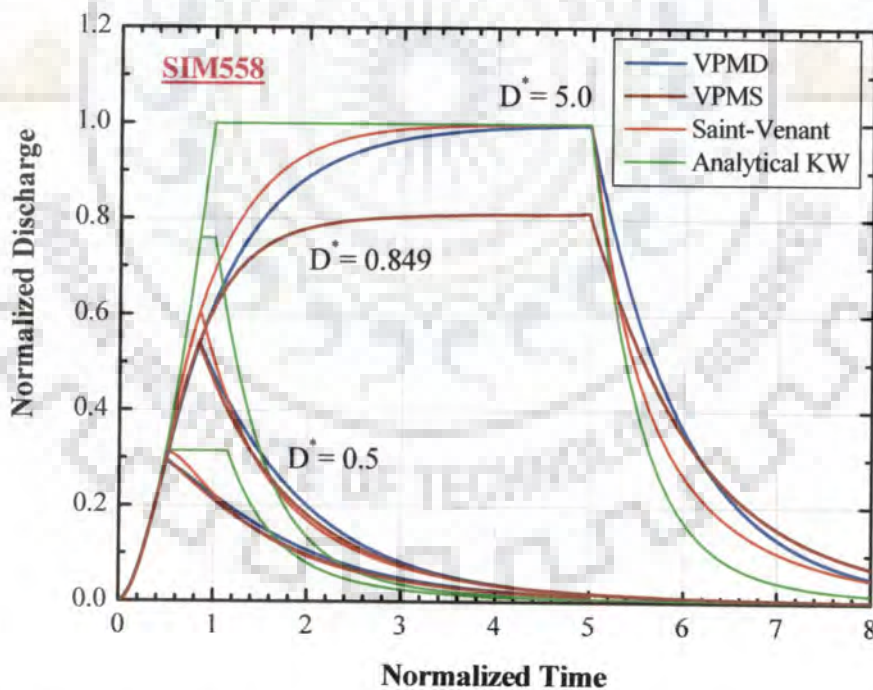
Figure 5.10 Solutions of the VPMD and VPMS methods to reproduce the corresponding solutions of the SVE and analytical KW equation for the flow conditions characterized by $k = 50.67$ and $F_{rp} = 0.11$ (test run SIM558). The normalized discharges are shown as the function of normalized time $t/t_e (KW)$ at various non-dimensional rainfall durations, D^*.

241
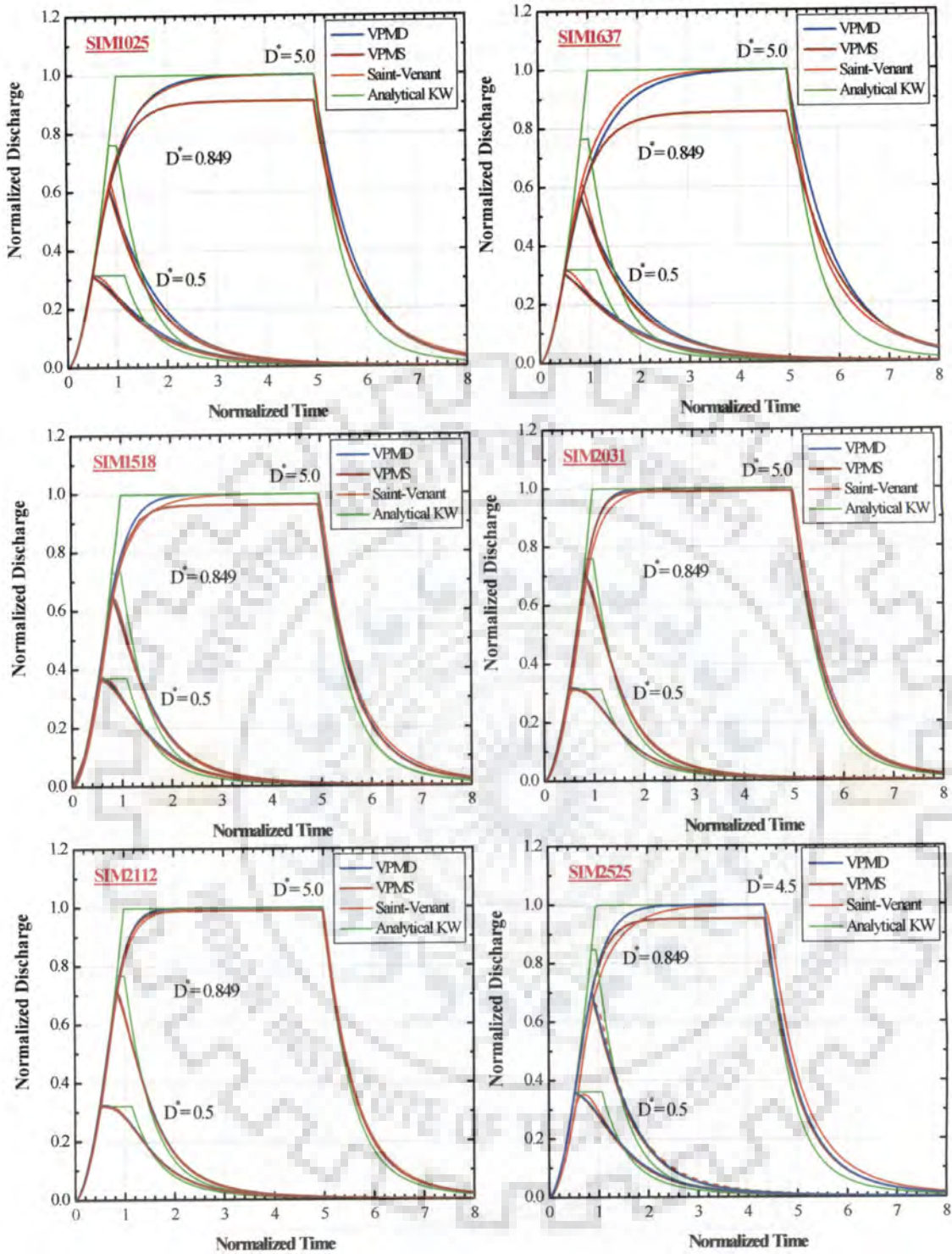
Figure 5.11 Solutions of the VPMD and VPMS methods to reproduce the corresponding solutions of the SVE and analytical KW equation for the flow conditions characterized by a) $k = 21.27$ and $F_{rp} = 0.21$ (SIM1025); b) $k = 20.40$ and $F_{rp} = 0.19$ (SIM1637); c) $k = 9.62$ and $F_{rp} = 0.42$ (SIM1518); d) $k = 9.35$ and $F_{rp} = 0.53$ (SIM2031); e) $k = 20.72$ and $F_{rp} = 0.37$ (SIM2112); and f) $k = 5.02$ and $F_{rp} = 0.53$ (SIM2525). The normalized discharges are shown as the function of normalized time at various non-dimensional rainfall durations, D^*.
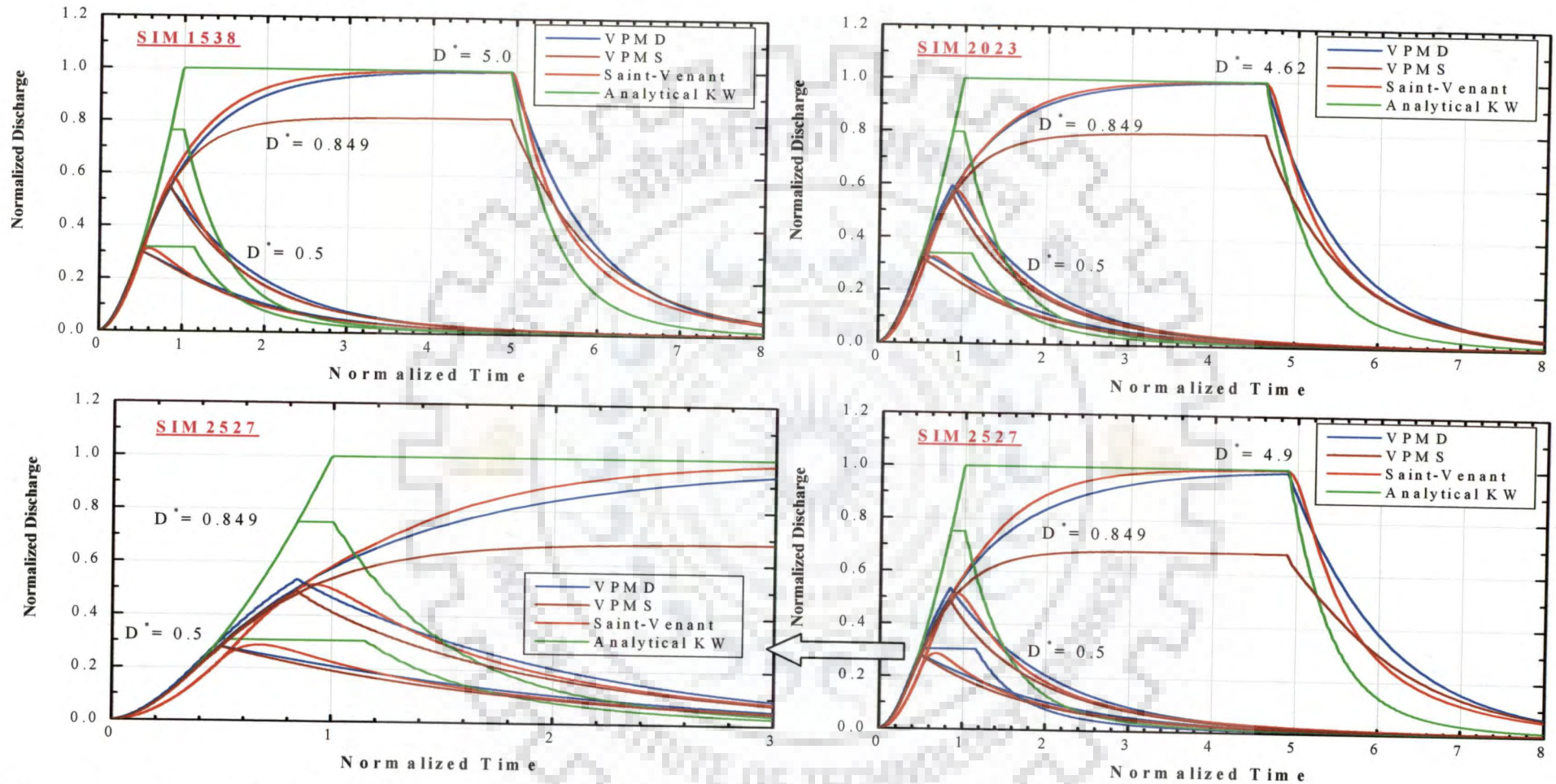
Figure 5.12 Normalized solutions of the VPMD and VPMS methods to reproduce the corresponding solutions of the SVE and analytical KW equation for the flow conditions with $(1/s_0)(\partial y/\partial x)_e > 1.2$ characterized by a) $k = 8.87$ and $F_{rp} = 0.27$ (SIM1538); b) $k = 5.21$ and $F_{rp} = 0.35$ (SIM2023); and c) $k = 3.58$ and $F_{rp} = 0.36$ (SIM2527).

Figure 5.13 illustrates the variation of Froude number F_{rp} with $(1/s_0)(\partial y/\partial x)_e$ from which it can be inferred that the test runs characterized by smaller F_{rp} and larger k values can be simulated successfully. For the test runs characterised by small kinematic wave number (i.e., $k \approx 5$), it is seen that the lower limit for the Froude number is approximately 0.35 and 0.5 for the VPMD and VPMS methods, respectively (Figures 5.10a and 5.13). Figures 5.14a–5.14d show the performance evaluation measures estimated by the VPMD and VPMS methods for the test runs studied in simulating the benchmark runoff hydrographs. While fixing the applicability criteria $(1/s_0)(\partial y/\partial x)_e \leq 1.2$ and $(1/s_0)(\partial y/\partial x)_e \leq 0.50$ for the VPMD and VPMS methods, respectively, the range of the error estimates CRM (%) by the VPMD and VPMS methods are evaluated as: -1.36 to -0.073% and -0.73 to 5.63%, respectively. Figure 5.14a reveals that for the test runs with $(1/s_0)(\partial y/\partial x)_e \leq 0.50$, $CRM <$ 5 % for the VPMS method, except the case of one test run. However, the VPMD method exhibits $CRM \ll 5\%$ for all the test runs. It is evident that for the established criteria of the VPMD and VPMS methods, the range of CD is 0.97–1.02 and 0.98–1.12, respectively (Figure 5.14b); the range of $EVOL$ is -0.033 to 1.08% and -4.56 to 0.30%, respectively (Figure 5.14c); and the range of q_{perr} is -0.74 to 1.79% and -5.0 to 1.86%, respectively (Figure 5.14d). Hence, the VPMD method is more volume conservative than the VPMS method. While selecting the applicability criterion for the VPMS method, the test runs with $EVOL < 5\%$, but $q_{perr} > 5\%$ are presented in Table 5.4 and these runs do not satisfy the established applicability criterion. Further, it was discussed earlier that the above established applicability criteria of the VPMD and VPMS methods, have been estimated using the equilibrium flow depths arrived at by these methods are the higher estimates when $(1/s_0)(\partial y/\partial x)_e \geq 0.43$ and, hence, the applicability criteria estimates $(1/s_0)(\partial y/\partial x)_e > 1$ of the applicable test runs apparently violate the limitation of the binomial series expansion particularly in case of the VPMD method. Further, the VPMS method has a better flow depth reproduction capability than the VPMD method. This inference is corroborated from Figure 5.2 wherein the VPMS method established relationship between $(1/s_0)(\partial y/\partial x)_e$ and (q_e/q^*) has tendency to adhere to the corresponding theoretical relationship based on the ACD momentum equation in comparison with that of the VPMD method.
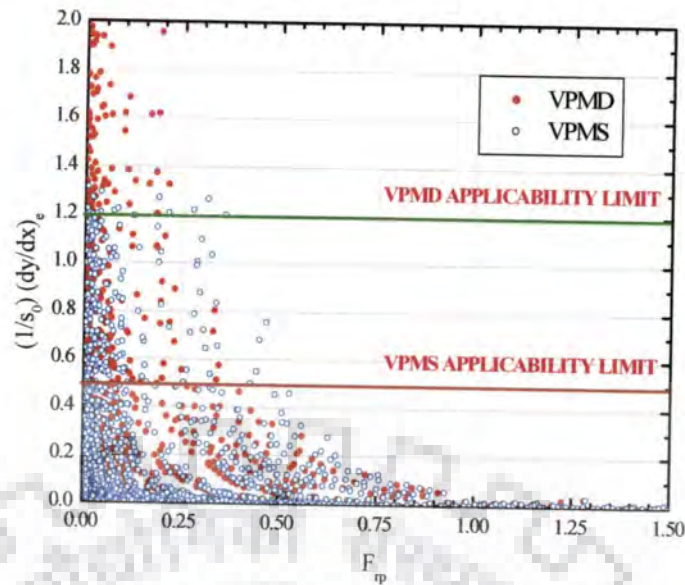
Figure 5.13 Variation of $(1/s_0)(\partial y/\partial x)_e$ with the Froude number (F_{rp}) for the test runs with $\eta_q > 99\,\%$.

Generally, the DW approximation is applicable, when $k \to \infty$ and $F_{rp} \to 0$ [*Daulz Vieira*, 1983]. Since the classical case presented by [*Daulz Vieira*, 1983] characterized by $k = 50$ and $F_{rp} = 0.1$ is commonly used to demonstrate its applicability, the test run SIM558 with $k = 50.67$ and $F_{rp} = 0.11$ is used herein to test the performance of the VPMD and VPMS methods. The non-dimensional runoff hydrographs by the VPMD, VPMS, SVE and analytical KW methods for the SIM558 test run are presented in Figure 5.10. It can be inferred from Figure 5.10 that the VPMD method is able to closely reproduce the benchmark runoff hydrographs, and the VPMS method significantly under-estimates these hydrographs; whereas the performance of the analytical KW solution is very poor. In the normalized time range of 0.6–3.5, the VPMD method hydrograph deviates from the runoff hydrograph of the SVE. Hence, if the rainfall ceases within this nondimensionalized time region, a slightly higher error in the estimated peak discharge by the VPMD method is expected. This inference can also be arrived at from Table 5.5, wherein for $D^* = 0.849$, the q_{perr} estimate is higher as compared to those for $D^* = 0.50$.

When the applicability criterion of $(1/s_0)(\partial y/\partial x)_e \leq 1.2$ is fixed for the VPMD method, the range of various parameters are estimated as: $k = 6.69$–624016.4, $\left(kF_{rp}^2\right)_e = 0.50$–10325.26, $F_{rp} = 0.0025$–1.49, $q_e/q^* = 0.59$–1.0, and $\eta_q = 99.52$–100 %; and the

245

Table 5.4 Typical test runs of the VPMS method with $(1/s_0)(\partial y/\partial x)_e > 0.5$ (simulation runs having $q_{perr} > 5\%$ and $EVOL < 5\%$)

Test Run Code	Plane Length L (m)	Manning's n	Slope s_0	Rain fall intensity r (cm/h)	$(1/s_0)(\partial y/\partial x)_e$		$(kF_{rp}^2)_e$ (KW Approach)	η_q (%)	q_{perr} (%)	$EVOL$ (%)
					ACD	VPMS				
SIM189	200	0.05	0.00005	0.1	-	0.64	1.11	99.67	-5.83	-4.68
SIM295	6	0.18	0.0003	0.1	0.62	0.53	1.29	99.71	-5.53	-4.72
SIM413	300	0.3	0.0001	0.1	-	0.64	1.09	99.68	-5.63	-4.80
SIM531	100	0.006	0.00005	0.4	0.61	0.52	1.30	99.73	-5.39	-4.75
SIM621	200	0.01	0.00005	0.4	0.65	0.54	1.26	99.71	-5.53	-4.71
SIM808	40	0.18	0.0003	0.4	-	0.57	1.20	99.67	-5.80	-4.86
SIM970	150	0.45	0.0003	0.4	-	0.59	1.18	99.73	-5.23	-4.53
SIM1115	150	0.01	0.0001	1.6	-	0.57	1.21	99.71	-5.70	-4.54
SIM1258	150	0.1	0.0003	1.6	0.65	0.54	1.26	99.74	-5.25	-4.38
SIM1348	300	0.18	0.0003	1.6	-	0.59	1.17	99.67	-5.83	-4.78
SIM1401	150	0.3	0.0005	1.6	0.64	0.54	1.27	99.75	-5.17	-4.30
SIM1770	200	0.1	0.0005	6	0.67	0.55	1.25	99.71	-5.52	-4.43
SIM1894	100	0.3	0.001	6	-	0.57	1.20	99.66	-5.87	-5.00
SIM1984	200	0.45	0.001	6	0.67	0.55	1.25	99.71	-5.35	-4.69
SIM2193	150	0.05	0.0005	10	0.68	0.55	1.24	99.69	-5.75	-4.61
SIM2264	150	0.1	0.0007	10	0.65	0.54	1.27	99.74	-5.32	-4.29
SIM2326	100	0.18	0.001	10	-	0.57	1.20	99.69	-5.77	-4.65
SIM2354	300	0.18	0.0007	10	-	0.59	1.18	99.66	-5.97	-4.78
SIM2626	150	0.01	0.0003	16	0.64	0.54	1.26	99.72	-5.21	-4.20
SIM2687	100	0.05	0.0007	16	0.69	0.56	1.23	99.71	-5.65	-4.53
SIM2715	300	0.05	0.0005	16	0.69	0.56	1.23	99.71	-5.59	-4.48
SIM2758	100	0.1	0.001	16	0.62	0.53	1.29	99.71	-5.56	-4.51
SIM2786	300	0.1	0.0007	16	0.65	0.54	1.26	99.75	-5.20	-4.20
SIM2848	200	0.18	0.001	16	-	0.58	1.20	99.71	-5.55	-4.43

corresponding estimates for the KW approach are: $k = 4.39$–624678.2, $(kF_{rp}^2)_e = 0.68$–10325.45, and $F_{rp} = 0.0039$–1.49. Therefore, it is interesting to see that the lower limit of $k \approx 5$ by the analytical KW approach. These results are compatible with the lower limit of k as suggested by *Daulz Vieira* [1983] for the DW approximation. Further, it can be concluded from the test runs presented in Tables 5.3 and 5.5 that the values of k is very small over the smooth surface that generally exists in the urban watersheds; whereas for the natural agricultural forest with rough surfaces, k is too large. Based on the present study and the study by *Daulz Vieira* [1983], it is concluded that on natural slopes, the values of $k > 50$ and, hence, the shallow subcritical flows can be accounted for within the applicability limits of the VPMD and VPMS methods. Under such circumstances, the possible impact
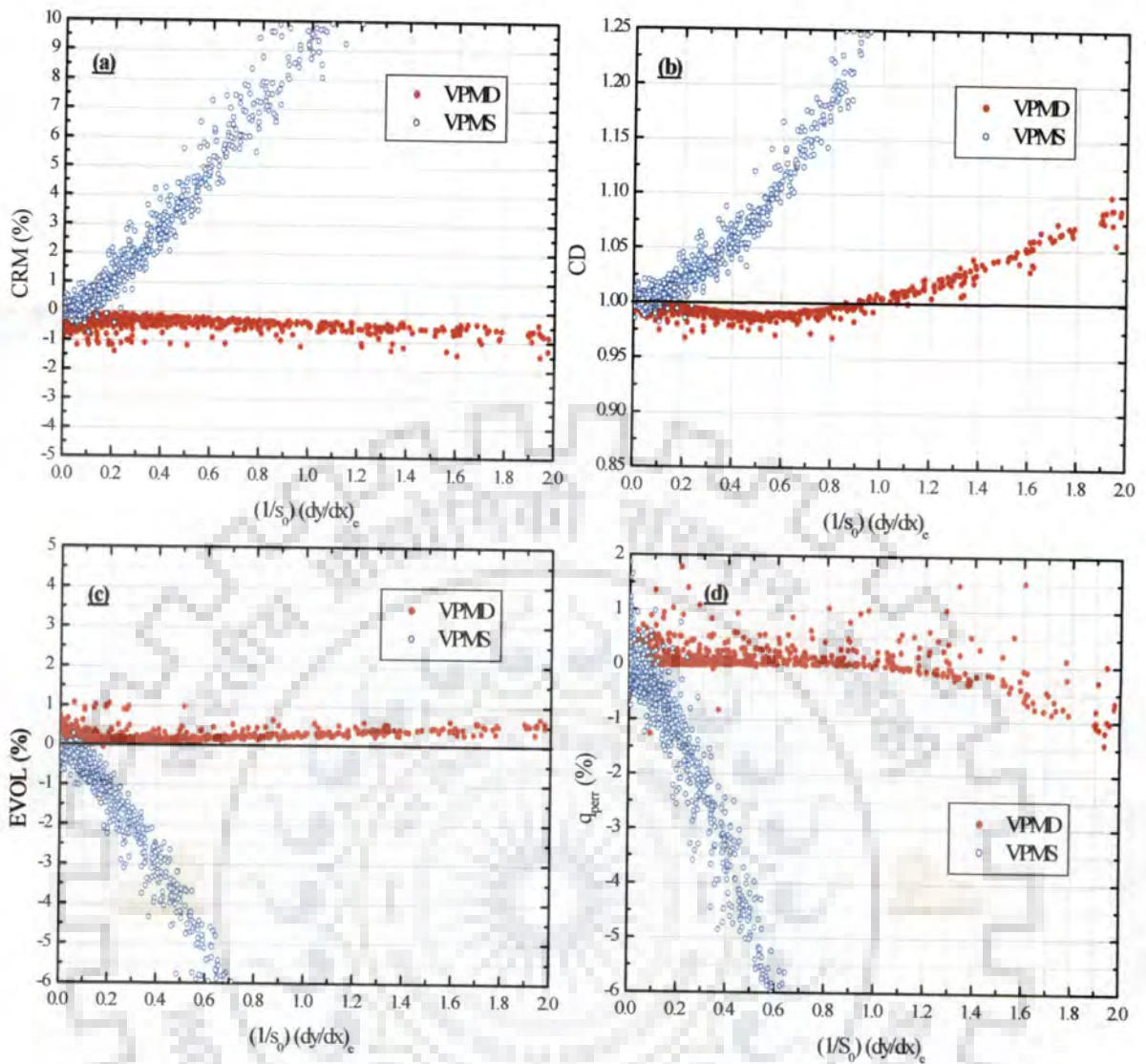
Figure 5.14 Various performance evaluation measures by the VPMD and VPMS methods with the proposed applicability criteria $(1/s_0)(\partial y/\partial x)_e$.

of the downstream boundary condition may be very marginal or almost negligible. Further, it was shown by *Daulz Vieira* [1983] that the solutions of the DW approximations to solve the zero-depth-gradient downstream boundary conditions are dependent on the parameter $(kF_{rp}^2)_e = 1/\mu$. The DW approximation is applicable for simulating the overland flow when $\mu \ll 2.0$, i.e., when $(kF_{rp}^2)_e \gg 0.5$, in which $(kF_{rp}^2)_e$ is estimated by the KW approach. The applicability criteria $(1/s_0)(\partial y/\partial x)_e \le 1.2$ fixed for the VPMD method results in the estimates of $(kF_{rp}^2)_e = 0.5$ and 0.68 by the VPMD and KW methods, respectively. Hence, the VPMD method is applicable almost in the entire range of the DW approximations (see Figure 5.8b).

247

Table 5.5 Performance evaluation of the VPMD and VPMS methods for the complete and partial non-dimensional runoff hydrographs using the test runs presented in Table 5.3.

Test Run code	Non-dimensional Rainfall Duration (D^*) $\times t_e$	KW approach			VPMD Method							VPMS Method						
		k	F_{rp}	$(kF_{rp}^2)_e$	k	F_{rp}	kF_{rp}^2	$(1/s_0)(\partial y/\partial x)$	η_q (%)	q_{perr} (%)	EVOL (%)	k	F_{rp}	kF_{rp}^2	$(1/s_0)(\partial y/\partial x)$	η_q (%)	q_{perr} (%)	EVOL (%)
SIM558	5	50.67	0.11	0.61	100.26	0.07	0.43	1.39	99.32	-0.25	0.39	35.1	0.12	0.47	1.29	95.93	-18.61	-10.35
	0.849				107.61	0.09	0.78	0.77	98.69	-10.60	-0.05	73.55	0.11	0.81	0.74	99.18	-10.23	-4.28
	0.5				144.31	0.09	1.23	0.49	98.96	-5.86	-4.72	130.35	0.10	1.25	0.48	99.34	-4.92	-9.27
SIM1025	5	21.27	0.21	0.97	32.45	0.16	0.78	0.77	99.96	0.02	0.29	16.63	0.22	0.79	0.73	99.25	-8.89	-6.96
	0.849				36.57	0.18	1.20	0.50	99.62	-3.52	0.32	29.51	0.20	1.24	0.49	99.69	-4.11	-5.82
	0.5				55.06	0.19	1.92	0.31	99.55	-1.10	-3.80	53.66	0.19	1.94	0.31	99.52	-1.54	-9.28
SIM1637	5	20.40	0.19	0.72	36.25	0.12	0.54	1.12	99.76	-0.07	0.26	14.95	0.19	0.57	1.05	97.89	-14.34	-9.8
	0.849				39.89	0.15	0.91	0.66	99.24	-7.67	-0.37	28.95	0.18	0.94	0.64	99.57	-6.33	-4.47
	0.5				55.58	0.16	1.43	0.42	99.33	-3.91	-2.91	51.71	0.17	1.45	0.41	99.50	-3.13	-7.18
SIM1518	5	9.62	0.42	1.66	12.06	0.35	1.48	0.40	99.88	0.02	0.41	8.39	0.42	1.47	0.4	99.80	-3.77	-3.16
	0.849				14.26	0.38	2.05	0.29	99.57	2.23	0.68	12.49	0.40	1.98	0.29	99.65	0.90	-1.98
	0.5				20.86	0.37	2.93	0.20	99.37	2.62	-0.43	20.77	0.38	2.94	0.20	99.58	0.36	-3.64
SIM2031	5	9.35	0.53	2.61	10.67	0.48	2.44	0.25	99.89	0.04	0.12	8.64	0.53	2.46	0.24	99.87	-0.95	-0.87
	0.849				12.70	0.50	3.14	0.19	99.47	3.92	0.47	12.02	0.51	3.14	0.19	99.61	2.57	-0.78
	0.5				23.26	0.47	5.17	0.12	99.54	1.83	-1.84	23.26	0.47	5.15	0.11	99.68	0.11	-2.23
SIM1538	5	8.87	0.27	0.63	17.04	0.16	0.45	1.33	99.74	-0.17	0.35	6.28	0.28	0.48	1.22	96.68	-17.99	-11.7
	0.849				18.49	0.21	0.80	0.75	99.13	-6.69	0.02	12.79	0.25	0.83	0.72	99.26	-5.72	-4.96
	0.5				24.81	0.22	1.25	0.48	98.65	-3.54	-4.29	22.54	0.24	1.27	0.47	98.87	-3.18	-7.68
SIM2112	5	20.72	0.37	2.77	23.69	0.33	2.59	0.23	99.97	0.01	0.24	19.12	0.37	2.6	0.23	99.97	-0.97	-0.84
	0.849				28.07	0.34	3.33	0.18	99.90	0.86	-0.41	26.60	0.35	3.34	0.18	99.93	0.56	-0.92
	0.5				50.62	0.33	5.41	0.11	99.85	1.34	-3.13	50.63	0.33	5.40	0.11	99.93	0.00	-2.28
SIM2525	4.5	5.02	0.53	1.43	6.47	0.44	1.26	0.48	99.61	0.06	0.15	4.33	0.54	1.25	0.46	99.43	-4.63	-3.78
	0.849				7.33	0.48	1.68	0.36	99.01	5.20	-0.14	6.09	0.52	1.62	0.35	98.81	4.51	-2.03
	0.5				11.49	0.48	2.63	0.23	98.71	1.61	-1.09	11.19	0.48	2.59	0.23	98.58	1.43	-3.44
SIM2023	4.62	5.21	0.35	0.63	9.95	0.21	0.45	1.33	99.87	-0.18	0.56	3.75	0.36	0.48	1.2	95.99	-19.72	-14.84
	0.849				10.42	0.27	0.75	0.80	98.85	3.37	4.63	7.36	0.33	0.81	0.74	98.62	-2.54	-7.27
	0.5				13.27	0.30	1.17	0.51	97.50	3.63	4.87	12.70	0.31	1.23	0.49	97.81	-2.14	-8.91
SIM2527	4.9	3.58	0.36	0.47	8.40	0.19	0.31	1.96	99.40	-1.03	0.72	2.38	0.38	0.34	1.69	89.43	-31.72	-22.32
	0.849				8.35	0.26	0.58	1.03	98.07	3.65	5.10	5.42	0.35	0.65	0.93	97.22	-4.82	-8.75
	0.5				11.07	0.30	0.96	0.62	96.43	-2.45	-2.05	9.58	0.32	0.99	0.60	95.30	-2.63	-11.78

It can be inferred from Table 5.5 that when the applicability criterion $(1/s_0)(\partial y/\partial x) \leq$ 1.2 is satisfied while simulating the partial hydrographs by the VPMD method, η_q is slightly less than 99% for those cases in which the applicability criteria $(1/s_0)(\partial y/\partial x)$ estimated for the complete runoff hydrographs are larger than 1.2 as in the case of SIM558, SIM1538, SIM2023 and SIM2527, except in SIM2525. Consequently, $EVOL < 5\%$ (except in SIM2527) and $q_{perr} > 5$ % as in SIM558, SIM1538 and SIM2525, where $(1/s_0)(\partial y/\partial x) > 0.75$ except in SIM2525 when the non-dimensional rainfall duration $D^* =$ 0.849. Similarly, when the applicability criteria $(1/s_0)(\partial y/\partial x) \leq 0.50$ is satisfied while simulating the partial hydrographs by the VPMS method, η_q is slightly less than 99%, q_{perr} varies in the range of -4.92 to 4.51, and $EVOL < -9.27\%$, wherein the higher error in these estimates arises when the value of k or F_{rp} is very small.

The typical test runs with $(1/s_0)(\partial y/\partial x) \leq 1.2$ are shown in Figure 5.11, which reveals that for the test runs SIM1025 and SIM1637, complete runoff hydrographs simulated using the VPMD method are in well agreement with the solutions of the SVE; whereas, the simulated runoff hydrographs by the VPMS method significantly underestimate the peak runoff. Consequently, when the applicability criterion is set as $(1/s_0)(\partial y/\partial x) \leq 0.50$, the partial hydrographs simulated by the VPMS method are in well agreement with the VPMD and SVE. The VPMD method is able to simulate the partial hydrographs slightly better than the VPMS method, particularly when $(1/s_0)(\partial y/\partial x) > 0.5$. The recession limbs simulated by the VPMD and VPMS methods are also well in agreement with the solutions of the SVE, rather than with the solutions of the analytical KW equation. For the test runs SIM1518, SIM2031, SIM2112, and SIM2525, the applicability criterion estimates obtained by the VPMD and VPMS methods are $(1/s_0)(\partial y/\partial x) < 0.5$ and, hence, the complete and partial runoff hydrographs simulated by both these methods are in well agreement with the solutions of the SVE. This inference can also be verified from the performance criteria of the VPMD and VPMS methods presented in Table 5.5. It can be noted that the hydrograph with the same values of $(1/s_0)(\partial y/\partial x)_e$, but different k and F_{rp} are identical as seen from Figure 5.11 (SIM2031 and SIM2112). This inference is consistent with the findings of *Daulz Vieira* [1983]. In case of SIM2525 (Figure 5.11), the kinematic wave number, $k =$ 5.0, and the slight overestimation of the rising limb and underestimation of the recession limb of the SVE solution by the VPMD, VPMS, and analytical KW solutions demonstrate

that the effect of inertial terms in the momentum equation is significant. Hence, the simulations of the partial runoff hydrographs by the VPMD and VPMS methods for this test run case, even with the applicability limit of $(1/s_0)(\partial y/\partial x) < 0.5$, leads to a higher error in the estimation of peak of the SVE solution.

Figure 5.12 shows the normalized runoff hydrographs by the VPMD, VPMS, SVE, and the analytical KW solutions for $(1/s_0)(\partial y/\partial x)_e > 1.2$. In SIM1538 and SIM2023, the performance of the VPMD method is in well agreement with the SVE, although in both the test runs, $(1/s_0)(\partial y/\partial x)_e = 1.33$, which is higher than the established upper limit of 1.2 for this method. As expected, the VPMS method reproduced the complete runoff hydrographs with underestimation of the peak, whereas the partial hydrographs are well in agreement with the VPMD and SVE solutions when $(1/s_0)(\partial y/\partial x) < 0.5$. Figure 5.12 (SIM2527) further demonstrates that the test runs characterized by small kinematic wave number $k = 3.58$ are not suitable for the application of the VPMD and VPMS methods for overland flow modelling. Similarly, for test run SIM2525, the rising and recession limbs of the VPMD, VPMS, and analytical KW solutions deviate from the solutions of the SVE due to the inability of these methods to properly account for the inertial effects in the momentum equation. The VPMS method yields slightly lower estimate of the KW number for the test runs SIM2525 and SIM2527 than those by the KW approach, especially in the DW range resulting in the KW number $k < 5$. However, the KW approach yields exactly $k = 5$. Therefore, it can be inferred from Figure 5.12 that to achieve the best simulation results with the VPMD and VPMS overland flow routing methods, $k \geq 5$. These results are in conformity with the work of *Daulz Vieira* [1983], who advocated that application of the DW and KW equations are not admissible when $k < 5$ and, under such a situation, only the use of gravity wave or dynamic wave solutions are advisable.

It is inferred from all these results that the VPMD and VPMS methods are suitable to apply in the full applicability range of the KW approximation and in the transition range of the DW and KW approximations. The VPMD method is found applicable in almost the full range of DW approximation. Since *Daulz Vieira* [1983] concluded that for $k < 5$, the downstream boundary conditions are important and, the present study based on the VPMD and VPMS methods are not suitable to use when $k < 5$. Further, if the applicability criteria established for these methods are satisfied, then the solutions of the complete and partial runoff hydrographs with the acceptable accuracy can be achieved.

5.7. SUMMARY AND CONCLUDING REMARKS

A novel applicability criterion based on the magnitude of the scaled flow depth gradient $(1/s_0)(\partial y/\partial x)_e$ at equilibrium is developed for quantifying and assessing the applicability limits of the VPMD and VPMS routing methods for overland flow modelling studies. In fact, a similar criterion was advocated by *Perumal and Sahoo* [2007] for river flood routing by the VPMD and VPMS methods. In practice, the applicability criteria, such as the KW number (k), Froude number (F_{rp}), and $(kF_{rp}^2)_e$ [*Morris and Woolhiser*, 1980; *Daluz Viera*, 1983] have been used to assess the appropriateness of various overland flow models. According to *Morris and Woolhiser* [1980], the KW models can be used for overland flow modelling instead of the solutions of the SVE, when $(kF_{rp}^2)_e \geq 5$ and $F_{rp} \geq 0.5$. Similarly, *Daluz Viera* [1983] demonstrated that the accuracy of the overland flow model is dependent on the parameter $(kF_{rp}^2)_e = 1/\mu$, and the DW equation is applicable only when $\mu << 2.0$, which are reconfirmed in this study. However, in order to maintain the uniformity between the criteria for classification of flood waves and the criteria for assessing the suitability of various approximations to the SVE, emphasis has been given to use a common form of criterion $(1/s_0)(\partial y/\partial x)_e$ for both the flow routing models i.e., the flow routing models in channels and on overland flow planes. Further, in this study, the physical basis of the applicability criterion 'μ' is established as: $\mu = (m+1)(1/s_0)(\partial y/\partial x)_e$, where m is the exponent of the Manning's ($\frac{2}{3}$) or Chezy's ($\frac{1}{2}$) friction law used, which brings out that the applicability criteria is also a function of the friction law used.

The assessment of the applicability limits for the VPMD and VPMS overland flow methods were made by comparing the routing results arrived at the outlet of an overland flow plane for 2268 hypothetical cases, each for the VPMD and VPMS methods, with the corresponding solutions of the full SVE, which form the benchmark solution. Considering 99% model efficiency (N-S efficiency) and 95% accuracy levels in the volume conservation and peak runoff computations, the numerical experiments demonstrate that the applicability limit of the VPMD and VPMS methods for overland flow modelling can be fixed at $(1/s_0)(\partial y/\partial x)_e \leq 1.2$ and $(1/s_0)(\partial y/\partial x)_e \leq 0.50$, respectively, when simulating the complete runoff hydrographs. The corresponding limits using the conventional applicability criteria are $(kF_{rp}^2)_e \geq 0.68$ and 1.34 for the VPMD and VPMS methods, respectively. However, the corresponding applicability limits prescribed by *Perumal and Sahoo* [2007]

251

for the VPMD and VPMS river flood routing methods (only discharge computation) without accounting for the lateral flow contribution are 0.43 and 0.63, respectively. Such a change in the applicability limits and performances of two approaches for routing in the river and on overland flow planes may be attributed to the degree of shallowness of flow and magnitude of the inertial and pressure gradient terms. Further, the study based on the partial runoff hydrograph cases reveals that at 5% error level in the performance evaluation measures, the applicability limits of the VPMD and VPMS methods for overland flow modelling can be fixed at $(1/s_0)(\partial y/\partial x) \leq 0.6$ and $(1/s_0)(\partial y/\partial x) \leq 0.35$, respectively. Considering the existing applicability criteria, these two methods are applicable when $k > 5$. Moreover, the smaller values of the kinematic wave number $(5 < k < 20)$ occurs for the flow over very smooth surfaces which generally exits in the urban catchments and, k is always greater than 50 in the natural catchments. The flow regime characterized by the combinations of low k and high F_{rp} values, and high k and low F_{rp} values falls under the established applicability criteria of these two methods. However, the satisfaction of the established applicability limits of these two methods may eliminate the need for examining the k and F_{rp} values separately for characterizing the flow regimes. The VPMD and VPMS overland flow routing methods are capable of modelling the flood waves in the transition range of the DW and KW approximation including the full range of the latter. Therefore, within the applicability range, the VPMS overland flow routing method can closely model the kinematic waves in all the situations and the diffusive waves in an approximate manner, while the VPMD method can be successfully used in the entire applicability range of the KW and DW models. Conclusively, these two overland flow routing methods possess a great potential to handle the flow regimes under varied field conditions when the downstream boundary condition effects on the overland flow are absent.

6 EVALUATION OF THE VPMD AND VPMS METHODS FOR HORTONIAN OVRLAND FLOW GENERATION

6.1 GENERAL

The necessity for the better understanding of the effect of anthropogenic activities on the hydrologic processes lead to the choice of physically based distributed models over the empirical models, since the past records may no longer be a reliable guide to forecast the hydrological processes, such as the future catchment runoff generation and sediment transport [*Sivapalan et al.*, 2003]. The overland flow routing models have high scope in many hydrological, agricultural, and civil engineering applications, viz., the impact of land use or land cover on runoff responses, runoff forecasting, soil and water conservation measures including the design of bunds, terraces, soil erosion, pollutant transport, surface irrigation, and drainage systems; their maintenance and operation. Although, the two forms of the runoff generation mechanism, viz., the infiltration excess (Hortonian) and saturation excess (Dunne) are often treated as separate mechanisms, they are interrelated and may co-exist due to uneven distribution of the soil hydraulic properties [*Kollet and Maxwell*, 2006]. Generally, the Hortonian runoff generation mechanism dominates over the basin in the dessert and semi-arid regions due to poor development of soil structure with the lack of dense vegetative cover and organic matter [*Sivapalan et al.*, 1987]. Since the Dunne runoff generation is not significant during single storm and short storm events as compared to the Hortonian overland flow mechanism, this mechanism is generally ignored in the event based overland flow models.

The present study aims at the development of two Hortonian overland flow models by coupling the VPMD and VPMS overland flow routing models with the one-dimensional Green-Ampt (GA) infiltration model accounting for spatial and temporal variability of the infiltration process. The performance of the proposed Hortonian overland flow models accounting for spatial heterogeneity in the form of varied hydraulic conductivity of the soil is evaluated by comparing the simulation results with those of the numerical models available in literature using various performance evaluation measures.

6.2 MODELLING THE SURFACE FLOW COMPONENT

The Hortonian overland flow model over a pervious plane is basically composed of surface and subsurface flow components. The VPMD and VPMS overland flow models have been employed herein for the simulation of shallow water flow over an infiltrating surface. This runoff generation condition is depicted in Figure 6.1 which presents the same definition sketch of the Muskingum sub-reach as employed in the development of the VPMD and VPMS overland flow routing methods described in Chapters 3 and 4, except for the additional lateral flow component in the form of infiltration. Therefore, the same assumptions as used in the derivation of the VPMD and VPMS overland flow routing models are also applicable in the development of the respective models considering infiltration.
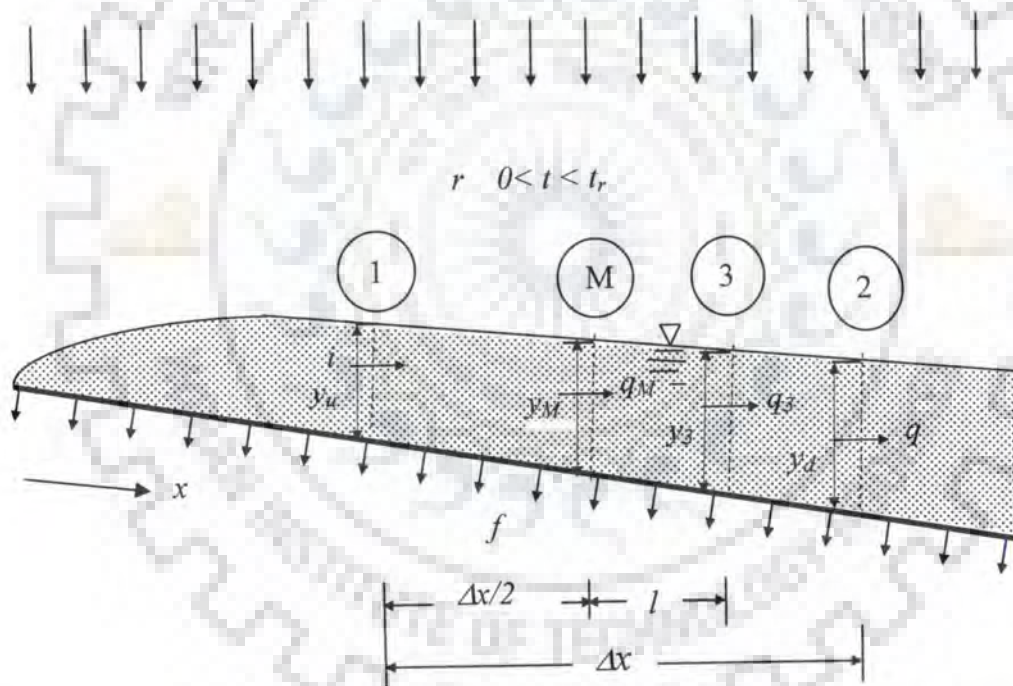
Figure 6.1 Definition sketch of the Muskingum reach of the VPMD and VPMS overland flow routing models for an infiltrating surface.

Assuming that the overland flow is occurring in a prismatic rectangular channel, the flow behavior described by the SVE consisting of continuity and momentum equations accounting for lateral flow can be given, respectively, as

$$\frac{\partial q}{\partial x} + \frac{\partial y}{\partial t} = q_L \qquad (6.1)$$

$$s_f = s_0 - \left(\frac{\partial y}{\partial x}\right) - \left(\frac{1}{g}\right)\left(\frac{\partial v}{\partial t}\right) - \left(\frac{v}{g}\right)\left(\frac{\partial v}{\partial x}\right) - \left(\frac{q_L v}{gy}\right) \qquad (6.2)$$

where q = flow rate per unit width of the flow plane $[L^2 T^{-1}]$; y = flow depth [L]; s_f = energy slope $[LL^{-1}]$; g = acceleration due to gravity $[LT^{-2}]$; v = flow velocity $[L\,T^{-1}]$; s_0 = bed slope $[LL^{-1}]$; q_L = net rate of lateral inflow per unit width $[L^2 T^{-1}]$ which can be expressed by ignoring the influence of the slope angle as

$$q_L = r - f \qquad (6.3)$$

in which r = rate of rainfall per unit area occurring for a duration t_r; and f = water infiltration rate into the soil. An order of magnitude analysis of equation (6.2) reveals that the momentum due to lateral inflow or outflow has a negligible effect on the flow dynamics [*Eagleson*, 1970; *Henderson*, 1966] and, hence, the term ($q_L v/gy$) is neglected in the analysis. This principle has been used in the surface irrigation hydraulics and the results are generally insensitive to inclusion of the term (vf/gy) in the momentum equation [*Walker and Skogerboe*, 1987]. The surface flow over an infiltrating plane surface can be considered as a case of gradually varied unsteady flow in a wide rectangular channel. The same algorithm as presented in Chapter 3 and 4 for the VPMD and VPMS overland flow routing models, respectively, are used herein to couple with the GA infiltration model required for determining the net rainfall as expressed by equation (6.3). A brief description of the GA infiltration model is appropriate herein.

6.3. MODELLING THE SUBSURFACE FLOW COMPONENT

The original GA model developed by *Green and Ampt* [1911] has undergone several modifications to describe the ponded infiltration with constant rainfall [*Mein and Larson*, 1973; *Swartzendruber*, 1974; *Chow, et al.*, 1988] and subsequently for variable rainfall [*Chu*, 1978]. Further modification were made to account for the model parameter variability with the initial water content [*Chu*, 1995], the effect of time varying ponded depths [*Warricks et al.*, 2005; *Hugo and Huang*, 2007] and the land slope on the infiltration and runoff generation processes [*Chen and Young*, 2006]. Many investigators prefer the use of GA infiltration model for overland flow modelling study due to its simplicity and robustness [*Fiedler and Ramirez*, 2000; *Esteves et al.*, 2000; *Castillo et al.*, 2003; *Liu and Singh*, 2004]. The governing equation of the GA model can be written as [*Chow et al.*, 1988]

$$f = \frac{dF}{dt} = K_s \left[1 + \frac{\psi \, \Delta\theta}{F} \right] \qquad (6.4)$$

where f = infiltration rate at the computational node (m/s); F = cumulative infiltration depth since start of infiltration (m); K_s = saturated hydraulic conductivity of soil (m/s); ψ = soil suction at water wetting front (m); Δt = computational time interval; and $\Delta\theta$ = volumetric soil water content at the soil wetting front which is equal to $(\theta_s - \theta_i)$; θ_s = saturated water content; and θ_i = initial water content.

Integrating equation (6.4) with the boundary conditions: $F = 0$ and $t = 0$, leads to

$$F - \psi \, \Delta\theta \ln \left[1 + \frac{F}{\psi \, \Delta\theta} \right] = K_s t \qquad (6.5)$$

Note that the effect of flow depth on the infiltration rate is assumed to be negligible [Schmid, 1989]. To account for the reduced infiltration rate due to air entrapment caused by the viscous resistance of wetted soil layer above the wetting front, Morel-Seytoux and Khanji [1974] introduced a correction factor to the GA model depending on the soil type and ponding depth, which ranges from 1.1 to 1.7 with an average of 1.4. However, the use of such a correction factor is not analyzed in this study.

The Hortonian overland flow generation process starts when the rainfall intensity, r exceeds the soil infiltrability, f. Therefore, during the pre-ponding condition, the average infiltration rate is expressed as

$$f^{(avg)} = r, \quad t \le t_p \qquad (6.6)$$

where t = time elapsed from the start of infiltration; and t_p = time to ponding. When $f = r$, the ponding occurs on the ground surface and the cumulative infiltration depth (F_p) can be computed by the GA model as

$$F_p = \frac{K_s \psi \, \Delta\theta}{(r - K_s)}, \quad t = t_p \qquad (6.7)$$

From equation (6.7), the ponding time can be calculated as

$$t_p = \frac{F_p}{r} \qquad (6.8)$$

In equations (6.6) and (6.7), if rainfall is uniformly distributed over the overland plane, then a uniform value of r can be used at all the spatial and temporal computational grid cells. During the post-ponding condition, the infiltration rate f at any time $t > t_p$ can be obtained by using equation (6.4), after computation of F using equation (6.5). However, since

ponding does not occur initially at $t = 0$, the use of equation (6.5) is not appropriate without modification. Therefore, equation (6.5) has been revised to account for the time lag between the actual ponding time t_p and the ponding time t_s $(t_s < t_p)$ at which the ponding occurs, when the infiltration takes place at a potential rate following the ponding from the start of the rainfall. Thus, the revised expression can be written as

$$K_s\left[t - \left(t_p - t_s\right)\right] = F - \psi\,\Delta\theta\,\ln\left[1 + \frac{F}{\psi\,\Delta\theta}\right] \tag{6.9}$$

The ponding time t_s at the potential infiltration rate can be expressed by using equation (6.7) as

$$t_s = \frac{F_p - \psi\,\Delta\theta\,\ln\left[1 + \dfrac{F_p}{\psi\,\Delta\theta}\right]}{K_s} \tag{6.10}$$

Since equation (6.9) is a nonlinear equation in F, it can be solved using the Newton-Raphson method after substituting the values of t_p and t_s from equations (6.8) and (6.10), respectively. Because of the spatially varying soil properties and the dynamic function of available water, the variables t_p and t_s vary spatially. Consequently, the average infiltration over a time interval Δt can be obtained as

$$f_2^{(avg)} = \frac{F_2 - F_1}{\Delta t} \tag{6.11}$$

where F_1 = cumulative infiltration depth at time $(t - \Delta t)$; and F_2 = cumulative infiltration depth at the current time level t for the considered sub-reach. Note that, the subroutine for the GA model to couple with the VPMD and VPMS overland flow routing models is given in Appendix-III.

6.4 COUPLING OF SURFACE AND SUBSURFACE FLOW COMPONENTS

In the coupling process, the surface water flow depth play an important role in deciding the upper boundary condition for the subsurface flow, whereas the subsurface flow condition controls the exchange flux term in the overland flow equation. In this study, the coupling of the surface and subsurface flow components is done using the sink type coupling (no-coupling) approach [*Gunduz*, 2006; *Tayfur et al.*, 1993; *Fiedler and Ramirez*, 2000; *Esteves et al.*, 2000; *Castillo et al.*, 2003; *Liu and Singh*, 2004], wherein these components are linked through a source/sink term (e.g., infiltration rate) in equation (6.3). In the mathematical sense, a net lateral inflow is controlled by rainfall intensity, surface and the

soil water conditions. The average rate of lateral inflow into each of the computational sub-reach at any time t as required in equation (6.3) can be estimated using the values of the infiltration rate computed by equations (6.6) or (6.11) depending on the status of ponding.

The following initial and boundary conditions are considered for coupling:

Upstream condition for surface flow: $\begin{cases} i(0,t) = 0; t \geq 0 \\ y(0,t) = 0; t \geq 0 \end{cases}$

where $t = \sum_{i=1}^{n} \Delta t_i$ and n = number of time intervals employed in the simulation process.

Initial condition for lateral surface inflow into each computational sub-reach is:

$\begin{cases} i(x,t) = q(x - \Delta x, t); \forall t > 0, \Delta x \leq x \leq L \\ q(x,t) = 0; \ 0 \leq x \leq L, 0 < t < t_p \\ y(x,t) = 0; \ 0 \leq x \leq L, \ 0 < t < t_p \end{cases}$

Initial condition for subsurface flow at any location x: $\psi(z,0) = \psi_0; 0 < z < Z_s$

Upper boundary condition for subsurface flow at any location x: $\psi(z,t) = \psi; 0 < z < Z_s$

where ψ_0 = initial suction at the wetting front; z = depth of the wetting front below the ground surface; and Z_s = depth below the ground surface where a stable water table may exist.

Lower boundary condition for subsurface flow at any location x:

$\psi(Z_s,t) = 0, 0 < t < \infty, z = Z_s$

The value of ψ can be obtained from the soil characteristics data or from the calibration of the GA parameters from the observed infiltration data. Note that *Smith and Woolhiser* [1971] have used similar boundary conditions in their model.

The VPMD-GA and VPMS-GA models developed for routing the Hortonian overland flow have the capability to refine their initial estimates of the model parameters for the considered sub-reach and to arrive at the refined estimates of outflow discharge and the corresponding depth. The VPMD or VPMS and GA models are solved simultaneously in a concurrent manner for each computational time and space intervals using the desired boundary conditions. Note that the assumption of linear variation of discharge or flow depth over a computational sub-reach is valid only when a small Δx is considered during the computation.

6.5. NUMERICAL APPLICATION

The numerical experiment data used by *Woolhiser et al.* [1996] is applied herein to evaluate the performance of the VPMD-GA and VPMS-GA conjunctive overland flow models. Since various field experimental data reveal that the trend in soil-hydraulic conductivity significantly impact the runoff hydrograph reproduction, especially for the small runoff events, the numerical experiments used by *Woolhiser* et al. [1996] for three scenarios of hydraulic conductivity variations are considered in the present study. The input data for all these three scenarios consisting of various soil parameters, hillslope parameters and rainfall conditions are given in Table 6.1. These three cases include: I) uniform soil hydraulic conductivity on the overland flow plane; II) linearly decreasing soil hydraulic conductivity along the plane in the downslope direction; and III) linearly increasing soil hydraulic conductivity along the plane in the downslope direction. The form of linear variation of K_s considered in the VPMD-GA and VPMS-GA model frameworks can be expressed as [*Smith and Hebbert*, 1979; *Woolhiser et al.*, 1996]

$$K_s = K_{av}(a + bx/L)$$
(6.12)

where K_{av} = average saturated hydraulic conductivity; a and b are the soil parameters; and x = locus of the point along the flow path, measured from the upstream end of the overland flow plane at which K_s is to be estimated at the midpoint of the considered computational sub-reach by using equation (6.12).

Table 6.1 Summary of input parameters used

Case	Rainfall Conditions		Hillslope parameters			Soil Parameters					
	Intensity r	Duration t_r	Length L	Slope S_0	Manning's n	K_{av}	B_{SP}	a	b	ψ	$\Delta\theta$
	cm/h	min	m			cm/s				cm	
I	17.76	20.0	50.0	0.04	0.10	0.000353	11.0	1.0	0	44.0	0.25
II	17.76	20.0	50.0	0.04	0.10	0.000353	11.0	1.3303	-0.6606	44.0	0.25
III	17.76	20.0	50.0	0.04	0.10	0.000353	11.0	0.6697	0.6606	44.0	0.25

The experimental set up used by *Woolhiser et al.* [1996] consists of a 50 m unit width overland flow plane characterized by a spatially variable infiltration surface. The runoff

hydrograph generated from this experiment is simulated using the KW overland flow model coupled with the Smith-Paralange infiltration model which is solved using a finite-difference scheme. *Fiedler and Ramirez* [2000] have also used the data sets of *Woolhiser et al.* [1996] to verify their developed hydrodynamic model for the coupled surface and subsurface flow equations, wherein the subsurface flow rate is simulated using the GA infiltration model. It has been shown by *Fiedler and Ramirez* [2000] that the adequately estimated Green-Ampt parameters, such as the soil-moisture suction at the wetting front, ψ and the volumetric soil-moisture deficit at the wetting front, $\Delta\theta$ corresponding to the Smith-Parlange parameter B_{SP} would essentially yield the identical results. A relationship between these parameters can be developed using the Youngs' approximation for the soil sorptivity, S_r [*Maidment*, 1993] as

$$S_r = \sqrt{2\Delta\theta K_s \psi} \tag{6.13}$$

Similarly, the relationship between the Smith-Parlange infiltration model parameters (B_{SP}) and S_r can be expressed as [*Smith and Parlange*, 1978]

$$B_{SP} = \frac{S_r^2}{2K_s} \tag{6.14}$$

Combining equations (6.13) and (6.14) results in:

$$B_{SP} = \psi\,\Delta\theta \tag{6.15}$$

Note that, by using the relationships expressed by equations (6.13)-(6.15), *Fiedler and Ramirez* [2000] used $\psi = 44$ cm and $\Delta\theta = 0.25$, corresponding to $B_{SP} = 11$ cm. The average, minimum and maximum values of K_s for all the three scenarios are considered as 3.53×10^{-4} cm/s, 2.37×10^{-4} cm/s, and 4.70×10^{-4} cm/s, respectively. It is further shown by *Woolhiser et al.* [1996] that the apparent coefficient of variation of hydraulic conductivity is 0.2, which is smaller as compared to its natural variability.

The performance of the developed models are evaluated using various performance evaluation measures, viz., Nash-Sutcliffe model efficiency (n_q) [*Nash and Sutcliffe*, 1970] (in %), percentage error in volume (*EVOL*), coefficient of residual mass (in %) (*CRM*), coefficient of determination (*CD*), percentage error in peak discharge reproduction (q_{perr}), and error in time to peak discharge reproduction (t_{perr}) as described in Chapter 3. Similarly, the applicability limits of the developed models are evaluated using the applicability criteria of kinematic wave number (k), Froude number (F_{rp}), and kF_{rp}^2.

6.6 RESULTS AND DISCUSSION

Figures 6.2a and 6.2b show the results of the average infiltration rate and cumulative infiltration depth, respectively, estimated at the end sub-reach of an infiltrating overland plane for three cases (I, II and III) of spatial heterogeneity as discussed in the previous section. It can be seen from Figure 6.2 that the decreasing trend of K_s along the downslope (Case II) resulted in a lower infiltration rate curve as well as cumulative infiltration depth as compared to those cases estimated with uniform K_s (Case I), and K_s increasing downslope (Case III). The K_s increasing downslope trend resulted in higher infiltration rate curve and higher cumulative infiltration depth curve than those estimated with the uniform K_s. These results shown in Figure 6.2 reveal that the GA infiltration model accounting for linear trends in K_s variation is correctly incorporated in the proposed model framework. Figures 6.3, 6.4 and 6.5 illustrate the comparison of the simulated runoff hydrographs from an infiltrating plane for the cases I, II and III, respectively, using the VPMD-GA and VPMS-GA overland flow models with those produced by using a characteristics based kinematic wave solution [*Woolhiser et al.* 1996] and the hydrodynamic wave model [*Fiedler and Ramirez*, 2000]. It is seen that the VPMD-GA and VPMS-GA model simulated runoff hydrographs are very close to those produced with the hydrodynamic model as compared to the kinematic wave solution, although the visual difference is not significant. In this context, it has been demonstrated by *Fiedler and Ramirez* [2000] that the GA infiltration model is predicting a slightly higher infiltration capacity implying less rainfall excess than the Smith-Parlange infiltration model as a function of the cumulative infiltration. Hence, it is expected that the VPMD and VPMS overland flow models coupled with the GA infiltration model would slightly underestimate the predicted discharge and flow depth than that simulated by the overland flow model coupled with the Smith-Parlange infiltration model. The slight differences between the solutions of the VPMD-GA and KW models, and VPMS-GA and KW models may be attributed to the use of different infiltration models. Further, it is important to note that the run-on phenomenon which occurs when the runoff generated in the upstream reach due to random variation of soil hydraulic conductivity is over-run the ponding locus. The rapid increase in K_s along the down-slope or the moving storm may be the adequate condition for occurrence of the run-on process. However, in the considered Case-III, the run-on phenomenon does not occur.
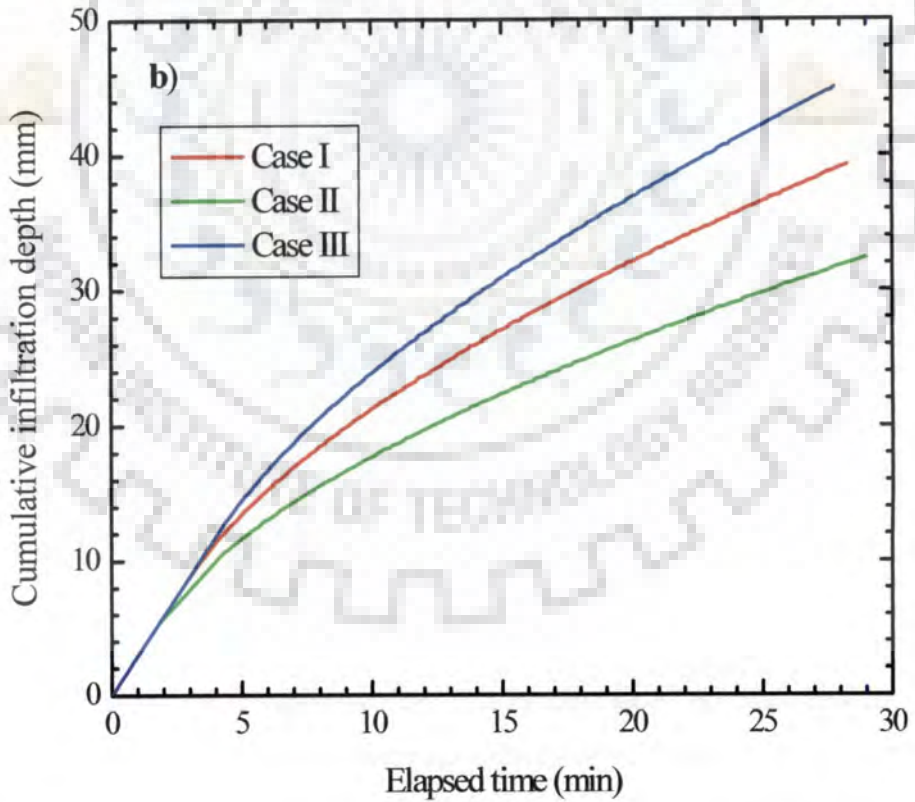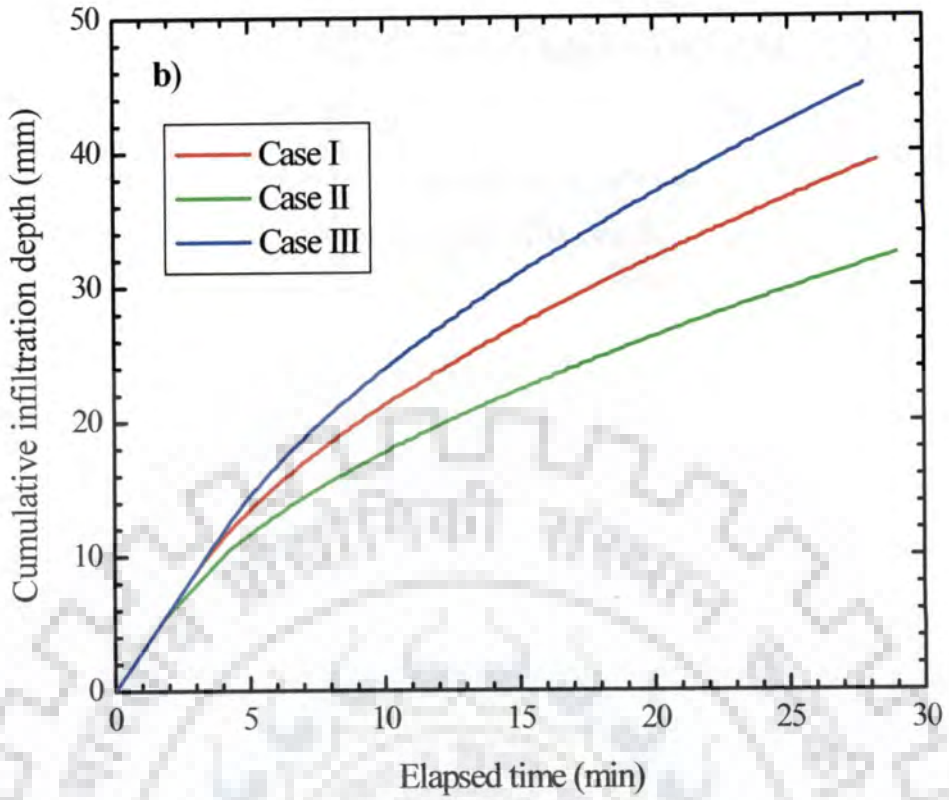
Figure 6.2 Infiltration rate and cumulative infiltration depth at the end of the overland flow plane for the three scenarios of spatial heterogeneity.
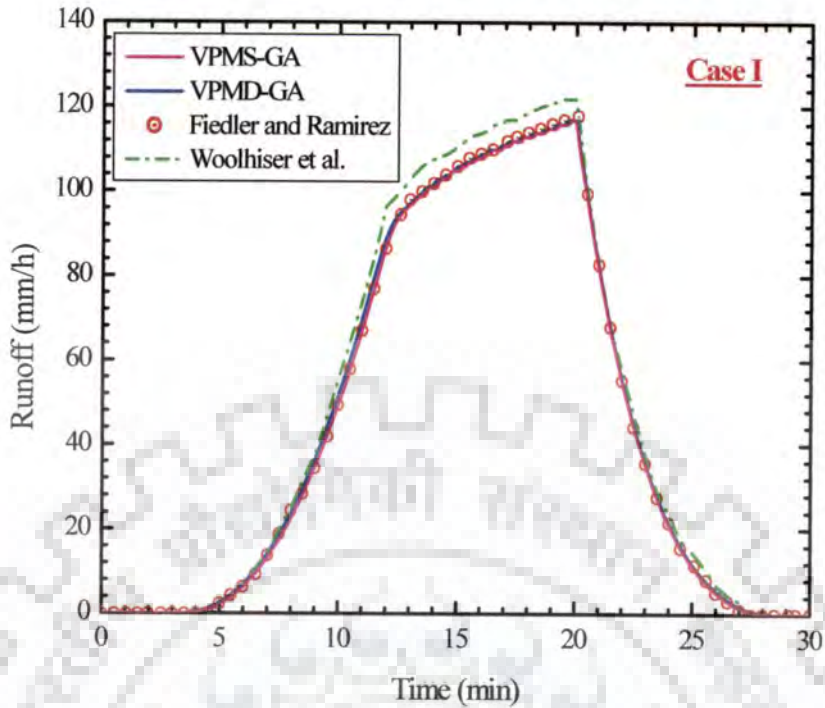
Figure 6.3 Comparison of the simulated runoff hydrographs by the VPMD-GA and VPMS-GA models from an infiltrating overland flow plane for Case I (uniform K_s).
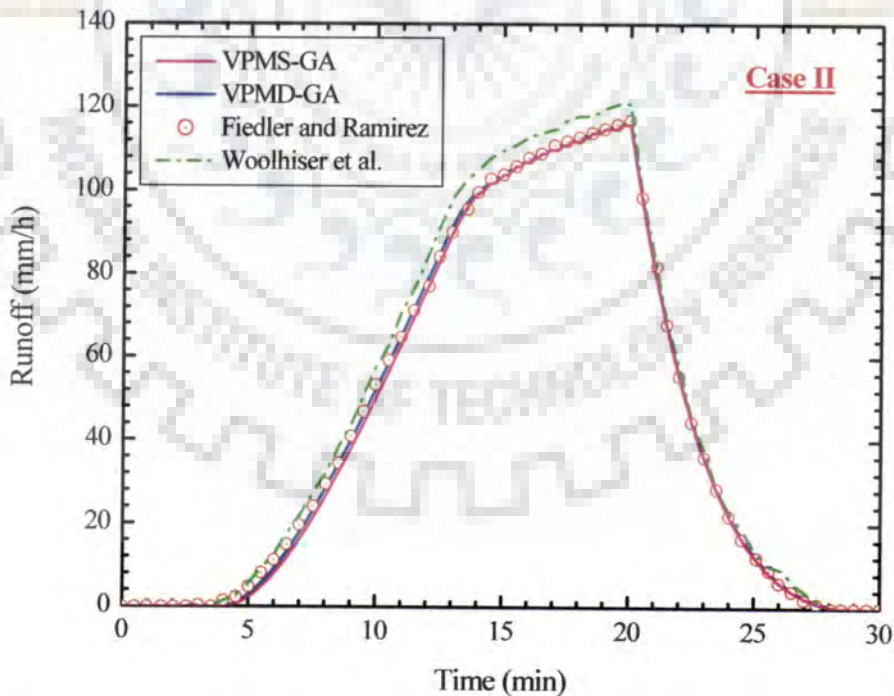
Figure 6.4 Comparison of the simulated runoff hydrographs by the VPMD-GA and VPMS-GA models from an infiltrating overland flow plane for Case II (K_s decreasing downslope).
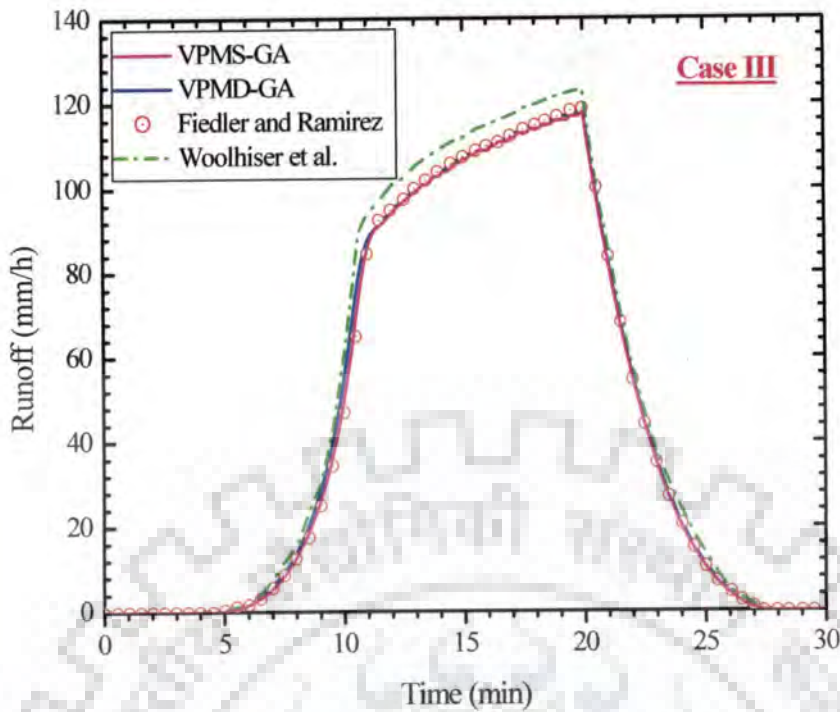
Figure 6.5 Comparison of the simulated runoff hydrographs by the VPMD-GA and VPMS-GA models from an infiltrating overland flow plane for Case III (K_s increasing downslope).

The various applicability criteria measures estimated corresponding to the equilibrium runoff discharges for all the three cases are presented in Table 6.2. It is seen from Table 6.2 that, for all the three cases considered herein, the flow regimes are well within the kinematic wave applicability range resulting in a close match between the simulation results of the VPMD-GA, VPMS-GA, and KW models as illustrated in Figures 6.3-6.5. Similarly, the estimates of different performance evaluation measures of the VPMD-GA and VPMS-GA models computed using the benchmark hydrodynamic model are presented in Tables 6.3 and 6.4, respectively. It can be seen from Tables 6.3 and 6.4 that the performances of the VPMD-GA and VPMS-GA models are very close to those of the benchmark hydrodynamic model with $n_q > 99.5\%$. The *CRM* estimates for both the models are nearly zero. Similarly, the *CD* estimates are very close to 1, representing the simulation accuracy of the proposed models with that of the benchmark model. The VPMD-GA and VPMS-GA models are capable of conserving the runoff volume very efficiently with $|EVOL| < 0.6\%$ and $|EVOL| < 1.5\%$, respectively, for both the cases of I and III. However, in Case II, *EVOL* is slightly higher which may be attributed to the type of coupling approach used between the surface and sub-surface flow models as the sink/source type coupling approach

Table 6.2 Estimated applicability criteria computed at the downstream end of the overland plane using VPMD-GA and VPMS-GA overland flow routing models for three cases of spatial heterogeneity

Case	Grid Ratio (m/s) $(\Delta x / \Delta t)$	Max. Celerity (m/s) c_{max}	Applicability Criteria					
			VPMD-GA			VPMS-GA		
			k	kF^2_{rp}	F_{rp}	k	kF^2_{rp}	F_{rp}
I	0.05	0.193	1450.93	141.41	0.31	1449.03	141.69	0.31
II	0.05	0.193	1458.17	141.89	0.31	1455.67	142.17	0.31
III	0.05	0.194	1440.73	140.71	0.31	1439.42	140.99	0.31

Table 6.3 Performance evaluation measures of the VPMD-GA model for three cases of spatial heterogeneity

Case	Δx (m)	Δt (s)	Performance Evaluation Criteria VPMD-GA				Error in Computed Peak Discharge and Time to Peak					
			η_q (%)	CRM (%)	CD	EVOL (%)	q_{pc} (cm/h)	t_{pc} (min)	q_{po} (cm/h)	t_{po} (min)	q_{perr} (%)	t_{perr} (min)
I	0.5	10	99.96	-0.57	1.01	-0.11	11.72	20.00	11.76	20.00	-0.32	0.00
II	0.5	10	99.96	0.41	0.99	-5.22	11.68	20.00	11.74	20.00	-0.53	0.00
III	0.5	10	99.85	-0.96	1.01	0.58	11.80	20.00	11.88	20.00	-0.68	0.00

q_{pc} = computed peak runoff by the proposed model; t_{pc} = computed time to peak runoff by the proposed model; q_{po} = computed peak runoff by the benchmark model; t_{po} = computed time to peak runoff by the benchmark model.

adopted herein may lead to some error in volume conservation. Further, this coupling approach does not guarantee very efficient volume conservation as in the case of the fully interactive coupling approach. The q_{perr} estimates show that the VPMD-GA and VPMS-GA models performs with $|q_{perr}| < 0.7\%$ and $|q_{perr}| \leq 1.0\%$, respectively, with $t_{perr} = 0$. Overall, it is surmised that the proposed VPMD-GA and VPMS-GA models are capable of modelling the Hortonian runoff process accurately. A comparative analysis of the performances of the VPMD-GA and VPMS-GA models shows that the latter model gives higher model efficiency (n_q) for the Cases-I and III, whereas for the Case II, the former model has better efficiency than the latter model. However, the VPMS-GA model shows slightly higher errors in the volume conservation ($EVOL$) and peak runoff discharge (q_{perr}) estimation as compared to the VPMD-GA model (see Tables 6.3 and 6.4).

6.7 SENSITIVITY ANALYSIS OF THE VPMD-GA AND VPMS-GA METHODS WITH COMPUTATIONAL GRID SIZES

The hydrologic behavior of a catchment is often approximated by employing the spatial and temporal lumping to reduce the data intensiveness of the distributed models. Hence, the timescales of surface runoff and infiltration processes have an important implication on the runoff generation process. Very rapid changes take place in soil infiltration and surface runoff processes and, thus, the timescale of the order of a few seconds or minutes is necessary to capture the micro-scale variability in the surface runoff flow dynamics [*Smith and Goodrich*, 2005]. Therefore, one of the most important steps in the simulation of overland flow with the VPMD-GA and VPMS-GA models is to determine the proper computational grid sizes to avoid inaccuracy of the solution.

6.7.1 Effect of Spatial Grid Sizes on the Performance of the VPMD-GA and VPMS-GA Methods

In order to examine the sensitivity of the VPMD-GA method to the computational spatial grid sizes, different space intervals ranging from 0.25–10.00 m are considered at a fixed

time interval of $\Delta t = 10$ s for all the numerical experiments. Figure 6.6 shows the simulation results of the VPMD-GA model at different spatial intervals. It can be surmised from Figure 6.6 that the simulated hydrographs are insensitive to different spatial intervals used when $\Delta x < 5$ m. However, with $\Delta x = 5$ m and $\Delta x = 10$ m, there is slight underestimation of the runoff hydrographs, as illustrated in Table 6.5. It can be inferred from the analysis of different performance evaluation measures illustrated in Table 6.5 that the accuracy of the VPMD-GA model is lower when $\Delta x = 5$ m and $\Delta x = 10$ m. However, it is interesting to note that although the performance of the VPMD-GA model is poor with these two spatial grid sizes, it is subjected to less volume conservation error which may be attributed to an increased estimates of the infiltrated volume; because, the use of larger Δx in the surface runoff computations using the VPMD method usually results in the overestimation of the predicted runoff volume. Hence, the difference in the effective rainfall volume and total combined volume of the computed runoff and accumulated infiltration is small as compared to those with the use of small space intervals in the computations.

Similarly, Figure 6.7 shows the simulation results of the VPMS-GA model for different computational spatial grid sizes. It can be surmised from Figure 6.7 and Table 6.6 that the same inference drawn from the analysis of the VPMD-GA model is also applicable for the VPMS-GA model. A comparative analysis of the VPMD-GA and VPMS-GA models as envisaged from Figures 6.6 and 6.7 and, Tables 6.5 and 6.6 reveal that the VPMD-GA model allows for using a slightly larger computational space step than that of the VPMS-GA model. The selection of a spatial grid size of $\Delta x < 5$ m can be considered appropriate for VPMS-GA routing study also.

6.7.2 Effect of Temporal Grid Sizes on the Performance of the VPMD-GA and VPMS-GA Methods

The sensitivity of the VPMD-GA and VPMS-GA models for different computational temporal grid sizes ranging from $5 - 90$ s is evaluated considering a fixed space step. Figure 6.8 shows the solution of the VPMD-GA model for different temporal grid sizes. It can be
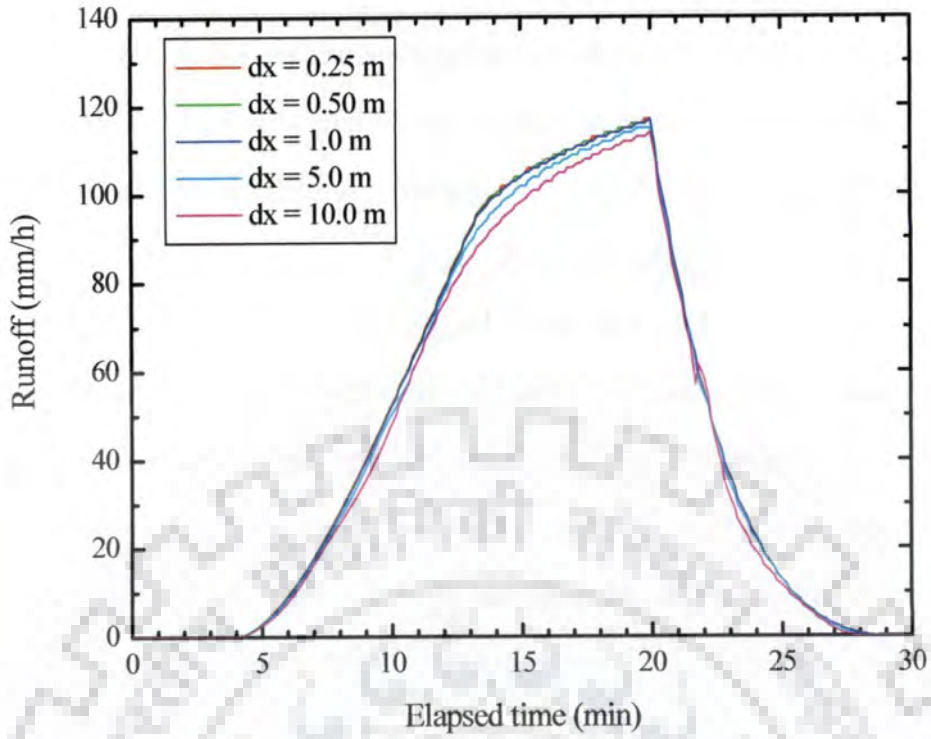
Figure 6.6 Effect of computational spatial grid sizes on the accuracy of the VPMD-GA model
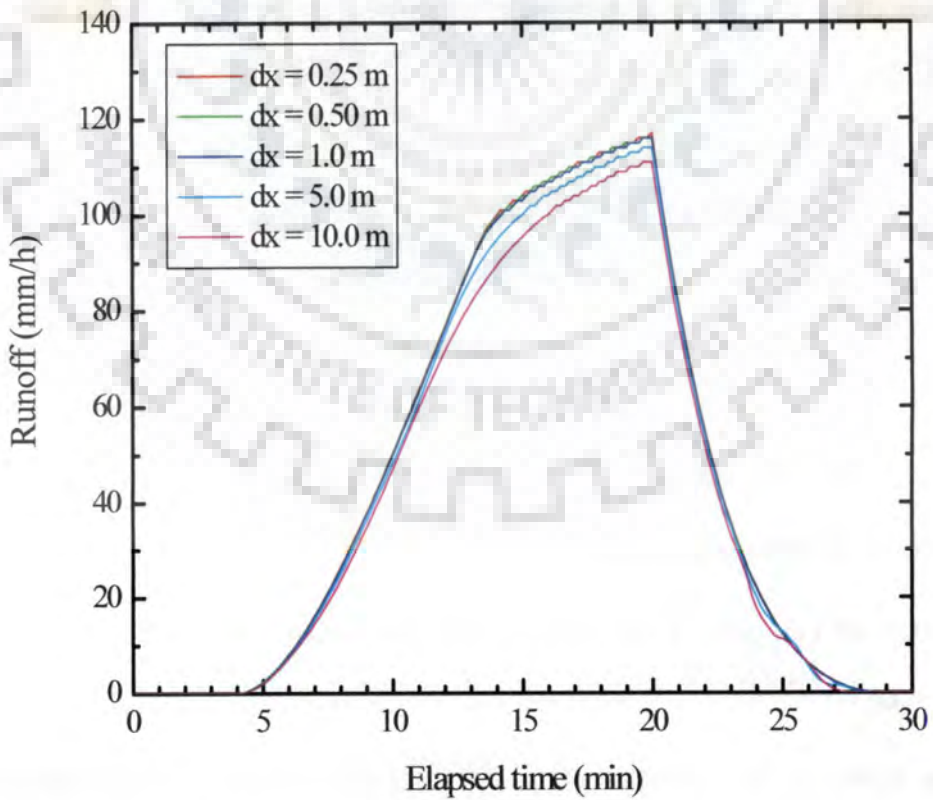
Figure 6.7 Effect of computational spatial grid sizes on the accuracy of the VPMS-GA model

Table 6.4 Performance evaluation measures of the VPMS-GA model for three cases of spatial heterogeneity

Case	Δx (m)	Δt (s)	Performance Evaluation Criteria				Error in Computed Peak Discharge and Time to Peak					
			VPMS-GA									
			η_q (%)	CRM (%)	CD	EVOL (%)	q_{pc} (cm/h)	t_{pc} (min)	q_{po} (cm/h)	t_{po} (min)	q_{perr} (%)	t_{perr} (min)
I	0.5	10	99.98	0.38	1.02	-1.29	11.68	20.00	11.80	20.00	-0.97	0.00
II	0.5	10	99.88	1.99	1.00	-6.50	11.64	20.00	11.74	20.00	-0.85	0.00
III	0.5	10	99.97	0.45	1.01	-0.87	11.76	20.00	11.88	20.00	-1.01	0.00

Table 6.5 Effect of computational spatial grid sizes on the performance of the VPMD-GA model

Δx (m)	$\dfrac{\Delta x}{\Delta t}$	c_{max}	Performance Evaluation Criteria				Error in Computed Peak Discharge and Time to Peak					
			VPMD-GA									
			η_q (%)	CRM (%)	CD	EVOL (%)	q_{pc} (cm/h)	t_{pc} (min)	q_{po} (cm/h)	t_{po} (min)	q_{perr} (%)	t_{perr} (min)
0.25	0.025	0.193	99.96	0.27	0.99	-5.20	11.68	20.00	11.74	20.00	-0.47	0.00
0.50	0.050	0.193	99.96	0.41	0.99	-5.22	11.68	20.00	11.74	20.00	-0.53	0.00
1.00	0.100	0.192	99.96	0.66	1.00	-5.21	11.66	20.00	11.74	20.00	-0.64	0.00
5.00	0.500	0.188	99.85	2.67	1.03	-4.95	11.55	20.00	11.74	20.00	-1.65	0.00
10.00	1.000	0.183	99.41	5.61	1.07	-4.64	11.37	20.00	11.74	20.00	-3.12	0.00

Table 6.6 Effect of computational spatial grid sizes on the performance of the VPMS-GA model

Δx (m)	$\dfrac{\Delta x}{\Delta t}$	c_{max}	Performance Evaluation Criteria				Error in Computed Peak Discharge and Time to Peak					
			VPMS-GA									
			η_q (%)	CRM (%)	CD	EVOL (%)	q_{pc} (cm/h)	t_{pc} (min)	q_{po} (cm/h)	t_{po} (min)	q_{perr} (%)	t_{perr} (min)
0.25	0.025	0.193	99.89	1.81	1.00	-6.29	11.66	20.00	11.74	20.00	-0.71	0.00
0.50	0.050	0.193	99.88	1.99	1.00	-6.50	11.64	20.00	11.74	20.00	-0.85	0.00
1.00	0.100	0.192	99.86	2.32	1.00	-6.98	11.61	20.00	11.74	20.00	-1.08	0.00
5.00	0.500	0.187	99.58	4.92	1.05	-10.62	11.42	20.00	11.74	20.00	-2.75	0.00
10.00	1.000	0.181	98.70	8.70	1.12	-15.54	11.15	20.00	11.74	20.00	-5.03	0.00

Table 6.7 Effect of computational temporal grid sizes on the performance of the VPMD-GA model

Δt (m)	$\dfrac{\Delta x}{\Delta t}$	c_{max}	Performance Evaluation Criteria				Error in Computed Peak Discharge and Time to Peak					
			VPMD-GA									
			η_q (%)	CRM (%)	CD	EVOL (%)	q_{pc} (cm/h)	t_{pc} (min)	q_{po} (cm/h)	t_{po} (min)	q_{perr} (%)	t_{perr} (min)
5	0.050	0.193	99.95	0.93	0.99	-5.37	11.68	20.00	11.74	20.00	-0.47	0.00
10	0.025	0.193	99.96	0.27	0.99	-5.20	11.68	20.00	11.74	20.00	-0.47	0.00
30	0.008	0.193	99.88	-2.06	0.99	-4.97	11.69	20.00	11.74	20.00	-0.47	0.00
60	0.004	0.193	99.48	-4.92	1.00	-4.87	11.69	20.00	11.74	20.00	-0.46	0.00
90	0.003	0.193	99.21	-2.40	0.99	-9.30	11.60	19.50	11.74	20.00	-1.19	-0.50
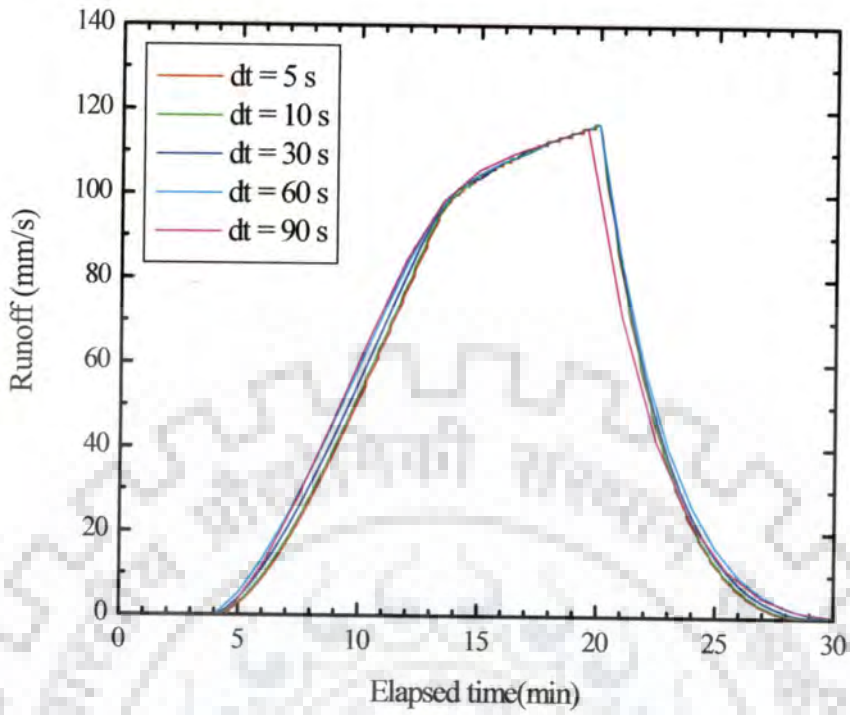
Figure 6.8 Effect of computational temporal grid sizes on the accuracy of the VPMD-GA model.
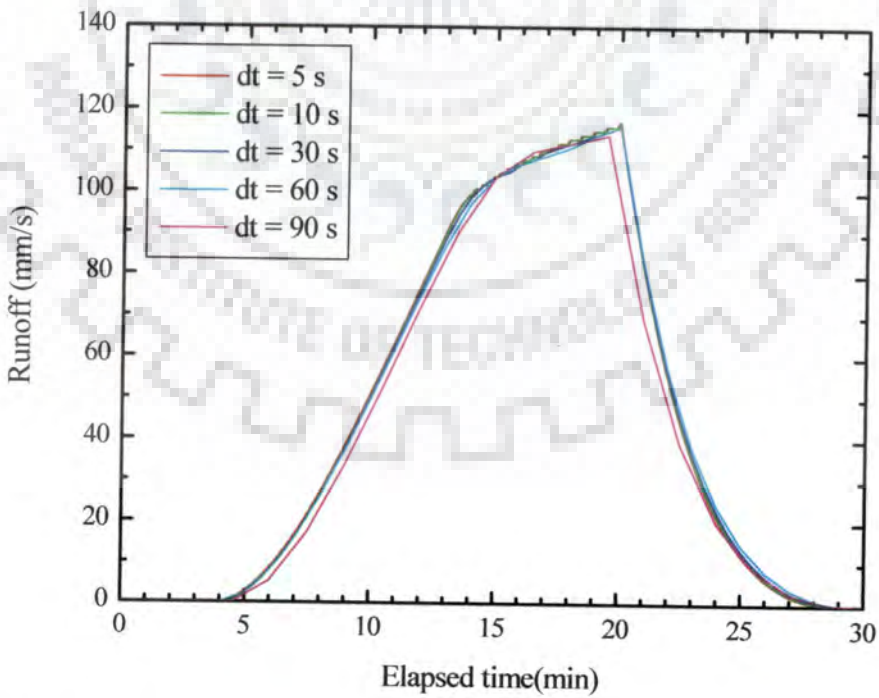
Figure 6.9 Effect of computational temporal grid sizes on the accuracy of the VPMS-GA model.

Table 6.8 Effect of computational temporal grid sizes on the performance of the VPMS-GA model

Δt (m)	$\dfrac{\Delta x}{\Delta t}$	c_{max}	Performance Evaluation Criteria				Error in Computed Peak Discharge and Time to Peak					
			VPMS-GA									
			η_q (%)	CRM (%)	CD	EVOL (%)	q_{pc} (cm/h)	t_{pc} (min)	q_{po} (cm/h)	t_{po} (min)	q_{perr} (%)	t_{perr} (min)
5	0.05	0.193	99.92	1.54	0.99	-5.66	11.67	20.00	11.74	20.00	-0.63	0.00
10	0.03	0.193	99.89	1.81	1.00	-6.29	11.66	20.00	11.74	20.00	-0.71	0.00
30	0.01	0.193	99.85	1.85	1.01	-7.17	11.62	20.00	11.74	20.00	-0.99	0.00
60	0.00	0.193	99.76	1.80	1.02	-8.51	11.62	20.00	11.74	20.00	-1.04	0.00
90	0.00	0.191	98.87	6.91	1.03	-14.22	11.39	19.50	11.74	20.00	-2.98	-0.50

seen from Figure 6.8 that the larger computational temporal grid sizes results in shifting of the simulated runoff hydrograph towards left both on the rising and recession limbs. The smaller the temporal grid size, the higher the model accuracy. However, the use of $\Delta t < 30$ s does not show any impact on the accuracy of the solution. This inference can also be seen from the analysis of the performance evaluation measures presented in Table 6.7. It is seen from Table 6.7 that larger the computational temporal grid sizes, the higher the volume conservation error and the error in the peak discharge, and lower the modelling efficiency.

Similarly, Figure 6.9 shows the simulated runoff hydrographs by the VPMS-GA model for various time steps and the performance evaluation measures estimated corresponding to each cases are presented in Table 6.8. It can be envisaged from Figure 6.9 and Table 6.8 that the use of larger time steps results in the underestimation of the runoff hydrograph. Further, the use of computational time interval $\Delta t \leq 60$ s does not show any impact on the accuracy of the solutions of the VPMS-GA model. It can be surmised from Figures 6.8 and 6.9 that both these models exhibit opposite behaviors to the variation of time steps, in which the VPMD-GA model overestimates the runoff and the VPMS-GA model underestimates the runoff with the increase of the temporal grid sizes. A comparative study of Tables 6.7 and 6.8 reveals that the VPMS-GA model allows for using a larger temporal grid size than that of the VPMD-GA model for achieving the same model efficiency.

6.8. SUMMARY AND CONCLUDING REMARKS

This chapter presents the application of the variable parameter Muskingum discharge-hydrograph (VPMD) and variable parameter Muskingum stage-hydrograph (VPMS) overland flow routing models for simulating the Hortonian overland flow by coupling with the Green-Ampt (GA) infiltration model. These models, respectively, termed as the VPMD-GA and VPMS-GA overland flow models are tested for three spatial heterogeneity conditions of infiltration viz., uniform, linearly decreasing and linearly increasing soil saturated hydraulic conductivity along the downslope direction. The simulation results of the conjunctive VPMD-GA and VPMS-GA Hortonian overland flow routing models reveal that these models are capable of closely reproducing the solutions of the hydrodynamic and characteristic-based kinematic wave models accounting for the spatial heterogeneity in the form of varied soil hydraulic conductivity. Furthermore, the developed models are very simple to formulate, unconditionally stable and accurate. The VPMD-GA model allows for using slightly a larger computational space grid size than the VPMS-GA model, whereas the

latter model allows for using a larger computational temporal grid size as compared to the former model to achieve the same level of model efficiency. Consequently, it is concluded that both the proposed models provide relatively wide flexibility in the computational grid size selection. Hence, these features of both the models hold a great promise for their coupling with the meso and micro scale catchment modelling.

7 CONCLUSIONS AND RECOMMENDATIONS FOR FUTURE STUDIES

7.1 GENERAL

The motivation for the present study formed from the realizations: 1) that the Variable Parameter Muskingum-Cunge (VPMC) method primarily developed for routing floods in channels, when suitably modified for accounting lateral flow in the form of rainfall has been found to be applicable for overland flow modelling and perform much better than the conventional numerical method based overland flow solution schemes in many aspects, by overcoming the problems of stability, convergence, numerical dispersion and the solutions being independent of spatial grid sizes used; and 2) the Variable Parameter Muskingum Discharge (VPMD) hydrograph and the Variable Parameter Muskingum stage (VPMS) hydrograph channel routing methods have been found to have much wider applicability limits than the VPMC method for routing flood hydrographs in channels, besides conserving mass. Taking cue from these realizations, it was surmised that both the VPMD and the VPMS methods when suitably modified for accounting rainfall along the reach may also have wider applicability limits than the corresponding VPMC method for modelling overland flow phenomenon. Accordingly, the study taken up with this consideration resulted in the development of the VPMD and VPMS solution schemes suitable for overland flow modelling using discharge and flow depth, respectively, as the operating variables. Apart from the objectives of development and extensive testing of these two models for hypothetical, experimental and field overland flow studies on impervious and pervious planes, the study also aimed at the development of applicability criteria for both of these models. The following are the conclusions arrived at from this study:

7.2 CONCLUSIONS

1. The study on the runoff generation process on impervious overland flow planes and level V-catchments reveals that the VPMD method simulated runoff hydrographs are unconditionally stable and in good agreement with the field and laboratory observed data and with solutions of the Saint-Venant, DW, and KW equations. Moreover, to ensure model accuracy and efficient mass conservation, specified by

the criterion $EVOL \ll 5\%$, the Courant condition for the VPMD method can be set in the range of $0.1 < C_{un} < 10.0$. It is also inferred from this study that it is more appropriate to select the computational grid sizes based on the requirement of the physical processes involved such as infiltration and rainfall variability rather than merely based on the mathematical requirement of the method. Hence, the proposed VPMD method is advantageous over the currently used overland flow models due to its structural simplicity, unconditional numerical stability, wide applicability, by fully covering the KW range and well into the DW range, and good accuracy of the solution even with the use of larger computational grid sizes, much larger than those employed in the conventional numerical solution based overland flow models.

2. Similarly, the VPMS overland flow method is found to be numerically stable, CPU run time efficient and accurate as compared to the field and laboratory observed data, hypothetical solutions of the SVE, DW, and KW equations. When applied beyond the KW range and well into the applicability range of the DW model, the VPMS method is also found to yield a better solution than the conventional numerical solution based overland flow models. To ensure the performance similar to the VPMD method, in preserving accuracy, and mass conservation specified by the criterion $EVOL \ll 5\%$, the Courant condition for the VPMS method can also be set in the range of $0.1 < C_{un} < 10.0$. A comparative study of the VPMS and VPMD overland flow methods reveals that the applicability range of the VPMS method is lower than the VPMD method. Moreover, the applicability limits of these methods are sensitive to the magnitude of overland flow depth that plays an important role in the flow dynamics. The VPMD method allows for using relatively a larger spatial grid size and a smaller temporal grid size than the VPMS method. The most pertinent features of the proposed VPMS method is its unconditional numerical stability, structural simplicity, and flexibility for a wide range of computational space and temporal grid sizes without compromising the accuracy of the method. Besides, like the VPMD method, the VPMS method is also computationally inexpensive and less data intensive in comparison with the currently used methods.

3. A novel applicability criterion, based on the magnitude of the dimensionless longitudinal flow depth gradient, $(1/s_0)(\partial y/\partial x)_e$, can be considered as a universal applicability criterion for quantifying and assessing the applicability limits of the

VPMD and VPMS overland flow routing methods and this criterion is commonly used in literature for classifying river flood waves. This applicability criterion can be an efficient one than the conventional applicability criteria, viz., KW number (k), Froude number (F_{rp}), and $(kF_{rp}^2)_e$. This study reconfirms the work of *Daluz Viera* [1983] that the DW equation for overland flow modelling is applicable only when $\mu \ll 2.0$, where $(kF_{rp}^2)_e = 1/\mu$. Further, the physical basis of the parameter 'μ' is established as: $\mu = (m+1)(1/s_0)(\partial y/\partial x)_e$, where m is the exponent of the Manning's (⅔) or Chezy's (½) friction law used, which also brings out the fact that the applicability criteria is a function of the friction law used. Considering 95% accuracy levels in model efficiency (N-S efficiency), volume conservation and in the peak runoff computations, the study reveals that when the complete and partial runoff hydrograph simulation cases are considered, the following applicability limits may be specified for these methods:

   i) VPMD method : $(1/s_0)(\partial y/\partial x)_e \leq 0.6$; and

   ii) VPMS method: $(1/s_0)(\partial y/\partial x)_e \leq 0.35$.

However, the corresponding applicability limits prescribed by *Perumal and Sahoo* [2007] for the VPMD and VPMS river flood routing methods (only for the discharge computation) without accounting for lateral flow contribution are 0.43 and 0.63, respectively. Such opposite characteristics of the applicability limits specified for the two approaches for routing in rivers and on overland flow planes may be attributed to the scale problem related to the magnitude of flow and that of the corresponding inertial and pressure gradient terms associated with these two phenomena. This inference is in corroboration with the inference arrived at by *Richardson and Julien* [1994] on the magnitude of different terms in the momentum equation while assessing the suitability of various overland and flood routing models. The VPMD method is able to model the overland flow in the close applicability range of the DW equations including the full applicability range of the KW equations; whereas, the VPMS method has a higher applicability limit than the KW equations, but less than that of the VPMD method.

4. It is inferred from this study that both the VPMD-GA and VPMS-GA methods are capable of modelling the Hortonian overland flow generation process effectively

accounting for the spatial heterogeneity in the form of varying hydraulic conductivity of the soil.

7.3 RECOMMENDATIONS FOR FUTURE STUDIES

The VPMD and VPMS overland flow routing methods possess a great potential to handle the flow regimes under varied field conditions where the downstream boundary conditions do not restrict their application. The limitations of the variable parameter Muskingum method in discharge and flow depth formulations proposed herein forms the basis for the future improved modifications as presented below.

1. The VPMD and VPMS simplified flood routing methods may be improved further by accounting the downstream boundary conditions in an approximate manner.

2. Taking cue from the study of *Perumal and Sahoo* [2007] that the applicability limits of the VPMD and VPMS routing methods are much higher than that of the VPMC method when applied for channel routing, the present study did not investigate the capabilities of the VPMC method for overland flow modelling in the manner as conducted herein for the VPMD and VPMS methods. Therefore, to arrive at a conclusive inference about the applicability limits of the VPMC method for overland flow modelling, a detailed investigation may be taken up to compare the performance of the VPMC, VPMD and VPMS methods for overland flow modelling.

3. The VPMD and VPMS methods are investigated only for the event based runoff simulation at the end of the unit width flow plane and at the outlet of the level V-catchment which could be extended for the continuous simulation of runoff and other hydrological processes (e.g., sediment transportation, distributed pollution modelling, etc.) in real world river basin studies and in hydrological land-surface schemes of the climate change models to ascertain their efficacy.

4. These methods could also be extended for surface irrigation modelling studies.

REFERENCES

1. Ababou, R., and Tr´egarot, G. (2002). Coupled modeling of partially saturated flow: macroporous media, interfaces, variability. In *Proceedings XIV Inter. Conf. on Computational Methods in Water Resources*, pp.8, Elsevier, Amsterdam, The Netherlands.

2. Abbott, M. B. (1979), *Computational Hydraulics: Elements of the Theory of Free Surface Flows*, 321 pp., Pitman Publishing Ltd., London.

3. Abbott, M. B., J. C. Bathurst, J. A. Cunge, P. E. O'Connell, and J. Rasmussen (1986a), An introduction to the European Hydrological System - Systeme Hydrologique Europeen, "SHE", 1: History and philosophy of a physically-based, distributed modeling system, *J. Hydrol., 87*, 45-59.

4. Abbott, M. B., J. C. Bathurst, J. A. Cunge, P. E. O'Connell, and J. Rasmussen (1986b), An introduction to the European Hydrologic System – System's Hydrologique Europeen "SHE"; 2. Structure of a physically based distributed modeling system, *J. Hydrol., 87*, 61-72.

5. Afouda, A. A. (1980a), Analysis of the rainfall-runoff transformation process, *Nordic Hydrol., 11*, 93-112.

6. Afouda, A. A. (1980b), A generalized kinematic approach to basin modeling, *Inter. Assoc. of Hydrol. Sci., Publ. 129*, pp. 105-114, Wallingford U. K.

7. Akan, A. O. (1988), Overland flow on pervious, converging surface, *Nordic Hydrol., 19*, 153-164.

8. Akan, A. O., and B. C. Yen, (1981). Mathematical model of shallow water flow over porous media, *J. Hydraul. Div., ASCE, 107*(4), 479-494.

9. Al-Mashidani, G., and C Taylor (1974), Finite element solutions of the shallow water equations- surface run-off, in Proc. Int. Symp. on Finite Element Methods in Flow Problems,Univ. of Alabama Press, Huntsville, Alabama.

10. Apollov, B. A., G. P. Kalinin, and V. D. Komarov (1964), Hydrological forecasting, translated from Russian, Israel Program for Scientific Translations, Jerusalem.

11. ASCE Task Committee (2000), Artificial neural networks in hydrology, 2. Hydrologic applications, *J. Hydrol. Engg., ASCE*, 5 (2), 124–137.

12. ASCE Task Committee on Definition of Criteria for Evaluation of Watershed Models of the Watershed Management Committee, Irrigation and Drainage Division (1993), Criteria for evaluation of watershed models, *J. Irrig. Drain. Engg., ASCE, 119*(3), 429-442.

13. Barros, A. P., and J. D. Colello (2001), surface roughness for shallow overland flow on crushed stone surfaces, *J. Hydraul. Eng.,ASCE, 127(1)*, 38-52.

14. Bathurst, J. S. (1986), Physically-based distributed modeling of an upland catchment using the Syst'eme Hydrologique Europ'een, *J. Hydrol., 87*, 79-102.

15. Bathurst J. C., J. M. Wicks, and P. E. O'Connell (1995), The SHE/SHESED basin scale water flow and sediment modelling system, in *Computer Models of Watershed Hydrology*, edited by V. P. Singh, pp. 563-594, Water Resources Publications, Highlands Ranch, Colo.

16. Bergström, S. (1991), Principles and confidence in hydrological modelling, *Nordic Hydrol., 22*, 123-136.

17. Beven, K. (1989), Changing ideas in hydrology–the case of physically based models, *J. Hydrol., 105*, 157–172.

18. Beven, K. (1993), Prophecy, reality and uncertainty in distributed hydrological modelling, *Adv. Water Resour., 16*(1), 41-51.

19. Beven, K. (2001), How far can we go in distributed hydrological modelling? *Hydrol. Earth Syst. Sci.*, 5, 1-12.

20. Beven, K. (2002a), Towards an alternative blue print for a physically based digitally simulated hydrologic response system, *Hydrol., Process., 16*, 189-206.

21. Beven, K. (2002b), Toward a coherent philosophy for modelling the environment, *Proc. R. Soc. Lon. A, 458*, 1-20.

22. Beven, K. J., and M. J. Kirkby (1979), A physically based variable contributing area model of basin hydrology, *Hydrol. Sci. Bull., 24*(1), 43-69.

23. Bhadra, A., N. Panigrahy, R. Singh, N. S. Raghuwanshi, B. C. Mal, M. P. Tripathi (2008), Development of a geomorphological instantaneous unit hydrograph model for scantily gauged watersheds, *Envir. Modelling & Software* 23, 1013-1025.

24. Brath, A., and A. Montanari (2003), Sensitivity of the peak flows to the spatial variability of the soil infiltration capacity for different climatic scenarios, *Phy. and Chem. Earth, 28*, 247–254.

25. Cameron, D., P. Kneale, and L. See (2002), An evaluation of a traditional and a neural net modeling approach to flood forecasting for an upland catchment, *Hydrol. Process., 16*, 1033-1046.

26. Camporese, M., C. Paniconi, M. Putti, and S. Orlandini (2010), Surface-subsurface flow modeling with path-based runoff routing, boundary condition-based coupling, and assimilation of multisource observation data, *Water Resour. Res., 46*, W02512, doi:10.1029/2008WR007536.

27. Carpena, R. M., C. T. Miller, and J. E. Parsons (1993), A quadratic-Garlerkin solution for kinematic wave overland flow, *Water Resour. Res., 29*(8), 2615-2627.

28. Castaings, W., D. Dartus, F.-X. Le Dimet, and G.-M. Saulnier (2009), Sensitivity analysis and parameter estimation for distributed hydrological modeling: potential of variational methods, *Hydrol. Earth Syst. Sci., 13*, 503-517.

29. Castillo, V. M., A. Gómez-Plaza, and M. Martinez-Mena, (2003), The role of antecedent soil water content in the runoff response of semiarid catchments: a simulation approach, *J. Hydrol., 284*, 114-130.

30. Chang, F.-J., and Y.-C. Chen (2001), A counterpropagation fuzzy-neural network modeling approach to real time streamflow prediction, *J. Hydrol., 245*, 153–164.

31. Chen, L., and M. H. Young (2006), Green-Ampt infiltration model for sloping surfaces, *Water Resour. Res.*, *42*, W07420, 1-9, doi:10.1029/2005WR004468.

32. Chow ,V. T. (1959), *Open-Channel Hydraulics*, 680 pp., McGraw-Hill, New York, USA.

33. Chow, V. T., D. R. Maidment, and L. W. Mays (1988), *Applied Hydrology*, 572 pp., McGraw-Hill Book Co., Singapore.

34. Chu, S. T. (1978), Infiltration during an unsteady rain, *Water Resour. Res.*, *14*(3), 461-466.

35. Chu, S. T. (1995), Effect of initial water content on Green-Ampt parameters, *Trans. ASAE*, *38*, 839-841.

36. Chua, L. H. C., T. S. W. Wong, and L. K. Sriramula (2008), Comparison between kinematic wave and artificial neural network models in event-based runoff simulation for an overland plane, *J. Hydrol.*, *357*, 337-348.

37. Craya, A. (1952), The criterion for the possibility of roll wave formation, Gravity Waves, *Circ.* 521, pp. 141-151, Natl. of Stand. And Technol., Gaithersburg, Md.

38. Croley, T. E., II, and B. Hunt (1981), Multiple-valued and non-convergent solutions in kinematic cascade models. *J. Hydrol.*, *49*, 121-138.

39. Cunge, J. A. (1969), On the subject of a flood propagation method (Muskingum method), *J. Hydraul. Res.*, *7*(2), 205-230.

40. Daluz Vieira, J. H. (1983), Conditions governing the use of approximations for the St. Venant Equations for shallow surface-water flow, *J. Hydrol.*, *60* (1-4), 43-58.

41. DiGiammarco, P., E. Todini, and P. A. Lamberti (1996), Conservative finite element approach to overland flow: the control volume finite element formulation, *J. Hydrol.*, *175*, 267–91.

42. Dooge, J. C. I. (1973), Linear theory of hydrologic systems, USDA, *Agric. Res. Serv., Tech. Bull., No.1468.*

43. Dooge, J. C. I., and B. M. Harley (1967), Linear routing in uniform open channel, paper presented at Int. Hydrol. Symp. Vol. 1, pp. 57–63., Fort Collins, Colorado, USA.

44. Dooge, J. C. I., and J. J. Napiórkowski (1987), Applicability of diffusion analogy in flood routing, *Acta Geophysica Polonica, 35*(1), 66–75.

45. Dooge, J .C. I., W. G. Strupczewski, and J. J. Napiorkowski (1982), Hydrodynamic derivation of storage parameters of the Muskingum model, *J. Hydrol.*, *54*(4), 371–387.

46. Downer, C. W., and F. L. Ogden (2003). Prediction of runoff and soil moistures at the watershed scale: Effects of model complexity and parameter assignment. *Water Resour.Res.*, *39*(3), 1045, doi:10.1029/2002WR001439.

47. Downer, C. W., F. L. Ogden, W. Martin, R. S. Harmon (2002), Theory, development, and applicability of the surface water hydrologic model CASC2D. *Hydrol. Processes*, *16*, 255-275.

48. Dunne, T. (1983), Relation of field studies and modelling in the prediction of storm runoff, *J. Hydrol. 65*, 25-48.

49. Eagleson P. S. (1970), *Dynamic Hydrology*, 462 pp., McGraw Hill, New York.

50. Engman, E. T. (1986), Roughness coefficients for routing surface runoff, *J. Irrig. Drain. Engg., ASCE, 112*(1), 39-53.

51. Este`ves, M., X. Faucher, S. Galle, M. Vauclin (2000), Overland flow and infiltration modelling for small plots during unsteady rain: numerical results versus observed values, *J. Hydrol., 228,* 265–288.

52. Ferrick, M. G. (1985), Analysis of river wave types, *Water Resour. Res., 21*(2), 209–220.

53. Fiedler, F. R., and J. A. Ramirez (2000), A numerical method for simulating discontinuous shallow flow over an infiltrating surface, *Int. J. Numer. Meth. Fluids, 32,* 219-240.

54. Franchini, M., and P. E. O'Connell (1996), An analysis of the dynamic component of the geomorphologic instantaneous unit hydrograph, *J. Hydrol., 175,* 407-428.

55. Fread, D. L. (1985), Applicability criteria for kinematic and diffusion routing models, Laboratory of Hydrology, National Weather Service, NOAA, U.S. Dept. of Commerce, Silver Spring, Md.

56. Fread D. L. and K. S. Hsu (1993), Applicability of two simplified flood routing methods: Level-pool and Muskingum-Cunge, paper presented at ASCE National Hydraulic Engineering Conference, San Fransisco, CA.

57. Freeze, R. A. (1974), Streamflow generation, *Rev. Geophys., 12,* 627– 647.

58. Freeze, R. A., and R. L. Harlan (1969), Blueprint for a physically based, digitally-simulated hydrologic response model, *J. Hydrol., 9,* 237–258.

59. Gandolf, C., and F. Savi, (2000), A mathematical model for the coupled simulation of surface runoff and infiltration, *J. Agril. Engrg. Res., 75,* 49-55.

60. Gaume, E., and R. Gosset (2003), Over-parameterisation, a major obstacle to the use of artificial neural networks in hydrology? *Hydrol. Earth Syst. Sci., 7,* 693-706.

61. Giannoni, F., G. Roth, and R. Rudari (2000), A semi-distributed rainfall-runoff model based on a geomorphologic approach, *Phys. Chem. Earth (B), 25*(7-8), 665-671.

62. Gill, M. A. (1984), Discussion of "Asymptotic solution for dam-break problem on sloping channel" by B. Hunt, *J. Hydraul. Engg., ASCE, 108*(HY1), 115-126.

63. Gonwa, W. S., and M. L. Kavvas, (1986), A modified diffusion wave equation for flood propagation in trapezoidal channels, *J. Hydrol., 83,* 119–136.

64. Gottardi, G., and M. Venutelli (2008), An accurate time integration method for simplified overland flow models, *Adv. Water Resour., 31*(1), 173-180.

65. Govindaraju, R. S., and M. L. Kavvas (1991), Dynamics of moving overland flows over infiltrating surfaces at hillslopes, *Water Resour. Res., 27*(8), 1885-1898.

66. Govindaraju R. S., S. E. Jones, and M. L. Kavvas (1988a), On the diffusion wave model for overland flow. 1: Solution for steep slopes, *Water Resour. Res., 24*(5), 734–744.

67. Govindaraju R. S., S. E. Jones, and M. L. Kavvas (1988b), On the diffusion wave model for overland flow. 2: Steady state analysis, *Water Resour. Res., 24*(5), 745–754.

68. Govindaraju, R. S., M. L. Kavvas, and S. E. Jones (1990). Approximate analytical solutions for overland flows, *Water Resour. Res., 26*(11), 2903–2912.

69. Govindaraju, R. S., M. L. Kavvas, and G. Tayfur, (1992), A simplified model for two-dimensional overland flows, *Adv. Water Resour., 15*, 133–141.

70. Graham, D. N., and M. B. Butts (2005), Flexible, integrated watershed modelling with MIKE SHE, in *Watershed Models*, edited by V. P. Singh and D. K. Frevert, pp. 245–272, CRC press, Boca Raton, FL.

71. Grayson, R. B., I. D. Moore, and T. A. McMahon (1992), Physically based hydrologic modelling. 2 – Is the concept realistic? *Water Resour. Res., 28*, 2659-2666.

72. Green, W. H., and G. A. Ampt (1911), Studies on soil physics, 1, The flow of air and water through soils, *J. Agri. Sci., 4*(1), 1-24.

73. Gresho P. M., and R. L. Lee (1981), Don't suppress the wiggles-they're telling you something! *Computers and Fluides, 9*(2), 223-255.

74. Gunduz O. (2006), Surface/subsurface interactions: coupling mechanisms and numerical solution procedures, in *Groundwater and Ecosystems*, edited by A. Baba, K. W. F. Howard, and O. Gunduz, pp. 121-130, Springer Netherlands.

75. Gupta, H.V., K. Hsu, and S. Sorooshian (2000), Effective and efficient modeling for streamflow forecasting, in *Artificial Neural Networks in Hydrology*, edited by Govindaraju, R.S, and A. R. Rao, pp. 7–22, Kluwer, Dordrecht.

76. Gyasi-Agyei, Y., F. P. de Troch, and P. A. Troch (1996), A dynamic hillslope response model in a geomorphology, *J. Hydrol., 178*, 1-18.

77. Hager, W. H., and K. Hager (1985), Application limits for the kinematic wave approximation, *Nordic Hydrol., 16*, 203-212.

78. Hayami, S. (1951), On the propagation of flood waves, *Bull. Dis. Preven. Res. Instit.,* Kyoto Univ., Japan, *1*(1), 1–16.

79. He Z., W. Wu, and S. S. Y. Wang (2008), Coupled finite-volume model for 2D surface and 3D subsurface flows, *J. Hydrol. Engg.*, ASCE, *13*(9), 835-845.

80. Heatherman, W. J. (2004), Muskingum–Cunge revisited, *World Water and Environmental Resources Congress 2004, ASCE,* Edited by G. Sehlke, D. F. Hayes, and D. K. Stevens (June 2– July 1, 2004), Salt Lake City, Utah, USA.

81. Heatherman, W. J. (2008), Flood routing on small streams: A review of Muskingum-Cunge, Cascading reservoirs and full dynamic solutions, PhD thesis, Dep. of Civil Engg., Univ. of Kansas, Overland Park, USA.

82. Henderson, F. M. (1966), *Open Channel Flow,* 522 pp., The Macmillan Co., New York.

83. Heng, B. C. P., G. C. Sander, and C. F. Scott (2009), Modeling overland flow and soil erosion on nonuniform hillslopes: A finite volume scheme, *Water Resour. Res., 45*, W05423, doi:10.1029/2008WR007502.

84. Hjelmfelt, A., and M. Wang (1933a), Artificial neural networks as unit hydrograph applicatons, in *Engineering Hydrology—Symposium*, edited by Kuo, C., Hydraulic Division/ASCE, ASCE, San Francisco, CA.

85. Hjelmfelt, A., and M. Wang (1933b), Runoff hydrograph estimation using artificial neural networks, in *Proceedings ASAE Conf.,* edited by Topping, B., A. I. Khan, 18–19 June 1993, ASAE, Spokane, Washington.

86. Hjelmfelt, A., and M. Wang (1993c), Runoff simulation using ANN, in Proc. of the Fourth International Conference in the Application of Artificial Intelligence in Civil and Structural Engineering: NN and Combinatorial Optimization in Civil and Structural Engineering, ASCE, CIVL-COMP'93, edited by Topping, B., A. I. Khan, pp. 517–522, Edinburgh, UK.

87. Holden, A. P., and D. Stephenson (1988), Improved four point solution of the kinematic equations, *J. Hydraul. Res., 26*(4), 413-423.

88. Holden, A. P., and D. Stephenson (1995), Finite difference formulations of kinematic equations, *J Hydraul. Engg., ASCE, 121*(5), 423–426.

89. Holzbecher, E., and O. F. Vasiliev (2005), Coupling aspects of heat and mass transfer, in *Coupled Models for the Hydrological Cycle: Integrating Atmosphere, Biosphere, and Pedosphere*, edited by A. Bronstert et al., pp. 175– 188, Springer, New York.

90. Holzbecher, E., M. Bonnell, A. Bronstert, and O. F. Vasiliev (2005), Fluxes, compartments and ordering of feedbacks, in *Coupled Models for the Hydrological Cycle: Integrating Atmosphere, Biosphere, and Pedosphere*, edited by A. Bronstert et al., pp. 76– 95, Springer, New York.

91. Horton R. E. (1938), The interpretation and application of runoff plate experiments with reference to soil erosion problems, *Soil Sci. Soc. Am. Proc., 1*, 401-437.

92. Hromadka, T. V. and J. J. DeVries (1988), Kinematic wave routing and computational error. *J. Hydrol. Engg., ASCE, 114* (2), 207–217.

93. Hsu, K., X. Gao, and S. Sorooshain, (1997), Precipitation estimation from remotely sensed information using artificial neural network, *J. Applied Meteo., 36*(9), 1176–1190.

94. Hsu, S. M., C. F. Ni, and P. F. Hung (2002), Assessment of three infiltration formulas based on model fitting on Richards's equation, *J. Hydrol. Engrg., ASCE, 7*(5), 373-379.

95. Huang J., and C. C. S. Song (1985), Stability of dynamic flood routing schemes, *J. Hydraul. Engg., ASCE, 111*(12), 1497-1505.

96. Huang G., and G. T. Yeh (2009), Comparative study of coupling approaches for surface water and subsurface interactions, *J. Hydrol. Engg., ASCE, 14*(5), 453-462.

97. Hugo A. L., and A. Huang (2007), Ponding analysis with Green-Ampt infiltration, *J. Irrig. and Drain. Engg., ASCE, 12*(1), 109-112.

98. Hunt B. (1982), Asymptotic solution for dam-break problem, *J. Hydraul. Engg., ASCE, 110*(10), 1515-1516.

99. Iwagaski, Y. (1955), Fundamental studies on the runoff analysis by characteristics, *Bull. Dis. Preven. Res. Instit.*, No.10, 25 pp., Kyoto, Japan.

100. Iwasa, Y. (1954), The criterion for instability of steady uniform flows in open channels, *Memoirs of the Facul. of Engg., Kyoto Univ., Japan, 16*(6), 264-275.

101. Izzard, C. F. (1942), Runoff from flight strips, *Proc. Highway Res. Board, 22*, 94-99.

102. Izzard, C. F. (1944), The surface-profile of overland flow, *Eos Trans. AGU, 25*(VI), 959-968.

103. Jaber, F., and R. H. Mohtar (2001), Stability and accuracy of numerical schemes for overland flow problems, *An ASAE Meeting Presentation 2001, Paper Number: 01-3067.*

104. Jaber, F., and R. H. Mohtar (2002), Dynamic time step for one-dimensional overland flow kinematic wave, *J. Hydrol. Engg., ASCE, 7*(1), 3-11.

105. Jain A., and S. K. V. Prasad Indurthy (2003), Comparative analysis of event-based rainfall-runoff modeling techniques—deterministic, statistical, and artificial neural networks, *J. Hydrol. Engg., ASCE, 8*(2), 93-98.

106. Jain M. K., and V. P. Singh (2005), DEM-based modelling of surface runoff using diffusion wave equation, *J. Hydrol., 302*, 107-126.

107. Jakeman, A. J., and G. M. Hornberger (1993), How much complexity is warranted in a rainfall-runoff model?, *Water Resour. Res., 29*(8), 2637–2649.

108. James, W. P., and K. W. Kim (1990), A distributed dynamic watershed model, *Water Resour. Bull., 26* (4), 587-596.

109. Johnson, D. L., and A. C. Miller (1997), A spatially distributed hydrologic model utilizing raster data structures, *Comp. & Geosci., 23*(3), 267-272.

110. Jolly, J. P., and V. Yevjevich (1971), Amplification criterion of gradually varied, single peaked waves, *Hydrol. Pap.* 51, Colo State Univ., Fort. Collins.

111. Jones, J. P., E. A. Sudicky, and R. G. McLaren (2008), Application of a fully-integrated surface-subsurface flow model at the watershed-scale: A case study. *Water Resour.Res., 44*, W03407, doi:10.1029/2006WR005603.

112. Kampf, S. K. and S. J. Burges (2007), A framework for classifying and comparing distributed hillslope and catchment hydrologic models, *Water Resour. Res., 43*, W05423, doi:10.1029/2006WR005370.

113. Karvonen T., H. Koivusalo, M. Jauhiainen, J. Palko, and K. Weppling (1999), A hydrological model for predicting runoff from different land use areas, *J. Hydrol., 217*, 253–265.b

114. Kazezyılmaz-Alhan, C. M., and M. A. Medina, Jr. (2007), Kinematic and diffusion waves: Analytical and numerical solutions to overland and channel flow, *J. Hydraul. Engg., 133*(2), 217-228.

115. Kazezyılmaz-Alhan, C. M., M. A. Medina, Jr., and P. Rao (2005), On numerical modeling of overland flow, *Appl. Math. and Comp., 166* (3) 724-740.

116. Klemeš, V. (1982), Stochastic models of rainfall-runoff relationship, in *Statistical Analysis of Rainfall and Runoff*, edited by V. P. Singh, *Water Resour. Publications*, Littleton, Colorado.

117. Klemeš, V. (1986), Dilettantism in hydrology: Tradition or destiny? *Water Resourc. Res., 22*, 177S-188S.

118. Kollet, S. J., and R. M. Maxwell (2006), Integrated surface–groundwater flow modeling: A free-surface overland flow boundary condition in a parallel groundwater flow model, *Adv. Water Resour., 29*, 945-958.

119. Koussis, A. D. (1976), An approximate dynamic flood routing method, *Proc. Int. Symp. On Unsteady Flow in Open Channels, Paper L1*, Newcastle-Upon Tyne, U.K.

120. Koussis, A. D. (1978), Theoretical estimation of flood routing parameters, *J. Hydraul. Div., ASCE, 104* (HY1), 109–115.

121. Koussis, A. D. (1980), Comparison of Muskingum method difference schemes, *J. Hydraul. Div., ASCE, 106*(HY5), 925–929.

122. Koussis, A. D. (1983), Unified theory for flood and pollution routing, *J. Hydraul. Eng., ASCE, 109*(HY12), 1652–1664.

123. Kundzewicz, Z. W. (1986), Physically based hydrological flood routing method, *Hydrol. Sci. J., IAHS, 31*(2), 237–261.

124. Lai, Y. G. (2009), Watershed runoff and erosion modelling with a hybrid mesh model, *J. Hydrol. Engg., ASCE, 14*(1), 15-26.

125. Lal, A. M. W. (1998a) Performance comparison of overland flow algorithms, *J. Hydraul. Engg., ASCE, 124*(4), 342–349.

126. Lal, A. M. W. (1998b), Weighted implicit finite-volume model for over- land flow, *J. Hydraul. Engg., ASCE, 124*(9), 941–950.

127. Lamberti P., and S. Pilati (1996), Flood propagation models for real-time forecasting, *J. Hydrol., 175*, 239-265.

128. Langford K. J., and A. K. Turner (1973), An experimental study of the application of kinematic wave theory to overland flow, *J. Hydrol., 18*, 125–145.

129. Laurenson, E. M. (1962), Hydrograph synthesis by runoff routing, *Water Research Laboratory, University of New South Wales Report No. 66.*

130. Liggett, J. A., and D. A. Woolhiser (1967), Difference solutions of the shallow-water equation, *J. Eng. Mech. Div., ASCE, 93*, 39-71.

131. Lighthill, M. J., and G. B. Witham (1955), On kinematic waves: 1. Flood movement in long rivers, *Proc. R. Soc. London, Ser. A, 229*, 281–316.

132. Liong, S. Y., T. R. Gautam, S. T. Khu, V. Babovic, and N. Muttil, (2002), Genetic programming: A new paradigm in rainfall-runoff modeling, *J. Am. Water Resour. Assoc., 38*(3), 705–718.

133. Liu, Q. Q., and V. P. Singh (2004), Effect of microtopography, slope length and gradient, and vegetative cover on overland flow through simulation, *J. Hydrol. Engg., ASCE, 9*(5), 375–382.

134. Liu Q. Q., L. Chen, J. C. Li, and V. P. Singh (2005), Roll waves in overland flow, *J. Hydrol. Engg., ASCE, 10*(2), 110-117.

135. Loague, K. (1990), Changing ideas in hydrology-The case of physically based models-Comment, *J. Hydrol., 120*, 405-407.

136. Loague, K. (1992), Impact of overland flow plane characterization on event simulations with a quasi-physically based rainfall-runoff model, *Water Resour. Res., 28*(9), 2541-2545.

137. Loague, K. M., and R. A. Freeze, (1985), A comparison of rainfall-runoff modelling techniques on small upland catchments, *Water Resour. Res., 21*, 229-248.

138. Loague, K., and R. E. Green (1991), Statistical and graphical methods for evaluating solute transport models: Overview and application, *J. Contaminant Hydrol., 7*, 51–73.

139. Loague K., and J. E. VanderKwaak (2004), Physics-based hydrologic response simulation: platinum bridge, 1958 Edsel, or useful tool, *Hydrol. Process., 18*, 2949–2956.

140. López, J. J., F. N. Gimena, M. Goñi, and U. Agirre (2005), Analysis of a unit hydrograph model based on watershed geomorphology represented as a cascade of reservoirs, *Agril. Water Manag.*, *77*, 128–143

141. Maidment D. R. (1993), *Handbook of Hydrology*, McGraw-Hill, New York.

142. Maksimović, Ć., and M. Radojković (1986), *Urban drainage catchments – selected worldwide rainfall-runoff data from experimental catchments*, pp. 313-330, Pregamon Press, Oxford.

143. McCarthy, G. T. (1938), The unit hydrograph and flood routing, *Conf. North Atlantic Division*, U.S. Army Corps of Engineers, New London, Conn.

144. McCarthy, J., O. Canziani, N. Leary, D. Dokken, and K. White (2002), Climate Change 2001: Impacts, adaptation, and vulnerability, Intergovernmental Panel on Climate Change. Cambridge University Press, Cambridge.

145. Mein, R. G., and C. L. Larson (1971), Modeling of the infiltration component of the rainfall-runoff process, Bull. 43, pp. 21-29, Water Resour. Res. Center, Univ. Minnesota, Minneapolis, Minn.

146. Mein, R. G., and C. L. Larson (1973), Modeling of the infiltration during a steady rain, Water Resour. Res., *9*(2), 384-394.

147. Meng, H., T. R. Green, , J. D. Salas, and L. R. Ahuja, (2008), Development and testing of a terrain-based hydrologic model for spatial Hortonian infiltration and runoff/on, *Envir. Modelling and Software*, *23*(6), 794-812.

148. Merkel, W. (2001), Reference on time of concentration with respect to sheet flow, unpublished manuscript, 17 Dec., 2001, USDA, NRSC, National Water and Climate Centre, Beltsville, MD (www.wsi.nrcs.usda.gov/products/w2q/h%26h/.../Sheet_Flow_**References**.doc).

149. Miller, J. E., and J. A. Cunge (1975), Simplified equations of unsteady flow, in *Unstedy flow in open channels,* edited by K. Mahmood, and V. Yevjevich, pp. 89-180, Water Resources Publication, Fort Collins, Colo.

150. Milly, P., C. D. R. T. Wetherald, K. A. Dune, and T. L. Delworth (2002), Increasing risk of great floods in a changing climate, *Nature, 415*, 514– 617.

151. Molnár, D. K., and P. Y. Julien (2000), Grid-size effects on surface runoff modelling, *J. Hydrol. Engg., ASCE, 5*(1), 8-16.

152. Moramarco T., and V. P. Singh (2002), Accuracy of kinematic wave and diffusion wave for spatial-varying rainfall excess over a plane, *Hydrol. Process., 16*, 3419–3435.

153. Moramarco, T., C. Pandolfo, and V. P. Singh (2008a), Accuracy of kinematic wave and diffusion wave approximations for flood routing. I: Steady analysis, *J. Hydrol. Engg., 13*(11), 1078-1088.

154. Moramarco, T., C. Pandolfo, and V. P. Singh (2008b), Accuracy of kinematic wave and diffusion wave approximations for flood routing. II: Unsteady analysis, *J. Hydrol. Engg., 13*(11), 1089-1095.

155. Morel-Seytoux, H. J., and J. Khanji (1974), Derivation of an equation of infiltration, *Water Resour. Res., 10*(4), 795-800.

156. Moretti G., and A. Montanari (2007), AFFDEF: A spatially distributed grid based rainfall-runoff model for continuous time simulations of river discharge, *Envir. Modelling and Software*, 22(6), 823-836.

157. Morgali, J. R., and R. K. Linsely (1965), Computer analysis of overland flow, *J. Hydraul. Div. ASCE*, 91(HY3), 81-100.

158. Morita, M., and B. C. Yen (2002), Modeling of conjunctive two-dimensional surface–three-dimensional subsurface flows, *J. Hydrau. Engrg., ASCE*, 128(2), 184–200.

159. Morris, E. M. (1979), The effect of the small-slope approximation and lower boundary conditions on solutions of the Saint-Venant equations, *J. Hydrol.*, 40, 31-47.

160. Morris, E. M. (1980), The propagation of waves in shallow water flow with lateral inflow, *Hydol. Sci. Bull., de Sciences Hydrologique*, 25(1,3), 25-32.

161. Morris, E. M., and D. A. Woolhiser (1980), Unsteady one-dimensional flow over a plane: partial equilibrium and recession hydrographs, *Water Resour. Res.*, 16, 355-360.

162. Moussa, R., and C. Bocquillon, (1996), Criteria for the choice of flood-routing methods in natural channels, *J. Hydrol.*, 186, 1-30.

163. Moussa, R., and Bocquillon C. (2000), Approximation zones of the Saint-Venant equations for flood routing with overbank flow, *Hydrol. and Earth Sys. Sci.*, 4(2), 251-261.

164. Mulvany, T. J. (1850), On the use of self registering rain and flood gauges, *Inst. Civ. Eng. Proc.*, 4, 1-8, Dublin, Ireland.

165. Naden, P. S. (1992), Spatial variability in flood estimation for large catchments: the exploitation of channel network structure, *Hydrol. Sci. J.*, 37(1–2), 53–71.

166. Nash, J. E. (1960), A unit hydrograph study with particular reference to British catchments, *Proc. Inst. Civ. Eng.*, 17, 249–282.

167. Nash, J. E., and J. V. Sutcliffe (1970), River flow forecasting through conceptual models. Part-1: A discussion of principles, *J. Hydrol.*, 10(3), 282-290.

168. Natale, L. and E.Todini (1976a), A stable estimation for linear models 1. Theoretical development and Monte-Corlo experiments, *Water Resour. Res.*, 12, 667-671.

169. Natale, L. and E. Todini (1976b), A stable estimation for linear models 2. Real world hydrologic applications, *Water Resour. Res.*, 12, 672-675.

170. Nawarathna, N. M. N. S. B., Y. Tachikawa, and K. Takara (2005), Water resources distribution of the lower Mekong region: distributed hydrological modelling approach, *Role of Water Sciences in Transboundary River Basin Management, Thailand*, 43–48, <http://www.mekongnet.org/images/b/bf/Bandara.pdf>.

171. Natural Environment Research Council (NERC) (1975), Flood Routing Studies, in *Flood Studies Report*, Vol. III, Institute of Hydrology, Wallingford, UK.

172. Nourani, V., V. P. Singh, and H. Delafrouz (2009), Three geomorphological rainfall–runoff models based on the linear reservoir concept, *Catena*, 76, 206–214.

173. Nunes, J. P., G. A. Nuno Vieira, J. Seixas, P. Goncalves, and N. Carvalhais (2005), Evaluating the MEFIDIS model for runoff and soil erosion prediction during rainfall events, *Catena*, 61, 210–228.

174. O'Donnell, T. (1966), Methods of computations in hydrograph analysis and synthesis, recent trends in hydrograph synthesis, *Proc. Tech meeting No., 21, T.N.O.*, The Hague, pp. 65-102.

175. Orlandini, S., and R. Rosso (1996), Diffusion wave modelling of distributed catchment dynamics, *J. Hydrol. Engg.*, ASCE, *1*(3), 103-113.

176. Orlandini S., and R. Rosso, (1998), Parameterization of stream channel geometry in the distributed modeling of catchment dynamics, *Water Resour. Res.*, *34*(8), 1971–1985.

177. Overton, D. E. (1972), Kinematic flow on long impermeable planes. *Water Resour. Bull.*, *8*(6), 1198-1204.

178. Overton, D. E., and D. L. Brakensiek, (1973), A kinematic model of surface runoff response. *IAHS Publ. 96* (1973), 100–112.

179. Overton, D. E., and M. E. Meadows (1976), *Stormwater Modeling*, 358 pp., Academic Press, Inc., New York.

180. Panday, S., and P. S. Huyakorn (2004), A fully coupled physically-based spatially-distributed model for evaluating surface/subsurface flow, *Adv. Water Resour.*, *27*, 361-382.

181. Paniconi, C., and E. F. Wood (1993), A detailed model for simulation of catchment scale subsurface hydrologic processes, *Water Resour. Res.*, *29*, 1601-1620.

182. Parlange J. Y., W. Hogarth, G. Sander, G. Rose, R., Haverkamp, A. Surin, and W. Brutsaert (1990), Asymptotic expansion for steady-state overland flow, *Water Resour. Res.*, *26*(4), 579-583.

183. Pearson, C. P. (1989), One-dimensional flow over a plane: criteria for kinematic wave modeling, *J. Hydrol.*, *111*, 39-48.

184. Perumal, M. (1989), Unification of Muskingum difference schemes, *J. Hydraul. Eng.*, ASCE, *115*(4), 536–543.

185. Perumal, M., (1992), Comments to "New perspective on the Vedernikov number" by V. M. Ponce, *Water Resour. Res.*, *28*, 1734.

186. Perumal, M. (1994a), Hydrodynamic derivation of a variable parameter Muskingum method- Part 1: Theory and solution procedure, *Hydrol. Sci. J.*, IASH, *39*(5), 431-442.

187. Perumal, M. (1994b), Hydrodynamic derivation of a variable parameter Muskingum method- Part 2: Verification, *Hydrol. Sci. J.*, IASH, *39*(5), 442-458.

188. Perumal, M. (1995), Variable parameter flood routing using hydrodynamic principles, Ph. D. Thesis, Department of Civil Engineering, University of Roorkee, India, 226 p.

189. Perumal, M. (2010), Discussions on "Assessment and review of the hydraulics of storage flood routing 70 years after the presentation of the Muskingum method", by Kousis, A. D., in *Hydrol. Sci. J., 54*(1), 43-60, *Hydrol. Sci. J. (in press)*.

190. Perumal, M., and K. G. Ranga Raju, (1998a), Variable parameter stage-hydrograph routing method: I. Theory, *J. Hydrol. Engg.*, ASCE, *3*(2), 109–114.

191. Perumal, M., and K. G. Ranga Raju, (1998b) Variable parameter stage-hydrograph routing method: II. Evaluation, *J. Hydrol. Engg.*, ASCE, *3*(2), 115–121.

192. Perumal, M., and K. G. Ranga Raju, (1999), Approximate Convection-Diffusion equations, *J. Hydrol. Engg.*, ASCE, *4*(2), 161-164.

193. Perumal, M., and B. Sahoo (2007), Applicability criteria of the variable parameter Muskingum stage and discharge routing methods, *Water Resour. Res., 43*(5), W05409, doi: 10.1029/2006WR004909, 1–20.

194. Perumal, M., and B. Sahoo (2008), Volume conservation controversy of variable parameter Muskingum-Cunge method, *J. Hydraul. Engg., ASCE, 134*(4), 475-485.

195. Perumal, M., P. E. O'Connell, and K. G. Ranga Raju, (2001), Field applications of a variable-parameter Muskingum method, *J. Hydrol. Engg., ASCE, 6*(3), 196-207.

196. Perumal, M., K. B. Shrestha, and U. C. Chaube (2004), Reproduction of hysteresis in rating curves. *J. Hydrau. Engg., ASCE, 130*(9), 870-878.

197. Perumal, M., T. Moramarco, B. Sahoo, and S. Barbetta (2007), A methodology for discharge estimation and rating curve development at ungaged river sites, *Water Resour. Res., 43*(2), W02412, doi:10.1029/2005WR004609, 1–22.

198. Perumal, M., T. Moramarco, B. Sahoo, and S. Barbetta (2010a), On the practical applicability of the VPMS routing method for rating curve development at ungauged river sites, *Water Resour. Res., 46*(3), W03522, doi:10.1029/2009WR008103, 1–9.

199. Perumal, M., T. Moramarco, S. Barbetta, F. Melone, and B. Sahoo (2010b), Real-time flood-stage forecasting by VPMS routing method, *Hydrol. Res. (Formerly Nordic Hydrol.)*, (in press).

200. Philip, J. R. (1983), Infiltration in one, two, and three dimensions, *Procs. National Conference on Advances in Infiltration*, ASAE, St. Joseph, Mich., 1-13.

201. Pilgrim, D. H., and I. Cordery (1993), Flood runoff, in *Handbook of Hydrology*, edited by D. R. Maidment, pp. 9.1-9.42, McGraw-Hill, New York.

202. Pohll, G. M., J. J. Warwick, and S. W. Tyler, (1996). Coupled surface–subsurface hydrologic model of a nuclear subsidence crater at the Nevada test site. *J. Hydrol., 186*, 43–62.

203. Ponce, V. M. (1986), Diffusion wave modeling of catchment dynamics, *J. Hydraul. Engg., ASCE, 112*(8), 716-727.

204. Ponce, V. M. (1989), *Engineering Hydrology, Principles and Practices*, 640 pp., Prentice Hall, Englewood Cliffs, NJ.

205. Ponce, V. M. (1991), New perspective on the Vedernikov number, *Water Resour.Res., 27*, 1777-1779.

206. Ponce, V. M. (1993), Modelling surface runoff with kinematic, diffusion, and dynamic waves, paper presented at International Conference on Hydrology and Water Resources, pp. 1-12, New Delhi, India.

207. Ponce, V. M., and P. V. Chaganti (1994), Variable parameter Muskingum–Cunge method revisited, *J. Hydrol., 162*(3–4), 433–439.

208. Ponce, V. M., and A. C. Klabunde (1999), Parking lot storage modelling using diffusion waves, *J. Hydrol. Engg., ASCE, 4*(4), 371-376.

209. Ponce, V. M., and V. Yevjevich (1978), Muskingum-Cunge method with variable parameters, *J. Hydraul. Div., ASCE, 104*(HY12), 1663–1667.

210. Ponce, V. M., D. B. Simons, and R. -M. Li, (1978), Applicability of kinematic and diffusion models, *J. Hydraul. Div., ASCE., 104*(3), 353–360.

211. Price, R. K. (1985), *Flood Routing, Chapter 4*, edited by P. Novak, pp. 129–173. Elsevier Applied Science Publishers, London.

212. Price, R. K. (2009), Volume conservative, non-linear flood routing, *J. Hydraul. Engg., ASCE, 135*(10), 838-845, doi:10.1061/(ASCE)HY.1943-7900.0000088.

213. Qu, Y. (2005), An integrated hydrologic model for multi-process simulation using semi-discrete finite volume approach, Ph.D. Thesis, 136 pp., Civ. And Environ. Eng. Dep., Pa. State Univ., Univ. Park.

214. Qu, Y. and C. J. Duffy (2007), A semidiscrete finite volume formulation for multiprocess watershed simulation. *Water Resour. Res., 43,* W08419, doi:10.1029/2006WR005752.

215. Reddy, K. V., T. I. Eldho, , E. P. Rao, and N. Hengade (2007), A kinematic-wave-based distributed watershed model using FEM, GIS and remotely sensed data, *Hydrol. Process., 21,* 2765-2777.

216. Richardson, J. R., and P. Y. Julien (1994), Suitability of simplified overland flow equations, *Water Resour. Res., 30*(3), 665-671.

217. Richtmyer R. D., and K. W. Morton (1967), *Difference Methods for Initial-Value Problems*, Wiley, New York.

218. Robinson, J. S., and M. Sivapalan, (1996), Instantaneous response functions of overland flow and subsurface stormflow for catchment models, *Hydol. Process, 10,* 845-862.

219. Rodriguez-Iturbe, I., and Valdes, J. B. (1979), The geomorphologic structure of hydrologic response, *Water Resour. Res., 15*(6), 1409–1420.

220. Rose, C. W., J. Y. Parlange, G. C. Sander, S. Y. Campbell, and D. A. Barry, (1982), Kinematic flow approximation to runoff on a plane: an approximate analytical solution, *J. Hydrol., 62,* 363-369.

221. Rovey, E. W., D. A. Woolhiser, and R. E. Smith (1977), A distributed kinematic model of upland watersheds, *Hydrol. Pap. 93,* 52 pp., Colo. State Univ., Fort Collins, Colo, USA.

222. Sahoo B., C. Chatterjee, N. S. Raghuwanshi, R. Singh, and R. Kumar (2006), Flood Estimation by GIUH-Based Clark and Nash Models, *J. Hydrol. Engg., ASCE, 11*(6), 515-525.

223. Sahoo, B. (2007), Variable parameter flood routing methods for hydrological analyses of ungauged basins, Ph. D. Thesis, Department of Hydrology, Indian Inst. Tech. Roorkee, India, 297 p.

224. Sajikumar N., and B. S. Thandaveswara (1999), A non-linear rainfall–runoff model using an artificial neural network, *J. Hydrol., 216,* 32-55.

225. Santillana, M., and C. Dawson (2009), A numerical approach to study the properties of solutions of the diffusive wave approximation of the shallow water equations, *Comput. Geosci.,* doi:10.1007/s10596-009-9131-4.

226. Savic, D. A., G. A.Walters, and G. W. Davidson (1999), A genetic programming approach to rainfall-runoff modeling, *Water Resour. Manage., 13,* 219–231.

227. Schmid, B. H. (1989), On overland flow modelling: can rainfall excess be treated as independent of flow depth? *J. Hydrol., 107,* 1 – 8.

228. Shamseldin, A. Y. (1997), Application of a neural network technique to rainfall-runoff modeling. *J. Hydrol., 199* (3–4), 272–294.

229. Sherman, L. K. (1932), Streamflow from rainfall by the unit graph method, *Engg. New Records, 108*, 501-505.

230. Singh, V. P. (1988), *Hydrologic Systems: Rainfall-Runoff Modeling,* Vol. I, Prentice Hall, Englewood Cliffs, New Jersy.

231. Singh, V. P. (1994a), Accuracy of kinematic-wave and diffusion-wave approximations for space-independent flows, *Hydrol. Process., 8*(1), 45-62.

232. Singh, V. P. (1994b), Accuracy of kinematic-wave and diffusion-wave approximations for space-independent flows with lateral inflow neglected in the momentum equation, *Hydrol. Process., 8*(4), 311-326.

233. Singh, V. P. (1995), *Computer Models of Watershed Hydrology,* pp. 1-1131, Water Resources Publications, Highlands Ranch, Colo.

234. Singh, V. P. (1996), *Kinematic Wave Modelling in Water Resources: Surface-Water Hydrology,* 1424 pp., John Wiley and Sons, Inc., New York.

235. Singh, V. P. (2001), Kinematic wave modeling in water resources: a historical perspective, *Hydrol. Process., 15*, 671-706.

236. Singh, V. P. (2002), Is hydrology kinematic? *Hydrol. Process., 16*, 667-716.

237. Singh, V. P. (2003), Kinematic wave modeling, in *Hydrology, World Water Congress 2003,* edited by P. Bizier and P. Debarry, June 23-26, 2003, Philadelphia, Pennsylvania. doi:10.1061/40685(2003)165.

238. Singh V. P., and V. Aravamuthan (1995), Errors of kinematic-wave and diffusion-wave approximations for time-independent flows, *Water Resour. Manage., 9*(3), 175-202.

239. Singh V. P., and V. Aravamuthan (1997), Accuracy of kinematic wave and diffusion wave approximations for time-independent flows with momentum exchange included, *Hydrol. Process., 11*(5), 511-532.

240. Singh, V., and S. M. Bhallamudi (1998), Conjunctive surface-subsurface modeling of overland flow, *Adv. Water Res., 21*, 567-579.

241. Singh, V. P., and D. A. Woolhiser (2002), Mathematical modelling of watershed hydrology, *J. Hydrol. Engg.,* ASCE, 7(4), 270-292.

242. Sivapalan, M., K. J. Beven, and E. F. Wood (1987), On hydrologic similarity, 2, A scaled model of storm runoff production, *Water Resour. Res.,* 23(12), 2266-2278.

243. Sivpalan, M., K. Takeuchi, S. W. Franks, V. K. Gupta, H. Karambiri, V. Lakshmi, X. Liang, J. J. McDonnell, E. M. Mendiondo, P. E. O'Connell, T. Oki, J. W. Pomeroy, D. Schertzer, S. Uhlenbrook, and E. Zehe (2003), IAHS decade on Predictions in Ungauged Basins (PUB), 2003-2012: Shaping an exciting future for the hydrologic sciences, *Hydrol. Sci. J., 48*(6), 857-880.

244. Smith, R. E., and R. H. B. Hebbert (1979), A Monte-Carlo analysis of the hydrologic effects of spatial variability of infiltration, *Water Resour. Res., 15*(2), 419–429.

245. Smith R. E., and J.-Y. Parlange (1978), A parameter-efficient hydrologic infiltration model, *Water Resour. Res., 14*, 533-538.

246. Smith, R. E., and D. A. Woolhiser (1971), Overland flow on an infiltrating surface, *Water Resour. Res.*, *7*(3), 899-913.

247. Smith, R. E., and D. C. Goodrich (2005), *Rainfall excess overland flow*, Encyclopedia of Hydrological Sciences, edited by M. G. Anderson, John Wiley & Sons, Ltd.

248. Smith, M. W., N. J. Cox, and L. J. Bracken (2007), Applying flow resistance equations to overland flows, *Progress in Phy. Geography.*, *31*(4), 363-387

249. Stephenson, D. and M. E. Meadows (1986), *Kinematic Hydrology and Modelling*, Elsevier, New York.

250. Stoker, J. J. (1957), Water waves, *Interscience*, New York, USA.

251. Strelkoff, T. (1970), Numerical solution of the Saint-Venant equations. *J. Hydraul. Div.*, ASCE, *96*(HY1), 223-252.

252. Swartzendruber, D. (1974), Infiltration of constant-flux rainfall into soil as analyzed by the approach of Green and Ampt, *Soil Sci.*, *117*, 272-281.

253. Talei, A., L. H. C. Chu, and C. Quek (2010), A novel application of a neuro-fuzzy computational technique in event-based rainfall–runoff modeling, *Expert Systems with Applications* (2010), doi:10.1016/j.eswa.2010.04.015.

254. Tan, W. (1992), *Shallow water hydrodynamics*, Elsevier Science Publishing Co., Inc., New York, USA.

255. Tayfur, G., M. L. Kavvas, R. S. Govindaraju, and D. E. Storm (1993), Two dimensional overland flows over rough infiltrating surfaces, J. *Hydraul. Eng., ASCE, 119*(1), 51-63.

256. Therrien, R., R. G. McLaren, E. A. Sudicky, and S. Panday (2003), HydroSphere: A three-dimensional numerical model describing fully-integrated subsurface and surface flow and solute transport, *User's Guide of HydroSphere*, pp. 273, *Univ.of Laval and Univ. of Waterloo, a draft.*

257. Todini, E. (1988), Rainfall-runoff modelling – past, present and future, *J. Hydrol. 100*, 341-352.

258. Todini, E. (2007), A mass conservative and water storage consistent variable parameter Muskingum-Cunge approach, *Hydrol. Earth Syst. Sci., 11*, 1645–1659.

259. Todini, E. (2009), History and perspectives of hydrological catchment modelling, *Proc. of Int. Conf. on Water, Environment, Energy and Society* (WEES-2009), pp.512-523, New Delhi, 12-16, Jan., 2009.

260. Tsai, C. W.-S. (2003), Applicability of kinematic, noninertia, and quasi-steady dynamic wave models to unsteady flow routing, *J. Hydraul. Engg., 129*(8), 613-627.

261. U.S. Army Corps of Engineers (USACE) (2000), Hydrologic modeling system HEC-HMS technical reference manual, *Rep. CPD-74B*, Hydrol. Eng. Cent., Davis, Calif.

262. U.S. Army Corps of Engineers (USACE) (2006), Hydrologic modeling system HEC-HMS user's manual (version 3.1.0), *Rep. CPD-74A*, Hydrol. Eng., Cent., Davis, Calif.

263. VanderKwaak, J. E., and K. Loague, (2001), Hydrologic-response simulations for the R-5 catchment with a comprehensive physics-based model. *Water Resour. Res.*, *37*(4), 999–1013.

264. Vieux, B. E. (2004a), *Distributed hydrologic modeling using GIS* (CDROM including model software and documentation), 2nd ed., Water Science Technology Series, Vol. 48, Kluwer Academic Publishers, Norwell, Mass.

265. Vieux, B. E. (2004b), Distributed hydrologic modelling for flood forecasting, paper presented at Three Gorges Dam Conference on GIS and remote sensing in hydrology, water resources and environment, IAHS Red Book Publication, No. 289, 1–10.

266. Vieux, B. E., J. H. Park, and B. Kang (2009), Distributed hydrologic prediction: Sensitivity to accuracy of initial soil moisture conditions and radar rainfall inputs, *J. Hydrol. Engg., ASCE, 14*(7), 671-689.

267. Walker, W. R., and G. V. Skogerboe (1987). *Surface Irrigation: Theory and Practice,* Prentice-Hall, Inc. Englewood Cliffs, New Jersey 07632.

268. Wang M., and A. T. Hjelmfelt (1998), DEM based overland flow routing Model, *J. Hydrol. Engg., ASCE, 3*(1), 1-8.

269. Wang, G. -T., and V. P. Singh (1992), Muskingum method with variable parameters for routing in channels, *J. Hydrol., 134*(1-4), 57–76.

270. Warrick, A. W., D. Zerihun, C. A. Sanchez, and A. Furman (2005), Infiltration under variable ponding depths of water, *J. Irrig. Drain. Engg., ASCE, 131*(4), 358-363.

271. Weill, S., Mouche, E., and Patin, J. (2009), A generalized Richards equation for surface/subsurface flow modeling, *J. Hydrol., 366*(1–4), 9–20.

272. Weinmann, P. E., and E. M. Laurenson (1979), Approximate flood routing methods: A review, *J. Hydrol. Div., ASCE,105*(HY12), 1521–1536.

273. Whigham P. A., and P. F. Crapper (2001), Modelling rainfall-runoff using genetic programming, *Math. & Comp. Modelling, 33,* 707-721.

274. Willmott, C. J., S. G. Ackleson, R. E. Davis, J. J. Feddema, K. M. Klink, D. R. Legates, J. O'Connell, and C. M. Rowe (1985), Statistics for the evaluation and comparison of the models, *J. Geophys. Res., 90*(C5), 8995-9005.

275. Wong, T. S. W. (1992). *An Introduction to Kinematic Wave Method for Storm Drainage Design,* 56 pp., Hillview Publications, Singapore.

276. Wong T.S.W. (2005), Kinematic Wave Method for Storm Drainage Design, in *Water Encyclopedia: Surface and Agricultural Water,* edited by J. H. Lehr and J. Keeley, pp. 242-245, John Wiley, Ostrander, Ohio, USA.

277. Wong, T. S. W. (2006), Physically based approach in Hydrology - What is the benefit? *J. Hydrol. Engg., ASCE , 11*(4), 293-295.

278. Wong T. S. W. (2008), Optimum rainfall interval and Manning's roughness coefficient for runoff simulation, *J. Hydrol. Engg.,* ASCE, *13*(11), 1097-1102.

279. Wong, T. S. W. (2009), Overland flow experimental data, Nanyang Tech. Univ., Nanyang Avenue, Singapore, (Personal communication).

280. Wong, T. S. W., and C. K. Lim (2006), Effect of loss model on evaluation of Manning roughness coefficient of experimental concrete catchment, *J. Hydrol., 331,* 205– 218.

281. Wooding, R. A. (1965a), A hydraulic model for the catchment-stream problem: 1. Kinematic wave theory, *J. Hydrol., 3*(3/4), 254–267.

282. Wooding, R. A. (1965b), A hydraulic model for the catchment-stream problem: 2. Numerical solutions, *J. Hydrol.,, 3*(3/4), 268–282.

283. Wooding R. A. (1966), A hydraulic model for the catchment-stream problem: 3. Comparisons with runoff observations. *J. Hydrol., 4,* 21–37.

284. Woolhiser, D.A. (1974), Unsteady free surface flow problems, in *Proc. of Institute on Unsteady Flow in Open Channels*, pp. 195–213, Colorado State Univ., Fort Collins, Colo, USA.

285. Woolhiser D. A. (1975), Simulation of Unsteady overland flow, in *Unsteady flow in open channels*, Vol. II, ediated by K. Mahmood and V. Yevjevich, pp. 485-508, Water Resources Publications, Fort Collins, Colo, USA.

286. Woolhiser, D. A. (1982), Physically based models of watershed runoff, in *Rainfall-Runoff Relationship*, edited by V. P. Singh, pp. 189-202, Water Resources Publications, Littleton, Colorado.

287. Woolhiser, D. A. (1996), Search for physically based runoff model—A hydrologic El Dorado? *J. Hydraul. Engg., 122*(3), 122–129.

288. Woolhiser, D. A., and J. A. Liggett (1967), Unsteady one-dimensional flow over a plane: the rising hydrograph, *Water Resour. Res., 3*(3), 753–771.

289. Woolhiser, D. A., R. E. Smith, and J.-V. Giraldez, (1996), Effects of spatial variability of saturated hydraulic conductivity on Hortonian overland flow, *Water Resour. Res., 32*(3), 671–678.

290. Yeh, G. T., H. P. Cheng, G. B. Huang, F. Zhang, H. C. Lin, E. Edris, and D. Richards (2004), A numerical model of flow, heat transfer, and salinity, sediment, and water quality transport in watershed systems of 1-D stream-river network, 2-D overland regime, and 3D subsurface media (WASH123D: version 2.0), *Tech. Rep.,* CHL Waterw. Exp. Stn.,U.S. Army Corps of Eng., Vicksburg, Miss.

291. Yeh, G. T., G. B. Huang, H. P. Cheng, F. Zhang, H. C. Lin, E. Edris, and D. Richards (2006), A first-principle, physics-based watershed model: WASH123D, in *Watershed Models*, edited by V. P. Singh, and D. K. Frevert, pp. 211– 244, CRC Press, Boca Raton, Fla.

292. Yen, B. C., and A. O. Akan (1984), Effect of soil property on overland flow and infiltration, paper presented at Third IAHR/IAWPRC Conference on Urban Storm Drainage, Goteborg, Sweden, 193-202.

293. Yu, Z. (2000), Assessing the response of subgrid hydrologic processes to atmospheric forcing with a hydrologic model system, *Global and Planetary Change, 25,* 1-11.

294. Zanuttigh, B., and A. Lamberti (2007), Instability and surge development in debris flows, *Rev. Geophys.,45,* RG3006, doi:10.1029/2005RG000175.

295. Zhang, B., and R. S. Govindaraju (2003), Geomorphology-based artificial neural networks (GANNs) for estimation of direct runoff over watersheds, *J. Hydrol., 273,* 18–34.

296. Zhang, B., and R. S. Govindaraju, (2000), Prediction of watershed runoff using Bayesian concepts and modular neural networks, *Water Resour. Res.,* 36 (3), 753–762.

297. Zhao, R. -J., and X. -R. Liu (1995), The Xinanjiang model, in *Computer Models of Watershed Hydrology*, Edited by V. P. Singh, *Water Resour. Publ.*, Littleton, Colorado, USA, 215–232.

298. Zienkiewicz, O. C. (1977), *The element methods*, 3rd ed., McGraw-Hill, New York.

299. Zoppou, C., and I. C. O'Neill (1982), Criteria for the choice of flood routing methods in natural channels, in *Proc. Hydrology and Water Resources Symposium, Melbourne*, Inst. of Eng., Barton, A.C.T., 75–81.

FORTRAN CODE FOR THE RUNOFF ESTIMATION AT THE OUTLET OF THE V-CATCHMENT USING THE VPMD METHOD FOR OVERLAND FLOW AND CHANNEL FLOW MODELLING

```
C***********************************************************************************
C     THE VARIABLE PARAMETER MUSKINGUM DISCHARGE ROUTING METHOD IS USED AS ROUTING SCHEME    *
C     PROGRAM FOR DISCHARGE ROUTING ON V-CATCHMENT (RECTANGULAR CHANNEL ASSUMED)             *
C     LAST MODIFIED ON 05.03.2009          Time:1:10 AM                                      *
C     NO BACK WATER EFFECT CONSIDERED.                                                       *
C     THE PROGRAMME IS WRITTEN IN MKS/FPS UNIT ALSO IT GIVES OUTFLOW DISCHARGE IN FT/SEC     *
C     CM/HR, (M/SEC)*10**5 AND INCH/HR                                                       *
C     COMPUTES ALSO THE DOWNSTREAM STAGE HYDROGRAPHS                                         *
C     THE TERM QL IS THE LATERAL INFLOW IN CUBIC METERS/CUBIC FEET PER SECOND.FOR ROUTING    *
C     IN THE PLANES, THE LATERAL INFLOW IS EQUAL TO THE EFFECTIVE RAINFALL(CENTIMETERS/      *
C     INCH PER HOUR)                                                                         *
C     TO CHECK THE SUITABILITY OF THE METHOD FOR THE GIVEN PROBLEM                           *
C     COMPUTED HYDROGRAPH TESTED WITH ERROR IN VOLUME CRITERION                              *
C     THE MODEL IS VERIFIED WITH GIVEN OTHER MODEL DATA OR OBSERVED DATA USING NASH-         *
C     SUTCLIFFE CRITERION                                                                    *
C     THE MODEL PREDICTED RESULTS ARE ANALYSED BY MEASURES OF RESIDUAL ERRORS (LOAGUE AND    *
C     GREEN,1991)SUCH AS                                                                     *
C     1. ROOT MEAN SQUARE ERROR                                                              *
C     2. COEFFIECENT OF RESIDUAL MASS                                                        *
C     3. COEFFIECENT OF DETERMINATION                                                        *
C     4. MODELLING EFFICIENCY                                                                *
C***********************************************************************************
C     DESCRIPTION OF VARIABLES USED IN THE PROGRAM.                                          *
C                                                                                            *
C***********************************************************************************
C     XLE      = PLANE LENGTH(METER/FEET)                                                    *
C     NDX      = NUMBER OF PLANE INCREMENTS                                                  *
C     TST      = TOTAL SIMULATION TIME(MIN)                                                  *
C     NDT      = NUMBER OF TIME INTERVALS                                                    *
C     RAINT    = AN ARRAY OF EFFECTIVE RAINFALL INTENSITY(CM/H OR INCH/HR)                   *
C                (FOR INPUT IT USED AS QEE)                                                  *
C     RADUR    = AN ARRAY OF EFFEVTIVE RAINFALL DURATION(MIN)(FOR INPUT IT USED AS PT)       *
C     CELP     = AVERAGE WAVE CELERITY IN THE PLANES (M/SEC OR FT/SEC)                       *
C     SLOPEP   = SLOPE OF THE PLANE (M/M OR FT/FT)                                           *
C     SLOPEC   = SLOPE OF THE CHANNEL (M/M OR FT/FT)                                         *
C     UQP      = AVERAGE UNIT-WIDTH FLOW OVER THE PLANES (SQUARE M/ SEC OR SQUARE FT/SEC)    *
C     N        = NUMBER OF VALUES OF OBSERVED DATA                                           *
C     QOBS     = OBSERVED OUTFLOW DISCHARGE AT EACH TIME INTERVAL TIOBS(MIN)                 *
C***********************************************************************************
      DIMENSION QP(2,3500),QLC(3500),RAIN(3500),QLCHN(3500)
      DIMENSION QP2(2,3500),QPR(2,3500),QPL(2,3500),QCH(2,3500)
      DIMENSION Y(3500),FUNC(3500),CELP(35000),QOBS(3500)
      DIMENSION Y1(3500),QL(3500),QP1(2,3500),CHLAT(3500)
      DIMENSION YCH(2,3500),VCH(3500)
      DIMENSION YP(2,3500),YM(3500),QCAL(3500),QP3(2,3500)
      DIMENSION QEE(3500),RADUR(200),PT(200),QES(31500),CELCH(3500)
      CHARACTER *3 RFC
      CHARACTER*4 UNITS
      CHARACTER*5 RCUNIT
      CHARACTER*3 KMS,PFS,AMN,HCE
      CHARACTER*6 BMDATA
      CHARACTER*4 MCPH
      CHARACTER*4 NIPH
      CHARACTER*4 PMSM
      REAL KNP,APCP,KFSQRP,APCMAXP,KFSQRMINP,KNMINP,AKKP,AKMAXP
      REAL KNP1,APCP1,KFSQRP1,APCMAXP1,KFSQRMINP1,KNMINP1,AKKP1,AKMAXP1
      REAL KN,APC,KFSQR,APCMAX,KFSQRMIN,KNMIN,AKK,AKMAX
      REAL KN1,APC1,KFSQR1,APCMAX1,KFSQRMIN1,KNMIN1,AKK1,AKMAX1
      REAL APPL,APPL1,APPC,APPC1,APPLMAX,APPLMAX1,APPCMAX,APPCMAX1
      KN=0
      KNP=0
      APC=0.0
      APPL=0.0
      APPC=0.0
      APCP=0.0
      KFSQR=0.0
      KFSQRP=0.0
      AKK=0.0
```

```
          AKKP=0.0
          APCMAX=0.0
          APCMAXP=0.0
          APPLMAX=0.0
          APPLMAX1=0.0
          APPCMAX=0.0
          APPCMAX1=0.0
          KFSQRMIN=0.0
          KFSQRMINP=0.0
          KNMIN=0.0
          KNMINP=0.0
          AKMAX=0.0
          AKMAXP=0.0
          KN1=0.0
          KNP1=0.0
          APC1=0.0
          APPL1=0.0
          APPC1=0.0
          APCP1=0.0
          KFSQR1=0.0
          KFSQRP1=0.0
          AKK1=0.0
          AKKP1=0.0
          APCMAX1=0.0
          APCMAXP1=0.0
          KFSQRMIN1=0.0
          KFSQRMINP1=0.0
          KNMIN1=0.0
          KNMINP1=0.0
          AKMAX1=0.0
          AKMAXP1=0.0
          QPKCMAX=0.0
          TPKCMAX=0.0
          QPKC=0.0
          TPKC=0.0
          GRIDRATIOP=0.0
          GRIDRATIOC=0.0
          MP=0
          MPP=0.0
          NAPP=0.0
          NAP=0
C*****************************************************************************************
C                 THE ARRAYS USED FOR STORAGE OF VARIABLES USED IN THE PROGRAM          *
C*****************************************************************************************
C     ARRAY QP(2,3500) STORES THE VALUES OF OUTFLOW FROM THE REACH                      +
C     ARRAY QLP(3500) STORES THE VALUES OF LATERALFLOW TO THE PLANE                     +
C     ARRAY QLC(3500) STORES THE VALUES OF LATERALFLOW FROM THE REACH                   +
C     VARIABLE QO STORES THE VALUE OF INTIAL ESTIMATES OF OUTFLOW DISCHARGE             +
C         FOR EACH TIME STEP AND EACH SUBREACH                                          +
C     ARRAY Y(3500) STORES THE VALUE OF COMPUTED FLOW DEPTH                             +
C     ARRAY FUNC(3500) STORES THE COMPUTED VALUES REQUIRED IN NEWTON-RAPHSON METHOD     +
C     ARRAY VP(3500) STORES THE VALUE OF FLOW VELOCITY FOR EACH TIME STEP AND SUBREACH  +
C     ARRAY CELP(3500) STORES THE VALUES OF CELERITY   FOR EACH TIME STEP AND SUBREACH  +
C     ARRAY QOBS(3500)STORES THE VALUES OF OBSERVED VALUES OF OUTFLOW DISCHARGE FROM     +
C         OVERLAND FLOW PLANE                                                           +
C     ARRAY YP(2,3500) STORES THE STAGE AT THE OUTFLOW SECTION                          +
C     ARRAY QP1(2,3500)STORES THE OUTFLOW DISCHARGE CONVERTED IN METRIC UNIT (cm/sec)   +
C     ARRAY QP3(2,3500)OUTFLOW DISCHARGE CONVERTED IN METRIC UNIT (m/sec)*10**5         +
C     ARRAY QP2(2,3500)STORES THE OUTFLOW DISCHARGE CONVERTED IN FPS UNIT      (ft/h)    +
C     ARRAY YM(3500) STORES THE STAGE AT THE  MIDDLE OF THE REACH                       +
C     ARRAY QCAL(3500) THE CALCULATED OUTFLOW                                           +
C     *****************************************************************************************
          OPEN(1,FILE='MOD_OVERLAND_FSIM.DAT',STATUS='OLD')
          OPEN(2,FILE='MOD_AVFC OVERLAND_FSIM.OUT',STATUS='unknown')
          OPEN(5,FILE='MOD_AVFC cmperhr.OUT',STATUS='unknown')
          OPEN(9,FILE='OUTPUT FOR GRAPH.OUT',STATUS='UNKNOWN')
          OPEN(4,FILE='OUTPUT CRITERIA.OUT',STATUS='UNKNOWN')
C         OPEN(3,FILE='AVFC reachwise hydrograph.OUT',STATUS='NEW')
C         OPEN(7,FILE='AVFC K AND THETA.OUT',STATUS='NEW')
C*****************************************************************************************
C                 INPUT AND OUTPUT FILES USED IN THE PROGRAM                            *
C*****************************************************************************************
C     'OVERLAND_FSIM.DAT' IS THE INPUT FILE STORES THE INPUT DATA SUCH AS ND,TIOBS AND  *
C     QOBS VALUES AND PARAMETERS SUCH AS XLE,NDX,CD,TST,NDT,ARAINT,RADUR,               *
C             SLOPEP,B,G                                                                *
C     "MOD_OVERLAND_FSIM" IS A OUTPUT FILE WHICH DISPLAY THE RUNOFF OUTFLOW AT DOWNSTREAM *
C     END OF THE OVERLAND FLOW PLANE IN (inch/h) AT EACH TIME INTERVAL DISPLAYED IN     *
```

```
C          SECOND AS WELL AS MINUTE.
C       "MOD_OVERLAND_FSIM_cmperh" IS A OUTPUT FILE WHICH DISPLAY THE RUNOFF OUTFLOW AT          *
C       DOWNSTREAM END OF THE OVERLAND FLOW PLANE IN (inch/h) AT EACH TIME INTERVAL              *
C       DISPLAYED IN SECOND AS WELL AS MINUTE.                                                   *
C       ND IS THE NUMBER OF OBSERVED DATA POINTS                                                 *
C       TIOBS IS THE TIME OF OBSERVATION FOR ONE MINUTE IT IS WRITTEN AS (1.0) AND SO ON         *
C       QOBS IN THIS PROGRAM SHOULD BE ENTERED AS OBSERVED VALUE IN M3/SEC OR FT3/SEC            *
C       BMDATA IS THE BENCHMARK DATA UNIT (ENTER "CMPH" IF DATA IS IN M**3/SEC, ENTER "INPH       *
C       "IF DATA IS IN FT3/SEC OR ENTER MPSM"IF DATA IS IN M3/SEC*10**5.                         *
C ****************************************************************************************************
         ELAPSED_TIME=TIMEF()
         READ(1,*)ND,TIOBS,BMDATA
         WRITE(5,11)ND
  11     FORMAT('NUMBER OF OBSERVATIONS/BENCH MARK PREDICTIONS='I7)
         WRITE(5,*)'BMDATA CMPH=M**3/SEC,INPH=INCH/HR,MPSM= M/SEC*10**5'
         WRITE(5,*)'UNIT OF RUNOFF DICHARGE=',BMDATA
         SUMQOBS=0.0
         TIME=0.0
         QPKOMAX=0.0
         TPKOMAX=0.0
         CELPMAX=0.0
         CELCMAX=0.0
         WRITE(5,*)'OBSERVED/BENCHMARK DATA USED FOR MODEL EVALUATION'
         WRITE(5,13)
  13     FORMAT(5X,'RUNOFF',7X,'TIME(MINUTE)')
         DO 101 J=1,ND
         READ(1,*)QOBS(J)
         WRITE(5,*)TIME,QOBS(J)
         IF(J.EQ.1)THEN
         QPKOMAX=QOBS(J)
         TPKOMAX=TIME
         ELSEIF(J.GT.1)THEN
         QPKO=QOBS(J)
         IF(QPKO.GT.QPKOMAX)THEN
         QPKOMAX=QPKO
         TPKOMAX=TIME
         ELSE
         ENDIF
         ELSE
         ENDIF
         SUMQOBS=SUMQOBS+QOBS(J)
C        WRITE(*,*)QOBS(J)
         TIME=TIME+TIOBS
 101     CONTINUE
         QMEAN=SUMQOBS/ND
C        WRITE(*,*)'QMEAN',QMEAN
         MCPH='CMPH'
         NIPH='INPH'
         PMSM='MPSM'
         READ(1,*)NPLANE   !write 1 if v-ctchment with uniform plane and 2 if uneven size planes
         READ(1,*)TST,NDT,NIER,G
         READ(1,*)XLER,NDXR,SOPR,BR
         READ(1,*)XLEL,NDXL,SOPL,BL
         READ(1,*)CHLEN,NDXCH,SOCH,BCH
         MSIGNAL=0
C ****************************************************************************************************
C  CHECKING UNITS OF PARAMETERS USED IN COMPUTATION AND IF NECESAARY CONVERSION                  *
C  INTO APPRORIATE UNIT FOR MANNINGS OR CHEZYS COEFFICIENT.                                      *
C ****************************************************************************************************
C  WRITE(*,*)'ENTER "MKS" IF SYSTEM UNIT EXCEPT ROUGHNESS COEFFICIENT
C  1        ARE IN MKS UNIT SYSTEM OR ENTER "FPS" IF SYSTEM OF
C  2             UNITS ARE IN FPS UNIT'
                  AMN='MAN'
                  HCE='CHE'
                  KMS='MKS'
                  PFS='FPS'
         READ(1,*)UNITS
C  WRITE(*,*)'UNITS=',UNITS
         UNITS=UNITS
         IF(UNITS.EQ.KMS)THEN
         WRITE(5,41)XLER
  41     FORMAT('LENGTH OF PLANE 1=',F15.5,' ','METER')
         WRITE(5,22)XLEL
  22     FORMAT('LENGTH OF PLANE 2=',F15.5,' ','METER')
         WRITE(5,23)CHLEN
  23     FORMAT('LENGTH OF CHANEEL=',F15.5,' ','METER')
C  WRITE(*,*)'ENTER "MAN" FOR MANNINGS ROUGHNESS COEFFICIENT OR
```

299

```
C     I               ENTER "CHE" FOR CHEZYS ROUGHNESS COEFFICIENT.'
      READ(1,*)RFC
       IF(RFC.EQ.AMN) THEN
         READ(1,*)AMNPR,AMNPL,AMNCH
       ELSEIF(RFC.EQ.HCE)THEN
            READ(1,*)CDR,CDL,CDCH
        ELSE
         WRITE (*,*)'WRONG UNIT ENTRY'
          ENDIF
C           WRITE(*,*)'ENTER "MKS" FOR ROUGHNESS COEFF.IN MKS UNIT SYSTEM
C     I           OR ENTER"FPS" FOR ROUGH. COEFF.IN FPS UNIT SYSTEM'
       READ(1,*)RCUNIT
          IF(RCUNIT.EQ.KMS)THEN
            IF(RFC.EQ.AMN)THEN
              AMNPR=AMNPR
              AMNPL=AMNPL
          AMNCH=AMNCH
        WRITE(5,43)AMNPR,SOPR
43    FORMAT('MANNINGS ROUGH.COEFF.PLANE 1 =',F10.5,' ','SLOPE=',F10.5)
        WRITE(5,24)AMNPL,SOPL
24    FORMAT('MANNINGS ROUGH.COEFF.PLANE 2 =',F10.5,' ','SLOPE=',F10.5)
        WRITE(5,26)AMNCH,SOCH
26    FORMAT('MANNINGS ROUGH.COEFF.CHANNEL =',F10.5,' ','SLOPE=',F10.5)
              ELSEIF(RFC.EQ.HCE)THEN
                CDR=CDR
                CDL=CDL
                CDCH=CDCH
        WRITE(5,47)CDR,SOPR
47    FORMAT('CHEZYS ROUGH. COEFF.PLANE 1 =',F10.5,' ','SLOPE=',F10.5)
        WRITE(5,27)CDL,SOPL
27    FORMAT('CHEZYS ROUGH. COEFF.PLANE 2 =',F10.5,' ','SLOPE=',F10.5)
        WRITE(5,28)CDCH,SOCH
28    FORMAT('CHEZYS ROUGH. COEFF. CHANNEL =',F10.5,' ','SLOPE=',F10.5)
          ELSE
           WRITE(*,*) 'WRONG UNIT ENTRY'
            ENDIF
          ELSEIF(RCUNIT.EQ.PFS)THEN
            IF(RFC.EQ.AMN)THEN
              AMNPR=AMNPR*1.486
              AMNPL=AMNPL*1.486
          AMNCH=AMNCH*1.486
        WRITE(5,44)AMNPR,SOPR
44    FORMAT('MANNINGS ROUG.COEFF PLANE 1 =',F10.5,' ','SLOPE=',F10.5)
        WRITE(5,29)AMNPL,SOPL
29    FORMAT('MANNINGS ROUGH.COEFF.PLANE 2 =',F10.5,' ','SLOPE=',F10.5)
        WRITE(5,32)AMNCH,SOCH
32    FORMAT('MANNINGS ROUGH.COEFF.CHANNEL =',F10.5,' ','SLOPE=',F10.5)
              ELSEIF(RFC.EQ.HCE)THEN
                CDR=CDR*SQRT(0.3048)
                CDL=CDL*SQRT(0.3048)
                CDCH=CDCH*SQRT(0.3048)
        WRITE(5,48)CDR,SOPR
48    FORMAT('CHEZYS ROUGH. COEFF.PLANE 1 =',F10.5,' ','SLOPE=',F10.5)
        WRITE(5,33)CDL,SOPL
33    FORMAT('CHEZYS ROUGH. COEFF.PLANE 2 =',F10.5,' ','SLOPE=',F10.5)
        WRITE(5,34)CDCH,SOCH
34    FORMAT('CHEZYS ROUGH. COEFF. CHANNEL =',F10.5,' ','SLOPE=',F10.5)
          ELSE
           WRITE(*,*) 'WRONG UNIT ENTRY'
             ENDIF
             ENDIF
          ELSEIF(UNITS.EQ.PFS)THEN
           WRITE(5,42)XLER
42    FORMAT('LENGTH OF PLANE 1=',F15.5,' ','FEET')
           WRITE(5,37)XLEL
37    FORMAT('LENGTH OF PLANE 2=',F15.5,' ','FEET')
           WRITE(5,38)CHLEN
38    FORMAT('LENGTH OF CHANEEL=',F15.5,' ','FEET')
        READ(1,*)RFC
         IF(RFC.EQ.AMN) THEN
           READ(1,*)AMNPR,AMNPL,AMNCH
         ELSEIF(RFC.EQ.HCE)THEN
              READ(1,*)CDR,CDL,CDCH
          ELSE
           WRITE(*,*) 'WRONG UNIT ENTRY'
            ENDIF
C           WRITE(*,*)'ENTER "MKS" FOR ROUGHNESS COEFF.IN MKS UNIT SYSTEM
```

```
C    1             OR ENTER"FPS" FOR ROUGH. COEFF.IN FPS UNIT SYSTEM'
       READ(1,*)RCUNIT
           IF(RCUNIT.EQ.KMS)THEN
              IF(RFC.EQ.AMN)THEN
                 AMNPR=AMNPR/1.486
                 AMNPL=AMNPL/1.486
                 AMNCH=AMNCH/1.486
          WRITE(5,45)AMNPR,SOPR
45    FORMAT('MANNINGS ROUG. COEFF.PLANE 1 =',F10.5,' ','SLOPE=',F10.5)
          WRITE(5,39)AMNPL,SOPL
39    FORMAT('MANNINGS ROUGH.COEFF.PLANE 2 =',F10.5,' ','SLOPE=',F10.5)
          WRITE(5,62)AMNCH,SOCH
62    FORMAT('MANNINGS ROUGH.COEFF.CHANNEL =',F10.5,' ','SLOPE=',F10.5)
                 ELSEIF(RFC.EQ.HCE)THEN
                 CDR=CDR/SQRT(0.3048)
                 CDL=CDL/SQRT(0.3048)
                 CDCH=CDCH/SQRT(0.3048)
          WRITE(5,49)CDR,SOPR
49    FORMAT('CHEZYS ROUGH. COEFF.PLANE 1 =',F10.5,' ','SLOPE=',F10.5)
          WRITE(5,63)CDL,SOPL
63    FORMAT('CHEZYS ROUGH. COEFF.PLANE 2 =',F10.5,' ','SLOPE=',F10.5)
          WRITE(5,64)CDCH,SOCH
64    FORMAT('CHEZYS ROUGH. COEFF. CHANNEL =',F10.5,' ','SLOPE=',F10.5)
             ELSE
                WRITE(*,*) 'WRONG UNIT ENTRY'
                ENDIF
           ELSEIF(RCUNIT.EQ.PFS)THEN
              IF(RFC.EQ.AMN)THEN
                 AMNPR=AMNPR
                 AMNPL=AMNPL
               AMNCH=AMNCH
          WRITE(5,46)AMNPR,SOPR
46    FORMAT('MANNINGS ROUGH.COEFF.PLANE 1 =',F10.5,' ','SLOPE=',F10.5)
          WRITE(5,66)AMNPL,SOPL
66    FORMAT('MANNINGS ROUGH.COEFF.PLANE 2 =',F10.5,' ','SLOPE=',F10.5)
          WRITE(5,67)AMNCH,SOCH
67    FORMAT('MANNINGS ROUGH.COEFF.CHANNEL =',F10.5,' ','SLOPE=',F10.5)
                 ELSEIF(RFC.EQ.HCE)THEN
                 CDR=CDR
                 CDL=CDL
                 CDCH=CDCH
          WRITE(5,52)CDR,SOPR
52    FORMAT('CHEZYS ROUGH. COEFF.PLANE 1 =',F10.5,' ','SLOPE=',F10.5)
          WRITE(5,68)CDL,SOPL
68    FORMAT('CHEZYS ROUGH. COEFF.PLANE 2 =',F10.5,' ','SLOPE=',F10.5)
          WRITE(5,69)CDCH,SOCH
69    FORMAT('CHEZYS ROUGH. COEFF. CHANNEL =',F10.5,' ','SLOPE=',F10.5)
             ELSE
                WRITE(*,*) 'WRONG UNIT ENTRY'
                ENDIF
              ENDIF
       ENDIF
       CELP=0.0
       LC=0
       DX1=0.0
       CFVOL=0.0
       RFVOL=0.0
       QCH(1,0)=0.0
       QCH(0,1)=0.0
       READ(1,*)(QEE(L),PT(L),L=1,NIER)
       DO 2 L=1,NIER
       RADUR(L)=PT(L)*60
        IF(UNITS.EQ.KMS)THEN
         SRFVOL=QEE(L)/(360000.0)*(RADUR(L)-RADUR(L-1))
         RFVOL=RFVOL+SRFVOL  !RAINFALL VOLUME IN CUBIC METER PER SEC
       WRITE(5,53)QEE(L),PT(L)
53    FORMAT('RAIN INTENSITY (CM/H) =',F10.5,5X,'DURATION(MIN)=',F10.2)
         ELSEIF(UNITS.EQ.PFS)THEN
         SRFVOL=QEE(L)/(3600.0*12.0)*(RADUR(L)-RADUR(L-1))
         RFVOL=RFVOL+SRFVOL  !RAINFALL VOLUME IN CUBIC FEET PER SEC
       WRITE(5,54)QEE(L),PT(L)
54    FORMAT('RAIN INTENSITY (IN/H) =',F10.5,5X,'DURATION(MIN)=',F10.2)
       ELSE
       WRITE(*,*)'ERROR IN COMPUTATION'
       ENDIF
       WRITE(*,*)RFVOL,SRFVOL,RADUR(L),QEE(L)
2     CONTINUE
```

```
      RADURS=RADUR(NIER)
      TSTS=TST*60. !SIMULATION TIME IN SEC
      DXR=XLER/NDXR   !SUBREACH LENGTH IN M/FT
      DXL=XLEL/NDXL   !SUBREACH LENGTH IN M/FT
      DXCH=CHLEN/NDXCH  !SUBREACH LENGTH IN M/FT
      DT=TSTS/NDT !TIME INTERVAL IN SEC
      GRIDRATIOP=DXR/DT
      GRIDRATIOC=DXCH/DT
      IF(UNITS.EQ.KMS)THEN
      WRITE(5,56)DXR,DT
56    FORMAT('SUB-REACH LENGTH DX (M), PLANE 1=', F10.6,',5X,
     1  'TIME STEP(SEC)=',F4.1)
      WRITE(5,72)DXL,DT
72    FORMAT('SUB-REACH LENGTH DX (M), PLANE 1=', F10.6,',5X,
     1  'TIME STEP(SEC)=',F4.1)
      WRITE(5,73)DXCH,DT
73    FORMAT('SUB-REACH LENGTH DX (M), CHNNEL=', F10.6,',5X,
     1  'TIME STEP(SEC)=',F4.1)
      ELSEIF(UNITS.EQ.PFS)THEN
      WRITE(5,57)DX,DT
57    FORMAT('SUB-REACH LENGTH DX (FEET)=', F10.6,',5X,
     1  'TIME STEP(SEC)=',F4.1)
      ELSE
      ENDIF
      WRITE(5,*)'*******************************************************'
      NRDT=RADURS+0.01
      IF((TIOBS*60.0).GE.DT)THEN
      TSKIP=(TIOBS*60)/DT
      ELSE
      DTSKIP=DT/60.0
      TTSKIP=DTSKIP/TIOBS
      ND=ND+1
      ND=(ND-1)/TTSKIP+1
      TIME=0.0
      SUMQOBS=0.0
      QMEAN=0.0
      DO 6 J=2,ND
      QOBS(J)=QOBS((J-1)*TTSKIP+1)
      TIME=TIME+DTSKIP
      SUMQOBS=SUMQOBS+QOBS(J)
C     WRITE(*,*)QOBS(J),TIME*60
6     CONTINUE
      QMEAN=SUMQOBS/ND
C          WRITE(*,*)'QMEAN',QMEAN
      TSKIP=1.0
      ENDIF
C     NS=0
      QP(1,0)=0.0
      QP(0,1)=0.0
C     QP1(1,0)=0.0
C     QP2(1,0)=0.0
C     QP3(1,0)=0.0
      QCAL(0)=0.0
      WRITE(5,600)
600   FORMAT(2X,'TIME INTERVAL',5X,'TIME (S)',5X,'TIME(MIN)',
     1 5X,'OUTFLOW(M**3/sec)',2X,'FLOW DEPTH (cm)')
      WRITE(2,500)
500   FORMAT(2X,'TIME INTERVAL',5X,'TIME (S)',5X,'TIME(MIN)',5X,
     1 'OUTFLOW(inch/hr)',2X,'LATERAL CHANNEL FLOW')
      WRITE(*,*)'NRDT,NDT,DT',NRDT,NDT,DT
      WRITE(*,*)'SKIP TIME=',TSKIP,NS
      WRITE(*,*)'IF SKIP TIME IS WHOLE NUMBER, PRESS 1 IF NOT PRESS 2'
C     READ(*,*)MSIGNAL
      MSIGNAL=1
      IF(MSIGNAL.EQ.2)THEN
      STOP
      ELSE
      NDX=NDXR
      BR=BR
C     B=BR
      B=1.0
      XLE=XLER
      DX=DXR
      SLOPEP=SOPR
      NNPLANE=NPLANE-1
      IF(RFC.EQ.AMN)THEN
      AMNP=AMNPR
```

302

```
        ELSEIF(RFC.EQ.HCE)THEN
        CD=CDR
        ELSE
        ENDIF
76  IF(NNPLANE.EQ.2)THEN
      NDX=NDXL
      B=1.0
      XLE=XLEL
      DX=DXL
      SLOPEP=SOPL
        IF(RFC.EQ.AMN)THEN
          AMNP=AMNPL
        ELSEIF(RFC.EQ.HCE)THEN
          CD=CDL
        ELSE
        ENDIF
      ELSE
      ENDIF
      AMNP=AMNP
      NS=0
      RRDUR=RADUR(1)
      DX1=0.0
      DO 10 J=1,NDX
C     DO 20 J=1,1
      DX1=DX1+DX
      T=0.0
      QP(2,0)=0.0
      RADUR(1)=RRDUR
      NN=1
      DO 20 N=1,NDT
      T=T+DT
      IF (T.LE.NRDT)THEN
      IF(T.LE.RADUR(NN))THEN
      RAINT=QEE(NN)
      IF(T.EQ.RADUR(NN))THEN
      NN=NN+1
      ELSE
      ENDIF
C     WRITE(*,*)'RAINT,NN',RAINT,NN
      ELSE
C     WRITE(*,*)'RADUR(NN+1)',RADUR(NN+1)
      IF(NN.LE.NIER)THEN
      IF(T.LE.(RADUR(NN+1)))THEN
      ANTC=T-RADUR(NN)
C     WRITE(*,*)'NTC,NN',NTC,NN,T,RADUR(NN)
      IF(ANTC.LT.DT)THEN
      ANTCC=DT-ANTC
      QES(NN)=QEE(NN)*ANTCC/3600.0
      NN=NN+1
      QES(NN)=QEE(NN)*ANTC/3600.0
      RAINT=(QES(NN-1)+QES(NN))/(DT/3600.0)
      ELSE
      NN=NN+1
      RAINT=QEE(NN)
      ENDIF
      ELSEIF(T.LE.RADUR(NN+2))THEN
      AKT=DT-RADUR(NN+1)
      QES(NN+2)=AKT/3600.0*QEE(NN+2)
      AKTT=RADUR(NN+1)-RADUR(NN)
      QES(NN+1)=AKTT*QEE(NN+1)/3600.0
      AKKT=DT-(AKT+AKTT)
      QES(NN)=AKKT/3600.0*QEE(NN)
      RAINT=(QES(NN)+QES(NN+1)+QES(NN+2))/(DT/3600.0)
      ELSE
      WRITE(*,*)'RECHECKING OF DATA IS REQUIRED AS TIME INTERVAL EXCEEDS
     1      CONSECUTIVE THREE EFFECTIVE RAINFALL TIME INTERVAL'
      ENDIF
      ELSE
      WRITE(*,*)'NUMBER OF EFFECTIVE RAINFALL TIME INTERVAL EXCEEDS
     1     THE NUMBER OF EFFECTIVE RAINFALL TIME INTERVAL SUPPLIED.'
      ENDIF
      ENDIF
      ELSE
        RAINT=0.0
        ENDIF
      IF(UNITS.EQ.KMS)THEN
       RAINT=RAINT/(3600.0*100.0) !RAINT INTENSITY IN M/SEC
```

```
         ELSEIF(UNITS.EQ.PFS)THEN
          RAINT=RAINT/(3600.0*12.0) !RAINT INTENSITY IN FT/SEC
         ELSE
          WRITE(*,*)'ERROR IN COMPUTATION'
          ENDIF
         IF(J.EQ.1)THEN
         RAIN(N)=RAINT
         ELSE
         ENDIF
         RCMS=(RAINT)*DX*B
         IF(T.LE.NRDT)THEN
         QLP=RCMS
         PP=(RAINT)*DX*B
         ELSE
         QLP=0.0
         PP=0.0
         ENDIF
C        Y(I+1)=0.0
C        WRITE(*,*)PP
         IF(J.EQ.1)THEN
         QO=(PP+QP(2,N-1))/2.
         write(2,*)qp(2,n-1),pp,n
         ELSEIF(J.GT.1)THEN
         QO=((QP(1,N)+QP(1,N-1)+QP(2,N-1))/3.)
         IF(j.EQ.2)THEN
         WRITE(2,*)QP(1,N),QP(1,N-1),QP(2,N-1)j,n
         ELSE
         ENDIF
         ELSE
         ENDIF
C        WRITE(*,*)'QO',QO,J,N
         IF(QO.LE.0.0) GOTO 20
         QL(N)=QLP
         IF(RFC.EQ.AMN)THEN
            CONST=(1./AMNP)*SQRT(SLOPEP)*B**(5./3.)
          YAV=(QO/((1./AMNP)*SQRT(SLOPEP)*B))**(3./5.)
          VEL=QO/(YAV*B)
          R=YAV
          CEL=(5./3.)*VEL
          AK=DX/CEL
          THETA=0.5-(QO*(1.-(4./9.)*((QO*QO)/(G*(YAV)**3))))
         1 /(2.*SLOPEP*CEL*DX)
          ELSEIF(RFC.EQ.HCE)THEN
          CONST=CD*SQRT(SLOPEP)
          YAV=(QO/(CONST*B))**(2./3.)
          VEL=QO/(YAV*B)
          R=YAV
          CEL=3./2.*VEL
          AK=DX/CEL
          THETA=0.5-(QO*(1.-(1./4.)*((QO*QO)/(G*(YAV)**3))))
         1 /(2.*SLOPEP*CEL*DX)
          ELSE
           ENDIF
     255 IF (J.EQ.1) THEN
          CDN1=AK+DT/2.
          CUP1=(AK-DT/2.)/CDN1
          CUP2=DT/CDN1
          QP(2,N)=CUP1*QP(2,N-1)+CUP2*QL(N)
          IF(QP(2,N).LE.0.0)THEN
          QP(2,N)=0.0
          ELSE
          ENDIF
          GOTO 20
          ELSE
          ENDIF
C
C        COUNTER M IS USED FOR UPDATING THE PARAMETERS AT ANY TIME
C
         M=0
      19 DNMTR=AK*(1.-THETA)+(DT/2.)
C        C1P, C2P,C3P AND C4P ARE THE COEFFICIENTS OF THE MUSKINGUM ROUTING EQUATION.
         C1P=(-(AK*THETA)+(DT/2.))/DNMTR
         C2P=(AK*THETA+DT/2.)/DNMTR
         C3P=(AK*(1.-THETA)-DT/2.)/DNMTR
         C4P=DT/DNMTR
       5 M=M+1
C        COMPUTATION OF OUTFLOW
```

304

```
        QP(2,N)=C1P*QP(1,N)+C2P*QP(1,N-1)+C3P*QP(2,N-1)+C4P*QL(N)
C           COMPUTATION OF WEIGHTED OUTFLOW.
        Q3=QP(2,N)+THETA*(QP(1,N)-QP(2,N))
        IF(Q3.LE.0.0)THEN
        GOTO 750
        ELSE
        Q3=Q3
        ENDIF
C    WRITE(*,*)'Q3=',Q3
C    WRITE(*,*)'YMID=',YMID
        IF(RFC.EQ.AMN)THEN
          CONST=(1./AMNP)*SQRT(SLOPEP)
        YMID=(Q3/(CONST*B))**(3./5.)
C    WRITE(*,*)'YMID=',YMID
C         COMPUTATION OF DISCHARGE AT THE MIDDLE OF THE REACH
        QMID=(QP(1,N)+QP(2,N))/2.
C         COMPUTATION OF THE SQUARE OF FROUDE NUMBER.
        FSQ=(QMID*QMID*B)/(G*(B*YMID)**3)
C         COMPUTATION OF THE STAGE AT THE OUTFLOW SECTION.
        YP(2,N)=YMID+(QP(2,N)-QMID)/((5./3.)*QMID/YMID)
C         COMPUTATION OF STAGE AT THE WEIGHTED OUTFLOW SECTION.
        Y3=YMID+(Q3-QMID)/((5./3.)*QMID/YMID)
C         COMPUTATION OF VELOCITY AT THE WEIGHTED OUTFLOW SECTION.
        V3=Q3/(B*Y3)
C         COMPUTATION OF WAVE CELERITY OF THE REACH.
        CELP(J)=(5./3.)*V3
C         COMPUTATION OF PARAMETERS AK AND THETA.
        AK=DX/CELP(J)
        R=YMID
        THETA=0.5-Q3*(1.-(4./9.)*FSQ)/(2.*SLOPEP*B*CELP(J)*DX)
C         COMPUTATION OF STAGE AT THE INLET OF THE REACH
        IF(DX1.EQ.DX) Y1(J)=YMID+(QP(J-1,N)-QMID)/((5./3.)*QMID/YMID)
        ELSEIF(RFC.EQ.HCE)THEN
          CONST=CD*SQRT(SLOPEP)
        YMID=(Q3/(CONST*B))**(2./3.)
C    WRITE(*,*)'YMID=',YMID
C         COMPUTATION OF DISCHARGE AT THE MIDDLE OF THE REACH
        QMID=(QP(1,N)+QP(2,N))/2.
C         COMPUTATION OF THE SQUARE OF FROUDE NUMBER.
        FSQ=(QMID*QMID*B)/(G*(B*YMID)**3)
C         COMPUTATION OF THE STAGE AT THE OUTFLOW SECTION.
        YP(2,N)=YMID+(QP(2,N)-QMID)/((3./2.)*QMID/YMID)
C         COMPUTATION OF STAGE AT THE WEIGHTED OUTFLOW SECTION.
        Y3=YMID+(Q3-QMID)/((3./2.)*QMID/YMID)
C         COMPUTATION OF VELOCITY AT THE WEIGHTED OUTFLOW SECTION.
        V3=Q3/(B*Y3)
C         COMPUTATION OF WAVE CELERITY OF THE REACH.
        CELP(J)=(3./2.)*V3
C         COMPUTATION OF PARAMETERS AK AND THETA.
        AK=DX/CELP(J)
        R=YMID
        THETA=0.5-Q3*(1.-(1./4.)*FSQ)/(2.*SLOPEP*CELP(J)*DX)
C    WRITE(*,*)AK,CELP(J),THETA
C    WRITE(*,*)'QP(J,N)=',QP(J,N)
C         COMPUTATION OF STAGE AT THE INLET OF THE REACH
C    IF(DX1.EQ.DX)Y1(J)=2.*YMID-YCOM(J)
        IF(DX1.EQ.DX) Y1(J)=YMID+(QP(1,N)-QMID)/
        1((3./2.-(YMID/(B+2.*YMID)))*QMID/YMID)
        ELSE
        WRITE(*,*)'WRONG FRICTION FORMULA USED IN COMPUTATION.'
        ENDIF
750     IF(M.LE.1) GOTO 19
        IF(QP(2,N).LE.0.0)THEN
        QP(2,N)=0.0
        GOTO 20
c    FC=0.0
        ELSE
        QP(2,N)=QP(2,N)
C    WRITE(5,*)QP(2,N)*3600.0*100.0/(XLE*B),N,nnplane,j
c    FC=FC
        ENDIF
C    ********************************************************************
C         APPLICABILITY CRITERIA TO CHECK SUITABILITY OF METHOD
C    ********************************************************************
C    APPLICABILITY CRITERIA AT ONE METER FROM U/S
C    ********************************************************************
        FET=1.0/0.3048
```

```
      FET2=1.2/0.3048
      MPP=MPP+N
      IF(UNITS.EQ.KMS)THEN
      IF(DX1.GE.0.97.AND.DX1.LE.(1.2))THEN
C     WRITE(*,*)'DX1,Y1(J),FSQ',DX1,YP(J,N),FSQ
      KNP=(SLOPEP*DX1)/((YP(2,N)*FSQ)) !WOOLISER AND LIGGETTEE (1967) CRITERIA
      KFSQRP=KNP*FSQ
C     IF(RFC.EQ.AMN)THEN
C     AM=5./3.
C     ELSE IF(RFC.EQ.HCE)THEN
C     AM=2./3.
C     ELSE
C     ENDIF
C     APC=-(1./(CELCH(J)*B)*((QCH(2,N)-QCH(2,N-1))/DT))
C     APC=(1.0/SLOPEC)*(YCH(2,N)/(DX1)) !PERUMAL AND SAHOO(2007) CRITERIA
      APPL=(1.0/SLOPEP)*(YP(2,N)/(DX1))
      IF(RFC.EQ.AMN)THEN
      APCP=1.-(QP(2,N)/((SQRT(SLOPEP)/AMNP)*YP(2,N)**(5./3.)))**2
      DISPR=(QP(2,N)/((SQRT(SLOPEP)/AMNP)*YP(2,N)**(5./3.)))**2
      IF(DISPR.GE.1.0)THEN
      APCP=(1.0/SLOPEP)*(YP(2,N)/(DX1))
      ELSE
      ENDIF
      ELSEIF(RFC.EQ.HCE)THEN
      APCP=1.-(QP(2,N)/((SQRT(SLOPEP)*CD)*YP(2,N)**(3./2.)))**2
      DISPR=(QP(2,N)/((SQRT(SLOPEP)*CD)*YP(2,N)**(3./2.)))**2
      IF(DISPR.GE.1.0)THEN
      APCP=(1.0/SLOPEP)*(YP(2,N)/(DX1))
      ELSE
      ENDIF
      ELSE
      ENDIF
      AKKP=AK
       IF(N.EQ.MPP.OR.KNMINP.EQ.0) THEN
         KNMINP=KNP
         KFSQRMINP=KFSQRP
         AKMAXP=AKKP
       ELSE
        ENDIF
       IF(KNMINP.GT.KNP)THEN
          KNMINP=KNP
       ELSE
       ENDIF
       IF(KFSQRMINP.GT.KFSQRP) THEN
          KFSQRMINP=KFSQRP
       ELSE
       ENDIF
       IF(APCMAXP.LT.APCP)THEN
         APCMAXP=APCP
       ELSE
       ENDIF
       IF(APPLMAX.LT.APPL)THEN
         APPLMAX=APPL
       ELSE
       ENDIF
       IF(AKMAXP.LT.AKKP)THEN
         AKMAXP=AKKP
       ELSE
       ENDIF
      ELSE
      GOTO 551
      ENDIF
      ELSEIF(UNITS.GE.PFS) THEN
      IF(DX1.GE.FET.AND.DX1.LE.FET2)THEN
      KNP=(SLOPEP*DX1)/((YP(2,N)*FSQ)) !WOOLISER AND LIGGETTEE (1967) CRITERIA
      KFSQRP=KNP*FSQ
      APPL=(1.0/SLOPEP)*(YP(2,N)/(DX1))
      IF(RFC.EQ.AMN)THEN
      APCP=1.-(QP(2,N)/((SQRT(SLOPEP)/AMNP)*YP(2,N)**(5./3.)))**2
      DISPR=(QP(2,N)/((SQRT(SLOPEP)/AMNP)*YP(2,N)**(5./3.)))**2
      IF(DISPR.GE.1.0)THEN
      APCP=(1.0/SLOPEP)*(YP(2,N)/(DX1))
      ELSE
      ENDIF
      ELSEIF(RFC.EQ.HCE)THEN
      APCP=1.-(QP(2,N)/((SQRT(SLOPEP)*CD)*YP(2,N)**(3./2.)))**2
      DISPR=(QP(2,N)/((SQRT(SLOPEP)*CD)*YP(2,N)**(3./2.)))**2
```

306

```
        IF(DISPR.GE.1.0)THEN
        APCP=(1.0/SLOPEP)*(YP(2,N)/(DX1))
        ELSE
        ENDIF
        ELSE
        ENDIF
        AKKP=AK
         IF(N.EQ.MPP.OR.KNMINP.EQ.0) THEN
           KNMINP=KNP
           KFSQRMINP=KFSQRP
           AKMAXP=AKKP
         ELSE
          ENDIF
         IF(KNMINP.GT.KNP)THEN
           KNMINP=KNP
        ELSE
        ENDIF
        IF(KFSQRMINP.GT.KFSQRP) THEN
          KFSQRMINP=KFSQRP
        ELSE
        ENDIF
        IF(APCMAXP.LT.APCP)THEN
          APCMAXP=APCP
        ELSE
        ENDIF
        IF(APPLMAX.LT.APPL)THEN
          APPLMAX=APPL
        ELSE
        ENDIF
        IF(AKMAXP.LT.AKKP)THEN
          AKMAXP=AKKP
        ELSE
        ENDIF
        ELSE
        GOTO 551
        ENDIF
        ELSE
        WRITE(*,*)'PROBLEM IN APPLICABILITY CRITERIA COMPUTATION'
        ENDIF
        continue
C   *************************************************************************
C   APPLICABILITY CRITERIA AT THE END OF THE PLANE
C   *************************************************************************
551 IF(DX1.GE.XLER)THEN   !USE DEPEND ON WHEATHER APPLICABILITY CRITERIA AT END OF REACH OR 1
        METER FROM UPSTREAM
        NAPP= NAPP+N
        KNP1=(SLOPEP*DX1)/((YP(2,N)*FSQ)) !WOOLISER AND LIGGETTEE (1967) CRITERIA
        KFSQRP1=KNP1*FSQ
        APPL1=(1.0/SLOPEP)*(YP(2,N)/(DX1))
        IF(RFC.EQ.AMN)THEN
        APCP1=1.-(QP(2,N)/((SQRT(SLOPEP)/AMNP)*YP(2,N)**(5./3.)))**2
        DISPR=(QP(2,N)/((SQRT(SLOPEP)/AMNP)*YP(2,N)**(5./3.)))**2
C   WRITE(*,*)'DISCR',DISCR
        IF(DISPR.GE.1.0)THEN
        APCP1=(1.0/SLOPEP)*(YP(2,N)/(DX1))
        ELSE
        ENDIF
        ELSEIF(RFC.EQ.HCE)THEN
        APCP1=1.-(QP(2,N)/((SQRT(SLOPEP)*CD)*YP(2,N)**(3./2.)))**2
        DISPR=(QP(2,N)/((SQRT(SLOPEP)*CD)*YP(2,N)**(3./2.)))**2
        IF(DISPR.GE.1.0)THEN
        APCP1=(1.0/SLOPEP)*(YP(2,N)/(DX1))
        ELSE
        ENDIF
        ELSE
        ENDIF
        AKKP1=AK      !DT<=K THIS CRITERIA FOR MUSKINGUM ROUTING METHOD
           IF(N.EQ.NAPP.AND.KNMINP1.EQ.0) THEN
            KNMINP1=KNP1
            KFSQRMINP1=KFSQRP1
        AKMAXP1=AKKP1
          ELSE
           ENDIF
          IF(KNMINP1.GT.KNP1)THEN
            KNMINP1=KNP1
          ELSE
          ENDIF
```

```
        IF(KFSQRMINP1.GT.KFSQRP1) THEN
          KFSQRMINP1=KFSQRP1
C          WRITE(*,*)'KFSQRP1',KFSQRMINP1
        ELSE
        ENDIF
        IF(APCMAXP1.LT.APCP1)THEN
          APCMAXP1=APCP1
        ELSE
        ENDIF
        IF(APPLMAX1.LT.APPL1)THEN
          APPLMAX1=APPL1
        ELSE
        ENDIF
        IF(AKMAXP1.LT.AKKP1)THEN
          AKMAXP1=AKKP1
        ELSE
        ENDIF
      IF(N.EQ.1)THEN
      IF(CELP(J).GT.CELPMAX)THEN
      CELPMAX=CELP(J)
      TIMEPCEL=N*DT
      ELSE
      ENDIF
      ELSEIF(N.GT.2)THEN
      IF(CELP(J).GT.CELPMAX)THEN
      CELPMAX=CELP(J)
      TIMEPCEL=N*DT
      ELSE
      ENDIF
      ELSE
      ENDIF
      ELSE
      ENDIF
20    CONTINUE
      DO 14 N=1,NDT
14    QP(1,N)=QP(2,N)
10    CONTINUE
      WRITE(*,*)
      IF(NPLANE.EQ.1.OR.NNPLANE.EQ.0.OR.NNPLANE.EQ.1)THEN
      DO 74 N=1,NDT
      QPR(2,N)=QP(2,N)
C      WRITE(2,*)'QPR(2,N)',N,(QPR(2,N)*3600.0*100.0/(XLE*B)),J
      WRITE(2,*)'QPR(2,N)',N,QPR(2,N),J
74    CONTINUE
      ELSE
      ENDIF
      NNPLANE=NNPLANE+1
      IF(NNPLANE.EQ.2)THEN
      QP(1,0)=0.0
      QP(0,1)=0.0
      DO 89 N=1,NDT
89    QP(2,N-1)=0.0
      GOTO 76
      ELSE
      ENDIF
      IF(NNPLANE.EQ.3)THEN
      DO 77 N=1,NDT
      QPL(2,N)=QP(2,N)
      WRITE(2,*)'QPL(2,N)',N,QPL(2,N),J
77    CONTINUE
      ELSE
      ENDIF
      CONTINUE
          DX1=0.0
      NDX=NDXCH
      B=BCH
      XLE=CHLEN
      DX=DXCH
      SLOPEC=SOCH
      IF(RFC.EQ.AMN)THEN
      AMNCH=AMNCH
      ELSEIF(RFC.EQ.HCE)THEN
      CD=CDCH
      ELSE
      ENDIF
      DO 92 I=1,NDT
      IF(NPLANE.EQ.1.OR.DXR.EQ.DXL)THEN
```

308

```
C      CHLAT(I)=((2.0*QPR(2,I))/BR)*DXCH
       CHLAT(I)=2.0*QPR(2,I)*DXCH
       ELSE
C      CHLAT(I)=((QPR(2,I)/BR)+(QPL(2,I)/BL))*DXCH
       CHLAT(I)=(QPR(2,I)+QPL(2,I))*DXCH
       ENDIF
C      WRITE(2,*)'CAT(I)',CHLAT(I),QPR(2,I),QPL(2,I),NPLANE,I,BR,BL,DXCH
92     CONTINUE
       DO 93 J=1,NDX
       DX1=DX1+DX
       T=0.0
       QCH(2,0)=0.0
       DO 94 N=2,NDT
       T=T+DT
       RAINT=RAIN(N)
       RCMS=(RAINT)*DXCH*BCH
C      CATCHMENT ROUTING CALCULATIONS
C      WRITE(*,*)NRDT,RADURS
c      IF(T.LE.NRDT)THEN
C      QLCH=RCMS+CHLAT(N)
       QLCH=CHLAT(N)
       PP=(RAINT)*DXCH*BCH
       IF(J.EQ.1)THEN
       QO=(QLCH+QCH(2,N-1))/2.
       ELSEIF(J.GT.1)THEN
C      QO=(((QP(1,N)+QP(1,N-1)+QP(2,N-1))/3.)+QLCH)/2.0
       QO=((QCH(1,N)+QCH(1,N-1)+QCH(2,N-1))/3.)
       ELSE
       ENDIF
       IF(QO.LE.0.0) GOTO 94
C      WRITE(*,*)'QO'
C      WRITE(*,*)QO
       QLCHN(N)=QLCH
C      WRITE(*,*)'QLCHN(N)'
C      WRITE(*,*)QLCHN(N),J,N
       IF(RFC.EQ.AMN)THEN
         CONST=(1./AMNCH)*SQRT(SLOPEC)*B**(5./3.)
       IF (J.EQ.1)      THEN
       YAV=(QO/((1./AMNCH)*SQRT(SLOPEC)*B))**(3./5.)
       VEL=QO/(YAV*B)
       R=YAV/(B+2.*YAV)
       CEL=5./3.*VEL
       CEL=(5./3.-(4./3.*R))*VEL
       AK=DX/CEL
       GOTO 257
         ELSE
         ENDIF
       I=1
       Y(I)=0.001
       FUNC(I)=QO-CONST*Y(I)**(5./3.)/(B+2*Y(I))**(2./3.)
       I=2
       Y(I)=Y(I-1)+0.2*Y(I-1)
C        WRITE(*,*)'Y(I)',Y(I)
96     FUNC(I)=QO-CONST*Y(I)**(5./3.)/(B+2*Y(I))**(2./3.)
       DYM=-FUNC(I)*(Y(I)-Y(I-1))/(FUNC(I)-FUNC(I-1))
       Y(I+1)=Y(I)+DYM
       IF(ABS((Y(I+1)-Y(I))/Y(I+1)).LT.0.00001) GOTO 97
       I=I+1
       GOTO 96
97     Y(I+1)=Y(I+1)
       CONTINUE
         ELSEIF(RFC.EQ.HCE)THEN
       CONST=CD*SQRT(SLOPEC)
         IF (J.EQ.1)      THEN
       YAV=(QO/(CONST*B))**(2./3.)
       VEL=QO/(YAV*B)
       R=YAV/(B+2.*YAV)
C      CEL=(3./2.-R)*VEL
       CEL=3./2.*VEL
       AK=DX/CEL
       GOTO 257
       ELSE
       ENDIF
       I=1
       Y(I)=0.001
       FUNC(I)=QO-CONST*(Y(I)*B)**(3./2.)/(B+2*Y(I))**(1./2.)
       I=2
```

309

```
      Y(I)=Y(I-1)+0.2*Y(I-1)
98    FUNC(I)=QO-CONST*(Y(I)*B)**(3./2.)/(B+2*Y(I))**(1./2.)
      DYM=-FUNC(I)*(Y(I)-Y(I-1))/(FUNC(I)-FUNC(I-1))
      Y(I+1)=Y(I)+DYM
      IF(ABS((Y(I+1)-Y(I))/Y(I+1)).LT.0.000001) GOTO 99
      I=I+1
      GOTO 98
99    Y(I+1)=Y(I+1)
      CONTINUE
        ELSE
      WRITE(*,*)'WRONG FRICTION FORMULA USED IN COMPUTATION.'
      ENDIF
      YIN=Y(I+1)
C*********************************************************************************
C           FSQ      - SQUARE OF FROUDE NUMBER.                                 *
C           R        - HYDRAULIC RADIUS.                                        *
C           THETA    - WEIGHTING PARAMETER.                                     *
C           THETAN   - NUMERATOR OF THE WEIGHTING PARAMETER.                    *
C           THETAD   - DENOMINATOR OF THE WEIGHTING PARAMETER.                  *
C*********************************************************************************
      IF(RFC.EQ.AMN)THEN
      VCH(J)=(1./AMNCH)*SQRT(SLOPEC)*(YIN*B)**(2./3.)/
1     ((B+2*YIN)**(2./3.))
      FSQ=VCH(J)**2.0*B/(G*(B*YIN))
      R=YIN/(B+2.*YIN)
      CELCH(J)=VCH(J)*(5./3.-(4./3.*R))
      AK=DX/CELCH(J)
      THETAN=YIN**(1.+4./9.*FSQ*(-1.+4.*R-4.*R*R))
      THETAD=2.*SLOPEC*(5./3.-4./3.*R)*DX
      ELSEIF(RFC.EQ.HCE)THEN
      VCH(J)=CONST*(YIN*B)**(1./2.)/((B+2*YIN)**(1./2.))
      FSQ=VCH(J)**2.0*B/(G*(B*YIN))
      R=YIN/(B+2.*YIN)
      CELCH(J)=VCH(J)*(3./2.-R)
      AK=DX/CELCH(J)
      THETAN=YIN*(1.+1./4.*FSQ*(-1.+4.*R-4.*R*R))
      THETAD=2.*SLOPEC*(3./2.-R)*DX
       ELSE
       WRITE(*,*)'WRONG FRICTION FORMULA USED IN COMPUTATION.'
       ENDIF
      THETA=0.5-THETAN/THETAD
257   IF (J.EQ.1) THEN
      CDN1=AK+DT/2.
      CUP1=(AK-DT/2.)/CDN1
      CUP2=DT/CDN1
      QCH(2,N)=CUP1*QCH(2,N-1)+CUP2*QLCHN(N)
      GOTO 94
      ELSE
      ENDIF
      YMID=YIN
C        COUNTER M IS USED FOR UPDATING THE PARAMETERS AT ANY TIME
      M=0
17    DNMTR=AK*(1.-THETA)+(DT/2.)
C         C1P, C2P,C3P AND C4P ARE THE COEFFICIENTS OF THE MUSKINGUM ROUTING EQUATION.
      C1P=(-(AK*THETA)+(DT/2.))/DNMTR
      C2P=(AK*THETA+DT/2.)/DNMTR
      C3P=(AK*(1.-THETA)-DT/2.)/DNMTR
      C4P=DT/DNMTR
18    M=M+1
C         COMPUTATION OF OUTFLOW
      QCH(2,N)=C1P*QCH(1,N)+C2P*QCH(1,N-1)+C3P*QCH(2,N-1)+C4P*QLCHN(N)
C         COMPUTATION OF WEIGHTED OUTFLOW.
      Q3=QCH(2,N)+THETA*(QCH(1,N)-QCH(2,N))
      IF(Q3.LE.0.0)THEN
      GOTO 751
      ELSE
      Q3=Q3
      ENDIF
       IF(RFC.EQ.AMN)THEN
         CONST=(1./AMNCH)*SQRT(SLOPEC)*B**(5./3.)
         I=1
         YM(I)=YMID
C         FINDING THE STAGE AT THE MIDDLE OF THE REACH
      FUNC(I)=Q3-CONST*YM(I)**(5./3.)/(B+2.*YM(I))**(2./3.)
         I=2
         YM(I)=YMID+0.2*YMID
702   FUNC(I)=Q3-CONST*YM(I)**(5./3.)/(B+2.*YM(I))**(2./3.)
```

```
          DYM=-FUNC(I)*(YM(I)-YM(I-1))/(FUNC(I)-FUNC(I-1))
          YM(I+1)=YM(I)+DYM
          IF(ABS((YM(I+1)-YM(I))/YM(I+1)).LT.0.00001)GOTO 703
          I=I+1
          GOTO 702
703       YMID=YM(I+1)
C     WRITE(*,*)'YMID=',YMID
C         COMPUTATION OF DISCHARGE AT THE MIDDLE OF THE REACH
      QMID=(QCH(1,N)+QCH(2,N))/2.
C         COMPUTATION OF THE SQUARE OF FROUDE NUMBER.
      FSQ=(QMID*QMID*B)/(G*(B*YMID)**3)
C         COMPUTATION OF THE STAGE AT THE OUTFLOW SECTION.
      YCH(2,N)=YMID+(QCH(2,N)-QMID)/
     1((5./3.-4./3.*(YMID/(B+2.*YMID)))*QMID/YMID)
C         COMPUTATION OF STAGE AT THE WEIGHTED OUTFLOW SECTION.
      Y3=YMID+(Q3-QMID)/
     1((5./3.-4./3.*(YMID/(B+2.*YMID)))*QMID/YMID)
C         COMPUTATION OF VELOCITY AT THE WEIGHTED OUTFLOW SECTION.
      V3=Q3/(B*Y3)
C         COMPUTATION OF WAVE CELERITY OF THE REACH.
      CELCH(J)=(5./3.-((4./3.)*Y3/(B+2.*Y3)))*V3
C         COMPUTATION OF PARAMETERS AK AND THETA.
      AK=DX/CELCH(J)
      R=YMID/(B+2.*YMID)
      THETAN=Y3*(1.+4./9.*FSQ*(-1.+4.*R-4.*R*R))
C     THETAN=Y3
      THETAD=2.*SLOPEC*(5./3.-4./3.*R)*DX
C     GM=(QCOM(J)-AI(J))*THETAN/(THETAD*Q3)
      GM=0.
      THETA=0.5-(THETAN/THETAD)*(0.5+0.125*GM+(1./16.)*GM*GM
     1 +(5./128.)*GM**3+(7./256.)*GM**4)
C     WRITE(*,*)AK,CELP(J),THETA
C     WRITE(*,*)'QP(J,N)=',QP(J,N)
C         COMPUTATION OF STAGE AT THE INLET OF THE REACH
C     IF(DX1.EQ.DX)Y1(J)=2.*YMID-YCOM(J)
      IF(DX1.EQ.DX) Y1(J)=YMID+(QP(J-1,N)-QMID)/
     1((5./3.-4./3.*(YMID/(B+2.*YMID)))*QMID/YMID)
      ELSEIF(RFC.EQ.HCE)THEN
          CONST=CD*SQRT(SLOPEC)*B**(3./2.)
          I=1
          YM(I)=YMID
C         FINDING THE STAGE AT THE MIDDLE OF THE REACH
          FUNC(I)=Q3-CONST*YM(I)**(3./2.)/(B+2.*YM(I))**(1./2.)
          I=2
          YM(I)=YMID+0.2*YMID
704       FUNC(I)=Q3-CONST*YM(I)**(3./2.)/(B+2.*YM(I))**(1./2.)
          DYM=-FUNC(I)*(YM(I)-YM(I-1))/(FUNC(I)-FUNC(I-1))
          YM(I+1)=YM(I)+DYM
          IF(ABS((YM(I+1)-YM(I))/YM(I+1)).LT.0.000001)GOTO 706
          I=I+1
          GOTO 704
706       YMID=YM(I+1)
C         COMPUTATION OF DISCHARGE AT THE MIDDLE OF THE REACH
      QMID=(QCH(1,N)+QCH(2,N))/2.
C         COMPUTATION OF THE SQUARE OF FROUDE NUMBER.
      FSQ=(QMID*QMID*B)/(G*(B*YMID)**3)
C         COMPUTATION OF THE STAGE AT THE OUTFLOW SECTION.
      YCH(2,N)=YMID+(QP(2,N)-QMID)/
     1((3./2.-(YMID/(B+2.*YMID)))*QMID/YMID)
C         COMPUTATION OF STAGE AT THE WEIGHTED OUTFLOW SECTION.
      Y3=YMID+(Q3-QMID)/
     1((3./2.-(YMID/(B+2.*YMID)))*QMID/YMID)
C         COMPUTATION OF VELOCITY AT THE WEIGHTED OUTFLOW SECTION.
      V3=Q3/(B*Y3)
C         COMPUTATION OF WAVE CELERITY OF THE REACH.
      CELCH(J)=(3./2.-(Y3/(B+2.*Y3)))*V3
C         COMPUTATION OF PARAMETERS AK AND THETA.
      AK=DX/CELCH(J)
      R=YMID/(B+2.*YMID)
      THETAN=Y3*(1.+1./4.*FSQ*(-1.+4.*R-4.*R*R))
C     THETAN=Y3
      THETAD=SLOPEC*(3./2.-R)*DX
C     GM=(QCOM(J)-AI(J))*THETAN/(THETAD*Q3)
      GM=0.
      THETA=0.5-(THETAN/THETAD)*(0.5+0.125*GM+(1./16.)*GM*GM
     1 +(5./128.)*GM**3+(7./256.)*GM**4)
C     WRITE(*,*)AK,CELP(J),THETA
```

311

```
C       WRITE(*,*)'QP(J,N)=',QP(J,N)
C           COMPUTATION OF STAGE AT THE INLET OF THE REACH
C       IF(DX1.EQ.DX)Y1(J)=2.*YMID-YCOM(J)
        IF(DX1.EQ.DX) Y1(J)=YMID+(QP(1,N)-QMID)/
       1((3./2.-(YMID/(B+2.*YMID)))*QMID/YMID)
        ELSE
         WRITE(*,*)'WRONG FRICTION FORMULA USED IN COMPUTATION.'
        ENDIF
751     IF(M.LE.1) GOTO 17
        IF(QCH(2,N).LE.0.0)THEN
        QCH(2,N)=0.0
        GOTO 94
        ELSE
        QCH(2,N)=QCH(2,N)
        ENDIF
C       ******************************************************************
C           APPLICABILITY CRITERIA TO CHECK SUITABILITY OF METHOD
C       ******************************************************************
C       APPLICABILITY CRITERIA AT ONE METER FROM U/S
C       ******************************************************************
        FET=1.0/0.3048
        FET2=1.2/0.3048
        MP=MP+N
        IF(UNITS.EQ.KMS)THEN
        IF(DX1.GE.0.97.AND.DX1.LE.(1.2))THEN
        KN=(SLOPEC*DX1)/((YCH(2,N)*FSQ)) !WOOLISER AND LIGGETTEE (1967) CRITERIA
        KFSQR=KN*FSQ
        APPC=(1.0/SLOPEC)*(YCH(2,N)/(DX1))
        IF(RFC.EQ.AMN)THEN
        APC=1.-((QCH(2,N)/BCH)/((SQRT(SLOPEC)/AMNCH)*YCH(2,N)
       1 **(5./3.)))**2
        DISCR=((QCH(2,N)/BCH)/((SQRT(SLOPEC)/AMNCH)*YCH(2,N)**(5./3.)))**2
        IF(DISCR.GE.1.0)THEN
        APC=(1.0/SLOPEC)*(YCH(2,N)/(DX1))
        ELSE
        ENDIF
        ELSEIF(RFC.EQ.HCE)THEN
        APC=1.-((QCH(2,N)/BCH)/((SQRT(SLOPEC)*CD)*YCH(2,N)**(3./2.)))**2
        DISCR=((QCH(2,N)/BCH)/((SQRT(SLOPEC)*CD)*YCH(2,N)**(3./2.)))**2
        IF(DISCR.GE.1.0)THEN
        APC=(1.0/SLOPEC)*(YCH(2,N)/(DX1))
        ELSE
        ENDIF
        ELSE
        ENDIF
        AKK=AK
          IF(N.EQ.MP.OR.KNMIN.EQ.0) THEN
            KNMIN=KN
           KFSQRMIN=KFSQR
           AKMAX=AKK
          ELSE
           ENDIF
          IF(KNMIN.GT.KN)THEN
            KNMIN=KN
          ELSE
          ENDIF
          IF(KFSQRMIN.GT.KFSQR) THEN
           KFSQRMIN=KFSQR
          ELSE
          ENDIF
          IF(APCMAX.LT.APC)THEN
           APCMAX=APC
          ELSE
          ENDIF
          IF(APPCMAX.LT.APPC)THEN
           APPCMAX=APPC
          ELSE
          ENDIF
          IF(AKMAX.LT.AKK)THEN
           AKMAX=AKK
          ELSE
          ENDIF
        ELSE
        GOTO 555
        ENDIF
        ELSEIF(UNITS.GE.PFS) THEN
        IF(DX1.GE.FET.AND.DX1.LE.FET2)THEN
```

312

```
       KN=(SLOPEC*DX1)/((YCH(2,N)*FSQ)) !WOOLISER AND LIGGETTEE (1967) CRITERIA
       KFSQR=KN*FSQ
       APPC=(1.0/SLOPEC)*(YCH(2,N)/(DX1))
       IF(RFC.EQ.AMN)THEN
       APC=1.-((QCH(2,N)/BCH)/((SQRT(SLOPEC)/AMNCH)*YCH(2,N)
     1 **(5./3.)))**2
       DISCR=((QCH(2,N)/BCH)/((SQRT(SLOPEC)/AMNCH)*YCH(2,N)**(5./3.)))**2
       IF(DISCR.GE.1.0)THEN
       APC=(1.0/SLOPEC)*(YCH(2,N)/(DX1))
       ELSE
       ENDIF
       ELSEIF(RFC.EQ.HCE)THEN
       APC=1.-((QCH(2,N)/BCH)/((SQRT(SLOPEC)*CD)*YCH(2,N)**(3./2.)))**2
       DISCR=((QCH(2,N)/BCH)/((SQRT(SLOPEC)*CD)*YCH(2,N)**(3./2.)))**2
       IF(DISCR.GE.1.0)THEN
       APC=(1.0/SLOPEC)*(YCH(2,N)/(DX1))
       ELSE
       ENDIF
       ELSE
       ENDIF
       AKK=AK
C      WRITE(4,*)T,KN,APC,KFSQR
       IF(N.EQ.MP.OR.KNMIN.EQ.0) THEN
         KNMIN=KN
         KFSQRMIN=KFSQR
         AKMAX=AKK
       ELSE
         ENDIF
       IF(KNMIN.GT.KN)THEN
         KNMIN=KN
       ELSE
       ENDIF
       IF(KFSQRMIN.GT.KFSQR) THEN
         KFSQRMIN=KFSQR
       ELSE
       ENDIF
       IF(APCMAX.LT.APC)THEN
         APCMAX=APC
       ELSE
       ENDIF
       IF(APPCMAX.LT.APPC)THEN
         APPCMAX=APPC
       ELSE
       ENDIF
       IF(AKMAX.LT.AKK)THEN
         AKMAX=AKK
       ELSE
       ENDIF
       ELSE
       GOTO 555
       ENDIF
       ELSE
       WRITE(*,*)'PROBLEM IN APPLICABILITY CRITERIA COMPUTATION'
       ENDIF
       continue
C      ***********************************************************************
C      APPLICABILITY CRITERIA AT THE END OF THE PLANE
C      ***********************************************************************
555    IF(DX1.GE.CHLEN)THEN          !USE DEPEND ON WHEATHER APPLICABILITY CRITERIA AT END OF REACH OR 1
       METER FROM UPSTREAM
       NAP= NAP+N
       KN1=(SLOPEC*DX1)/((YCH(2,N)*FSQ)) !WOOLISER AND LIGGETTEE (1967) CRITERIA
       KFSQR1=KN1*FSQ
       APPC1=(1.0/SLOPEC)*(YCH(2,N)/(CHLEN))
       IF(RFC.EQ.AMN)THEN
       APC1=1.-((QCH(2,N)/BCH)/((SQRT(SLOPEC)/AMNCH)*YCH(2,N)
     1 **(5./3.)))**2
       DISCR=((QCH(2,N)/BCH)/((SQRT(SLOPEC)/AMNCH)*YCH(2,N)**(5./3.)))**2
C      WRITE(*,*)'DISCR',DISCR
       IF(DISCR.GE.1.0)THEN
       APC1=(1.0/SLOPEC)*(YCH(2,N)/(CHLEN))
       ELSE
       ENDIF
       ELSEIF(RFC.EQ.HCE)THEN
       APC1=1.-((QCH(2,N)/BCH)/((SQRT(SLOPEC)*CD)*YCH(2,N)**(3./2.)))**2
       DISCR=((QCH(2,N)/BCH)/((SQRT(SLOPEC)*CD)*YCH(2,N)**(3./2.)))**2
       IF(DISCR.GE.1.0)THEN
```

313

```
        APC1=(1.0/SLOPEC)*(YCH(2,N)/(CHLEN))
        ELSE
        ENDIF
        ELSE
        ENDIF
        AKK1=AK        !DT<=K THIS CRITERIA FOR MUSKINGUM ROUTING METHOD
C       WRITE(4,*)T,KN1,APC1,KFSQR1
            IF(N.EQ.NAP.AND.KNMIN1.EQ.0) THEN
            KNMIN1=KN1
            KFSQRMIN1=KFSQR1
            AKMAX1=AKK1
C       WRITE(*,*)'KFSQRMIN1',KFSQRMIN1
            ELSE
            ENDIF
            IF(KNMIN1.GT.KN1)THEN
            KNMIN1=KN1
            ELSE
            ENDIF
            IF(KFSQRMIN1.GT.KFSQR1) THEN
            KFSQRMIN1=KFSQR1
c       WRITE(*,*)'KFSQR1',KFSQRMIN1
            ELSE
            ENDIF
            IF(APCMAX1.LT.APC1)THEN
            APCMAX1=APC1
            ELSE
            ENDIF
            IF(APPCMAX1.LT.APPC1)THEN
            APPCMAX1=APPC1
            ELSE
            ENDIF
            IF(AKMAX1.LT.AKK1)THEN
            AKMAX1=AKK1
            ELSE
            ENDIF
C       WRITE(*,*)'KFSQR1',KFSQRMIN1
            ELSE
            GOTO 565
            ENDIF
565     IF(UNITS.EQ.KMS)THEN
        QP1(2,N)=QCH(2,N)
        QP2(2,N)=QP1(2,N)/2.54
        QP3(2,N)=QP1(2,N)/360000.0*10.0**5.
        ELSEIF(UNITS.EQ.PFS)THEN
        QP1(2,N)=QCH(2,N)*3600.0*100.0*0.3048
        QP2(2,N)=QP1(2,N)/2.54
        QP3(2,N)=QP1(2,N)/360000.0*10.0**5.
        ELSE
        WRITE(*,*)'WRONG OUTPUT HYDROGRAPH'
        ENDIF
        IF(QP1(2,N).LT.0.000001)THEN
        QP1(2,N)=0.0
        ELSE
        QP1(2,N)=QP1(2,N)
        ENDIF
        IF(N.EQ.1)THEN
        IF(CELCH(J).GT.CELCMAX)THEN
        CELCMAX=CELCH(J)
        TIMECCEL=N*DT
        ELSE
        ENDIF
        ELSEIF(N.GT.2)THEN
        IF(CELCH(J).GT.CELCMAX)THEN
        CELCMAX=CELCH(J)
        TIMECCEL=N*DT
        ELSE
        ENDIF
        ELSE
        ENDIF
15      FORMAT(1X,'SUBREACH=',I5,5X,'Y('I5')=',F10.6,5X,'QP('I3,',',I5,
     1   ')=',F12.9)
94      CONTINUE
        DO 16 N=1,NDT
16      QCH(1,N)=QCH(2,N)
93      CONTINUE
25      FORMAT(4X,'TIME STEP',2X,'LATER FLOW (M3/SEC OR FT3/SEC)',F10.8)
        DO 40 N=1,NDT
```

```fortran
      QLC(N)=QCH(2,N-1)+QCH(2,N)
 40   CONTINUE
      qp1(2,0)=0.0
      qp2(2,0)=0.0
      qp3(2,0)=0.0
      DO 55 L=1, NDT
      Runoffvol=Runoffvol+QCH(2,L)*DT
      IF(BMDATA.EQ.MCPH)THEN
      QP1(2,L)=QP1(2,L)
      QCAL(L)=QP1(2,L)
      ELSEIF(BMDATA.EQ.NIPH)THEN
      QP2(2,L)=QP2(2,L)
      QCAL(L)=QP2(2,L)
      ELSEIF(BMDATA.EQ.PMSM)THEN
      QP3(2,L)=QP3(2,L)
      QCAL(L)=QP3(2,L)
C     WRITE(6,*)QCMP(L),QP3(2,L),N
      ELSE
      WRITE(*,*)'WRONG UNITS OF PREDICTED AND BENCH MARK DATA'
      ENDIF
      IF(L.EQ.I)THEN
      QPKCMAX=QCAL(L)
      TPKCMAX=(L*DT)/60.0
C     WRITE(*,*)QPKCMAX,TPKCMAX
      ELSE
      ENDIF
      IF(L.GT.1)THEN
      QPKC=QCAL(L)
c     write(*,*)'qpkc',qpkc,L
      IF(QPKC.GT.QPKCMAX.AND.QPKC.NE.QPKCMAX)THEN
      QPKCMAX=QPKC
      TPKCMAX=(L*DT)/60.0
c     WRITE(*,*)QPKCMAX,TPKCMAX
      ELSE
      ENDIF
      ELSE
      ENDIF
 55   CONTINUE
      DO 60 L=1,NDT-1,2
 60   SUMA=SUMA+QCH(2,L)
C     WRITE(*,*)'SUMA'
C     WRITE(*,*)SUMA
      DO 70 L=2, NDT-2,2
 70   SUMB=SUMB+QCH(2,L)
      VOL=(DT/3.)*(QCH(2,0)+4*SUMA+2*SUMB+QCH(2,NDT))+CFVOL
 250  FORMAT(2X,'SUMA=',F12.6,2X,'SUMB=',F12.6,2X,'VOL=',F12.6)
      TIMESEC=-DT
      DO 80 N=0,NDT
      TIMESEC=TIMESEC+DT
      TIMEMIN=TIMESEC/60.
      IF(N.GT.NDT.AND.QCH(2,N).LT.0.00001)THEN
      GOTO 90
      ELSE
      WRITE(2,*)N,TIMESEC,TIMEMIN,QP2(2,N),QP3(2,N)
      WRITE(5,*)N,TIMESEC,TIMEMIN,QP1(2,N),YCH(2,N)*100.0
      IF (N.EQ.NS.AND.NS.LE.(ND*TSKIP))THEN
C     WRITE(*,*)QP1(NDX,NS)
C************************************************************************
C     CHECKING OF UNITS OUTPUT HYDROGRAPH AND BENCHMARK OUTPUT HYDROGRAPH        *
C************************************************************************
      IF(BMDATA.EQ.MCPH)THEN
      QP1(2,NS)=QP1(2,NS)
      QCAL(LC)=QP1(2,NS)
      ELSEIF(BMDATA.EQ.NIPH)THEN
      QP2(2,NS)=QP2(2,NS)
      QCAL(LC)=QP2(2,NS)
      ELSEIF(BMDATA.EQ.PMSM)THEN
      QP3(2,NS)=QP3(2,NS)
      QCAL(LC)=QP3(2,NS)
      ELSE
      WRITE(*,*)'WRONG UNITS OF PREDICTED AND BENCH MARK DATA'
      ENDIF
C     WRITE(7,*)QCAL(LC),LC
      LC=LC+1
      NS=N+(TSKIP)
C     WRITE (*,*)'NS',NS, QCAL(LC)
      ELSE
```

315

```
      ENDIF
      ENDIF
 80  CONTINUE
 90  CONTINUE
C***********************************************************************
C    USING NASH-SUTCLIFFE CRITERION FOR VERIFICATION            *
C***********************************************************************
      NEM=0.0
      SUMQCAL=0.0
      IF(DT.LE.TIOBS*60.0)THEN
      IF(TST.LT.(ND*TIOBS))THEN
      ND=NDT/TSKIP+1
      ELSE
      ENDIF
      ELSE
      ENDIF
      IF(ND.LE.NDT)THEN
      ND=ND
      ELSE
      ND=NDT+1
      ENDIF
      DO 201 ND=1,ND
      WRITE(*,*)QCAL(ND-1),QOBS(ND),ND
      IF(DT.LE.(TIOBS*60.0))THEN
      ANC=((TIOBS*60.0)/DT)*TIOBS
      WRITE(9,*)((ND-1)*TIOBS),(((ND-1)*TIOBS)*60.0),QCAL(ND-1),QOBS(ND)
c     WRITE(9,*)(((ND-1)*TIOBS)*60.0),QCAL(ND-1)
      ELSEIF(DT.GE.(TIOBS*60.0))THEN
      ANC=(DT/(TIOBS*60.0))*TIOBS
      WRITE(9,*)((ND-1)*ANC),QCAL(ND-1),QOBS(ND)
      ELSE
      ENDIF
      QMEAN=QMEAN
      SUMQCAL=SUMQCAL+QCAL(ND-1)
      ANEM=ANEM+(QOBS(ND)-QCAL(ND-1))**2
      DEN=DEN+(QOBS(ND)-QMEAN)**2
      RDEN=RDEN+(QCAL(ND-1)-QMEAN)**2
      RNEM=RNEM+(QCAL(ND-1)-QOBS(ND))**2
C     WRITE(*,*)DEN,ANEM
201  CONTINUE
c     WRITE(*,*)NEM,DEN
      ANEM=ANEM
      DEN=DEN
     EFFNS=(1-(ANEM/DEN))*100
C *********************************************************************
C    MEASURES FOR ANALYSIS OF RESIDUAL ERRORS (LOAGUE AND GREEN, 1991)  *
C    ROOT MEAN SQUARE ERROR                                             *
C*********************************************************************
      RMSE=(RNEM/(ND))**(0.5)*(100./QMEAN)
      CRM=(SUMQOBS-SUMQCAL)/SUMQOBS*100
      CD=(DEN/RDEN)
      EF=(DEN-RNEM)/DEN*100
C *********************************************************************
      WRITE(*,*)'EFFNS',EFFNS,ANEM,DEN,QMEAN,KNMIN1,KFSQR1
      CONTINUE
      DO 3 L=1,NIER
      RADUR(L)=PT(L)*60
       IF(UNITS.EQ.KMS)THEN
        SRFVOL=QEE(L)/(360000.0)*(RADUR(L)-RADUR(L-1))
        RFVOL=RFVOL+SRFVOL  !RAINFALL VOLUME IN CUBIC METER PER SEC
       ELSEIF(UNITS.EQ.PFS)THEN
        SRFVOL=QEE(L)/(3600.0*12.0)*(RADUR(L)-RADUR(L-1))
        RFVOL=RFVOL+SRFVOL  !RAINFALL VOLUME IN CUBIC FEET PER SEC
       ELSE
       WRITE(*,*)'ERROR IN COMPUTATION'
       ENDIF
      WRITE(*,*)RFVOL,SRFVOL,RADUR(L),QEE(L)
 3    CONTINUE
C*********************************************************************
C    USE THIS FORMULA WHEN RAINFALLING ON CHANNEL IS CONSIDERED       *
C*********************************************************************
      RFVOL=RFVOL*(XLER*BR+XLEL*BL) !RAINFALL VOLUME IN CUBIC FEET PER SEC
      EVOL=(VOL-RFVOL)/RFVOL*100.
      QPKER=((QPKCMAX/QPKOMAX)-1.0)*100.0
      TPKER=(TPKCMAX-TPKOMAX)
C     FROUDE NUMBER COMPUTATIONS FOR PLANE
      IF(KFSQRMINP.GT.0.0.AND.KNMINP.GT.0.0)THEN
```

316

```
        F0UPP=SQRT(KFSQRMINP/KNMINP)
        ELSE
        F0UPP=0.0
        ENDIF
        IF(KFSQRMINP1.GT.0.0.AND.KNMINP1.GT.0.0)THEN
        F0DOWNP=SQRT(KFSQRMINP1/KNMINP1)
        ELSE
        F0DOWNP=0.0
        ENDIF
C    FROUDE NUMBER COMPUTATIONS FOR CHANNEL
        IF(KFSQRMIN.GT.0.0.AND.KNMIN.GT.0.0)THEN
        F0UP=SQRT(KFSQRMIN/KNMIN)
        ELSE
        F0UP=0.0
        ENDIF
        IF(KFSQRMIN1.GT.0.0.AND.KNMIN1.GT.0.0)THEN
        F0DOWN=SQRT(KFSQRMIN1/KNMIN1)
        ELSE
        F0DOWN=0.0
        ENDIF
        WRITE(*,*)'EVOL',EVOL,VOL,RFVOL,KNMIN1,KFSQR1
        WRITE(2,400)SUMA,SUMB,CFVOL,EFFNS
        WRITE(*,*)SUMA,SUMB,CFVOL,EFFNS
        WRITE(5,*)'
        WRITE(5,*)'ALLICABILITY CRITERIA FOR PLANE
        WRITE(5,*)'
        WRITE(5,*)' APPLICABILITY CRITERIA AT APPROX.1 METER FROM U/S'
        WRITE(5,456)KNMINP,APCMAXP,KFSQRMINP,F0UPP,AKMAXP
456 FORMAT(2X,'KW NUMBER (MINIMUM)=',F12.4,2X,'MAX [(1/SO)*dY/dX]=',
   1 F12.4,2X,'MIN [KN*SQURE F0]=',F12.4,2X,'MAX [K]=',F12.6)
        WRITE(5,*)' APPLICABILITY CRITERIA AT THE END OF PLANE'
        WRITE(5,457)KNMINP1,APCMAXP1,KFSQRMINP1,F0DOWNP,AKMAXP1
457 FORMAT(2X,'KW NUMBER (MINIMUM)=',F12.4,2X,'MAX [(1/SO)*dY/dX]=',
   1 F12.4,2X,'MIN [KN*SQURE F0]=',F12.4,2X,'MAX [K]=',F12.6)
        WRITE(5,*)'$$$$$$$$$$$$$$$$$$$$$$$$$$$$$$$$$$$$$$$$$$$$$$$$$$$$$$$$$$$$$$'
        WRITE(5,*)'    APPLICABILITY CRITERIA USING 1/SO*DY/DX  PLANE '
        WRITE(5,*)'$$$$$$$$$$$$$$$$$$$$$$$$$$$$$$$$$$$$$$$$$$$$$$$$$$$$$$$$$$$$$$'
        WRITE(5,*)'APC AT APPR. 1M FROM U/S=',APPLMAX
        WRITE(5,*)'APC AT D/S END=',APPLMAX1
400 FORMAT(2X,'SUMA=',F10.5,2X,'SUMB=',F10.5,2X,'Cumul.Infiltration
   1  volume=',F10.5,2X,'NASH-SUTCLIFFE EFFICIENCY=',F12.6)
        WRITE(2,425)VOL,RFVOL,EVOL,Runoffvol,EFFNS
425 FORMAT(2X,'VOL=',F12.6,2X,'RFVOL=',F12.6,2X,'EVOL=',F12.6,2X,
   1'Runoffvol=',F12.6,2X,'NASH-SUTCLIFFE EFFICIENCY=',F12.6)
        WRITE(2,415)RMSE,CRM,CD,EF,EFFNS
415 FORMAT(2X,'ROOT MEAN SQUARE ERROR=',F12.6,2X,'COEFFICIENT OF
   1 RESIDUAL MASS=',F12.6,2X,'COEFF. DETERMINATION=',F12.6,2X,'
   1MODELING EFFICIENCY=',F12.6,2X,'NASH-SUTCLIFFE EFFICIENCY=',F12.6)
        WRITE(5,455)SUMA,SUMB,CFVOL
455 FORMAT(2X,'SUMA=',F10.5,2X,'SUMB=',F10.5,2X,'Cumul.Infiltration
   1  volume=',F10.5)
        WRITE(5,452)VOL,RFVOL,EVOL,Runoffvol
452 FORMAT(2X,'VOL=',F12.6,2X,'RFVOL=',F12.6,2X,'EVOL=',F12.6,2X,
   1'Runoffvol=',F12.6)
        WRITE(5,*)' MODEL PERFORMANCE CRITERIA'
        WRITE(5,451)RMSE,CRM,CD,EF,EFFNS
451 FORMAT(2X,'ROOT MEAN SQUARE ERROR=',F12.6,2X,'COEFFICIENT OF
   1RESIDUAL MASS=',F12.6,/,2X,'COEFF. DETERMINATION=',F12.6,2X,'
   1MODELING EFFICIENCY=',F12.6,/,2X'NASH-SUTCLIFFE EFFICIENCY='
   2,F12.6)
        WRITE(5,*)' APPLICABILITY CRITERIA AT APPROX.1 METER FROM U/S'
        WRITE(5,453)KNMIN,APCMAX,KFSQRMIN,AKMAX
453 FORMAT(2X,'KW NUMBER (MINIMUM)=',F12.4,2X,'MAX [(1/SO)*dY/dX]=',
   1 F12.4,2X,'MIN [KN*SQURE F0]=',F12.4,2X,'MAX [K]=',F12.6)
        WRITE(5,*)' APPLICABILITY CRITERIA AT THE END OF CHHANEL'
        WRITE(5,454)KNMIN1,APCMAX1,KFSQRMIN1,AKMAX1
454 FORMAT(2X,'KW NUMBER (MINIMUM)=',F12.4,2X,'MAX [(1/SO)*dY/dX]=',
   1 F12.4,2X,'MIN [KN*SQURE F0]=',F12.4,2X,'MAX [K]=',F12.6)
        ELAPSED_TIME=TIMEF()
        WRITE(5,*)'EXCUTION_TIME',ELAPSED_TIME,' SEC'
        WRITE(5,*)'QPKCMAX,TPKCMAX',QPKCMAX,' BMDATA',TPKCMAX,' MIN'
C51 CONTINUE
        WRITE(5,*)'QPKOMAX,TPKOMAX',QPKOMAX,' BMDATA',TPKOMAX,' MIN'
        WRITE(5,*)'QPKCERROR,TPKCERROR',QPKER,' %',TPKER,' MIN'
        WRITE(5,*)' COURANT CONDITION CHECK FOR PLANE'
        WRITE(5,366)CELPMAX,(TIMEPCEL/60.0),GRIDRATIOP
366 FORMAT(2X,'MAX CELERITY=',F10.8,7X,'TIME OF MAX CELERITY (MIN)='
```

```
   1 ,F10.4,7X,'GRID RATIO=',F10.8)
     WRITE(5,*)' COURANT CONDITION CHECK FOR CHANNEL'
     WRITE(5,367)CELCMAX,(TIMECCEL/60.0),GRIDRATIOC
 367 FORMAT(2X,'MAX CELERITY=',F10.8,7X,'TIME OF MAX CELERITY (MIN)='
   1 ,F10.4,7X,'GRID RATIO=',F10.8)
         write(5,*)'GRIDRATIOP=',GRIDRATIOP
         write(5,*)'GRIDRATIOC=',GRIDRATIOC
     WRITE(5,*)'$$$$$$$$$$$$$$$$$$$$$$$$$$$$$$$$$$$$$$$$$$$$$$$$$$$$$$$$$$$'
     WRITE(5,*)'    APPLICABILITY CRITERIA USING 1/SO*DY/DX CHANNEL'
     WRITE(5,*)'$$$$$$$$$$$$$$$$$$$$$$$$$$$$$$$$$$$$$$$$$$$$$$$$$$$$$$$$$$$'
     WRITE(5,*)'APC AT APPR. 1M FROM U/S=',APPCMAX
     WRITE(5,*)'APC AT D/S END=',APPCMAX1
     write(4,955)DXR,dt,GRIDRATIOP,CELPMAX,(TIMEPCEL/60.0)
 955 format(2x,F12.6,2x,F12.2,2x,F10.8,2x,F10.8,2x,F10.4)
     write(4,960)DXCH,dt,GRIDRATIOC,CELCMAX,(TIMECCEL/60.0)
 960 format(2x,F12.6,2x,F12.2,2x,F10.8,2x,F10.8,2x,F10.4)
     WRITE(4,951)EF,RMSE,CRM,CD,EVOL
 951 FORMAT(F12.6,2X,F12.6,2X,F12.6,2X,F12.6,2X,F10.6)
     WRITE(4,952)QPKCMAX,(TPKCMAX),QPKOMAX,TPKOMAX,QPKER,TPKER
 952 FORMAT(F12.6,2X,F12.4,2X,F12.6,2X,F12.6,2X,1X,F12.6,F12.4)
     WRITE(4,953)KNMINP,APCMAXP,APPLMAX,KFSQRMINP,F0UPP,AKMAXP
 953 FORMAT(F12.6,2X,F12.4,2X,F12.6,F12.6,2X,F12.6,1X,F10.4)
     WRITE(4,954)KNMINP1,APCMAXP1,APPLMAX1,KFSQRMINP1,F0DOWNP,AKMAXP1
 954 FORMAT(F12.6,2X,F12.4,2X,F12.6,F12.6,2X,F12.6,1X,F10.4)
     WRITE(4,958)KNMIN,APCMAX,APPCMAX,KFSQRMIN,F0UP,AKMAX
 958 FORMAT(F12.6,2X,F12.4,2X,F12.6,F12.6,2X,F12.6,1X,F10.4)
     WRITE(4,959)KNMIN1,APCMAX1,APPCMAX1,KFSQRMIN1,F0DOWN,AKMAX1
 959 FORMAT(F12.6,2X,F12.4,2X,F12.6,F12.6,2X,F12.6,1X,F10.4)
     WRITE(4,*)ELAPSED_TIME
c    DO 51 N=1,NPK
c    WRITE(5,*)'QPKC,TPKC',QPKC(N),TPKC(N),N
c 51 CONTINUE
     ENDIF
     STOP
     END
C ****************************************************************************
C              THE END OF THE PROGRAM                                      *
C****************************************************************************
```

318

APPENDIX-II

```
C*********************************************************************************
C     THE VARIABLE PARAMETER MUSKINGUM STAGE ROUTING METHOD IS USED AS ROUTING SCHEME   *
C     PROGRAM    FOR DISCHARGE ROUTING ON V-CATCHMENT (RECTANGULAR CHANNEL ASSUMED)     *
c     LAST MODIFIED ON 02.12.2009        Time:1:10 AM                                   *
C     NO BACK WATER EFFECT CONSIDERED.                                                  *
C     THE PROGRAMME IS WRITTEN IN MKS/FPS UNIT ALSO IT GIVES OUTFLOW DISCHARGE IN FT/SEC *
C     CM/HR, (M/SEC)*10**5 AND INCH/HR                                                  *
C     COMPUTES ALSO THE DOWNSTREAM STAGE HYDROGRAPHS                                    *
C     THE TERM QL IS THE LATERAL INFLOW IN CUBIC METERS/CUBIC FEET PER SECOND.FOR ROUTING *
C     IN THE PLANES, THE LATERAL INFLOW IS EQUAL TO THE EFFECTIVE RAINFALL(CENTIMETERS/ *
C     INCH PER HOUR)                                                                    *
C     TO CHECK THE SUITABILITY OF THE METHOD FOR THE GIVEN PROBLEM                      *
C     COMPUTED HYDROGRAPH TESTED WITH ERROR IN VOLUME CRITERION                         *
C     THE MODEL IS VERIFIED WITH GIVEN OTHER MODEL DATA OR OBSERVED DATA USING NASH-    *
C     SUTCLIFFE CRITERION                                                               *
C     THE MODEL PREDICTED RESULTS ARE ANALYSED BY MEASURES OF RESIDUAL ERRORS (LOAGUE AND *
C     GREEN,1991)SUCH AS                                                                *
C     1. ROOT MEAN SQUARE ERROR                                                         *
C     2. COEFFIECENT OF RESIDUAL MASS                                                   *
C     3. COEFFIECENT OF DETERMINATION                                                   *
C     4. MODELLING EFFICIENCY                                                           *
C*********************************************************************************
C     DESCRIPTION OF VARIABLES USED IN THE PROGRAM.                                     *
C*********************************************************************************
C     XLE       = PLANE LENGTH(METER/FEET)                                             *
C     NDX       = NUMBER OF PLANE INCREMENTS                                           *
C     TST       = TOTAL SIMULATION TIME(MIN)                                           *
C     NDT       = NUMBER OF TIME INTERVALS                                             *
C     RAINT     = AN ARRAY OF EFFECTIVE RAINFALL INTENSITY(CM/H OR INCH/HR)            *
C               (FOR INPUT IT USED AS QEE)                                             *
C     RADUR     = AN ARRAY OF EFFEVTIVE RAINFALL DURATION(MIN)(FOR INPUT IT USED AS PT) *
C     CELP      = AVERAGE WAVE CELERITY IN THE PLANES (M/SEC OR FT/SEC)                *
C     SLOPEP    = SLOPE OF THE PLANE (M/M OR FT/FT)                                    *
C     SLOPEC    = SLOPE OF THE CHANNEL (M/M OR FT/FT)                                  *
C     UQP       = AVERAGE UNIT-WIDTH FLOW OVER THE PLANES (SQUARE M/ SEC OR SQUARE FT/SEC) *
C     N         = NUMBER OF VALUES OF OBSERVED DATA                                    *
C     QOBS      = OBSERVED OUTFLOW DISCHARGE AT EACH TIME INTERVAL TIOBS(MIN)          *
C*********************************************************************************
      DOUBLE PRECISION YP,DNMTR,THETA,AK,DX,DT
      DIMENSION QP(2,3500),QLC(3500),RAIN(3500),QLCHN(3500)
      DIMENSION QP2(2,3500),QPR(2,3500),QPL(2,3500),QCH(2,3500)
      DIMENSION CELP(3500),QOBS(3500)
      DIMENSION Y1(3500),QL(3500),QP1(2,3500),CHLAT(3500)
      DIMENSION YCH(2,3500),VCH(3500),YIND(3500)
      DIMENSION YP(2,3500),QCAL(3500),QP3(2,3500)
      DIMENSION QEE(3500),RADUR(200),PT(2000),QES(315000),CELCH(3500)
      DIMENSION YPR(2,3500),YPL(2,3500)
c     DIMENSION QPKO(100),TPKO(100),QPKC(100),TPKC(100),Y(35000),FUNC(3500),VP(35000)
      CHARACTER *3 RFC
      CHARACTER*4 UNITS
      CHARACTER*5 RCUNIT
      CHARACTER*3 KMS,PFS,AMN,HCE
      CHARACTER*6 BMDATA
      CHARACTER*4 MCPH
      CHARACTER*4 NIPH
      CHARACTER*4 PMSM
      REAL KNP,APCP,KFSQRP,APCMAXP,KFSQRMINP,KNMINP,AKKP,AKMAXP
      REAL KNP1,APCP1,KFSQRP1,APCMAXP1,KFSQRMINP1,KNMINP1,AKKP1,AKMAXP1
      REAL KN,APC,KFSQR,APCMAX,KFSQRMIN,KNMIN,AKK,AKMAX
      REAL KN1,APC1,KFSQR1,APCMAX1,KFSQRMIN1,KNMIN1,AKK1,AKMAX1
      REAL APPL,APPL1,APPC,APPC1,APPLMAX,APPLMAX1,APPCMAX,APPCMAX1
      KN=0
      KNP=0
      APC=0.0
      APPL=0.0
      APPC=0.0
      APCP=0.0
      KFSQR=0.0
```

```
       KFSQRP=0.0
       AKK=0.0
       AKKP=0.0
       APCMAX=0.0
       APCMAXP=0.0
       APPLMAX=0.0
       APPLMAX1=0.0
       APPCMAX=0.0
       APPCMAX1=0.0
       KFSQRMIN=0.0
       KFSQRMINP=0.0
       KNMIN=0.0
       KNMINP=0.0
       AKMAX=0.0
       AKMAXP=0.0
       KN1=0.0
       KNP1=0.0
       APC1=0.0
       APPL1=0.0
       APPC1=0.0
       APCP1=0.0
       KFSQR1=0.0
       KFSQRP1=0.0
       AKK1=0.0
       AKKP1=0.0
       APCMAX1=0.0
       APCMAXP1=0.0
       KFSQRMIN1=0.0
       KFSQRMINP1=0.0
       KNMIN1=0.0
       KNMINP1=0.0
       AKMAX1=0.0
       AKMAXP1=0.0
       QPKCMAX=0.0
       TPKCMAX=0.0
       QPKC=0.0
       TPKC=0.0
       GRIDRATIOP=0.0
       GRIDRATIOC=0.0
       MP=0
       MPP=0.0
       NAPP=0.0
       NAP=0
C**************************************************************************
C            THE ARRAYS USED FOR STORAGE OF VARIABLES USED IN THE PROGRAM      *
C**************************************************************************
C    ARRAY QP(2,3500) STORES THE VALUES OF OUTFLOW FROM THE REACH             +
C    ARRAY QLP(3500) STORES THE VALUES OF LATERALFLOW TO THE PLANE            +
C    ARRAY QLC(3500) STORES THE VALUES OF LATERALFLOW FROM THE REACH          +
C    VARIABLE QO STORES THE VALUE OF INTIAL ESTIMATES OF OUTFLOW DISCHARGE     +
C        FOR EACH TIME STEP AND EACH SUBREACH                                 +
C    ARRAY Y(5000) STORES THE VALUE OF COMPUTED FLOW DEPTH                     +
C    ARRAY FUNC(3500) STORES THE COMPUTED VALUES REQUIRED IN NEWTON-RAPHSON METHOD  +
C    ARRAY VP(3500) STORES THE VALUE OF FLOW VELOCITY FOR EACH TIME STEP AND SUBREACH  +
C    ARRAY CELP(3500) STORES THE VALUES OF CELERITY   FOR EACH TIME STEP AND SUBREACH  +
C    ARRAY QOBS(3500)STORES THE VALUES OF OBSERVED VALUES OF OUTFLOW DISCHARGE FROM     +
C        OVERLAND FLOW PLANE                                                  +
C    ARRAY YP(2,3500) STORES THE STAGE AT THE OUTFLOW SECTION                 +
C    ARRAY QP1(2,3500)STORES THE OUTFLOW DISCHARGE CONVERTED IN METRIC UNIT (cm/sec)  +
C    ARRAY QP3(2,3500)OUTFLOW DISCHARGE CONVERTED IN METRIC UNIT (m/sec)*10**5  +
C    ARRAY QP2(2,3500)STORES THE OUTFLOW DISCHARGE CONVERTED IN FPS UNIT    (ft/h)  +
C    ARRAY QCAL(3500) THE CALCULATED OUTFLOW                                  *
C  **************************************************************************
       OPEN(1,FILE='MOD_OVERLAND_FSIM.DAT',STATUS='OLD')
       OPEN(2,FILE='MOD_AVFC OVERLAND_FSIM.OUT',STATUS='unknown')
       OPEN(5,FILE='MOD_AVFC cmperhr.OUT',STATUS='unknown')
       OPEN(9,FILE='OUTPUT FOR GRAPH.OUT',STATUS='UNKNOWN')
       OPEN(4,FILE='OUTPUT CRITERIA.OUT',STATUS='UNKNOWN')
C      OPEN(3,FILE='AVFC reachwise hydrograph.OUT',STATUS='NEW')
C      OPEN(7,FILE='AVFC K AND THETA.OUT',STATUS='NEW')
C**************************************************************************
C            INPUT AND OUTPUT FILES USED IN THE PROGRAM                        *
C**************************************************************************
C  'OVERLAND_FSIM.DAT' IS THE INPUT FILE STORES THE INPUT DATA SUCH AS ND,TIOBS AND  *
C  QOBS VALUES AND PARAMETERS SUCH AS XLE,NDX,CD,TST,NDT,ARAINT,RADUR,
C        SLOPEP,B,G                                                        *
C  "MOD_OVERLAND_FSIM" IS A OUTPUT FILE WHICH DISPLAY THE RUNOFF OUTFLOW AT DOWNSTREAM  *
```

320

```
C      END OF THE OVERLAND FLOW PLANE IN (inch/h) AT EACH TIME INTERVAL DISPLAYED IN        *
C      SECOND AS WELL AS MINUTE.                                                            *
C      "MOD_OVERLAND_FSIM_cmperh" IS A OUTPUT FILE WHICH DISPLAY THE RUNOFF OUTFLOW AT      *
C       DOWNSTREAM END OF THE OVERLAND FLOW PLANE IN (inch/h) AT EACH TIME INTERVAL         *
C      DISPLAYED IN SECOND AS WELL AS MINUTE.                                               *
C      ND IS THE NUMBER OF OBSERVED DATA POINTS                                             *
C      TIOBS IS THE TIME OF OBSERVATION FOR ONE MINUTE IT IS WRITTEN AS (1.0) AND SO ON     *
C      QOBS IN THIS PROGRAM SHOULD BE ENTERED AS OBSERVED VALUE IN M3/SEC OR FT3/SEC        *
C      BMDATA IS THE BENCHMARK DATA UNIT (ENTER "CMPH" IF DATA IS IN M**3/SEC, ENTER "INPH" *
C      IF DATA IS IN FT3/SEC OR ENTER MPSM"IF DATA IS IN M3/SEC*10**5.                      *
C ***********************************************************************************************
       ELAPSED_TIME=TIMEF()
       READ(1,*)ND,TIOBS,BMDATA
       WRITE(5,11)ND
11     FORMAT('NUMBER OF OBSERVATIONS/BENCH MARK PREDICTIONS='I7)
       WRITE(5,*)'BMDATA CMPH=M**3/SEC,INPH=INCH/HR,MPSM= M/SEC*10**5'
       WRITE(5,*)'UNIT OF RUNOFF DICHARGE=',BMDATA
       SUMQOBS=0.0
       TIME=0.0
       QPKOMAX=0.0
       TPKOMAX=0.0
       CELPMAX=0.0
       CELCMAX=0.0
       WRITE(5,*)'OBSERVED/BENCHMARK DATA USED FOR MODEL EVALUATION'
       WRITE(5,13)
13     FORMAT(5X,'RUNOFF',7X,'TIME(MINUTE)')
c      READ(1,*)NPK
c      READ(1,*)(QPKO(K),TPKO(K),K=1,NPK)
       DO 101 J=1,ND
       READ(1,*)QOBS(J)
       WRITE(5,*)TIME,QOBS(J)
       IF(J.EQ.1)THEN
       QPKOMAX=QOBS(J)
       TPKOMAX=TIME
       ELSEIF(J.GT.1)THEN
       QPKO=QOBS(J)
       IF(QPKO.GT.QPKOMAX)THEN
       QPKOMAX=QPKO
       TPKOMAX=TIME
       ELSE
        ENDIF
       ELSE
       ENDIF
       SUMQOBS=SUMQOBS+QOBS(J)
C      WRITE(*,*)QOBS(J)
       TIME=TIME+TIOBS
101    CONTINUE
       QMEAN=SUMQOBS/ND
C      WRITE(*,*)'QMEAN',QMEAN
       MCPH='CMPH'
       NIPH='INPH'
       PMSM='MPSM'
       READ(1,*)NPLANE    !write 1 if v-ctchment with uniform plane and 2 if uneven size planes
       READ(1,*)TST,NDT,NIER,G
       READ(1,*)XLER,NDXR,SOPR,BR
       READ(1,*)XLEL,NDXL,SOPL,BL
       READ(1,*)CHLEN,NDXCH,SOCH,BCH
       MSIGNAL=0
C ***********************************************************************************************
C      CHECKING UNITS OF PARAMETERS USED IN COMPUTATION AND IF NECESAARY CONVERSION         *
C      INTO APPRORIATE UNIT FOR MANNINGS OR CHEZYS COEFFICIENT.                             *
C ***********************************************************************************************
C      WRITE(*,*)'ENTER "MKS" IF SYSTEM UNIT EXCEPT ROUGHNESS COEFFICIENT
C      1     ARE IN MKS UNIT SYSTEM OR ENTER "FPS" IF SYSTEM OF
C      2            UNITS ARE IN FPS UNIT'
                AMN='MAN'
                HCE='CHE'
                KMS='MKS'
                PFS='FPS'
       READ(1,*)UNITS
C      WRITE(*,*)'UNITS=',UNITS
       UNITS=UNITS
       IF(UNITS.EQ.KMS)THEN
       WRITE(5,41)XLER
41     FORMAT('LENGTH OF PLANE 1=',F15.5,' ','METER')
       WRITE(5,22)XLEL
22     FORMAT('LENGTH OF PLANE 2=',F15.5,' ','METER')
```

321

```
        WRITE(5,23)CHLEN
23    FORMAT('LENGTH OF CHANEEL=',F15.5,' ','METER')
C       WRITE(*,*)'ENTER "MAN" FOR MANNINGS ROUGHNESS COEFFICIENT OR
C    1           ENTER "CHE" FOR CHEZYS ROUGHNESS COEFFICIENT.'
        READ(1,*)RFC
C     WRITE (*,*)'RFC=',RFC
      IF(RFC.EQ.AMN) THEN
        READ(1,*)AMNPR,AMNPL,AMNCH
C     WRITE (*,*)'AMNPR=',AMNPR
      ELSEIF(RFC.EQ.HCE)THEN
           READ(1,*)CDR,CDL,CDCH
        ELSE
          WRITE (*,*)'WRONG UNIT ENTRY'
          ENDIF
       READ(1,*)RCUNIT
           IF(RCUNIT.EQ.KMS)THEN
            IF(RFC.EQ.AMN)THEN
                AMNPR=AMNPR
                AMNPL=AMNPL
          AMNCH=AMNCH
      WRITE(5,43)AMNPR,SOPR
43    FORMAT('MANNINGS ROUGH.COEFF.PLANE 1 =',F10.5,' ','SLOPE=',F10.5)
      WRITE(5,24)AMNPL,SOPL
24    FORMAT('MANNINGS ROUGH.COEFF.PLANE 2 =',F10.5,' ','SLOPE=',F10.5)
      WRITE(5,26)AMNCH,SOCH
26    FORMAT('MANNINGS ROUGH.COEFF.CHANNEL =',F10.5,' ','SLOPE=',F10.5)
               ELSEIF(RFC.EQ.HCE)THEN
               CDR=CDR
               CDL=CDL
               CDCH=CDCH
      WRITE(5,47)CDR,SOPR
47    FORMAT('CHEZYS ROUGH. COEFF.PLANE 1 =',F10.5,' ','SLOPE=',F10.5)
      WRITE(5,27)CDL,SOPL
27    FORMAT('CHEZYS ROUGH. COEFF.PLANE 2 =',F10.5,' ','SLOPE=',F10.5)
      WRITE(5,28)CDCH,SOCH
28    FORMAT('CHEZYS ROUGH. COEFF. CHANNEL =',F10.5,' ','SLOPE=',F10.5)
          ELSE
             WRITE(*,*) 'WRONG UNIT ENTRY'
             ENDIF
          ELSEIF(RCUNIT.EQ.PFS)THEN
            IF(RFC.EQ.AMN)THEN
               AMNPR=AMNPR*1.486
               AMNPL=AMNPL*1.486
               AMNCH=AMNCH*1.486
      WRITE(5,44)AMNPR,SOPR
44    FORMAT('MANNINGS ROUG.COEFF PLANE 1 =',F10.5,' ','SLOPE=',F10.5)
      WRITE(5,29)AMNPL,SOPL
29    FORMAT('MANNINGS ROUGH.COEFF.PLANE 2 =',F10.5,' ','SLOPE=',F10.5)
      WRITE(5,32)AMNCH,SOCH
32    FORMAT('MANNINGS ROUGH.COEFF.CHANNEL =',F10.5,' ','SLOPE=',F10.5)
               ELSEIF(RFC.EQ.HCE)THEN
               CDR=CDR*SQRT(0.3048)
               CDL=CDL*SQRT(0.3048)
               CDCH=CDCH*SQRT(0.3048)
      WRITE(5,48)CDR,SOPR
48    FORMAT('CHEZYS ROUGH. COEFF.PLANE 1 =',F10.5,' ','SLOPE=',F10.5)
      WRITE(5,33)CDL,SOPL
33    FORMAT('CHEZYS ROUGH. COEFF.PLANE 2 =',F10.5,' ','SLOPE=',F10.5)
      WRITE(5,34)CDCH,SOCH
34    FORMAT('CHEZYS ROUGH. COEFF. CHANNEL =',F10.5,' ','SLOPE=',F10.5)
          ELSE
             WRITE(*,*) 'WRONG UNIT ENTRY'
             ENDIF
             ENDIF
       ELSEIF(UNITS.EQ.PFS)THEN
       WRITE(5,42)XLER
42    FORMAT('LENGTH OF PLANE 1=',F15.5,' ','FEET')
      WRITE(5,37)XLEL
37    FORMAT('LENGTH OF PLANE 2=',F15.5,' ','FEET')
      WRITE(5,38)CHLEN
38    FORMAT('LENGTH OF CHANEEL=',F15.5,' ','FEET')
C       WRITE(*,*)'ENTER "MAN" FOR MANNINGS ROUGHNESS COEFFICIENT OR
C    1           ENTER "CHE" FOR CHEZYS ROUGHNESS COEFFICIENT.'
       READ(1,*)RFC
       IF(RFC.EQ.AMN) THEN
         READ(1,*)AMNPR,AMNPL,AMNCH
       ELSEIF(RFC.EQ.HCE)THEN
```

322

```fortran
                READ(1,*)CDR,CDL,CDCH
            ELSE
              WRITE(*,*) 'WRONG UNIT ENTRY'
              ENDIF
C           WRITE(*,*)'ENTER "MKS" FOR ROUGHNESS COEFF.IN MKS UNIT SYSTEM
C     1           OR ENTER"FPS" FOR ROUGH. COEFF.IN FPS UNIT SYSTEM'
          READ(1,*)RCUNIT
            IF(RCUNIT.EQ.KMS)THEN
              IF(RFC.EQ.AMN)THEN
                 AMNPR=AMNPR/1.486
                 AMNPL=AMNPL/1.486
                 AMNCH=AMNCH/1.486
            WRITE(5,45)AMNPR,SOPR
 45     FORMAT('MANNINGS ROUG. COEFF.PLANE 1 =',F10.5,' ','SLOPE=',F10.5)
            WRITE(5,39)AMNPL,SOPL
 39     FORMAT('MANNINGS ROUGH.COEFF.PLANE 2 =',F10.5,' ','SLOPE=',F10.5)
            WRITE(5,62)AMNCH,SOCH
 62     FORMAT('MANNINGS ROUGH.COEFF.CHANNEL =',F10.5,' ','SLOPE=',F10.5)
                ELSEIF(RFC.EQ.HCE)THEN
                 CDR=CDR/SQRT(0.3048)
                 CDL=CDL/SQRT(0.3048)
                 CDCH=CDCH/SQRT(0.3048)
            WRITE(5,49)CDR,SOPR
 49     FORMAT('CHEZYS ROUGH. COEFF.PLANE 1 =',F10.5,' ','SLOPE=',F10.5)
            WRITE(5,63)CDL,SOPL
 63     FORMAT('CHEZYS ROUGH. COEFF.PLANE 2 =',F10.5,' ','SLOPE=',F10.5)
            WRITE(5,64)CDCH,SOCH
 64     FORMAT('CHEZYS ROUGH. COEFF. CHANNEL =',F10.5,' ','SLOPE=',F10.5)
              ELSE
                WRITE(*,*) 'WRONG UNIT ENTRY'
                ENDIF
              ELSEIF(RCUNIT.EQ.PFS)THEN
                IF(RFC.EQ.AMN)THEN
                 AMNPR=AMNPR
                 AMNPL=AMNPL
                AMNCH=AMNCH
            WRITE(5,46)AMNPR,SOPR
 46     FORMAT('MANNINGS ROUGH.COEFF.PLANE 1 =',F10.5,' ','SLOPE=',F10.5)
            WRITE(5,66)AMNPL,SOPL
 66     FORMAT('MANNINGS ROUGH.COEFF.PLANE 2 =',F10.5,' ','SLOPE=',F10.5)
            WRITE(5,67)AMNCH,SOCH
 67     FORMAT('MANNINGS ROUGH.COEFF.CHANNEL =',F10.5,' ','SLOPE=',F10.5)
                ELSEIF(RFC.EQ.HCE)THEN
                  CDR=CDR
                  CDL=CDL
                  CDCH=CDCH
            WRITE(5,52)CDR,SOPR
 52     FORMAT('CHEZYS ROUGH.COEFF.PLANE 1 =',F10.5,' ','SLOPE=',F10.5)
            WRITE(5,68)CDL,SOPL
 68     FORMAT('CHEZYS ROUGH. COEFF.PLANE 2 =',F10.5,' ','SLOPE=',F10.5)
            WRITE(5,69)CDCH,SOCH
 69     FORMAT('CHEZYS ROUGH. COEFF. CHANNEL =',F10.5,' ','SLOPE=',F10.5)
                ELSE
                  WRITE(*,*) 'WRONG UNIT ENTRY'
                  ENDIF
                ENDIF
            ENDIF
C     ***************************************************************************
      CELP=0.0
      LC=0
      DX1=0.0
      CFVOL=0.0
      RFVOL=0.0
      QCH(1,0)=0.0
      QCH(0,1)=0.0
     READ(1,*)(QEE(L),PT(L),L=1,NIER)
      DO 2 L=1,NIER
      RADUR(L)=PT(L)*60
       IF(UNITS.EQ.KMS)THEN
        SRFVOL=QEE(L)/(360000.0)*(RADUR(L)-RADUR(L-1))
        RFVOL=RFVOL+SRFVOL !RAINFALL VOLUME IN CUBIC METER PER SEC
      WRITE(5,53)QEE(L),PT(L)
 53    FORMAT('RAIN INTENSITY (CM/H) =',F10.5,5X,'DURATION(MIN)=',F10.2)
       ELSEIF(UNITS.EQ.PFS)THEN
        SRFVOL=QEE(L)/(3600.0*12.0)*(RADUR(L)-RADUR(L-1))
        RFVOL=RFVOL+SRFVOL !RAINFALL VOLUME IN CUBIC FEET PER SEC
      WRITE(5,54)QEE(L),PT(L)
```

```
 54    FORMAT('RAIN INTENSITY (IN/H) =',F10.5,5X,'DURATION(MIN)=',F10.2)
       ELSE
       WRITE(*,*)'ERROR IN COMPUTATION'
       ENDIF
       WRITE(*,*)RFVOL,SRFVOL,RADUR(L),QEE(L)
  2    CONTINUE
       RADURS=RADUR(NIER)
  C    RAINT=ARAINT/(3600.0*100.0)  !RAINT INTENSITY IN M/SEC
       TSTS=TST*60.  !SIMULATION TIME IN SEC
       DXR=XLER/NDXR   !SUBREACH LENGTH IN M/FT
       DXL=XLEL/NDXL   !SUBREACH LENGTH IN M/FT
       DXCH=CHLEN/NDXCH   !SUBREACH LENGTH IN M/FT
       DT=TSTS/NDT  !TIME INTERVAL IN SEC
       GRIDRATIOP=DXR/DT
       GRIDRATIOC=DXCH/DT
       IF(UNITS.EQ.KMS)THEN
       WRITE(5,56)DXR,DT
 56    FORMAT('SUB-REACH LENGTH DX (M), PLANE 1=', F10.6,'',5X,
      1 'TIME STEP(SEC)=',F4.1)
       WRITE(5,72)DXL,DT
 72    FORMAT('SUB-REACH LENGTH DX (M), PLANE 1=', F10.6,'',5X,
      1 'TIME STEP(SEC)=',F4.1)
       WRITE(5,73)DXCH,DT
 73    FORMAT('SUB-REACH LENGTH DX (M), CHNNEL=', F10.6,'',5X,
      1 'TIME STEP(SEC)=',F4.1)
       ELSEIF(UNITS.EQ.PFS)THEN
       WRITE(5,57)DX,DT
 57    FORMAT('SUB-REACH LENGTH DX (FEET)=', F10.6,'',5X,
      1 'TIME STEP(SEC)=',F4.1)
       ELSE
       ENDIF
       WRITE(5,*)'*******************************************************'
       NRDT=RADURS+0.01
       IF((TIOBS*60.0).GE.DT)THEN
       TSKIP=(TIOBS*60)/DT
       ELSE
       DTSKIP=DT/60.0
       TTSKIP=DTSKIP/TIOBS
       ND=ND+1
       ND=(ND-1)/TTSKIP+1
       TIME=0.0
       SUMQOBS=0.0
       QMEAN=0.0
       DO 6 J=2,ND
       QOBS(J)=QOBS((J-1)*TTSKIP+1)
       TIME=TIME+DTSKIP
       SUMQOBS=SUMQOBS+QOBS(J)
  C    WRITE(*,*)QOBS(J),TIME*60
  6    CONTINUE
       QMEAN=SUMQOBS/ND
  C         WRITE(*,*)'QMEAN',QMEAN
       TSKIP=1.0
       ENDIF
  C    NS=0
       QP(1,0)=0.0
       QP(0,1)=0.0
       YP(1,0)=0.0          !newly added
       YP(0,1)=0.0          !newly added
       QP1(1,0)=0.0    !previously off(VPMD)
       QP2(1,0)=0.0    !previously off
       QP3(1,0)=0.0    !previously off
       QCAL(0)=0.0
       WRITE(5,600)
 600   FORMAT(2X,'TIME INTERVAL',5X,'TIME (S)',5X,'TIME(MIN)',
      1 5X,'OUTFLOW(M**3/sec)',2X,'Flow Depth (cm)')
       WRITE(2,500)
 500   FORMAT(2X,'TIME INTERVAL',5X,'TIME (S)',5X,'TIME(MIN)',5X,
      1 'OUTFLOW(inch/hr)',2X,'LATERAL CHANNEL FLOW')
       WRITE(*,*)'NRDT,NDT,DT',NRDT,NDT,DT
       WRITE(*,*)'SKIP TIME=',TSKIP,NS
       WRITE(*,*)'IF SKIP TIME IS WHOLE NUMBER, PRESS 1 IF NOT PRESS 2'
  c    READ(*,*)MSIGNAL
       MSIGNAL=1
       IF(MSIGNAL.EQ.2)THEN
       STOP
       ELSE
       NDX=NDXR
```

324

```
         BR=BR
c        B=BR
         B=1.0
         XLE=XLER
         DX=DXR
         SLOPEP=SOPR
         NNPLANE=NPLANE-1
c        WRITE(*,*)'AMNPR',AMNPR,BR,BL
         IF(RFC.EQ.AMN)THEN
         AMNP=AMNPR
         ELSEIF(RFC.EQ.HCE)THEN
         CD=CDR
         ELSE
         ENDIF
76    IF(NNPLANE.EQ.2)THEN
         NDX=NDXL
         B=1.0
         XLE=XLEL
         DX=DXL
         SLOPEP=SOPL
             IF(RFC.EQ.AMN)THEN
               AMNP=AMNPL
             ELSEIF(RFC.EQ.HCE)THEN
               CD=CDL
             ELSE
             ENDIF
         ELSE
         ENDIF
         AMNP=AMNP
         NS=0
         RRDUR=RADUR(1)
         DX1=0.0000
         DO 10 J=1,NDX
         DX1=DX1+DX
         T=0.0
         QP(2,0)=0.0
         YP(2,0)=0.0
         RADUR(1)=RRDUR
         NN=1
         DO 20 N=1,NDT
         T=T+DT
         IF (T.LE.NRDT)THEN
         IF(T.LE.RADUR(NN))THEN
         RAINT=QEE(NN)
         IF(T.EQ.RADUR(NN))THEN
         NN=NN+1
         ELSE
         ENDIF
         ELSE
         IF(NN.LE.NIER)THEN
         IF(T.LE.(RADUR(NN+1)))THEN
         ANTC=T-RADUR(NN)
         IF(ANTC.LT.DT)THEN
         ANTCC=DT-ANTC
         QES(NN)=QEE(NN)*ANTCC/3600.0
         NN=NN+1
         QES(NN)=QEE(NN)*ANTC/3600.0
         RAINT=(QES(NN-1)+QES(NN))/(DT/3600.0)
         ELSE
         NN=NN+1
         RAINT=QEE(NN)
         ENDIF
         ELSEIF(T.LE.RADUR(NN+2))THEN
         AKT=DT-RADUR(NN+1)
         QES(NN+2)=AKT/3600.0*QEE(NN+2)
         AKTT=RADUR(NN+1)-RADUR(NN)
         QES(NN+1)=AKTT*QEE(NN+1)/3600.0
         AKKT=DT-(AKT+AKTT)
         QES(NN)=AKKT/3600.0*QEE(NN)
         RAINT=(QES(NN)+QES(NN+1)+QES(NN+2))/(DT/3600.0)
         ELSE
         WRITE(*,*)'RECHECKING OF DATA IS REQUIRED AS TIME INTERVAL EXCEEDS
         1       CONSECUTIVE THREE EFFECTIVE RAINFALL TIME INTERVAL'
         ENDIF
         ELSE
         WRITE(*,*)'NUMBER OF EFFECTIVE RAINFALL TIME INTERVAL EXCEEDS
         1     THE NUMBER OF EFFECTIVE RAINFALL TIME INTERVAL SUPPLIED.'
```

```
      ENDIF
C     NN=NN+1
C     GOTO 111
      ENDIF
      ELSE
      RAINT=0.0
      ENDIF
       IF(UNITS.EQ.KMS)THEN
         RAINT=RAINT/(3600.0*100.0) !RAINT INTENSITY IN M/SEC
        ELSEIF(UNITS.EQ.PFS)THEN
         RAINT=RAINT/(3600.0*12.0) !RAINT INTENSITY IN FT/SEC
        ELSE
        WRITE(*,*)'ERROR IN COMPUTATION'
        ENDIF
       IF(J.EQ.1)THEN
       RAIN(N)=RAINT
C      WRITE(*,*)RAIN(N),N
       ELSE
       ENDIF
       RCMS=(RAINT)
       QLP=RCMS
       PP=(RAINT)*DT
       IF(J.EQ.1)THEN
       YO=(PP+YP(2,N-1))/2.
       ELSEIF(J.GT.1.AND.N.EQ.1)THEN
       YO=(PP+YP(1,N))/2.
       ELSEIF(J.GT.1)THEN
       YO=((YP(1,N)+YP(1,N-1)+YP(2,N-1))/3.)
       ELSE
       ENDIF
       IF(YO.LE.0.0) GOTO 20
       QL(N)=QLP
       IF(J.EQ.1)THEN        !(CHANGE ON 22.12.2008)
      IF(RFC.EQ.AMN)THEN
         CONST=(1./AMNP)*SQRT(SLOPEP)
       VEL=(1./AMNP)*SQRT(SLOPEP)*YO**(2./3.)
       R=YO
        CEL=(5./3.)*VEL
        AK=DX/CEL
       ELSEIF(RFC.EQ.HCE)THEN
         CONST=CD*SQRT(SLOPEP)
       VEL=CD*SQRT(SLOPEP)*YO**(1./2.)
       R=YO
       CEL=(3./2.)*VEL
        AK=DX/CEL
       ELSE
        ENDIF
  255 IF (J.EQ.1) THEN
       CDN1=AK+DT/2.
       CUP1=(AK-DT/2.)/CDN1
       CUP2=DT/CDN1
       YP(2,N)=CUP1*YP(2,N-1)+CUP2*QL(N)*AK
       IF(RFC.EQ.AMN)THEN
       QP(2,N)=(1./AMNP)*SQRT(SLOPEP)*(YO)**(5./3.)*B
       ELSEIF(RFC.EQ.HCE)THEN
       QP(2,N)=CONST*(YO)**(3./2.)*B
       ELSE
       ENDIF
       if(yp(2,n).le.0)yp(2,n)=0.0          ! added on 06.02.2009
       GOTO 20
       ELSE
       ENDIF
       ELSE                  !(CHANGE ON 22.12.2008)
       ENDIF                 !(CHANGE ON 22.12.2008)
       IF(N.LE.NDT)THEN
       IF(RFC.EQ.AMN)THEN
       CONST=(1./AMNP)*SQRT(SLOPEP)
       VEL=(1./AMNP)*SQRT(SLOPEP)*YO**(2./3.)
        R=YO
        CEL=5./3.*VEL
        AK=DX/CEL
        THETA=0.5-((YO*VEL)*(1.-(4./9.)*(((YO*VEL)*(YO*VEL))
      1 /(G*(YO)**3))))/(2.*SLOPEP*CEL*DX)
          ELSEIF(RFC.EQ.HCE)THEN
           CONST=CD*SQRT(SLOPEP)
           VEL=CD*SQRT(SLOPEP)*YO**(1./2.)
        R=YO
```

326

```
      CEL=3./2.*VEL
      AK=DX/CEL
      THETA=0.5-((YO*VEL)*(1.-(1./4.)*(((YO*VEL)*(YO*VEL))
    1 /(G*(YO)**3))))/(2.*SLOPEP*CEL*DX)
      ELSE
      ENDIF
      ELSE
      ENDIF
C         COUNTER M IS USED FOR UPDATING THE PARAMETERS AT ANY TIME
      M=0
19    DNMTR=AK*(1.-THETA)+(DT/2.)
C         C1P, C2P,C3P AND C4P ARE THE COEFFICIENTS OF THE MUSKINGUM ROUTING EQUATION.
      C1P=(-(AK*THETA)+(DT/2.))/DNMTR
      C2P=(AK*THETA+DT/2.)/DNMTR
      C3P=(AK*(1.-THETA)-DT/2.)/DNMTR
      C4P=DT/DNMTR
5     M=M+1
C         COMPUTATION OF OUTFLOW
      YP(2,N)=C1P*YP(1,N)+C2P*YP(1,N-1)+C3P*YP(2,N-1)+C4P*QL(N)*AK
      IF(YP(2,N).LE.0.0)THEN
      YP(2,N)=0.0
      GOTO 750
      ELSE
      YP(2,N)=YP(2,N)
      ENDIF
      YNOR=YP(2,N)+THETA*(YP(1,N)-YP(2,N))
      YMID=(YP(1,N)+YP(2,N))/2.
      IF(RFC.EQ.AMN)THEN
      VNOR=(1./AMNP)*(YMID/YNOR)*(YMID)**(2./3.)
      VNOR=VNOR*SQRT(SLOPEP)
      VMID=(1./AMNP)*(YMID)**(2./3.)*SQRT(SLOPEP)
      QMID=YMID*VMID
      FSQM=QMID*QMID/(G*(YMID)**3)
      FSQ=FSQM
C     COMPUTATION OF WEIGHTED OUTFLOW.
      Q3=YNOR*VNOR
      V3=VNOR
      R=(YMID)  !REQUIRE CHANGE
      THETA=0.5-Q3*(1.-(4./9.)*FSQ)/(2.*SLOPEP*((5./3.)*V3)*DX)
      AK=DX/((5./3.)*V3)
C         COMPUTATION OF STAGE AT THE INLET OF THE REACH
      IF(DX1.EQ.DX) Y1(J)=2*YMID-YP(2,N)
      ELSEIF(RFC.EQ.HCE)THEN
      YNOR=YP(2,N)+THETA*(YP(1,N)-YP(2,N))
      YMID=(YP(1,N)+YP(2,N))/2.
      VNOR=CD*(YMID/YNOR)*(YMID)**(1./2.)
      VNOR=VNOR*SQRT(SLOPEP)
      VMID=CD*(YMID)**(1./2.)*SQRT(SLOPEP)
      QMID=YMID*VMID
      FSQM=QMID*QMID/(G*(YMID)**3)
      FSQ=FSQM
C     COMPUTATION OF WEIGHTED OUTFLOW.
      Q3=YNOR*VNOR
      V3=VNOR
      THETA=0.5-Q3*(1.-(1./4.)*FSQ)/(2.*SLOPEP*((3./2.)*V3)*DX)
      AK=DX/((3./2.)*V3)
C         COMPUTATION OF STAGE AT THE INLET OF THE REACH
      ELSE
       WRITE(*,*)'WRONG FRICTION FORMULA USED IN COMPUTATION.'
      ENDIF
750   IF(M.LE.1) GOTO 19
      IF(RFC.EQ.AMN)THEN
      CELNOR=(5./3.)*VNOR
      CELMID=(5./3.)*VMID
      ELSEIF(RFC.EQ.HCE)THEN
      CELNOR=(3./2.)*VNOR
      CELMID=(3./2.)*VMID
      ELSE
      ENDIF
      QP(2,N)=Q3+B*CELNOR*(YP(2,N)-YNOR)
c     ENDIF
C     Q3=THETA*QP(1,N)+(1.-THETA)*QP(2,N)
      DYDX=(YP(2,N)-YP(1,N))/DX
      IF(QP(2,N).LE.0.0)THEN
      QP(2,N)=0.0
      GOTO 20
      ELSE
```

327

```
          QP(2,N)=QP(2,N)
          ENDIF
          CONTINUE
C    ********************************************************************
C         APPLICABILITY CRITERIA TO CHECK SUITABILITY OF METHOD
C    ********************************************************************
C    APPLICABILITY CRITERIA AT ONE METER FROM U/S
C    ********************************************************************
          FET=1.0/0.3048
          FET2=1.2/0.3048
          MPP=MPP+N
          IF(UNITS.EQ.KMS)THEN
          IF(DX1.GE.0.97.AND.DX1.LE.(1.2))THEN
          KNP=(SLOPEP*DX1)/((YP(2,N)*FSQ)) !WOOLISER AND LIGGETTEE (1967) CRITERIA
          KFSQRP=KNP*FSQ
          APPL=(1.0/SLOPEP)*(YP(2,N)/(DX1))
          IF(RFC.EQ.AMN)THEN
          APCP=1.-(QP(2,N)/((SQRT(SLOPEP)/AMNP)*YP(2,N)**(5./3.)))**2
          DISPR=(QP(2,N)/((SQRT(SLOPEP)/AMNP)*YP(2,N)**(5./3.)))**2
          IF(DISPR.GE.1.0)THEN
          APCP=(1.0/SLOPEP)*(YP(2,N)/(DX1))
          ELSE
          ENDIF
          ELSEIF(RFC.EQ.HCE)THEN
          APCP=1.-(QP(2,N)/((SQRT(SLOPEP)*CD)*YP(2,N)**(3./2.)))**2
          DISPR=(QP(2,N)/((SQRT(SLOPEP)*CD)*YP(2,N)**(3./2.)))**2
          IF(DISPR.GE.1.0)THEN
          APCP=(1.0/SLOPEP)*(YP(2,N)/(DX1))
          ELSE
          ENDIF
          ELSE
          ENDIF
          AKKP=AK
            IF(N.EQ.MPP.OR.KNMINP.EQ.0) THEN
              KNMINP=KNP
              KFSQRMINP=KFSQRP
              AKMAXP=AKKP
            ELSE
            ENDIF
            IF(KNMINP.GT.KNP)THEN
              KNMINP=KNP
            ELSE
            ENDIF
            IF(KFSQRMINP.GT.KFSQRP) THEN
              KFSQRMINP=KFSQRP
            ELSE
            ENDIF
            IF(APCMAXP.LT.APCP)THEN
              APCMAXP=APCP
            ELSE
            ENDIF
            IF(APPLMAX.LT.APPL)THEN
              APPLMAX=APPL
            ELSE
            ENDIF
            IF(AKMAXP.LT.AKKP)THEN
              AKMAXP=AKKP
            ELSE
            ENDIF
          ELSE
          GOTO 551
          ENDIF
          ELSEIF(UNITS.GE.PFS) THEN
          IF(DX1.GE.FET.AND.DX1.LE.FET2)THEN
          KNP=(SLOPEP*DX1)/((YP(2,N)*FSQ)) !WOOLISER AND LIGGETTEE (1967) CRITERIA
          KFSQRP=KNP*FSQ
          APPL=(1.0/SLOPEP)*(YP(2,N)/(DX1))
          IF(RFC.EQ.AMN)THEN
          APCP=1.-(QP(2,N)/((SQRT(SLOPEP)/AMNP)*YP(2,N)**(5./3.)))**2
          DISPR=(QP(2,N)/((SQRT(SLOPEP)/AMNP)*YP(2,N)**(5./3.)))**2
          IF(DISPR.GE.1.0)THEN
          APCP=(1.0/SLOPEP)*(YP(2,N)/(DX1))
          ELSE
          ENDIF
          ELSEIF(RFC.EQ.HCE)THEN
          APCP=1.-(QP(2,N)/((SQRT(SLOPEP)*CD)*YP(2,N)**(3./2.)))**2
          DISPR=(QP(2,N)/((SQRT(SLOPEP)*CD)*YP(2,N)**(3./2.)))**2
```

328

```
        IF(DISPR.GE.1.0)THEN
        APCP=(1.0/SLOPEP)*(YP(2,N)/(DX1))
        ELSE
        ENDIF
        ELSE
        ENDIF
        AKKP=AK
          IF(N.EQ.MPP.OR.KNMINP.EQ.0) THEN
            KNMINP=KNP
            KFSQRMINP=KFSQRP
            AKMAXP=AKKP
          ELSE
            ENDIF
          IF(KNMINP.GT.KNP)THEN
            KNMINP=KNP
          ELSE
          ENDIF
          IF(KFSQRMINP.GT.KFSQRP) THEN
            KFSQRMINP=KFSQRP
          ELSE
          ENDIF
          IF(APCMAXP.LT.APCP)THEN
            APCMAXP=APCP
          ELSE
          ENDIF
          IF(APPLMAX.LT.APPL)THEN
            APPLMAX=APPL
          ELSE
          ENDIF
          IF(AKMAXP.LT.AKKP)THEN
            AKMAXP=AKKP
          ELSE
          ENDIF
        ELSE
        GOTO 551
      ENDIF
      ELSE
      WRITE(*,*)'PROBLEM IN APPLICABILITY CRITERIA COMPUTATION'
      ENDIF
      continue
C     ****************************************************************************
C     APPLICABILITY CRITERIA AT THE END OF THE PLANE
C     ****************************************************************************
551   IF(DX1.GE.XLER)THEN   !USE DEPEND ON WHEATHER APPLICABILITY CRITERIA AT END OF REACH OR 1
      METER FROM UPSTREAM
      NAPP= NAPP+N
      KNP1=(SOPR*DX1)/((YP(2,N)*FSQ)) !WOOLISER AND LIGGETTEE (1967) CRITERIA
      KFSQRP1=KNP1*FSQ
      APPL1=(1.0/SLOPEP)*(YP(2,N)/(DX1))
      IF(RFC.EQ.AMN)THEN
      APCP1=1.-(QP(2,N)/((SQRT(SLOPEP)/AMNP)*YP(2,N)**(5./3.)))**2
      DISPR=(QP(2,N)/((SQRT(SLOPEP)/AMNP)*YP(2,N)**(5./3.)))**2
C     WRITE(*,*)'DISCR',DISCR
      IF(DISPR.GE.1.0)THEN
      APCP1=(1.0/SLOPEP)*(YP(2,N)/(DX1))
      ELSE
      ENDIF
      ELSEIF(RFC.EQ.HCE)THEN
      APCP1=1.-(QP(2,N)/((SQRT(SLOPEP)*CD)*YP(2,N)**(3./2.)))**2
      DISPR=(QP(2,N)/((SQRT(SLOPEP)*CD)*YP(2,N)**(3./2.)))**2
      IF(DISPR.GE.1.0)THEN
      APCP1=(1.0/SLOPEP)*(YP(2,N)/(DX1))
      ELSE
      ENDIF
      ELSE
      ENDIF
      AKKP1=AK        !DT<=K THIS CRITERIA FOR MUSKINGUM ROUTING METHOD
          IF(N.EQ.NAPP.AND.KNMINP1.EQ.0) THEN
            KNMINP1=KNP1
            KFSQRMINP1=KFSQRP1
            AKMAXP1=AKKP1
          ELSE
            ENDIF
          IF(KNMINP1.GT.KNP1)THEN
            KNMINP1=KNP1
          ELSE
          ENDIF
```

329

```
       IF(KFSQRMINP1.GT.KFSQRP1) THEN
         KFSQRMINP1=KFSQRP1
       ELSE
       ENDIF
       IF(APCMAXP1.LT.APCP1)THEN
         APCMAXP1=APCP1
       ELSE
       ENDIF
       IF(APPLMAX1.LT.APPL1)THEN
         APPLMAX1=APPL1
       ELSE
       ENDIF
       IF(AKMAXP1.LT.AKKP1)THEN
         AKMAXP1=AKKP1
       ELSE
       ENDIF
     IF(QP(2,N).LT.0.000001)THEN
     QP(2,N)=0.0
     ELSE
     QP(2,N)=QP(2,N)
     ENDIF
     IF(N.EQ.1)THEN
     IF(CELNOR.GT.CELPMAX)THEN
     CELPMAX=CELNOR
     TIMEPCEL=N*DT
     ELSE
     ENDIF
     ELSEIF(N.GT.2)THEN
     IF(CELNOR.GT.CELPMAX)THEN
     CELPMAX=CELNOR
     TIMEPCEL=N*DT
     ELSE
     ENDIF
     ELSE
     ENDIF
     ELSE
     ENDIF
20   CONTINUE
     DO 14 N=1,NDT
     YP(1,N)=YP(2,N)
14   CONTINUE
10   CONTINUE
     IF(NPLANE.EQ.1.OR.NNPLANE.EQ.0.OR.NNPLANE.EQ.1)THEN
     DO 74 N=1,NDT
     QPR(2,N)=QP(2,N)
     YPR(2,N)=YP(2,N)
     WRITE(2,*)'QPR(2,N)',N,QPR(2,N),YP(2,N),J
74   CONTINUE
     ELSE
     ENDIF
     NNPLANE=NNPLANE+1
     IF(NNPLANE.EQ.2)THEN
     QP(1,0)=0.0
     QP(0,1)=0.0
     YP(1,0)=0.0
     YP(0,1)=0.0
     DO 89 N=1,NDT
     QP(2,N-1)=0.0
     YP(2,N-1)=0.0
89   CONTINUE
     GOTO 76
     ELSE
     ENDIF
     IF(NNPLANE.EQ.3)THEN
     DO 77 N=1,NDT
     QPL(2,N)=QP(2,N)
     YPL(2,N)=YP(2,N)
77   CONTINUE
     ELSE
     ENDIF
     CONTINUE
         DX1=0.0
     NDX=NDXCH
     B=BCH
     XLE=CHLEN
     DX=DXCH
     SLOPEC=SOCH
```

330

```
      IF(RFC.EQ.AMN)THEN
      AMNCH=AMNCH
      ELSEIF(RFC.EQ.HCE)THEN
      CD=CDCH
      ELSE
      ENDIF
      DO 92 I=1,NDT
      IF(NPLANE.EQ.1.OR.DXR.EQ.DXL)THEN
      CHLAT(I)=2.0*QPR(2,I)*DXCH          ! discharge for unit width plane
      YIND(I)=2.0*YPR(2,I)
      ELSE
      CHLAT(I)=(QPR(2,I)+QPL(2,I))*DXCH    ! discharge for unit width plane
      YIND(I)=(YPL(2,I)+YPR(2,I))/2
      ENDIF
92    CONTINUE
      DO 93 J=1,NDX
      DX1=DX1+DX
      T=0.0
      QCH(2,0)=0.0
      YCH(2,N)=0.0
      DO 94 N=2,NDT
      T=T+DT
      RAINT=RAIN(N)
      RCMS=(RAINT)
      QLCH=CHLAT(N)
      PP=(RAINT)*DXCH*BCH
      IF(J.EQ.1)THEN
      YO=(YIND(N)+YCH(2,N-1))/2.
      ELSEIF(J.GT.1.AND.N.EQ.1)THEN
      YO=(YIND(N)+YCH(1,N))/2.
      ELSEIF(J.GT.1)THEN
      YO=((YCH(1,N)+YCH(1,N-1)+YCH(2,N-1))/3.)
      ELSE
      ENDIF
      IF(YO.LE.0.0) GOTO 94
      QLCHN(N)=QLCH
      IF(J.LT.1)THEN         !(CHANGE ON 22.12.2008)
      IF(RFC.EQ.AMN)THEN
        CONST=(1./AMNCH)*SQRT(SLOPEC)*B**(5./3.)
       VEL=(1./AMNP)*SQRT(SLOPEP)*YO**(2./3.)
       R=YO
       CEL=5./3.*VEL
       AK=DX/CEL
       GOTO 257
       ELSEIF(RFC.EQ.HCE)THEN
        CONST=CD*SQRT(SLOPEC)
       VEL=CD*SQRT(SLOPEP)*YO**(1./2.)
       R=YO
       CEL=3./2.*VEL
       AK=DX/CEL
       GOTO 257
       ELSE
        WRITE(*,*)'WRONG FRICTION FORMULA USED IN COMPUTATION.RAVI'
       ENDIF
      ELSE
      ENDIF
      YIN=YO
C****************************************************************************************
C        FSQ      - SQUARE OF FROUDE NUMBER.                                            *
C             R      - HYDRAULIC RADIUS.                                                *
C             THETA    - WEIGHTING PARAMETER.                                           *
C             THETAN   - NUMERATOR OF THE WEIGHTING PARAMETER.                          *
C             THETAD   - DENOMINATOR OF THE WEIGHTING PARAMETER.                        *
C****************************************************************************************
    IF(RFC.EQ.AMN)THEN
    VCH(J)=(1./AMNCH)*SQRT(SLOPEC)*(YIN*B)**(2./3.)/
   1  ((B+2*YIN)**(2./3.))
   FSQ=VCH(J)**2.0*B/(G*(B*YIN))
    R=YIN/(B+2.*YIN)
    CELCH(J)=VCH(J)*(5./3.-(4./3.*R))
    AK=DX/CELCH(J)
    THETAN=YIN**(1.+4./9.*FSQ*(-1.+4.*R-4.*R*R))
    THETAD=2.*SLOPEC*(5./3.-4./3.*R)*DX
    ELSEIF(RFC.EQ.HCE)THEN
    VCH(J)=CONST*(YIN*B)**(1./2.)/((B+2*YIN)**(1./2.))
    FSQ=VCH(J)**2.0*B/(G*(B*YIN))
    R=YIN/(B+2.*YIN)
```

331

```
        CELCH(J)=VCH(J)*(3./2.-R)
        AK=DX/CELCH(J)
        THETAN=YIN*(1.+1./4.*FSQ*(-1.+4.*R-4.*R*R))
        THETAD=2.*SLOPEC*(3./2.-R)*DX
        ELSE
          WRITE(*,*)'WRONG FRICTION FORMULA USED IN COMPUTATION.'
        ENDIF
        THETA=0.5-THETAN/THETAD
257     IF (J.EQ.1) THEN
        CDN1=AK+DT/2.
        CUP1=(AK-DT/2.)/CDN1
        CUP2=DT/CDN1
        YCH(2,N)=CUP1*YCH(2,N-1)+CUP2*(QLCHN(N)/(DXCH*BCH))*AK
        IF(RFC.EQ.AMN)THEN
        QCH(2,N)=(1./AMNCH)*SQRT(SLOPEC)*(YO*BCH)**(2./3.)/
    1   ((BCH+2*YO)**(2./3.))*YO*BCH
        ELSEIF(RFC.EQ.HCE)THEN
        QCH(2,N)=CONST*(YO*BCH)**(1./2.)/((BCH+2*YO)**(1./2.))*YO*BCH
        ELSE
        ENDIF
        if(YCH(2,n).le.0)YCH(2,n)=0.0          ! added on 24.03.2009
        GOTO 94
        ELSE
        ENDIF
        YMID=YIN

C           COUNTER M IS USED FOR UPDATING THE PARAMETERS AT ANY TIME
        M=0
17      DNMTR=AK*(1.-THETA)+(DT/2.)
C           C1P, C2P,C3P AND C4P ARE THE COEFFICIENTS OF THE MUSKINGUM ROUTING EQUATION.
        C1P=(-(AK*THETA)+(DT/2.))/DNMTR
        C2P=(AK*THETA+DT/2.)/DNMTR
        C3P=(AK*(1.-THETA)-DT/2.)/DNMTR
        C4P=DT/DNMTR
18      M=M+1
C           COMPUTATION OF OUTFLOW
        YCH(2,N)=C1P*YCH(1,N)+C2P*YCH(1,N-1)+C3P*YCH(2,N-1)
    1   +C4P*(QLCHN(N)/(DXCH*BCH))*AK
        IF(YCH(2,N).LE.0.0)THEN
        YCH(2,N)=0.0
        GOTO 751
        ELSE
        YCH(2,N)=YCH(2,N)
        ENDIF
        YNOR=YCH(2,N)+THETA*(YCH(1,N)-YCH(2,N))
        YMID=(YCH(1,N)+YCH(2,N))/2.
        IF(RFC.EQ.AMN)THEN
        VNOR=(1./AMNCH)*(YMID/YNOR)*(B*YMID/(B+2.*YMID))**(2./3.)
        VNOR=VNOR*SQRT(SLOPEC)
        VMID=(1./AMNCH)*(B*YMID/(B+2.*YMID))**(2./3.)*SQRT(SLOPEC)
        VMID=VMID*SQRT(1.-(YP(2,N)-YP(1,N))/(SLOPEP*DX))
        QMID=B*YMID*VMID
        FSQM=QMID*QMID*B/(G*(B*YMID)**3)
        FSQ=FSQM
C           COMPUTATION OF WEIGHTED OUTFLOW.
        Q3=B*YNOR*VNOR
        V3=VNOR
        R=(YMID)/(B+2.0*YMID)  !REQUIRE CHANGE
        ELNUM=Q3*(1.-4./9.*FSQM*(B/(B+2.*YMID))**2)
        ELDIN=SLOPEC*B*(5./3.-4./3.*YNOR/(B+2.*YNOR))*V3
        GM=(YCH(2,N)-YCH(1,N))/(SLOPEC*DX)
        GM=GM*(1.-4./9.*FSQM*(B/(B+2.*YMID))**2)
        GM=0.0
        THETA=0.5-ELNUM/(ELDIN*DX)*(0.5+0.125*GM+0.0625*GM*GM)
        AK=DX/((5./3.-4./3.*YNOR/(B+2.*YNOR))*VNOR)
C           COMPUTATION OF STAGE AT THE INLET OF THE REACH
        IF(DX1.EQ.DX) Y1(J)=2*YMID-YCH(2,N)
        ELSEIF(RFC.EQ.HCE)THEN
        YNOR=YCH(2,N)+THETA*(YCH(1,N)-YCH(2,N))
        YMID=(YCH(1,N)+YCH(2,N))/2.
        VNOR=CD*(YMID/YNOR)*(B*YMID/(B+2.*YMID))**(1./2.)
        VNOR=VNOR*SQRT(SLOPEC)
        VMID=CD*(B*YMID/(B+2.*YMID))**(1./2.)*SQRT(SLOPEC)
        VMID=VMID*SQRT(1.-(YP(2,N)-YP(1,N))/(SLOPEP*DX))
        QMID=B*YMID*VMID
        FSQM=QMID*QMID*B/(G*(B*YMID)**3)
        FSQ=FSQM
```

```
C         COMPUTATION OF WEIGHTED OUTFLOW.
          Q3=B*YNOR*VNOR
          V3=VNOR
C    R=(B*YMID)/(B+2.0*YMID)
          ELNUM=Q3*(1.-1./4.*FSQM*(B/(B+2.*YMID))**2)
          ELDIN=SLOPEC*B*(3./2.-YNOR/(B+2.*YNOR))*VNOR
          GM=(YCH(2,N)-YCH(1,N))/(SLOPEC*DX)
          GM=GM*(1.-1./4.*FSQM*(B/(B+2.*YMID))**2)
          GM=0.0
C    CONSIDERATION OF 4TH OR 5TH POWER IN bINOMIAL SERIES EXPANSION REDUCES THE ERRO IN VOLUME OR
     MASS CONSERVATION
          THETA=0.5-ELNUM/(ELDIN*DX)*(0.5+0.125*GM+0.0625*GM*GM)
          AK=DX/((3./2.-YNOR/(B+2.*YNOR))*VNOR)
          ELSE
           WRITE(*,*)'WRONG FRICTION FORMULA USED IN COMPUTATION.'
          ENDIF
751  IF(M.LE.1) GOTO 17
          IF(RFC.EQ.AMN)THEN
          CELNOR=(5./3.-4./3.*YNOR/(B+2.*YNOR))*VNOR
          CELMID=(5./3.-4./3.*YMID/(B+2.*YMID))*VMID
          ELSEIF(RFC.EQ.HCE)THEN
          CELNOR=(3./2.-YNOR/(B+2.*YNOR))*VNOR
          CELMID=(3./2.-YMID/(B+2.*YMID))*VMID
          ELSE
          ENDIF
          QCH(2,N)=Q3+B*CELNOR*(YCH(2,N)-YNOR)
C    Q3=THETA*QCH(1,N)+(1.-THETA)*QCH(2,N)
          DYDX=(YCH(2,N)-YCH(1,N))/DX
          IF(QCH(2,N).LE.0.0)THEN
          QCH(2,N)=0.0
          GOTO 94
          ELSE
          QCH(2,N)=QCH(2,N)
          ENDIF
C    *******************************************************************
C         APPLICABILITY CRITERIA TO CHECK SUITABILITY OF METHOD
C    *******************************************************************
C    APPLICABILITY CRITERIA AT ONE METER FROM U/S
C    *******************************************************************
          FET=1.0/0.3048
          FET2=1.2/0.3048
          MP=MP+N
          IF(UNITS.EQ.KMS)THEN
          IF(DX1.GE.0.97.AND.DX1.LE.(1.2))THEN
          KN=(SLOPEC*DX1)/((YCH(2,N)*FSQ)) !WOOLISER AND LIGGETTEE (1967) CRITERIA
          KFSQR=KN*FSQ
          APPC=(1.0/SLOPEC)*(YCH(2,N)/(DX1))
          IF(RFC.EQ.AMN)THEN
          APC=1.-((QCH(2,N)/BCH)/((SQRT(SLOPEC)/AMNCH)*YCH(2,N)
     1 **(5./3.)))**2
          DISCR=((QCH(2,N)/BCH)/((SQRT(SLOPEC)/AMNCH)*YCH(2,N)**(5./3.)))**2
          IF(DISCR.GE.1.0)THEN
          APC=(1.0/SLOPEC)*(YCH(2,N)/(DX1))
          ELSE
          ENDIF
          ELSEIF(RFC.EQ.HCE)THEN
          APC=1.-((QCH(2,N)/BCH)/((SQRT(SLOPEC)*CD)*YCH(2,N)**(3./2.)))**2
          DISCR=((QCH(2,N)/BCH)/((SQRT(SLOPEC)*CD)*YCH(2,N)**(3./2.)))**2
          IF(DISCR.GE.1.0)THEN
          APC=(1.0/SLOPEC)*(YCH(2,N)/(DX1))
          ELSE
          ENDIF
          ELSE
          ENDIF
          AKK=AK
           IF(N.EQ.MP.OR.KNMIN.EQ.0) THEN
             KNMIN=KN
             KFSQRMIN=KFSQR
             AKMAX=AKK
           ELSE
             ENDIF
           IF(KNMIN.GT.KN)THEN
             KNMIN=KN
           ELSE
           ENDIF
           IF(KFSQRMIN.GT.KFSQR) THEN
             KFSQRMIN=KFSQR
```

```
        ELSE
        ENDIF
        IF(APCMAX.LT.APC)THEN
          APCMAX=APC
        ELSE
        ENDIF
        IF(APPCMAX.LT.APPC)THEN
          APPCMAX=APPC
        ELSE
        ENDIF
        IF(AKMAX.LT.AKK)THEN
          AKMAX=AKK
        ELSE
        ENDIF
      ELSE
      GOTO 555
       ENDIF
      ELSEIF(UNITS.GE.PFS) THEN
      IF(DX1.GE.FET.AND.DX1.LE.FET2)THEN
      KN=(SLOPEC*DX1)/((YCH(2,N)*FSQ)) !WOOLISER AND LIGGETTEE (1967) CRITERIA
      KFSQR=KN*FSQ
      APPC=(1.0/SLOPEC)*(YCH(2,N)/(DX1))
      IF(RFC.EQ.AMN)THEN
      APC=1.-((QCH(2,N)/BCH)/((SQRT(SLOPEC)/AMNCH)*YCH(2,N)
     1 **(5./3.)))**2
      DISCR=((QCH(2,N)/BCH)/((SQRT(SLOPEC)/AMNCH)*YCH(2,N)**(5./3.)))**2
      IF(DISCR.GE.1.0)THEN
      APC=(1.0/SLOPEC)*(YCH(2,N)/(DX1))
      ELSE
      ENDIF
      ELSEIF(RFC.EQ.HCE)THEN
      APC=1.-((QCH(2,N)/BCH)/((SQRT(SLOPEC)*CD)*YCH(2,N)**(3./2.)))**2
      DISCR=((QCH(2,N)/BCH)/((SQRT(SLOPEC)*CD)*YCH(2,N)**(3./2.)))**2
      IF(DISCR.GE.1.0)THEN
      APC=(1.0/SLOPEC)*(YCH(2,N)/(DX1))
      ELSE
      ENDIF
      ELSE
      ENDIF
      AKK=AK
        IF(N.EQ.MP.OR.KNMIN.EQ.0) THEN
          KNMIN=KN
          KFSQRMIN=KFSQR
          AKMAX=AKK
        ELSE
          ENDIF
        IF(KNMIN.GT.KN)THEN
          KNMIN=KN
        ELSE
        ENDIF
        IF(KFSQRMIN.GT.KFSQR) THEN
          KFSQRMIN=KFSQR
        ELSE
        ENDIF
        IF(APCMAX.LT.APC)THEN
          APCMAX=APC
        ELSE
        ENDIF
        IF(APPCMAX.LT.APPC)THEN
          APPCMAX=APPC
        ELSE
        ENDIF
        IF(AKMAX.LT.AKK)THEN
          AKMAX=AKK
        ELSE
        ENDIF
      ELSE
      GOTO 555
      ENDIF
      ELSE
      WRITE(*,*)'PROBLEM IN APPLICABILITY CRITERIA COMPUTATION'
      ENDIF
      continue
C     *************************************************************************
C     APPLICABILITY CRITERIA AT THE END OF THE PLANE
C     *************************************************************************
```

334

```
555  IF(DX1.GE.CHLEN)THEN        !USE DEPEND ON WHEATHER APPLICABILITY CRITERIA AT END OF REACH OR 1
     METER FROM UPSTREAM
     NAP= NAP+N
     KN1=(SLOPEC*DX1)/((YCH(2,N)*FSQ)) !WOOLISER AND LIGGETTEE (1967) CRITERIA
     KFSQR1=KN1*FSQ
     APPC1=(1.0/SLOPEC)*(YCH(2,N)/(CHLEN))
     IF(RFC.EQ.AMN)THEN
     APC1=1.-((QCH(2,N)/BCH)/((SQRT(SLOPEC)/AMNCH)*YCH(2,N)
     1 **(5./3.)))**2
     DISCR=((QCH(2,N)/BCH)/((SQRT(SLOPEC)/AMNCH)*YCH(2,N)**(5./3.)))**2
     IF(DISCR.GE.1.0)THEN
     APC1=(1.0/SLOPEC)*(YCH(2,N)/(CHLEN))
     ELSE
     ENDIF
     ELSEIF(RFC.EQ.HCE)THEN
     APC1=1.-((QCH(2,N)/BCH)/((SQRT(SLOPEC)*CD)*YCH(2,N)**(3./2.)))**2
     DISCR=((QCH(2,N)/BCH)/((SQRT(SLOPEC)*CD)*YCH(2,N)**(3./2.)))**2
     IF(DISCR.GE.1.0)THEN
     APC1=(1.0/SLOPEC)*(YCH(2,N)/(CHLEN))
     ELSE
     ENDIF
     ELSE
     ENDIF
     AKK1=AK        !DT<=K THIS CRITERIA FOR MUSKINGUM ROUTING METHOD
C    WRITE(4,*)T,KN1,APC1,KFSQR1
         IF(N.EQ.NAP.AND.KNMIN1.EQ.0) THEN
         KNMIN1=KN1
         KFSQRMIN1=KFSQR1
         AKMAX1=AKK1
C    WRITE(*,*)'KFSQRMIN1',KFSQRMIN1
     ELSE
      ENDIF
     IF(KNMIN1.GT.KN1)THEN
       KNMIN1=KN1
     ELSE
     ENDIF
     IF(KFSQRMIN1.GT.KFSQR1) THEN
       KFSQRMIN1=KFSQR1
     ELSE
     ENDIF
     IF(APCMAX1.LT.APC1)THEN
      APCMAX1=APC1
     ELSE
     ENDIF
     IF(APPCMAX1.LT.APPC1)THEN
      APPCMAX1=APPC1
     ELSE
     ENDIF
     IF(AKMAX1.LT.AKK1)THEN
      AKMAX1=AKK1
     ELSE
     ENDIF
     ELSE
     GOTO 565
     ENDIF
565  IF(UNITS.EQ.KMS)THEN
     QP1(2,N)=QCH(2,N)
     QP2(2,N)=QP1(2,N)/2.54
     QP3(2,N)=QP1(2,N)/360000.0*10.0**5.
     ELSEIF(UNITS.EQ.PFS)THEN
     QP1(2,N)=QCH(2,N)*3600.0*100.0*0.3048
     QP2(2,N)=QP1(2,N)/2.54
     QP3(2,N)=QP1(2,N)/360000.0*10.0**5.
     ELSE
     WRITE(*,*)'WRONG OUTPUT HYDROGRAPH'
     ENDIF
     IF(QP1(2,N).LT.0.000001)THEN
     QP1(2,N)=0.0
     ELSE
     QP1(2,N)=QP1(2,N)
     ENDIF
     IF(N.EQ.1)THEN
     IF(CELNOR.GT.CELCMAX)THEN
     CELCMAX=CELNOR
     TIMECCEL=N*DT
     ELSE
     ENDIF
```

```
       ELSEIF(N.GT.2)THEN
       IF(CELNOR.GT.CELCMAX)THEN
       CELCMAX=CELNOR
       TIMECCEL=N*DT
       ELSE
       ENDIF
       ELSE
       ENDIF
C      WRITE(3,15)J,N,YP(2,N),J,N,QP(2,N)
  15   FORMAT(1X,'SUBREACH=',I5,5X,'Y(''I5'')=',F10.6,5X,'QP(''I3'','','',I5,
     1 ')=',F12.9)
  94   CONTINUE
       DO 16 N=1,NDT
  16   YCH(1,N)=YCH(2,N)
  93   CONTINUE
C
  25   FORMAT(4X,'TIME STEP',2X,'LATER FLOW (M3/SEC OR FT3/SEC)',F10.8)
       DO 40 N=1,NDT
       QLC(N)=QCH(2,N-1)+QCH(2,N)
  40   CONTINUE
       DO 55 L=1, NDT
       Runoffvol=Runoffvol+QCH(2,L)*DT
       IF(BMDATA.EQ.MCPH)THEN
       QP1(2,L)=QP1(2,L)
       QCAL(L)=QP1(2,L)
       ELSEIF(BMDATA.EQ.NIPH)THEN
       QP2(2,L)=QP2(2,L)
       QCAL(L)=QP2(2,L)
       ELSEIF(BMDATA.EQ.PMSM)THEN
       QP3(2,L)=QP3(2,L)
       QCAL(L)=QP3(2,L)
       ELSE
       WRITE(*,*)'WRONG UNITS OF PREDICTED AND BENCH MARK DATA'
       ENDIF
       IF(L.EQ.1)THEN
       QPKCMAX=QCAL(L)
       TPKCMAX=(L*DT)/60.0
       ELSE
       ENDIF
       IF(L.GT.1)THEN
       QPKC=QCAL(L)
c      write(*,*)'qpkc',qpkc,L
       IF(QPKC.GT.QPKCMAX.AND.QPKC.NE.QPKCMAX)THEN
       QPKCMAX=QPKC
       TPKCMAX=(L*DT)/60.0
c      WRITE(*,*)QPKCMAX,TPKCMAX
       ELSE
       ENDIF
       ELSE
       ENDIF
  55   CONTINUE
       DO 60 L=1,NDT-1,2
  60   SUMA=SUMA+QCH(2,L)
       DO 70 L=2, NDT-2,2
  70   SUMB=SUMB+QCH(2,L)
       VOL=(DT/3.)*(QCH(2,0)+4*SUMA+2*SUMB+QCH(2,NDT))+CFVOL
 250   FORMAT(2X,'SUMA=',F12.6,2X,'SUMB=',F12.6,2X,'VOL=',F12.6)
       TIMESEC=-DT
       DO 80 N=0,NDT
       TIMESEC=TIMESEC+DT
       TIMEMIN=TIMESEC/60.
       IF(N.GT.NDT.AND.QCH(2,N).LT.0.00001)THEN
       GOTO 90
       ELSE
       WRITE(2,*)N,TIMESEC,TIMEMIN,QP2(2,N),QP3(2,N)
       WRITE(5,*)N,TIMESEC,TIMEMIN,QP1(2,N),YCH(2,N)*100.0
       IF (N.EQ.NS.AND.NS.LE.(ND*TSKIP))THEN
C***********************************************************************************************
C      CHECKING OF UNITS OUTPUT HYDROGRAPH AND BENCHMARK OUTPUT HYDROGRAPH               *
C***********************************************************************************************
       IF(BMDATA.EQ.MCPH)THEN
       QP1(2,NS)=QP1(2,NS)
       QCAL(LC)=QP1(2,NS)
       ELSEIF(BMDATA.EQ.NIPH)THEN
       QP2(2,NS)=QP2(2,NS)
       QCAL(LC)=QP2(2,NS)
       ELSEIF(BMDATA.EQ.PMSM)THEN
```

```
      QP3(2,NS)=QP3(2,NS)
      QCAL(LC)=QP3(2,NS)
      ELSE
      WRITE(*,*)'WRONG UNITS OF PREDICTED AND BENCH MARK DATA'
      ENDIF
C     WRITE(7,*)QCAL(LC),LC
      LC=LC+1
      NS=N+(TSKIP)
C     WRITE (*,*)'NS',NS, QCAL(LC)
      ELSE
      ENDIF
      ENDIF
 80   CONTINUE
 90   CONTINUE
C*******************************************************************************
C     USING NASH-SUTCLIFFE CRITERION FOR VERIFICATION                        *
C*******************************************************************************
      NEM=0.0
      SUMQCAL=0.0
      IF(DT.LE.TIOBS*60.0)THEN
      IF(TST.LT.(ND*TIOBS))THEN
      ND=NDT/TSKIP+1
      ELSE
      ENDIF
      ELSE
      ENDIF
      IF(ND.LE.NDT)THEN
      ND=ND
      ELSE
      ND=NDT+1
      ENDIF
      DO 201 ND=1,ND
      WRITE(*,*)QCAL(ND-1),QOBS(ND),ND
      IF(DT.LE.(TIOBS*60.0))THEN
      ANC=((TIOBS*60.0)/DT)*TIOBS
      WRITE(9,*)((ND-1)*TIOBS),(((ND-1)*TIOBS)*60.0),QCAL(ND-1),QOBS(ND)
c     WRITE(9,*)(((ND-1)*TIOBS)*60.0),QCAL(ND-1)
      ELSEIF(DT.GE.(TIOBS*60.0))THEN
      ANC=(DT/(TIOBS*60.0))*TIOBS
      WRITE(9,*)((ND-1)*ANC),QCAL(ND-1),QOBS(ND)
      ELSE
      ENDIF
      QMEAN=QMEAN
      SUMQCAL=SUMQCAL+QCAL(ND-1)
      ANEM=ANEM+(QOBS(ND)-QCAL(ND-1))**2
      DEN=DEN+(QOBS(ND)-QMEAN)**2
      RDEN=RDEN+(QCAL(ND-1)-QMEAN)**2
      RNEM=RNEM+(QCAL(ND-1)-QOBS(ND))**2
201   CONTINUE
c     WRITE(*,*)NEM,DEN
      ANEM=ANEM
      DEN=DEN
      EFFNS=(1-(ANEM/DEN))*100
C *******************************************************************************
C     MEASURES FOR ANALYSIS OF RESIDUAL ERRORS (LOAGUE AND GREEN, 1991)        *
C     ROOT MEAN SQUARE ERROR                                                   *
C*******************************************************************************
      RMSE=(RNEM/(ND))**(0.5)*(100./QMEAN)
      CRM=(SUMQOBS-SUMQCAL)/SUMQOBS*100
      CD=(DEN/RDEN)
      EF=(DEN-RNEM)/DEN*100
C *******************************************************************************
      WRITE(*,*)'EFFNS',EFFNS,ANEM,DEN,QMEAN,KNMIN1,KFSQR1
      CONTINUE
      DO 3 L=1,NIER
      RADUR(L)=PT(L)*60
       IF(UNITS.EQ.KMS)THEN
        SRFVOL=QEE(L)/(360000.0)*(RADUR(L)-RADUR(L-1))
        RFVOL=RFVOL+SRFVOL   !RAINFALL VOLUME IN CUBIC METER PER SEC
       ELSEIF(UNITS.EQ.PFS)THEN
        SRFVOL=QEE(L)/(3600.0*12.0)*(RADUR(L)-RADUR(L-1))
        RFVOL=RFVOL+SRFVOL   !RAINFALL VOLUME IN CUBIC FEET PER SEC
       ELSE
       WRITE(*,*)'ERROR IN COMPUTATION'
       ENDIF
      WRITE(*,*)RFVOL,SRFVOL,RADUR(L),QEE(L)
3     CONTINUE
```

```
C*********************************************************************************
C      USE THIS FORMULA WHEN RAINFALLING ON CHANNEL IS CONSIDERED                *
C*********************************************************************************
       RFVOL=RFVOL*(XLER*BR+XLEL*BL) !RAINFALL VOLUME IN CUBIC FEET PER SEC
       EVOL=(VOL-RFVOL)/RFVOL*100.
C      ERROR IN TIME TO PEAK AND PEAK DISCHARGE
       QPKER=((QPKCMAX/QPKOMAX)-1.0)*100.0
       TPKER=(TPKCMAX-TPKOMAX)
C      FROUDE NUMBER COMPUTATIONS FOR PLANE
       IF(KFSQRMINP.GT.0.0.AND.KNMINP.GT.0.0)THEN
       F0UPP=SQRT(KFSQRMINP/KNMINP)
       ELSE
       F0UPP=0.0
       ENDIF
       IF(KFSQRMINP1.GT.0.0.AND.KNMINP.GT.0.0)THEN
       F0DOWNP=SQRT(KFSQRMINP1/KNMINP1)
       ELSE
       F0DOWNP=0.0
       ENDIF
C      FROUDE NUMBER COMPUTATIONS FOR CHANNEL
       IF(KFSQRMIN.GT.0.0.AND.KNMIN.GT.0.0)THEN
       F0UP=SQRT(KFSQRMIN/KNMIN)
       ELSE
       F0UP=0.0
       ENDIF
       IF(KFSQRMIN1.GT.0.0.AND.KNMIN1.GT.0.0)THEN
       F0DOWN=SQRT(KFSQRMIN1/KNMIN1)
       ELSE
       F0DOWN=0.0
       ENDIF
       WRITE(*,*)'EVOL',EVOL,VOL,RFVOL,KNMIN1,KFSQR1
       WRITE(2,400)SUMA,SUMB,CFVOL,EFFNS
       WRITE(*,*)SUMA,SUMB,CFVOL,EFFNS
       WRITE(5,*)'
       WRITE(5,*)'ALLICABILITY CRITERIA FOR PLANE
       WRITE(5,*)'
       WRITE(5,*)' APPLICABILITY CRITERIA AT APPROX.1 METER FROM U/S'
       WRITE(5,456)KNMINP,APCMAXP,KFSQRMINP,AKMAXP
456    FORMAT(2X,'KW NUMBER (MINIMUM)=',F12.4,2X,'MAX [(1/SO)*dY/dX]=',
      1 F12.4,2X,'MIN [KN*SQURE F0]=',F12.4,2X,'MAX [K]=',F12.6)
       WRITE(5,*)' APPLICABILITY CRITERIA AT THE END OF PLANE'
       WRITE(5,457)KNMINP1,APCMAXP1,KFSQRMINP1,AKMAXP1
457    FORMAT(2X,'KW NUMBER (MINIMUM)=',F12.4,2X,'MAX [(1/SO)*dY/dX]=',
      1 F12.4,2X,'MIN [KN*SQURE F0]=',F12.4,2X,'MAX [K]=',F12.6)
       WRITE(5,*)'$$$$$$$$$$$$$$$$$$$$$$$$$$$$$$$$$$$$$$$$$$$$$$$$$$$$$$$$$$$'
       WRITE(5,*)'    APPLICABILITY CRITERIA USING 1/SO*DY/DX  PLANE '
       WRITE(5,*)'$$$$$$$$$$$$$$$$$$$$$$$$$$$$$$$$$$$$$$$$$$$$$$$$$$$$$$$$$$$'
       WRITE(5,*)'APC AT APPR. 1M FROM U/S=',APPLMAX
       WRITE(5,*)'APC AT D/S END=',APPLMAX1
400    FORMAT(2X,'SUMA=',F10.5,2X,'SUMB=',F10.5,2X,'Cumul.Infiltration
      1  volume=',F10.5,2X,'NASH-SUTCLIFFE EFFICIENCY=',F12.6)
       WRITE(2,425)VOL,RFVOL,EVOL,Runoffvol,EFFNS
425    FORMAT(2X,'VOL=',F12.6,2X,'RFVOL=',F12.6,2X,'EVOL=',F12.6,2X,
      1'Runoffvol=',F12.6,2X,'NASH-SUTCLIFFE EFFICIENCY=',F12.6)
       WRITE(2,415)RMSE,CRM,CD,EF,EFFNS
415    FORMAT(2X,'ROOT MEAN SQUARE ERROR=',F12.6,2X,'COEFFICIENT OF
      1 RESIDUAL MASS=',F12.6,2X,'COEFF. DETERMINATION=',F12.6,2X,'
      1MODELING EFFICIENCY=',F12.6,2X,'NASH-SUTCLIFFE EFFICIENCY=',F12.6)
       WRITE(5,455)SUMA,SUMB,CFVOL
455    FORMAT(2X,'SUMA=',F10.5,2X,'SUMB=',F10.5,2X,'Cumul.Infiltration
      1  volume=',F10.5)
       WRITE(5,452)VOL,RFVOL,EVOL,Runoffvol
452    FORMAT(2X,'VOL=',F12.6,2X,'RFVOL=',F12.6,2X,'EVOL=',F12.6,2X,
      1'Runoffvol=',F12.6)
       WRITE(5,*)' MODEL PERFORMANCE CRITERIA'
       WRITE(5,451)RMSE,CRM,CD,EF,EFFNS
451    FORMAT(2X,'ROOT MEAN SQUARE ERROR=',F12.6,2X,'COEFFICIENT OF
      1 RESIDUAL MASS=',F12.6,/,2X,'COEFF. DETERMINATION=',F12.6,2X,'
      1 MODELING EFFICIENCY=',F12.6,/,2X'NASH-SUTCLIFFE EFFICIENCY='
      2 ,F12.6)
       WRITE(5,*)' APPLICABILITY CRITERIA AT APPROX.1 METER FROM U/S'
       WRITE(5,453)KNMIN,APCMAX,KFSQRMIN,AKMAX
453    FORMAT(2X,'KW NUMBER (MINIMUM)=',F12.4,2X,'MAX [(1/SO)*dY/dX]=',
      1 F12.4,2X,'MIN [KN*SQURE F0]=',F12.4,2X,'MAX [K]=',F12.6)
       WRITE(5,*)' APPLICABILITY CRITERIA AT THE END OF CHHANEL'
       WRITE(5,454)KNMIN1,APCMAX1,KFSQRMIN1,AKMAX1
454    FORMAT(2X,'KW NUMBER (MINIMUM)=',F12.4,2X,'MAX [(1/SO)*dY/dX]=',
```

338

```
      1 F12.4,2X,'MIN [KN*SQURE F0]=',F12.4,2X,'MAX [K]=',F12.6)
        ELAPSED_TIME=TIMEF()
        WRITE(5,*)'EXCUTION_TIME',ELAPSED_TIME,'   SEC'
        WRITE(5,*)'QPKCMAX,TPKCMAX',QPKCMAX,' BMDATA',TPKCMAX,'  MIN'
        WRITE(5,*)'QPKOMAX,TPKOMAX',QPKOMAX,' BMDATA',TPKOMAX,'  MIN'
        WRITE(5,*)'QPKCERROR,TPKCERROR',QPKER,' %',TPKER,'  MIN'
        WRITE(5,*)' COURANT CONDITION CHECK FOR PLANE'
        WRITE(5,366)CELPMAX,(TIMEPCEL/60.0),GRIDRATIOP
    366 FORMAT(2X,'MAX CELERITY=',F10.8,7X,'TIME OF MAX CELERITY (MIN)='
      1 ,F10.4,7X,'GRID RATIO=',F10.8)
        WRITE(5,*)' COURANT CONDITION CHECK FOR CHANNEL'
        WRITE(5,367)CELCMAX,(TIMECCEL/60.0),GRIDRATIOC
    367 FORMAT(2X,'MAX CELERITY=',F10.8,7X,'TIME OF MAX CELERITY (MIN)='
      1 ,F10.4,7X,'GRID RATIO=',F10.8)
        WRITE(5,*)'$$$$$$$$$$$$$$$$$$$$$$$$$$$$$$$$$$$$$$$$$$$$$$$$$$$$$$$$$$$$$$'
        WRITE(5,*)'     APPLICABILITY CRITERIA USING 1/SO*DY/DX CHANNEL'
        WRITE(5,*)'$$$$$$$$$$$$$$$$$$$$$$$$$$$$$$$$$$$$$$$$$$$$$$$$$$$$$$$$$$$$$$'
        WRITE(5,*)'APC AT APPR. 1M FROM U/S=',APPCMAX
        WRITE(5,*)'APC AT D/S END=',APPCMAX1
        write(4,955)DXR,dt,GRIDRATIOP,CELPMAX,(TIMEPCEL/60.0)
    955 format(2x,F12.6,2x,F12.2,2x,F10.8,2x,F10.8,2x,F10.4)
        write(4,960)DXCH,dt,GRIDRATIOC,CELCMAX,(TIMECCEL/60.0)
    960 format(2x,F12.6,2x,F12.2,2x,F10.8,2x,F10.8,2x,F10.4)
        WRITE(4,951)EF,RMSE,CRM,CD,EVOL
    951 FORMAT(F12.6,2X,F12.6,2X,F12.6,2X,F12.6,2X,F10.6)
        WRITE(4,952)QPKCMAX,(TPKCMAX),QPKOMAX,TPKOMAX,QPKER,TPKER
    952 FORMAT(F12.6,2X,F12.4,2X,F12.6,2X,F12.6,2X,1X,F12.6,F12.4)
        WRITE(4,953)KNMINP,APCMAXP,APPLMAX,KFSQRMINP,F0UPP,AKMAXP
    953 FORMAT(F12.6,2X,F12.4,2X,F12.6,F12.6,2X,F12.6,1X,F10.4)
        WRITE(4,954)KNMINP1,APCMAXP1,APPLMAX1,KFSQRMINP1,F0DOWNP,AKMAXP1
    954 FORMAT(F12.6,2X,F12.4,2X,F12.6,F12.6,2X,F12.6,1X,F10.4)
        WRITE(4,958)KNMIN,APCMAX,APPCMAX,KFSQRMIN,F0UP,AKMAX
    958 FORMAT(F12.6,2X,F12.4,2X,F12.6,F12.6,2X,F12.6,1X,F10.4)
        WRITE(4,959)KNMIN1,APCMAX1,APPCMAX1,KFSQRMIN1,F0DOWN,AKMAX1
    959 FORMAT(F12.6,2X,F12.4,2X,F12.6,F12.6,2X,F12.6,1X,F10.4)
        WRITE(4,*)ELAPSED_TIME
        ENDIF
        STOP
        END
C *******************************************************************************
C                                      THE END OF THE PROGRAM                  *
C *******************************************************************************
```

APPENDIX-III

```
      SUBROUTINE GAINF(EK,SI,DLTHETA,FP,RAINT,T,TP,CFF)
      DIMENSION CF(1000),FUNCF(1000)
c     WRITE(*,*)'T,TP',T,TP
      RAINT=RAINT
      EK=EK
      SIDT=(SI/100.0)*DLTHETA
C     FP=SIDT/(RAINT/EK-1.0)
C     WRITE(*,*)'SIDT',SIDT
C     WRITE(*,*)'FP,RAINT,T,TP,EK,SI,DLTHE',FP,RAINT,T,TP,EK,SI,DLTHETA
C     TP=FP/(RAINT)
      TS=(FP-SIDT*ALOG(1.0+(FP/SIDT)))/EK
      EKT=EK*(T-(TP-TS))
C     WRITE(*,*)'TS,EKT'
C     WRITE(*,*)TS,EKT
      M=1
      CF(M)=EKT
      FUNCF(M)=EKT-(CF(M)-(SIDT*ALOG(1.0+(CF(M)/SIDT))))
      M=2
      CF(M)=CF(M-1)+0.2*CF(M-1)
200   FUNCF(M)=EKT-(CF(M)-(SIDT*ALOG(1.0+(CF(M)/SIDT))))
      DCF=-FUNCF(M)*(CF(M)-CF(M-1))/(FUNCF(M)-FUNCF(M-1))
      CF(M+1)=CF(M)+DCF
C     WRITE(*,*)CF(M+1)
      IF(ABS((CF(M+1)-CF(M))/CF(M+1)).LT.0.001) GOTO 300
      M=M+1
      GOTO 200
300   CF(M+1)=CF(M+1)
      CFF=CF(M+1)
C     WRITE(*,*)'CFF',CFF
      RETURN
      END
```

341

APPENDIX-IV

UDM CODE: US1L
CATCHMENT: IZZARD(Author)
LOCATION: USA

RAINFALL -RUNOFF DATA

NUMBER OF FLOW GAUGES: 1
NUMBER OF EVENTS IN UDM FILES: 146
NUMBER OF EVENTS PRESENTED HERE: 8
----

event number: 34	event number: 35	event number: 36	event number: 50
number of rainfall data: 1	number of rainfall data: 2	number of rainfall data: 3	number of rainfall data: 6
number of flow data : 44	number of flow data : 61	number of flow data : 76	number of flow data : 116

----

event number: 301	event number: 302	event number: 318	event number: 319
number of rainfall data: 1	number of rainfall data: 1	number of rainfall data: 2	number of rainfall data: 3
number of flow data : 210	number of flow data : 175	number of flow data : 213	number of flow data : 260

Event Number: 34

Elapsed time [sec]	Flow [l/sec]	Elapsed time [sec]	Flow [l/sec]	Elapsed time [sec]	Flow [l/sec]	Elapsed time [sec]	Flow [l/sec]	Elapsed time [sec]	Flow [l/sec]
10	0	110	0.527	220	1.089	490	0.51	765	0.043
20	0.006	120	0.652	420	1.089	500	0.431	870	0.028
30	0.011	130	0.748	425	1.14	510	0.357	1200	0.014
40	0.023	140	0.828	430	1.208	520	0.306	1620	0.009
50	0.045	150	0.896	435	1.276	530	0.261		
60	0.074	160	0.958	440	1.191	540	0.227		
70	0.108	170	1.004	450	1.009	560	0.173		
80	0.164	180	1.043	460	0.856	580	0.139		
90	0.272	190	1.066	470	0.726	600	0.119		
100	0.403	200	1.077	480	0.607	620	0.099		

Event Number : 35

Elapsed time [sec]	Flow [l/sec]	Elapsed time [sec]	Flow [l/sec]	Elapsed time [sec]	Flow [l/sec]	Elapsed time [sec]	Flow [l/sec]	Elapsed time [sec]	Flow [l/sec]
80	0	220	0.459	690	0.887	1120	0.825	1260	0.113
100	0.006	230	0.488	700	0.927	1130	0.7	1280	0.096
110	0.011	240	0.516	710	0.961	1140	0.581	1300	0.085
120	0.023	247	0.53	720	0.989	1150	0.496	1330	0.071
130	0.045	600	0.53	730	1.012	1160	0.422	1375	0.057
140	0.085	610	0.507	740	1.029	1170	0.36	1445	0.043
150	0.142	620	0.53	760	1.052	1180	0.303	1580	0.028
160	0.21	630	0.57	770	1.057	1190	0.264	1920	0.014
170	0.261	640	0.615	1080	1.057	1200	0.226	2280	0.006
180	0.283	650	0.672	1090	1.211	1210	0.196		
190	0.318	660	0.729	1095	1.233	1220	0.173		
200	0.369	670	0.785	1100	1.188	1230	0.156		
210	0.42	680	0.825	1110	0.989	1240	0.139		

Event Number : 36

Elapsed time [sec]	Flow [l/sec]	Elapsed time [sec]	Flow [l/sec]	Elapsed time [sec]	Flow [l/sec]	Elapsed time [sec]	Flow [l/sec]	Elapsed time [sec]	Flow [l/sec]
20	0	180	1.032	560	0.442	710	1.06	900	0.227
30	0.006	190	1.055	565	0.442	720	1.072	920	0.176
40	0.011	200	1.068	570	0.448	730	1.083	940	0.145
50	0.028	215	1.077	580	0.465	780	1.083	960	0.119
60	0.057	225	1.083	590	0.499	790	1.242	980	0.099
70	0.102	480	1.083	600	0.587	795	1.287	1000	0.085
80	0.17	485	1.208	610	0.652	800	1.219	1030	0.071
90	0.278	490	1.315	620	0.72	810	1.004	1070	0.057
100	0.397	495	1.31	630	0.782	820	0.839	1130	0.043
110	0.482	500	1.242	640	0.833	830	0.697	1290	0.028
120	0.635	510	1.021	650	0.885	840	0.59	1680	0.014
130	0.731	520	0.845	660	0.924	850	0.505	1920	0.009
140	0.822	530	0.692	670	0.958	860	0.425		
150	0.902	540	0.587	680	0.987	870	0.357		
160	0.97	550	0.465	690	1.015	880	0.301		
170	1.009	555	0.448	700	1.038	890	0.261		

Event Number : 50

Elapsed time [sec]	Flow [l/sec]	Elapsed time [sec]	Flow [l/sec]	Elapsed time [sec]	Flow [l/sec]	Elapsed time [sec]	Flow [l/sec]	Elapsed time [sec]	Flow [l/sec]
60	0	430	1.191	660	0.839	980	0.17	1380	0.38
70	0.014	438	1.253	670	0.89	1000	0.179	1390	0.309
80	0.028	445	1.117	680	0.941	1010	0.196	1400	0.269
90	0.043	450	0.987	690	0.981	1020	0.218	1410	0.235
100	0.065	460	0.805	700	1.015	1030	0.241	1420	0.207
110	0.094	470	0.669	710	1.038	1040	0.269	1440	0.159
120	0.13	480	0.567	720	1.049	1050	0.303	1460	0.13
130	0.181	490	0.482	740	1.066	1060	0.332	1480	0.108
140	0.238	500	0.414	770	1.072	1070	0.354	1500	0.091
150	0.312	510	0.352	840	1.072	1080	0.383	1520	0.077
160	0.386	520	0.301	850	1.185	1100	0.422	1540	0.065
170	0.465	530	0.255	858	1.27	1120	0.458	1570	0.057
180	0.544	540	0.221	865	1.123	1140	0.488	1630	0.043
190	0.652	550	0.198	870	1.015	1160	0.507	1680	0.034
200	0.748	560	0.21	880	0.833	1180	0.522	1730	0.028
210	0.833	570	0.232	890	0.697	1200	0.53	1810	0.023
220	0.907	580	0.266	900	0.584	1230	0.536	1910	0.017
230	0.964	590	0.318	910	0.499	1320	0.538	1990	0.014
240	1.004	600	0.38	920	0.425	1330	0.576	2120	0.011
250	1.038	610	0.465	930	0.374	1335	0.593	2280	0.009
260	1.055	620	0.556	940	0.306	1340	0.581		
270	1.066	630	0.641	950	0.255	1350	0.541		
280	1.072	640	0.709	960	0.215	1360	0.473		
420	1.072	650	0.782	970	0.187	1370	0.417		

Event Number : 301

Elapsed time [sec]	Flow [l/sec]	Elapsed time [sec]	Flow [l/sec]	Elapsed time [sec]	Flow [l/sec]	Elapsed time [sec]	Flow [l/sec]	Elapsed time [sec]	Flow [l/sec]
40	0	570	0.456	990	0.933	1910	0.593	2350	0.23
50	0.003	580	0.473	1000	0.944	1920	0.581	2360	0.224
150	0.009	590	0.485	1010	0.961	1930	0.57	2380	0.218
160	0.014	600	0.496	1020	0.972	1940	0.553	2390	0.213
170	0.02	610	0.513	1030	0.995	1950	0.541	2410	0.207
180	0.026	620	0.53	1040	1.006	1960	0.524	2420	0.201
190	0.031	630	0.541	1050	1.012	1970	0.513	2440	0.196
200	0.037	640	0.558	1070	1.018	1980	0.502	2450	0.19
210	0.043	650	0.57	1080	1.023	1990	0.49	2470	0.184
220	0.048	660	0.587	1110	1.029	2000	0.473	2490	0.179

240	0.065	670	0.598	1130	1.035	2010	0.468	2510	0.173
250	0.071	680	0.61	1160	1.04	2020	0.456	2520	0.167
270	0.088	690	0.627	1180	1.046	2030	0.445	2540	0.162
280	0.099	700	0.638	1200	1.052	2040	0.434	2560	0.156
290	0.105	710	0.655	1220	1.057	2050	0.428	2590	0.15
300	0.128	720	0.666	1240	1.063	2060	0.417	2620	0.145
310	0.139	730	0.678	1260	1.069	2070	0.405	2640	0.139
320	0.156	740	0.689	1290	1.074	2080	0.4	2670	0.133
330	0.173	750	0.7	1320	1.08	2090	0.388	2700	0.128
340	0.19	760	0.712	1680	1.08	2100	0.383	2740	0.122
350	0.207	770	0.723	1690	1.097	2110	0.371	2780	0.116
360	0.224	780	0.734	1700	1.069	2120	0.36	2810	0.111
370	0.235	790	0.751	1710	1.035	2130	0.354	2840	0.105
380	0.252	800	0.763	1720	1.006	2140	0.343	2880	0.099
390	0.264	810	0.774	1730	0.978	2150	0.337	2920	0.094
400	0.275	820	0.785	1740	0.95	2160	0.332	2960	0.088
410	0.286	830	0.797	1750	0.921	2170	0.326	3000	0.082
420	0.298	840	0.808	1760	0.893	2180	0.315	3070	0.077
430	0.303	850	0.814	1770	0.87	2190	0.309	3180	0.071
440	0.315	860	0.825	1780	0.842	2200	0.303	3220	0.065
450	0.326	870	0.836	1790	0.819	2210	0.298	3300	0.06
460	0.332	880	0.848	1800	0.797	2220	0.292	3400	0.054
470	0.343	890	0.853	1810	0.774	2230	0.286	3500	0.048
480	0.349	900	0.865	1820	0.751	2240	0.281	3630	0.043
490	0.36	910	0.87	1830	0.734	2250	0.275	3830	0.037
500	0.371	920	0.876	1840	0.712	2260	0.269	4110	0.031
510	0.383	930	0.882	1850	0.695	2270	0.264	4470	0.026
520	0.388	940	0.887	1860	0.672	2280	0.258	4680	0.023
530	0.4	950	0.893	1870	0.655	2290	0.252	4960	0.02
540	0.417	960	0.904	1880	0.638	2310	0.247	5320	0.017
550	0.434	970	0.91	1890	0.621	2320	0.241		
560	0.439	980	0.921	1900	0.61	2340	0.235		

Event Number : 302

Elapsed time [sec]	Flow [l/sec]	Elapsed time [sec]	Flow [l/sec]	Elapsed time [sec]	Flow [l/sec]	Elapsed time [sec]	Flow [l/sec]	Elapsed time [sec]	Flow [l/sec]
10.00	0.003	560.00	0.207	980.00	0.405	1940.00	0.383	2460.00	0.162
80.00	0.009	570.00	0.213	990.00	0.411	1950.00	0.377	2480.00	0.156
100.00	0.011	590.00	0.218	1010.00	0.417	1960.00	0.366	2500.00	0.150
120.00	0.020	600.00	0.224	1030.00	0.422	1970.00	0.360	2530.00	0.145
150.00	0.026	610.00	0.230	1050.00	0.428	1980.00	0.354	2580.00	0.139
160.00	0.031	630.00	0.235	1070.00	0.434	1990.00	0.349	2600.00	0.133
180.00	0.037	640.00	0.241	1090.00	0.439	2000.00	0.337	2620.00	0.128
200.00	0.043	650.00	0.247	1110.00	0.445	2010.00	0.332	2660.00	0.122
220.00	0.048	660.00	0.252	1140.00	0.445	2020.00	0.326	2690.00	0.116
240.00	0.054	670.00	0.258	1170.00	0.456	2030.00	0.315	2720.00	0.111
260.00	0.060	680.00	0.264	1200.00	0.462	2040.00	0.309	2760.00	0.105

270.00	0.065	700.00	0.269	1230.00	0.468	2050.00	0.303	2800.00	0.099
280.00	0.071	710.00	0.275	1260.00	0.473	2070.00	0.298	2840.00	0.094
290.00	0.077	720.00	0.281	1290.00	0.479	2080.00	0.292	2890.00	0.088
300.00	0.082	730.00	0.286	1320.00	0.485	2090.00	0.286	2950.00	0.077
310.00	0.088	740.00	0.292	1360.00	0.490	2100.00	0.281	3030.00	0.077
320.00	0.094	750.00	0.298	1400.00	0.496	2110.00	0.275	3140.00	0.071
330.00	0.099	760.00	0.303	1440.00	0.502	2120.00	0.269	3240.00	0.065
340.00	0.105	770.00	0.309	1490.00	0.507	2140.00	0.264	3350.00	0.060
350.00	0.111	780.00	0.315	1540.00	0.513	2160.00	0.258	3450.00	0.054
360.00	0.116	800.00	0.320	1620.00	0.519	2180.00	0.247	3540.00	0.048
370.00	0.128	810.00	0.326	1800.00	0.519	2200.00	0.241	3690.00	0.043
380.00	0.133	820.00	0.332	1810.00	0.524	2210.00	0.235	3780.00	0.040
390.00	0.139	830.00	0.337	1820.00	0.507	2230.00	0.230	3900.00	0.037
400.00	0.145	840.00	0.343	1830.00	0.496	2240.00	0.224	4020.00	0.034
410.00	0.150	850.00	0.349	1840.00	0.479	2250.00	0.218	4170.00	0.031
430.00	0.156	870.00	0.354	1850.00	0.468	2270.00	0.213	4340.00	0.026
440.00	0.162	880.00	0.360	1860.00	0.462	2290.00	0.207	4540.00	0.026
460.00	0.167	890.00	0.366	1870.00	0.451	2310.00	0.201	4780.00	0.023
470.00	0.173	900.00	0.371	1880.00	0.439	2330.00	0.196	5130.00	0.020
490.00	0.179	910.00	0.377	1890.00	0.428	2350.00	0.190	5560.00	0.017
500.00	0.184	930.00	0.383	1900.00	0.417	2370.00	0.184	6070.00	0.014
520.00	0.190	940.00	0.388	1910.00	0.411	2390.00	0.179	6780.00	0.011
530.00	0.196	950.00	0.394	1920.00	0.400	2410.00	0.173	7700.00	0.009
550.00	0.201	960.00	0.400	1930.00	0.394	2430.00	0.167	7800.00	0.006

Event Number : 318

Elapsed time [sec]	Flow [l/sec]	Elapsed time [sec]	Flow [l/sec]	Elapsed time [sec]	Flow [l/sec]	Elapsed time [sec]	Flow [l/sec]	Elapsed time [sec]	Flow [l/sec]
80	0	980	0.255	1530	0.726	2090	0.726	2530	0.238
180	0.006	1000	0.278	1540	0.731	2100	0.70	2540	0.232
240	0.011	1010	0.295	1550	0.743	2110	0.68	2550	0.227
270	0.017	1020	0.312	1560	0.754	2120	0.66	2560	0.221
300	0.023	1030	0.323	1570	0.765	2130	0.635	2570	0.215
330	0.028	1040	0.346	1580	0.78	2140	0.618	2580	0.21
350	0.034	1050	0.383	1590	0.78	2150	0.601	2600	0.204
380	0.04	1060	0.38	1600	0.79	2160	0.584	2640	0.187
400	0.045	1070	0.397	1610	0.811	2170	0.567	2660	0.181
420	0.051	1080	0.41	1620	0.822	2180	0.55	2680	0.176
440	0.057	1090	0.43	1630	0.828	2190	0.539	2690	0.17
460	0.062	1100	0.44	1640	0.839	2200	0.527	2710	0.16
470	0.068	1110	0.448	1650	0.85	2220	0.505	2730	0.16
480	0.074	1120	0.459	1660	0.862	2230	0.488	2740	0.153
490	0.082	1130	0.485	1670	0.873	2240.00	0.48	2760	0.147
500	0.085	1140	0.471	1680	0.885	2250.00	0.47	2790	0.142
510	0.091	1160	0.478	1690	0.896	2260.00	0.45	2810	0.136
520	0.096	1170	0.482	1700	0.907	2270.00	0.442	2840	0.13
530	0.102	1180	0.488	1710	0.92	2280	0.431	2860	0.125

540	0.108	1190	0.493	1720	0.93	2290	0.425	2890	0.119
550	0.119	1210	0.499	1730	0.94	2300	0.414	2910	0.113
560	0.125	1250	0.505	1740	0.947	2310	0.403	2940	0.108
570	0.13	1320	0.51	1750	0.953	2320	0.391	2980	0.102
580	0.136	1330	0.51	1760	0.964	2330	0.386	3020	0.10
590	0.142	1340	0.52	1770	0.97	2340	0.374	3060	0.09
600	0.147	1350	0.522	1780	0.975	2350	0.369	3100	0.09
610	0.153	1360	0.539	1790	0.987	2360	0.357	3150	0.079
620	0.159	1370	0.556	1800	0.992	2370	0.35	3200	0.074
640	0.164	1380	0.567	1810	0.998	2380	0.34	3260	0.068
650	0.17	1390	0.578	1830	1.004	2390	0.33	3330	0.062
670	0.178	1400	0.584	1840	1.009	2400	0.323	3400	0.057
700	0.181	1410	0.595	1860	1.02	2410	0.318	3490	0.051
730	0.187	1420	0.607	1980	1.02	2420	0.306	3600	0.045
780	0.193	1430	0.624	1990	1.01	2430	0.301	3740	0.04
810	0.198	1440	0.629	2000	0.998	2440	0.289	3970	0.034
830	0.204	1450	0.65	2010	0.97	2450	0.283	4230	0.026
870	0.21	1460	0.65	2020	0.941	2460	0.278	4380	0.03
900	0.215	1470	0.66	2030	0.907	2470	0.272	4540	0.02
920	0.221	1480	0.675	2040	0.873	2480	0.266	4740	0.02
930	0.23	1490	0.68	2050	0.839	2490	0.261	4920	0.017
950	0.23	1500	0.692	2060	0.805	2500	0.26	8520	0
960	0.24	1510	0.703	2070	0.777	2510	0.25		
970	0.249	1520	0.714	2080	0.748	2520	0.24		

Event Number : 319

Elapsed time [sec]	Flow [l/sec]	Elapsed time [sec]	Flow [l/sec]	Elapsed time [sec]	Flow [l/sec]	Elapsed time [sec]	Flow [l/sec]	Elapsed time [sec]	Flow [l/sec]
40	0	700	0.587	1240	0.771	1770	0.737	2300	0.329
80	0.008	710	0.584	1250	0.748	1780	0.743	2320	0.312
150	0.011	720	0.601	1260	0.726	1790	0.748	2340	0.306
170	0.017	730	0.612	1270	0.703	1800	0.754	2360	0.289
190	0.023	740	0.624	1280	0.68	1810	0.765	2380	0.278
210	0.028	750	0.641	1290	0.663	1820	0.771	2400	0.272
220	0.034	760	0.652	1300	0.641	1830	0.777	2410	0.266
240	0.04	770	0.663	1310	0.624	1840	0.788	2420	0.261
250	0.045	780	0.675	1320	0.607	1850	0.794	2430	0.255
260	0.051	790	0.686	1330	0.59	1860	0.799	2450	0.249
270	0.057	800	0.697	1340	0.573	1870	0.805	2480	0.244
280	0.062	810	0.709	1350	0.556	1890	0.811	2490	0.232
290	0.074	820	0.72	1360	0.544	1890	0.811	2500	0.227
300	0.079	830	0.731	1370	0.533	1900	0.805	2520	0.221
310	0.091	840	0.743	1380	0.522	1910	0.782	2530	0.215
320	0.102	850	0.748	1390	0.51	1920	0.765	2540	0.21
330	0.113	860	0.76	1400	0.499	1930	0.743	2580	0.204
340	0.125	870	0.765	1410	0.488	1940	0.72	2580	0.198
350	0.142	880	0.777	1420	0.476	1950	0.697	2600	0.193

348

360	0.159	890	0.782	1430	0.465	1960	0.68	2620	0.187
370	0.17	900	0.794	1440	0.448	1970	0.658	2640	0.181
380	0.187	910	0.799	1450	0.442	1980	0.641	2660	0.176
390	0.204	920	0.811	1460	0.448	1990	0.624	2680	0.17
400	0.221	930	0.822	1470	0.454	2000	0.607	2700	0.164
410	0.232	940	0.828	1480	0.465	2020	0.578	2720	0.159
420	0.244	950	0.833	1490	0.414	2030	0.567	2750	0.153
430	0.255	960	0.845	1500	0.493	2040	0.556	2780	0.147
440	0.266	970	0.856	1510	0.505	2050	0.544	2810	0.142
450	0.278	980	0.868	1520	0.516	2060	0.533	2840	0.136
460	0.289	990	0.879	1530	0.527	2070	0.522	2870	0.13
470	0.301	1000	0.896	1540	0.539	2080	0.51	2900	0.125
480	0.308	1010	0.902	1560	0.567	2090	0.499	2940	0.119
490	0.318	1020	0.907	1570	0.578	2100	0.488	2980	0.113
500	0.329	1030	0.907	1580	0.584	2110	0.476	3020	0.108
510	0.335	1040	0.919	1590	0.595	2120	0.471	3080	0.102
520	0.346	1050	0.924	1600	0.601	2130	0.459	3110	0.096
530	0.357	1060	0.941	1610	0.612	2140	0.448	3180	0.091
540	0.363	1070	1.015	1620	0.624	2150	0.437	3220	0.085
550	0.374	1080	1.009	1630	0.629	2160	0.431	3280	0.079
560	0.386	1090	1.026	1640	0.641	2170	0.42	3340	0.074
570	0.397	1100	1.038	1650	0.652	2180	0.414	3410	0.068
580	0.397	1130	1.043	1660	0.663	2190	0.403	3500	0.062
590	0.42	1140	1.043	1670	0.675	2200	0.397	3810	0.057
600	0.445	1150	1.032	1680	0.68	2210	0.391	3780	0.051
620	0.459	1160	1.004	1690	0.686	2220	0.38	3920	0.045
630	0.471	1170	0.97	1700	0.692	2230	0.374	4110	0.04
640	0.482	1180	0.936	1710	0.697	2240	0.369	4320	0.034
650	0.499	1190	0.907	1720	0.703	2250	0.363	4880	0.028
660	0.51	1200	0.879	1730	0.709	2260	0.352	4880	0.026
670	0.527	1210	0.85	1740	0.714	2270	0.346	5080	0.023
680	0.539	1220	0.822	1750	0.726	2280	0.34	5280	0.02
690	0.556	1230	0.794	1760	0.731	2290	0.335	9080	0